Detection Techniques and Performance Analysis for Fading Multipath Channels with Unresolved Components

Florence A. Danilo

Department of Electrical & Computer Engineering
McGill University
Montreal, Canada

July 2000

A thesis submitted to the Faculty of Graduate Studies and Research in partial fulfillment to the requirements for the degree of Doctor of Philosophy.

Abstract

Personal communication services (PCS) is one of the fastest growing sectors in telecommunications. PCS can be provided by wireless cellular communication systems, that operate in radio environments characterized as multipath fading channels. This thesis addresses the subject of signal detection and performance analysis over multipath Ricean/Rayleigh fading channels, when the multipath delays are known and the path resolvability assumption is not satisfied. The path resolvability condition asserts that the signal autocorrelation function vanishes ("strict") or it is small ("approximate") at inter-path delays. The strict path resolvability assumption is rarely satisfied, and even the approximate path resolvability condition is not always satisfied in practice. For example, the approximate path resolvability is not satisfied for narrow-band systems such as GSM, IS136, or their third generation derivatives and it is neither satisfied for wide-band systems, such as IS95 or W-CDMA, in indoors due to the relatively small multipath delays of these environments.

Existing demodulation schemes for multipath fading channels, such as Rake receivers, provide diversity gains but they are based on the path resolvability assumption. This thesis shows the severe limitations of the classical Rake receiver over unresolved multipath fading channels, and generalizes the Rake concept to improve performance. The optimal receiver that assumes knowledge of the specular component (specular coherent), and the optimal scheme that assumes knowledge of the specular component magnitudes only (non-coherent), are derived for unresolved Ricean multipath fading channels. It is shown that both include an orthogonalization (or decorrelation) stage that vanishes when the multipath is resolved. This thesis presents explicit forms of the Minimum Mean-Square Error estimator of the likelihood ratio estimator-correlator forms, and shows that the decorrelation operation is present in the estimation process. Based on the insight provided by these optimal schemes, suboptimal receivers more suitable for implementation are proposed.

Performance analysis results, for several binary modulation formats, demonstrate the importance of the decorrelation operation in yielding diversity gains and eliminating error floors under multipath unresolvability conditions. It is also shown that the knowledge of the specular component phase does not provide significant gains at high SNR for orthogonal FSK. Finally, it is shown that SNR gains can be obtained by exploiting the knowledge of the specular component magnitude.

Sommaire

Le domaine des services de communications personnelles (PCS) est l'un des secteurs des télécommunications ayant un taux de croissance des plus élevés. Les PCS peuvent être fournis par des systèmes de communications cellulaires. Ces systèmes opèrent dans des environnements qui peuvent être décrits comme des canaux à évanouissements multiples ("multipath fading channels"). Cette thèse porte sur la détection de signaux et l'analyse de performance à travers des canaux à évanouissements multiples de Ricean ou de Rayleigh lorsque les retards des trajets sont connus et l'hypothèse de trajets multiples séparés ("path resolvability assumption") n'est pas satisfaite. L'hypothèse de trajets multiples séparés suppose que la fonction d'autocorrélation du signal évaluée aux retards entre deux trajets, est nulle ('stricte') ou faible ('approximative'). L'hypothèse de trajets multiples séparés stricte est rarement satisfaite, et même l'hypothèse de trajets multiples séparés approximative n'est pas toujours satisfaite en pratique. Par exemple, l'hypothèse de trajets multiples séparés approximative n'est pas satisfaite pour des systèmes à bande étroite tels que GSM, IS136 ou les systèmes équivalents de troisième génération. L'hypothèse de trajets multiples séparés approximative n'est pas non plus satisfaite pour des systèmes à large bande, tels que IS95 ou W-CDMA, dans des environnements à l'intérieur des bâtiments à cause des retards relativement faibles de ces environnements.

Les systèmes existants de démodulation pour des canaux à évanouissements multiples tels que les récepteurs de type Rake, fournissent des gains en diversité mais supposent l'hypothèse de trajets multiples séparés. Cette thèse montre les limites sévères du récepteur Rake classique pour les canaux à évanouissements multiples non séparés et généralise le concept du Rake afin d'améliorer la performance. Ce document présente le récepteur optimal qui connait les valeurs des amplitudes et phases du composant fixe ("specular coherent") ainsi que le récepteur optimal qui dispose simplement de la valeur des amplitudes du composant fixe ("non-coherent"). Ces deux récepteurs optimaux sont calculés pour des canaux à évanouissements multiples de Ricean. Cette thèse montre que les deux récepteurs effectuent un processus d'orthogonalisation (ou de décorrélation) qui disparait dans le cas où le canal est séparé. Ce document donne des expressions explicites de l'estimateur qui est présent dans la forme estimation-correlation du rapport de vraisemblance, où l'estimateur minimise l'erreur quadratique moyenne. Il est aussi montré que l'opération de décor-

rélation est présente dans le processus d'estimation. Cette thèse propose également des récepteurs sous-optimaux plus appropriés pour une conception pratique, obtenus à partir des connaissances acquises lors de l'étude des récepteurs optimaux.

Des résultats d'analyse de performance pour plusieurs modulations binaires montrent à quel point l'opération de décorrélation est importante afin d'obtenir des gains en diversité et d'éliminer les seuils d'erreurs lorsque le canal n'est pas séparé. Cette thèse montre également que la connaissance de la phase du composant fixe n'apporte pas de gains significatifs pour des rapports signal-sur-bruit élevés et une modulation par variation de fréquence orthogonale ("orthogonal Frequency-Shift Keying"). Il est montré finallement qu'il est possible d'obtenir des gains du rapport signal-sur-bruit en tirant bénéfice de la connaissance de l'amplitude du composant fixe.

Acknowledgments

My Ph.D. studies were supported by Research Assistantships from the Natural Sciences and Engineering Research Council of Canada (NSERC), and the Canadian Institute of Telecommunications Research (CITR) in relation with the "Anti-Multipath Modulation" project, through grants awarded to my supervisor Prof. Harry Leib. I thank very much my supervisor and these organizations for their financial support. The prize of the Canadian Advanced Technology Alliance (CATA Alliance), and the financial support of the Helsinki University of Technology during the summer of 1996 are also highly appreciated.

I would like to express my deep gratitude to Prof. Harry Leib for the careful guidance, constant support and the many encouragements he provided through my graduate studies. His patience, critical insight and his advice were instrumental in the completion of this work.

I would also like to thank the late Prof. Georges Zames, Prof. Charalambos Charalambous, and Prof. Maier Blostein, members of my Ph.D. committee, as well as Prof. Peter Kabal for their expertise and advice in completing the research and the manuscript of the thesis.

I would also like to thank my external examiner Prof. Norman Beaulieu from Queen's University in Kingston Ontario, and the members of my Ph.D. Defense committee Prof. Monroe Newborn, Prof. Jonathan Webb, Prof. Harry Leib, Prof. Michael Kaplan, Prof. Maier Blostein and Prof. Paul Mermelstein from INRS-Telecommunications for their suggestions and comments.

My research has also profited from many discussions with my fellow graduate students including Jean-Paul Chaib, Michaël Godbout, Dr. Marc Kimpe, Dr. Raymond Knopp, Ang Li, Rami Mehio, Nader Sheikholeslami, Dr. Jacek Stachurski, Dr. Young Yoon and other fellow members of the Telecommunications and Signal Processing Lab (TSP). I thank them for their help and friendship during these years at McGill.

Je tiens à remercier chaleureusement mes parents, mes sœurs Sylvie et Emmanuelle, mon beau-frère, mes beaux-parents et mon parrain pour leur soutien constant. Je tiens finalement à remercier tout spécialement mon mari Alain, pour s'être tenu toujours à mes côtés et m'avoir encouragée tout au long de ce doctorat, et sans qui ce travail n'aurait pas été possible. C'est pourquoi je lui dédie cette thèse. Je souhaite également remercier tous nos amis pour leur amitié.

Contents

List of Figures

List of Tables

List of Abbreviations

a.s.	Almost surely
AMPS	Advanced Mobile Phone Service
AR	AutoRegressive
ARIB	Association of Radio Industries and Businesses
BEP	Bit-error probabilities
BW	Bandwidth
cdf	Probability (cumulative) distribution function
CDG	CDMA Development Group
CDMA	Code Division Multiple Access
CMMSE	Conventional Minimum Mean-Square Error receiver
CSI	Channel State Information
DECT	Digital European Cordless Telecommunications
DP	Dominant Paths
DPSK	Differential Phase-Shift Keying
DSSS	Direct-Sequence Spread-Spectrum
EDGE	Enhanced Data Rates for Global Evolution
EGC	Equal-Gain Combining
EKF	Extended Kalman Filter
ETSI	European Telecommunications Standards Institute
FSK	Frequency-Shift Keying

FSK(v)	FSK with frequency separation equal to $\frac{v}{T}$
GSM	Global System for Mobile communications
HT100	Hilly Terrain model in GSM
IMMSE	Improved Minimum Mean-Square Error receiver
IPP	Inter-Path Interference
IS136	Interim Standard 136
ISI	Inter-Symbol Interference
LS	Least-Squares (estimation for example)
LSE	Least-Squares Error
l.i.m.	Mean square limit
MAI	Multiple Access Interference
MSE	Mean-Square Error
MAP	Maximum A Posteriori
MAPSD	Maximum A Posteriori Symbol Detector
MMSE	Minimum Mean-Square Error
MEM	Maximum Entropy Method
MFD	Matched Filter Deconvolution
ML	Maximum-Likelihood
MLSD	Maximum-Likelihood Sequence Detector
MPDI	Masked Post-Detection Integrating (receiver)
MQDR	Multi-receiver composed of QDR ($\beta = 0.5, 1, 1.3, 1.5$), R OPT and QR ($\beta = 0$) schemes
MRC	Maximal-Ratio Combining
MUSIC	MUltiple SIgnal Classification method
OPT	Non-coherent optimal receiver over Ricean multipath fading channels
PCS	Personal Communication Services

pdf	Probability density function
PDI	Post-Detection Integrating (receiver)
PN	Pseudo-Noise (codes or sequences)
QR	Quadratic Receiver (or QDR when the multipath is resolved)
R OPT	Rayleigh fading channel non-coherent optimum receiver
R QR	Rayleigh channel Quadratic Receiver (or R OPT when the multipath is resolved)
RA250	Rural Area model in GSM
rms	Root-mean-square
SC	Selection diversity (Combining)
SDPSK	Symmetrical Differential Phase-Shift Keying
SMPDI	Sidelobe-Masked Post-Detection Integrating (receiver)
SNR	Signal-to-Noise Ratio
SPECCOH	Specular-coherent optimal receiver over Ricean multipath fading channels
SSE	Sequential Sequence Estimator
WSSUS	Wide-Sense Stationary Uncorrelated Scattering
TDMA	Time Division Multiple Access
TIA	Telecommunications Industry Association
TU50	Typical Urban model in GSM
W-CDMA	Wide-CDMA

List of Symbols

Symbol	Explanation	page where symbol is defined
^{T}	Transposition of a matrix or vector	
*	Complex conjugation of a matrix or vector	
†	Hermitian conjugation of a matrix or vector	
A	Bias term, see Table 4.2	139
A'	$= -A$	140
A_γ	$= A$, where the dependence on the SNR γ is specified	147
A_{up}	Bound on $\lvert A_\gamma \rvert$ for $\gamma > 1$, see (4.10)	147
$\mathcal{A}$	"Boundary" set of a time-limited function	236
$\mathsf{a}(s)$	Non-anticipating real process jointly measurable in the product σ-algebra $\mathcal{L} \otimes \mathcal{F}$	209
$\mathsf{a}_k(s)$	Time-varying amplitude of the k^{th} path (infinite time resolution)	7
a_k	Complex gain of the k^{th} path (finite time resolution)	14
$\breve{a}_{lm}(\boldsymbol{\theta})$	l^{th} multipath gain of the equivalent decorrelated channel on $[0, T_o]$ when $\boldsymbol{\theta}$ is held fixed $\left(= \sum_{k=0}^{L-1} a_k e^{j\theta_k} \frac{\sqrt{\epsilon_{km}}}{\sqrt{\epsilon_{lm}}} y_{kl}^m\right)$	62
a_k'	k^{th} zero mean multipath gain $(= (a_k - \alpha_k)\, e^{j\theta_k})$	54
$\widehat{a_k'(t\,\vert\,\boldsymbol{\theta})}$	Estimate of a_k' on $[0, t]$ (specular coherent detection), see (3.48)	73

$\widehat{a'_k(t)}$	Estimate of a'_k on $[0,t]$ (non-coherent detection), see (3.131) ..	102
$a''_{lm}(t)$	l^{th} zero mean path gain of the equivalent decorrelated channel on $[0,t]$, see (3.52)	74
$\widehat{a''_{lm}(t\|\boldsymbol{\theta})}$	Estimate of $a''_{lm}(t)$ (specular coherent detection), see (3.54) ...	74
$\widehat{a''_{lm}(t)}$	Estimate of $a''_{lm}(t)$ (non-coherent detection), see (3.133)	103
α_k	Mean of a_k	54
$\boldsymbol{\alpha}$	Column L-vector of means $\{\alpha_l\}_l$ (L-path channel), see (3.13) .	60
$\boldsymbol{\alpha}_k$	$= [\alpha_0, \ldots, \alpha_{k-1}]^T$, valid also if $k = i_t$	89
B_d	Doppler spread of the channel	8
$\mathcal{B}$	"Boundary" set of a time-limited function	236
$\boldsymbol{B}_m$	Matrix with entries equal to the m^{th} signal autocorrelation function at inter-path delays	24
$\boldsymbol{B}$	Matrix used in various contexts	
$\mathsf{b}(s)$	Lebesgue measurable function square integrable (Appendix A.1)	208
	Non-anticipating real process jointly measurable in the product σ-algebra $\mathcal{L} \otimes \mathcal{F}$ (Appendix A.2)	213
$b_{km}(\boldsymbol{\theta}_{k-1})$	A term in $f_m(\boldsymbol{\theta})$ (non-coherent optimal detection), see (3.65)	79
$b^{i_t}_{km}(\boldsymbol{\theta}'_{k-1}, t)$	Equivalent to $b_{km}(\boldsymbol{\theta}_{k-1}) = b_{km}(\boldsymbol{\theta}'_{k-1})$ on $[0,t]$ instead of $[0,T_o]$	90
$b_{km}(\boldsymbol{\theta}'_{k-1}, t)$	Grouping of $b^{i_t}_{km}(\boldsymbol{\theta}'_{k-1}, t)$ into one function, or see (3.101)	92
β	Parameter in the QDR scheme decision variable, see (3.175) ..	125
$\mathfrak{B}_k(s)$	Time-varying phase of the k^{th} path (infinite time resolution) .	7
$\boldsymbol{C}$	Covariance matrix of the channel ($= \boldsymbol{C}_L$)	58
$\boldsymbol{C}_k$	$k \times k$ diagonal matrix with $[\boldsymbol{C}_k]_{ll} = 2\sigma_l^2$, also valid for $k = i_t$	70
$\boldsymbol{C}'_m$	Covariance of $\left[\breve{a}_{0m}(\boldsymbol{\theta}), \ldots, \breve{a}_{L-1m}(\boldsymbol{\theta})\right]^T$ when $\boldsymbol{\theta}$ is held fixed, see (3.20)	64

c	$= \gamma_m^{-\beta}$ in the QDR scheme decision variable, see (3.174)	125
$\chi_A(s)$	Characteristic (or indicator) function of a set A	207
$\chi_m(\dot{z};T_o)$	Decision variable of the QDR scheme on $[0,T_o]$, see (3.175)	125
$\chi_m(\dot{z};t)$	Decision variable of the QDR scheme on $[0,t]$	127
$\chi_m^{'}(\dot{z};t)$	$= \exp\{\chi_m(\dot{z};t)\}$	127
$\chi_m^{''}(\dot{z};T_o)$	Decision variable of the QR scheme on $[0,T_o]$, see (3.184)	130
$\chi_m^{e}(\dot{z};T_o)$	Equivalent non-coherent optimal decision variable for mixed mode Ricean/Rayleigh channels assuming large $\lvert\alpha_0\rvert$ and small γ_m	113
$\boldsymbol{D}_m$	Matrix of eigenvalues of $\boldsymbol{\epsilon}_m\boldsymbol{C}\boldsymbol{\Gamma}_m^*$, see (3.8)	59
$\boldsymbol{D}_{i_t m}(t)$	Matrix of eigenvalues of $\boldsymbol{\epsilon}_{i_t m}(t)\boldsymbol{C}_{i_t}\boldsymbol{\Gamma}_{i_t m}^*(t)$, see (3.35)	70
d_{km}	Term in $b_{km}(\boldsymbol{\theta}_{k-1})$ that is independent of $\boldsymbol{\theta}_{k-1}$, see (3.68)	80
$d_{km}^{i_t}(t)$	Equivalent to d_{km} on $[0,t]$ instead of $[0,T_o]$, see (3.87)	89
$d_{km}(t)$	Grouping of $d_{km}^{i_t}(t)$ into one function, or equivalently see (3.100)	92
$\boldsymbol{d}_m$	Column L-vector formed of the magnitudes and phases of $\{d_{km}\}_k$	83
$\boldsymbol{d}_{i_t m}(t)$	Column i_t-vector formed of the magnitudes and phases of $\{d_{km}^{i_t}(t)\}_k$	88
$\boldsymbol{d}_m(t)$	Column L-vector formed of the magnitudes and phases of $\{d_{km}(t)\}_k$, see (3.95)	91
Δ	Quadratic form (performance evaluation)	137
$\Delta^{'}$	$= -\Delta$	140
Δ_∞	Almost sure limit of Δ when γ tends towards infinity	146
$(\Delta f)_c$	Coherence bandwidth of the channel	8
$(\Delta s)_c$	Coherence time of the channel	8
$\delta(s)$	Dirac delta function	
δ_{lk}	Kronecker delta: $\forall\, l \neq k\ \delta_{lk} = 0$ and $\delta_{ll} = 1$	
δ_n	Phase of α_n	250

$\{\boldsymbol{B}\}_d$	Diagonal matrix composed of the main diagonal entries of $\boldsymbol{B}$	
$\tilde{E}_m$	Energy of the complex signal $\tilde{s}_m(s)$ $\left(=\int_{-\infty}^{\infty}\lvert\tilde{s}_m(s)\rvert^2\,ds\right)$ ..	57
E_b/N_0	Received SNR per bit $\left(=\sum_{k=0}^{L-1}(2\sigma_k^2+\lvert\alpha_k\rvert^2)\,\mathcal{E}_b/N_0\right)$	
$E_{\mathcal{T}}$	Bound on the error of truncation $e_{\mathcal{T}}$ $\left(\text{integration of } \frac{\sin(\Theta_1(t))}{t\Theta_2(t)}\right)$	143
e_{kn}^m	A term in $b_{km}(\boldsymbol{\theta}_{k-1})$, see (3.69)	80
$e_{kn}^{i_t m}(t)$	Equivalent to e_{kn}^m on $[0,t]$ instead of $[0,T_o]$, see (3.91)	90
$e_{kn}^m(t)$	Grouping of $e_{kn}^{i_t m}(t)$ into one function defined piecewise	92
	or equivalently, see (3.102)	92
$e_{\mathcal{T}}$	Performance evaluation: error of truncation	143
$e'_{\mathcal{T}}$	Performance evaluation : error of integration	143
e'_n	Relative error of integration for $\int_{\mathcal{T}_n}^{\mathcal{T}_{n+1}}\frac{\sin(\Theta_1(t))}{t\Theta_2(t)}dt$ (n^{th} sub-integral)	145
$\boldsymbol{\epsilon}_m(t)$	Diagonal matrix with k^{th} diagonal entry $\epsilon_{km}(t)$	58
$\boldsymbol{\epsilon}_m$	Short notation for $\boldsymbol{\epsilon}_m(T_o)$ when $[0,T_o]$ is long or intermediate	58
$\boldsymbol{\epsilon}_{i_t m}(t)$	$i_t \times i_t$ diagonal matrix with $[\boldsymbol{\epsilon}_{i_t m}(t)]_{kk}=\epsilon_{km}(t)$	70
$\epsilon_{km}(t)$	Energy of $\tilde{s}_m(s-\tau_k)$ on $[0,t]$ divided by $\tilde{E}_m$ $(0\le\epsilon_{km}(t)\le 1)$	57
ϵ_{km}	Short notation for $\epsilon_{km}(T_o)$ when $[0,T_o]$ is long or intermediate	58
$\mathcal{E}_b$	Energy per bit of the real signal $s_m(s)$, $m=1,2$	148
η_r	rr^{th} entry of $\boldsymbol{N}_d$	141
η''_r	Equivalent to η_r when γ tends towards infinity	146
$F_\gamma(x)$	Probability distribution function (cdf) of Δ	146
$F_\infty(x)$	Cdf of Δ_∞	146
$F(s,x)$	Denotes various functions used in the proofs of Appendix A	

$\mathcal{F}$	σ-algebra of subsets of a sample space Ω	209
$\mathcal{F}_t$	Smallest σ-algebra containing all the events $\{w(s) < x, x \in \mathbb{R}\}$ for each $s \in [0,t]$	209
$\mathcal{F}_m(\dot{z};t)$	Function of the form $J_m(t)g(\boldsymbol{d}_m(t),t)$	96
$\mathcal{F}'_m(t)$	A term in $d\mathcal{F}_m(\dot{z};t)$, see (3.118)	97
$\mathcal{F}''_m(t)$	A term in $d\mathcal{F}_m(\dot{z};t)$, see (3.118)	97
$f_m(\boldsymbol{\theta})$	Nonlinear term in the product form of $\Lambda_m(\dot{z};T_o\|\boldsymbol{\theta})$, see (3.64)	79
f'_m	Upper-bound of $f_m(\boldsymbol{\theta})$	85
$\mathsf{f}(s)$	Denotes a function (used in various parts of the document)	
$\mathsf{f}_l(z)$	Part of $\mathsf{h}_k(z)$ that is non-analytic at $z = \eta_l^{-1}$, see (G.1)	303
$G(u,s,x)$	Various functions used in the proofs of Appendix A	
$g(\boldsymbol{d}_m)$	Nonlinear term in the product form of $\Lambda_m(\dot{z};T_o)$, see Table 3.1	83
$g_{i_t}(\boldsymbol{d}_{i_t m}(t),t)$	Equivalent to $g(\boldsymbol{d}_m)$ on $[0,t]$ instead of $[0,T_o]$	90
$g(\boldsymbol{d}_m(t),t)$	Grouping of $g_{i_t}(\boldsymbol{d}_{i_t m}(t),t)$ into one function, see (3.94)	91
$\mathsf{g}_l(z)$	Part of $\mathsf{h}_k(z)$ that is analytic at $z = \eta_l^{-1}$, see (G.1)	303
$\boldsymbol{\Gamma}_{rl}(t)$	Cross-correlation matrix of $\tilde{s}_r(s)$ with $\tilde{s}_l(s)$ $\left([\boldsymbol{\Gamma}_{rl}(t)]_{kj} = \rho^{rl}_{kj}(t)\right)$	57
$\boldsymbol{\Gamma}_m(t)$	Correlation matrix of $\tilde{s}_m(s)$ $(= \boldsymbol{\Gamma}_{mm}(t))$	57
$\boldsymbol{\Gamma}_{i_t m}(t)$	$i_t \times i_t$ correlation matrix of $\tilde{s}_m(s)$, see (3.36)	70
$\boldsymbol{\Gamma}_{rl}$	Short notation for $\boldsymbol{\Gamma}_{rl}(T_o)$ when $[0,T_o]$ is long or intermediate	58
$\boldsymbol{\Gamma}_m$	Short notation for $\boldsymbol{\Gamma}_m(T_o)$	58
γ_m	Signal-to-Noise Ratio of the m^{th} transmitted signal $s_m(s)$, see (3.11)	60
$H_c(f,s)$	Transfer function of the channel	9
$H_W(f,s)$	Equivalent channel transfer function (band-limited signals)	11

$H_{cW}(f,s)$	$= \frac{1}{W}\sum_{n=-\infty}^{\infty} h_W\left(\frac{n}{W},s\right) e^{-j2\pi f\frac{n}{W}}$ (i.e. $= H_W(f,s)$ $\lvert f\rvert \leq \frac{W}{2}$) .	12
$H_{\text{LPF}}(f)$	Ideal low-pass filter of bandwidth $W/2$	11
H_m	Hypothesis H_m, $m = 1,\ldots,M$	53
$H_m(\tau,s,t)$	Resolvent kernel of $K_m(s,u)$, see (3.42)	71
$H''_m(\tau,s,t)$	Resolvent kernel of $K''_m(s,u)$	133
$H_{sm}(s,u,t)$	Reversible whitening filter used to whiten $n_c(s)$	105
$\mathcal{H}_m(\tau,s,t)$	Resolvent kernel of $\mathcal{K}_m(s,u)$, see (3.41)	71
$\mathcal{H}'_m(\tau,s,t)$	Linear filter implementing the QDR linear estimate, see (3.180)	128
$\mathcal{H}''_m(\tau,s,t)$	Resolvent kernel of $\mathcal{K}''_m(s,u)$, see (3.191)	132
$h_c(\tau,s)$	Low-pass complex impulse of a multipath fading channel (infinite time resolution), see (2.1)	7
$h_c(\tau)$	Low-pass complex impulse response of the channel assuming slow fading and a finite time resolution, see (2.7)	14
$h_W(\tau,s)$	Equivalent low-pass complex channel impulse response (band-limited signals)	11
$h_{cW}(\tau,s)$	Low-pass complex impulse response of the channel using the sampling model (band-limited signals), see (2.6)	12
$h_{cW}(\tau)$	Low-pass complex impulse response of the channel assuming slow fading and using the sampling model, see (2.8)	14
$h_{\text{LPF}}(\tau)$	Impulse response of the low-pass filter $H_{\text{LPF}}(f)$, $(= W\text{sinc}W\tau)$	12
$h_m(t,s)$	Unique square integrable solution of the Wiener Hopf equation with $K_m(s,u)$, see (3.28)	67
	also equal to $H_m(t,s,t) = H_m(s,t,t) = \Re\left\{2\mathcal{H}^*_m(s,t,t)e^{j\omega_c(t-s)}\right\}$	71
$h''_m(t,s)$	Unique square integrable solution of the Wiener Hopf equation with $K''_m(s,u)$, see (3.187)	132
$\mathsf{h}_k(z)$	$= \dfrac{\varphi_{\Delta\mid H_k}(z)}{z}e^{-zA}$	138

$\{I_k(h,t)\}_k$ Various integrals used in the proofs of Appendix A

$\{I'_k(h,t)\}_k$	Various integrals used in the proofs of Appendix A	
I_{comp}	Numerical value of $\int_0^{\mathcal{T}} \frac{\sin(\Theta_1(t))}{t\Theta_2(t)}dt$	143
I_n	Computed value of $\int_{\mathcal{T}_n}^{\mathcal{T}_{n+1}} \frac{\sin(\Theta_1(t))}{t\Theta_2(t)}dt$ (n^{th} sub-integral)	145
$\boldsymbol{I}$	$L \times L$ identity matrix	59
$\boldsymbol{I}_k$	$k \times k$ identity matrix, also valid for $k = i_t$	70
$\Im\{\cdot\}$	Imaginary part of the argument	
i_t	Number of non-zero time-shifted signals included in $[0,t]$	235
J_m	Quadratic term in the product form of $\Lambda_m(\dot{z};T_o)$, see (3.63)	79
$J_{i_t m}(t)$	Equivalent to J_m on $[0,t]$ instead of $[0,T_o]$	89
$J_m(t)$	Grouping of $J_{i_t m}(t)$ into one function, equivalently see (3.93)	91
$K_m(s,u)$	Covariance function of $v_m(s)$ when $\boldsymbol{\theta}$ is held fixed, see (3.5)	59
$K''_m(s,u)$	Covariance function of $v_m(s)$ when $\boldsymbol{\theta}$ is random, see (3.188)	132
$K^s_m(s,u)$	Term in $K''_m(s,u)$ related to the specular component, see (3.190)	132
$K_{cm}(s,u)$	Covariance function of the colored noise $n_c(s)$, see (3.138)	105
$\mathcal{K}_m(s,u)$	Covariance function of $\tilde{v}_m(s)$ when $\boldsymbol{\theta}$ is held fixed, see (3.6)	59
$\mathcal{K}''_m(s,u)$	Covariance function of $\tilde{v}_m(s)$ when $\boldsymbol{\theta}$ is random, see (3.189)	132
$\mathcal{K}^s_m(s,u)$	Term in $\mathcal{K}''_m(s,u)$ related to the specular component	132
$\mathcal{K}^{i_t}_m(s,u)$	Restriction of the covariance function $\mathcal{K}_m(s,u)$ to $[0,t]^2$ where $T'_m + \tau_0 < t < \infty$, see (3.32)	69
K	Ricean parameter ($=\lvert\alpha_0\rvert^2/2\sigma_0^2$)	148
κ_{lm}	l^{th} eigenvalue of $K_m(s,u)$ on $[0,T_o]$, see (3.9)	60
$\kappa^{i_t}_{lm}(t)$	l^{th} eigenvalue of $K_m(s,u) = K^{i_t}_m(s,u)$ on $[0,t]$	89
$\kappa_{lm}(t)$	Grouping of $\kappa^{i_t}_{lm}(t)$ into one function, or equivalently see (3.43)	72

L	Number of paths of the channel, see (3.1)	54
$\mathcal{L}$	σ-algebra of Lebesgue measurable sets in $[0, b]$	209
$l_{km}(s)$	Filter implementing d_{km}, see (3.72)	82
$l_{km}^{i_t}(s,t)$	Equivalent to $l_{km}(s)$ on $[0,t]$ instead of $[0,T_o]$, see (3.88)	89
$l_{km}(s,t)$	Filter implementing $\widehat{a_k'(t)}$, see (3.49)	73
	also grouping of $l_{km}^{i_t}(s,t)$ into one function, see (3.103)	92
	or correlation of $Q_{*m}(s,v,t)$ with $\tilde{s}_m^*(v-\tau_k)e^{-j\omega_c v}$, see (3.141)	106
$\mathfrak{l}_{i_t m}(t)$	A term in the product form of $J_{i_t m}(t)$	89
$\mathfrak{l}_m(t)$	Grouping of $\mathfrak{l}_{i_t m}(t)$ into one function, or equivalently a term in the product form of $J_m(t)$, see (3.105)	93
$\boldsymbol{\ell}'(t)$	A term in $d\boldsymbol{\varpi}$ (dependence on H_m omitted), see (E.2)	279
$\boldsymbol{\ell}''(t)$	A term in $d\boldsymbol{\varpi}$ (dependence on H_m omitted), see (E.5)	279
$\ell(t)$	A term in $d\boldsymbol{\varpi}$ (dependence on H_m omitted), see (E.8)	279
$\ell_k'(t)$	k^{th} component of $\boldsymbol{\ell}'(t)$ (dependence on H_m omitted), see (E.3)	279
$\ell_k''(t)$	k^{th} component of $\boldsymbol{\ell}''(t)$ (dependence on H_m omitted), see (E.6)	279
$\{\boldsymbol{B}\}_l$	Lower triangular matrix composed of the lower triangular elements of $\boldsymbol{B}$ with zero main diagonal entries	
$\Lambda_m(\dot{z}; T_o \mid \boldsymbol{\theta})$	Likelihood ratio of SPECCOH on $[0,T_o]$, see (3.10)	60
$\Lambda_m(\dot{z}; T_o)$	Likelihood ratio of OPT on $[0,T_o]$, see (3.67)	79
$\Lambda_m(\dot{z}; t)$	Likelihood ratio of OPT on $[0,t]$, see (3.92)	91
λ_{lm}	l^{th} eigenvalue of $\mathcal{K}_m(s,u)$ on $[0,T_o]$, or equivalently l^{th} eigenvalue of $\boldsymbol{\epsilon}_m \tilde{E}_m \boldsymbol{C} \boldsymbol{\Gamma}_m^*$	59
$\lambda_{lm}^{i_t}(t)$	l^{th} eigenvalue of $\mathcal{K}_m(s,u) = \mathcal{K}_m^{i_t}(s,u)$ on $[0,t]$, or equivalently l^{th} eigenvalue of $\tilde{E}_m \boldsymbol{\epsilon}_{i_t m}(t) \boldsymbol{C}_{i_t} \boldsymbol{\Gamma}_{i_t m}^*(t)$	69
$\lambda_{lm}(t)$	Grouping of $\lambda_{lm}^{i_t}(t)$ into one function, see (3.37)	70
M	Number of possible transmitted signals	53

P_e''	Exact bit-error probability of a second receiver denoted for example REC2 (used for comparison between REC1 and REC2)	165
$\hat{P}_e'$	Computed value of P_e'	165
$\hat{P}_e''$	Computed value of P_e''	165
$\mathcal{P}$	Probability measure of a complete probability space $(\Omega, \mathcal{F}, \mathcal{P})$	209
$p_k'(t)$	A term in $q_k'(t)$ (dependence on H_m omitted), see (E.12)	280
$p_k''(t)$	A term in $q_k''(t)$ (dependence on H_m omitted), see (E.15)	280
$p_k^c(t)$	A term in $d\boldsymbol{v}_k$ (dependence on H_m omitted), see (E.19)	281
$p_k^s(t)$	A term in $d\boldsymbol{v}_k$ (dependence on H_m omitted), see (E.20)	281
$\Pi_{i_t m}(t)$	A term in the product form of $J_{i_t m}(t)$	89
$\Pi_m(t)$	Grouping of $\Pi_{i_t m}(t)$ into one function, or equivalently a term in the product form of $J_m(t)$, see (3.104)	93
$\phi_{lm}(s)$	l^{th} eigenfunction of $\mathcal{K}_m(s,u)$ on $[0,T_o]$, see (3.7)	59
$\phi_{lm}^{i_t}(s,t)$	l^{th} eigenfunction of $\mathcal{K}_m(s,u) = \mathcal{K}_m^{i_t}(s,u)$ on $[0,t]$, see (3.34)	69
"$\phi_{lm}(s,t)$"	Grouping of "$\phi_{lm}^{i_t}(s,t)$" into one function, see (3.39)	71
$\varphi_{km}(\boldsymbol{\theta}_{k-1})$	$= \arg[b_{km}(\boldsymbol{\theta}_{k-1})] - \arg[\alpha_k]$, see (3.66)	79
$\varphi_{km}^{i_t}(\boldsymbol{\theta}_{k-1}', t)$	Equivalent to $\varphi_{km}(\boldsymbol{\theta}_{k-1}) = \varphi_{km}(\boldsymbol{\theta}_{k-1}')$ on $[0,t]$ instead of $[0,T_o]$	90
$\varphi_{km}(\boldsymbol{\theta}_{k-1}', t)$	$= \arg\left[b_{km}(\boldsymbol{\theta}_{k-1}', t)\right] - \arg[\alpha_k]$	92
$\varphi_{\Delta\|H_k}(jt)$	Characteristic function of Δ under H_k when $\boldsymbol{\theta}$ is held fixed	137
$Q_{*m}(u,v,t)$	Inverse kernel of $K_{cm}(s,u)$, see (3.144)	107
$\boldsymbol{Q}_m$	Combining diagonal matrix in SPECCOH and OPT, see (3.16)	61
$\boldsymbol{Q}_m'$	Combining diagonal matrix of the quadratic receivers	138
$\boldsymbol{Q}$	Matrix associated with the quadratic form Δ (block diagonal matrix with diagonal blocks $\boldsymbol{Q}_1'$ and $-\boldsymbol{Q}_2'$)	137
$\boldsymbol{q}'(t)$	A term in $d\boldsymbol{\varpi}$ (dependence on H_m omitted), see (E.10)	280

$\boldsymbol{q}''(t)$	A term in $d\boldsymbol{\varpi}$ (dependence on H_m omitted), see (E.13)	280
$q(t)$	A term in $d\boldsymbol{\varpi}$ (dependence on H_m omitted), see (E.16)	280
$q_k'(t)$	k^{th} component of $\boldsymbol{q}'(t)$ (depend. on H_m omitted), see (E.11)	280
$q_k''(t)$	k^{th} component of $\boldsymbol{q}''(t)$ (depend. on H_m omitted), see (E.14)	280
$R_h(\tau, \Delta s)$	$R_h(\tau, \Delta s)\delta(\tau-\tau')$: Autocorrelation of the impulse response of a WSSUS channel	8
$R_h(\tau)$	Multipath intensity profile or delay power spectrum	8
$R_H(\Delta f, \Delta s)$	Spaced-frequency spaced-time correlation function of the channel	8
$R_H(\Delta f)$	Fourier transform of the multipath intensity profile $R_h(\tau)$	8
$R_{mp}(\tau)$	(Time) cross-correlation function of $\tilde{s}_m(s)$ and $\tilde{s}_p(s)$, see (2.10)	21
$R_m(\tau)$	(Time) autocorrelation function of $\tilde{s}_m(s)$, see (2.16)	32
$R_e(s)$	(Time) autocorrelation function of the sounding signal $\tilde{s}_e(s)$	41
$\mathcal{R}(t)$	A term in $\frac{d\mathcal{F}(\dot{z};t)}{\mathcal{F}(\dot{z};t)}$ (dependence on H_m omitted), see (E.46)	292
$\mathcal{R}_1(t)$	A term in $\mathcal{R}(t)$ (dependence on H_m omitted), see (E.47)	293
$\mathcal{R}_2(t)$	A term in $\mathcal{R}(t)$ (dependence on H_m omitted), see (E.50)	293
$\mathcal{R}_{2m}(t)$	$= \mathcal{R}_2(t)$ for the QDR scheme over mixed mode Ricean/Rayleigh channels, see (3.178)	128
$\mathcal{R}_k'(t)$	A term in $\mathcal{R}(t)$ (dependence on H_m omitted), see (E.48)	293
$\mathcal{R}_k''(t)$	A term in $\mathcal{R}(t)$ (dependence on H_m omitted), see (E.49)	293
$\Re\{\cdot\}$	Real part of the argument	
$\mathbb{R}^n$	$= \mathbb{R} \overbrace{\times \ldots \times}^{n} \mathbb{R}$, where $\mathbb{R} = \mathbb{R}^1$ is the set of real numbers	
$\mathcal{R}_{ab}'$	Domain of $\mathbb{R}^2$: $(s,t) \in \mathbb{R}^2$; $0 \le s \le t,\ \ a \le t \le b$, see (A.4)	210
$\mathcal{R}_u'$	Domain of $\mathbb{R}^2$: $(s,x) \in \mathbb{R}^2$; $0 \le s \le x,\ \ 0 \le x \le u$, see (A.17)	220
$\mathcal{R}''$	Domain of $\mathbb{R}^3$, $(u,s,x) \in \mathbb{R}^3$; $0 \le u, s \le x,\ \ 0 \le x \le t$, see (A.34)	230
$\mathcal{R}_r$	Domain of $\mathbb{R}^2$: $(s,t) \in \mathbb{R}^2; 0 \le s \le t,\ \ T' + \tau_{r-1} < t \le T' + \tau_r$	262

$\mathcal{R}_r(\epsilon)$	Domain of $\mathbb{R}^2$: $(s,t) \in \mathbb{R}^2; 0 \le s \le t,\ T' + \tau_{r-1} + \epsilon \le t \le T' + \tau_r$	263
$\mathcal{R}_r''(\epsilon)$	Domain of $\mathbb{R}^3$: $(\tau,s,t) \in \mathbb{R}^3$; $0 \le \tau, s \le t,\ T' + \tau_{r-1} + \epsilon \le t \le T' + \tau_r$	263
$\boldsymbol{R}_k$	Covariance matrix of $\boldsymbol{r}$ under H_k when $\boldsymbol{\theta}$ is held fixed	137
$\boldsymbol{R}$	Short notation for $\boldsymbol{R}_k$	141
$\boldsymbol{R}_d$	Diagonal form of $\boldsymbol{R}_k = \boldsymbol{R}$	141
$\boldsymbol{R}_{sq}$	Square root of $\boldsymbol{R}_d$	141
$\text{rect}(u)$	Rectangular pulse of unit duration centered at the origin	11
$r(s)$	Received signal (common notation) $= \dot{z}(s)$ (thesis notation) ..	33
$\tilde{r}(s)$	Complex envelope of the received signal (common notation) ..	18
$\boldsymbol{r}_m$	Vector of correlations of the received signal with $2\frac{\phi_{lm}(s)}{\sqrt{E_m}} e^{j\omega_c s}$.	60
$\boldsymbol{r}_{i_t m}(t)$	Equivalent to $\boldsymbol{r}_m$ on $[0,t]$ instead of $[0,T_o]$	89
$\boldsymbol{r}$	Vector representing the sufficient statistic for binary signaling	138
$\overline{\boldsymbol{r}}^k$	Mean of $\boldsymbol{r}$ under H_k when $\boldsymbol{\theta}$ is held fixed	137
$\overline{\boldsymbol{r}}$	Short notation for $\overline{\boldsymbol{r}}^k$	141
$\overline{\boldsymbol{r}}'$	$= \frac{\overline{\boldsymbol{r}}}{\alpha_{r_0} \exp\{j\theta_{r_0}\}}$ where $\alpha_{r_0} \neq 0$	141
$\rho_{kj}^{rl}(t)$	Complex correlation coefficient between $\tilde{s}_r(s-\tau_k)$ and $\tilde{s}_l(s-\tau_j)$	57
$\rho_{kj}^{m}(t)$	$\triangleq \rho_{kj}^{mm}(t)$	57
ρ_{kj}^{rl}	Short notation for $\rho_{kj}^{rl}(T_o)$ when $[0,T_o]$ is long or intermediate	58
$\boldsymbol{\varrho}(\boldsymbol{\theta})$	Mean of $\left[a_0 e^{j\theta_0}, \ldots, a_{L-1} e^{j\theta_{L-1}}\right]^T$ when $\boldsymbol{\theta}$ is held fixed, see (3.12)	60
$\boldsymbol{\varrho}'_m(\boldsymbol{\theta})$	Mean of $\left[\breve{a}_{0m}(\boldsymbol{\theta}), \ldots, \breve{a}_{L-1m}(\boldsymbol{\theta})\right]^T$ when $\boldsymbol{\theta}$ is held fixed	62
$S(\tau,\lambda)$	Scattering function of the channel	10
$S(\lambda)$	Doppler power spectrum	8
$\tilde{S}_m(f)$	Fourier transform of $\tilde{s}_m(s)$	10

$\boldsymbol{S}_k$	Matrix diagonalizing the characteristic function $\varphi_{\Delta\|H_k}(jt)$ $(= \boldsymbol{U}_1 \boldsymbol{R}_{sq} \boldsymbol{U}_2)$	141
$\boldsymbol{S}$	Short notation for $\boldsymbol{S}_k$	141
$s_m(s)$	m^{th} transmitted signal	8
$\tilde{s}_m(s)$	Complex envelope of $s_m(s)$	8
$s'_{lm}(s)$	Impulse response of the matched filter used to implement u_{lm}	61
$s'_m(s)$	Approximation of $s'_{lm}(s)$ when $T_o \gg \tau_l$ and $\epsilon_{lm} = 1$ for all l	61
$s_e(s)$	Sounding signal	41
$\tilde{s}_e(s)$	Complex envelope of the sounding signal $s_e(s)$	41
s	Rayleigh path's strength of the second path relative to the first	148
s'	Rayleigh path's strength of the third path relative to the first	183
$\boldsymbol{\Sigma}_0$	Covariance matrix of $\boldsymbol{z}_m$ under H_0	245
$\boldsymbol{\Sigma}_m$	Covariance matrix of $\boldsymbol{z}_m$ under H_m when $\boldsymbol{\theta}$ is held fixed	245
σ_k^2	Variance of the complex Gaussian random variable a_k $(= E\left[\|a_k - \alpha_k\|^2 / 2\right])$	54
σ	$= 2\sigma_k^2$ when all the Rayleigh path strengths are assumed equal	65
σ_τ	Root-mean-square delay spread	48
$S_1(n)$	A term in the sum form of $I(t) = \int_0^t \mathrm{f}(s,t)dw(s)$, see (A.19)	221
$S_2(n)$	A term in the sum form of $I(t) = \int_0^t \mathrm{f}(s,t)dw(s)$, see (A.20)	221
T	$[0, T]$: Numerical range of integration of $\int_0^\infty \frac{\sin(\Theta_1(t))}{t\Theta_2(t)}dt$	143
T_m	Multipath spread of the channel	8
T	Duration of time-limited signaling waveforms	10
T'	"Initial" time of a waveform, see (3.3)	56
T''	"Final" time of a waveform, see (3.4)	56
T'_m	"Initial" time of $\tilde{s}_m(s)$, see (3.30)	68

T_m''	"Final" time of $\tilde{s}_m(s)$, see (3.31)	68
$T_R^{(m)}$	Autocorrelation time of $R_m(\tau)$, see summary in Table 2.1	35
T_o	Refers to the observation interval $[0, T_o]$ such that the L-order linear independency assumption is satisfied on $[0, T_o]$	55
t	Refers to an arbitrary observation interval $[0, t]$, $t > 0$ (no L-order linear independency assumption on $[0, t]$)	68
θ_k	Multipath component phase shifts, see (3.1)	54
θ_k'	$= \theta_k + \arg[\alpha_k] = \theta_k + \delta_k$, see (3.71)	82
$\boldsymbol{\theta}$	Vector of multipath component phase shifts $(= [\theta_0, \ldots, \theta_{L-1}]^T)$	57
$\boldsymbol{\theta}_k$	$= [\theta_0, \ldots, \theta_k]^T$	57
$\boldsymbol{\theta}_k'$	$= [\theta_0', \ldots, \theta_k']^T$	90
$\Theta_1(t)$	$= \sum_{r=0}^{2L-1} \left[\tan^{-1}(\eta_r t) + \frac{\lvert v_r\rvert^2 \eta_r t}{1+\eta_r^2 t^2}\right] - tA$	142
$\Theta_2(t)$	$= \prod_{r=0}^{2L-1} (1+\eta_r^2 t^2)^{1/2} \exp\left\{\frac{\lvert v_r\rvert^2 \eta_r^2 t^2}{1+\eta_r^2 t^2}\right\}$	143
$\Theta_1''(t,x)$	$= \sum_{r=0}^{2L-1} \left[\tan^{-1}(\eta_r'' t) + \frac{\lvert v_r''\rvert^2 \eta_r'' t}{1+\eta_r''^2 t^2}\right] - tx$	146
$\Theta_2''(t)$	$= \prod_{r=0}^{2L-1} (1+\eta_r''^2 t^2)^{1/2} \exp\left\{\frac{\lvert v_r''\rvert^2 \eta_r''^2 t^2}{1+\eta_r''^2 t^2}\right\}$	146
$\tau_k(s)$	Time-varying multipath delay of the k^{th} path (infinite time resolution)	7
τ_k	Multipath delay of the k^{th} path (finite time resolution)	14
τ	Relative delay between the first and the second path $(= \tau_1 - \tau_0)$	148
τ'	Relative delay between the first and the third path $(= \tau_2 - \tau_0)$.	183
τ_R	Theoretical minimum resolution time of time delay estimation techniques $(\tau_R = 0)$	13
τ_R'	Practical minimum resolution time of time delay estimation techniques $(\tau_R' > 0)$	13
$\boldsymbol{U}_1$	Unitary matrix which diagonalizes the matrix $\boldsymbol{R}_k = \boldsymbol{R}$	141

$\boldsymbol{U}_2$	Unitary matrix which diagonalizes the matrix $\boldsymbol{N}$	141
$u_m(s)$	Output of the matched filter matched to $s_m(s)$ under H_m	33
$u_e(s)$	Output of a filter matched to $s_e(s)$ assuming that $s_e(s)$ is transmitted	41
$\tilde{u}_e(s)$	Complex envelope of $u_e(s)$	42
u_{lm}	Correlation of the received signal with $2\frac{\tilde{s}_m(s-\tau_l)e^{j\omega_c s}}{\sqrt{\tilde{E}_m}\sqrt{\tilde{E}_m\epsilon_{lm}}}$, see (3.18)	61
$\boldsymbol{u}_m$	$= [u_{0m}, \ldots, u_{L-1m}]^T$ or equivalently $= (\boldsymbol{X}_m^*)^{-1}\boldsymbol{r}_m$, see (3.18)	61
$\Upsilon_{lm}(s)$	l^{th} eigenfunction of $K_m(s,u)$ on $[0,T_o]$, see (3.9)	60
$\Upsilon_{lm}^{i_t}(s,t)$	l^{th} eigenfunction of $K_m(s,u) = K_m^{i_t}(s,u)$ on $[0,t]$	90
"$\Upsilon_{lm}(s,t)$"	Grouping of "$\Upsilon_{lm}^{i_t}(s,t)$" into one function, or equivalently see (3.44)	72
V_{km}	Magnitude of d_{km}, see (3.73)	83
$V_{km}^{i_t}(t)$	Equivalent to V_{km} on $[0,t]$ instead of $[0,T_o]$, see (3.85)	89
$V_{km}(t)$	Magnitude of $d_{km}(t)$ (and grouping of $V_{km}^{i_t}(t)$), see (3.98)	91
$V_k^c(t)$	Real part of $d_{km}^*(t)$, see (E.17)	280
$V_k^s(t)$	Imaginary part of $d_{km}^*(t)$, see (E.18)	280
$V_A(t)$	Equivalent to $V_{km}(t)$ for a random phase channel, see (3.134)	104
$\boldsymbol{V}_{i_t m}(t)$	Column vector formed of $\left\{V_{km}^{i_t}(t)\right\}_{k=0,\ldots,i_t-1}$, see (3.83)	88
$\boldsymbol{V}_m(t)$	Column vector formed of $\{V_{km}(t)\}_{k=0,\ldots,L-1}$, see (3.96)	91
ϑ_{km}	Phase of d_{km}, see (3.74)	83
$\vartheta_{km}^{i_t}(t)$	Equivalent to ϑ_{km} on $[0,t]$ instead of $[0,T_o]$, see (3.86)	89
$\vartheta_{km}(t)$	Phase of $d_{km}(t)$ (and grouping of $\vartheta_{km}^{i_t}(t)$), see (3.99)	91
$\vartheta_A(t)$	Equivalent to $\vartheta_{km}(t)$ for a random phase channel, see (3.134)	104
$\boldsymbol{\vartheta}_{i_t m}(t)$	Column vector formed of $\left\{\vartheta_{km}^{i_t}(t)\right\}_{k=0,\ldots,i_t-1}$, see (3.84)	89
$\boldsymbol{\vartheta}_m(t)$	Column vector formed of $\{\vartheta_{km}(t)\}_{k=0,\ldots,L-1}$, see (3.97)	91

V_{kn}^m	Magnitude of e_{kn}^m, see (3.75)	83
ϑ_{kn}^m	Phase of e_{kn}^m, see (3.76)	83
$v_m(s)$	Noiseless received signal assuming that $s_m(s)$ is transmitted	8
$\tilde{v}_m(s)$	Complex envelope of $v_m(s)$	8
$v_{km}^d(s)$	Specular component excluding the k^{th} path, see (3.137)	105
$v_{*k}^d(s)$	Whitened $v_{km}^d(s)$, see (3.140)	106
$\tilde{v}_A(s)$	Complex envelope of the noiseless received signal of a random phase channel	104
$\check{v}_m(t\|\boldsymbol{\theta})$	Conditional mean for specular coherent detection, see (3.27)	67
$\check{v}_{L-1m}(t,\boldsymbol{\theta}')$	Other notation for $\check{v}_m(t\|\boldsymbol{\theta})$, see (3.109)	94
$\check{v}_{lm}(t,\boldsymbol{\theta}_l')$	Conditional mean given $\boldsymbol{\theta}_l'$, see (3.110)	94
$\check{v}_m(t)$	Conditional mean for non-coherent detection (definition)	93
	Expressions of $\check{v}_m(t)$, see (3.124)	100
	Other expressions of $\check{v}_m(t)$, see (3.125)	100
$\check{v}_{Rm}(t)$	Part of $\check{v}_m(t)$ associated with the Rayleigh component	116
$\check{v}_{Sm}(t)$	Part of $\check{v}_m(t)$ associated with the specular component	116
$\widehat{v_m(t)}$	Estimator in the quasi estimator-correlator form of a suboptimum receiver, see (3.120)	97
$\widehat{v_{*k}^d(s)}$	Estimate of $v_{*k}^d(s)$ $(= E\left[v_{*k}^d(s)\right] = 0)$	106
$\boldsymbol{v}_k$	$= \left[V_k^c(t)\ V_k^s(t)\right]^T$ (dependence on H_m omitted)	280
$\boldsymbol{v}_{kw}(t)$	A term in $d\boldsymbol{v}_k$ (dependence on H_m omitted), see (E.21)	281
$\boldsymbol{v}^k$	$= \boldsymbol{S}_k^{-1}\overline{\boldsymbol{r}}^k$	141
$\boldsymbol{v}(\boldsymbol{\theta})$	Short notation for $\boldsymbol{v}^k$ specifying the dependence on $\boldsymbol{\theta}$	141
$v_r(\boldsymbol{\theta})$	r^{th} component of $\boldsymbol{v}(\boldsymbol{\theta})$	141
v_r	$v_r(\boldsymbol{\theta})$ for mixed mode Ricean/Rayleigh channels	142
v_r''	Equivalent to v_r when γ tends towards infinity	146

$w(s)$	Wiener process	54
$\dot{w}(s)$	Channel noise: a zero mean white Gaussian process	54
$\boldsymbol{X}_m$	Matrix of eigenvectors of $\boldsymbol{\epsilon}_m \boldsymbol{C} \boldsymbol{\Gamma}_m^*$ (or $[\boldsymbol{X}_m]_{lk} = x_{lk}^m$), see (3.8)	59
$\boldsymbol{X}_{i_t m}(t)$	Matrix of eigenvectors of $\boldsymbol{\epsilon}_{i_t m}(t) \boldsymbol{C}_{i_t} \boldsymbol{\Gamma}_{i_t m}^*(t)$, see (3.35)	70
x_{lk}^m	$= [\boldsymbol{X}_m]_{lk}$ or equivalently k^{th} component of $\boldsymbol{x}_l^m$	59
$x_{lk}^{i_t m}(t)$	Equivalent to x_{lk}^m on $[0,t]$ instead of $[0,T_o]$, $\left(= \left[\boldsymbol{X}_{i_t m}(t)\right]_{lk} \right)$.	70
"$x_{lk}^m(t)$"	Grouping of "$x_{lk}^{i_t m}(t)$" into one function, see (3.38)	70
$\boldsymbol{x}_l^m$	l^{th} eigenvector of $\tilde{E}_m \boldsymbol{\epsilon}_m \boldsymbol{C} \boldsymbol{\Gamma}_m^*$ (or $\boldsymbol{\epsilon}_m \boldsymbol{C} \boldsymbol{\Gamma}_m^*$)	241
$\boldsymbol{x}^m$	Short notation for $\boldsymbol{x}_l^m$	241
$\boldsymbol{x}'$	$= \boldsymbol{\Gamma}_m^* \boldsymbol{x}^m$ (dependence on H_m omitted)	242
y_{kl}^m	$= \left[\boldsymbol{X}_m^{-1}\right]_{kl}$	62
$y_m^{\mathrm{c}}(s)$	Unknown part of the received signal (specular coherent detection), see (3.29)	67
$y_m^{\mathrm{nc}}(s)$	Unknown part of the received signal (non-coherent detection), see (3.126)	101
$Z_{i_t m}(t)$	A term in the product form of $J_{i_t m}(t)$	89
$Z_m(t)$	Grouping of $Z_{i_t m}(t)$ into one function, or equivalently a term in the product form of $J_m(t)$, see (3.106)	93
$\dot{z}(s)$	Received signal, see (3.1)	54
$\dot{z}_*(s)$	Whitened received signal, see (3.139)	106
z_{lm}	Correlation of the received signal with $\Upsilon_{lm}(s)$, see (3.15)	61
$\boldsymbol{z}_m$	$= [z_{0m}, \ldots, z_{L-1m}]^T$	61
$z_{lm}^{i_t}(t)$	Equivalent to z_{lm} on $[0,t]$ instead of $[0,T_o]$, see (3.89)	89
"$z_{lm}(t)$"	Grouping of "$z_{lm}^{i_t}(t)$" into one function, see (3.107)	93

Chapter 1

Introduction

In the last decade we have witnessed a phenomenal interest in Personal Communication Services (PCS). The aim of PCS is to provide communications in the form of voice, data and video services anywhere and anytime. This objective can be achieved by wireless cellular communication systems that operate in indoor and outdoor radio environments. In such environments, the transmitted signal reaches the receiver not only by a direct line-of-sight but by ways of many paths, due to reflection, diffraction and scattering of radio waves by terrains, buildings and walls. Therefore, the received signal consists of the sum of multiple delayed and attenuated versions of the transmitted signal in addition to the thermal noise present in any practical communication systems [1, 2]. Generally, due to time variations of the environment (motion of vehicles, people, ...), the attenuations and delays in this multipath propagation model are time-variant, resulting in a fading phenomenon. Fading is the terminology used to denote any random amplitude variations (in this case, in the received signal). These amplitudes variations in the received signal are created by the successive constructive or destructive vector additions of the multiple attenuated and delayed versions of the transmitted signal.

The effect of multipath fading, and consequently the choice (or validity) of a particular channel model, depends on the signal transmission bandwidth. For narrow-band transmission (compared to the channel coherence bandwidth), the multiple versions of the transmitted signal cannot be distinguished one from another; thus they are all combined together (constructively or destructively) resulting in a flat fading channel. In this case, the noiseless received signal is simply a randomly attenuated and carrier phase-shifted version of the transmitted signal. Optimal detection over such a

channel in the presence of additive white Gaussian noise and Rayleigh fading results in bit-error probabilities inversely proportional to the Signal-to-Noise Ratio (SNR), yielding no diversity gains.

For wide-band transmission, different frequency components of the transmitted signal undergo different attenuations and phase shifts yielding the so-called frequency selective channels. Two classical models are investigated in detail in Section 2.1.1 of Chapter 2, one that assumes band-limited signals and the other one that assumes known multipath delays. When the transmitted signal is assumed to be strictly band-limited, a tapped-delay line model with tap spacing at multiples of the reciprocal of the signal bandwidth is obtained by using the sampling theorem [2]. The sampling model does not make any assumption on the channel multipath delays, but is valid only for strictly band-limited signals and has, in theory, an infinite number of taps. Practically, due to the finite multipath spread of the channel, the tapped-delay line can be truncated to a finite length. When the multipath delays are known at the receiver (in practice estimated), a multipath fading channel model is obtained with paths at each known multipath delay. Each path is composed of the sum of sub-paths which cannot be separated (i.e. cannot be resolved).

It is well known that diversity gains (illustrated by bit-error probabilities inversely proportional to higher powers of the SNR) can be obtained for these wide-band systems by the use of Rake receivers [3, 4, 5]. However Rake structures are based on the path resolvability assumption in one form or another. A detailed description of the various forms of the path resolvability, their implications and use in the literature is provided in Section 2.2 of Chapter 2. The classical Rake receiver [5], implicitly based on the sampling model, assumes a very large bandwidth yielding very narrow signal autocorrelation functions that do not overlap when time-shifted by the channel multipath delays. This first form of the path resolvability condition ensures proper estimation of the amplitudes and phases of the multipath components that are used to form a replica of the noiseless received signal. Since this estimated signal is composed of several versions of the transmitted signal, it provides a diversity effect.

Rake receivers based on the known multipath channel model [4] assume that the signal autocorrelation function vanishes at inter-path delays, a condition satisfied if the inter-path delays are larger than the signal autocorrelation time[1]. Equivalently,

[1]The signal autocorrelation time is defined as the width of the signal autocorrelation function. More details on those two definitions are given in Section 2.2.1.

this second form of path resolvability says that any two versions of the transmitted signal that are time-shifted by two different multipath delays are orthogonal. For wide-band signals, path resolvability is often stated as the inter-path delays being much larger than the reciprocal of the signal bandwidth since their autocorrelation time is approximately equal to the inverse of their bandwidth. After matched filtering to the transmitted signal, a weighted sum of time-shifted versions of the signal autocorrelation function plus noise is obtained. Sampling the matched filter output at the multipath delays yields samples that can be combined to generate a higher SNR. Therefore, Rake receivers combat multipath by exploiting the inherent diversity provided by the time-shifted versions of the transmitted signal.

The path resolvability assumption when the multipath delays are known is generally satisfied for spread-spectrum systems in outdoor environments but cannot be ensured in indoor environments due to smaller inter-path delays (order of tens to hundreds of nanoseconds [6, 7]). Numerical examples based on existing standards showing that the path resolvability assumption is not always satisfied are provided in Section 2.3.1. For example, a bandwidth of 50MHz would be needed to resolve an indoor multipath fading channel [8].

Assuming known multipath delays, the objective of this thesis is to derive receiver structures that yield diversity gains without the path resolvability assumption over multipath fading channels. Notice that the multipath delays can be estimated with a time resolution greater than the reciprocal of the information signal bandwidth. Such a time resolution can be achieved by using a sounding signal of bandwidth larger than that of the information signal, or by using super-resolution techniques [9]-[19]. The concepts of this thesis are applicable to existing as well as future generation wide-band systems in indoor and outdoor environments. They are also applicable to narrow-band systems that "see" a flat fading channel provided that the channel multipath delays, identified with wide-band signals, are known. A detailed formulation of the problem is given in Section 2.3.1.

In this thesis, the multipath gains are assumed to be Ricean distributed; Rayleigh fading is viewed as a special case of Ricean. For Ricean fading, each path can be considered as the phasor sum of a Rayleigh component with a uniformly distributed phase and a fixed (specular) component. Two classes of detection techniques are considered: specular coherent and non-coherent. Specular coherent detection assumes knowledge of the specular component magnitudes and phases. Non-coherent detection assumes

knowledge of the specular component magnitudes only. Part of this work has been previously published in [20]. This thesis also includes a thorough literature review (Section 2.1.2) of existing detection techniques over multipath fading channels, with an emphasis on the assumptions related to path resolvability used in the derivation and performance analysis of receiver structures. The issue of path resolvability and its effects on receiver structures for fading multipath channels has not been given proper attention in existing literature surveys. Finally, since this thesis considers multipath fading channels models that assume known multipath delays, existing sounding techniques are also reviewed (Section 2.2.3).

1.1 Original Contributions

The main contribution of this thesis is the derivation of the specular coherent and non-coherent optimal receiver structures, respectively SPECCOH and OPT, over unresolved Ricean multipath fading channels, and identification of multipath decorrelation as essential to eliminating error floors. These novel structures are generalizations of the Rake receiver to unresolved multipath fading channels. This thesis also presents explicit forms of the Minimum Mean-Square Error (MMSE) estimate included in the estimator-correlator structure [21] of the SPECCOH as well as in the OPT, and provides an interpretation of the operations performed by these schemes. Based on the insight provided by these optimal structures, non-coherent suboptimal receivers implementing the decorrelation operation, such as the Quadratic Decorrelation Receiver (QDR), are derived. These receivers can be used in narrow-band and wide-band systems in indoor and outdoor environments since they are especially designed to handle path unresolvability. The results illustrate that diversity gains can be obtained on multipath fading channels without spreading the signal bandwidth. A list of the original contributions of this thesis follows:

Detection over unresolved multipath fading channels; generalization of the Rake:

- Derivation of the specular coherent and non-coherent optimal receiver structures (SPECCOH and OPT) over unresolved Ricean multipath fading channels (respectively Section 3.2.1 and Section 3.3.1).
- Identification of an orthogonalization (or decorrelation) stage as crucial to eliminating error floors over unresolved multipath fading channels (Sections 3.2.2,

3.3.2 and Sections 4.2.2-4.2.3, 4.3).

- Derivation of a simpler quadratic non-coherent suboptimal receiver implementing the decorrelation operation, over mixed mode Ricean/Rayleigh channels[2], with performance close to optimal at high SNR: the Quadratic Decorrelation Receiver (QDR) (Section 3.7.2).

Estimator-correlator interpretation; presence of the decorrelation operation:

- Derivation of explicit forms of the MMSE estimates (conditional means) for the SPECCOH and OPT schemes, and relation of these structures to a multipath channel (respectively Section 3.2.3 and Sections 3.3.3, 3.4.3).
- Interpretation of the QDR as an estimator-correlator with a linear estimate (Section 3.7.3).
- Derivation of the linear MMSE estimate (Section 3.7.6).

Performance analysis (one-shot transmission):

- Presentation of asymptotically tight upper and lower-bounds to the bit-error probabilities of OPT (methodology: Section 4.1, results: Section 4.2.2).
- Numerical evaluation of the bit-error probabilities of SPECCOH, QDR and various receivers previously derived, over mixed mode Ricean/Rayleigh and Rayleigh fading channels for binary Frequency-Shift Keying (FSK) and variants of Differential Phase-Shift Keying (DPSK) (SPECCOH: Section 4.2.2, QDR: Section 4.2.3).
- Identification of the cases where knowledge of the specular component phase shifts provides significant gains and where it does not, with emphasis on the comparison of two quadratic schemes, SPECCOH and QDR (effect of the modulation scheme choice) (Section 4.2.2: Table 4.4, Section 4.2.3).
- Demonstration that SNR gains can be obtained by the knowledge of the specular component magnitude that assumes an intermediate value, for FSK and variants of DPSK (Section 4.2.3).

[2]A channel is said to be mixed mode Ricean/Rayleigh if the first path is Ricean distributed and the other paths gains are Rayleigh distributed.

1.2 Outline of the thesis

- Chapter 2 reviews the modeling of multipath fading channels and existing detection techniques. Assumptions related to path resolvability used in the derivation and performance analysis of receivers structures are elucidated. A detailed description of the various forms of the path resolvability assumption and their implications is provided. Since this thesis considers multipath fading channels models that assume known multipath delays, existing sounding techniques are also reviewed. Then the objectives and methodology of the thesis are formulated.

- Chapter 3 presents the channel model and then derives optimal and suboptimal receiver structures without the path resolvability assumption. The interpretation as an estimator-correlator is investigated and explicit forms of the estimators are derived.

- Chapter 4 analyses the one-shot transmission performance of the receivers developed in Chapter 3 for commonly used binary modulation schemes such as FSK and variants of DPSK over mixed mode Ricean/Rayleigh and Rayleigh fading channels. The effects of path unresolvability and the effectiveness of the decorrelation operation to eliminate error floors is demonstrated.

- Chapter 5 discusses practical applications of results and gives possible extension of the work.

- Chapter 6 presents a summary and conclusions to this thesis.

- Appendices A-G present the mathematical details of this thesis.

Chapter 2

Background and Rationale

2.1 Receivers for multipath fading channels

2.1.1 Modeling of multipath fading channels

This section presents models for multipath fading channels and the influence of the transmission bandwidth on the choice of a particular model. Multipath fading is a common phenomenon present in many different types of environments, such as land cellular [8, 22] as well as indoor cellular communication systems [1], short-wave ionospheric radio communications in the $3-30$MHz frequency band (HF), ionospheric forward scatter in the $30-300$MHz frequency band (VHF), and tropospheric scatter (beyond-the-horizon) radio communications in the $300-3000$MHz frequency band (UHF) and $3-30$GHz frequency band (SHF) [2]. Finally, multipath fading affects microwave line-of-sight links [2, 23, 24], and one-path fading affects satellite communications [25]-[28].

A multipath fading channel can be modeled as a linear time-varying filter with low-pass complex impulse response given by [1, 2, 29, 30]

$$h_c(\tau, s) = \sum_k \mathsf{a}_k(s) e^{j\mathsf{ß}_k(s)} \delta\big(\tau - \tau_k(s)\big) \tag{2.1}$$

where s and $s-\tau$ are respectively the observation time[1] and application time of the impulse, $\{\mathsf{a}_k(s)\}$, $\{\tau_k(s)\}$ and $\{\mathsf{ß}_k(s)\}$ are the random time-varying amplitude, arrival-

[1] The notation s is used throughout this thesis as the observation time instead of the classical letter t since this letter is reserved to denote an arbitrary finite observation interval $[0, t]$.

time and phase sequences. In other words, if the signal $s_m(s) = \Re\{\tilde{s}_m(s)e^{j\omega_c s}\}$ is transmitted over the channel, the noiseless received signal is $v_m(s) = \Re\{\tilde{v}_m(s)e^{j\omega_c s}\}$ where

$$\tilde{v}_m(s) = \int_{-\infty}^{\infty} h_c(\tau, s)\tilde{s}_m(s-\tau)d\tau = \sum_k \mathsf{a}_k(s)e^{j\beta_k(s)}\tilde{s}_m\big(s-\tau_k(s)\big)$$

The coefficients $\{\mathsf{a}_k(s)\}$, $\{\tau_k(s)\}$ and $\{\beta_k(s)\}$ can be estimated and characterized statistically. The most common statistical characterization of the channel is obtained under the assumptions that the impulse response $h_c(\tau, s)$ is wide sense stationary and the scattering is uncorrelated [31]-[33]. The term Wide-Sense Stationary Uncorrelated Scattering (WSSUS) channels is generally used. A WSSUS channel can be described either in the time or frequency domain by several correlation functions, coined Bello functions [31, 34], as shown in Fig. 2.1.

As seen in Fig. 2.1, the autocorrelation of the impulse response of a WSSUS channel is given by

$$E\left[h_c^*(\tau, s)h_c\big(\tau', s+\Delta s\big)/2\right] = R_h(\tau, \Delta s)\delta\big(\tau-\tau'\big)$$

The multipath intensity profile of the channel or the delay power spectrum denoted in Fig. 2.1 by $R_h(\tau)$ is obtained by setting Δs to zero in $R_h(\tau, \Delta s)$. The range of values of τ over which $R_h(\tau)$ is *essentially* non-zero is called the multipath spread of the channel and is denoted by T_m [2, ch. 7]. The Fourier transform of the multipath intensity profile is denoted $R_H(\Delta f)$ in Fig. 2.1. The range of values of Δf over which $R_H(\Delta f)$ is *essentially* non-zero is called the coherence bandwidth of the channel and is denoted $(\Delta f)_c$. Due to the Fourier transform relationship between $R_h(\tau)$ and $R_H(\Delta f)$, the coherence bandwidth is approximately equal to the reciprocal of the multipath spread. The autocorrelation of the transfer function $H_c(f, s)$ of a WSSUS channel is called the spaced-frequency spaced-time correlation function of the channel and is denoted in Fig. 2.1 by $R_H(\Delta f, \Delta s)$. When $\Delta f = 0$, its Fourier transform with respect to Δs is called the Doppler power spectrum and is denoted $S(\lambda)$ in Fig. 2.1. The range of values of λ over which $S(\lambda)$ is *essentially* non-zero is called the Doppler spread of the channel and is denoted by B_d. The range of values of Δs over which $R_H(\Delta s)$ is *essentially* non-zero is called the coherence time of the channel and is denoted by $(\Delta s)_c$. The coherence time is approximately equal to the reciprocal

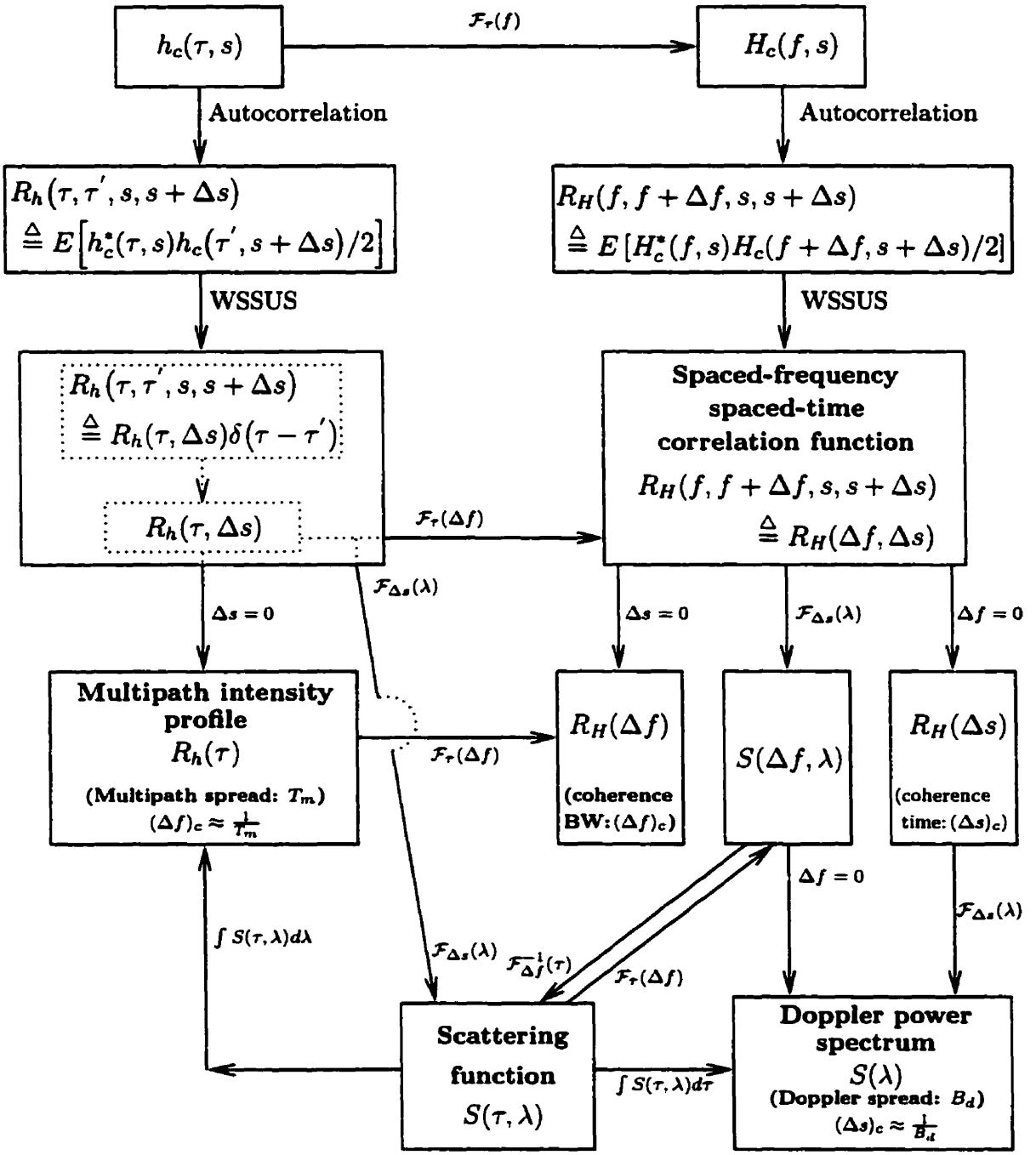

Fig. 2.1 Relations between Bello functions: $\mathcal{F}_x(y)$ denotes the Fourier transform with respect to x and yields a function of the variable y, for example $\mathcal{F}_x(y)\{f(x,z)\} = \int_{-\infty}^{\infty} f(x,z) e^{-j2\pi yx} dx = F(y,z)$

of the Doppler spread. Relationships between the multipath intensity profile and the Doppler power spectrum exist via the so-called scattering function $S(\tau, \lambda)$ which is the Fourier transform of $R_h(\tau, \Delta s)$ with respect to Δs. Other methods of obtaining the scattering function through Fourier transform relationships are illustrated in Fig. 2.1. The channel coherence time and bandwidth along with the transmission bandwidth and the duration of the signaling waveform provide a way to classify fading channels. Common classifications of fading channels are frequency selective versus flat fading (frequency nonselective) and slow versus fast fading [2].

If the signaling waveform is time-limited and its duration T is such that $T \ll (\Delta s)_c$, the channel attenuation, delay and phase shift of each path are essentially fixed for the duration of at least one signaling interval and the channel is slowly varying. In that case the channel becomes linear time invariant with low-pass complex impulse response given by [1]

$$h_c(\tau) = \sum_k \mathsf{a}_k e^{j\beta_k} \delta(\tau - \tau_k) \tag{2.2}$$

If the transmitted signal bandwidth W is such that $W \ll (\Delta f)_c$, the channel is said to be flat or frequency nonselective. In that case the noiseless received signal is simply the transmitted signal multiplied by a complex-valued random process as seen in the following [2]

$$\begin{aligned}\tilde{v}_m(s) &= \int_{-\infty}^{\infty} h_c(\tau, s)\tilde{s}_m(s-\tau)d\tau = \int_{-\infty}^{\infty} H_c(f, s)\tilde{S}_m(f)e^{j2\pi fs}df \\ &= \int_{-\frac{W}{2}}^{\frac{W}{2}} H_c(f, s)\tilde{S}_m(f)e^{j2\pi fs}df \approx H_c(0, s)\int_{-\frac{W}{2}}^{\frac{W}{2}} \tilde{S}_m(f)e^{j2\pi fs}df = H_c(0, s)\tilde{s}_m(s)\end{aligned}$$

where $H_c(0, s) = \mathcal{F}_\tau \left\{ \sum_k \mathsf{a}_k(s) e^{j\beta_k(s)} \delta(\tau - \tau_k(s)) \right\} \Big|_{f=0} = \sum_k \mathsf{a}_k(s) e^{j\beta_k(s)}$ and $\tilde{S}_m(f)$ is the Fourier transform of $\tilde{s}_m(s)$. When the number of paths is large, $H_c(0, s)$ is Gaussian by virtue of the central limit theorem. If $H_c(0, s)$ is modeled as a zero mean Gaussian process, its magnitude $|H_c(0, s)|$ is Rayleigh distributed for any fixed s and its phase $\arg[H_c(0, s)]$ is uniformly distributed between $-\pi$ and π. In that case the channel is said to undergo Rayleigh fading. If $H_c(0, s)$ is modeled as a non-zero mean Gaussian process, its magnitude $|H_c(0, s)|$ is Ricean distributed for any fixed s resulting in a Ricean channel.

When $W \gg (\Delta f)_c$, the channel is said to be frequency selective since the Fourier transform of the transmitted signal is subject to different gains and phase shifts across the frequency band. Note that according to this definition no channel classification is given when W is of the order of $(\Delta f)_c$. Some authors define a channel as frequency selective if W is of the order of or exceeds $(\Delta f)_c$ [35, p. 338]. For convenience in the following, the second definition for frequency selective channels will be used with an explicit mention of the more strict assumption whenever required. Several models can be derived for frequency selective channels depending whether or not the transmitted signal is strictly band-limited, the fading is slow and the multipath delays are characterized deterministically or statistically.

Let us first derive the sampling channel model that assumes a strictly band-limited transmitted signal. This model based on the sampling theorem is valid regardless of the channel temporal variations and does not explicitly characterize the multipath delays. Let $s_m(s)$ be the transmitted signal strictly band-limited to W. Then $\tilde{s}_m(s)$, its complex envelope, is strictly band-limited to $W/2$ and an equivalent channel model can be obtained by introducing an ideal low-pass filter $H_{\text{LPF}}(f)$ as illustrated in Fig. 2.2 [31].

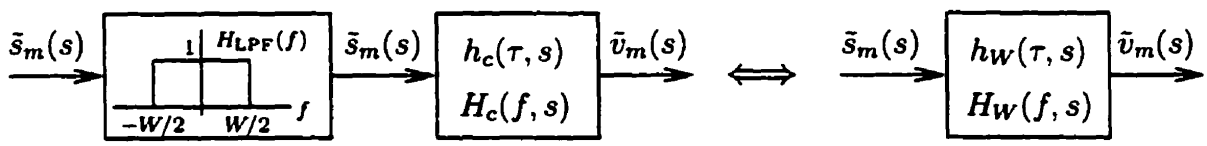

Fig. 2.2 Equivalent band-limited channel model

The equivalent filter $h_W(\tau, s)$ is band-limited with transfer function given by

$$H_W(f, s) = H_c(f, s)\text{rect}\left(\frac{f}{W}\right)$$

where $\text{rect}(u)$ is defined as

$$\text{rect}(u) = \begin{cases} 1 & |u| \leq \frac{1}{2}, \\ 0 & \text{else.} \end{cases} \tag{2.3}$$

Using the sampling theorem, the band-limited channel impulse response is given by

$$h_W(\tau, s) = \sum_{n=-\infty}^{\infty} h_W\left(\frac{n}{W}, s\right) \operatorname{sinc}\left[W\left(\tau - \frac{n}{W}\right)\right] \tag{2.4}$$

where the equality in (2.4) is in the mean square sense [36] and $\operatorname{sinc}(x) = \frac{\sin(\pi x)}{\pi x}$. Using the convolution in the τ variable $h_W(\tau, s) = h_{\text{LPF}}(\tau) * h_c(\tau, s)$, $h_{\text{LPF}}(\tau) = W\operatorname{sinc}(W\tau)$ and (2.1) yields

$$h_W\left(\frac{n}{W}, s\right) = \sum_k \mathsf{a}_k(s) e^{j\beta_k(s)} W \operatorname{sinc}\left[W\left(\frac{n}{W} - \tau_k(s)\right)\right] \tag{2.5}$$

From (2.4), the transfer function of the band-limited channel is given by

$$H_W(f, s) = \mathcal{F}_\tau\left\{h_W(\tau, s)\right\} = \frac{1}{W} \sum_{n=-\infty}^{\infty} h_W\left(\frac{n}{W}, s\right) e^{-j2\pi f \frac{n}{W}} \operatorname{rect}\left(\frac{f}{W}\right)$$

Define

$$H_{cW}(f, s) = \frac{1}{W} \sum_{n=-\infty}^{\infty} h_W\left(\frac{n}{W}, s\right) e^{-j2\pi f \frac{n}{W}} \quad \left(\text{i.e. } H_{cW}(f, s) = H_W(f, s) \quad |f| \le \frac{W}{2}\right)$$

$$h_{cW}(\tau, s) \triangleq \mathcal{F}_f^{-1}\left\{H_{cW}(f, s)\right\} = \frac{1}{W} \sum_{n=-\infty}^{\infty} h_W\left(\frac{n}{W}, s\right) \delta\left(\tau - \frac{n}{W}\right) \tag{2.6}$$

From (2.6), whenever the transmitted signal is strictly band-limited to W, the channel can be modeled as a tapped-delay-line with tap spacing $1/W$ and tap weight coefficients $\left\{h_W\left(\frac{n}{W}, s\right)\right\}$ [2, 37]. In other words, the resolution in time delay of the model is $1/W$. Note that such a model requires an infinite observation interval and an infinite number of taps. However in practice, if the multipath delay spread is T_m, the channel model can be approximated by truncation at $N = [T_m W] + 1$, resulting in the low-pass complex impulse response

$$h_{cW}(\tau, s) = \frac{1}{W} \sum_{n=1}^{N} h_W\left(\frac{n}{W}, s\right) \delta\left(\tau - \frac{n}{W}\right)$$

where $[T_m W]$ is the integer part of $T_m W$. From the central limit theorem evoked in (2.5), $h_W\left(\frac{n}{W}, s\right)$ for all n can be statistically modeled as jointly Gaussian random

processes in the s variable when the number of paths is large.

Channel models for slowly fading or time-invariant multipath fading channels are considered next. These channels are assumed to be time-invariant over at least one symbol duration with low-pass complex impulse response given by (2.2). The multipath delays in (2.2) can be characterized statistically or assumed known at the receiver. The first proposed distribution of the sequence of path arrival times $\{\tau_k - \tau_0\}_1^\infty$ was Poisson [1, 38]. However, inadequacy of this distribution has been observed. Therefore, a modified Poisson distribution, the so-called $\Delta - K$ model was subsequently proposed [1],[38]-[40]. Such a model takes into account the clustering property of paths caused by the grouping property of scatterers.

Other types of models assume that the multipath delays are known at the receiver. In principle, such a model is given by (2.2), where the multipath delays are assumed to be known. In practice, however, the multipath delays are estimated with a finite resolution in time (or finite time resolution). The minimum resolution time of an estimation method τ_R corresponds to the minimum required time difference between two multipath delays (i.e. minimum inter-path delays) so that the estimator identifies these two time delays as distinct. Methods of estimation are summarized in Section 2.2.3. In order to estimate all the inter-path delays present in (2.2), where some of them could be arbitrarily small, one needs to sound the channel with an impulse received with an infinite bandwidth yielding an infinite time resolution (i.e $\tau_R = 0$). In that case, all the multipath delays can be estimated or equivalently the multipath is completely resolved and the output of the channel to $\delta(s)$ is given by (2.2) and illustrated in Fig. 2.3(a). However only a finite time resolution or equivalently

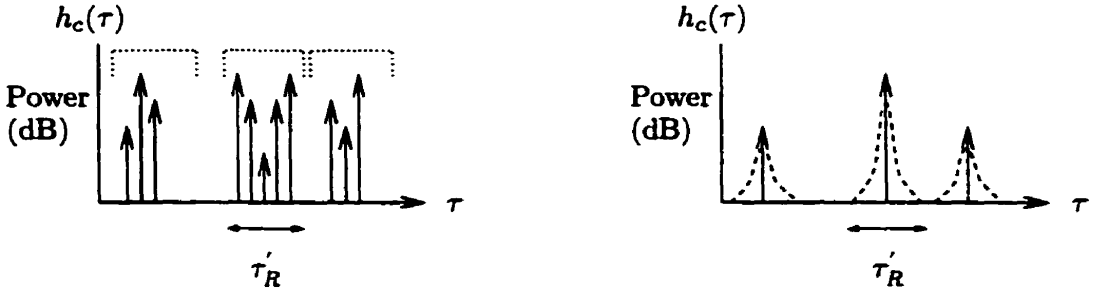

(a) Channel impulse response (infinite time resolution: $\tau_R = 0$)

(b) Channel impulse response (finite time resolution: $\tau_R' > 0$)

Fig. 2.3 Channel impulse responses

a non-zero minimum resolution time $\tau_R' > 0$ can be obtained in practice. Classical sounding techniques using pulse compression (for example the convolution matched-filter technique) [41, 42] yield a time resolution of $1/W$ where W is the bandwidth of the sounding pulse. However super-resolution techniques may yield a time resolution better than $1/W$ but still finite [9]-[19]. Note that in models found in the literature, the time resolution is usually considered to be $1/W$ [1, 43]. This finite time resolution, specific to each estimation technique, has to be taken into account in the representation of channels with known delays yielding the classical model of multipath fading channels. Rewriting (2.2) with a double summation the noiseless received signal $v_m(s) = \Re\{\tilde{v}_m(s)e^{j\omega_c s}\}$ can be expressed as (see Fig. 2.3)

$$v_m(s) = \Re\left\{\left(\sum_{k=0}^{L-1}\sum_{l=-\infty}^{\infty} a_{k,l}e^{j\beta_{k,l}}\tilde{s}_m(s-\tau_{k,l})\right)e^{j\omega_c s}\right\} \approx \Re\left\{\left(\sum_{k=0}^{L-1} a_k\tilde{s}_m(s-\tau_k)\right)e^{j\omega_c s}\right\}$$

where all the "sub-paths" within a cluster, which cannot be resolved (when $|\tau_{k,l} - \tau_{k,r}| \ll \tau_R'$) are grouped together. Therefore $a_k \triangleq \sum_l a_{k,l}e^{j\beta_{k,l}}$ and $\tau_k \approx \tau_{k,l}$ are respectively the complex gain and the time delay of the k^{th} "resolved" multipath component. The low-pass complex impulse response of the channel is then given by

$$h_c(\tau) = \sum_{k=0}^{L-1} a_k\delta(\tau - \tau_k) \tag{2.7}$$

For band-limited signals, the channel model given by (2.7) is completely equivalent to the linear time-invariant version of the tapped-delay-line model (2.6) given by

$$h_{cW}(\tau) = \frac{1}{W}\sum_{n=-\infty}^{\infty} h_W\left(\frac{n}{W}\right)\delta\left(\tau - \frac{n}{W}\right) \tag{2.8}$$

where the tap weight coefficients of the tapped-delay-line are given by

$$h_W\left(\frac{n}{W}\right) = \sum_{k=0}^{L-1} a_k W\mathrm{sinc}\left[W\left(\frac{n}{W} - \tau_k\right)\right] \tag{2.9}$$

since $h_W(\tau) = h_{\mathrm{LPF}}(\tau) * h_c(\tau) = \sum_{k=0}^{L-1} a_k W\mathrm{sinc}\left[W(\tau - \tau_k)\right]$.

In both models, the amplitudes and phases of the path gains can be assumed known or characterized statistically. Several amplitude distributions can be chosen to

characterize the path gains. Well-accepted models employ the Rayleigh and Ricean distributions with the Rayleigh distribution modeling the small-scale rapid amplitude fluctuations in absence of a strong received component and the Ricean distribution modeling the presence of a strong path [1]. Their justification comes from the central limit theorem which states that the sum of a large number of random variables tends to a Gaussian random variable. Measurements in indoor environments showed good fit to Rayleigh and Ricean at various frequencies, i.e. 900MHz, 1.5GHz, $2.3-2.4$GHz and 60GHz [1, 44, 45]. Measurements in micro-cellular urban radio environment showed good fit to Rayleigh and Ricean at 1.8GHz [46]. Good fit to Ricean was also observed in straight sections of tunnels environment at 900MHz and 1.8GHz [47]. However other measurements studies showed better fit to log-normal distributions even for local areas data [40]. Other amplitude distributions include Nakagami [48], Suzuki [39], extended Suzuki [49] and the new so-called POCA distribution [50].

2.1.2 Detection techniques for multipath fading channels

Detection techniques over multipath fading channels have been thoroughly studied since the fifties. In this work, only the subject of single-user systems is addressed. Fundamentals of single-user detection over multipath fading channels are well covered in several reference books [29, 30, 35, 51, 52]. A more recent literature review of this subject is presented in [53].

Two basic types of single-user receivers can be identified, one-shot receivers and multi-shot receivers. One-shot receivers assume that a single symbol signal is transmitted. The decision regarding the transmitted signal is based on an observation interval that spans the duration of the received signal corresponding to the single transmitted symbol [51, p. 80]. Over Gaussian or one-path fading channels, the observation interval is the transmitted signal duration; however over multipath channels, the observation interval should be chosen to be longer to take into account the multipath spread. The key assumption of one-shot receivers is that the transmitter is idle outside the transmitted signal interval. Performance analysis of one-shot receivers yields single-pulse performance or matched filter bounds. It is equivalent to neglecting any Inter-Symbol Interference (ISI) and hence provides a lower-bound on bit-error probabilities if ISI is present. Multi-shot receivers assume that a sequence of symbol signals is transmitted and make decisions concerning all the transmitted symbols [51, p. 80].

Optimality of a receiver is defined with respect to a criteria such as minimization of a cost, or risk, function (Bayes criterion). In detection theory, common optimality criteria is minimization of the average probability of symbol error. Any receiver structure (optimum or suboptimum) depends on knowledge of channel parameters. For example, a receiver may know some parameters exactly or may know only their second order statistical description.

One-shot receivers for multipath fading channels, optimum in the minimum average probability of symbol error sense, have been first presented in [3]-[5], including the well known Rake receiver [5]. In [3], the channel is time-varying, multipath delays are assumed to be arbitrary but known and the path gains are zero mean Gaussian random variables (Rayleigh fading). Representing the continuous time transmitted and received signals using the sampling theorem, the likelihood ratio is expressed in terms of filters defined by integral equations. These integral equations are solved in closed-form only for special cases such as the slowly fading multipath and the single path channels. Using Neumann's series expansion of the integral equations, a structure has been proposed using a tapped-delay-line that approximates the optimum decision rule at low SNR. In [4], optimal receivers are derived assuming that the multipath delays are known at the receiver and satisfy the resolvability condition defined by

$$|\tau_l - \tau_k| \gg \frac{1}{W}, \qquad l \neq k$$

where W is the transmission bandwidth. The resolvability condition implies that the signal autocorrelation function is approximately zero at inter-path delays (i.e at $\tau_l - \tau_k$ for example). Path gains are assumed to be Ricean or Rayleigh distributed and the phases of the specular term are assumed to be either known or uniformly distributed. A one-shot optimum receiver using the same resolvability assumption was derived in [48] with Nakagami distributed multipath gains. Essentially, these receivers employ the Rake technique [5]. The optimal receiver that assumes a statistical characterization of the multipath delays, was derived in [4] with Ricean or Rayleigh path gains, and in [48] with Nakagami gains. In [48], structures assuming a statistical characterization of the multipath delays were derived under the assumption that with high probability $|\tau_l - \tau_k| > \delta$ for all $l \neq k$, where δ is approximately the reciprocal of the transmission bandwidth.

The well known Rake receiver was first introduced in [5], although its concept has

been used already in the suboptimal structure of [3]. Optimality of the Rake receiver was studied in detail in [54]. The approximate finite tapped-delay-line model obtained from the sampling theorem was implicitly used to obtain the Rake structure in [5]. In the original Rake structure, the amplitudes and phases of the multipath components are first estimated based on the received signal and then the estimates are used to form a replica of the noiseless received signal. Once this replica has been formed, detection is equivalent to the detection of a known signal in white Gaussian noise which is basically a correlation of the received signal with the replica. The estimation of the channel coefficients or its channel impulse response is accomplished using correlation. In the absence of noise, the correlation of the received signal with the sum of both possible transmitted waveforms yields the channel impulse response when the long-term cross-correlation function of the transmitted signals is zero for all τ shifts and each transmitted signal autocorrelation function is approximately equal to a delta function. Practically, the second condition yields very narrow signal autocorrelation functions that do not overlap when time-shifted by the channel multipath delays. The signal is then said to resolve the multipath. This "resolvability" condition, defined more rigorously in Section 2.2.1, is satisfied for wide-band signals of sufficiently large bandwidth.

Fig. 2.4 illustrates an example of the m^{th} hypothesis block diagram of a Rake receiver with weighted combining that employs matched filtering. The actual receiver is composed of several such blocks, one for each possible transmitted signal followed by a decision device that takes the largest output. The combining weights can be either equal to the estimated values of the amplitudes and phases of the multipath components as in [5], or based on the channel statistical characterization as in [4]. The received signal is passed through a matched filter associated with the m^{th} possible transmitted signal. The output of the matched filter is passed through a tapped-delay-line (Fig. 2.4), whose tap outputs, corresponding to inter-path delays, are combined and the result sampled. Basically, the receiver attempts to collect the signal energy present at each of the tap outputs, hence the name Rake [2]. In other words, it combats multipath by exploiting the inherent channel diversity yielding diversity gains. In addition to being essential for channel estimation, the resolvability condition (i.e. non-overlapping of time-shifted versions of the signal autocorrelation function) has important implications for the interpretation of the Rake receiver. Whenever the resolvability condition is satisfied, the multipath channel provides several replicas of

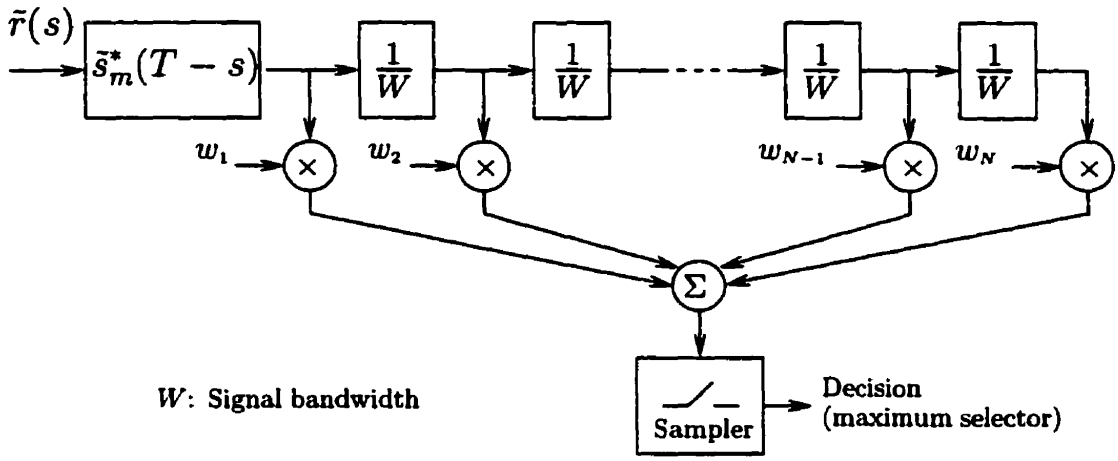

Fig. 2.4 Rake receiver: block diagram for the m^{th} hypothesis using complex envelope notation.

the transmitted signal at the corresponding tapped-delay-line outputs. Therefore the Rake receiver can be viewed as a time diversity combiner. This shows that results in multichannel or diversity reception over fading channels are applicable to resolved multipath channels [55]-[57], providing ways of combining the tapped-delay-line outputs.

Linear diversity techniques for fading channels have been studied in detail since the fifties. In [58], Selection diversity (SC), Maximal-Ratio Combining (MRC) and Equal-Gain Combining (EGC) were compared based on their SNRs. As expected, MRC yielded the highest output SNR. Non-coherent and coherent diversity combining techniques were derived in [59], and analyzed in terms of their bit-error probabilities when the amplitudes are Rayleigh distributed (Rayleigh fading). In [59] the term non-coherent refers to the receiver absence of knowledge of the phases and instantaneous signal amplitudes. Coherent diversity assumes that such a knowledge is available to the receiver. It was shown that square-law combining is the optimum non-coherent combining for Rayleigh fading. MRC, similar to [58], was found to be the optimum coherent diversity technique. The optimal one-shot diversity receiver for Ricean fading, assuming only a statistical characterization of the channel with a known specular term, was derived in [55]. This receiver represents a generalization of the square-law combiner of [59]. It was also derived in [60] for a more general channel based on a

sampling model. Performance of the receiver derived in [55] was analyzed in [56] when no specular term is present. Minimum error rates achievable by optimization of the number of diversity branches have been determined for predetection MRC and post-detection EGC with frequency and time-diversity [61]. For both combining schemes, detection was performed using bandpass matched filters followed by square-envelope detectors (non-coherent). It was shown that the minimum required transmitted power for a given error rate is strictly larger than zero for both diversity techniques (even if an infinite number of diversity branches is used). MRC with correlated diversity branches and arbitrary average powers in each was studied in [62] in term of the probability density function (pdf) of the combined power. In [63], the probability distribution of the post-combination SNR is calculated for SC, MRC, EGC and constant combining without assuming equal mean SNR on the various diversity branches. Binary error probabilities of square-law combiners and differentially coherent diversity receivers with EGC were studied in [64] for a frequency selective multi-channel. The existence of an irreducible error probability due to the selective fading was demonstrated. Results were later extended in [65] to multi-channels with a specular term. Error probabilities for the optimum coherent receiver over Ricean/Rayleigh fading multi-channels were derived in [57] for signals with identical cross-correlation coefficients on each diversity channel. Error probabilities for orthogonal signaling were also derived for a (non-coherent) square-law combiner. Extension of these results to nonorthogonal signaling was done in [66]. Square-law envelope diversity combining was studied in [67] for FSK and DPSK where each channel is composed of two specular terms and a scatter (diffuse) term. Adaptive diversity receivers using a noisy reference signal derived either from the previously received signal or from a pilot signal, were analyzed in [68]. Closed-form expressions for the probabilities of error of these diversity receivers with M-phase signaling and Rayleigh fading in each diversity branch were given. Equivalent results were derived for Ricean channels with 2-4 phase signaling.

More recently, analysis of the performance of equal-gain diversity receivers with coherent, differentially coherent and non-coherent detection on Nakagami fading channels was performed using a Chernoff-bound type of approximation [69]. One method to determine the average bit-error probability consists of averaging the conditional error rate, conditioned on the predetection SNR. For EGC, the predetection SNR is equal to $\gamma_{EGC} = \left[\sum_{k=0}^{L-1} |a_k|\right]^2 / (2LN_0)$ where L is the number of diversity channels,

N_0 is the noise power of one channel and $|a_k|$ are Nakagami random variables corresponding to the signal amplitudes at the output of each diversity channel. Therefore, the first step is the computation of the pdf of $\sum_{k=0}^{L-1} |a_k|$. In [69], such a pdf is approximated within a specified accuracy by the convergent infinite series derived in [70]. Bit-error probabilities of an equal-gain combiner with coherent detection over Rayleigh fading channels were derived in [71] in the form of one-fold integrals. Error probabilities for MRC and post-detection combining over Nakagami fading channels were also studied by the same author [72, 73]. A unified approach to the performance analysis of digital communications over slow fading multi-links channels, possibly correlated was proposed in [74, 75]. This framework allows evaluation of the average bit-error rate either in closed-form or in the form of a single integral with finite limits readily calculable numerically. The results included MRC and EGC with coherent detection as well as square-law combining. Error probabilities with square-law combining were computed over fast Ricean fading channels in [76]. Symbol error probabilities for various coherent 8-ary and 16-ary modulations were computed in [77] for slow Rayleigh, Ricean and Nakagami fadings with SC, MRC and EGC. These results enabled accurate optimization of modulation constellation parameters. In particular it was shown that the CCITT V.29 constellation can be improved by adjusting the amplitude ratios of the constellation points.

Another implementation of the Rake receiver using a channel estimator based on periodic integration approximated by a first order recursive structure (re-circulation loop) was given in [78]. It was assumed that the signal and noise autocorrelation functions are essentially zero at all inter-paths delays (i.e. at $\tau_l - \tau_k$). Variations of the Rake receiver were later derived. For example, an optimum receiver for reception of Direct-Sequence Spread-Spectrum (DSSS) signals on WSSUS fading channels was presented in [79]. A discrete-time multipath channel model (with a discrete set of Rayleigh-faded paths) was derived and resulted in a receiver very similar to [4]. Since the paths are assumed to be Rayleigh fading (zero mean signal component), the obtained optimum receiver is quadratic and hence non-coherent. The obtained channel model can be viewed as a discrete-time version of the continuous-time tapped-delay-line model derived from the sampling theorem. Although the channel was formed by a continuum of multipaths, the spread-spectrum processing produced the discrete multipath components (delayed versions of the transmitted signal). Because Pseudo-Noise (PN) codes with ideal autocorrelation properties are assumed, the discrete-time

delayed versions of the input signal form orthogonal sequences. In other words, the discrete-time delayed versions of the input are resolvable similar to the resolvability of the continuous-time delayed versions of the input signal from [5]. An optimum non-coherent one-shot receiver for detection of band-limited DSSS signals over Rayleigh multipath fading channels was derived in [80] using chip rate sampling of the received signal. Non-coherent here means that the receiver knows the channel statistics rather than the channel impulse response. A DSSS coherent Rake receiver that estimates the phases and combining factors of the receiving paths was presented in [81]. The inter-paths delays were assumed to be larger than the length of a code chip. The effect of imperfect phase estimates of a coherent Rake receiver that employs a Phase Lock Loop for phase recovery was studied for DSSS signaling in [82]. The channel model of [82] is a sampling model (finite-length tapped-delay-line) where the tap weights are assumed to be perfect estimates of the channel parameters. Self noise arising from non ideal PN sequences is neglected.

In [83], the "partially coherent" binary optimum receiver for multipath Rayleigh fading channels under uniform orthogonality conditions was derived. This receiver knows the multipath coefficient phases but has only statistical knowledge of their magnitudes (the term "partially coherent" is not accurate here, and the receiver should be called coherent). Uniform orthogonality means that the complex envelopes of the transmitted signals $\tilde{s}_m(s)$ satisfy

$$R_{mp}(\tau_l - \tau_k) \triangleq \int_{-\infty}^{\infty} \tilde{s}_m^*(u)\tilde{s}_p(u-(\tau_l-\tau_k))du = \int_{-\infty}^{\infty} \tilde{s}_m^*(u-\tau_k)\tilde{s}_p(u-\tau_l)du = \tilde{E}_m\delta_{lk}\delta_{mp} \tag{2.10}$$

where δ_{lk} is the Kronecker delta ($\forall\, l \neq k\ \delta_{lk} = 0$ and $\delta_{ll} = 1$). As seen previously, optimal receivers over multipath fading channels that are related to Rake structures have always assumed resolved multipath. The optimal one-shot receiver for multipath Rayleigh channels with known delays without the path resolvability assumption has been derived in [84]. The analysis included a Doppler phase shift f_p, and the set $\left\{b_p(s) = e^{j2\pi f_p s}\tilde{s}_m(s-\tau_p)\right\}_p$ was assumed to be linearly independent over the observation interval. Later, optimal receivers over two-path Rayleigh channels were derived with known delays and different levels of channel knowledge assuming "uniform au-

tocorrelation" without path resolvability [85]. Uniform autocorrelation is defined as

$$|R_m(\tau_1 - \tau_0)| \triangleq \left| \int_{-\infty}^{\infty} \tilde{s}_m^*(u)\tilde{s}_m(u - (\tau_1 - \tau_0))du \right| \quad \text{independent of } m \qquad (2.11)$$

Optimum receivers, even of one-shot type, may be difficult to implement or difficult to analyze; therefore suboptimum receivers are often considered. A quadratic suboptimum receiver structure over two-path Rayleigh channels with known delays was derived in [86] for signals with uniform orthogonality for the cross-correlation function, i.e.

$$R_{mp}(\tau_1 - \tau_0) \triangleq \int_{-\infty}^{\infty} \tilde{s}_m^*(u)\tilde{s}_p(u - (\tau_1 - \tau_0))du = 0 \quad m, p = 1, 2 \quad m \neq p \qquad (2.12)$$

Such a condition states that the signal cross-correlation function is zero at the channel inter-path delays. The decision variable of the proposed receiver is an optimum (in the minimum probability of error sense) linear combination of two quadratic forms. The first quadratic form is the sum of the outputs of two envelope detector receivers with filters matched respectively to the first and second possible transmitted signals. The second quadratic form is equivalent to the first one, except that filters are matched to the delayed versions of the possible transmitted signals. "Partially coherent" and non-coherent BiQuadratic and Bilinear, suboptimal receivers were derived in [83, 87] for uniformly orthogonal signals as defined by (2.10).

Since performance analysis of one-shot receivers (matched filter bound) assumes no ISI, it provides in general a lower-bound to the bit or symbol error performance. Nevertheless, such analysis is important to provide benchmarks. Analytical matched filter bounds of the optimal receiver for resolved multipath Rayleigh fading channel have been derived in [88] for uniformly orthogonal signals. The result was equivalent to the one found in [59] in the context of multi-channel reception. It was shown that for a resolved multipath channel diversity gains can be obtained by using the contributions of all paths. Furthermore, it was shown that even a low power path should not be discarded in the decision variable. Since the optimum decision variable in that case is a Hermitian quadratic form in complex Gaussian random variables, the bit-error probability is found by inverting the characteristic function of the quadratic form [88]- [92]. This method of computing the bit-error probability applies to any quadratic receiver. New methods based on the evaluation of the Laplace transform of

the pdf of the difference between the metrics of two competing signal sequences have been proposed in [93, 94]. For diversity detection, the unified approach proposed in [74, 75] can be used. In [48], analytical bit-error probabilities over Nakagami multipath fading channels were only obtained for suboptimal receivers and under the assumption of uniform orthogonal signals and complete resolvability, equivalent to the following assumptions:

$$R_{12}(\tau) \triangleq \int_{-\infty}^{\infty} \tilde{s}_1^*(u)\tilde{s}_2(u-\tau)du = 0 \quad \forall \tau$$

$$\left|\int_{-\infty}^{\infty} \tilde{s}_1^*(u)\tilde{s}_1(u-\tau)du\right| = \left|\int_{-\infty}^{\infty} \tilde{s}_2^*(u)\tilde{s}_2(u-\tau)du\right| \quad \text{(i.e. } |R_1(\tau)| = |R_2(\tau)|) \quad \forall \tau$$

$$\left|\int_{-\infty}^{\infty} \tilde{s}_m^*(u)\tilde{s}_m(u-\tau+\tau_l)du\right| \left|\int_{-\infty}^{\infty} \tilde{s}_m^*(u)\tilde{s}_m(u-\tau+\tau_k)du\right| = 0 \quad l \neq k, m=1,2 \quad \forall \tau$$

It was shown that diversity gains are obtained even for suboptimum receivers. Diversity gains were also pointed out in [79]-[81] for Spread-Spectrum single-user transmission with receivers based on Rake structures. In [95], both single-user and multi-user transmissions employing a single-user Rake receiver with perfect measurement of the channel parameters (coherent multipath combining) were considered. The channel is characterized as a linear time-invariant filter with randomly distributed complex gains and multipath delays. Based on approximations to the average bit-error probability using SNRs, diversity gains were observed for single-user transmission, however large performance degradations were observed for multi-user transmission. Although in the receiver design no particular assumption was made on the inter-path delays, in the performance analysis, the probability that the inter-path delays are less than the chip duration was assumed to be very small. In [96], based on a Gaussian approximation, performance of DSSS Rake receivers with random spreading sequences, several diversity combining schemes and two finger assignment strategies, was assessed. It was assumed that the inter-path delays are larger than the chip duration. For diversity combining it was shown that instantaneous amplitude-based finger assignment is much better than the average power-based finger assignment. This was to be expected since instantaneous amplitude-based finger assignment corresponds to a complete (instantaneous) knowledge of the channel, whereas power-based finger assignment corresponds to a statistical characterization of the channel. More recently, the impact of the number of Rake fingers, spreading bandwidth and multipath spread

on the total Rake receiver output SNR for Spread-Spectrum systems was assessed in [97]. A representative result indicates that for Spread-Spectrum systems with 5MHz bandwidth and a constant power delay profile channel having $5\mu s$, increasing the number of Rake fingers from one to three yields 3.8dB SNR gain and 1.5dB if the number of Rake fingers is further increased by two.

Performance of the optimum receiver for unresolved multipath Rayleigh fading channels based on bounds to the bit-error probability was considered in [98] for binary widely orthogonal signals. Binary signals are said to be widely orthogonal if any time-Doppler-shifted version of one signal is orthogonal to any time-Doppler-shifted version of the other, i.e.

$$\int \tilde{s}_1(u-\tau_l)e^{j2\pi f_l u}\tilde{s}_2^*(u-\tau_k)e^{-j2\pi f_k u}du = 0 \tag{2.13}$$

The channel was modeled as a linear time-invariant filter composed of L discrete paths with complex amplitudes equal to a_l. Let $\boldsymbol{B}_m$ and $\boldsymbol{C}$ be $L \times L$ matrices with lk^{th} entries equal to

$$[\boldsymbol{B}_m]_{lk} = \int \tilde{s}_m(u-\tau_l)e^{j2\pi f_l u}\tilde{s}_m^*(u-\tau_k)e^{-j2\pi f_k u}du \tag{2.14a}$$

$$[\boldsymbol{C}]_{lk} = E\left[(a_l-\bar{a}_l)(a_k-\bar{a}_k)^*\right] = 2\sigma_l^2\delta_{lk} \quad (\boldsymbol{C} \text{ is a diagonal matrix}) \tag{2.14b}$$

Upper and lower spectral bounds on the error probability were derived assuming that the spectra of the matrices $\boldsymbol{B}_m\boldsymbol{C}, m = 1, 2$ are narrow about the nominal value $\frac{1}{L}$. When $\boldsymbol{B}_m$ is diagonal or approximately diagonal (i.e. $\sum_{l\neq k}|[\boldsymbol{B}_m]_{lk}| \ll 1$) and $\boldsymbol{C} \approx \sigma\boldsymbol{I}$, these bounds are found to be sharp. Note that the sharpness of the bounds depends on the spread of the spectrum of $\boldsymbol{B}_m\boldsymbol{C}$, and only results with small values of this spread have been presented in [98]. Results for the special case of resolvable signals, i.e. any time-Doppler-shifted version of a signal is orthogonal to any version of itself ($\boldsymbol{B}_m = \boldsymbol{I}$), in addition to the widely orthogonality assumption, were also briefly compared to previous diversity results [56]. In [85], bit-error probabilities corresponding to the optimum receiver are evaluated for two-path Rayleigh fading channels with known delays under the assumption of "uniform autocorrelation" defined by (2.11). Two-fold diversity-like effects in the performance of envelope orthogonal FSK and variants of chirp or linear frequency sweep modulation were observed. In [86], bit-error probabilities of the suboptimum quadratic receiver mentioned previously have only

been derived over two-path unresolved Rayleigh fading channels under the assumption of uniformly orthogonality for the cross-correlation function defined by (2.12). This receiver also achieves diversity-like effects using the same type of modulation schemes as in [85]. Similarly bit-error probabilities (BEP) and asymptotical BEP were derived in [87, 99] for suboptimal receivers under the assumption of uniform orthogonality.

All these performance results are matched filter bounds associated with receivers that know the channel only partially. Some authors define the matched filter bound as the performance of the optimal receiver that assumes perfect equalization (no ISI) and perfect channel estimation [100, 101]. Assuming single transmission, the considered receiver is composed of filters matched to all possible noiseless received signals. The matched filter performance bound assuming the channel to be known exactly provides a ultimate lower-bound on the probability of error and can be found without the resolvability assumption. Matched filter bounds have been evaluated for two-path Rayleigh fading channels in [102], for multipath Rayleigh channels in [100, 101],[103]-[106] and for mixed mode Ricean/Rayleigh fading channels[2] in [107]. All matched filter bounds showed that diversity-like improvement can be achieved at high SNR. Performance degradation due to noisy channel estimation in the adapted matched filter receiver was assessed in [108] for various channel estimation techniques assuming no ISI. Bit-error probability of a matched filter receiver assuming perfect channel estimation in a multipath Rayleigh fading channel that includes the effects of Inter-Path Interference (IPP) and ISI, was determined for a binary antipodal system [109].

Since decisions of optimal one-shot receivers are based only on the current received symbol and assume single transmission, the performance of these receivers is not optimal if the channel has memory or if ISI is present (introduced by the channel or by the type of modulation used). Memory for a multipath fading channel means that the fading coefficients, over two consecutive symbol intervals or more, are correlated. Transmission over multipath fading channel most often results in ISI due to the channel multipath spread, T_m. The only case where ISI can be neglected occurs when spread spectrum signals of duration much larger than T_m are used [33]. In that case only a small portion of adjacent symbols (in the order of numbers of chips) interferes with the detection of a particular symbol. However, frequently ISI is taken

[2] A mixed mode Ricean/Rayleigh fading channel denotes a multipath channel where the first path gain is Ricean distributed and all the other path gains are Rayleigh distributed.

into account in Spread-Spectrum Code Division Multiple Access (CDMA) systems along with other type of interference such as Multiple Access Interference (MAI), see for example [110]. Performance degradation due channel memory and ISI may be overcome by using sequential detection, i.e multi-shot receivers, or equalizers [2].

One can distinguish between two types of multi-shot receivers: symbol-by-symbol-decision structures, including equalizers, and sequence detection structures. Symbol-by-symbol decision receivers make an individual decision on each transmitted symbol based on the entire received sequence. The optimal symbol-by-symbol decision receiver, in the sense of minimizing the probability of symbol error, is the Maximum A Posteriori (MAP) Symbol Detector (MAPSD) [2, 51, 111]. Two types of MAPSD algorithms were developed at the end of the sixties; a forward and backward recursions algorithm [112], and a forward recursions only algorithm [113]. Later a algorithm similar in concept to the one proposed in [112] was derived for the decoding of error control codes [114]. Recently a new MAP algorithm has been derived [115] that generates optimum soft-outputs; it requires only a forward recursion and memory that increases only linearly with the decision delay.

Sequence decision receivers make a decision on the transmitted sequence based on the received signal. The optimal sequence detector in the sense of minimizing the probability of sequence error when the data sequence a-priori probabilities are equal, is the Maximum-Likelihood (ML) sequence detector (MLSD) [33, 53, 116]. MLSDs for a known time-invariant deterministic channel causing ISI have been studied in the seventies [117]-[119]. The detection technique employed the Viterbi algorithm [120]. Unification of these receivers and extension to time-varying known as well as unknown channels with decision-directed channel estimation was considered in [121]. An extension of the MLSD from [119] to linear time-varying dispersive channels with diversity appeared in [122]. The resulting receiver is optimum only for ideal Channel State Information (CSI) but can also be used with high-quality CSI estimates. The MLSD when the channel is completely unknown (blind MLSD) was considered in [123]. In [124] the MLSD was derived for linear modulations with band-limited signals over a frequency selective Rayleigh fading channel with a known continuous time multipath intensity profile (second-order statistical characterization of the channel). The received signal was filtered and sampled according to the sampling theorem yielding a discrete channel model. An irreducible error floor due to ISI was observed. The Maximum-Likelihood sequence estimation (MLSE) was achieved by using Kalman fil-

tering and the Viterbi algorithm. MLSD receivers were analyzed either analytically [118, 119, 122] or by using simulations [118, 121, 124]. In [125], a combined MLSE equalizer and decoder was analyzed analytically for slowly time-varying frequency selective Rayleigh fading channels. A new upper-bound on the decoded bit-error probability was derived. Pairwise probability of sequence or event errors of the MLSD with perfect knowledge of the impulse response of a WSSUS channel was later derived in closed-form without any resolvability assumption [126]. Union bounds and approximations were used to obtain the total average probability of error. Slow fading was assumed and sequence by sequence reception was performed making this structure equivalent to a one-shot receiver where each sequence is considered as a symbol.

Since both the MAPSD and the MLSD receivers are computationally complex, suboptimum symbol-by-symbol and sequence decision receivers have also been derived. One can distinguish between two suboptimal detection methods applicable for multipath fading channels and any dispersive channel in general. The first method consists of using an equalizer followed by a one-shot decision [127]; the purpose of the equalizer is to remove the effect of ISI on the received signal. The second method consists of using a suboptimal symbol-by-symbol detector, or a suboptimal sequence detector. These suboptimal detectors are derived either by approximating the optimum decision rule [128] or by imposing a type of structure on the receiver (for example reduced complexity channel estimator [129], sequential sequence estimation [124], decision feedback [130, 131]) or by combining both methods [132].

Literature reviews of adaptive equalization are given in [33, 53, 133, 134]. Equalizers can be linear or nonlinear, although linear equalizers are usually not used in multipath fading channels since they do not perform well due to spectral nulls in channel frequency-response characteristics [33]. A popular nonlinear equalizer for multipath fading channels is the Decision Feedback Equalizer (DFE) [127, 135]. The ISI caused by previously detected symbols can be estimated using the previous decisions and removed from the received signal before detection of the present symbol [2]. In [127], a DFE consisting of a feed-forward and a feedback filter, assuming absence of decision errors and optimized for a MMSE criterion was derived. Although the MMSE criterion may yield higher probability of error than the minimum probability of error criterion, in many situations both criteria yield close performance. More often than not, linear modulation is assumed when equalizers are employed. An adaptive receiver that does not require any training sequence nor statistical estimation was also

proposed for unknown slowly time-varying channels (decision-directed scheme). The achieved error probabilities in a dispersive channel were lower than the non-dispersive fading channel error probabilities, showing that diversity gains are obtained by the equalizer in absence of decision errors. The DFE is attractive due to its relatively low complexity and has been extensively studied [135] (see also references in [53]). However it has limitations as shown for example in [136] where the impact of channel estimation errors on its performance is studied. The principle of DFE can also be combined with MAP or MLSD detection techniques. For example, a generalized DFE related to the MAPSD has been proposed independently in [116] and [130] and analyzed in dispersive mobile radio channels [131]. A jointly adaptive fractionally spaced DFE and diversity combiner was derived in [137]. The current estimates of the channel impulse response at each diversity branch are used to compute the receiver parameters periodically. The performance is limited at high SNR by the channel impulse response estimation. In [138], diversity reception and various adaptive equalization techniques are combined. A MMSE criterion is used and expressions for the attainable MMSE's as well as upper-bounds to average probabilities of error are presented. An adaptive nonlinear equalizer for fast time-varying multipath channels that consists of a symbol-by-symbol detector and a single Kalman-type nonlinear channel estimator was presented in [139]. Another type of equalizer is based on channel precoding or pre-equalization. The transmitted signal is precoded to achieve an ISI-free received signal [140]. This is feasible only in slow fading multipath channels since the channel characteristic has to be known.

Usually, suboptimum receivers are designed using a combination of concepts. For example in [132], the MAP algorithm of Abend and al [113] was combined with an Extended Kalman Filter algorithm (EKF) to jointly estimate the multipath coefficients, the symbol timing and the data sequence in a TDMA system. The system included a training mode followed by a blind equalization mode. Due to the exponential complexity of the EKF-MAPSD, approximate algorithms were proposed. A suboptimal sequence estimation receiver was derived in [129] for frequency selective channels with linearly modulated signals. The proposed receiver consists of a sequence estimator implemented using the Viterbi algorithm with a parallel channel estimator. Similar to the flat fading channel estimator, the channel estimator employs linear predictive filters instead of Kalman filters. Jointly maximum-likelihood synchronization, equalization and detection of linearly modulated signals over a time-varying frequency

selective Ricean channel were studied in [141]. An approximation of the MLSD was presented in [124] in the form of a Sequential Sequence Estimator (SSE). The SSE has a much lower computational complexity than the MLSD while giving almost identical error performance.

Most equalizers presented earlier are designed to combat ISI that occurs even in the presence of a single user. Receivers may also be designed to take into account the presence of several users and they are referred as multi-user receivers. In the context of CDMA systems that suffer from MAI, popular suboptimal multi-user receivers are the linear multi-user decorrelating receivers [142, 143]. Multi-user decorrelating principles have been later applied to asynchronous CDMA slow fading frequency selective channels [144, 145]. A K users sampling channel model composed of L resolvable paths (each separated by the reciprocal of the signal bandwidth) was assumed. The front-end of the multipath decorrelating receiver consists of KL filters, matched to the (K) users normalized signature waveforms delayed by the (L) channel inter-paths delays. Note that the term multipath decorrelating receiver is used since the users are decorrelated. However no decorrelation of the multipath samples is performed. When the sequence length tends to infinity (infinite horizon detector), the vector formed of the KL matched filters output sampled at bit rate can be written as the sum of a signal vector component and a noise vector component. The signal vector component can be viewed as the output of a linear time-invariant filter when the input is the vector of the K users data scaled by the complex channel multipath gains. The principle of the decorrelating receiver is to pass this output vector through the corresponding inverse filter (decorrelating filter) in order to decouple the contribution of each user in the received signal. Coherent or differentially coherent single-user structures can then be used to form the decisions.

The interpretation of optimum receivers as estimator-correlators will conclude this literature review. This will provide directions for design of suboptimum receivers. In [146], it was shown that the optimum receiver over a Gaussian random linear time-varying channel of finite memory can be interpreted as an estimator-correlator. Over a deterministic channel with additive white Gaussian noise, the receiver cross-correlates the received signal with all possible noiseless received signals. For a random channel, the receiver uses the same decision rule, except that it employs estimates of the noiseless received signals. This result was also shown in [3] for a single path channel and was verified in [111] for multipath time-varying fading channels modeled using

the sampling theorem. The MAP symbol detector was also derived in [111] and it was shown that if the number of samples representing each symbol is large and all possible transmitted symbols are of equal energy, the approximately MAP symbol detector has also an estimator-correlator interpretation. The estimator-correlator interpretation from [146], explained earlier in this paragraph, was generalized to any random channel in the presence of additive noise with a Gaussian component [21]. The estimate of the noiseless received signal is the MMSE estimate or conditional mean. Furthermore, the cross-correlation operation involves a special stochastic integral called the Itô integral and denoted $\int$ in this thesis. In [21], the structure of the estimator-correlator is illustrated for purely random amplitude and purely random phase channels with conditional means that are relatively simple to find in closed-form. A tutorial on the subject is presented in [147].

The interpretation of the optimum receiver in Gaussian noise has several implications in terms of the implementation of optimal as well as the design of suboptimal receivers. In principle, the estimator-correlator structure can be implemented, however the number of sequence waveform estimator and log-likelihoods to be evaluated grows exponentially with the message length N. If a random dispersive channel has a finite memory of duration L in the sense that the channel output causal MMSE estimate at any given time is a function of only the most recent LT seconds of observations, a reduced complexity implementation of the optimal receiver can be derived [148]. The channel output sequence can be treated as a finite state process having 2^{L+1} states. Furthermore, the 2^N waveform estimates required in the implementation of the estimator-correlator structure can be pieced together using only 2^{L+1} subsequence estimators. A Viterbi algorithm having only 2^L metrics can be employed to determine the transmitted sequence. Therefore the complexity of the optimal receiver has been reduced from exponential in N (message length) to exponential in L (channel memory independent of N). In [149], optimal and suboptimal receivers that have an estimator-correlator structure have been derived for linearly phase modulated signals over a flat Rayleigh fading channel. Optimal receivers in additive white Gaussian noise have an estimator-correlator structure, including a MMSE estimator. Often such a structure is difficult to implement especially the estimation part of the receiver. But this structure leads naturally to suboptimum receivers that can be obtained by using a simpler approximation to the MMSE estimator. Such design examples will be proposed in this thesis.

The assumptions used in the design and performance evaluation of receivers in relation to path resolvability are summarized in Tables 2.2 and 2.3. For example the authors in [5] assumed a large transmission bandwidth. The inter-path delays were assumed to be (much) larger than the reciprocal of the transmission bandwidth in [4, 48, 81, 88, 95, 96]. In [78, 83, 86, 87, 99] the signal autocorrelation function was assumed to be essentially zero at all inter-paths delays. In fact all these assumptions are equivalent and represent the so-called path resolvability assumption defined in Section 2.2.1. This assumption yields important simplifications in the derivation of receiver structures for multipath fading channels and their performance analysis. However it is not always satisfied, hence optimal receivers derived assuming path resolvability are often suboptimal. The aim of this thesis is to derive receiver structures without assuming path resolvability. To start with, the various forms of the path resolvability assumption are studied next. For purpose of comparison and completeness, references based on sampling models such as [79, 80, 82] and classic references related to the thesis results have also been included in Tables 2.2 and 2.3.

2.2 Path resolvability in multipath fading channels

2.2.1 Definitions of path resolvability

In this thesis, only receiver structures that assume knowledge of the channel inter-path delays over slow fading multipath channels are studied. Therefore discussion of path resolvability will be carried out in that framework. As seen in Section 2.1.1, two different models can be used to describe a multipath fading channel: the classical wide-band model (2.7) and the sampling model (2.8) that is valid only for band-limited signals. However, for band-limited signals these models are equivalent and the path resolvability assumptions are the same.

Let us first consider the classical wide-band model that yields a channel impulse response given by (2.7). Let $\tilde{s}_m(s)$ be the m^{th} possible transmitted signal and let $\tau_0, \ldots, \tau_{L-1}$ be the L distinct delays of the multipath fading channel. Mathematically the strict path resolvability assumption is defined by the following orthogonality condition

$$\int_a^b \tilde{s}_m(u-\tau_l)\tilde{s}_m^*(u-\tau_k)du = 0 \qquad l \neq k \qquad m = 1, \ldots, M \tag{2.15}$$

where $[a, b]$ is the observation interval. The term strict has been introduced to distinguish the rigorous path resolvability assumption from the approximate path resolvability that is defined next (2.19). Note from (2.15) that the path resolvability condition depends on the observation interval. Let us show that assumptions from the literature are equivalent to the orthogonality condition (2.15). From (2.10), it is seen that a uniform orthogonality condition implies the path resolvability condition for an infinite observation interval. Therefore, any result obtained under the assumption of uniform orthogonal signals implicitly implies the path resolvability assumption as in [83]. The signal (time) autocorrelation function is given by

$$R_m(\tau) = \int_{-\infty}^{\infty} \tilde{s}_m^*(u)\tilde{s}_m(u-\tau)du \tag{2.16}$$

The transmitted signals can be either time-limited or band-limited. Assume first that the transmitted signals are time-limited to $[0, T]$. Let the observation interval be chosen to be sufficiently long to include all the received signal energy, i.e. $[a, b] = [0, T + \max_l \tau_l]$. Then, (2.15) can be equivalently expressed as

$$R_m(\tau_l - \tau_k) = 0 \qquad l \neq k \qquad\qquad m = 1, \ldots, M \tag{2.17}$$

which is satisfied if the absolute values of the inter-path delays are larger than the autocorrelation time $T_R^{(m)}$, defined as the width of the autocorrelation function, i.e

$$\forall\ |\tau| \geq \frac{T_R^{(m)}}{2} \qquad R_m(\tau) = 0. \tag{2.18}$$

Since $\tilde{s}_m(s)$ is time-limited, $T_R^{(m)}$ is well defined and is less or equal to $2T$. Therefore (2.17) gives the second definition of the path resolvability. Equivalently, for time-limited signals, the multipath is said to be resolved if the inter-path delays are larger than the autocorrelation time.

Consider now signals band-limited to W (in theory of infinite duration). Therefore, to exploit all the received signal energy, the observation interval needs to be infinite ($[a, b] = (-\infty, \infty)$). The strict multipath resolvability is still given by (2.15) or (2.17). Since the signals are not time-limited, the autocorrelation is also not time-limited, therefore there is no $T_R^{(m)}$ such that (2.18) is satisfied. Assume that the

autocorrelation function is composed of a main lobe and lower side lobes. Let $\frac{T_R^{(m)}}{2}$ be defined as the minimal time after which the autocorrelation is *essentially* zero, i.e.

$$\forall\ |\tau| \geq \frac{T_R^{(m)}}{2} \qquad |R_m(\tau)| < \epsilon$$

where ϵ is a small number determined by the application and the design requirements. The approximate path resolvability assumption is defined as

$$|R_m(\tau_l - \tau_k)| < \epsilon \qquad l \neq k \qquad m = 1, \ldots, M. \tag{2.19}$$

Such approximate path resolvability condition is often found in the literature for band-limited signals although receivers are usually designed assuming strict path resolvability. For spread-spectrum signals, W is very large and $T_R^{(m)} \approx \frac{1}{W}$. Hence for wide-band signals, the multipath is said to be (approximately) resolved if the inter-path delays are much larger than the reciprocal of the signal bandwidth. Such a definition appears for example in [4, 48]. The approximate path resolvability assumption can also be visualized graphically as follows. From (2.7) under H_m, the complex envelope of the noiseless received signal is given by $\tilde{v}_m(s) = \sum_{k=0}^{L-1} a_k \tilde{s}_m(s - \tau_k)$. Assuming that $s_m(s)$ is transmitted, the output of the matched filter matched to the m^{th} possible transmitted signal $\tilde{s}_m(t)$ ("m^{th} matched filter output") is given by[3]

$$\begin{aligned} u_m(s) &= \int_{-\infty}^{\infty} r(u) s_m(-s+u)du \\ &= \int_{-\infty}^{\infty} \left[\Re\left\{ \left(\sum_{k=0}^{L-1} a_k \tilde{s}_m(u-\tau_k) \right) e^{j\omega_c u} \right\} + n(u) \right] \Re\left\{ \tilde{s}_m(-s+u) e^{j\omega_c(-s+u)} \right\} du \end{aligned}$$

Neglecting integrals containing double frequency terms (from Lemma C.1) and assuming no noise, $u_m(s)$ is given by

$$u_m(s) \approx \frac{1}{2} \Re\left\{ \sum_{k=0}^{L-1} a_k R_m^*(s - \tau_k) e^{j\omega_c s} \right\} \tag{2.20}$$

[3]The notation $u_m(s)$ is used since $u_m(\tau_l) = \Re\left\{ u_{lm} e^{j\omega_c \tau_l} \frac{\tilde{E}_m}{2} \right\}$ where the variables $\{u_{lm}\}_{l=0,\ldots,L-1}$, first stage of the optimum receivers, are given by (3.18b), $\tilde{E}_m$ is the energy of $\tilde{s}_m(s)$ and the observation interval is $(-\infty, \infty)$.

where $R_m(s)$ is the autocorrelation function of $\tilde{s}_m(s)$ given by (2.16). The complex envelope of $u_m(s)$ is illustrated in Fig. 2.5 for a two-path noiseless channel. Fig. 2.5(a)

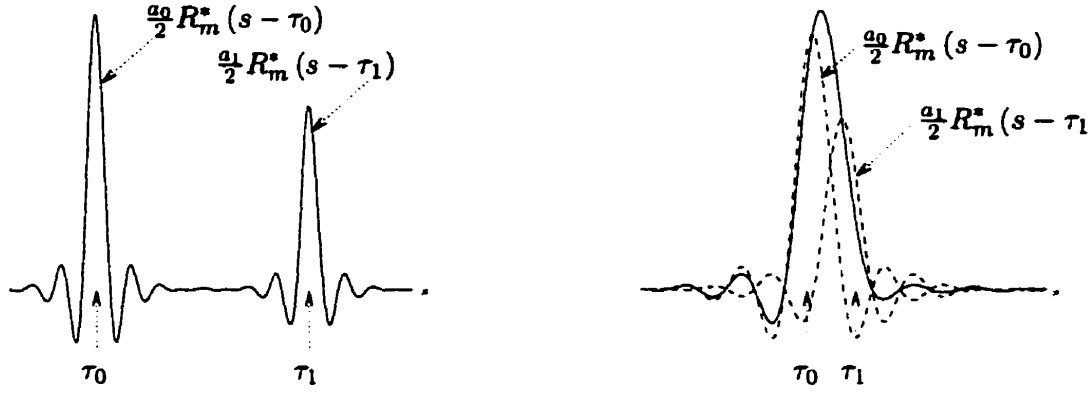

(a) Resolved multipath, $|\tau_1 - \tau_0| \geq T_R^m$

(b) Unresolved multipath, $|\tau_1 - \tau_0| \leq T_R^m$

Fig. 2.5 Complex envelope of the noiseless m^{th} matched filter output assuming that $s_m(s)$ is transmitted. The autocorrelation time $T_R^{(m)}$ is the width of the autocorrelation function.

shows that if $|\tau_1 - \tau_0| \geq T_R^{(m)}$, the two autocorrelation functions *approximately* do not overlap. In other words, the two paths are separated or resolved and one can be distinguished from the other. Such a terminology is used in [5]. Furthermore, for fixed inter-path delays, separation (or path resolvability) can be obtained by choosing W sufficiently large since $T_R^{(m)} \approx \frac{1}{W}$ for wide-band signals. Such visualization of the path resolvability is also used in [5]. Fig. 2.5 could also correspond to the first stage of a channel estimator based on pulse compression ("convolution method"). Fig. 2.5 clearly shows that if the path resolvability assumption is satisfied, the inter-path delays and amplitude path gains can be easily estimated whereas if the path resolvability assumption is not satisfied, no straightforward estimation is possible. This shows the importance of the path resolvability (i.e. of large bandwidth) in early days of detection theory as recognized by Price and Green in [5].

Let us consider now strict path resolvability for sampling channel models. The channel is modeled as a tapped-delay-line with equally spaced taps at $\frac{n}{W}$ and an impulse response given by (2.8). But recall that this model is just another representation of a wide-band channel model given by (2.7) valid for the case of band-limited signals

only. Therefore, the path resolvability assumption can still be expressed as (2.15) or (2.17); however, the signals are band-limited. In other words, for resolvability, the inter-paths delays must correspond to zero-crossings of the signal autocorrelation function. For example if $\tilde{s}_m(s) = \text{sinc}(Ws)$, from Parseval theorem applied to (2.16), its autocorrelation function is given by

$$R_m(\tau) = \int_{-\infty}^{\infty} \tilde{S}_m^*(f)\tilde{S}_m(f)e^{-j2\pi f\tau}df = \left(\frac{1}{W}\right)^2 \int_{-\frac{W}{2}}^{\frac{W}{2}} e^{-j2\pi f\tau}df = \frac{1}{W}\text{sinc}(W\tau)$$

Therefore from (2.17), strict path resolvability is satisfied in that case if and only if the inter-path delays are integer multiples of $\frac{1}{W}$ ($\tau_l - \tau_k = \frac{n}{W}$).

Conditions where path resolvability is satisfied are summarized in Table 2.1.

Table 2.1 Conditions where path resolvability is satisfied

	Time-limited signals	Band-limited signals[4]
autocorrelation time ($T_R^{(m)}$)	$\forall \lvert\tau\rvert \geq \frac{T_R^{(m)}}{2} \quad R_m(\tau) = 0$	$\forall \lvert\tau\rvert \geq \frac{T_R^{(m)}}{2} \quad \lvert R_m(\tau)\rvert < \epsilon$
strict path resolvability	$R_m(\tau_l - \tau_k) = 0, l \neq k$ or $\lvert\tau_l - \tau_k\rvert \geq T_R^{(m)}$	$R_m(\tau_l - \tau_k) = 0, l \neq k$ for specific values of $\{\tau_l\}_l$
approximate path resolvability	* $\lvert R_m(\tau_l - \tau_k)\rvert < \epsilon$ * $\lvert\tau_l - \tau_k\rvert \geq T_R^{(m)}$ * $\lvert\tau_l - \tau_k\rvert < T_R^{(m)}$ for specific values of $\{\tau_l\}_l$ such that $\lvert R_m(\tau_l - \tau_k)\rvert < \epsilon$	$\lvert R_m(\tau_l - \tau_k)\rvert < \epsilon$ or $\lvert\tau_l - \tau_k\rvert \geq T_R^{(m)}$

2.2.2 Path resolvability assumption in the literature

Comparing results of Tables 2.2 and 2.3 with the conditions where the path resolvability is satisfied summarized in Table 2.1, shows that path resolvability is often assumed in the literature although sometimes not mentioned explicitly. A receiver structure depends mainly on two factors, the channel model and its level of knowledge. One can

[4]For wide-band signals band-limited to W, $T_R^{(m)} \approx \frac{1}{W}$. Thus the approximate path resolvability assumption in that case may also expressed as $\lvert\tau_l - \tau_k\rvert \gtrsim \frac{1}{W}$. Since $T_R^{(m)}$ is only approximately equal to $\frac{1}{W}$, $\lvert\tau_l - \tau_k\rvert \gg \frac{1}{W}$ is often mentioned in the literature for safe guard purpose.

distinguish between perfect channel knowledge and knowledge of channel statistics. The optimum receiver assuming perfect channel knowledge includes filters matched to all possible noiseless received signals (including the channel filtering effects), regardless of whether path resolvability is assumed or not. Therefore papers that assume perfect channel knowledge do not assume path resolvability [100]-[109],[126]. This applies both to wide-band and sampling channel models. Note that papers that include the channel estimator in their receiver design such as [5, 78] assume path resolvability (large W in [5], $R_m(\tau_l - \tau_k) \approx 0 \quad l \neq k$ in [78]). These resolvability assumptions are only required for the channel estimator. Sometimes path resolvability is assumed even with perfect channel knowledge in order to simplify performance analysis [95]. In [81], path resolvability is assumed to derive an equivalent discrete time model with samples at the symbol rate.

For knowledge of channel statistics, wide-band and sampling channel models have to be considered separately. For wide-band channel models, path resolvability assumption yields simpler optimum and suboptimum structures and also simpler performance analysis. Therefore such assumption has often been considered in the literature under various forms (see Tables 2.2 and 2.3). For example, Rake and Rake-type receivers presented in [4, 48, 96] assume that the inter-path delays are (much) larger than the reciprocal of the transmission bandwidth. Uniform orthogonality which implies path resolvability was assumed in [83]. Receivers without the path resolvability assumption have been derived in [3],[84]-[86] for Rayleigh fading. The Ricean fading was not studied. The path resolvability assumption is also often assumed in performance analysis. For example $|\tau_l - \tau_k| \gg 1/W$ is assumed in [88], uniform orthogonality was assumed in [87, 99]. In [98] path resolvability is not assumed, but uniform orthogonality for the cross-correlation function (including the Doppler shift), (2.13), is requested. Furthermore, sharp bounds to the bit-error probabilities are obtained only if the matrix $\boldsymbol{B}_m\boldsymbol{C}, m = 1, 2$ (see (2.14)) has a narrow spectra. This assumption is not related to path resolvability but imposes additional constraints on the channel and the transmitted signals in addition to the uniform orthogonality for the cross-correlation function. Recently, performance analysis of non-coherent and coherent delay lock loop chip time trackers in the presence of unresolved multipath components has been presented [150]. In [150], path unresolvability such that the multipath delays satisfy $0 < \frac{\tau_k}{T_c} \leq 1.5$ is considered. It was shown that the non-coherent delay lock loop outperforms the coherent one in terms of demodulated signal power loss.

Table 2.2 Various assumptions found in the literature in receiver design and performance analysis, W is the signal bandwidth.

Reference		Modulation	Channel knowledge (amplitude/phase)	Fading distributions	Slow & Fast fading	One shot	Resolvability assumptions
[3]	Price(1956)	M-ary	second order	zero mean Gaussian	S/F	X	arbitrary known delays
[4]	Turin(1956)	M-ary	second order with known or unknown specular phase shift	Gaussian	S	X	known delays satisfying $\lvert\tau_l - \tau_k\rvert \gg 1/W.\ l \neq k$
[5]	Price & Green(1958)	Binary FSK	perfect measurement		S	X	large W
[88]	Turin(1959) (performance evaluation)	Binary	second order with known specular phase shift	Gaussian	S	X	known delays satisfying $\lvert\tau_l - \tau_k\rvert \gg 1/W.\ l \neq k$
[78]	Sussman (1960)	Binary wide-band	perfect measurement		S	X	$R(\tau_l - \tau_k) \approx 0.\ l \neq k$
[54]	Kailath (1963)	M-ary	second order with known mean	Gaussian	F		discrete-time model $\Longleftrightarrow$ sampling model
[84]	Aiken(1967)	M-ary	second order	zero mean Gaussian	S	X	arbitrary known delays with Doppler shifts
[98]	Aiken(1967) (performance evaluation)	Binary widely orthogonal	second order	zero mean Gaussian	S	X	$\int \tilde{s}_1(u-\tau_l)e^{j2\pi f_l u}\cdot \tilde{s}_2^*(u-\tau_k)e^{-j2\pi f_k u}du = 0$ narrow spectra
[48]	Charash (1979)	M-ary	known or unknown amplitudes & phases	Nakagami	S	X	known and random delays with $\Pr\left[\lvert\tau_l - \tau_k\rvert > \frac{1}{W}\right] \approx 1.\ l \neq k$
[79]	Ochsner (1987)	BPSK (DSSS)	second order	zero mean Gaussian	S		discrete-time model rect. spread. function $c(t)$ $\sum_{j=0}^{J-1} c(jT)c((j+k)T) = C\delta_{0k}$
[95]	Lehnert & Pursley (1987)	PSK(B,Q) MSK (DSSS)	perfect measurement		S		$P\left[\lvert\tau_l - \tau_k\rvert < T_c\right] \ll 1$ (assumed for performance only)

Table 2.3 Various assumptions found in the literature in receiver design and performance analysis (cont.)

Reference		Modulation	Channel knowledge (amplitude/phase)	Fading distributions	Slow & Fast fading	One shot	Resolvability assumptions
[80]	Hagmanns & Hespelt(1994)	M-ary (DSSS)	second order	zero mean Gaussian	S	X	sampling model band-limited signals
[81]	Fawer(1994)	M-PSK (DSSS)	ML phase estimation assuming known amplitudes	Gaussian	S		$\lvert\tau_l - \tau_k\rvert \geq T_c, l \neq k$ equivalent discrete-time model
[83]	Abdel-Ghaffar & Pasupathy (1994)	Binary uniformly orthogonal	unknown amplitudes & known phases	zero mean Gaussian (2-path)	S	X	$R_m(\tau_l - \tau_k) = 0,\ {}_{l\neq k,m=1,2}$ $R_{12}(\tau_l - \tau_k) = 0,\ {}_{l\neq k}$ (cross correlation funct.)
[85]	Alles & Pasupathy (1994)	Binary Envelope orthogonal FSK & Chirp	* second order * perfect direct path measurement * perfect measurement	zero mean Gaussian (2-path)	S	X	arbitrary known delays such that $\lvert R_m(\tau_l - \tau_0)\rvert$ is independent of m
[86]	Alles & Pasupathy (1994)		second order	zero mean Gaussian	X	S	* $\lvert R_m(\tau_l - \tau_0)\rvert$ ind. of m * $R_{mp}(\tau_l - \tau_0) = 0$ ${}_{m,p=1,2;m\neq p}$(for P_e only)
[87]	Abdel-Ghaffar & Pasupathy (1995), (perf.)	M-ary uniformly orthogonal	* perfect measurement * known amplitude	Gaussian	S	X	$R_m(\tau_l - \tau_k) = 0, l \neq k$ $R_{12}(\tau_l - \tau_k) = 0, l \neq k$ (cross correlation funct.)
[99]	Abdel-Ghaffar & Pasupathy (1995) (performance)	M-ary uniformly orthogonal	* perfect measurement * known phase * second order	Gaussian	S	X	$R_m(\tau_l - \tau_k) = 0, l \neq k$ $R_{12}(\tau_l - \tau_k) = 0, l \neq k$ (cross correlation funct.)
[82]	Eng & Milstein (1997)	BPSK (DSSS)	perfect amplitude & unperfect phase measurements	Rayleigh	S		sampling model $\left\lvert\sum_j c_j c_{j+k}\right\rvert \ll \left\lvert\sum_j c_j^2\right\rvert$ $\{c_j\}$: code sequence
[96]	Cheun(1997)	BPSK QPSK (DSSS)	known phases known or unknown amplitudes	Rayleigh	S		known delays such that $\lvert\tau_l - \tau_k\rvert > T_c, l \neq k$

But no tracking scheme designed to handle the path unresolvability was proposed.

Sampling channel models are usually represented in the literature [2, pp. 728-731], [80, 82, 145] by (2.8) without referring to (2.9). In other words, the multipath delays are not generally specified. Therefore, the derived structures using those models do not use the knowledge of the multipath delays. Hence the issue of path resolvability defined by (2.15) is irrelevant for the derivation of the receiver. Receivers designed to minimize the probability of error are optimal but only if the transmitted signals are strictly band-limited since the sampling channel model holds only in that case. If the observation interval is finite (ex. $[a, b]$), the so-called optimal receivers are in fact suboptimal since band-limited signals are of infinite duration. Path resolvability yields simplifications in receiver design. An equivalent assumption for purpose of simplification with the sampling channel model is

$$\int_a^b \tilde{s}_m\left(t-\frac{n}{W}\right)\tilde{s}_m^*\left(t-\frac{k}{W}\right)dt=0 \quad n\neq k \qquad\qquad m=1,\ldots,M$$

which is for example assumed in [2] to simplify performance analysis of the Rake receiver. Similar assumption in the context of DSSS transmission$\Big(\left|\sum_j c_j c_{j+k}\right| \ll \left|\sum_j c_j^2\right| \iff \left|\sum_j c_j c_{j+k}\right| \approx 0$, where $\{c_j\}$ is the code sequence$\Big)$ is considered in [82]. In [79], the dispersive WSSUS channel is reduced to a discrete-time multipath fading channel with samples at the chip rate and path resolvability defined by (2.15) is irrelevant. However a discrete-time condition similar to path resolvability ($\sum_{j=0}^{J-1} c(jT)c\left((j+k)T\right) = C\delta_{0k}$), where $c(t)$ is the spreading function composed of rectangular chips) has been assumed. Finally note the discrete-time model used in [54] can be obtained by sampling the channel output at $\frac{n}{W}$ as explained in [111], so it is equivalent to the sampling channel model.

When the channel is modeled as a dispersive ISI channel, the received signal is generally first passed through a matched filter, matched to the channel impulse response and sampled at the bit rate, to yield an equivalent discrete-time model. Such operation assumes that the channel is known to the receiver and as already mentioned in that case the path resolvability assumption does not affect the receiver design. In other cases, since the channel impulse response is unknown, the received signal is passed through a filter with rectangular low-pass transfer function and sampled at bit rate yielding a discrete-time signal that depends on the samples of the channel impulse response. Therefore similarly to the sampling channel model, the path resolvability

assumption is irrelevant in the design of equalizers.

As seen in Table 2.1, path resolvability is closely related to the channel inter-path delays assumed known to the receiver. Those inter-path delays are in practice estimated using sounding techniques. A summary of the principal sounding methods for radio channel estimation, including the more recent super-resolution techniques is given next.

2.2.3 Channel sounding techniques

Multipath fading channels are characterized by their impulse responses such as (2.7). However a channel can also be characterized by its frequency domain transfer function. Based on these two characterizations, one can identify two classes of sounding techniques: those that estimate the channel impulse response in the time domain and those that estimate the channel transfer function. When a narrow-band characterization of the channel is required, the estimation is often done in the frequency domain. The most common technique consists of exciting the channel by an un-modulated radio frequency carrier (single-tone) and measuring the amplitude and phase of the received signal [42]. By sequentially stepping the tone across a band of frequencies, measurements of the channel transfer function can be obtained (frequency-sweep methods). A similar method (multi-tone) is based on simultaneous transmission of multiple independently generated sinusoids [41]. Multiple receivers can then be used to measure the amplitude and phase of each received tone. These methods are mainly used for narrow-band characterization; for wide-band measurements, the number of tones must be large to maintain good frequency resolution. Therefore, the single-tone method is time consuming for wide-band measurements and cannot be used in fast fading environments since the characteristics of the channel may have changed by the time the last tone of the frequency sweep is transmitted. The multi-tone or frequency-sweep methods yield a very complex receiver for wide-band measurements. Therefore for wide-band channel characterization, time domain wide-band sounding techniques such as pulse methods, are preferable.

In the time domain, two types of pulses can be used, either periodic short duration pulses (simulating delta functions) or long pulses that have an autocorrelation function with a very narrow central peak that contains most of the energy (pulse compression). The major drawback of short duration pulses is their inefficient use of transmission power. Their total energy has to be sufficiently high such that the SNR at the output

of the matched filter is high. For a narrow pulse, this requirement translates into a high amplitude peak. Therefore, pulse compression methods with lower amplitude peaks for the same received SNR are usually preferred.

Pulse compression techniques are based on the principle that the impulse response of a system can be obtained by cross-correlating the output of the channel excited by white noise with a delayed replica of the input [42]. Usually pseudo-random sequences are used to replace the white noise that is not implementable. This method is usually implemented using a matched filter matched to the sounding waveform (convolution matched-filter technique) or a sliding correlator [17, 151]. Assume that the channel to be estimated is a linear time-invariant system with low-pass complex impulse response given by (2.7) and that estimates of the amplitudes and multipath delays are required. Let $\tilde{s}_e(s)$ be the complex envelope of a wide-band sounding signal of bandwidth W (for example a pseudo-random sequence as illustrated in Fig. 2.6(a)). Similar to the

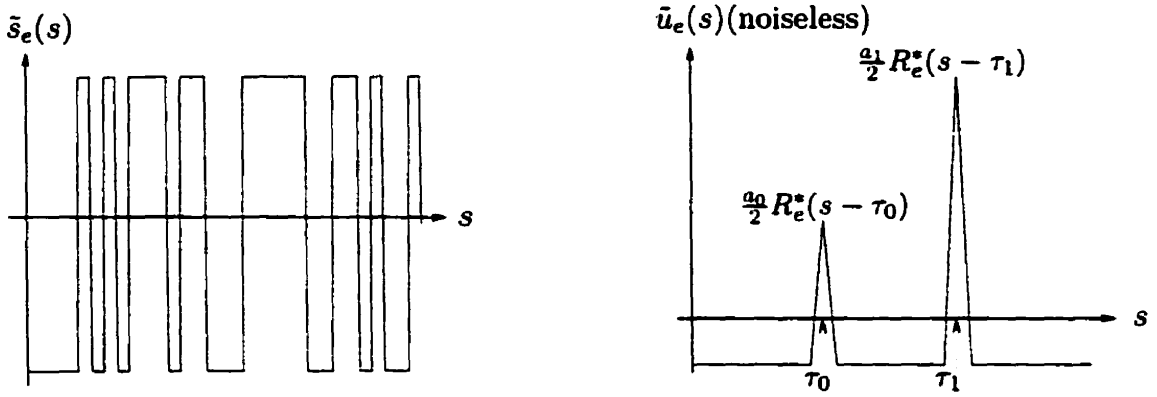

(a) Complex envelope of the sounding signal (time domain)

(b) Complex envelope of the noiseless output of the matched filter, matched to the sounding signal

Fig. 2.6 Sounding signal and its matched filter output

steps yielding (2.20), the noiseless output of a filter matched to the sounding signal $s_e(s)$ is given by

$$u_e(s) \approx \frac{1}{2}\Re\left\{\sum_{k=0}^{L-1} a_k R_e^*(s-\tau_k)e^{j\omega_c s}\right\} \tag{2.21}$$

where $R_e(s)$ is the autocorrelation function of $\tilde{s}_e(s)$. When the inter-path delays are much larger than the autocorrelation time or the reciprocal of the sounding signal

bandwidth (resolved multipath), the complex envelope of the noiseless output of the matched filter $\tilde{u}_e(s)$ exhibits peaks at τ_k with amplitudes proportional to the multipath gains amplitudes as illustrated in Fig. 2.6(b). And the straightforward approach to determine the amplitudes and multipath delays is to use the amplitudes and locations of the peaks of the matched filter output [152]. Such approach is not optimal unless the individual peaks are separated by times greater than the autocorrelation time (such as in Fig. 2.6(b)). In that special case, the obtained values correspond to the ML estimates calculated by considering each path separately. This pure convolution method provides accurate estimates of a_k and τ_k only if the path resolvability assumption is satisfied for the sounding signal. For smaller inter-path delays, errors into the amplitudes and delays occur due to the overlapping of the matched filter outputs associated with each path.

Better accuracy of the amplitudes and delays can be obtained from another time domain method based on the ML approach considering all the paths together [152]. Modifying results of [152] to consider the channel low-pass complex impulse response given by (2.7) instead of a real impulse response, the ML estimates of the amplitudes and multipath delays are obtained by

$$[\hat{a_k}, \hat{\tau_k}] = \arg\max_{a_k, \tau_k} \{\Lambda[r, \{a_k, \tau_k\}; T_o]\} = \arg\max_{a_k, \tau_k} \{\ln \Lambda[r, \{a_k, \tau_k\}; T_o]\}$$

where $\Lambda[r, \{a_k, \tau_k\}; T_o]$, the likelihood ratio over the observation interval $[0, T_o]$ assuming known a_k and τ_k, is given by

$$\Lambda[r, \{a_k, \tau_k\}; T_o] = \exp\left\{ \frac{2}{N_0} \int_0^{T_o} r(t) \Re\left\{ \left(\sum_{k=0}^{L-1} a_k \tilde{s}_e(t - \tau_k) \right) e^{j\omega_c t} \right\} dt \right.$$
$$\left. - \frac{1}{N_0} \int_0^{T_o} \left[\Re\left\{ \left(\sum_{k=0}^{L-1} a_k \tilde{s}_e(t - \tau_k) \right) e^{j\omega_c t} \right\} \right]^2 dt \right\}$$

Since this method does not require multipath resolvability, it can be used to improve accuracy in case overlapping of the delayed path responses occurs due to very small inter-path delays. However it requires knowledge of the number of paths. In [152], a suboptimum procedure is proposed to determine the number of multipath components. First estimates of the amplitudes and multipath delays are determined successively assuming there is only one path, two paths and so on. Secondly the

smaller number of paths that gives an integrated Mean-Square Error (MSE) between the actual and the estimated signal approximately equal to the MSE due to noise alone, is chosen.

In the more general case of an arbitrary time invariant channel impulse response, sounding methods are equivalent to deconvolution techniques. The purpose of sounding methods is to solve the following problem: find the system real impulse response $h_{cR}(\tau)$ from the channel output $r(s)$ given by

$$r(s) = \int_{-\infty}^{\infty} h_{cR}(s-\tau)s_e(\tau)d\tau + n(s) = \int_{-\infty}^{\infty} h_{cR}(\tau)s_e(s-\tau)d\tau + n(s) \qquad (2.22)$$

where $s_e(s)$, the sounding signal is known, and $n(s)$ is a random process (noise). From (2.22), it is seen that the convolution of $h_{cR}(\tau)$ with $s_e(\tau)$ yields $r(s)$. The problem of deconvolution is then to find $h_{cR}(\tau)$ given $r(t)$ and $s_e(\tau)$ [153]. Several solutions to perform deconvolution have been derived. For example, a discrete-time solution based on constrained linear regression has been derived in [153]. If deconvolution is transposed in the frequency domain, then the problem becomes inverse filtering [152, 154]. In the absence of noise the straightforward approach is to use an inverse filter but in the presence of noise the "ideal" inverse filter may not be suitable since it amplifies the noise. Therefore an estimate of the system real impulse response is given by $\widehat{h_{cR}}(s) = r(s) * \mathsf{f}(s)$ where the linear estimating filter $\mathsf{f}(s)$ is chosen such that the MSE, $E\left[\left(\widehat{h_{cR}}(s) - h_{cR}(s)\right)^2\right]$, is minimized and a known sounding signal $s_e(s)$ is transmitted (i.e. $r(s) = h_{cR}(s) * s_e(s) + n(s)$) (Wiener theory) [152]. The solution is usually given in the frequency domain. Note this does not provide a MMSE estimate of the amplitudes and multipath delays. However, multipath resolvability is not required. Once the channel transfer function has been reconstructed, the amplitudes and multipath delays could be retrieved from it by using an adapted version of Prony's method [155].

As shown in the following, multipath fading channel estimation in the frequency domain is closely related to the estimation of the amplitudes, phases and frequencies of sums of f-complex sinusoids (i.e. f-exponentials), the multipath delays being interpreted as the frequencies of the sinusoids. Let us assume that the low-pass complex impulse response $h_c(\tau) = \sum_{k=0}^{L-1} a_k \delta(\tau - \tau_k)$ is to be estimated. Equivalently the low-pass complex channel transfer function $H_c(f) = \mathcal{F}\{h_c(\tau)\} = \sum_{k=0}^{L-1} a_k e^{-j2\pi f \tau_k}$ needs to be estimated where the τ_k's appear as frequencies. Let $x[n] = H_c(n) + n'(n)$, $n = 0, 1, \ldots, N-1$ be N observations of $H_c(f)$ in complex additive white Gaussian

noise. Assuming L known and widely separated frequencies, the ML frequencies estimates of $H_c(n)$ in complex additive white Gaussian noise correspond to the frequencies at which the periodogram, $1/N \left|\sum_{n=0}^{N-1} x[n] \exp(-j2\pi fn)\right|^2$, attains its maximum [156]. However for closely spaced sinusoids, the periodogram cannot be used and optimal ML estimation approaches are not practical yielding to the use of suboptimal methods based on spectral estimation techniques. Spectral estimation techniques are methods that estimate the power spectral density of a stationary signal based on a finite set of observations from that process. Three types of modern spectral estimation methods can be used for frequency estimation [156], AutoRegressive (AR) spectral methods such as the Maximum Entropy Method (MEM) [157], principal component frequency estimation, and noise subspace frequency estimation such as the MUltiple SIgnal Classification method (MUSIC) [158]. If the SNR is high enough, the peaks of the estimated AR power spectral density provide good estimate of the frequencies [156].

The MEM is based on the principle that the spectral estimate must be the most random (or equivalently have the maximum entropy) among all power spectra which are consistent with the measured data. It was shown that for Gaussian random processes and known samples of the autocorrelation function, the maximum-entropy process is an AR process. The solution is obtained by solving linear Yule-Walker equations [159]. The MEM method gives accurate AR spectral estimates for truly AR data but has difficulties such as phase dependence of the peak locations for sinusoidal data [156, p. 231]. A better AR spectral method less sensitive to sinusoidal phases and peaks shifts due to noise effects is the modified covariance method [156, pp. 225-228].

Principal component frequency estimation retains only the principal eigenvector components (i.e. associated with large eigenvalues) in the estimate of the observations autocorrelation matrix, thus eliminating noise eigenvectors [156, pp. 425-428].

Noise subspace frequency estimation methods are based on the eigendecomposition of the observation covariance matrix into orthogonal signal and noise subspaces. One of them, the MUSIC method, generates an estimated power spectrum $\hat{P}_{\mathrm{MU}}(f)$ that becomes by definition infinity at the sinusoidal frequencies [156, 158]. Therefore, the frequencies estimates are found as the frequencies corresponding to the L largest peaks of $\hat{P}_{\mathrm{MU}}(f)$, where $\hat{P}_{\mathrm{MU}}(f)$ is the inverse of the Euclidean distance from the vector $V = \left[1, e^{j2\pi f}, \ldots, e^{j2\pi f(L-1)}\right]^T / \sqrt{L}$ to the signal subspace. In general, the multipath amplitudes are estimated using another method. For example, once the

multipath delays are determined, the Least-Squares Error (LSE) MUSIC [14] can be used to estimate the multipath amplitudes. Many other spectral estimation methods do exist, additional references on the subject can be found in [156, 160].

To summarize, it is seen that earlier sounding techniques such as the convolution method [41, 42] could only achieve a time resolution equal to $1/W$ the reciprocal of the sounding signal bandwidth. However super-resolution techniques may yield a time resolution better than $1/W$ [9]- [19]. Similar to classical sounding techniques, super-resolution techniques can operate in time domain or frequency domain. In general they achieve better time resolution by combining several methods based on the classical sounding techniques. For example, a sounding technique yielding better resolution than correlation and inverse filtering techniques combines Wiener filtering similar to [153] and windowing [9].

A time domain technique that combines the concept of convolution and inverse filtering, called Matched Filter Deconvolution (MFD) and including sequential bin tuning, is proposed in [14]. The multipath delays and amplitudes are estimated in two steps. First, the Dominant Paths (DP) are extracted by minimizing the sum of the square-errors between the received signal samples and the output samples of a preliminary channel impulse estimate excited by the sounding signal (LSE method). The preliminary estimate is obtained by applying a moving amplitude threshold to a combined function formed by the matched filter and the matched filter deconvolution (based on inverse filtering) channel estimates. The LSE method yields a preliminary approximation of the DP and forms the core of MFD techniques. The DP amplitudes are determined more accurately using a sequential bin tuning algorithm also based on LSE but applied on a reduced channel response obtained by removing the dominant paths. The second step is the extraction of the lower amplitude paths (reinforcement tuning). The main concept of the second iterative step is to form a reduced channel estimate by removing the paths that have already been estimated and redo LSE to identify lower amplitude paths. A minimum resolution time (τ_R'), lower than the chip duration, was obtained with good performance. Improvement in accuracy was observed compared to the MEM and MUSIC methods. However MFD techniques yields deconvolution noise that has to be compensated [15, 161] to eliminate the SNR floor.

Several super-resolution techniques have an initial matched filtering stage similar to pulse compression methods [10, 11, 13]. For example, higher resolution can be

obtained by sampling the matched filter output at K discrete delay times and applying principles of the MUSIC algorithm to the data vector formed with the samples [10]. Another technique involves the direct Least-Squares (LS) estimation of the amplitudes and the multipath delays [13]. The initial matched filtering stage enables the identification of the regions of potential presence of multipath delays (region with large energy). Then LS estimation of the amplitudes and multipath delays is performed using an error function based on the positive frequency part of the discrete signal spectra.

The time domain super-resolution technique presented in [11] employs matched filtering, set-theoretic deconvolution and AR modeling. Similar to pulse compression methods, the received signal is passed through a matched filter, matched to the sounding signal. Signals with autocorrelation functions having narrow main lobes and low side lobes are used to facilitate the deconvolution stage. The output of the matched filter is the sum of the convolution of the signal autocorrelation function (known function) with the channel impulse response and a noise component. Deconvolution methods give an estimate of the channel impulse response from which estimates of the multipath parameters can be obtained. Here deconvolution is performed using the method of projections onto convex sets. This method is an iterative technique that yields a solution satisfying a set of predetermined constraints (variance of the residual, amplitude, support and real-valuedness constraints). The solution is found by successively projecting an initial estimate on the constraint sets. The multipath parameters are then estimated from the final channel impulse response estimate using a simple thresholding or using an AR model with the Prony algorithm. Comparisons with matched filtering and inverse filtering techniques showed improvement in the time resolution of multipath delays that were very close to each other. This method was later extended for use in DS-CDMA communications by replacing the variance of the residual constraint with a modified residual covariance constraint which is based on the exact statistic of the noise at the output of the matched filter [19].

Recently a super-resolution technique based on substrative deconvolution is compared with a modified inverse filtering technique [18]. The main idea of the substrative deconvolution algorithm is similar to the sequential bin tuning of [14] in the sense that initial multipath estimates are made and dominant paths are iteratively subtracted from the received signal to generate a residual signal that is used in the next estimation iteration. However the estimation in [18] is obtained by correlating the residual

signal with a band-limited replica of the sounding pulse that includes the distortion induced by the transmitter and the receiver. Amplitudes and locations of the peaks at the output of the correlator give the amplitudes and multipath delays estimates. The modified inverse filtering technique does not consider spectral nulls of the sounding pulse in its frequency transfer function estimation. For both algorithms, the obtained impulse response is reduced by keeping only the significant peaks. The amplitudes and multipath delays left are then optimized using a MMSE criterion. It was shown that although the inverse filtering technique performs better in the absence of noise, deconvolution performs better in the presence of noise before the MMSE optimization step. However after the MMSE optimization step, the modified inverse filtering technique gives better results.

Super-resolution techniques operating in the frequency domain can make use of the Root-MUSIC algorithm [12]. In [16], a super-resolution modeling of the indoor radio propagation channel that matches the measured channel frequency response $H_c(f)$ $\left(\text{i.e. } H_c(f) = \sum_{k=0}^{L-1} a_k e^{-j2\pi f \tau_k}\right)$ to the transfer function of a finite impulse response (FIR) filter $H_F\left(e^{j2\pi f}\right)$ $\left(\text{i.e. } H_F\left(e^{j2\pi f}\right) = e^{-j2\pi\tau_b} \sum_{k=0}^{M-1} b_k e^{-j2\pi f k}\right)$, where the delay term $e^{-j2\pi f \tau_b}$ is used to lower the filter order. The filter tap weights b_k are obtained by solving an over-determined system of N equations in the least squares sense similar to the one used in the extended Prony's method.

Although the information conveying signal bandwidth may be equal to W, inter-path delays smaller than $1/W$ can be estimated by using super-resolution sounding techniques. In this case, the receiver can have a super-resolution model of a multi-path fading channel that is not resolved by the information conveying signal. The implication of this observation on detection techniques is the general subject of this thesis.

2.3 The subject of this thesis

2.3.1 Formulation of the problem

As seen in Section 2.1.1, the effect of multipath fading depends on the signal transmission bandwidth. For narrow-band transmission, i.e when the transmission bandwidth is much less than the channel coherence bandwidth, the channel can be modeled as flat fading. Without any diversity technique, the bit error rate will be inversely pro-

portional to the SNR [2]. This occurs for example in GSM[5] or IS136[6] (digital AMPS[7]) [162] systems with signal bandwidths of 200kHz and 30kHz respectively. Typical values of the channel root-mean-square (rms) delay spread, σ_τ are $3\mu s$ in urban areas, $0.5\mu s$ in suburban areas, less than $0.2\mu s$ in open areas and less than $0.1\mu s$ in office buildings [6]. These values depend on the transmission frequency band and site. For example, the delay spread in office buildings at 850MHz was measured to be $270ns$ maximum [7]. Using a common rule of thumb, $(\Delta f)_c \approx 1/(5 * \sigma_\tau)$ [163], the coherence bandwidths of the urban, suburban, open areas and office buildings channels are roughly equal to 67kHz, 400kHz, 1000kHz and 2000kHz. Therefore, suburban, open areas and office building channels appear as flat fading for the GSM and IS136 signals. In order to decrease the bit error probability, various forms of diversity techniques such as time, frequency, spatial, polarization diversity or frequency hopping can be used. Other powerful techniques such as interleaving and error correction coding can also be combined with diversity. All of these techniques, excluding error correction coding, involve several transmissions of the same signal and require additional equipment. When a wide-band signal is transmitted, the channel becomes frequency selective, a form of time diversity that can be exploited without several transmissions of the same signal (Rake receiver). It is widely believed that this inherent time diversity can only be taken advantage of, using a wide-band signal [2, 164, 165], but is it so ? This yields the following question:

When a narrow-band signal is transmitted over a channel that "appears" to be flat fading, is it possible to exploit the channel inherent time diversity that is identified with wide-band transmission ?

With wide-band signaling, this inherent channel time diversity can be exploited by a class of detection structures known as Rake receivers. As seen in Section 2.1.2, Rake receivers assume path resolvability (either strict or approximate although the literature does not really differentiate between the two). But strict path resolvability (orthogonality condition (2.15)) is rarely satisfied and even approximate path resolvability (defined by (2.19)) is not always satisfied in practice. For example, for band-limited signals the classical assumption that the inter-path delays are much larger than the reciprocal of the signal bandwidth [4] implies only approximate path resolv-

[5]GSM: Global System for Mobile communications
[6]IS136: Interim Standard 136
[7]AMPS: Advanced Mobile Phone Service

ability since the reciprocal of the signal bandwidth takes into consideration only the main lobe of the autocorrelation function. However practical autocorrelation functions have low side lobe(s) that generates IPP [109]. Therefore optimum receiver structures derived under the strict path resolvability assumption are in fact not optimum under these realistic conditions in the sense that they neglect IPP. Optimum receivers designed without the path resolvability by definition take into consideration the IPP and thus could improve performance. Up to now, analyses that include the effect of IPP have been done only for matched filter receivers, i.e. receivers that have complete knowledge of the channel [100, 102, 105, 108, 109].

Let us give examples of situations where even the (approximate) path resolvability is not satisfied. Consider first the IS95 standard, that is based on CDMA [162]. The basic user channel rate is 9.6kb/s or 14.4kb/s for the IS95 second generation. Bandwidth spreading yields a channel chip rate of 1.2288 Mchip/s, of bandwidth 1.25MHz. For wide-band signals, the autocorrelation time is approximately the reciprocal of the bandwidth that is $0.8\mu s$. The outdoor inter-path delays are in the order of magnitude of $1 - 10\mu s$ [8], thus the approximate path resolvability assumption is satisfied. However, indoor inter-path delays are of the order of magnitude of tens to hundreds of ns, which prevents the approximate path resolvability from being satisfied. In fact a bandwidth of 50MHz will be required to resolve the multipath in an indoor environment [8]. Thus even third generation "wideband" CDMA systems [166] (CDMA2000 [167], UTRA[8] [168], W-CDMA[9] [169]) employing $5 - 15$MHz signals will not be able to resolve the indoor multipath. For GSM and IS136 systems based on Time Division Multiple Access (TDMA) that have even smaller bandwidths, approximate path resolvability assumption cannot be ensured to be satisfied in the outdoor as well as the indoor environment. Therefore, it is seen that neither strict nor approximate path resolvability are always satisfied, thus making Rake receivers not necessarily optimal. This yields the following questions:

In a frequency selective channel, what is the optimal structure when the path resolvability is not satisfied ? Can diversity gains still be obtained without the path resolvability ? These are issues that will be addressed in this thesis.

[8]UTRA: UTMS Terrestrial Radio Access
[9]W-CDMA: Wide-CDMA

2.3.2 Goals

The first goal of this thesis is to derive optimal (in the minimum probability of error sense) one-shot receivers for multipath fading channels that do not satisfy the path resolvability condition (strict and approximate) and to provide insight in the operations performed by these receivers. In particular, this thesis focuses on the estimator-correlator interpretation of receivers and studies the effect of path un-resolvability on their structures. The second goal is to assess performance of the optimal receivers and to show that diversity gains can be obtained even without path resolvability. Optimal receivers provide the best performance. However they are not necessarily implementable or cost effective. Therefore, the final goal of this thesis is to derive suboptimal receivers more suitable for implementation that can also yield diversity gains, and to assess their performance.

2.3.3 Methodology

In this thesis, slow fading is assumed. The assumption of stationarity or quasi-stationarity of the indoor channel in a time span of a few seconds is reasonable for residential buildings or office environments in which small movements are expected yielding a small Doppler spread (order of a few Hz in the 800/900MHz) [1]. The channel is not assumed to be fully tracked, while the multipath gains follow Rayleigh and Ricean distributions. Two classes of detection techniques will be considered; specular coherent and non-coherent. Specular coherent receivers assume knowledge of the magnitudes and phases of the specular component. Non-coherent receivers assume knowledge of the specular component magnitudes only. Therefore, in order to design non-coherent receivers, the channel impulse response will be given by (2.7), except that the multipath gains a_k will be replaced by $a_k e^{j\theta_k}$, where $\{\theta_k\}_{k=0,\ldots,L-1}$ are independent uniformly distributed phases between $-\pi$ and π. Whenever the θ_k's are known, the new model will represent a multipath fading channel model that implicitly assumes that the specular components magnitudes and phases are known at the receiver (specular coherent detection). The path gains a_k are independent circularly complex Gaussian random variables [170] with arbitrary means, modeling Ricean as well as Rayleigh fading. To illustrate results, this thesis will consider two channels of practical interest: the Rayleigh channel and the mixed mode Ricean/Rayleigh channel. The Rayleigh channel corresponds to wireless transmission with no line-of-

sight [1]. The mixed mode Ricean/Rayleigh channel is characterized by having its first path gain Ricean distributed and all the other path gains Rayleigh distributed. This channel corresponds to wireless transmission with a line-of-sight [1] and appears in the literature. For example, one of the typical channel impulse responses suggested by GSM standard, the so-called Rural environment (RA), is a mixed mode Ricean/Rayleigh channel with six paths equally spaced, the first one being Ricean distributed [171]. Additive white Gaussian noise will be assumed. A detailed channel model appears in Chapter 3.

Let $\{\tilde{s}_m(t)\}_{m=1,\ldots,M}$ denote the complex envelopes of the possible transmitted finite energy bandpass signals. In this thesis, path resolvability assumption is defined by the orthogonality condition

$$\int_0^{T_o} \tilde{s}_m(u-\tau_l)\tilde{s}_m^*(u-\tau_k)du = 0 \qquad l \neq k$$

which corresponds to what was called previously strict path resolvability where $[0, T_o]$ is the observation interval. This assumption was very often implicitly used for receiver design in the literature [4] while the "stated" assumption was only approximate path resolvability. In this thesis, this assumption is **not used**, instead it is assumed that the delayed signals $\tilde{s}_m(t-\tau_0), \tilde{s}_m(t-\tau_1), \ldots, \tilde{s}_m(t-\tau_{L-1})$ are linearly independent over the observation interval, $[0, T_o]$. This linear independence condition is a much weaker constraint compared to orthogonality as will be shown in Chapter 3. Because the path resolvability assumption is not made, the results of this thesis apply to narrow-band as well as wide-band signals. For narrow-band signal detection, the use of a wide-band channel model with known (in practice estimated) multipath delays will result in structures yielding diversity gains that could not be obtained if a narrow-band channel model (flat fading) would be used. The wide-band multipath estimates can be obtained either by sounding the channel with a pulse of much larger bandwidth than the information conveying signal or by using super-resolution techniques. In both cases, the achieved time resolution of the estimation method is better than the reciprocal of the information conveying signal bandwidth. For wide-band signals, path unresolvability enables to take into account IPP.

The optimal receivers (specular coherent and non-coherent) in the minimum probability of error sense are derived for general Ricean channels using classical statistical theory tools. They form the likelihood ratio between each of the hypotheses corre-

sponding to the possible transmitted signals and a null hypothesis. The decision is made in the favor of the largest likelihood ratio [172, p. 11]. For Ricean channels, the specular coherent optimal receiver is quadratic. Unlike the specular coherent optimal scheme, the non-coherent optimal receiver is nonlinear and involves a quadratic form and infinite series of Bessel functions. For Rayleigh channels it becomes quadratic. It is well known that these receivers can be interpreted as estimator-correlators provided that the "correlation" integral is interpreted as an Itô integral. The estimate is the causal MMSE estimate of the signal from the observation. These MMSE estimates, generally difficult to express in closed-form, have been found only for the general Gaussian channel [173] and the random phase non-fading channel [21]. In this thesis using Itô differentiation of the likelihood ratio, closed-form expressions are found for the MMSE estimate for mixed mode Ricean/Rayleigh with known and random phase as well as Rayleigh channels.

Single-pulse performance of these receivers is assessed. This corresponds to neglecting any ISI, a reasonable assumption for small inter-path delays. For mixed mode Ricean/Rayleigh channels, the receiver structure is nonlinear, therefore, its performance is assessed by upper and lower bounding the bit-error probability. These upper and lower-bounds are obtained by considering performance of quadratic receivers that can be evaluated more easily. For Rayleigh channels, the receiver structure is quadratic, hence exact bit error probabilities can be evaluated numerically. The importance of the knowledge of the Ricean specular term phase will be assessed.

Since the non-coherent optimal structure for mixed mode Ricean/Rayleigh channels is not easily implementable, non-coherent quadratic suboptimal structures more suitable for implementation such as the Quadratic Decorrelation receiver (QDR) and the Quadratic Receiver (QR) are considered. Based on the insight provided by the special case of Rayleigh channels, these suboptimal receivers are obtained by replacing the nonlinear parts of the non-coherent optimal receivers (unresolved and resolved) with quadratic forms. Exact single pulse bit-error probabilities of these suboptimal receivers are evaluated numerically.

The receiver structures in this thesis are derived for M-ary modulations without assuming specific modulation format, except the continuity of the signaling waveforms on the observation interval. The receiver performances will be assessed for binary FSK, DPSK and SDPSK [174]. These modulations schemes have been chosen because they are simple and commonly used.

Chapter 3

Receiver structures

3.1 Channel modeling

Assume transmission of one of M possible bandpass signals of finite energy over a fading multipath channel. For convenience, the M possible transmitted signals will be represented by their complex envelope $\tilde{s}_m(s)$. Assume furthermore that $\forall\, k = 0, \ldots, L-1$, $\tilde{s}_m(s-\tau_k)$ is continuous on the observation interval $[0, T_o]$. The continuity hypothesis is not too limiting since any square-integrable function can be approximated arbitrarily closely in the Euclidean norm by a continuous function [175, p. 71]. As will be seen in Section 3.2.1, the continuity assumption ensures the mean square continuity of the noiseless received signal required for the existence of its Karhunen-Loève expansion. Equivalently instead of the continuity hypothesis of the transmitted signal, the random process defined by the noiseless received signal could have been assumed to be second order and mean square continuous. The mean square continuity assumption is also not too limiting since any random process measurable in (s, ω) and square integrable on $(\mathbb{R} \times \Omega)$ where Ω denotes the sample space of a probability space can be approximately arbitrarily closely (in mean square) by a mean square continuous process [176]. However since continuity of $\tilde{s}_m(s-\tau_k)$ has several other implications, such assumption will be used in this thesis. For example continuity of the signals $\tilde{s}_m(s-\tau_k)$ implies that they are also bounded on $[0, T_o]$ [177, p. 72] for any finite T_o. In this thesis, $\Re\{\cdot\}$ denotes the real part, and $\Im\{\cdot\}$ denotes the imaginary part of the argument. Under hypothesis H_m, the received signal is

given by

$$\dot{z}(s) = \Re\left\{\left[\sum_{k=0}^{L-1} a_k e^{j\theta_k}\tilde{s}_m(s-\tau_k)\right] e^{j\omega_c s}\right\} + \dot{w}(s) \qquad 0 \le s \le T_o \qquad m = 1,2,...,M \tag{3.1}$$

where a_k are independent circularly complex Gaussian random variables [170] with mean $E[a_k] = \alpha_k$, variance $E[(a_k - \alpha_k)(a_k - \alpha_k)^*/2] = \sigma_k^2$, and θ_k, the multipath component phase shifts, are either fixed and known, or unknown independent uniformly distributed random variables between $-\pi$ and π. The multipath delays τ_k are assumed to be known and $\tau_k \neq \tau_j$ if $k \neq j$. The effect of the channel noise is modeled by an additive zero mean White Gaussian process $\dot{w}(s)$ ($w(s)$ is a Wiener process) satisfying $E[\dot{w}(u)\dot{w}(s)] = \frac{N_0}{2}\delta(u-s)$. Dot notation is used for $\dot{w}(s)$ and $\dot{z}(s)$ to facilitate conversion to the integrated form, e.g. $z(s) = \int_0^s v_m(\tau)d\tau + w(s)$ used in subsequent sections. For example $\dot{z}(s)$ and $\dot{w}(s)$ replace the more common notation $r(s)$ and $n(s)$ used in Chapter 2. For Ricean multipath channels each path can be considered as the phasor sum of two components: a Rayleigh component with a uniformly distributed phase, and a fixed (specular) component. In order to design receivers that do not have any reference phase information (non-coherent detection), an additional completely random phase needs to be added to each multipath component, $a_k\tilde{s}_m(s-\tau_k)$, yielding the model (3.1). By definition the complex gains present in (3.1), $a_k e^{j\theta_k}$, can be expressed as $a_k e^{j\theta_k} = a_k' + \alpha_k e^{j\theta_k}$ where $a_k' = (a_k - \alpha_k)\, e^{j\theta_k}$. Since $\{a_k - \alpha_k\}_{k=0,\ldots,L-1}$ are zero mean circularly complex Gaussian random variables, a_k' and $a_k - \alpha_k$ are identically distributed. Therefore, whenever the θ_k's are known, (3.1) represents a multipath Ricean fading channel model that implicitly assumes that the specular component phases and amplitudes are known at the receiver (specular coherent detection). For all m, conditioned on $\theta_0, \theta_1, \ldots, \theta_{L-1}$, the signal process $v_m(s) = \Re\left\{\left[\sum_{k=0}^{L-1} a_k e^{j\theta_k}\tilde{s}_m(s-\tau_k)\right] e^{j\omega_c s}\right\}$ is Gaussian, and has a finite mean-square value on the observation interval $[0, T_o]$. Furthermore, the signal is assumed to be statistically independent of $\dot{w}(s)$ and a non-anticipating process measurable in (s,ω) [178, p. 90]. Note that a non-anticipating signal $v_m(s)$ is statistically independent of future values of the Wiener process $\{w(u), u > s\}$ (if s is considered to be the present) [179, p. 22], [180, p. 72], [181]. In this thesis statistical independence with respect to past values is also required. Since by continuity assumption $\tilde{s}_m(s-\tau_k)$ is bounded

on $[0,T_o]$, $\int_0^{T_o}|\Re\{\tilde{s}_m(s-\tau_k)e^{j\omega_c s}\}|\,ds<\infty$ and $\int_0^{T_o}|\Im\{\tilde{s}_m(s-\tau_k)e^{j\omega_c s}\}|\,ds<\infty$. It is shown below that this implies that $\int_0^{T_o}E\,|v_m(s)|\,ds<\infty$.

$$
\begin{aligned}
E\,|v_m(s)| &= E\left|\sum_{k=0}^{L-1}\Big[\Re\left\{\tilde{s}_m(s-\tau_k)e^{j\omega_c s}\right\}\Re\left\{a_k e^{j\theta_k}\right\}-\Im\left\{\tilde{s}_m(s-\tau_k)e^{j\omega_c s}\right\}\Im\left\{a_k e^{j\theta_k}\right\}\Big]\right| \\
&\le \sum_{k=0}^{L-1}\Big[\left|\Re\left\{\tilde{s}_m(s-\tau_k)e^{j\omega_c s}\right\}\right|E\left|\Re\left\{a_k e^{j\theta_k}\right\}\right|+\left|\Im\left\{\tilde{s}_m(s-\tau_k)e^{j\omega_c s}\right\}\right|E\left|\Im\left\{a_k e^{j\theta_k}\right\}\right|\Big] \\
&\le \sum_{k=0}^{L-1}E\,|a_k|\left[\left|\Re\left\{\tilde{s}_m(s-\tau_k)e^{j\omega_c s}\right\}\right|+\left|\Im\left\{\tilde{s}_m(s-\tau_k)e^{j\omega_c s}\right\}\right|\right] \qquad (3.2)\\
&\int_0^{T_o}E\,|v_m(s)|\,ds \\
&\le \sum_{k=0}^{L-1}E\,|a_k|\left[\int_0^{T_o}\left|\Re\left\{\tilde{s}_m(s-\tau_k)e^{j\omega_c s}\right\}\right|ds+\int_0^{T_o}\left|\Im\left\{\tilde{s}_m(s-\tau_k)e^{j\omega_c s}\right\}\right|ds\right]<\infty
\end{aligned}
$$

Furthermore the delayed signals $\tilde{s}_m(s-\tau_0),\tilde{s}_m(s-\tau_1),\ldots,\tilde{s}_m(s-\tau_{L-1})$ are assumed to be linearly independent over the observation interval $[0,T_o]$ (called L-order linear independency assumption). Let's recall from Chapter 2 that the resolvability condition requires that all time-shifted versions of the signals are orthogonal, $(\int_0^{T_o}\tilde{s}_m(s-\tau_k)\tilde{s}_m^*(s-\tau_j)ds=0,k\neq j)$. In this thesis, only linear independency is required that is a much weaker constraint compared to orthogonality as shown in the following. Note also that although a finite observation interval $[0,T_o]$ is assumed throughout this thesis, receiver structures derived in Section 3.2.1 and Section 3.3.1 are still valid for infinite observation intervals with only slight modifications in the matched filtering implementation of the decision variables $\{u_{lm}\}_{l=0,\ldots,L-1}$ provided that the signals $\tilde{s}_m(s-\tau_k)$ are assumed bounded and the L-order linear independency condition is satisfied. To assess what the L-order linear independency assumption implies, let us first define three types of observation intervals.

Definition 3.1.1. Let $\mathsf{f}(s)$ be a square integrable complex signal of energy $\tilde{E}=\int_{-\infty}^{\infty}|\mathsf{f}(s)|^2\,ds$. Let $n\in\mathbb{N}$. An observation interval $[u,t]$ is said to be "long" (with respect to $\mathsf{f}(s)$ and $\{\tau_k\ge 0\}_k$) if the signals $\mathsf{f}(s-\tau_0),\mathsf{f}(s-\tau_1),\ldots,\mathsf{f}(s-\tau_{n-1})$ are contained within the observation interval, i.e.

$$
\forall k=0,\ldots,n-1\quad\forall s\in(-\infty,\infty)\qquad \mathsf{f}(s-\tau_k)\,\mathrm{rect}\left(\frac{s-\frac{u+t}{2}}{t-u}\right)=\mathsf{f}(s-\tau_k)
$$

$$\text{hence} \qquad \epsilon_k(u,t) \triangleq \frac{1}{\bar{E}} \int_u^t |\mathrm{f}(s-\tau_k)|^2 \, ds = 1$$

where from (2.3) $\mathrm{rect}\left(\frac{s-\frac{u+t}{2}}{t-u}\right)$ is a unit magnitude rectangular pulse spanning the interval $[u,t]$.

An observation interval $[u,t]$ is said to be "intermediate" if

$$\forall\, k = 0, \ldots, n-1 \qquad \epsilon_k(u,t) > 0 \quad \text{and} \quad \exists\, k_0 \in \{0, \ldots, n-1\} \quad \epsilon_{k_0}(u,t) < 1$$

An observation interval $[u,t]$ is said to be "short" if

$$\exists\, k_0 \in \{0, \ldots, n-1\} \qquad \epsilon_{k_0}(u,t) = 0$$

These definitions are relative to the number of time-shifted signals, the values of the time shifts and depend on the signal itself. An observation interval can be long for one waveform and short for another, long for some time shifts and short for others. For example from Lemma B.1, it can be shown that for a continuous waveform time-limited to $[0,T]$ (i.e. $\mathrm{f}(s) = 0$ for $s \notin [0,T]$) and ordered time delays $(\tau_0 < \tau_1 < \ldots < \tau_{n-1})$ an observation interval of the form $[0,t]$ is long iff $t \geq T'' + \tau_{n-1}$, intermediate iff $T' + \tau_{n-1} < t < T'' + \tau_{n-1}$ and short iff $t \leq T' + \tau_{n-1}$, where T' and T'' are the "initial" and "final" times of the waveform defined mathematically as

$$T' = \sup_v \left\{ v \in I\!R, \ \int_{-\infty}^{v} |\mathrm{f}(s)|^2 \, ds = 0 \right\} \tag{3.3}$$

$$T'' = \inf_v \left\{ v \in I\!R, \ \int_{-\infty}^{v} |\mathrm{f}(s)|^2 \, ds = \int_{-\infty}^{\infty} |\mathrm{f}(s)|^2 \, ds \right\} \tag{3.4}$$

The "times" T' and T'' are defined to take into consideration the case where the m possible transmitted signals, although time-limited to $[0,T]$, or $[0,2T]$ do not have the same "initial" or "final" times (as in return-to-zero or biphase signaling for example). Nevertheless, using the continuous approximations of FSK, DPSK and SDPSK [174] considered in Chapter 4 of this thesis, for FSK $T' = 0$, and $T'' = T$, while for (S)DPSK $T' = 0$ and $T'' = 2T$.

It is shown in Theorem B.1 that a square integrable complex signal that has a non-zero energy will satisfy the L-order linear independency condition over a long observation interval $[u,t]$ for any arbitrary non-zero integer L and distinct multipath

delays. Consider a second case where $\tilde{s}_m(s)$ is time-limited to $[0,T]$ such that $\tilde{E}_m = \int_0^T |\tilde{s}_m(s)|^2\,ds \neq 0$ and the L delays $\{\tau_k\}_{k=0,\ldots,L-1}$ are distinct and sorted in increasing order ($\tau_0 < \tau_1 < \ldots$). Let $[0,T_o]$ be an observation interval where $T_o > T' + \tau_{L-1}$ corresponding to a long or intermediate observation interval. Then Theorem B.2 shows that the signals $\tilde{s}_m(s-\tau_0), \ldots, \tilde{s}_m(s-\tau_{L-1})$ are linearly independent over $[0,T_o]$. Therefore the L-order linear independency condition assumed in receiver design's sections such as Section 3.2.1 and Section 3.3.1 is not too restricting.

However results from Section 3.2.1 and Section 3.3.1 do not apply to short observation intervals since one of the time-shifted signals has zero energy failing the linear independency assumption. But receiver structures for short observation intervals can be easily deduced from Sections 3.2.1, 3.3.1 results in the special case of time-limited waveforms. In that case, Section 3.2.3 (topic: "Eigenvalues and eigenfunctions of $K_m(s,u)$ ... ") shows that the L-path channel model (3.1) assuming a short observation interval, $[0,t]$ can be reduced to a multipath channel model similar to (3.1) except that it includes a smaller number of paths. And the reduced set of time-shifted waveforms forms a linear independent set. Therefore results obtained in Sections 3.2.1, 3.3.1 can be readily applied using the reduced channel model.

In this thesis the following notation is used: Bold capital letters denote matrices and bold lowercase letters denote vectors, ^{T}, * and † denote respectively the transposition, complex conjugation and Hermitian conjugation of a matrix or vector. The kj^{th} entry of a matrix $\boldsymbol{B}$ is denoted as $[\boldsymbol{B}]_{kj}$, and the k^{th} entry of a vector $\boldsymbol{v}$ is denoted as $[\boldsymbol{v}]_k$. The diagonal matrix composed of the main diagonal entries of $\boldsymbol{B}$ is denoted by $\{\boldsymbol{B}\}_d$, and the lower triangular matrix composed of the lower triangular elements of $\boldsymbol{B}$ with zero main diagonal entries is denoted by $\{\boldsymbol{B}\}_l$. Let us define $\boldsymbol{\theta} = [\theta_0, \theta_1, \ldots, \theta_{L-1}]^T$, $\boldsymbol{\theta}_k = [\theta_0, \theta_1, \ldots, \theta_k]^T$ for $k \leq L-1$ where $\boldsymbol{\theta}_{-1} = [\cdot]$ (*null set*) by convention. Let $\tilde{E}_m = \int_{-\infty}^{\infty} |\tilde{s}_m(s)|^2\,ds$ be the baseband signal energy under H_m. The energies of the signals $\tilde{s}_m(s-\tau_k)$ over the interval $[0,t]$ are defined as fractions of their total energy, i.e. $\int_0^t |\tilde{s}_m(s-\tau_k)|^2 ds = \epsilon_{km}(t)\tilde{E}_m$ where $0 \leq \epsilon_{km}(t) \leq 1$. The duration of time-limited signaling waveforms is denoted by T. Furthermore, $\rho_{kj}^{rl}(t)$, $(r,l \in \{1,2,\ldots,M\}, k,j \in \{0,1,\ldots,L-1\})$ denotes the complex cross-correlation coefficient between $\tilde{s}_r(s-\tau_k)$ and $\tilde{s}_l(s-\tau_j)$, $\rho_{kj}^{rl}(t) = \frac{1}{\sqrt{\tilde{E}_r \tilde{E}_l \epsilon_{kr}(t)\epsilon_{jl}(t)}} \int_0^t \tilde{s}_r(s-\tau_k)\tilde{s}_l^*(s-\tau_j)ds$. Then the signal cross-correlation matrix between the hypothesis H_r and H_l, $\boldsymbol{\Gamma}_{rl}(t)$ is defined as $[\boldsymbol{\Gamma}_{rl}(t)]_{kj} = \rho_{kj}^{rl}(t)$. The correlation matrix of the signal under H_m, $\boldsymbol{\Gamma}_m(t)$ is defined as $[\boldsymbol{\Gamma}_m(t)]_{kj} = \rho_{kj}^{m}(t)$ where $\rho_{kj}^{m}(t) = \rho_{kj}^{mm}(t) = \frac{1}{\tilde{E}_m \sqrt{\epsilon_{km}(t)\epsilon_{jm}(t)}} \int_0^t \tilde{s}_m(s -$

$\tau_k)\tilde{s}_m^*(s-\tau_j)ds$. Let $\boldsymbol{\epsilon}_m(t)$ be the diagonal matrix with k^{th} diagonal entry $\epsilon_{km}(t)$, and $\boldsymbol{C}$ be the covariance matrix of the channel defined as $[\boldsymbol{C}]_{kj} = E\left[(a_k - \alpha_k)(a_j - \alpha_j)^*\right]$. Since the path gains are uncorrelated, $\boldsymbol{C}$ is diagonal with k^{th} diagonal entry $2\sigma_k^2$. For sake of simplicity, whenever the L-order linear independency condition is assumed over an observation interval $[0, T_o]$, the index T_o in $\epsilon_{km}(T_o)$, $\boldsymbol{\epsilon}_m(T_o)$, $\rho_{kj}^{rl}(T_o)$, $\boldsymbol{\Gamma}_{rl}(T_o)$ and $\boldsymbol{\Gamma}_m(T_o)$ will be omitted.

3.2 Specular coherent optimal decision rule for an L-path Ricean channel

3.2.1 L-path Ricean specular coherent optimum receiver structure (SPECCOH)

Let us consider an observation interval $[0, T_o]$ such that the L-order linear independency condition is satisfied. From Section 3.1, $[0, T_o]$ is necessarily long or intermediate as defined in Definition 3.1.1. The specular component phases and amplitudes are assumed to be known at the receiver hence the term specular coherent detection. In this thesis the specular coherent optimal receiver is denoted the SPECCOH scheme. As explained in Section 3.1, known specular component phases is equivalent to assuming that $\boldsymbol{\theta}$ is known. The likelihood ratio associated with the SPECCOH scheme corresponds to the conditional likelihood ratio (given $\boldsymbol{\theta}$) associated with the non-coherent optimal receiver. Multipath Ricean channels, when $\boldsymbol{\theta}$ is fixed yield the classical problem of detecting a continuous time Gaussian random signal $v_m(s) = \Re\left\{\left[\sum_{k=0}^{L-1} a_k e^{j\theta_k}\tilde{s}_m(s-\tau_k)\right]e^{j\omega_c s}\right\}$ in additive white Gaussian noise [172, pp. 419-421]. A minimum probability of error receiver forms the likelihood ratio between each one of the hypotheses $H_m : \dot{z}(s) = v_m(s) + \dot{w}(s)$, $_{m=1,2,...M}$ and a null hypothesis $H_0 : \dot{z}(s) = \dot{w}(s)$. With equiprobable hypotheses, the decision is made in the favor of the largest likelihood ratio [172, p. 11]. The discrete representation of $\dot{z}(s)$ when $\boldsymbol{\theta}$ is held fixed, follows from Karhunen-Loève expansion and exists since given $\boldsymbol{\theta}$ the signal $v_m(s)$ is a second-order mean square continuous random process [182, p. 86], [183, p. 271] as shown in the following:

From Appendix B.2.1, the covariance function of the bandpass signal process $v_m(s)$ under H_m given $\boldsymbol{\theta}$ is

$$K_m(s,u) \triangleq E\Big[\big(v_m(s) - E\left[v_m(s)|\boldsymbol{\theta}\right]\big)\big(v_m(u) - E\left[v_m(u)|\boldsymbol{\theta}\right]\big)\Big|\boldsymbol{\theta}\Big]$$

$$K_m(s,u) = \Re\left\{\frac{1}{2}\mathcal{K}_m(s,u)e^{j\omega_c(s-u)}\right\} \tag{3.5}$$

where $\mathcal{K}_m(s,u)$, the covariance function of the complex signal process $\tilde{v}_m(s) = \sum_{k=0}^{L-1} a_k e^{j\theta_k}\tilde{s}_m(s-\tau_k)$ with $\boldsymbol{\theta}$ held fixed, is given by

$$\begin{aligned}\mathcal{K}_m(s,u) &\triangleq E\Big[\big(\tilde{v}_m(s) - E[\tilde{v}_m(s)|\boldsymbol{\theta}]\big)\big(\tilde{v}_m(u) - E[\tilde{v}_m(u)|\boldsymbol{\theta}]\big)^*|\boldsymbol{\theta}\Big] \\ &= \sum_{k=0}^{L-1} 2\sigma_k^2\tilde{s}_m(s-\tau_k)\tilde{s}_m^*(u-\tau_k)\end{aligned} \tag{3.6}$$

Since from Section 3.1 $\forall k = 0,\ldots,L-1$, $\tilde{s}_m(s-\tau_k)$ is bounded, (3.5-3.6) yield $\forall (s,u) \in [0,T_o]^2 \quad K_m(s,u) < \infty$, and $v_m(s)$ is a second order process when $\boldsymbol{\theta}$ is held fixed [182, p. 74]. Since $\forall k = 0,\ldots,L-1 \quad \tilde{s}_m(s-\tau_k)$ is continuous, $K_m(s,u)$ given by (3.5) is also continuous. Therefore from [182, p. 77], [183, p. 226], $v_m(s)$ is mean square continuous.

From (3.6), it is recognized that $\mathcal{K}_m(s,u)$, the covariance function of the complex signal process $\tilde{v}_m(s)$, is independent of $\boldsymbol{\theta}$ and it is a finite dimensional kernel with well known eigenvalues and eigenfunctions [184, p. 55]. Notice that in this thesis the definition of the eigenvalues is similar to [172, pp. 379-380]. As shown in Appendix B.2.2 $\mathcal{K}_m(s,u)$, given by (3.6), has at most L positive eigenvalues $\{\lambda_{lm}\}_{l=0,1,\ldots,L-1}$ and L corresponding eigenfunctions. Its eigenvalues are those of the matrix $\tilde{E}_m\boldsymbol{\epsilon}_m\boldsymbol{C}\boldsymbol{\Gamma}_m^*$, where $\boldsymbol{C}$ is the channel covariance matrix, and $\boldsymbol{\Gamma}_m$ is the signal correlation matrix defined in Section 3.1. Since $\mathcal{K}_m(s,u)$ in (3.6) is a finite dimensional kernel, its eigenfunctions $\{\phi_{lm}(s)\}_{l=0,\ldots,L-1}$, that form an orthogonal set, are given by

$$\phi_{lm}(s) = \frac{1}{\sqrt{\tilde{E}_m}}\sum_{k=0}^{L-1}\frac{x_{lk}^m}{\sqrt{\epsilon_{km}}}\tilde{s}_m(s-\tau_k) \qquad 0 \le s \le T_o \quad l = 0,\ldots,L-1 \tag{3.7}$$

where[1] $x_{lk}^m = [\boldsymbol{X}_m]_{lk}$, $\boldsymbol{X}_m$ is an $L \times L$ matrix that satisfies the equations:

$$\boldsymbol{X}_m^*\boldsymbol{\Gamma}_m^*\boldsymbol{X}_m^T = \boldsymbol{I} \tag{3.8a}$$

$$\boldsymbol{\epsilon}_m\boldsymbol{C}\boldsymbol{\Gamma}_m^*\boldsymbol{X}_m^T = \boldsymbol{X}_m^T\boldsymbol{D}_m \tag{3.8b}$$

$\boldsymbol{I}$ is the $L \times L$ identity matrix and $\boldsymbol{D}_m$ denotes the $L \times L$ diagonal matrix of the

[1]The superscript m is not an exponent and refers to the hypothesis H_m.

energy normalized eigenvalues of $\mathcal{K}_m(s,u)$, defined by $[\boldsymbol{D}_m]_{kk} = \lambda_{km}/\tilde{E}_m$.

Furthermore (3.5) and the signal narrow-band assumption imply that the eigenvalues κ_{lm} and eigenfunctions $\Upsilon_{lm}(s)$ of the bandpass signal process covariance function $K_m(s,u)$ can be expressed in terms of the eigenvalues and eigenfunctions of the covariance function of the complex signal process $\tilde{v}_m(s)$. It is shown in Appendix B.2.3 that $K_m(s,u)$ has $2L$ eigenvalues and $2L$ eigenfunctions given by

$$\Upsilon_{lm}(s) = \Re\left\{\sqrt{2}\phi_{lm}(s)e^{j\omega_c s}\right\} \qquad l=0,\ldots,L-1 \quad \text{associated with } \kappa_{lm} = \frac{\lambda_{lm}}{4} \tag{3.9a}$$

$$\Upsilon_{lm}(s) = \Im\left\{\sqrt{2}\phi_{l-Lm}(s)e^{j\omega_c s}\right\} \qquad l=L,\ldots,2L-1 \quad \text{associated with } \kappa_{lm} = \frac{\lambda_{l-Lm}}{4} \tag{3.9b}$$

The detailed mathematical derivation of the conditional likelihood ratio associated with the non-coherent optimal receiver can be found in Appendix B.3.1. Here only the final result is presented. By substituting $\boldsymbol{\Omega}_m = N_0\boldsymbol{I} + \frac{\tilde{E}_m}{2}\boldsymbol{D}_m$, $\boldsymbol{\Omega}_0 = N_0\boldsymbol{I}$ and (B.25) into (B.30), the conditional likelihood ratio or the SPECCOH likelihood ratio $\Lambda_m\left(\dot{z}(s); s\in[0,T_o]|\boldsymbol{\theta}\right)$ or $\Lambda_m\left(\dot{z};T_o|\boldsymbol{\theta}\right)$ for short is given by

$$\Lambda_m\left(\dot{z};T_o|\boldsymbol{\theta}\right) = \left[\det\left(\boldsymbol{I}+\gamma_m\boldsymbol{D}_m\right)\right]^{-1}\exp\left\{-\boldsymbol{\alpha}^\dagger\boldsymbol{C}^{-1}\boldsymbol{\alpha}\right\}\cdot$$
$$\exp\left\{\gamma_m\left(\boldsymbol{r}_m+\frac{1}{\gamma_m}\boldsymbol{X}_m^*\boldsymbol{C}^{-1}\boldsymbol{\epsilon}_m^{-1/2}\boldsymbol{\varrho}(\boldsymbol{\theta})\right)^\dagger\boldsymbol{Q}_m\left(\boldsymbol{r}_m+\frac{1}{\gamma_m}\boldsymbol{X}_m^*\boldsymbol{C}^{-1}\boldsymbol{\epsilon}_m^{-1/2}\boldsymbol{\varrho}(\boldsymbol{\theta})\right)\right\} \tag{3.10}$$

where γ_m is the SNR given by

$$\gamma_m = \frac{\tilde{E}_m}{2N_0} \tag{3.11}$$

$$\boldsymbol{\varrho}(\boldsymbol{\theta}) = \left[\alpha_0 e^{j\theta_0},\ldots,\alpha_{L-1}e^{j\theta_{L-1}}\right]^T \tag{3.12}$$

$$\boldsymbol{\alpha} = \left[\alpha_0,\ldots,\alpha_{L-1}\right]^T \tag{3.13}$$

the vector $\boldsymbol{r}_m$ is defined as

$$[\boldsymbol{r}_m]_l \triangleq \frac{2}{\sqrt{\tilde{E}_m}}\int_0^{T_o}\phi_{lm}^*(s)e^{-j\omega_c s}dz(s) \qquad l=0,\ldots,L-1 \tag{3.14}$$

$$= \sqrt{\frac{2}{\tilde{E}_m}}\left\{[\boldsymbol{z}_m]_l - j\,[\boldsymbol{z}_m]_{l+L}\right\} \qquad l=0,\ldots,L-1$$

$$[\boldsymbol{z}_m]_l = \int_0^{T_o} \Upsilon_{lm}(s)dz(s) \triangleq z_{lm} \qquad l = 0, \ldots, 2L-1 \tag{3.15}$$

and the integrals in (3.14) and (3.15) are Wiener integrals (see Appendix A.1). The matrix $\boldsymbol{Q}_m$ is given by

$$\boldsymbol{Q}_m = \gamma_m \left[\boldsymbol{D}_m^{-1} + \gamma_m \boldsymbol{I}\right]^{-1} \tag{3.16a}$$

$$= \gamma_m \left(\boldsymbol{X}_m^T\right)^{-1} \left[(\boldsymbol{\epsilon}_m \boldsymbol{C})^{-1} + \gamma_m \boldsymbol{\Gamma}_m^*\right]^{-1} (\boldsymbol{X}_m^*)^{-1} \tag{3.16b}$$

where (3.16b) is obtained from (3.16a) by using (3.8). Using (3.8b) and (3.16b), the SPECCOH likelihood ratio is also given by

$$\Lambda_m(\dot{z}; T_o|\boldsymbol{\theta}) = \left[\det\left(\boldsymbol{I} + \gamma_m \boldsymbol{\epsilon}_m \boldsymbol{C} \boldsymbol{\Gamma}_m^*\right)\right]^{-1} \exp\left\{-\boldsymbol{\alpha}^\dagger \boldsymbol{C}^{-1} \boldsymbol{\alpha}\right\} \cdot$$
$$\exp\left\{\gamma_m^2 \left(\boldsymbol{u}_m + \frac{1}{\gamma_m} \boldsymbol{C}^{-1} \boldsymbol{\epsilon}_m^{-1/2} \boldsymbol{\varrho}(\boldsymbol{\theta})\right)^\dagger \left[(\boldsymbol{\epsilon}_m \boldsymbol{C})^{-1} + \gamma_m \boldsymbol{\Gamma}_m^*\right]^{-1} \left(\boldsymbol{u}_m + \frac{1}{\gamma_m} \boldsymbol{C}^{-1} \boldsymbol{\epsilon}_m^{-1/2} \boldsymbol{\varrho}(\boldsymbol{\theta})\right)\right\} \tag{3.17}$$

where

$$\boldsymbol{u}_m = \left(\boldsymbol{X}_m^*\right)^{-1} \boldsymbol{r}_m = [u_{0m}, u_{1m}, \ldots, u_{L-1m}]^T \tag{3.18a}$$

$$u_{lm} \triangleq \frac{2}{\sqrt{\tilde{E}_m}} \int_0^{T_o} \frac{\tilde{s}_m^*(s - \tau_l)}{\sqrt{\tilde{E}_m \epsilon_{lm}}} e^{-j\omega_c s} dz(s) \qquad l = 0, \ldots, L-1 \tag{3.18b}$$

The decision variable u_{lm} (3.18b) can be obtained by using a bank of matched filters. For example, the following bank of matched filter $\{s'_{lm}(s)\}_{l=0,\ldots,L-1}$ can be used with a sampling time at $T_{el} = T_o + \tau_l$

$$s'_{lm}(s) = \begin{cases} \dfrac{2}{\sqrt{\tilde{E}_m}} \dfrac{\tilde{s}_m^*(T_o - s)\, e^{j\omega_c(s - T_o - \tau_l)}}{\sqrt{\tilde{E}_m \epsilon_{lm}}} & \tau_l \le s \le T_o + \tau_l, \\ 0 & \text{else.} \end{cases}$$

Since the term $\exp\left\{-\boldsymbol{\alpha}^\dagger \boldsymbol{C}^{-1} \boldsymbol{\alpha}\right\}$ is independent of the hypothesis H_m, an equivalent decision variable $\Lambda'_m(\dot{z}; T_o|\boldsymbol{\theta})$ is obtained by removing this term from (3.17). When the observation interval $[0, T_o]$ is assumed to be much longer than the multipath delays ($T_o \gg \tau_l$ for all l) and $\epsilon_{lm} = 1$ for all l, $s'_{lm}(s) \approx s'_m(s) = 2\tilde{s}_m^*(T_o - s)\, e^{j\omega_c(s - T_o)}/\tilde{E}_m$ for

$0 \leq s \leq T_o$. Then the receiver illustrated in Fig. 3.1 is obtained. In this special case, the decision variable u_{lm} can be generated by sampling the output of the matched filter $s'_m(s)$ at $T_o + \tau_l$, as shown in Fig. 3.1, or by using a tapped-delay-line after the matched filter.

3.2.2 SPECCOH: a quadratic decorrelator

As seen in Section 3.2.1, the likelihood ratio of the SPECCOH scheme is given by (3.10) or by (3.17). The second form of the likelihood (3.17) is convenient to use when the multipath is resolved. The first form of the likelihood (3.10) provides an important insight to the operations performed by the optimal specular coherent receiver. Recall that under the m^{th} hypothesis, the received signal is given by (3.1). In Section 3.2.1 a linear transformation on the signals $\tilde{s}_m(s-\tau_k)$, (3.7), is performed to obtain an orthogonal basis $\{\phi_{lm}(s)\}_l$. Therefore the m^{th} hypothesis can be equivalently expressed (since the linear transformation (3.7) is invertible) as

$$\begin{aligned}\dot{z}(s) &= \Re\left\{\sum_{k=0}^{L-1} a_k e^{j\theta_k}\left[\sqrt{\tilde{E}_m}\sum_{l=0}^{L-1}\sqrt{\epsilon_{km}}\,y_{kl}^m\phi_{lm}(s)\right]e^{j\omega_c s}\right\} + \dot{w}(s)\\ &= \Re\left\{\sum_{l=0}^{L-1}\breve{a}_{lm}(\boldsymbol{\theta})\sqrt{\epsilon_{lm}\tilde{E}_m}\phi_{lm}(s)e^{j\omega_c s}\right\} + \dot{w}(s) \qquad (3.19)\end{aligned}$$

where $y_{kl}^m = \left[\boldsymbol{X}_m^{-1}\right]_{kl}$, $\breve{a}_{lm}(\boldsymbol{\theta}) = \sum_{k=0}^{L-1} a_k e^{j\theta_k}\frac{\sqrt{\epsilon_{km}}}{\sqrt{\epsilon_{lm}}}y_{kl}^m$, while $\sqrt{\epsilon_{lm}\tilde{E}_m}\phi_{lm}(s)$ are orthogonal signals of same energy as $\tilde{s}_m(s-\tau_l)$. When $\boldsymbol{\theta}$ is held fixed, under each hypothesis the new random vector $\left[\breve{a}_{0m}(\boldsymbol{\theta}),\ldots,\breve{a}_{L-1m}(\boldsymbol{\theta})\right]^T$ is Gaussian with mean $\boldsymbol{\varrho}'_m(\boldsymbol{\theta}) = \boldsymbol{\epsilon}_m^{-1/2}\boldsymbol{D}_m\boldsymbol{X}_m^*\boldsymbol{C}^{-1}\boldsymbol{\epsilon}_m^{-1/2}\boldsymbol{\varrho}(\boldsymbol{\theta})$ and covariance $\boldsymbol{C}'_m = \boldsymbol{\epsilon}_m^{-1}\boldsymbol{D}_m$ as shown in the following.

$$\begin{aligned}\left[\boldsymbol{\varrho}'_m(\boldsymbol{\theta})\right]_{l0} &\triangleq E\left[\breve{a}_{lm}(\boldsymbol{\theta})\,|\boldsymbol{\theta}\right] = \sum_{k=0}^{L-1} E\left[a_k\right]e^{j\theta_k}\frac{\sqrt{\epsilon_{km}}}{\sqrt{\epsilon_{lm}}}y_{kl}^m = \sum_{k=0}^{L-1}\alpha_k e^{j\theta_k}\frac{\sqrt{\epsilon_{km}}}{\sqrt{\epsilon_{lm}}}y_{kl}^m\\ &= \left[\boldsymbol{\epsilon}_m^{-1/2}\left(\boldsymbol{X}_m^{-1}\right)^T\boldsymbol{\epsilon}_m^{1/2}\boldsymbol{\varrho}(\boldsymbol{\theta})\right]_{l0}\\ &= \left[\boldsymbol{\epsilon}_m^{-1/2}\left(\boldsymbol{\Gamma}_m^*\boldsymbol{X}_m^T\right)^\dagger\boldsymbol{\epsilon}_m^{1/2}\boldsymbol{\varrho}(\boldsymbol{\theta})\right]_{l0} \qquad \text{using (3.8a)}\\ &= \left[\boldsymbol{\epsilon}_m^{-1/2}\boldsymbol{D}_m\boldsymbol{X}_m^*\boldsymbol{C}^{-1}\boldsymbol{\epsilon}_m^{-1/2}\boldsymbol{\varrho}(\boldsymbol{\theta})\right]_{l0} \qquad \text{using (3.8b)}\end{aligned}$$

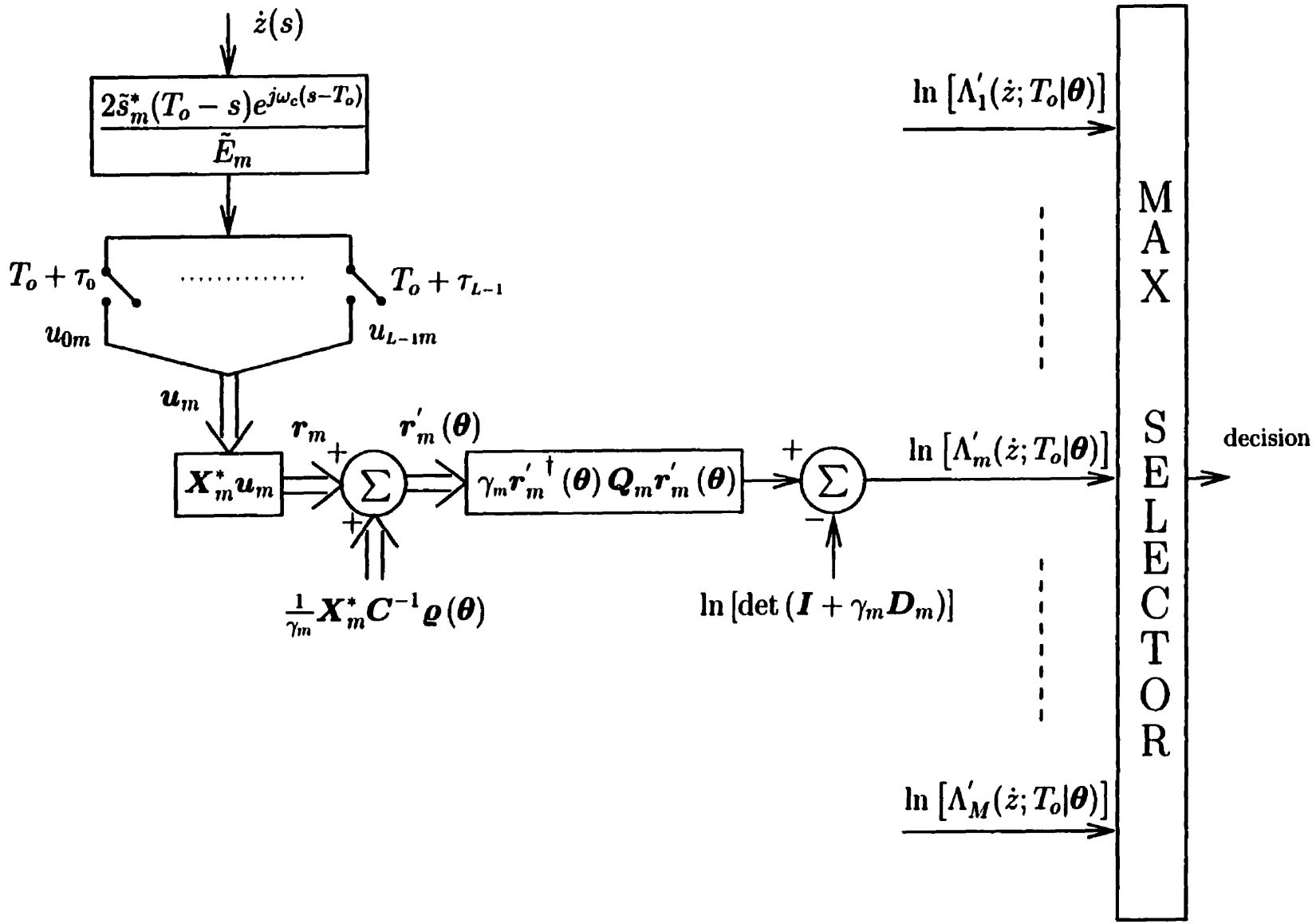

Fig. 3.1 Specular coherent optimum receiver for an L-path Ricean channel (SPECCOH) assuming $T_o \gg \tau_l$ & $\epsilon_{lm} = 1$ for all l

$$\left[\boldsymbol{C}'_m\right]_{rl} \triangleq E\Big[\left(\breve{a}_{rm}(\boldsymbol{\theta}) - E\left[\breve{a}_{rm}(\boldsymbol{\theta})\,|\boldsymbol{\theta}\right]\right)\left(\breve{a}_{lm}(\boldsymbol{\theta}) - E\left[\breve{a}_{lm}(\boldsymbol{\theta})\,|\boldsymbol{\theta}\right]\right)^*|\boldsymbol{\theta}\Big]$$
$$= \sum_{k=0}^{L-1}\sum_{j=0}^{L-1} E\left[(a_k - \alpha_k)(a_j - \alpha_j)^*\right] e^{j(\theta_k-\theta_j)} \frac{\sqrt{\epsilon_{km}}}{\sqrt{\epsilon_{rm}}} y_{kr}^m \frac{\sqrt{\epsilon_{jm}}}{\sqrt{\epsilon_{lm}}} (y_{jl}^m)^*$$

Hence

$$\begin{aligned}
\left[\boldsymbol{C}'_m\right]_{rl} &= \sum_{k=0}^{L-1} 2\sigma_k^2 \epsilon_{km} \frac{y_{kr}^m}{\sqrt{\epsilon_{rm}}} \frac{(y_{kl}^m)^*}{\sqrt{\epsilon_{lm}}} \\
&= \left[\left(\boldsymbol{X}_m^{-1}\boldsymbol{\epsilon}_m^{-1/2}\right)^T \boldsymbol{\epsilon}_m \boldsymbol{C} \left(\boldsymbol{X}_m^{-1}\right)^* \boldsymbol{\epsilon}_m^{-1/2}\right]_{rl} \\
&= \left[\boldsymbol{\epsilon}_m^{-1/2}\left(\boldsymbol{X}_m^T\right)^{-1} \boldsymbol{\epsilon}_m \boldsymbol{C} \boldsymbol{\Gamma}_m^* \boldsymbol{X}_m^T \boldsymbol{\epsilon}_m^{-1/2}\right]_{rl} \qquad \text{using (3.8a)} \\
&= \left[\boldsymbol{\epsilon}_m^{-1/2} \boldsymbol{D}_m \boldsymbol{\epsilon}_m^{-1/2}\right]_{rl} = \left[\boldsymbol{\epsilon}_m^{-1} \boldsymbol{D}_m\right]_{rl} = 0 \quad \text{if } r \neq l \qquad \text{using (3.8b)}
\end{aligned} \tag{3.20}$$

Therefore, under each hypothesis, the received signal can be represented as a linear combination of orthogonal functions weighted by uncorrelated circularly complex Gaussian random variables, similar to the resolvable multipath case. Substituting $\boldsymbol{X}_m = \boldsymbol{I}$, $\boldsymbol{\Gamma}_m = \boldsymbol{I}$ into (3.17), yields the likelihood ratio for a resolved multipath Ricean fading channel with specular coherent detection given by

$$\Lambda_m(\dot{z}; T_o|\boldsymbol{\theta}) = \left[\det\left(\boldsymbol{I} + \gamma_m \boldsymbol{\epsilon}_m \boldsymbol{C}\right)\right]^{-1} \exp\left\{-\boldsymbol{\alpha}^\dagger \boldsymbol{C}^{-1}\boldsymbol{\alpha}\right\} \cdot$$
$$\exp\left\{\gamma_m^2 \left(\boldsymbol{u}_m + \frac{1}{\gamma_m}\boldsymbol{C}^{-1}\boldsymbol{\epsilon}_m^{-1/2}\boldsymbol{\varrho}(\boldsymbol{\theta})\right)^\dagger \left[(\boldsymbol{\epsilon}_m\boldsymbol{C})^{-1} + \gamma_m \boldsymbol{I}\right]^{-1} \left(\boldsymbol{u}_m + \frac{1}{\gamma_m}\boldsymbol{C}^{-1}\boldsymbol{\epsilon}_m^{-1/2}\boldsymbol{\varrho}(\boldsymbol{\theta})\right)\right\} \tag{3.21}$$

where $\boldsymbol{\varrho}(\boldsymbol{\theta})$, given by (3.12), and $\boldsymbol{C}$, given by $[\boldsymbol{C}]_{kj} = 2\sigma_k^2\delta_{kj}$, can also be defined as

$$[\boldsymbol{\varrho}(\boldsymbol{\theta})]_{k0} \triangleq E\left[a_k e^{j\theta_k}|\boldsymbol{\theta}\right] \qquad [\boldsymbol{C}]_{kj} \triangleq E\Big[\left(a_k e^{j\theta_k} - [\boldsymbol{\varrho}(\boldsymbol{\theta})]_{k0}\right)\left(a_j e^{j\theta_j} - [\boldsymbol{\varrho}(\boldsymbol{\theta})]_{j0}\right)^*|\boldsymbol{\theta}\Big]$$

Note that (3.21) with $\boldsymbol{\epsilon}_m = \boldsymbol{I}$ is presented in [4, 88]. Using (3.8) with several matrix manipulations, the first form of the likelihood ratio when the multipath is unresolved (3.10) can be rewritten as

$$\Lambda_m(\dot{z}; T_o|\boldsymbol{\theta}) = \left[\det\left(\boldsymbol{I} + \gamma_m \boldsymbol{\epsilon}_m \boldsymbol{C}'_m\right)\right]^{-1} \exp\left\{-\boldsymbol{\varrho}'^\dagger_m(\boldsymbol{\theta})\left(\boldsymbol{C}'_m\right)^{-1}\boldsymbol{\varrho}'_m(\boldsymbol{\theta})\right\} \cdot$$

$$\exp\left\{\gamma_m^2\left(\boldsymbol{r}_m+\frac{1}{\gamma_m}\left(\boldsymbol{C}_m'\right)^{-1}\boldsymbol{\epsilon}_m^{-1/2}\boldsymbol{\varrho}'_m(\boldsymbol{\theta})\right)^{\dagger}\left[\left(\boldsymbol{\epsilon}_m\boldsymbol{C}_m'\right)^{-1}+\gamma_m\boldsymbol{I}\right]^{-1}\right.$$
$$\left.\cdot\left(\boldsymbol{r}_m+\frac{1}{\gamma_m}\left(\boldsymbol{C}_m'\right)^{-1}\boldsymbol{\epsilon}_m^{-1/2}\boldsymbol{\varrho}'_m(\boldsymbol{\theta})\right)\right\} \qquad (3.22)$$

From (3.21) and (3.22) it is seen that the Ricean channel specular coherent optimal receiver for unresolved multipath channels consists of an orthogonalization (or decorrelation) stage that transforms $\boldsymbol{u}_m$ into $\boldsymbol{r}_m=\boldsymbol{X}_m^*\boldsymbol{u}_m$ and then implements a resolved multipath channel specular coherent optimal decision rule for $\boldsymbol{r}_m$. The new random variable $\check{a}_{lm}(\boldsymbol{\theta})$ is referred as the l^{th} multipath gain of the equivalent decorrelated (resolved) channel (on $[0,T_o]$ when $\boldsymbol{\theta}$ is held fixed). Note that the term decorrelation is employed since besides the orthogonalization of the signals $\{\tilde{s}_m(s-\tau_k)\}_{k=0,\ldots,L-1}$, the matrix $\boldsymbol{X}_m$ also performs a statistical decorrelation stage in the sense that the new variables $\{[\boldsymbol{r}_m]_l\}_{l=0,\ldots,L-1}$, unlike $\left\{u_{lm}\triangleq[\boldsymbol{u}_m]_l\right\}_{l=0,\ldots,L-1}$, are uncorrelated as coefficients of the Karhunen-Loève expansion of $\dot{z}(s)$.

The decorrelation in (3.10) vanishes if the instantaneous values of the multipath gains a_k are known to the receiver in addition to the specular component phases as shown in the following. It is to be expected since in that case, the problem reduces to the detection of a known signal in additive white Gaussian noise. It is well known that the optimum receiver consists of a matched filter, matched to the signal filtered by the known channel. A receiver that has knowledge of the instantaneous values of the multipath gains a_k is obtained by setting $\sigma_k=0$ for all k yielding $a_k=\alpha_k$. For sake of simplicity all σ_k are assumed equal, therefore $\boldsymbol{C}\triangleq\sigma\boldsymbol{I}$ where $\sigma=2\sigma_k^2$. Then $\left[(\boldsymbol{\epsilon}_m\boldsymbol{C})^{-1}+\gamma_m\boldsymbol{\Gamma}_m^*\right]^{-1}$ reduces to

$$\left[(\boldsymbol{\epsilon}_m\boldsymbol{C})^{-1}+\gamma_m\boldsymbol{\Gamma}_m^*\right]^{-1}=\sigma\left[\boldsymbol{I}+\sigma\gamma_m\boldsymbol{\epsilon}_m\boldsymbol{\Gamma}_m^*\right]^{-1}\boldsymbol{\epsilon}_m$$

and (3.17) is given by

$$\Lambda_m(\dot{z};T_o|\boldsymbol{\theta})=\left[\det\left(\boldsymbol{I}+\sigma\gamma_m\boldsymbol{\epsilon}_m\boldsymbol{\Gamma}_m^*\right)\right]^{-1}\exp\left\{\sigma\gamma_m^2\boldsymbol{u}_m^{\dagger}\left[\boldsymbol{I}+\sigma\gamma_m\boldsymbol{\epsilon}_m\boldsymbol{\Gamma}_m^*\right]^{-1}\boldsymbol{\epsilon}_m\boldsymbol{u}_m\right.$$
$$+\gamma_m\boldsymbol{\varrho}^{\dagger}(\boldsymbol{\theta})\boldsymbol{\epsilon}_m^{-1/2}\left[\boldsymbol{I}+\sigma\gamma_m\boldsymbol{\epsilon}_m\boldsymbol{\Gamma}_m^*\right]^{-1}\boldsymbol{\epsilon}_m\boldsymbol{u}_m+\gamma_m\boldsymbol{u}_m^{\dagger}\left[\boldsymbol{I}+\sigma\gamma_m\boldsymbol{\epsilon}_m\boldsymbol{\Gamma}_m^*\right]^{-1}\boldsymbol{\epsilon}_m^{1/2}\boldsymbol{\varrho}(\boldsymbol{\theta})$$
$$\left.+\frac{1}{\sigma}\boldsymbol{\varrho}^{\dagger}(\boldsymbol{\theta})\left[\boldsymbol{\epsilon}_m^{-1/2}\left(\boldsymbol{I}+\sigma\gamma_m\boldsymbol{\epsilon}_m\boldsymbol{\Gamma}_m^*\right)^{-1}\boldsymbol{\epsilon}_m^{1/2}-\boldsymbol{I}\right]\boldsymbol{\varrho}(\boldsymbol{\theta})\right\}$$

Hence

$$\lim_{\sigma \to 0} \Lambda_m\left(\dot{z}; T_o|\boldsymbol{\theta}\right) = \exp\left\{2\gamma_m \Re\left[\boldsymbol{\varrho}^\dagger(\boldsymbol{\theta})\boldsymbol{\epsilon}_m^{1/2}\boldsymbol{u}_m\right] - \gamma_m \boldsymbol{\varrho}^\dagger(\boldsymbol{\theta})\boldsymbol{\epsilon}_m^{1/2}\boldsymbol{\Gamma}_m^*\boldsymbol{\epsilon}_m^{1/2}\boldsymbol{\varrho}(\boldsymbol{\theta})\right\}$$
$$= \exp\left\{\frac{2}{N_0}\int_0^{T_o} v_m(s)dz(s) - \frac{1}{2N_0}\int_0^{T_o} |\tilde{v}_m(s)|^2 ds\right\} \qquad (3.23)$$

where $v_m(s) = \Re\left\{\tilde{v}_m(s)e^{j\omega_c s}\right\}$, $\tilde{v}_m(s) = \sum_{k=0}^{L-1} a_k e^{j\theta_k}\tilde{s}_m(s-\tau_k)$ and (3.23) is obtained by using (3.12) with $\alpha_k = a_k$ and (3.18b). From (C.1) in Lemma C.1, (3.23) is also given by

$$\lim_{\sigma \to 0} \Lambda_m\left(\dot{z}; T_o|\boldsymbol{\theta}\right) = \exp\left\{\frac{2}{N_0}\left[\int_0^{T_o} v_m(s)dz(s) - \frac{1}{2}\int_0^{T_o} v_m^2(s)ds\right]\right\} \qquad (3.24)$$

which is the classical estimator-correlator form of the likelihood ratio of a known channel corrupted by additive white Gaussian noise. $\int_0^{T_o} v_m(s)dz(s)$ corresponds to the correlation of the signal filtered by the known channel with the received signal or equivalently to a matched filtering operation. From (3.24) it is seen that when a_k and θ_k are known, there is no decorrelation since the matrices $\boldsymbol{X}_m$ or $\boldsymbol{\Gamma}_m$ are not present in the decision rule. It is known that the estimator-correlator form applies also for random channels in additive white Gaussian noise [173]. Such a form derived next will give further insight on the operations of the specular coherent optimum receiver.

3.2.3 Specular coherent estimator-correlator for an L-path Ricean channel

The mathematical background used in this section appears in Appendix A and the mathematical details appear in Appendix D.

Since $v_m(t)$ has a finite mean-square value on the observation interval $[0, T_o]$ and $\int_0^{T_o} E\left|v_m(t)\right| dt < \infty$ (see Section 3.1), from Appendix A, under each hypothesis (including H_0) the received signal is an Itô process [181] that can be written as

$$dz(t) = v_m(t)dt + dw(t) \quad 0 \le t \le T_o \qquad m = 0, \ldots, M \qquad (3.25)$$

with $v_0(t) = 0$. Furthermore, note that the detection problem $H_m : \dot{z}(t) = v_m(t) + \dot{w}(t)$ with $E\left[\dot{w}(t)\dot{w}(u)\right] = \frac{N_0}{2}\delta(t-u)$ is equivalent to $H_m : \frac{\dot{z}(t)}{\sqrt{\frac{N_0}{2}}} = \frac{v_m(t)}{\sqrt{\frac{N_0}{2}}} + \frac{\dot{w}(t)}{\sqrt{\frac{N_0}{2}}}$ with

$E\left[\frac{\dot{w}(t)}{\sqrt{\frac{N_0}{2}}}\frac{\dot{w}(u)}{\sqrt{\frac{N_0}{2}}}\right] = \delta(t-u)$. Therefore, from [21], the likelihood ratio $\Lambda_m\left(\dot{z};T_o|\boldsymbol{\theta}\right)$ can be expressed as

$$\Lambda_m\left(\dot{z};T_o|\boldsymbol{\theta}\right) = \exp\left\{\frac{2}{N_0}\left[\int_0^{T_o}\breve{v}_m\left(t|\boldsymbol{\theta}\right)dz(t) - \frac{1}{2}\int_0^{T_o}\breve{v}_m^2\left(t|\boldsymbol{\theta}\right)dt\right]\right\} \tag{3.26}$$

where $\breve{v}_m\left(t|\boldsymbol{\theta}\right) \triangleq E\left[v_m(t)|\dot{z}(s), 0\le s\le t, H_m, \boldsymbol{\theta}\right]$. In other words, $\breve{v}_m\left(t|\boldsymbol{\theta}\right)$ is the conditional mean (or equivalently the MMSE estimate) of $v_m(t)$ from the observations $\dot{z}(s)$ (given H_m) on the interval $[0,t]$ when $\boldsymbol{\theta}$ is known. This illustrates the interpretation of the L-path Ricean channel specular coherent optimum receiver as an estimator-correlator with a MMSE estimator. The mathematical derivation of the conditional mean is carried out in Appendix D.1. From (D.7), the conditional mean for an L-path Ricean channel with specular coherent detection is given by

$$\breve{v}_m\left(t|\boldsymbol{\theta}\right) = \int_0^t h_m(t,s)dy_m^{\mathrm{c}}(s) + \Re\left\{\left(\sum_{k=0}^{L-1}|\alpha_k|\,e^{j\theta_k'}\tilde{s}_m(t-\tau_k)\right)e^{j\omega_c t}\right\} \tag{3.27a}$$

$$= \Re\left\{\left(2\int_0^t \mathcal{H}_m^*(s,t,t)e^{-j\omega_c s}dy_m^{\mathrm{c}}(s) + \sum_{k=0}^{L-1}|\alpha_k|\,e^{j\theta_k'}\tilde{s}_m(t-\tau_k)\right)e^{j\omega_c t}\right\} \tag{3.27b}$$

where $h_m(t,s) = \Re\left\{2\mathcal{H}_m^*(s,t,t)e^{j\omega_c(t-s)}\right\}$ is the unique square integrable solution of the Wiener Hopf equation

$$h_m(t,s) + \frac{2}{N_0}\int_0^t h_m(t,\tau)K_m(\tau,s)d\tau = \frac{2}{N_0}K_m(t,s) \qquad 0\le s\le t<\infty \tag{3.28}$$

and $y_m^{\mathrm{c}}(s)$, the unknown part of the received signal, is given by[2]

$$dy_m^{\mathrm{c}}(s) = dz(s) - \Re\left\{\sum_{k=0}^{L-1}|\alpha_k|\,e^{j\theta_k'}\tilde{s}_m(s-\tau_k)e^{j\omega_c s}\right\}ds \tag{3.29}$$

where $\theta_k' = \theta_k + \arg\left[\alpha_k\right]$. It is seen from (3.27a) that the MMSE signal estimate for a multipath fading channel with known Ricean specular component is obtained by filtering the unknown part of the received signal by a linear time-varying filter $h_m(t,s)$.

[2]The superscript c is not an exponent.

From (3.28), since $K_m(s,u)$ is a finite dimensional kernel (3.5-3.6), $h_m(t,s)$ can be expressed in terms of the eigenfunctions and eigenvalues of $K_m(s,u)$ over an arbitrary observation interval $[0,t]$. However, since over $[0,t]$ the time-shifted signals $\tilde{s}_m(s-\tau_k)$ are not necessarily linearly independent (see Appendix B.1), it is not possible to find closed-form solutions for these eigenfunctions and eigenvalues valid for arbitrary waveforms. But such closed-form solutions can be obtained for the special case of time-limited waveforms yielding additional insight on the physical interpretation of the MMSE estimate. The M possible transmitted signals $\{\tilde{s}_m(s)\}_{m=1,\ldots,M}$ are assumed to be time-limited to $[0,T]$ for the remainder of this section (Section 3.2.3).

Eigenvalues and eigenfunctions of $K_m(s,u)$ over an arbitrary observation interval $[0,t], t > T'_m + \tau_0$ assuming that $\tilde{s}_m(s)$ is time-limited

Let us assume that the multipath delays τ_k are ordered as follows $0 \leq \tau_0 < \tau_1 < \ldots < \tau_{L-1}$. Following (3.3-3.4) let T'_m and T''_m be defined as

$$T'_m = \sup_v \left\{ v \in I\!R, \quad \int_{-\infty}^{v} |\tilde{s}_m(s)|^2 \, ds = 0 \right\} \tag{3.30}$$

$$T''_m = \inf_v \left\{ v \in I\!R, \quad \int_{-\infty}^{v} |\tilde{s}_m(s)|^2 \, ds = \int_{-\infty}^{\infty} |\tilde{s}_m(s)|^2 \, ds \right\} \tag{3.31}$$

Recall that in Section 3.2.1 (and Appendix B.2), the eigenfunctions $\phi_{lm}(s)$ and eigenvalues λ_{lm} of the covariance function $\mathcal{K}_m(s,u)$ of the complex signal process $\tilde{v}_m(s) = \sum_{k=0}^{L-1} a_k e^{j\theta_k} \tilde{s}_m(s-\tau_k)$ are derived under the L-order linear independency condition (i.e. the time-shifted signals $\tilde{s}_m(s-\tau_0), \tilde{s}_m(s-\tau_1), \ldots, \tilde{s}_m(s-\tau_{L-1})$ are linearly independent over $[0,T_o]$). This assumption ensures that $\mathcal{K}_m(s,u)$ has L eigenfunctions. However, as seen in Appendix B.1, over an arbitrary observation interval $[0,t]$, the signals $\tilde{s}_m(s-\tau_0), \tilde{s}_m(s-\tau_1), \ldots, \tilde{s}_m(s-\tau_{L-1})$ are not necessarily linearly independent and actually the number of linear independent time-shifted signals depends on t. This is to be expected since as the observation interval is decreased, some time-shifted signals have no contribution on the observation interval (i.e. are identically zero on $[0,t]$), thus they cannot be part of a linear independent set.

Over $[0,t]$, the covariance function of the complex signal process $\tilde{v}_m(s)$, given by

$\mathcal{K}_m(s,u) = \sum_{k=0}^{L-1} 2\sigma_k^2 \tilde{s}_m(s-\tau_k)\tilde{s}_m^*(u-\tau_k)$, reduces to[3]

$$\mathcal{K}_m^{i_t}(s,u) = \sum_{k=0}^{i_t-1} 2\sigma_k^2 \tilde{s}_m(s-\tau_k)\tilde{s}_m^*(u-\tau_k) \qquad 0 \le s,u \le t \quad T_m' + \tau_0 < t < \infty \quad (3.32)$$

where i_t[4], defined in (B.3) of Appendix B.1.2 with T' replaced by T_m' given by (3.30), is the number of non-zero multipath time-shifted signals in $[0,t]$. Similarly, over $[0,t]$ the received signal (3.1) reduces to

$$\dot{z}(s) = \Re\left\{\left[\sum_{k=0}^{i_t-1} a_k e^{j\theta_k}\tilde{s}_m(s-\tau_k)\right] e^{j\omega_c s}\right\} + \dot{w}(s) \quad 0 \le s \le t \quad m = 1,2,...,M \quad (3.33)$$

Furthermore, from Theorem B.2 the signals $\tilde{s}_m(s-\tau_0)$, $\tilde{s}_m(s-\tau_1), \ldots, \tilde{s}_m(s-\tau_{i_t-1})$ are linearly independent on $[0,t]$. Thus comparing (3.33) with (3.1) shows that for time-limited transmitted signals and an arbitrary observation interval $[0,t]$, $t > T_m' + \tau_0$, an L-path channel model (3.1) that satisfies the L-order linear independency condition can be reduced to an equivalent i_t-path channel model (3.33) that satisfies the i_t-order linear independency condition. Therefore, it is seen that the methods used in Appendix B.2 and Appendix B.3 to derive the eigenfunctions, eigenvalues and likelihood ratios can be also used in this section except that the number of signals is i_t instead of L where $1 \le i_t \le L$. In particular, modifying results from Section 3.2.1 (or Appendix B.2), $\forall\, t > T_m' + \tau_0$, over $[0,t]$, the covariance function $\mathcal{K}_m(s,u) \triangleq \mathcal{K}_m^{i_t}(s,u)$ has i_t eigenvalues, $\lambda_{lm}^{i_t}(t)$ which are the eigenvalues of the $i_t \times i_t$ matrix $\tilde{E}_m \boldsymbol{\epsilon}_{i_t m}(t) \boldsymbol{C}_{i_t} \boldsymbol{\Gamma}_{i_t m}^*(t)$, and has i_t eigenfunctions $\phi_{lm}^{i_t}(s,t)$ given by[5]

$$\phi_{lm}^{i_t}(s,t) = \frac{1}{\sqrt{\tilde{E}_m}} \sum_{k=0}^{i_t-1} \frac{x_{lk}^{i_t m}(t)}{\sqrt{\epsilon_{km}(t)}} \tilde{s}_m(s-\tau_k) \quad 0 \le s \le t \qquad l = 0,\ldots,i_t-1 \quad (3.34)$$

[3]The superscript i_t is not an exponent: $\mathcal{K}_m^{i_t}$ is just a designation for the function $\mathcal{K}_m^{i_t}(s,u)$ whose value at (s,u) is $\sum_{k=0}^{i_t-1} 2\sigma_k^2 \tilde{s}_m(s-\tau_k)\tilde{s}_m^*(u-\tau_k)$.

[4]Generally i_t depends on H_m through T_m', however, for most modulation schemes T_m' is independent of H_m. Thus to simplify notation the index m will be omitted in i_t.

[5]The superscript i_t in $\lambda_{lm}^{i_t}(t)$ and $\phi_{lm}^{i_t}(s,t)$ is not an exponent.

where $x_{lk}^{i_t m}(t) = [\boldsymbol{X}_{i_t m}(t)]_{lk}$, $\boldsymbol{X}_{i_t m}(t)$ is an $i_t \times i_t$ matrix that satisfies the equations:

$$\boldsymbol{X}_{i_t m}^*(t)\boldsymbol{\Gamma}_{i_t m}^*(t)\boldsymbol{X}_{i_t m}^T(t) = \boldsymbol{I}_{i_t} \tag{3.35a}$$

$$\boldsymbol{\epsilon}_{i_t m}(t)\boldsymbol{C}_{i_t}\boldsymbol{\Gamma}_{i_t m}^*(t)\boldsymbol{X}_{i_t m}^T(t) = \boldsymbol{X}_{i_t m}^T(t)\boldsymbol{D}_{i_t m}(t) \tag{3.35b}$$

$\boldsymbol{I}_{i_t}$ is the $i_t \times i_t$ identity matrix, $\boldsymbol{D}_{i_t m}(t)$ denotes the $i_t \times i_t$ diagonal matrix with $[\boldsymbol{D}_{i_t m}(t)]_{kk} = \lambda_{km}^{i_t}(t)/\tilde{E}_m$, $\boldsymbol{\epsilon}_{i_t m}(t)$ is the $i_t \times i_t$ diagonal matrix with $[\boldsymbol{\epsilon}_{i_t m}(t)]_{kk} = \epsilon_{km}(t) = \frac{1}{\tilde{E}_m}\int_0^t |\tilde{s}_m(s-\tau_k)|^2\, ds$, $\boldsymbol{C}_{i_t}$ is the $i_t \times i_t$ diagonal matrix with $[\boldsymbol{C}_{i_t}]_{kk} = 2\sigma_k^2$ and $\boldsymbol{\Gamma}_{i_t m}(t)$ is the $i_t \times i_t$ correlation matrix of the signal under H_m when the observation interval is $[0,t]$ with kj^{th} entry equal to $\rho_{kj}^m(t)$, i.e.

$$[\boldsymbol{\Gamma}_{i_t m}(t)]_{kj} = \frac{1}{\tilde{E}_m\sqrt{\epsilon_{km}(t)\epsilon_{jm}(t)}}\int_0^t \tilde{s}_m(s-\tau_k)\tilde{s}_m^*(s-\tau_j)ds \quad k,j = 0,\ldots,i_t-1 \tag{3.36}$$

Since the integer function i_t is a staircase function (see Appendix B.1.2), the eigenvalues $\{\lambda_{lm}^{i_t}(t)\}_{l=0,\ldots,i_t-1}$ and the functions $\{x_{lk}^{i_t m}(t)\}_{l,k=0,\ldots,i_t-1}$ are defined on $(T_m' + \tau_0, +\infty)$. Grouping the results together, functions $\{\lambda_{lm}(t)\}_{l=0,\ldots,L-1}$ and $\left\{\sqrt{\frac{\lambda_{lm}(t)}{\epsilon_{km}(t)}}x_{lk}^m(t)\right\}_{l,k=0,\ldots,L-1}$ can be defined on $[0,+\infty)$ as follows:

$$\lambda_{lm}(t) = \begin{cases} \lambda_{lm}^{i_t}(t) & T_m' + \tau_0 < t < \infty \quad l = 0,\ldots,i_t-1, \\ 0 & \text{else.} \end{cases} \tag{3.37}$$

$$\sqrt{\frac{\lambda_{lm}(t)}{\epsilon_{km}(t)}}x_{lk}^m(t) = \begin{cases} \sqrt{\frac{\lambda_{lm}^{i_t}(t)}{\epsilon_{km}(t)}}x_{lk}^{i_t m}(t) & T_m' + \tau_0 < t < \infty \quad l,k = 0,\ldots,i_t-1, \\ 0 & \text{else.} \end{cases} \tag{3.38}$$

where $\lambda_{lm}^{i_t m}(t) = \tilde{E}_m[\boldsymbol{D}_{i_t m}(t)]_{ll}$, $x_{lk}^{i_t m}(t) = [\boldsymbol{X}_{i_t m}(t)]_{lk}$ and $\{\boldsymbol{D}_{i_t m}(t), \boldsymbol{X}_{i_t m}(t)\}$ satisfy (3.35).

Similarly, the eigenfunctions $\{\phi_{lm}^{i_t}(s,t)\}_{l=0,\ldots,i_t-1}$ are functions of (s,t) defined on $[0,t] \times (T_m' + \tau_0, +\infty)$. Grouping the results together, functions

$\left\{\sqrt{\lambda_{lm}(t)}\phi_{lm}(s,t)\right\}_{l=0,\ldots,L-1}$ can be defined on $[0,+\infty)\times[0,+\infty)$ as follows:

$$\sqrt{\lambda_{lm}(t)}\phi_{lm}(s,t)=\begin{cases}\sqrt{\lambda_{lm}^{i_t}(t)}\phi_{lm}^{i_t}(s,t) & \begin{matrix}0\le s\le t\\ T_m'+\tau_0<t<\infty\end{matrix} \quad l=0,\ldots,i_t-1,\\ 0 & \text{else.}\end{cases} \tag{3.39a}$$

$$=\frac{1}{\sqrt{\tilde{E}_m}}\sum_{k=0}^{L-1}\sqrt{\frac{\lambda_{lm}(t)}{\epsilon_{km}(t)}}x_{lk}^m(t)\tilde{s}_m(s-\tau_k) \quad \begin{matrix}0\le s\le t\\ 0\le t<\infty\end{matrix} \tag{3.39b}$$

where $\phi_{lm}^{i_t}(s,t)$ and $\sqrt{\frac{\lambda_{lm}(t)}{\epsilon_{km}(t)}}x_{lk}^m(t)$ are given by (3.34) and (3.38). Using the inverse linear transformation of (3.34)[6], $\tilde{s}_m(s-\tau_k)$ can be expressed in terms of $\phi_{lm}(s,t)$ as

$$\tilde{s}_m(s-\tau_k)=\begin{cases}\frac{1}{2\sigma_k^2\sqrt{\epsilon_{km}(t)\tilde{E}_m}}\sum_{l=0}^{i_t-1}\lambda_{lm}^{i_t}(t)\left[x_{lk}^{i_tm}(t)\right]^*\phi_{lm}^{i_t}(s,t) & \begin{matrix}0\le s\le t\\ T_m'+\tau_0<t<\infty\end{matrix}\\ 0 & \text{else.}\end{cases} \tag{3.40a}$$

$$=\frac{1}{2\sigma_k^2\sqrt{\epsilon_{km}(t)\tilde{E}_m}}\sum_{l=0}^{L-1}\lambda_{lm}(t)\left[x_{lk}^m(t)\right]^*\phi_{lm}(s,t) \quad \begin{matrix}0\le s\le t\\ 0\le t<\infty\end{matrix} \tag{3.40b}$$

Furthermore it is shown in Appendix C (C.14-C.18) that the unique solution of (3.28), $h_m(t,s)$, can be written $h_m(t,s)=H_m(s,t,t)=\Re\left\{2\mathcal{H}_m^*(s,t,t)e^{j\omega_c(t-s)}\right\}$ where the kernels $\mathcal{H}_m(\tau,s,t)=\mathcal{H}_m^*(s,\tau,t)$ and $H_m(\tau,s,t)=H_m(s,\tau,t)$ are given by

$$\mathcal{H}_m(\tau,s,t)\triangleq\begin{cases}\sum_{l=0}^{L-1}\frac{\frac{\lambda_{lm}(t)}{2N_0}}{1+\frac{\lambda_{lm}(t)}{2N_0}}\phi_{lm}(\tau,t)\phi_{lm}^*(s,t) & \begin{matrix}0\le\tau,s\le t\\ 0\le t<\infty\end{matrix}\\ 0 & \text{else.}\end{cases} \tag{3.41}$$

$$H_m(\tau,s,t)\triangleq\begin{cases}\sum_{l=0}^{2L-1}\frac{\frac{2}{N_0}\kappa_{lm}(t)}{1+\frac{2}{N_0}\kappa_{lm}(t)}\Upsilon_{lm}(\tau,t)\Upsilon_{lm}(s,t) & \begin{matrix}0\le\tau,s\le t\\ 0\le t<\infty\end{matrix}\\ 0 & \text{else.}\end{cases} \tag{3.42}$$

[6]The inverse linear transformation of (3.34) involves the matrix $\boldsymbol{X}_{i_tm}^{-1}(t)$. It can be shown using (3.35) that $\boldsymbol{X}_{i_tm}^{-1}(t)=\left(\boldsymbol{\epsilon}_{i_tm}(t)\boldsymbol{C}_{i_t}\right)^{-1}\boldsymbol{X}_{i_tm}^{\dagger}(t)\boldsymbol{D}_{i_tm}(t)$.

and for $l = 0, \ldots, L-1$

$$\kappa_{lm}(t) = \frac{\lambda_{lm}(t)}{4} \qquad \kappa_{l+Lm}(t) = \frac{\lambda_{lm}(t)}{4} \tag{3.43}$$

$$\begin{aligned} \sqrt{\kappa_{lm}(t)}\Upsilon_{lm}(s,t) &= \Re\left\{\sqrt{\frac{\lambda_{lm}(t)}{2}}\phi_{lm}(s,t)e^{j\omega_c s}\right\} \\ \sqrt{\kappa_{l+Lm}(t)}\Upsilon_{l+Lm}(s,t) &= \Im\left\{\sqrt{\frac{\lambda_{lm}(t)}{2}}\phi_{lm}(s,t)e^{j\omega_c s}\right\} \end{aligned} \tag{3.44}$$

where $\lambda_{lm}(t)$ and $\sqrt{\lambda_{lm}(t)}\phi_{lm}(s,t)$ are given by (3.37) and (3.39).

Next section will focus on giving physical interpretations of the expression for the conditional mean estimator $\breve{v}_m(t|\boldsymbol{\theta})$.

Interpretation of the expression for the conditional mean estimator $\breve{v}_m(t|\boldsymbol{\theta})$

In order to understand the expression of $\breve{v}_m(t|\boldsymbol{\theta})$, let us first investigate the signal that it estimates, that is the noiseless received signal, $v_m(t)$. From (3.1), the noiseless received signal is given by

$$\begin{aligned} v_m(t) &= \Re\left\{\left(\sum_{k=0}^{L-1} a_k e^{j\theta_k}\tilde{s}_m(t-\tau_k)\right)e^{j\omega_c t}\right\} \\ &= \Re\left\{\left(\sum_{k=0}^{L-1}(a_k-\alpha_k)e^{j\theta_k}\tilde{s}_m(t-\tau_k) + \sum_{k=0}^{L-1}|\alpha_k|e^{j\theta'_k}\tilde{s}_m(t-\tau_k)\right)e^{j\omega_c t}\right\} \\ &= \Re\left\{\left(\sum_{k=0}^{L-1} a'_k\tilde{s}_m(t-\tau_k) + \sum_{k=0}^{L-1}|\alpha_k|e^{j\theta'_k}\tilde{s}_m(t-\tau_k)\right)e^{j\omega_c t}\right\} \end{aligned} \tag{3.45}$$

where $a'_k \triangleq (a_k - \alpha_k)\, e^{j\theta_k}$ and $\theta'_k = \theta_k + \arg[\alpha_k]$. Since $a_k - \alpha_k$, $_{k=0,\ldots,L-1}$ are zero mean circularly complex Gaussian variables, a'_k and $a_k - \alpha_k$ are identically distributed for $_{k=0,\ldots,L-1}$. From (3.45), it is seen that the signal $\tilde{v}_m(t) = \sum_{k=0}^{L-1} a'_k\tilde{s}_m(t-\tau_k) + \sum_{k=0}^{L-1}|\alpha_k|e^{j\theta'_k}\tilde{s}_m(t-\tau_k)$ is to be estimated. Since the θ'_k's are known, only $\sum_{k=0}^{L-1} a'_k\tilde{s}_m(t-\tau_k)$ has to be estimated. From (3.41)

$$2\int_0^t \mathcal{H}^*_m(s,t,t)e^{-j\omega_c s}dy^c_m(s) = 2\int_0^t \sum_{l=0}^{L-1}\frac{\frac{\lambda_{lm}(t)}{2N_0}}{1+\frac{\lambda_{lm}(t)}{2N_0}}\phi^*_{lm}(s,t)\phi_{lm}(t,t)e^{-j\omega_c s}dy^c_m(s) \tag{3.46}$$

Replacing $\sqrt{\lambda_{lm}(t)}\phi_{lm}(t,t)$ with (3.39b) yields

$$2\int_0^t \mathcal{H}_m^*(s,t,t)e^{-j\omega_c s}dy_m^c(s) = \sum_{k=0}^{L-1} \widehat{a_k'(t|\boldsymbol{\theta})}\,\tilde{s}_m(t-\tau_k) \tag{3.47}$$

where $\widehat{a_k'(t|\boldsymbol{\theta})}$, estimates of a_k' with known $\boldsymbol{\theta}$ based on the observation interval $[0,t]$, are defined as

$$\widehat{a_k'(t|\boldsymbol{\theta})} = \frac{2}{\sqrt{\epsilon_{km}(t)\tilde{E}_m}} \sum_{l=0}^{L-1} \frac{\frac{\lambda_{lm}(t)}{2N_0}}{1+\frac{\lambda_{lm}(t)}{2N_0}} x_{lk}^m(t) \int_0^t \phi_{lm}^*(s,t)e^{-j\omega_c s}dy_m^c(s) \tag{3.48a}$$

$$= \frac{2\sigma_k^2}{N_0}\int_0^t \frac{l_{km}^*(s,t)}{|\alpha_k|}e^{-j\omega_c s}dy_m^c(s) \tag{3.48b}$$

where $y_m^c(s)$ is given by (3.29), for $k=0,\ldots,L-1$, $l_{km}(s,t)$ is given by

$$l_{km}(s,t) = \frac{N_0|\alpha_k|}{\sigma_k^2\sqrt{\epsilon_{km}(t)\tilde{E}_m}} \sum_{l=0}^{L-1} \frac{\frac{\lambda_{lm}(t)}{2N_0}}{1+\frac{\lambda_{lm}(t)}{2N_0}} \left[x_{lk}^m(t)\right]^* \phi_{lm}(s,t) \quad \begin{matrix} 0\le s\le t \\ 0\le t<\infty \end{matrix} \tag{3.49}$$

and $\lambda_{lm}(t)$, $\sqrt{\frac{\lambda_{lm}(t)}{\epsilon_{km}(t)}}x_{lk}^m(t)$ and $\sqrt{\lambda_{lm}(t)}\phi_{lm}(s,t)$ are given by (3.37), (3.38) and (3.39). Substituting (3.47) into (3.27b) yields

$$\check{v}_m(t|\boldsymbol{\theta}) = \Re\left\{\left(\sum_{k=0}^{L-1} \widehat{a_k'(t|\boldsymbol{\theta})}\,\tilde{s}_m(t-\tau_k) + \sum_{k=0}^{L-1} |\alpha_k|\,e^{j\theta_k'}\tilde{s}_m(t-\tau_k)\right)e^{j\omega_c t}\right\} \tag{3.50}$$

where $\widehat{a_k'(t|\boldsymbol{\theta})}$ are given by (3.48). Comparing (3.50) and (3.45) shows that the MMSE estimate of a random amplitude multipath signal has the same "multipath" form with the amplitudes replaced by estimates. From (3.48b) it is seen that the amplitude estimates are obtained by filtering the unknown part of the received signal (3.29) using the filter $\frac{2\sigma_k^2}{N_0}\frac{l_{km}^*(s,t)}{|\alpha_k|}e^{-j\omega_c s}$. This filter takes into account both the multipath unresolvability and fading as seen in the following.

Similarly to (3.19) except that an observation interval $[0,t]$ is considered and the phases θ_k have been included in a_k', by substituting (3.40b) into (3.45), the noiseless

received signal can be rewritten as

$$v_m(t) = \Re\left\{\left(\sum_{l=0}^{L-1} a''_{lm}(t)\sqrt{\epsilon_{lm}(t)\tilde{E}_m}\phi_{lm}(t,t) + \sum_{l=0}^{L-1}|\alpha_l|\, e^{j\theta'_l}\tilde{s}_m(t-\tau_l)\right) e^{j\omega_c t}\right\} \quad (3.51)$$

with zero mean path gains of the equivalent decorrelated (resolved) channel defined as

$$a''_{lm}(t) = \sum_{k=0}^{L-1} \frac{\lambda_{lm}(t)\,[x^m_{lk}(t)]^*}{2\sigma_k^2\sqrt{\epsilon_{km}(t)\epsilon_{lm}(t)\tilde{E}_m}} a'_k \qquad l = 0, \ldots, L-1 \quad (3.52)$$

Furthermore, substituting (3.39b) into (3.51) and comparing with (3.45) yields

$$a'_k = \sum_{l=0}^{L-1}\sqrt{\frac{\epsilon_{lm}(t)}{\epsilon_{km}(t)}}\, x^m_{lk}(t)\, a''_{lm}(t) \quad (3.53)$$

which constitutes the inverse linear transformation of (3.52). Since $\boldsymbol{X}_m^{-1}(T_o) = [\boldsymbol{\epsilon}_m(T_o)\boldsymbol{C}]^{-1}\,\boldsymbol{X}_m^{\dagger}(T_o)\boldsymbol{D}_m(T_o)$, from (3.52) $\breve{a}_{lm}(\boldsymbol{\theta})$ defined in Section 3.2.2, satisfies $\breve{a}_{lm}(\boldsymbol{\theta}) - E\left[\breve{a}_{lm}(\boldsymbol{\theta})|\boldsymbol{\theta}\right] = a''_{lm}(T_o)$ where $[0, T_o]$ is an interval such that the L-order linear independency condition holds. Note that the random processes $\{a''_{lm}(t)\}_{l=0,\ldots,L-1}$ are correlated, but similarly to $\{\breve{a}_{lm}(\boldsymbol{\theta})\}_{l=0,\ldots,L-1}$, the random variables $\{a''_{lm}(t)\}_{l=0,\ldots,L-1}$ obtained when t is fixed are uncorrelated. Substituting (3.46) into (3.27b), the conditional mean $\breve{v}_m(t|\boldsymbol{\theta})$ can be rewritten as

$$\breve{v}_m(t|\boldsymbol{\theta}) = \Re\left\{\left(\sum_{l=0}^{L-1}\widehat{a''_{lm}(t|\boldsymbol{\theta})}\sqrt{\epsilon_{lm}(t)\tilde{E}_m}\phi_{lm}(t,t) + \sum_{l=0}^{L-1}|\alpha_l|\, e^{j\theta'_l}\tilde{s}_m(t-\tau_l)\right) e^{j\omega_c t}\right\}$$

where

$$\widehat{a''_{lm}(t|\boldsymbol{\theta})} = \frac{2}{\sqrt{\epsilon_{lm}(t)\tilde{E}_m}}\frac{\frac{\lambda_{lm}(t)}{2N_0}}{1+\frac{\lambda_{lm}(t)}{2N_0}}\int_0^t \phi^*_{lm}(s,t)e^{-j\omega_c s}dy^c_m(s) \quad (3.54)$$

From (3.54) it is seen that $\widehat{a''_{lm}(t|\boldsymbol{\theta})}$, the gain estimate of $a''_{lm}(t)$, employs only the information related to the l^{th} path of the decorrelated channel. Furthermore although the random processes $\{\widehat{a''_{lm}(t|\boldsymbol{\theta})}\}_{l=0,\ldots,L-1}$ are correlated, the corresponding random

variables obtained by fixing t are uncorrelated. Comparing (3.48a) with (3.54) yields

$$\widehat{a_k'(t|\boldsymbol{\theta})} = \sum_{l=0}^{L-1} \frac{\sqrt{\epsilon_{lm}(t)}}{\sqrt{\epsilon_{km}(t)}} x_{lk}^m(t)\, \widehat{a_{lm}''(t|\boldsymbol{\theta})} \tag{3.55}$$

consistent with (3.53). Note that $\forall l = i_t, \ldots, L-1 \quad \widehat{a_{lm}''(t|\boldsymbol{\theta})} = 0$. Thus the estimate of the k^{th} zero mean gain of the unresolved multipath channel, $\widehat{a_k'(t|\boldsymbol{\theta})}$ is obtained by passing the zero mean path gain estimates of the decorrelated (resolved) multipath channel, $\left\{ \widehat{a_{lm}''(t|\boldsymbol{\theta})} \right\}_{l=0,\ldots,i_t-1}$ through the matrix $\boldsymbol{\epsilon}_{i_t m}^{1/2}(t)\boldsymbol{X}_{i_t m}(t)\boldsymbol{\epsilon}_{i_t m}^{-1/2}(t) = \boldsymbol{\epsilon}_{i_t m}^{1/2}(t)\boldsymbol{C}_{i_t}\left(\boldsymbol{X}_{i_t m}^*(t)\right)^{-1}\boldsymbol{D}_{i_t m}^{-1}(t)\boldsymbol{\epsilon}_{i_t m}^{1/2}(t)$, yielding correlated random processes $\left\{ \widehat{a_k'(t|\boldsymbol{\theta})} \right\}_{k=0,\ldots,L-1}$. Unlike $\{a_k'\}_{k=0,\ldots,L-1}$, $\{a_{lm}''(t)\}_{l=0,\ldots,L-1}$ and $\left\{ \widehat{a_{lm}''(t|\boldsymbol{\theta})} \right\}_{l=0,\ldots,L-1}$ (with t fixed), the random variables $\left\{ \widehat{a_k'(t|\boldsymbol{\theta})} \right\}_{k=0,\ldots,L-1}$, obtained by fixing t, are correlated. Since $a_k' = (a_k - \alpha_k)\, e^{j\theta_k}$ are uncorrelated random variables with $E\left[a_k' a_k'^*/2\right] = \sigma_k^2$, from (3.52) the variance of $a_{lm}''(t)$ is given by

$$E\left[\left|a_{lm}''(t)\right|^2\right] = \sum_{k=0}^{L-1} \frac{\lambda_{lm}^2(t)\left|x_{lk}^m(t)\right|^2}{2\sigma_k^2 \epsilon_{km}(t)\epsilon_{lm}(t)\tilde{E}_m^2} = \frac{\lambda_{lm}(t)}{\epsilon_{lm}(t)\tilde{E}_m} \tag{3.56}$$

where the last step is obtained using (C.24). For an $l \in \{0, \ldots, i_t - 1\}$, if the average energy of the complex signal $a_{lm}''(t)\sqrt{\epsilon_{lm}(t)\tilde{E}_m}\phi_{lm}(s,t)$ over $[0,t]$ is much smaller than the noise power density, i.e.

$$E\left[\int_0^t \left|a_{lm}''(t)\sqrt{\epsilon_{lm}(t)\tilde{E}_m}\phi_{lm}(s,t)\right|^2 ds\right] \ll 2N_0$$

or equivalently using (3.56) and the orthonormality of $\left\{\phi_{jm}(s,t) = \phi_{jm}^{i_t}(s,t)\right\}_{j=0,\ldots,i_t-1}$ on $[0,t]$

$$\lambda_{lm}(t) \ll 2N_0$$

then from (3.54) $\widehat{a_{lm}''(t|\boldsymbol{\theta})} \approx 0 = E\left[a_{lm}''(t)\right]$. Since the noise level is high, observations are very likely to be unreliable thus the best estimate bases its estimation on a-priori knowledge (in this case the a-priori mean which is equal to 0 since $E\left[a_k'\right] = 0$), and it reduces the effect of this noisy component. If $\lambda_{lm}(t) \gg 2N_0$, then $\widehat{a_{lm}''(t|\boldsymbol{\theta})}$ is

based on the observations and from (3.54) is approximately

$$\widehat{a''_{lm}(t|\boldsymbol{\theta})} \approx \frac{2}{\sqrt{\epsilon_{lm}(t)\tilde{E}_m}} \int_0^t \phi^*_{lm}(s,t) e^{-j\omega_c s} dy^{\mathsf{c}}_m(s) = \frac{2\int_0^t \sqrt{\epsilon_{lm}(t)\tilde{E}_m}\phi^*_{lm}(s,t)e^{-j\omega_c s}dy^{\mathsf{c}}_m(s)}{\int_0^t \left|\sqrt{\epsilon_{lm}(t)\tilde{E}_m}\phi^*_{lm}(s,t)\right|^2 ds} \tag{3.57}$$

where the second equation in (3.57) valid for $l = 0, \ldots, i_t - 1$ is obtained using the orthonormality of $\left\{\phi_{jm}(s,t) = \phi^{i_t}_{jm}(s,t)\right\}_{j<i_t}$ on $[0,t]$. Hence from (3.57) it is seen that $\widehat{a''_{lm}(t|\boldsymbol{\theta})}$ is the correlation of the unknown part of the received signal with the signal $\sqrt{\epsilon_{lm}(t)\tilde{E}_m}\phi_{lm}(s,t)$ associated with the l^{th} path of the decorrelated channel, normalized by its energy $\left(\int_0^{T_o}\left|\sqrt{\epsilon_{lm}(t)\tilde{E}_m}\phi_{lm}(s,t)\right|^2 ds\right)$. Since $\{\phi_{jm}(s,t)\}_{j=0,\ldots,L-1}$ are "orthogonal" on $[0,t]$ (C.20), in the limit when no noise is present ($\dot{w}(s) = 0$), from (3.45), (3.52), (3.54) and (3.40b) under H_m $\widehat{a''_{lm}(t|\boldsymbol{\theta})} = a''_{lm}(t)$.

Let us study next the special case of resolved multipath over $[0,t]$.

Conditional mean when the multipath is resolved

From (2.15), the resolvability assumption is satisfied over $[0,t]$ if

$$\forall\, l \neq k \quad \int_0^t \tilde{s}_m(u-\tau_l)\tilde{s}^*_m(u-\tau_k)du = 0 \qquad m = 1, \ldots, M \tag{3.58a}$$

or equivalently if

$$\forall\, l \neq k \quad R_m(\tau_l - \tau_k, t-\tau_k) = 0 \quad \text{or} \quad R^*_m(\tau_k - \tau_l, t-\tau_l) = 0 \tag{3.58b}$$

where $R_m(\tau,t)$ is the partial autocorrelation function defined as

$$R_m(\tau,t) = \int_0^t \tilde{s}^*_m(u)\tilde{s}_m(u-\tau)du$$

assuming that $\tilde{s}_m(s) = 0, \forall\, s < 0$. Let us investigate conditions when (3.58b) holds. Let $T^+_R(t)$ and $T^-_R(t)$ denote respectively the "positive" and "negative" autocorrelation

time functions defined as

$$T_R^+(t) = \inf_\tau \{\tau \geq 0; R_m(\tau, t) = 0\}$$
$$T_R^-(t) = \sup_\tau \{\tau \leq 0; R_m(\tau, t) = R_m^*(-\tau, t-\tau) = 0\}$$

The autocorrelation time function is defined as $T_R(t) = 2\sup\left(T_R^+(t), |T_R^-(t)|\right)$ and $\forall |\tau| \geq \frac{T_R(t)}{2}$, $R_m(\tau, t) = 0$. Note that $T_R(t)$ can be infinity. From (3.58b) if $\forall l \neq k, |\tau_l - \tau_k| \geq \max\{T_R(t-\tau_l), T_R(t-\tau_k)\}$ the resolvability assumption is satisfied over $[0, t]$. When signals, time-limited to $[0, T]$, are considered, a simplified sufficient condition of path resolvability over $[0, t]$ can be obtained. By definitions of T_m' and T_m'' given respectively in (3.30) and (3.31)

$$0 \leq s \leq T_m' \quad \text{or} \quad T_m'' \leq s \leq T \qquad \tilde{s}_m(s) = 0$$

hence if $\forall l \neq k, |\tau_l - \tau_k| \geq T_m'' - T_m'$, the path resolvability assumption is satisfied on $[0, t]$.

Whenever (3.58) is satisfied, from (3.36), $\boldsymbol{\Gamma}_{i_t m}(t) = \boldsymbol{I}_{i_t}$, hence from (3.35), $\boldsymbol{D}_{i_t m}(t) = \boldsymbol{\epsilon}_{i_t m}(t)\boldsymbol{C}_{i_t}$ and $\boldsymbol{X}_{i_t m}(t) = \boldsymbol{I}_{i_t}$. Therefore from (3.37-3.38)

$$\lambda_{lm}(t) = \begin{cases} 2\sigma_l^2 \epsilon_{lm}(t) \tilde{E}_m & T_m' + \tau_0 < t < \infty \quad l = 0, \ldots, i_t - 1 \\ 0 & \text{else.} \end{cases} \tag{3.59}$$

$$\sqrt{\frac{\lambda_{lm}(t)}{\epsilon_{km}(t)}} x_{lk}^m(t) = \begin{cases} \sqrt{\frac{2\sigma_l^2 \epsilon_{lm}(t)\tilde{E}_m}{\epsilon_{km}(t)}} \delta_{lk} & T_m' + \tau_0 < t < \infty \quad l, k = 0, \ldots, i_t - 1 \\ 0 & \text{else.} \end{cases} \tag{3.60}$$

and from (3.39b)

$$\begin{aligned} \sqrt{\lambda_{lm}(t)}\phi_{lm}(s,t) &= \frac{1}{\sqrt{\tilde{E}_m}} \sum_{k=0}^{i_t-1} \sqrt{\frac{2\sigma_l^2 \epsilon_{lm}(t)\tilde{E}_m}{\epsilon_{km}(t)}} \delta_{lk} \tilde{s}_m(s - \tau_k) \left[\prod_{j=i_t}^{L-1} (1 - \delta_{lj})\right] \\ &= \sqrt{2\sigma_l^2} \tilde{s}_m(s - \tau_l) \end{aligned} \tag{3.61}$$

since $\forall 0 \leq s \leq t, \forall l \geq i_t \quad \tilde{s}_m(s-\tau_l) = 0$. Substituting (3.59-3.61) into (3.48a) yields

$$\widehat{a_k'(t|\boldsymbol{\theta})} = \frac{2}{\sqrt{\epsilon_{km}(t)\tilde{E}_m}} \frac{2\sigma_k^2\epsilon_{km}(t)\gamma_m}{1+2\sigma_k^2\epsilon_{km}(t)\gamma_m} \int_0^t \frac{\tilde{s}_m^*(s-\tau_k)}{\sqrt{\epsilon_{km}(t)\tilde{E}_m}} e^{-j\omega_c s} dy_m^c(s)$$

hence whenever the multipath is resolved over $[0,t]$, there is no need for decorrelation, the estimate of the k^{th} zero mean multipath gain $a_k'(t)$ employs only the information related to that k^{th} multipath gain and the effect of fading is taken into account similarly to the unresolved case (3.54) with the signal $\tilde{s}_m(s-\tau_k)/\sqrt{\epsilon_{km}(t)\tilde{E}_m}$ replacing $\phi_{km}(s,t)$.

The next section will consider non-coherent optimal detection that does not assume knowledge of the Ricean specular component phases.

3.3 Non-coherent optimal decision rule for an L-path Ricean channel

3.3.1 L-path Ricean non-coherent optimum receiver structure (OPT)

Similarly to Section 3.2.1, let us consider an observation $[0,T_o]$ such that the L-order linear independency condition is satisfied. Such observation interval is necessarily long or intermediate. In this section the phases θ_k are assumed uniformly distributed between $-\pi$ and π modeling a receiver that does not have any reference phase information (non-coherent receiver). The non-coherent optimum receiver is denoted OPT in this thesis. From Section 3.2.1 the conditional likelihood ratio with $\boldsymbol{\theta}$ held fixed associated with the OPT scheme is given by (3.10). The likelihood ratio $\Lambda_m(\dot{z};T_o)$ is obtained by integrating successively (3.10) over all components of the vector $\boldsymbol{\theta}$ between $-\pi$ and π. To do the integration, terms inside (3.10) that are independent of $\boldsymbol{\theta}$ are grouped together and after simplification the conditional likelihood ratio can also be written as (see (B.31)).

$$\Lambda_m(\dot{z};T_o|\boldsymbol{\theta}) = J_m f_m(\boldsymbol{\theta}) \tag{3.62}$$

where by substituting (B.28) into (B.32) and using (3.8) J_m is given by

$$J_m = \left[\det(\boldsymbol{I} + \gamma_m \boldsymbol{D}_m)\right]^{-1} \exp\left\{\gamma_m \boldsymbol{r}_m^\dagger \boldsymbol{Q}_m \boldsymbol{r}_m - \boldsymbol{\alpha}^\dagger \left\{(\boldsymbol{X}_m^*)^{-1} \boldsymbol{Q}_m \boldsymbol{X}_m^*\right\}_d \boldsymbol{C}^{-1} \boldsymbol{\alpha}\right\} \tag{3.63a}$$

or equivalently using (3.8), (3.16b) and (3.18a)

$$\begin{aligned} J_m = {} & \left[\det(\boldsymbol{I} + \gamma_m \boldsymbol{\epsilon}_m \boldsymbol{C} \boldsymbol{\Gamma}_m^*)\right]^{-1} \\ & \cdot \exp\left\{\gamma_m^2 \boldsymbol{u}_m^\dagger \left[(\boldsymbol{\epsilon}_m \boldsymbol{C})^{-1} + \gamma_m \boldsymbol{\Gamma}_m^*\right]^{-1} \boldsymbol{u}_m - \boldsymbol{\alpha}^\dagger \left\{(\boldsymbol{X}_m^*)^{-1} \boldsymbol{Q}_m \boldsymbol{X}_m^*\right\}_d \boldsymbol{C}^{-1} \boldsymbol{\alpha}\right\} \end{aligned} \tag{3.63b}$$

and from (B.34) $f_m(\boldsymbol{\theta})$ is given by

$$f_m(\boldsymbol{\theta}) = \exp\left\{\sum_{k=0}^{L-1} \frac{|\alpha_k|}{\sigma_k^2 \sqrt{\epsilon_{km}}} |b_{km}(\boldsymbol{\theta}_{k-1})| \cos\left(\theta_k - \varphi_{km}(\boldsymbol{\theta}_{k-1})\right)\right\} \tag{3.64}$$

$$b_{km}(\boldsymbol{\theta}_{k-1}) = \left[\boldsymbol{X}_m^T \boldsymbol{Q}_m \boldsymbol{r}_m - \left\{\boldsymbol{X}_m^T \boldsymbol{Q}_m \left(\boldsymbol{X}_m^T\right)^{-1} \boldsymbol{\epsilon}_m^{1/2}\right\}_l \boldsymbol{\varrho}(\boldsymbol{\theta})\right]_k \quad b_{0m} = \left[\boldsymbol{X}_m^T \boldsymbol{Q}_m \boldsymbol{r}_m\right]_0 \tag{3.65}$$

$$\varphi_{km}(\boldsymbol{\theta}_{k-1}) = \arg\left[b_{km}(\boldsymbol{\theta}_{k-1})\right] - \arg[\alpha_k] \quad \varphi_{0m} = \arg\left[b_{0m}\right] - \arg[\alpha_0] \tag{3.66}$$

where γ_m is given by (3.11), $\boldsymbol{D}_m$ and $\boldsymbol{X}_m$ are given by (3.8), $\boldsymbol{Q}_m$ is given by (3.16), $\boldsymbol{\alpha}$ and $\boldsymbol{\varrho}(\boldsymbol{\theta})$ are respectively given by (3.13) and (3.12), $\boldsymbol{r}_m$ and $\boldsymbol{u}_m$ are respectively given by (3.14) and (3.18a). Integrating successively (3.62) over all components of the vector $\boldsymbol{\theta}$ between $-\pi$ and π, the log-likelihood ratio $\ln\left[\Lambda_m\left(\dot{z}; T_o\right)\right]$ is given by

$$\ln\left[\Lambda_m\left(\dot{z}; T_o\right)\right] = \ln\left(J_m\right) + \ln\left[\frac{1}{(2\pi)^L} \int_{-\pi}^{\pi} \cdots \int_{-\pi}^{\pi} f_m\left(\boldsymbol{\theta}\right) d\boldsymbol{\theta}\right] \tag{3.67}$$

where J_m and $f_m\left(\boldsymbol{\theta}\right)$ are respectively given by (3.63) and (3.64).

From (3.63-3.67) it is seen that the OPT scheme uses the same decision variables $\{u_{lm}\}_{l=0,\ldots,L-1}$ (3.18b) as the SPECCOH scheme does. Implementation of u_{lm} can be found in Section 3.2.1. In particular when the observation interval $[0, T_o]$ is assumed to be much longer than the inter-path delays ($T_o \gg \tau_l$ for all l), and $\epsilon_{lm} = 1$ for all l, the decision variable u_{lm} (3.18b) can be generated by sampling the output of the matched filter $s_m'(s) = 2\tilde{s}_m^*\left(T_o - s\right) e^{j\omega_c(s-T_o)} / \tilde{E}_m$ at $T_o + \tau_l$. Then the receiver

illustrated in Fig. 3.2 is obtained.

The first term in the right side of (3.67), $\ln J_m$, is a biased quadratic form of the input signal samples. In this thesis a biased quadratic form refers to the sum of a quadratic form and a bias term. The second term in the right side of (3.67), however, is nonlinear and depends on the multi-dimensional integral of the function $f_m(\boldsymbol{\theta})$ defined in (3.64). Section 3.4.1 shows how a closed-form solution for the integral of $f_m(\boldsymbol{\theta})$ can be found for L-path channels with one Ricean path (mixed mode Ricean/Rayleigh channels) in terms of a modified Bessel function of zero order. Similarly Appendix B.3.2 shows how a closed-form solution for the integral of $f_m(\boldsymbol{\theta})$ can be found for L-path channels with two Ricean paths (2 Ricean/L-2 Rayleigh channels) in terms of an infinite series of products of Bessel and trigonometric functions. The technique used in Appendix B.3.2 can be extended to provide a closed-form solution for the integral of $f_m(\boldsymbol{\theta})$ for the L-path case. For the L-path Ricean channel, an L-fold path integral need to be solved since $f_m(\boldsymbol{\theta})$ is to be integrated over $\theta_0, \ldots, \theta_{L-1}$. First integration with respect to θ_{L-1} is performed yielding $I_0\left(\frac{|\alpha_{L-1}|}{\sigma^2_{L-1}\sqrt{\epsilon_{L-1m}}}\,|b_{L-1m}(\boldsymbol{\theta}_{L-2})|\right)$. Then integration with respect to θ_{L-2} is done as follows. Let us define

$$d_{km} = \frac{|\alpha_k|}{\sigma_k^2\sqrt{\epsilon_{km}}}\left[\boldsymbol{X}_m^T\boldsymbol{Q}_m\boldsymbol{r}_m\right]_k \tag{3.68a}$$

$$= \frac{2}{N_0}\int_0^{T_o} l_{km}^*(s)e^{-j\omega_c s}dz(s) \tag{3.68b}$$

and[7]

$$e_{kn}^m = \frac{|\alpha_k||\alpha_n|}{\sigma_k^2\sqrt{\epsilon_{km}}}\left[\boldsymbol{X}_m^T\boldsymbol{Q}_m\left(\boldsymbol{X}_m^T\right)^{-1}\boldsymbol{\epsilon}_m^{1/2}\right]_{kn} \tag{3.69a}$$

$$= \frac{1}{N_0}\int_0^{T_o} l_{nm}(s)\,|\alpha_k|\,\tilde{s}_m^*(s-\tau_k)ds \tag{3.69b}$$

$$= \frac{1}{N_0}\int_0^{T_o} l_{km}^*(s)\,|\alpha_n|\,\tilde{s}_m(s-\tau_n)ds \tag{3.69c}$$

$$\approx \frac{2}{N_0}\int_0^{T_o} l_{km}^*(s)e^{-j\omega_c s}\Re\left\{|\alpha_n|\tilde{s}_m(s-\tau_n)e^{j\omega_c s}\right\}ds \tag{3.69d}$$

[7]The superscript m in e_{kn}^m is not an exponent.

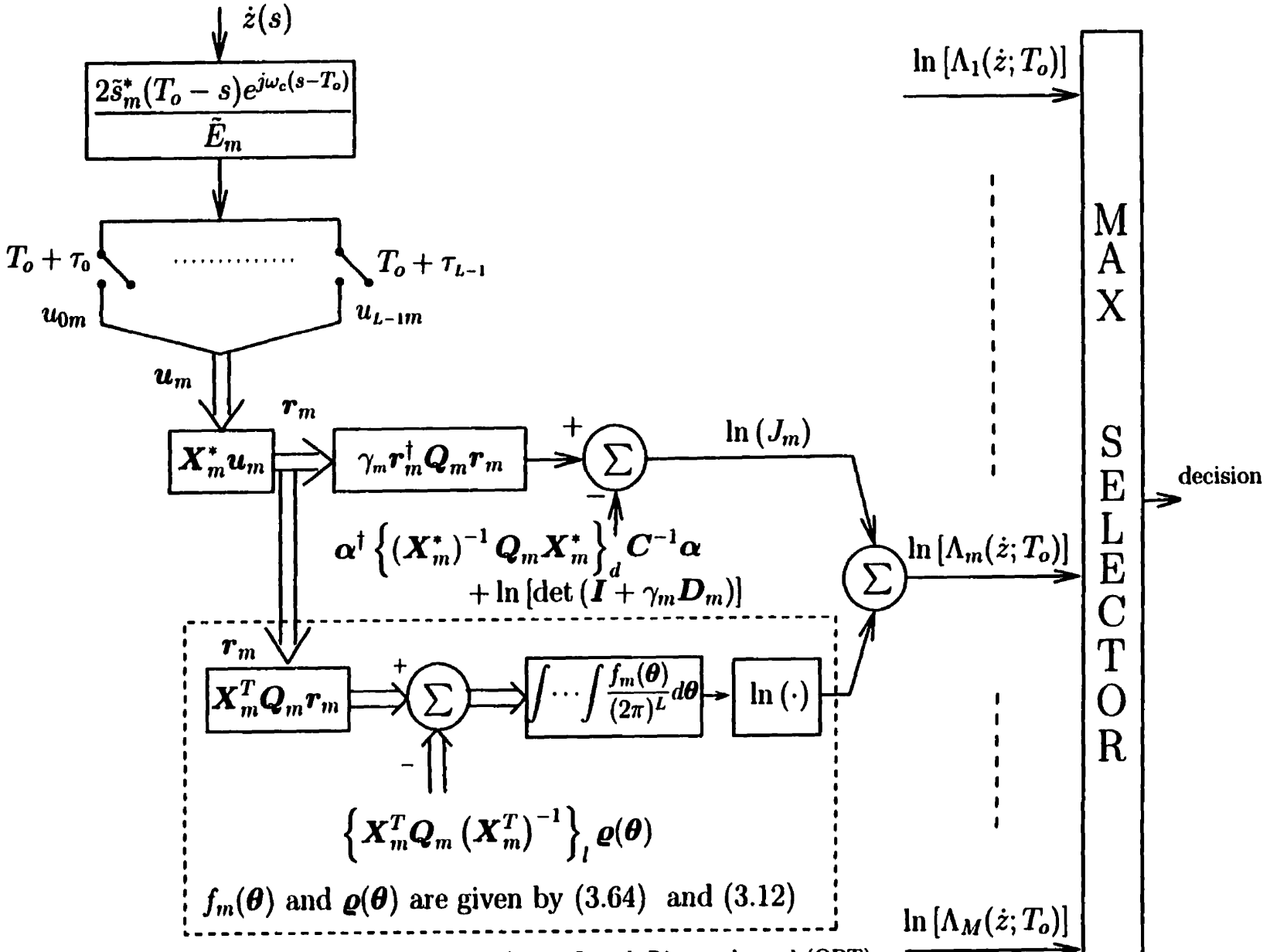

Fig. 3.2 Non-coherent optimum receiver for an L-path Ricean channel (OPT) assuming $T_o \gg \tau_l$ & $\epsilon_{lm} = 1$ for all l

such that

$$\frac{|\alpha_k|}{\sigma_k^2\sqrt{\epsilon_{km}}}b_{km}(\boldsymbol{\theta}_{k-1}) = d_{km} - \sum_{n=0}^{k-1} e_{kn}^m e^{j\theta_n'} \qquad \frac{|\alpha_0|}{\sigma_0^2\sqrt{\epsilon_{0m}}}b_{0m} = d_{0m} \tag{3.70}$$

$$\theta_k' = \theta_k + \arg[\alpha_k] \tag{3.71}$$

where $l_{km}(s)$ is given by

$$l_{km}(s) = \frac{N_0|\alpha_k|}{\sigma_k^2\sqrt{\epsilon_{km}\tilde{E}_m}} \sum_{l=0}^{L-1} \frac{\frac{\lambda_{lm}}{2N_0}}{1+\frac{\lambda_{lm}}{2N_0}} (x_{lk}^m)^* \phi_{lm}(s) \tag{3.72}$$

(3.68b) is obtained by straightforward substitution of (3.14) and (3.16a). Equations (3.69b) and (3.69c) can be derived using (3.8) and the fact that the eigenfunctions $\phi_{lm}(s)$ are orthonormal. A similar proof is done in Appendix C for (C.29a) and (C.29b). Equation (3.69d) is obtained from (3.69c) by neglecting integrals containing double frequency terms (use conjugate of (C.1) in Lemma C.1). Comparison between (3.68b) and (3.69d) shows that (3.68b) is the correlation of the received signal with $l_{km}(s)e^{j\omega_c s}$ and (3.69d) is the correlation of the specular term $\Re\{|\alpha_n|\,\tilde{s}_m(s-\tau_n)e^{j\omega_c s}\}$ with $l_{km}(s)e^{j\omega_c s}$. From (3.70)

$$\frac{|\alpha_{L-1}|}{\sigma_{L-1}^2\sqrt{\epsilon_{L-1m}}}b_{L-1m}(\boldsymbol{\theta}_{L-2}) = \left(d_{L-1m} - \sum_{n=0}^{L-3} e_{L-1n}^m e^{j\theta_n'}\right) - e_{L-1L-2}^m e^{j(\theta_{L-2}+\delta_{L-2})}$$

where $\delta_{L-2} = \arg[\alpha_{L-2}]$. Hence $\frac{|\alpha_{L-1}|}{\sigma_{L-1}^2\sqrt{\epsilon_{L-1m}}}b_{L-1m}(\boldsymbol{\theta}_{L-2})$ can be expressed as the difference of a complex term dependent on $\boldsymbol{\theta}_{L-3}$ and a complex term independent of $\boldsymbol{\theta}_{L-3}$ rotated by $\theta_{L-2}+\delta_{L-2}$. By applying Neumann's addition theorem (D.34a) [185, p. 358], $I_0\left(\frac{|\alpha_{L-1}|}{\sigma_{L-1}^2\sqrt{\epsilon_{L-1m}}}|b_{L-1m}(\boldsymbol{\theta}_{L-2})|\right)$ is replaced so that its dependence on θ_{L-2} appears only in cosine terms. Hence integration with respect to θ_{L-2} can be performed, and the result involves modified Bessel functions of integer orders. Integration with respect to θ_{L-3} is quite similar to the previous integration. All Bessel functions arguments that depend on $\boldsymbol{\theta}_{L-3}$ should be expressed as the difference of a complex term dependent on $\boldsymbol{\theta}_{L-4}$ and a complex term independent of $\boldsymbol{\theta}_{L-4}$ rotated by $\theta_{L-3}+\delta_{L-3}$. Then Graf's generalization of Neumann's theorem (D.34b-D.34c) [185, p. 361] should be applied individually to all Bessel functions that depend on $\boldsymbol{\theta}_{L-3}$. The dependence on θ_{L-3} appears then in cosine or sine terms and integration with respect to

θ_{L-3} can be performed. By performing similar steps for integration over θ_{L-4} and so on, it can be shown that the closed-form solution of the integral of $f_m(\boldsymbol{\theta})$ for the L-path Ricean channel is the sum of multi-dimensional infinite series of products of Bessel and trigonometric functions that depends on $V_{km}, \vartheta_{km}, k = 0, \ldots, L-1$ and $V_{kn}^m, \vartheta_{kn}^m, k = 0, \ldots, L-1, n = 0, \ldots, k-1$, where

$$V_{km} \triangleq |d_{km}| = \left| \frac{2}{N_0} \int_0^{T_o} l_{km}^*(s) e^{-j\omega_c s} dz(s) \right| \tag{3.73}$$

$$\vartheta_{km} \triangleq \arg[d_{km}] = \arg\left[\frac{2}{N_0} \int_0^{T_o} l_{km}^*(s) e^{-j\omega_c s} dz(s) \right] \tag{3.74}$$

$$V_{kn}^m \triangleq |e_{kn}^m| = \left| \frac{1}{N_0} \int_0^{T_o} l_{nm}(s) |\alpha_k| \tilde{s}_m^*(s - \tau_k) ds \right| \tag{3.75}$$

$$\vartheta_{kn}^m \triangleq \arg[e_{kn}^m] = \arg\left[\frac{1}{N_0} \int_0^{T_o} l_{nm}(s) |\alpha_k| \tilde{s}_m^*(s - \tau_k) ds \right] \tag{3.76}$$

and alternative expressions of d_{km} and e_{kn}^m can be found in (3.68) and (3.69). Therefore from (3.67) the L-path Ricean likelihood ratio can be written as

$$\Lambda_m(\dot{z}; T_o) = J_m g(\boldsymbol{d}_m) \tag{3.77}$$

where J_m is given by (3.63), $\boldsymbol{d}_m = [V_{0m}, \ldots, V_{L-1m}, \vartheta_{0m}, \ldots, \vartheta_{L-1m}]^T$ and $g(\boldsymbol{d}_m) \triangleq \frac{1}{(2\pi)^L} \int_{-\pi}^{\pi} \cdots \int_{-\pi}^{\pi} f_m(\boldsymbol{\theta}) d\boldsymbol{\theta}$. Table 3.1 summarizes the various expressions of $g(\boldsymbol{d}_m)$ for multipath Ricean channels.

Table 3.1 Expression of $g(\boldsymbol{d}_m) = \frac{1}{(2\pi)^L} \int_{-\pi}^{\pi} \cdots \int_{-\pi}^{\pi} f_m(\boldsymbol{\theta}) d\boldsymbol{\theta}$

L-path Ricean channel	sum of multi-dimensional infinite series of products of Bessel and trigonometric functions that depends on $\{V_{km}, \vartheta_{km}\}_{k=0,\ldots,L-1}$ and $\{V_{kn}^m, \vartheta_{kn}^m\}_{k=0,\ldots,L-1, n=0,\ldots,k-1}$
L-path channel with two Ricean paths	$I_0(V_{0m}) I_0(V_{10}^m) I_0(V_{1m}) + \sum_{p=1}^{\infty} (-1)^p I_p(V_{0m}) I_p(V_{10}^m) I_p(V_{1m}) \cos\left(p(\vartheta_{0m} + \vartheta_{10}^m - \vartheta_{1m})\right)$
L-path channel with one Ricean path	$I_0(V_{0m})$

Note that although the phase of α_k appears in (3.66), the optimum non-coherent re-

ceiver does not require the knowledge of the phases of the specular term since they are integrated out. In fact cancellation of the phases occurs after the integration of $f_m(\boldsymbol{\theta})$ (see example of likelihood for 2 Ricean/L-2 Rayleigh channels in Appendix B.3.2). Notice that when the multipath is resolved, $\boldsymbol{D}_m$ reduces to $\boldsymbol{\epsilon}_m \boldsymbol{C}$, $\boldsymbol{X}_m$ is the identity matrix and $b_{km}(\boldsymbol{\theta}_{k-1})$ is independent of $\boldsymbol{\theta}$ and equals to $[\boldsymbol{Q}_m \boldsymbol{r}_m]_k$. If in addition to path resolvability, a long observation interval is assumed, the matrix $\boldsymbol{\epsilon}_m$ is independent of the hypothesis and equal to $\boldsymbol{I}$, the optimal receiver reduces to that derived in [4] when the multipath is assumed to be resolved, yielding the classical Rake receiver. The behavior of the SPECCOH and OPT schemes at high SNR is illustrated in the following proposition.

Proposition 3.3.1. *The SPECCOH and OPT scheme log-likelihood ratios "converge" almost surely (a.s.) to the same term as γ_m goes to infinity, i.e.*

$$\lim_{\gamma_m \to \infty} a.s. \ \frac{1}{\gamma_m} \ln \left[\Lambda_m \left(\dot{z}; T_o \left| \boldsymbol{\theta} \right. \right) \right] = \lim_{\gamma_m \to \infty} a.s. \ \frac{1}{\gamma_m} \ln \left[\Lambda_m \left(\dot{z}; T_o \right) \right] = \boldsymbol{r}_m^{\dagger} \boldsymbol{r}_m$$

This asymptotical property will also be confirmed analytically and numerically in terms of the receivers performance in Chapter 4.

Proof of Proposition 3.3.1. $\boldsymbol{X}_m$, $\boldsymbol{C}$ and $\boldsymbol{\varrho}(\boldsymbol{\theta})$ are independent of γ_m. Therefore since the term $\frac{1}{\gamma_m} \boldsymbol{X}_m^* \boldsymbol{C}^{-1} \boldsymbol{\epsilon}_m^{-1/2} \boldsymbol{\varrho}(\boldsymbol{\theta})$ is deterministic, $\boldsymbol{r}_m + \frac{1}{\gamma_m} \boldsymbol{X}_m^* \boldsymbol{C}^{-1} \boldsymbol{\epsilon}_m^{-1/2} \boldsymbol{\varrho}(\boldsymbol{\theta})$ converges a.s. to $\boldsymbol{r}_m$ as γ_m tends to infinity. Furthermore, from (3.16a)

$$\lim_{\gamma_m \to \infty} \boldsymbol{Q}_m = \boldsymbol{I} \tag{3.78}$$

Hence from (3.10) the log-likelihood ratio for the SPECCOH scheme satisfies

$$\lim_{\gamma_m \to \infty} \text{a.s.} \ \frac{1}{\gamma_m} \ln \left[\Lambda_m \left(\dot{z}; T_o \left| \boldsymbol{\theta} \right. \right) \right] = \boldsymbol{r}_m^{\dagger} \boldsymbol{r}_m \tag{3.79}$$

From (3.63a) and (3.78) $\ln(J_m)$ in (3.67) satisfies

$$\lim_{\gamma_m \to \infty} \text{a.s.} \ \frac{1}{\gamma_m} \ln \left[J_m \right] = \boldsymbol{r}_m^{\dagger} \boldsymbol{r}_m \tag{3.80}$$

The function $f_m(\boldsymbol{\theta})$ given by (3.64) depends on the Gaussian random vector $\boldsymbol{r}_m$.

Using the joint pdf of $\boldsymbol{r}_m$, from (B.33) it can be shown that

$$E\left[|f_m(\boldsymbol{\theta})|\,|\boldsymbol{\theta}, H_k\right] = \exp\left\{(\overline{\boldsymbol{r}_m}^k)^\dagger \boldsymbol{\varrho}''(\boldsymbol{\theta}) + \boldsymbol{\varrho}''^\dagger(\boldsymbol{\theta})\overline{\boldsymbol{r}_m}^k + 2\boldsymbol{\varrho}''^\dagger(\boldsymbol{\theta})\tilde{E}_m^{-1}\boldsymbol{\Omega}_{mk}\boldsymbol{\varrho}''(\boldsymbol{\theta}) - b'(\boldsymbol{\theta})\right\}$$

where $\overline{\boldsymbol{r}_m}^k \triangleq E\left[\boldsymbol{r}_m|\boldsymbol{\theta}, H_k\right]$ and $\tilde{E}_m^{-1}\boldsymbol{\Omega}_{mk} \triangleq E\left[\frac{1}{2}\left(\boldsymbol{r}_m - \overline{\boldsymbol{r}_m}^k\right)\left(\boldsymbol{r}_m - \overline{\boldsymbol{r}_m}^k\right)^\dagger|\boldsymbol{\theta}, H_k\right]$

$$\overline{\boldsymbol{r}_m}^k = \sqrt{\frac{\tilde{E}_k}{\tilde{E}_m}}\boldsymbol{X}_m^*\boldsymbol{\Gamma}_{km}^T\boldsymbol{\epsilon}_k^{1/2}\boldsymbol{\varrho}(\boldsymbol{\theta}) \quad \boldsymbol{\Omega}_{mk} = \frac{\tilde{E}_k}{2}\boldsymbol{X}_m^*\boldsymbol{\Gamma}_{km}^T\boldsymbol{\epsilon}_k^{1/2}\boldsymbol{C}\boldsymbol{\epsilon}_k^{1/2}\boldsymbol{\Gamma}_{mk}^T\boldsymbol{X}_m^T + N_0\boldsymbol{I}$$

$$\boldsymbol{\varrho}''(\boldsymbol{\theta}) = \boldsymbol{Q}_m\boldsymbol{X}_m^*\boldsymbol{\epsilon}_m^{-1/2}\boldsymbol{C}^{-1}\boldsymbol{\varrho}(\boldsymbol{\theta}) \quad b'(\boldsymbol{\theta}) = \Re\left\{\boldsymbol{\varrho}^\dagger(\boldsymbol{\theta})2\boldsymbol{\epsilon}_m^{-1/2}\boldsymbol{C}^{-1}\left\{\boldsymbol{X}_m^T\boldsymbol{Q}_m\boldsymbol{X}_m^{T^{-1}}\boldsymbol{\epsilon}_m^{1/2}\right\}_l\boldsymbol{\varrho}(\boldsymbol{\theta})\right\}$$

Therefore $\forall\,\boldsymbol{\theta} \in [-\pi, \pi]^L$, $E\left[|f_m(\boldsymbol{\theta})|\,|\boldsymbol{\theta}, H_k\right] < \infty$ and

$$\forall\, l = 0, \ldots, L-1 \qquad \int_{-\pi}^{\pi}\cdots\int_{-\pi}^{\pi} E\left[|f_m(\boldsymbol{\theta})|\,|\boldsymbol{\theta}, H_k\right]d\boldsymbol{\theta}_l < \infty$$

Furthermore since $f_m(\boldsymbol{\theta})$ is measurable in (θ_0, ω) when $\theta_1, \ldots, \theta_{L-1}$ are held fixed and $\forall\, l = 0, \ldots, L-2$ $\int_{-\pi}^{\pi}\cdots\int_{-\pi}^{\pi} f_m(\boldsymbol{\theta})d\boldsymbol{\theta}_l$ is measurable in (θ_{l+1}, ω) when $\theta_{l+1}, \ldots, \theta_{L-1}$ are held fixed, the integral $\int_{-\pi}^{\pi}\cdots\int_{-\pi}^{\pi} f_m(\boldsymbol{\theta})d\boldsymbol{\theta}$ can be defined as a Lebesgue integral of the sample functions of $f_m(\boldsymbol{\theta})$ for almost all sample functions [182, p. 45]. From (3.16a) $\forall\, l = 0, \ldots, L-1$ $0 \le [\boldsymbol{Q}_m]_{ll} \le 1$, therefore

$$\frac{|\alpha_l|}{\sigma_l^2\sqrt{\epsilon_{lm}}}|b_{lm}(\boldsymbol{\theta}_{l-1})| \le |d_{lm}| + \sum_{n=0}^{l-1}|e_{ln}^m|\left|e^{j\theta_n'}\right| = |d_{lm}| + \sum_{n=0}^{l-1}|e_{ln}^m| \qquad \text{from (3.70)}$$

$$|d_{lm}| \le \frac{|\alpha_l|}{\sigma_l^2\sqrt{\epsilon_{lm}}}\left[|\boldsymbol{X}_m^T|\,|\boldsymbol{r}_m|\right]_l \qquad \text{from (3.68a)}$$

$$|e_{ln}^m| \le \frac{|\alpha_l||\alpha_n|}{\sigma_l^2\sqrt{\epsilon_{lm}}}\left[|\boldsymbol{X}_m^T|\,|(\boldsymbol{X}_m^T)^{-1}|\boldsymbol{\epsilon}_m^{1/2}\right]_{ln} \qquad \text{from (3.69a)}$$

$$f_m(\boldsymbol{\theta}) \le \exp\left\{\sum_{l=0}^{L-1}\frac{|\alpha_l|}{\sigma_l^2\sqrt{\epsilon_{lm}}}|b_{lm}(\boldsymbol{\theta}_{l-1})|\right\} \le f_m' \qquad \text{from (3.64)}$$

where for any matrix $\boldsymbol{B}$ $|\boldsymbol{B}|$ is defined in this thesis as $\left[|\boldsymbol{B}|\right]_{lj} \triangleq |[\boldsymbol{B}]_{lj}|$ and f_m' is independent of γ_m and given by

$$f_m' = \exp\left\{\sum_{l=0}^{L-1}\left[\frac{|\alpha_l|}{\sigma_l^2\sqrt{\epsilon_{lm}}}\left[|\boldsymbol{X}_m^T|\,|\boldsymbol{r}_m|\right]_l + \sum_{n=0}^{l-1}\frac{|\alpha_l||\alpha_n|}{\sigma_l^2\sqrt{\epsilon_{lm}}}\left[|\boldsymbol{X}_m^T|\,|(\boldsymbol{X}_m^T)^{-1}|\boldsymbol{\epsilon}_m^{1/2}\right]_{ln}\right]\right\}$$

Since f'_m is independent of γ_m and $\int_{-\pi}^{\pi}\cdots\int_{-\pi}^{\pi}|f'_m|\,d\boldsymbol{\theta} = (2\pi)^L f'_m < \infty$, from the Lebesgue dominated convergence theorem

$$\lim_{\gamma_m\to\infty} \text{a.s. } \frac{1}{(2\pi)^L}\int_{-\pi}^{\pi}\cdots\int_{-\pi}^{\pi} f_m(\boldsymbol{\theta})\,d\boldsymbol{\theta} = \frac{1}{(2\pi)^L}\int_{-\pi}^{\pi}\cdots\int_{-\pi}^{\pi}\lim_{\gamma_m\to\infty} \text{a.s. } f_m(\boldsymbol{\theta})\,d\boldsymbol{\theta}$$

$$= \frac{1}{(2\pi)^L}\int_{-\pi}^{\pi}\cdots\int_{-\pi}^{\pi}\exp\left\{\sum_{l=0}^{L-1}\frac{|\alpha_l|}{\sigma_l^2\sqrt{\epsilon_{lm}}}\left|\left[\boldsymbol{X}_m^T\boldsymbol{r}_m\right]_l\right|\cos\left(\theta_l-\varphi'_{lm}\right)\right\}d\boldsymbol{\theta} \quad \begin{matrix}\text{from (3.78)}\\ \text{\& (3.64-3.66)}\end{matrix}$$

$$= \prod_{l=0}^{L-1} I_0\left(\frac{|\alpha_l|}{\sigma_l^2\sqrt{\epsilon_{lm}}}\left|\left[\boldsymbol{X}_m^T\boldsymbol{r}_m\right]_l\right|\right) < \infty$$

where $\varphi'_{lm} = \arg\left[\left[\boldsymbol{X}_m^T\boldsymbol{r}_m\right]_l\right] - \arg\left[\alpha_l\right]$. Hence from (3.67) and (3.80) the log-likelihood ratio for the OPT scheme satisfies

$$\lim_{\gamma_m\to\infty} \text{a.s. } \frac{1}{\gamma_m}\ln\left[\Lambda_m(\dot{z};T_o)\right] = \boldsymbol{r}_m^\dagger\boldsymbol{r}_m \tag{3.81}$$

Comparing (3.79) and (3.81) completes the proof. **Q.E.D**

3.3.2 OPT: a decorrelator

From (3.63), it is seen that the first term in the right side of (3.67), $\ln(J_m)$, is a biased quadratic form of the input signal samples and includes the matrix $\boldsymbol{X}_m$ acting on the matched filter samples u_{lm}. Section 3.2.2 showed that this matrix has an interpretation as a decorrelating matrix. Such an interpretation will also be given in Section 3.5.2 for Rayleigh fading channels. Therefore from (3.67) it is seen that the optimum non-coherent receiver performs a decorrelation on the input samples as well as nonlinear operations related to the Ricean specular term. Note that for low γ_m, from (3.16b) and (3.8a) regardless of $\boldsymbol{\alpha}$, $\{(\boldsymbol{X}_m^*)^{-1}\boldsymbol{Q}_m\boldsymbol{X}_m^*\}_d \approx \gamma_m\{\boldsymbol{\Gamma}_m^*\boldsymbol{\epsilon}_m\boldsymbol{C}\}_d = \gamma_m\boldsymbol{\epsilon}_m\boldsymbol{C}$, thus from (3.63b) $\ln(J_m) \approx \gamma_m^2\boldsymbol{u}_m^\dagger\boldsymbol{\epsilon}_m\boldsymbol{C}\boldsymbol{u}_m - \gamma_m\boldsymbol{\alpha}^\dagger\boldsymbol{\epsilon}_m\boldsymbol{\alpha}$. Similarly the equations $\boldsymbol{X}_m^T\boldsymbol{Q}_m\boldsymbol{r}_m = \gamma_m\left[(\boldsymbol{\epsilon}_m\boldsymbol{C})^{-1} + \gamma_m\boldsymbol{\Gamma}_m^*\right]^{-1}\boldsymbol{u}_m \approx \gamma_m\boldsymbol{\epsilon}_m\boldsymbol{C}\boldsymbol{u}_m$ and $\boldsymbol{X}_m^T\boldsymbol{Q}_m\left(\boldsymbol{X}_m^T\right)^{-1}\boldsymbol{\epsilon}_m^{1/2} \approx \gamma_m\boldsymbol{\epsilon}_m\boldsymbol{C}\boldsymbol{\Gamma}_m^*\boldsymbol{\epsilon}_m^{1/2}$ are obtained from (3.16b), (3.18a) and (3.8a) thus from (3.65) $b_{km}(\boldsymbol{\theta}_{k-1}) \approx \left[\gamma_m\boldsymbol{\epsilon}_m\boldsymbol{C}\boldsymbol{u}_m - \gamma_m\left\{\boldsymbol{\epsilon}_m\boldsymbol{C}\boldsymbol{\Gamma}_m^*\boldsymbol{\epsilon}_m^{1/2}\right\}_l\boldsymbol{\varrho}(\boldsymbol{\theta})\right]_k$. Thus it is seen that at low γ_m, for the Ricean channel optimal receiver the decorrelation operation on the input signal vanishes. This is to be expected since a side effect of the decorrelation operation is to enhance the white background channel noise. The decorrelating matrix is still used in the bias term $\gamma_m\left\{\boldsymbol{\epsilon}_m\boldsymbol{C}\boldsymbol{\Gamma}_m^*\boldsymbol{\epsilon}_m^{1/2}\right\}_l\boldsymbol{\varrho}(\boldsymbol{\theta}) =$

$\gamma_m \left\{ \boldsymbol{X}_m^T \boldsymbol{D}_m \left(\boldsymbol{X}_m^T \right)^{-1} \boldsymbol{\epsilon}_m^{1/2} \right\}_l \boldsymbol{\varrho}(\boldsymbol{\theta})$.

Section 3.3.3 will give further insight on the operations of the optimum non-coherent receiver. The mathematical framework appears in Appendix A.

3.3.3 Non-coherent estimator-correlator for an L-path Ricean channel

Likelihood ratio expressed in an estimator-correlator form

Independently of the characterization of $\boldsymbol{\theta}$ (known or random), $v_m(t)$ has a finite mean-square value on the observation interval $[0, T_o]$ and $\int_0^{T_o} E\,|v_m(t)|\,dt < \infty$ (see Section 3.1). Therefore, from Appendix A, under each hypothesis (including H_0) when $\boldsymbol{\theta}$ is random the received signal is an Itô process [181] and can be written as (3.25) with $v_0(t) = 0$. Similar to Section 3.2.3 from [21], the likelihood ratio $\Lambda_m(\dot{z}; T_o)$ can be expressed as

$$\Lambda_m(\dot{z}; T_o) = \exp\left\{ \frac{2}{N_0} \left[\int_0^{T_o} \check{v}_m(t)\, dz(t) - \frac{1}{2} \int_0^{T_o} \check{v}_m^2(t)\, dt \right] \right\} \tag{3.82}$$

where $\check{v}_m(t)$ is the conditional mean or equivalently the MMSE estimate of $v_m(t)$ from the observations $\dot{z}(s)$ (given H_m) on the interval $[0, t]$. This illustrates the interpretation of the L-path Ricean channel non-coherent optimum receiver as an estimator-correlator with a MMSE estimator.

The conditional mean can be found by two methods. The first method consists of using its definition. This requires finding conditional probability density functions which depend on the likelihood ratio and conditional likelihood ratios, all of them considered over an observation interval $[0, t]$. The second method derived from (3.82) involves Itô differentiation with respect to t of the likelihood ratio considered over an observation interval $[0, t]$. Therefore, both methods require the expression of the likelihood ratio considered over an arbitrary observation interval $[0, t]$. This issue is considered next for continuous time-limited waveforms. For waveforms of infinite duration, no closed-form solution of the likelihood ratio has been found for an arbitrary observation interval $[0, t]$ and an arbitrary waveform since time-shifted versions of an infinite duration signal are not necessarily independent over an observation interval $[0, t]$ (see Appendix B.1). Hence the form of the eigenfunctions of the covariance function $\mathcal{K}_m(s, u)$ over $[0, t]$ is waveform specific in that case. The M possible transmitted signals $\{\tilde{s}_m(s)\}_{m=1,\ldots,M}$ are assumed to be time-limited to $[0, T]$ for the remainder of

this section (Section 3.3.3).

Likelihood ratio over an arbitrary observation interval $[0,t]$ assuming that $\tilde{s}_m(s)$ is time-limited

In this section, the likelihood ratio over an arbitrary finite observation interval $[0,t]$ $(0 \leq t < \infty)$ is derived when the M possible transmitted signals $\{\tilde{s}_m(s)\}_{m=1,\ldots,M}$ are time-limited to $[0,T]$ and continuous on $[0,t]$. Let us assume that the multipath delays τ_k are ordered as follows $\tau_0 < \tau_1 < \ldots < \tau_{L-1}$. Let T_m' be defined as (3.30). If $0 \leq t \leq T_m' + \tau_0$, from Lemma B.2 $\forall\, s \in [0,t], \forall\, k = 0, \ldots, L-1$, $\tilde{s}_m(s-\tau_k) = 0$, therefore the likelihood ratio is given by

$$\Lambda_m(\dot{z};t) = 1$$

where the t denotes the dependence of the likelihood ratio on the observation interval. Let us assume now that $t > T_m' + \tau_0$. As seen in Section 3.2.3 (topic: "Eigenvalues and eigenfunctions of $K_m(s,u)$ over an arbitrary observation interval $[0,t]$, $t > T_m' + \tau_0$ assuming that $\tilde{s}_m(s)$ is time-limited"), for time-limited transmitted signals, when the observation interval is $[0,t]$, $t > T_m' + \tau_0$, an L-path channel model (3.1) that satisfies the L-order linear independency condition can be reduced to an equivalent i_t-path channel model (3.33) that satisfies the i_t-order linear independency condition. Therefore, it is seen that the methods previously used to derive the likelihood ratios[8] can be also used in this section except that the number of signals is i_t instead of L where $1 \leq i_t \leq L$. Modifying the results from Section 3.3.1 (and Appendix B.3.1) from (3.77) $\forall\, T_m' + \tau_0 < t < \infty$, the likelihood ratio associated with an observation interval equal to $[0,t]$ is given by

$$\Lambda_m(\dot{z};t) = J_{i_t m}(t)\, g_{i_t}\left(\boldsymbol{d}_{i_t m}(t), t\right) \quad T_m' + \tau_0 < t < \infty \qquad m = 1, \ldots, M$$

where from (3.72-3.76) the vector $\boldsymbol{d}_{i_t m}(t)$ is defined as[9]

$$\begin{aligned} \boldsymbol{d}_{i_t m}(t) &= \left[\left(\boldsymbol{V}_{i_t m}(t)\right)^T, \left(\boldsymbol{\vartheta}_{i_t m}(t)\right)^T\right]^T \\ \boldsymbol{V}_{i_t m}(t) &= \left[V_{0m}^{i_t}(t), \ldots, V_{i_t-1 m}^{i_t}(t)\right]^T \end{aligned} \tag{3.83}$$

[8] For the derivation of likelihood ratios on $[0,t]$, continuity of the signals $\tilde{s}_m(s-\tau_k)$ needs also to be assumed on $[0,t]$ to ensure existence of the associated Karhunen-Loève expansion.

[9] The superscript i_t in (3.83-3.88) is not an exponent.

$$\boldsymbol{\vartheta}_{i_t m}(t) = \left[\vartheta_{0m}^{i_t}(t), \ldots, \vartheta_{i_t-1m}^{i_t}(t)\right]^T \tag{3.84}$$

$$V_{km}^{i_t}(t) = |d_{km}^{i_t}(t)| \tag{3.85}$$

$$\vartheta_{km}^{i_t}(t) = \arg\left[d_{km}^{i_t}(t)\right] \tag{3.86}$$

$$d_{km}^{i_t}(t) = \frac{2}{N_0}\int_0^t \left[l_{km}^{i_t}(s,t)\right]^* e^{-j\omega_c s} dz(s) \quad k = 0, \ldots, i_t - 1 \tag{3.87}$$

$$l_{km}^{i_t}(s,t) = \frac{N_0|\alpha_k|}{\sigma_k^2\sqrt{\epsilon_{km}(t)\tilde{E}_m}} \sum_{l=0}^{i_t-1} \frac{\frac{\lambda_{lm}^{i_t}(t)}{2N_0}}{1+\frac{\lambda_{lm}^{i_t}(t)}{2N_0}} \left[x_{lk}^{i_t m}(t)\right]^* \phi_{lm}^{i_t}(s,t) \quad 0 \le s \le t \tag{3.88}$$

and from (3.63a), (3.16a) and (3.35) $J_{i_t m}(t)$ is given by[10]

$$\begin{aligned} J_{i_t m}(t) &= \left[\det\left(\boldsymbol{I}_{i_t} + \tfrac{\tilde{E}_m}{2N_0}\boldsymbol{D}_{i_t m}(t)\right)\right]^{-1} \\ &\quad \cdot \exp\left\{-\boldsymbol{\alpha}_{i_t}^{\dagger}\tfrac{\tilde{E}_m}{2N_0}\left\{\boldsymbol{\epsilon}_{i_t m}^{-1}(t)\boldsymbol{C}_{i_t}^{-1}\boldsymbol{X}_{i_t m}^T(t)\boldsymbol{D}_{i_t m}^2(t)\left[\boldsymbol{I}_{i_t} + \tfrac{\tilde{E}_m}{2N_0}\boldsymbol{D}_{i_t m}(t)\right]^{-1}\boldsymbol{X}_{i_t m}^*(t)\right\}_d \boldsymbol{C}_{i_t}^{-1}\boldsymbol{\alpha}_{i_t}\right\} \\ &\quad \cdot \exp\left\{\tfrac{\tilde{E}_m}{2N_0}\boldsymbol{r}_{i_t m}^{\dagger}(t)\tfrac{\tilde{E}_m}{2N_0}\boldsymbol{D}_{i_t m}(t)\left(\boldsymbol{I}_{i_t} + \tfrac{\tilde{E}_m}{2N_0}\boldsymbol{D}_{i_t m}(t)\right)^{-1}\boldsymbol{r}_{i_t m}(t)\right\} \\ &= \Pi_{i_t m}(t)\exp\left\{-\mathrm{l}_{i_t m}(t)\right\}\exp\left\{\frac{1}{2}\frac{2}{N_0}Z_{i_t m}(t)\right\} \end{aligned}$$

where

$$\Pi_{i_t m}(t) = \prod_{k=0}^{i_t-1}\left(1+\frac{\lambda_{km}^{i_t}(t)}{2N_0}\right)^{-1} = \prod_{k=0}^{2i_t-1}\left(1+\frac{2}{N_0}\kappa_{km}^{i_t}(t)\right)^{-1/2}$$

$$\mathrm{l}_{i_t m}(t) = \sum_{l=0}^{i_t-1}\frac{\left(\lambda_{lm}^{i_t}(t)\right)^2}{2N_0\left(1+\frac{\lambda_{lm}^{i_t}(t)}{2N_0}\right)}\sum_{k=0}^{i_t-1}\frac{|\alpha_k|^2|x_{lk}^{i_t m}(t)|^2}{(2\sigma_k^2)^2\epsilon_{km}(t)\tilde{E}_m}$$

$$Z_{i_t m}(t) = \sum_{k=0}^{i_t-1}\frac{\frac{\tilde{E}_m}{2}\frac{\lambda_{km}^{i_t}(t)}{2N_0}\left|\left[\boldsymbol{r}_{i_t m}(t)\right]_k\right|^2}{1+\frac{\lambda_{km}^{i_t}(t)}{2N_0}} = \sum_{k=0}^{2i_t-1}\frac{\frac{2}{N_0}\kappa_{km}^{i_t}(t)\left(z_{km}^{i_t}(t)\right)^2}{1+\frac{2}{N_0}\kappa_{km}^{i_t}(t)}$$

$$\left[\boldsymbol{r}_{i_t m}(t)\right]_k = \frac{2}{\sqrt{\tilde{E}_m}}\int_0^t\left[\phi_{km}^{i_t}(s,t)\right]^* e^{-j\omega_c s}dz(s) = \sqrt{\frac{2}{\tilde{E}_m}}\left\{z_{km}^{i_t}(t) - jz_{k+i_t m}^{i_t}(t)\right\}$$

$$z_{km}^{i_t}(t) = \int_0^t \Upsilon_{km}^{i_t}(s,t)dz(s) \qquad k = 0, \ldots, 2i_t - 1 \tag{3.89}$$

$$\kappa_{km}^{i_t}(t) = \frac{\lambda_{km}^{i_t}(t)}{4} \qquad \kappa_{k+i_t m}^{i_t}(t) = \frac{\lambda_{km}^{i_t}(t)}{4} \qquad k = 0, \ldots, i_t - 1$$

[10] The subscript i_t indicates that the dimension of a vector or a matrix is i_t instead of L. For example $\boldsymbol{\alpha}_{i_t} = [\alpha_0, \ldots, \alpha_{i_t-1}]^T$ whereas $\boldsymbol{\alpha} = [\alpha_0, \ldots, \alpha_{L-1}]^T$.

$$\Upsilon^{i_t}_{km}(s,t) = \Re\left\{\sqrt{2}\phi^{i_t}_{km}(s,t)e^{j\omega_c s}\right\} \quad \Upsilon^{i_t}_{k+i_t m}(s,t) = \Im\left\{\sqrt{2}\phi^{i_t}_{km}(s,t)e^{j\omega_c s}\right\}$$

where $\lambda^{i_t}_{km}(t) = \tilde{E}_m\left[\boldsymbol{D}_{i_t m}(t)\right]_{kk}$, $\phi^{i_t}_{km}(s,t)$ is given by (3.34). The function $g_{i_t}\left(\boldsymbol{d}_{i_t m}(t),t\right)$ is given by

$$g_{i_t}\left(\boldsymbol{d}_{i_t m}(t),t\right) = \frac{1}{(2\pi)^{i_t}}\int_{-\pi}^{\pi}\cdots\int_{-\pi}^{\pi}\exp\left\{\sum_{k=0}^{i_t-1}\frac{|\alpha_k||b^{i_t}_{km}(\boldsymbol{\theta}'_{k-1},t)|}{\sigma_k^2\sqrt{\epsilon_{km}(t)}}\cos\left(\theta_k - \varphi^{i_t}_{km}(\boldsymbol{\theta}'_{k-1},t)\right)\right\}d\boldsymbol{\theta}'_{i_t-1}$$

where

$$\frac{|\alpha_k|b^{i_t}_{km}(\boldsymbol{\theta}'_{k-1},t)}{\sigma_k^2\sqrt{\epsilon_{km}(t)}} = d^{i_t}_{km}(t) - \sum_{n=0}^{k-1}e^{i_t m}_{kn}(t)e^{j\theta'_n} \qquad \frac{|\alpha_0|b^{i_t}_{0m}(t)}{\sigma_0^2\sqrt{\epsilon_{0m}(t)}} = d^{i_t}_{0m}(t)$$

$$\varphi^{i_t}_{km}(\boldsymbol{\theta}'_{k-1},t) = \arg\left[b^{i_t}_{km}(\boldsymbol{\theta}'_{k-1},t)\right] - \arg\left[\alpha_k\right] \qquad \varphi^{i_t}_{0m}(t) = \arg\left[b^{i_t}_{0m}(t)\right] - \arg\left[\alpha_0\right]$$

$$\boldsymbol{\theta}'_k = \left[\theta'_0,\ldots,\theta'_k\right]^T \qquad k = 0,\ldots,L-1 \tag{3.90}$$

θ'_k is given by (3.71) and from (C.29)

$$\begin{aligned} e^{i_t m}_{kn}(t) &\triangleq \gamma_m\frac{|\alpha_k||\alpha_n|}{\sigma_k^2\sqrt{\epsilon_{km}(t)}}\left[\boldsymbol{X}^T_{i_t m}(t)\left[\boldsymbol{D}^{-1}_{i_t m}(t) + \gamma_m\boldsymbol{I}_{i_t}\right]^{-1}\left(\boldsymbol{X}^T_{i_t m}(t)\right)^{-1}\boldsymbol{\epsilon}^{1/2}_{i_t m}(t)\right]_{kn} \\ &= \frac{1}{N_0}\int_0^t l^{i_t}_{nm}(s,t)\,|\alpha_k|\,\tilde{s}^*_m(s-\tau_k)ds = \frac{1}{N_0}\int_0^t\left[l^{i_t}_{km}(s,t)\right]^*|\alpha_n|\,\tilde{s}_m(s-\tau_n)ds \end{aligned} \tag{3.91}$$

Similar to results obtained in Section 3.3.1, the function $g_{i_t}\left(\boldsymbol{d}_{i_t m}(t),t\right)$ is the sum of multi-dimensional infinite series of products of Bessel and trigonometric functions associated with the likelihood ratio of an i_t-path Ricean channel. For example, modifying results from Table 3.1 $g_1\left(\boldsymbol{d}_{1m}(t),t\right)$ and $g_2\left(\boldsymbol{d}_{2m}(t),t\right)$ are given by[11]

$$\forall\,\tau_0 < t - T'_m \le \tau_1, \quad g_1\left(\boldsymbol{d}_{1m}(t),t\right) = I_0\left(V^1_{0m}(t)\right) \quad \left(g_1\left(\boldsymbol{d}_{1m}(t),t\right)\text{ depends only on }V^1_{0m}(t)\right)$$

$$\begin{aligned} \forall\,\tau_1 < t - T'_m \le \tau_2, \quad & g_2\left(\boldsymbol{d}_{2m}(t),t\right) = I_0\left(V^2_{0m}(t)\right)I_0\left(V^{2m}_{10}(t)\right)I_0\left(V^2_{1m}(t)\right) \\ & + \sum_{p=1}^{\infty}(-1)^p I_p\left(V^2_{0m}(t)\right)I_p\left(V^{2m}_{10}(t)\right)I_p\left(V^2_{1m}(t)\right)\cos\left(p\left(\vartheta^2_{0m}(t) + \vartheta^{2m}_{10}(t) - \vartheta^2_{1m}(t)\right)\right) \end{aligned}$$

Remark. The energy $\tilde{E}_m$ is independent of t since $\tilde{E}_m = \int_0^T|\tilde{s}_m(s)|^2ds$. The term

[11] The superscripts are not exponents.

$J_{i_t m}(t)$ is equivalent to J_m given in (3.63a) except that the observation interval is considered to be $[0,t]$ instead of $[0,T_o]$, L is replaced by i_t and the bias term has been written differently using (3.35). Similarly (3.87), (3.88) and (3.89) are equivalent respectively to (3.68b), (3.72) and (3.15) except for the new observation interval $[0,t]$ that is specified explicitly as a new parameter t and i_t that replaces L.

Since the integer function i_t is a staircase function of t, the likelihood ratio over $[0,t]$ is a function of t defined piecewise. Grouping the piecewise definitions together, the likelihood ratio is given by

$$\Lambda_m(\dot{z};t) = J_m(t) g\big(\boldsymbol{d}_m(t),t\big) \quad 0 \le t < \infty \qquad m = 1,\ldots,M \tag{3.92}$$

where $J_m(t)$ is given by

$$\begin{aligned} J_m(t) &= \begin{cases} 1 & 0 \le t \le T_m' + \tau_0 \\ J_{i_t m}(t) & T_m' + \tau_0 < t < \infty \end{cases} \\ &= \Pi_m(t) \exp\{-l_m(t)\} \exp\left\{\frac{1}{2}\frac{2}{N_0} Z_m(t)\right\} \quad 0 \le t < \infty \end{aligned} \tag{3.93}$$

and $g\big(\boldsymbol{d}_m(t),t\big)$ is given by

$$\begin{aligned} g\big(\boldsymbol{d}_m(t),t\big) &= \begin{cases} 1 & 0 \le t \le T_m' + \tau_0 \\ g_{i_t}\big(\boldsymbol{d}_{i_t m}(t),t\big) & T_m' + \tau_0 < t < \infty \end{cases} \\ &= \frac{1}{(2\pi)^L} \int_{-\pi}^{\pi} \cdots \int_{-\pi}^{\pi} \exp\left\{ \sum_{k=0}^{L-1} \frac{|\alpha_k| |b_{km}(\boldsymbol{\theta}_{k-1}',t)|}{\sigma_k^2 \sqrt{\epsilon_{km}(t)}} \cos\big(\theta_k - \varphi_{km}(\boldsymbol{\theta}_{k-1}',t)\big) \right\} d\boldsymbol{\theta}_{L-1}' \end{aligned} \tag{3.94}$$

The vector $\boldsymbol{d}_m(t)$ is defined as

$$\boldsymbol{d}_m(t) = \Big[\big(\boldsymbol{V}_m(t)\big)^T, \big(\boldsymbol{\vartheta}_m(t)\big)^T \Big]^T \tag{3.95}$$

$$\boldsymbol{V}_m(t) = [V_{0m}(t),\ldots,V_{L-1m}(t)]^T \tag{3.96}$$

$$\boldsymbol{\vartheta}_m(t) = [\vartheta_{0m}(t),\ldots,\vartheta_{L-1m}(t)]^T \tag{3.97}$$

$$V_{km}(t) = |d_{km}(t)| \tag{3.98}$$

$$\vartheta_{km}(t) = \arg\left[d_{km}(t)\right] \tag{3.99}$$

$$d_{km}(t) = \frac{2}{N_0}\int_0^t l^*_{km}(s,t)e^{-j\omega_c s}dz(s) \quad 0 \le t < \infty \tag{3.100}$$

the scalar $b_{km}(\boldsymbol{\theta}'_{k-1}, t)$ and phase $\varphi_{km}(\boldsymbol{\theta}'_{k-1}, t)$ are defined as

$$\frac{|\alpha_k| b_{km}(\boldsymbol{\theta}'_{k-1}, t)}{\sigma_k^2\sqrt{\epsilon_{km}(t)}} = d_{km}(t) - \sum_{n=0}^{k-1} e^m_{kn}(t)e^{j\theta'_n} \qquad \frac{|\alpha_0| b_{0m}(t)}{\sigma_0^2\sqrt{\epsilon_{0m}(t)}} = d_{0m}(t) \tag{3.101}$$

$$\varphi_{km}(\boldsymbol{\theta}'_{k-1}, t) = \arg\left[b_{km}(\boldsymbol{\theta}'_{k-1}, t)\right] - \arg\left[\alpha_k\right] \qquad \varphi_{0m}(t) = \arg\left[b_{0m}(t)\right] - \arg\left[\alpha_0\right]$$

and $e^m_{kn}(t)$ is given by

$$e^m_{kn}(t) = \begin{cases} e^{i_t m}_{kn}(t) & T'_m + \tau_0 < t < \infty \quad k,n = 0,\ldots,i_t - 1, \\ 0 & \text{else.} \end{cases}$$

$$= \frac{1}{N_0}\int_0^t l_{nm}(s,t)\,|\alpha_k|\,\tilde{s}^*_m(s-\tau_k)ds \quad 0 \le t < \infty \tag{3.102a}$$

$$= \frac{1}{N_0}\int_0^t l^*_{km}(s,t)\,|\alpha_n|\,\tilde{s}_m(s-\tau_n)ds \tag{3.102b}$$

$$\approx \frac{2}{N_0}\int_0^t l^*_{km}(s,t)e^{-j\omega_c s}\Re\left\{|\alpha_n|\tilde{s}_m(s-\tau_n)e^{j\omega_c s}\right\}ds \tag{3.102c}$$

where (3.102c) is obtained by taking the conjugate of (C.1) in Lemma C.1. This approximation corresponds to neglecting integrals containing double frequency terms. For $k = 0,\ldots,L-1$ $l_{km}(s,t)$ is given by[12]

$$l_{km}(s,t) = \begin{cases} l^{i_t}_{km}(s,t) & \begin{matrix} 0 \le s \le t \\ T'_m + \tau_0 < t < \infty \end{matrix} \quad k = 0,\ldots,i_t - 1, \\ 0 & \text{else.} \end{cases} \tag{3.103a}$$

$$= \frac{N_0|\alpha_k|}{\sigma_k^2\sqrt{\epsilon_{km}(t)\tilde{E}_m}}\sum_{l=0}^{L-1}\frac{\frac{\lambda_{lm}(t)}{2N_0}}{1+\frac{\lambda_{lm}(t)}{2N_0}}\left[x^m_{lk}(t)\right]^*\phi_{lm}(s,t) \quad \begin{matrix} 0 \le s \le t \\ 0 \le t < \infty \end{matrix} \tag{3.103b}$$

where $\lambda_{lm}(t)$, $\sqrt{\frac{\lambda_{lm}(t)}{\epsilon_{km}(t)}}x^m_{lk}(t)$ and $\sqrt{\lambda_{lm}(t)}\phi_{lm}(s,t)$ are respectively given by (3.37),

[12]Note that $l_{km}(s,t)$ defined as (3.103a) is equal to the $l_{km}(s,t)$ defined as (3.49) in Section 3.2.3. For convenience (3.49) is reprint as (3.103b).

(3.38) and (3.39b). The terms of $J_m(t)$ in (3.93) are defined as

$$\Pi_m(t) = \begin{cases} 1 & 0 \le t \le T_m' + \tau_0 \\ \Pi_{i_t m}(t) & T_m' + \tau_0 < t < \infty \end{cases}$$
$$= \prod_{k=0}^{2L-1} \left(1 + \frac{2}{N_0}\kappa_{km}(t)\right)^{-1/2} \qquad 0 \le t < \infty \qquad (3.104)$$

$$\mathfrak{l}_m(t) = \begin{cases} 0 & 0 \le t \le T_m' + \tau_0 \\ \mathfrak{l}_{i_t m}(t) & T_m' + \tau_0 < t < \infty \end{cases}$$
$$= \sum_{l=0}^{L-1} \frac{\lambda_{lm}^2(t)}{2N_0\left(1 + \frac{\lambda_{lm}(t)}{2N_0}\right)} \sum_{k=0}^{L-1} \frac{|\alpha_k|^2 |x_{lk}^m(t)|^2}{(2\sigma_k^2)^2 \epsilon_{km}(t)\tilde{E}_m} \qquad 0 \le t < \infty \qquad (3.105)$$

$$Z_m(t) = \begin{cases} 0 & 0 \le t \le T_m' + \tau_0 \\ Z_{i_t m}(t) & T_m' + \tau_0 < t < \infty \end{cases}$$
$$= \sum_{k=0}^{2L-1} \frac{\frac{2}{N_0}\kappa_{km}(t) z_{km}^2(t)}{1 + \frac{2}{N_0}\kappa_{km}(t)} \qquad 0 \le t < \infty \qquad (3.106)$$

For $k = 0, \ldots, 2L-1$ $\sqrt{\kappa_{km}(t)}z_{km}(t)$ is given by

$$\sqrt{\kappa_{km}(t)}z_{km}(t) = \begin{cases} \sqrt{\kappa_{km}^{i_t}(t)}z_{km}^{i_t}(t) & T_m' + \tau_0 < t < \infty \quad k = 0, \ldots, 2i_t - 1, \\ 0 & \text{else.} \end{cases}$$
$$= \sqrt{\kappa_{km}(t)} \int_0^t \Upsilon_{km}(s,t) dz(s) \qquad (3.107)$$

where $\kappa_{km}(t)$ and $\sqrt{\kappa_{km}(t)}\Upsilon_{km}(s,t)$ are given by (3.43) and (3.44).

Computation of the conditional mean using its definition

Due to the properties of conditional expectations, the conditional mean $\check{v}_m(t)$ can be found by using the equations:

$$\check{v}_m(t) \triangleq E\left[v_m(t)|\dot{z}(s), 0 \le s \le t, H_m\right] = E_{\boldsymbol{\theta}'}\left[\check{v}_{L-1m}(t, \boldsymbol{\theta}')|\dot{z}(s), 0 \le s \le t, H_m\right]$$
$$= E_{\theta_0'}\left[\check{v}_{0m}(t, \theta_0')|\dot{z}(s), 0 \le s \le t, H_m\right] \qquad (3.108)$$

where (3.108) is obtained by using iteratively the property of conditional expectation $E[Y] = E[E[Y|X]]$, and $\boldsymbol{\theta}'$, θ_0', $\breve{v}_{L-1m}(t,\boldsymbol{\theta}')$ and $\breve{v}_{0m}(t,\theta_0')$ are defined as follows:

$$\begin{aligned}
\boldsymbol{\theta}' &= \left[\theta_0', \ldots, \theta_{L-1}'\right]^T (= \boldsymbol{\theta}_{L-1}') \quad \theta_l' = \theta_l + \arg[\alpha_l] \quad {\scriptstyle l=0,\ldots,L-1} \\
\breve{v}_{L-1m}(t,\boldsymbol{\theta}') &= E_{\boldsymbol{a}}\left[v_m(t)|\boldsymbol{\theta}', \dot{z}(s), 0 \le s \le t, H_m\right] \triangleq \breve{v}_m(t|\boldsymbol{\theta}) \qquad (3.109) \\
\boldsymbol{a} &= [a_0, \ldots, a_{L-1}]^T \\
\breve{v}_{0m}(t,\theta_0') &\triangleq \breve{v}_{0m}(t,\boldsymbol{\theta}_0') \\
\breve{v}_{l-1m}(t,\boldsymbol{\theta}_{l-1}') &= E_{\theta_l'}\left[\breve{v}_{lm}(t,\boldsymbol{\theta}_l')|\boldsymbol{\theta}_{l-1}', \dot{z}(s), 0 \le s \le t, H_m\right] \quad {\scriptstyle l=1,\ldots,L-1} \quad {\scriptstyle L\ge 2} \qquad (3.110)
\end{aligned}$$

$\boldsymbol{\theta}_l'$ is given by (3.90), $E(\cdot|Y)$ denotes expectation with respect to $\boldsymbol{a}$ and $\boldsymbol{\theta}'$ given Y, and $E_x(\cdot|Y)$ denotes expectation with respect to x, given Y. By definition $\breve{v}_{L-1m}(t,\boldsymbol{\theta}')$ is the specular coherent conditional mean $\breve{v}_m(t|\boldsymbol{\theta})$ whose derivation can be found in Appendix D.1. Appendix D.2 presents an iterative method to derive $\breve{v}_{lm}(t,\boldsymbol{\theta}_l')$ for general L-path Ricean channels. Complete derivation of the conditional mean using (3.108) can be found in Appendix D.3 and Appendix D.4 for the special cases of mixed mode Ricean/Rayleigh channels and 2 Ricean/L-2 Rayleigh channels. From (D.20) the conditional mean for a mixed mode Ricean/Rayleigh channel is given by

$$\breve{v}_m(t) = \Re\left\{\left(2\int_0^t \mathcal{H}_m^*(s,t,t)e^{-j\omega_c s}dz(s) + V_{0m}'(t)e^{j\vartheta_{0m}'(t)}l_{0m}(t,t)e^{j\vartheta_{0m}(t)}\right)e^{j\omega_c t}\right\} \qquad (3.111)$$

where $\mathcal{H}_m(\tau,s,t)$ is given by (3.41), $l_{0m}(t,t)$ is given by (3.103), $V_{0m}(t)$ and $\vartheta_{0m}(t)$ are given by (3.98) and (3.99), $V_{0m}'(t)e^{j\vartheta_{0m}'(t)}$ is given by

$$V_{km}'(t)e^{j\vartheta_{km}'(t)} = \frac{\dfrac{\partial g(\boldsymbol{d}_m(t),t)}{\partial V_{km}(t)}}{g(\boldsymbol{d}_m(t),t)} + j\frac{\dfrac{1}{V_{km}(t)}\dfrac{\partial g(\boldsymbol{d}_m(t),t)}{\partial \vartheta_{km}(t)}}{g(\boldsymbol{d}_m(t),t)} \quad \begin{array}{l} V_{km}'(t)\text{: real, positive.} \\ k = 0, \ldots, L-1 \end{array} \qquad (3.112)$$

and $g(\boldsymbol{d}_m(t),t) = I_0(V_{0m}(t))$ while $\boldsymbol{d}_m(t)$ is given by (3.95). From (D.44) the condi-

tional mean for a 2 Ricean/L-2 Rayleigh channel is given by

$$\check{v}_m(t) = \Re\left\{\left(2\int_0^t \mathcal{H}_m^*(s,t,t)e^{-j\omega_c s}dz(s) + \sum_{k=0}^{1} V'_{km}(t)e^{j\vartheta'_{km}(t)}l_{km}(t,t)e^{j\vartheta_{km}(t)}\right)e^{j\omega_c t}\right\} \tag{3.113}$$

where $V'_{km}(t)e^{j\vartheta'_{km}(t)}$ is given by (3.112) and $g\big(\boldsymbol{d}_m(t),t\big)$ is given by

$$\begin{aligned} g\big(\boldsymbol{d}_m(t),t\big) &= I_0\big(V_{0m}(t)\big)I_0\big(V_{10}^m(t)\big)I_0\big(V_{1m}(t)\big) \\ &+ \sum_{p=1}^{\infty}(-1)^p I_p\big(V_{0m}(t)\big)I_p\big(V_{10}^m(t)\big)I_p\big(V_{1m}(t)\big)\cos\left(p\big(\vartheta_{0m}(t)+\vartheta_{10}^m(t)-\vartheta_{1m}(t)\big)\right) \end{aligned}$$

where $V_{km}(t)$, $\vartheta_{km}(t)$ are given by (3.98) and (3.99),

$$V_{kn}^m(t) = |e_{kn}^m(t)| = \left|\frac{1}{N_0}\int_0^t l_{nm}(s,t)\,|\alpha_k|\,\tilde{s}_m^*(s-\tau_k)ds\right| \tag{3.114}$$

$$\vartheta_{kn}^m(t) = \arg\left[e_{kn}^m(t)\right] = \arg\left[\frac{1}{N_0}\int_0^t l_{nm}(s,t)\,|\alpha_k|\,\tilde{s}_m^*(s-\tau_k)ds\right] \tag{3.115}$$

and alternative expressions of $e_{kn}^m(t)$ can be found in (3.102). Extrapolating the expressions of the conditional mean for these two special cases (3.111-3.113), it is to be conjectured that the expression of the conditional mean for an L-path Ricean channel is given by

$$\check{v}_m(t) = \Re\left\{\left(2\int_0^t \mathcal{H}_m^*(s,t,t)e^{-j\omega_c s}dz(s) + \sum_{k=0}^{L-1} V'_{km}(t)e^{j\vartheta'_{km}(t)}l_{km}(t,t)e^{j\vartheta_{km}(t)}\right)e^{j\omega_c t}\right\} \tag{3.116}$$

where $\mathcal{H}_m(\tau,s,t)$ is given by (3.41), $l_{km}(t,t)$ is given by (3.103), $\vartheta_{km}(t)$ is given by (3.99), $V'_{km}(t)e^{j\vartheta'_{km}(t)}$ is given by (3.112) and $g\big(\boldsymbol{d}_m(t),t\big)$ of (3.112) is the function present in $\Lambda_m(\dot{z};t)$ that is formed by multi-dimensional infinite series of products of Bessel and trigonometric functions that depends on $\{V_{km}(t),\vartheta_{km}(t)\}_{k=0,\ldots,L-1}$ and $\{V_{kn}^m(t),\vartheta_{kn}^m(t)\}_{k=0,\ldots,L-1,n<k}$ given respectively by (3.98-3.99) and (3.114-3.115). Note that the validity of (3.116) for a general L-path Ricean channel using the direct method has not been proven. Nevertheless (3.116) has been derived by using the Itô differentiation method as seen next (3.124a). The Itô differentiation method requires stronger assumptions, but the fact that (3.116) is still accurate for mixed mode

and 2 Ricean/L-2 Rayleigh channels without those extra assumptions motivates the conjecture that (3.116) is valid for any number of paths even without those stronger assumptions.

Computation of the conditional mean by using Itô differentiation of the likelihood ratio

Provided that the likelihood ratio is known over any observation interval $[0, t]$ (denoted $\Lambda_m(\dot{z}; t)$), the conditional mean $\breve{v}_m(t)$ can be obtained by the formula [186]

$$\breve{v}_m(t) = \sqrt{\frac{N_0}{2}} \frac{d\Lambda_m(\dot{z}; t)}{\Lambda_m(\dot{z}; t)} \frac{1}{\frac{dz(t)}{\sqrt{\frac{N_0}{2}}}} = \frac{N_0}{2} \frac{d\Lambda_m(\dot{z}; t)}{\Lambda_m(\dot{z}; t)\, dz(t)} \tag{3.117}$$

where $d(\cdot)$ denotes the Itô differential (see Appendix A). Equation (3.117) is obtained by Itô differentiating the log-likelihood ratio over an observation $[0, t]$ given by

$$\ln \Lambda_m(\dot{z}; t) = \frac{2}{N_0} \left[\int_0^t \breve{v}_m(s) dz(s) - \frac{1}{2} \int_0^t \breve{v}_m^2(s) ds \right]$$

For convenience differentiation of a slightly more general function than the likelihood ratio is performed such that the obtained results can be used for optimum as well as suboptimum receivers. Specifically a function of the following type is considered.

$$\mathcal{F}_m(\dot{z}; t) = J_m(t) g\big(\boldsymbol{d}_m(t), t\big)$$

where $J_m(t)$ is given by (3.93), the vector $\boldsymbol{d}_m(t)$ is given by (3.95) and $g\big(\boldsymbol{d}_m(t), t\big)$ is an arbitrary scalar function of $\boldsymbol{d}_m(t)$ and t satisfying $g\big(\boldsymbol{d}_m(0), 0\big) = 1$ that possesses continuous first and second order partial derivatives with respect to any components of $\boldsymbol{d}_m(t)$ and a continuous first order partial derivative with respect to t. As seen earlier in this section (topic: "Likelihood ratio over an arbitrary observation interval $[0, t]$ assuming that $\tilde{s}_m(s)$ is time-limited"), when $\mathcal{F}_m(\dot{z}; t)$ is the m^{th} likelihood ratio for an L-path Ricean channel, $g(\boldsymbol{d}_m(t), t)$ is the sum of multi-dimensional infinite series of products of Bessel and trigonometric functions. Suboptimal receiver structures are derived in subsequent sections. For example modifying results from Section 3.7.2 to take into account the arbitrary observation interval $[0, t]$, from (3.174) it can be shown that $\mathcal{F}_m(\dot{z}; t)$ represents the m^{th} decision variable for the Quadratic Decor-

relation Receiver (QDR) scheme over mixed mode Ricean/Rayleigh channels when $g(\boldsymbol{d}_m(t), t) = \exp\{cV_{0m}^2(t)\}$. Since the decision variable $J_m(t)\exp\{cV_{0m}^2(t)\}$ for the QDR scheme is not a likelihood ratio, it does not have an estimator-correlator form as defined in (3.82), however, a quasi estimator-correlator form, as called in this thesis, can be defined based on the following proposition.

Proposition 3.3.2. *Assume that an arbitrary function $\mathcal{F}_m(\dot{z};t)$ can be written as*

$$d\mathcal{F}_m(\dot{z};t) = \mathcal{F}_m'(t)dt + \mathcal{F}_m''(t)dz(t) \tag{3.118}$$

where $d(\cdot)$ represents the Itô differentiation of $\mathcal{F}_m(\dot{z};t)$, $\mathcal{F}_m'(t)$ and $\mathcal{F}_m''(t)$ are non-anticipating processes jointly measurable in (t,ω) satisfying $\forall\, t \in [0,T_o]$ $\int_0^t E\left|\mathcal{F}_m'(s)\right| ds < \infty$, $\int_0^t E\left|\mathcal{F}_m''(s)\right|^2 ds < \infty$ and $z(t)$ is an Itô process of the form $dz(t) = v_m(t) + dw(t)$, $_{m=0,\ldots,L-1}$. Then if $\mathcal{F}_m(\dot{z};0) = 1$

$$\mathcal{F}_m(\dot{z};T_o) = \exp\left\{\frac{2}{N_0}\left[\int_0^{T_o} \widehat{v_m(t)}\, dz(t) - \frac{1}{2}\int_0^{T_o}\left(\widehat{v_m(t)}\right)^2 dt + \frac{N_0}{2}\int_0^{T_o}\frac{\mathcal{F}_m'(t)}{\mathcal{F}_m(\dot{z};t)}dt\right]\right\} \tag{3.119}$$

where the estimate $\widehat{v_m(t)}$ is equal to $\frac{N_0}{2}\frac{\mathcal{F}_m''(t)}{\mathcal{F}_m(\dot{z};t)}$ and can be obtained from $\mathcal{F}_m(\dot{z};t)$ by using

$$\widehat{v_m(t)} = \frac{N_0}{2}\left[\frac{d\mathcal{F}_m(\dot{z};t)}{\mathcal{F}_m(\dot{z};t)\,dz(t)} - \frac{\mathcal{F}_m'(t)dt}{\mathcal{F}_m(\dot{z};t)\,dz(t)}\right] \tag{3.120}$$

In this thesis (3.119) is called the quasi estimator-correlator form of a receiver (sub-optimum as well as optimum) whose m^{th} decision variable is equal to $\mathcal{F}_m(\dot{z};t)$. If $\mathcal{F}_m(\dot{z};t)$ is a likelihood ratio, from [21], it can expressed as (3.82) which is the true estimator-correlator form of any optimum receiver. In that case $\int_0^{T_o}\frac{\mathcal{F}_m'(t)}{\mathcal{F}_m(\dot{z};t)}dt = 0$ and $\widehat{v_m(t)} = \breve{v}_m(t)$ is the MMSE estimator.

Proof. Substituting $dz(t) = v_m(t)dt + dw(t)$ into (3.118) yields

$$d\mathcal{F}_m(\dot{z};t) = \left(\mathcal{F}_m''(t)v_m(t) + \mathcal{F}_m'(t)\right)dt + \mathcal{F}_m''(t)dw(t) \tag{3.121}$$

Let $\widehat{v_m(t)} = \frac{N_0}{2}\frac{\mathcal{F}_m'(t)}{\mathcal{F}_m(\dot{z};t)}$, from (3.118)

$$\frac{d\mathcal{F}_m(\dot{z};t)}{\mathcal{F}_m(\dot{z};t)} = \frac{2}{N_0}\widehat{v_m(t)}\,dz(t) + \frac{\mathcal{F}_m'(t)}{\mathcal{F}_m(\dot{z};t)}dt$$

which is a symbolic notation for

$$\int_0^{T_o}\frac{d\mathcal{F}_m(\dot{z};t)}{\mathcal{F}_m(\dot{z};t)} = \frac{2}{N_0}\int_0^{T_o}\widehat{v_m(t)}\,dz(t) + \int_0^{T_o}\frac{\mathcal{F}_m'(t)}{\mathcal{F}_m(\dot{z};t)}dt \qquad (3.122)$$

Using (3.121) and the Itô differentiation rule (A.13) on $\ln\big(\mathcal{F}_m(\dot{z};t)\big)$, the left-end side of (3.122) can also be written as

$$\int_0^{T_o}\frac{d\mathcal{F}_m(\dot{z};t)}{\mathcal{F}_m(\dot{z};t)} = \ln\big[\mathcal{F}_m(\dot{z};T_o)\big] - \ln\big[\mathcal{F}_m(\dot{z};0)\big] + \frac{1}{2}\frac{N_0}{2}\int_0^{T_o}\frac{\mathcal{F}_m''^2(t)}{\mathcal{F}_m^2(\dot{z};t)}dt \qquad (3.123)$$

If $\mathcal{F}_m(\dot{z};0) = 1$, substituting (3.122) into (3.123) and using $\widehat{v_m(t)} = \frac{N_0}{2}\frac{\mathcal{F}_m'(t)}{\mathcal{F}_m(\dot{z};t)}$ yields (3.119) the quasi estimator-correlator form for an arbitrary receiver whose decision variable under H_m is given by $\mathcal{F}_m(\dot{z};t)$. **Q.E.D**

The Itô differentiation of $\mathcal{F}_m(\dot{z};t) = J_m(t)g\big(\boldsymbol{d}_m(t),t\big)$ present in (3.117) and (3.120) is carried out in Appendix E under the following assumptions

1. $\forall r = 1,\ldots,L$ there exists functions[13] $\{x_{lk}^{rm}(t)\}_{l,k=0,\ldots,r-1}$ continuously differentiable on $\big(T_m' + \tau_{r-1}, T_m' + \tau_r\big]$ such that the $r\times r$ matrix $\boldsymbol{X}_{rm}(t)$ defined as $[\boldsymbol{X}_{rm}(t)]_{lk} = x_{lk}^{rm}(t)$ satisfies the equations $\boldsymbol{X}_{rm}^*(t)\boldsymbol{\Gamma}_{rm}^*(t)\boldsymbol{X}_{rm}^T(t) = \boldsymbol{I}_r$ and $\boldsymbol{\epsilon}_{rm}(t)\boldsymbol{C}_r\boldsymbol{\Gamma}_{rm}^*(t)\boldsymbol{X}_{rm}^T(t) = \boldsymbol{X}_{rm}^T(t)\boldsymbol{D}_{rm}(t)$ where $\boldsymbol{I}_r$ is the $r\times r$ identity matrix, $\boldsymbol{D}_{rm}(t)$ is an $r\times r$ diagonal matrix whose diagonal entries are the eigenvalues of $\boldsymbol{\epsilon}_{rm}(t)\boldsymbol{C}_r\boldsymbol{\Gamma}_{rm}^*(t)$, $\boldsymbol{\epsilon}_{rm}(t)$ and $\boldsymbol{C}_r$ are $r\times r$ diagonal matrices such that $[\boldsymbol{\epsilon}_{rm}]_{ll} = \epsilon_{lm}(t) = \frac{1}{\tilde{E}_m}\int_0^t|\tilde{s}_m(s-\tau_l)|^2\,ds$, $[\boldsymbol{C}_r]_{ll} = 2\sigma_l^2$, $\boldsymbol{\Gamma}_{rm}(t)$ is the $r\times r$ signal correlation matrix defined by[13] $[\boldsymbol{\Gamma}_{rm}(t)]_{lk} = \rho_{lk}^m(t) = \frac{1}{\sqrt{\epsilon_{lm}(t)\epsilon_{km}(t)\tilde{E}_m}}\int_0^t\tilde{s}_m(s-\tau_l)\tilde{s}_m^*(s-\tau_k)ds$.

2. $\forall r = 1,\ldots,L$ the eigenvalues of $\boldsymbol{\epsilon}_{rm}(t)\tilde{E}_m\boldsymbol{C}_r\boldsymbol{\Gamma}_{rm}^*(t)$, $\{\lambda_{lm}^r(t)\}_{l=0,\ldots,r-1}$ are distinct.

These assumptions are not too restrictive. For example it is shown in Appendix E.3.2 that they are satisfied in the case of non-degenerate two-path channels (i.e. $2\sigma_0^2 \neq$

[13]The superscripts are not exponents.

$0, 2\sigma_1^2 \neq 0$) such that $\forall\, t > T_m' + \tau_1$, the complex correlation coefficient between the signals $\tilde{s}_m(s-\tau_0)$ and $\tilde{s}_m(s-\tau_1)$ $\rho_{01}^m(t)$ over any observation interval $[0,t]$ is non-zero. More precisely $\forall\, t \in \left(T_m' + \tau_0, T_m' + \tau_1\right]$, there is only one eigenvalue $\lambda_{0m}^1(t)$ that is necessarily distinct and there exists at least one continuously differentiable function $x_{00}^{1m}(t)$ satisfying conditions described in Assumption 1, namely $x_{00}^{1m}(t) = 1$. Assume that $\forall\, t > T_m' + \tau_1$, $\rho_{01}^m(t) \neq 0$. Then $\boldsymbol{\epsilon}_{2m}(t)\tilde{\boldsymbol{E}}_m \boldsymbol{C}_2 \boldsymbol{\Gamma}_{2m}^*(t)$ has two distinct eigenvalues $\{\lambda_{lm}^2(t)\}_{l=0,1}$ given for example by (E.56)[14]. There also exists continuously differentiable functions $\{x_{lk}^{2m}(t)\}_{l,k=0,1}$ (given by (E.58)) satisfying conditions described in Assumption 1. The assumption that $\forall\, t > T_m' + \tau_1$, $\rho_{01}^m(t) \neq 0$ is not too restricting. It can be shown for example that for FSK, $\rho_{01}^m(t) = 0$ necessarily implies that $\tau_1 - \tau_0 \geq T$ which corresponds to resolved multipath. Similarly it can be shown that for DPSK or SDPSK, $\rho_{01}^m(t) = 0$ necessarily implies that $\tau_1 - \tau_0 \geq 2T$ which corresponds to resolved multipath for that modulation.

Assumption 1 ensures that the eigenfunctions $\left\{\phi_{lm}^{i_t}(s,t)\right\}_{l=0,\ldots,i_t-1}$ defined by (3.34) can be chosen to be differentiable. Since i_t is a t-staircase function defined by (B.3), there are only a finite number of eigenfunctions denoted $\phi_{1m}^1(s,t)$, $\{\phi_{lm}^2(s,t)\}_{l=0,1}, \ldots,$ $\left\{\phi_{lm}^L(s,t)\right\}_{l=0,\ldots,L-1}$. These functions are expressed in terms of $x_{11}^{1m}(t)$, $\{x_{lk}^{2m}(t)\}_{l,k=0,1}$, $\ldots, \left\{x_{lk}^{Lm}(t)\right\}_{l,k=0,\ldots,L-1}$ which are not unique. If $\forall\, r = 1, \ldots, L$, the chosen functions $\{x_{lk}^{rm}(t)\}_{l,k=0,\ldots,r-1}$ are continuously differentiable then $\{\phi_{lm}^r(s,t)\}_{l=0,\ldots,r-1}$ are also continuously differentiable. Assumption 1 ensures that such a choice is possible. Assumption 2 is used for consistency since differentiability of the functions $\{x_{lk}^{rm}(t)\}_{l,k=0,\ldots,r-1}$ is very likely not to be guaranteed whenever the corresponding eigenvalues $\lambda_{lm}^r(t)$ are not distinct even for the simple case of two-path Ricean channels.

The L-path Ricean channels likelihood ratio, $\Lambda_m(\dot{z};t)$, is of the form $J_m(t)g\big(\boldsymbol{d}_m(t),t\big)$ where $g\big(\boldsymbol{d}_m(t),t\big)$ is the sum of multi-dimensional infinite series of products of Bessel and trigonometric functions. Hence results of Appendix E can be used. From (E.53) the Itô derivative of $\Lambda_m(\dot{z};t)$ is of the form (3.118) where $\mathcal{F}_m'(t) = \mathcal{R}_{2m}(t)\Lambda_m(\dot{z};t)$. Since $\Lambda_m(\dot{z};t)$ is a likelihood ratio, $\int_0^{T_o} \frac{\mathcal{F}_m'(t)}{\Lambda_m(\dot{z};t)}dt = 0$ (symbolically $\mathcal{R}_{2m}(t) = 0$). Combining (3.117) and (E.53) with $\mathcal{R}_{2m}(t) = 0$, $\forall\, t > T_m' + \tau_0$ the conditional mean $\check{v}_m(t)$

[14]The expression of the set $\left\{\lambda_{lm}^2(t)\right\}_{l=0,1}$ is unique but the numbering of the elements in the set is not, (E.56) is an example of numbering.

for an L-path Ricean channel with non-coherent detection is given by[15]

$$\check{v}_m(t) = \Re\left\{\left(2\int_0^t \mathcal{H}_m^*(s,t,t)e^{-j\omega_c s}dz(s) + \sum_{k=0}^{L-1} V_{km}'(t)e^{j\vartheta_{km}'(t)}l_{km}(t,t)e^{j\vartheta_{km}(t)}\right)e^{j\omega_c t}\right\} \tag{3.124a}$$

where $\mathcal{H}_m(s,t,t)$ is given by (3.41), $V_{km}'(t)e^{j\vartheta_{km}'(t)}$ is given by (3.112), $l_{km}(t,t)$ is given by (3.103) and $\vartheta_{km}(t)$ is given by (3.99). Note that (3.124a) obtained by Itô differentiation reduces to (3.111) for mixed mode Ricean/Rayleigh channels and (3.113) for 2 Ricean/L-2 Rayleigh channels, both obtained by the direct method. Substituting $h_m(t,s) = \Re\left\{2\mathcal{H}_m^*(s,t,t)e^{j\omega_c(t-s)}\right\}$ into (3.124a) yields

$$\check{v}_m(t) = \int_0^t h_m(t,s)dz(s) + \Re\left\{\left(\sum_{k=0}^{L-1} V_{km}'(t)e^{j\vartheta_{km}'(t)}l_{km}(t,t)e^{j\vartheta_{km}(t)}\right)e^{j\omega_c t}\right\} \tag{3.124b}$$

where $h_m(t,s) = H_m(s,t,t) = H_m(t,s,t)$ is given by (3.42).

Substituting (C.27) into (3.124b) and using $h_m(t,s) = H_m(t,s,t)$ yield

$$\begin{aligned}\check{v}_m(t) &= \int_0^t h_m(t,s)dz(s) + \Re\left\{\sum_{k=0}^{L-1} V_{km}'(t)e^{j\vartheta_{km}'(t)}e^{j\vartheta_{km}(t)}\,|\alpha_k|\,\tilde{s}_m(t-\tau_k)e^{j\omega_c t}\right\} \\ &\quad - \Re\left\{\int_0^t \sum_{k=0}^{L-1} V_{km}'(t)e^{j\vartheta_{km}'(t)}e^{j\vartheta_{km}(t)}\,|\alpha_k|\,\tilde{s}_m(s-\tau_k)e^{j\omega_c s}h_m(t,s)ds\right\} \\ &= \int_0^t h_m(t,s)dy_m^{\mathrm{nc}}(s) + \Re\left\{\sum_{k=0}^{L-1} V_{km}'(t)e^{j\vartheta_{km}'(t)}e^{j\vartheta_{km}(t)}\,|\alpha_k|\,\tilde{s}_m(t-\tau_k)e^{j\omega_c t}\right\}\end{aligned} \tag{3.125a}$$

and $y_m^{\mathrm{nc}}(s)$ is given by (3.126). Substituting $h_m(t,s) = \Re\left\{2\mathcal{H}_m^*(s,t,t)e^{j\omega_c(t-s)}\right\}$ into (3.125a) and using that $y_m^{\mathrm{nc}}(s)$ is real yield

$$\check{v}_m(t) = \Re\left\{\left(2\int_0^t \mathcal{H}_m^*(s,t,t)e^{-j\omega_c s}dy_m^{\mathrm{nc}}(s) + \sum_{k=0}^{L-1} |\alpha_k|\,V_{km}'(t)e^{j\vartheta_{km}'(t)}e^{j\vartheta_{km}(t)}\tilde{s}_m(t-\tau_k)\right)e^{j\omega_c t}\right\} \tag{3.125b}$$

[15]Since for $t < T_m' + \tau_0$, $v_m(t) = 0$ then $\check{v}_m(t) = 0$. Therefore (3.124) is valid for any $t \geq 0$.

where $y_m^{\mathrm{nc}}(s)$ is given by[16]

$$dy_m^{\mathrm{nc}}(s) = dz(s) - \Re\left\{\sum_{k=0}^{L-1} V_{km}'(t)e^{j\vartheta_{km}'(t)}e^{j\vartheta_{km}(t)}\,|\alpha_k|\,\tilde{s}_m(s-\tau_k)e^{j\omega_c s}\right\}ds \qquad (3.126)$$

$\mathcal{H}_m(s,t,t)$ is given by (3.41), $V_{km}'(t)e^{j\vartheta_{km}'(t)}$ is given by (3.112) and $\vartheta_{km}(t)$ is given by (3.99).

The next section will focus on giving physical interpretations of the expression for the conditional mean estimator $\check{v}_m(t)$.

Interpretation of the expression for the conditional mean estimator $\check{v}_m(t)$

An interpretation of $y_m^{\mathrm{nc}}(s)$ is as follows: let us define the estimate of $e^{j\theta_k'}$ based on an observation on $[0,t]$, $\widehat{e^{j\theta_k'}(t)}$ as

$$\widehat{e^{j\theta_k'}(t)} = V_{km}'(t)e^{j\vartheta_{km}'(t)}e^{j\vartheta_{km}(t)} \qquad (3.127)$$

where $V_{km}'(t)e^{j\vartheta_{km}'(t)}$ and $\vartheta_{km}(t)$ are given by (3.112) and (3.99). Then (3.126) is also given by

$$dy_m^{\mathrm{nc}}(s) = dz(s) - \Re\left\{\sum_{k=0}^{L-1} |\alpha_k|\ \widehat{e^{j\theta_k'}(t)}\ \tilde{s}_m(s-\tau_k)e^{j\omega_c s}\right\}ds \qquad (3.128)$$

From (3.128) it is seen that $y_m^{\mathrm{nc}}(s)$ represents the remaining unknown part of the observation (or received signal) after the specular component phasors[17] $\left\{e^{j\theta_k'}\right\}_k$ have been estimated. From (3.41)

$$2\int_0^t \mathcal{H}_m^*(s,t,t)e^{-j\omega_c s}dy_m^{\mathrm{nc}}(s) = 2\int_0^t \sum_{l=0}^{L-1} \frac{\frac{\lambda_{lm}(t)}{2N_0}}{1+\frac{\lambda_{lm}(t)}{2N_0}}\phi_{lm}^*(s,t)\phi_{lm}(t,t)e^{-j\omega_c s}dy_m^{\mathrm{nc}}(s) \qquad (3.129)$$

[16]The superscript nc is not an exponent.

[17]The k^{th} specular component phasor is defined in this thesis as $e^{j\theta_k'}$ where $\theta_k' = \theta_k + \arg[\alpha_k]$ is the k^{th} specular component phase.

Replacing $\sqrt{\lambda_{lm}(t)}\phi_{lm}(t,t)$ with (3.39b) yields

$$2\int_0^t \mathcal{H}_m^*(s,t,t)e^{-j\omega_c s}dy_m^{\mathrm{nc}}(s) = \sum_{k=0}^{L-1} \widehat{a_k'(t)}\ \tilde{s}_m(t-\tau_k) \tag{3.130}$$

where $\widehat{a_k'(t)}$, estimate of a_k' based on the observation interval $[0,t]$, is defined as

$$\widehat{a_k'(t)} = \frac{2}{\sqrt{\epsilon_{km}(t)\tilde{E}_m}} \sum_{l=0}^{L-1} \frac{\frac{\lambda_{lm}(t)}{2N_0}}{1+\frac{\lambda_{lm}(t)}{2N_0}} x_{lk}^m(t) \int_0^t \phi_{lm}^*(s,t)e^{-j\omega_c s}dy_m^{\mathrm{nc}}(s) \tag{3.131a}$$

$$= \frac{2\sigma_k^2}{N_0}\int_0^t \frac{l_{km}^*(s,t)}{|\alpha_k|}e^{-j\omega_c s}dy_m^{\mathrm{nc}}(s) \quad \text{from (3.103b)} \tag{3.131b}$$

while $l_{km}(s,t)$ and $y_m^{\mathrm{nc}}(s)$ are respectively given by (3.103) and (3.128). Substituting (3.127) and (3.130) into (3.125b) yields

$$\check{v}_m(t) = \Re\left\{\left(\sum_{k=0}^{L-1} \widehat{a_k'(t)}\ \tilde{s}_m(t-\tau_k) + \sum_{k=0}^{L-1}|\alpha_k|\ \widehat{e^{j\theta_k'(t)}}\ \tilde{s}_m(t-\tau_k)\right)e^{j\omega_c t}\right\} \tag{3.132}$$

where $\widehat{a_k'(t)}$ and $\widehat{e^{j\theta_k'(t)}}$ are respectively given by (3.131) and (3.127). From Section 3.2.3 the noiseless received signal is given by (3.45). Comparing (3.132) and (3.45) shows that the MMSE estimate of a multipath fading signal has the same "multipath" form with the amplitudes $\{a_k'\}_k$ and specular component phasors $\left\{e^{j\theta_k'}\right\}_k$ replaced by estimates. From (3.131b) it is seen that the amplitude estimates are obtained by filtering of the unknown part of the received signal (3.128) by the filter $\frac{2\sigma_k^2}{N_0}\frac{l_{km}^*(s,t)}{|\alpha_k|}e^{-j\omega_c s}$. Similarly to Section 3.2.3 the filter takes into account both the multipath unresolvability and fading as seen in the following.

From Section 3.2.3 the noiseless received signal can be rewritten as (3.51). Substituting (3.129) and (3.127) into (3.125b), the conditional mean $\check{v}_m(t)$ can be rewritten as

$$\check{v}_m(t) = \Re\left\{\left(\sum_{l=0}^{L-1} \widehat{a_{lm}''(t)}\ \sqrt{\epsilon_{lm}(t)\tilde{E}_m}\phi_{lm}(t,t) + \sum_{l=0}^{L-1}|\alpha_l|\ \widehat{e^{j\theta_l'(t)}}\ \tilde{s}_m(t-\tau_l)\right)e^{j\omega_c t}\right\}$$

where

$$\widehat{a''_{lm}(t)} = \frac{2}{\sqrt{\epsilon_{lm}(t)\tilde{E}_m}} \frac{\frac{\lambda_{lm}(t)}{2N_0}}{1+\frac{\lambda_{lm}(t)}{2N_0}} \int_0^t \phi^*_{lm}(s,t) e^{-j\omega_c s} dy^{nc}_m(s) \qquad (3.133)$$

Comparing (3.133) with (3.54) and (3.131) with (3.48) shows that the multipath amplitude estimations for specular coherent and non-coherent detection are similar, except that the remaining unknown part of the observation for specular coherent detection, (3.29), is obtained by subtracting the known specular term from the received signal, whereas for non-coherent detection (3.128) is obtained by subtracting an estimate of the specular term. This was to be expected since the non-coherent estimator does not have the knowledge of the specular component phases, thus it uses an estimate of the specular term. From (3.131a) and (3.133), $\widehat{a'_k(t)}$ and $\widehat{a''_{lm}(t)}$ are linked by the same equation as (3.55) links $\widehat{a'_k(t|\boldsymbol{\theta})}$ and $\widehat{a''_{lm}(t|\boldsymbol{\theta})}$. The estimates of the unresolved multipath fading channel gains $\{a'_k\}_k$ are formed by first transforming the unresolved multipath channel into an equivalent decorrelated channel with zero mean multipath gains given by (3.52), and then estimating the zero mean path gains of the decorrelated multipath channel $\{a''_{lm}(t)\}_l$ by matched filtering as for a resolved multipath channel. From (3.133) it is seen that the gain estimate $\widehat{a''_{lm}(t)}$ employs only the information related to the l^{th} path of the decorrelated multipath channel. At low SNR a-priori information is used and $\widehat{a''_{lm}(t)} \approx 0$ which corresponds to the mean of $a''_{lm}(t)$. At high SNR, a-posteriori information is used as in Section 3.2.3. In the limit of no noise ($\dot{w}(s) = 0$) and perfect phasor estimation (i.e. $\forall k \ \widehat{e^{j\theta'_k}(t)} = e^{j\theta'_k}$), from (3.40b), (3.45), (3.52), (3.133) and the orthogonality of $\{\phi_{lm}(s,t) = \phi^{i_t}_{lm}(s,t)\}_{l=0,\ldots,i_t-1}$, under $H_m \ \ \forall l = 0,\ldots,i_t-1 \ \ \widehat{a''_{lm}(t)} = a''_{lm}(t)$.

The MMSE estimate of the specular term composed of the sum of random phase fixed amplitude signals is a little more complex. From (3.132) it is seen that the MMSE specular component estimate is obtained not by estimating individually the random specular component phases $\{\theta'_k\}_k$ but by estimating the specular component phasors $\left\{e^{j\theta'_k}\right\}_k$. Equation (3.127) shows that the k^{th} specular component phasor estimate involves a phase estimator of the k^{th} random phase (in this case $\vartheta_{km}(t) + \vartheta'_{km}(t)$) that is substituted for the k^{th} random phase θ'_k. But the k^{th} obtained signal estimate is then scaled by the factor $V'_{km}(t)$ that takes into account the presence of all the other randomly phase-shifted specular components since the multipath is unre-

solved. By definition the MMSE estimate for a signal minimizes the error between the estimate and the actual signal. Hence it can be expected that the scaling term $V'_{km}(t)$ reduces the difference between the signal estimate and the actual phasor in case the phase estimate is far from the actual value. In order to provide insight to $\widehat{e^{j\theta'_k}(t)} = V'_m(t)e^{j(\vartheta'_m(t)+\vartheta_m(t))}$ let us consider a simple random phase channel with received signal $\dot{z}(s) = \Re\left\{\tilde{v}_A(s)e^{j\theta}e^{j\omega_c s}\right\} + \dot{w}(s), 0 \leq s \leq T_o$, where $\tilde{v}_A(s)$ is a known complex low-pass function and $E\left[\dot{w}(s)\dot{w}(u)\right] = \delta(s-u)$.

Modifying results from [21], the MMSE estimate (conditional mean) of $v(t) = \Re\left\{\tilde{v}_A(t)e^{j\theta}e^{j\omega_c t}\right\}$ is given by

$$\check{v}(t) = \Re\left\{\frac{I_1(V_A(t))}{I_0(V_A(t))}\tilde{v}_A(t)e^{j\vartheta_A(t)}e^{j\omega_c t}\right\}$$

where $V_A(t)$ is a real non-negative function obtained from

$$V_A(t)e^{j\vartheta_A(t)} = \int_0^t \tilde{v}_A^*(s)e^{-j\omega_c s}dz(s) \tag{3.134}$$

Hence the conditional mean of a random phase channel can be written as

$$\check{v}(t) = \Re\left\{\tilde{v}_A(t)\,\widehat{e^{j\theta}(t)}\,e^{j\omega_c t}\right\}$$

where

$$\widehat{e^{j\theta}(t)} = \frac{I_1(V_A(t))}{I_0(V_A(t))}e^{j\vartheta_A(t)} \tag{3.135}$$

From (3.134) it is seen that $V_A(t)$ and $\vartheta_A(t)$ are obtained by taking respectively the amplitude (or absolute value) and phase of the correlation of the preenvelope (complex analytic) of the noiseless received signal excluding the random phase θ, $\tilde{v}_A(s)e^{j\omega_c s}$, with the received signal.

Compared to the simple random phase channel, two difficulties appear in the case of an unresolved multipath Ricean channel. First the multipath is unresolved which implies that the phases of each path specular component cannot be estimated individually. This can be observed from (3.127) where the term $V'_{km}(t)e^{j\vartheta'_{km}(t)}$ given by (3.112) depends on all the multipath components. As will be seen later, when the

multipath is resolved this term reduces to $\frac{I_1(V_{km}(t))}{I_0(V_{km}(t))}$ which corresponds to the non-fading random phase channel (3.135). Secondly, besides the unresolvability difficulty, the received signal has a fading component part. The simpler approach to take into account the channel fading in the phase estimation is to consider the Rayleigh component as noise and whiten it. This approach is followed by the phase estimator as shown by the presence of the filter $\frac{2}{N_0} l^*_{km}(s,t)e^{-j\omega_c s}$ in the expression of $V_{km}(t)$ and $\vartheta_{km}(t)$ (see 3.98-3.100).

From (3.45) the received signal can be rewritten as

$$dz(s) = \left[\Re\left\{\left(|\alpha_k|\,\tilde{s}_m(s-\tau_k)e^{j\theta'_k}\right)e^{j\omega_c s}\right\} + v^d_{km}(s) + n_c(s)\right]ds \tag{3.136}$$

where $v^d_{km}(s)$ (the specular component excluding the k^{th} path) is given by[18]

$$v^d_{km}(s) = \Re\left\{\left(\sum_{\substack{r=0\\ r\neq k}}^{L-1} |\alpha_r|\,\tilde{s}_m(s-\tau_r)e^{j\theta'_r}\right)e^{j\omega_c s}\right\} \tag{3.137}$$

and $n_c(s)$ is a zero mean colored Gaussian noise defined as

$$n_c(s) \triangleq \Re\left\{\left(\sum_{r=0}^{L-1} a'_r \tilde{s}_m(s-\tau_r)\right)e^{j\omega_c s}\right\} + \dot{w}(s)$$

The covariance function of $n_c(s)$ is given by

$$K_{cm}(s,u) \triangleq E\left[n_c(s)n_c(u)\right] = \frac{N_0}{2}\delta(s-u) + K_m(s,u) \tag{3.138}$$

Since $n_c(s)$ is not white, a new equivalent estimation problem can be obtained by passing the received signal through a whitening filter $H_{*m}(s,u,t)$ such that [187, pp. 290-297]

$$E\left[n_{*c}(s)n_{*c}(u)\right] = \delta(s-u)$$

where $n_{*c}(s) \triangleq \int_0^t H_{*m}(s,u,t)n_c(u)du$. From (3.136) the whitened received signal

[18]The superscript d is not an exponent.

$\dot{z}_*(s)$ is given by

$$\dot{z}_*(s) \triangleq \int_0^t H_{*m}(s,u,t)dz(u) \tag{3.139a}$$

$$= \int_0^t H_{*m}(s,u,t)\Re\left\{\left(|\alpha_k|\,\tilde{s}_m(u-\tau_k)e^{j\theta'_k}\right)e^{j\omega_c u}\right\}du + v^d_{*k}(s) + n_{*c}(s) \tag{3.139b}$$

$$= \Re\left\{\left(\int_0^t H_{*m}(s,u,t)\,|\alpha_k|\,\tilde{s}_m(u-\tau_k)e^{j\omega_c(u-s)}du\right)e^{j\theta'_k}e^{j\omega_c s}\right\} + v^d_{*k}(s) + n_{*c}(s) \tag{3.139c}$$

where from (3.137) $v^d_{*k}(s)$ is given by

$$v^d_{*k}(s) \triangleq \int_0^t H_{*m}(s,u,t)v^d_{km}(u)du \tag{3.140a}$$

$$= \int_0^t H_{*m}(s,u,t)\,\Re\left\{\left(\sum_{\substack{r=0\\ r\neq k}}^{L-1}|\alpha_r|\,\tilde{s}_m(u-\tau_r)e^{j\theta'_r}\right)e^{j\omega_c u}\right\}du \tag{3.140b}$$

One interpretation of the phase estimator is obtained by using a whitening approach for $v^d_{*k}(s)+n_{*c}(s)$ that is generally a non Gaussian random process due to the presence of $\boldsymbol{\theta}'$ (see (3.140b)). Another simpler interpretation of the phase estimator follows. Considering the new received signal $\dot{z}_*(s) - v^d_{*k}(s)$, (3.139c) is similar to the random phase channel. Since the term $v^d_{*k}(s)$ is unknown, the phase estimator uses an estimate of that signal, $\widehat{v^d_{*k}(s)}$. The simplest estimate of a random process is its a-priori mean. Hence $\widehat{v^d_{*k}(s)} = E\left[v^d_{*k}(s)\right] = 0$. Recall that the phasor estimate (3.127) depends nonlinearly on the terms $V_{km}(t)$ and $\vartheta_{km}(t)$. From (C.27)

$$\frac{2}{N_0}l^*_{km}(u,t)e^{-j\omega_c u} = \frac{2}{N_0}\left[|\alpha_k|\tilde{s}^*_m(u-\tau_k)e^{-j\omega_c u} - |\alpha_k|\int_0^t \tilde{s}^*_m(v-\tau_k)e^{-j\omega_c v}H_m(u,v,t)dv\right]$$

$$= \int_0^t Q_{*m}(u,v,t)\,|\alpha_k|\,\tilde{s}^*_m(v-\tau_k)e^{-j\omega_c v}dv \tag{3.141}$$

where $Q_{*m}(u,v,t)$ given by

$$Q_{*m}(u,v,t) = \frac{2}{N_0}\Big[\delta(u-v) - H_m(u,v,t)\Big] \qquad 0 \le u,v \le t \tag{3.142}$$

and $H_m(u,v,t)$ is given by (3.42). Substituting (3.141) into (3.100) yields

$$d_{km}(t) = V_{km}(t)e^{j\vartheta_{km}(t)} = \int_0^t \left[\int_0^t Q_{*m}(u,v,t)\,|\alpha_k|\,\tilde{s}_m^*(v-\tau_k)e^{-j\omega_c v}dv\right] dz(u) \quad (3.143a)$$

$$= \int_0^t \left(\int_0^t H_{*m}(s,v,t)\,|\alpha_k|\,\tilde{s}_m^*(v-\tau_k)e^{-j\omega_c v}dv\right)\left(\int_0^t H_{*m}(s,u,t)dz(u)\right) ds \quad (3.143b)$$

where (3.143b) is obtained by noting that $Q_{*m}(u,v,t)$ in (3.142) is the so-called inverse kernel satisfying [187, pp. 290-297]

$$\delta(s-u) = \int_0^t K_{cm}(v,s)Q_{*m}(u,v,t)dv$$

and given by

$$Q_{*m}(u,v,t) \triangleq \int_0^t H_{*m}(s,u,t)H_{*m}(s,v,t)ds \quad (3.144)$$

and $H_{*m}(s,u,t)$ is the whitening filter for $n_c(s)$ with $K_{cm}(v,s)$ given by (3.138). Since $K_m(s,u)$ is positive semi-definite (3.144) can be easily obtained from (3.142) by using (C.18). Thus from (3.141) the filter $\frac{2}{N_0}l_{km}(u,t)e^{j\omega_c u}$ can be interpreted as the concatenation of the inverse kernel (3.144) with a filter matched to the k^{th} specular component. Similar to (3.134) valid for the random phase channel, from (3.139c) it is seen that (3.143b) is the correlation of the preenvelope of the whitened noiseless received signal (excluding the random phase) with the whitened received signal $\dot{z}_*(s) - \widehat{v_{*k}^d(s)} \triangleq \dot{z}_*(s) = \int_0^t H_{*m}(s,u,t)dz(u)$.

Now that the impact of signal fading on the specular phasor estimate has been clarified, let us consider the difficulty associated with path unresolvability. Path unresolvability induces a form of interaction between the specular components associated with different paths. It is to expected that the k^{th} phasor estimate depends on the information related to the other paths, and indeed substituting (3.112) into (3.127) shows that the k^{th} specular component phasor estimate depends on "cross-correlation" factors such as $\{V_{kn}^m(t), \vartheta_{kn}^m(t)\}_{k=0,\ldots,L-1,n=0,\ldots,k-1}$ given respectively by

(3.114) and (3.115). Substituting (3.141) into (3.102c) yields

$$
\begin{aligned}
e_{kn}^{m}(t) &= V_{kn}^{m}(t)e^{j\vartheta_{kn}^{m}(t)} \\
&= \int_0^t \left[\int_0^t Q_{*m}(u,v,t)\,|\alpha_k|\,\tilde{s}_m^*(v-\tau_k)e^{-j\omega_c v}dv\right] \Re\left\{|\alpha_n|\,\tilde{s}_m(u-\tau_n)e^{j\omega_c u}\right\}du \qquad (3.145a) \\
&= \int_0^t \left(\int_0^t H_{*m}(s,v,t)\,|\alpha_k|\,\tilde{s}_m^*(v-\tau_k)e^{-j\omega_c v}dv\right) \\
&\qquad \cdot \left(\int_0^t H_{*m}(s,u,t)\Re\left\{|\alpha_n|\,\tilde{s}_m(u-\tau_n)e^{j\omega_c u}\right\}du\right)ds \qquad (3.145b)
\end{aligned}
$$

where $Q_{*m}(s,u,t)$ is given by (3.144). From (3.145b), similar to the interpretation of (3.143b), $V_{kn}^{m}(t)$ and $\vartheta_{kn}^{m}(t)$ are obtained by taking the amplitude and phase of the correlation between the preenvelope of k^{th} whitened specular component (excluding the random phase) and the n^{th} whitened specular component.

Further insight on the nonlinear function $V_{km}^{'}(t)e^{j[\vartheta_{km}^{'}(t)+\vartheta_{km}(t)]}$ can be obtained in the special case of resolved multipath.

Conditional mean when the multipath is resolved

From Section 3.2.3 (topic: "Conditional mean when the multipath is resolved"), the resolvability assumption is satisfied over $[0,t]$ if (3.58) is satisfied. In that case $\lambda_{lm}(t)$, $\sqrt{\frac{\lambda_{lm}(t)}{\epsilon_{km}(t)}}x_{lk}^{m}(t)$ and $\sqrt{\lambda_{lm}(t)}\phi_{lm}(s,t)$ are respectively given by (3.59), (3.60) and (3.61). Substituting (3.59-3.61) into (3.131a) and (3.103b) yields

$$
\widehat{a_k^{'}(t)} = \frac{2}{\sqrt{\epsilon_{km}(t)\tilde{E}_m}}\frac{2\sigma_k^2\epsilon_{km}(t)\gamma_m}{1+2\sigma_k^2\epsilon_{km}(t)\gamma_m}\int_0^t \frac{\tilde{s}_m^*(s-\tau_k)}{\sqrt{\epsilon_{km}(t)\tilde{E}_m}}e^{-j\omega_c s}dy_m^{\mathrm{nc}}(s) \qquad (3.146)
$$

$$
l_{nm}(s,t) = \frac{|\alpha_n|}{1+2\sigma_n^2\epsilon_{nm}(t)\gamma_m}\tilde{s}_m(s-\tau_n) \qquad (3.147)
$$

Therefore substituting (3.147) into (3.102a) and (3.101) and using (3.58) yield

$$
\forall\, k \neq n \quad e_{kn}^{m}(t) = \frac{1}{N_0}\int_0^t l_{nm}(s,t)\,|\alpha_k|\,\tilde{s}_m^*(s-\tau_k)ds = 0 \qquad (3.148)
$$

$$
\frac{|\alpha_k|b_{km}(\boldsymbol{\theta}_{k-1}^{'},t)}{\sigma_k^2\sqrt{\epsilon_{km}(t)}} = d_{km}(t) \qquad (3.149)
$$

From (3.149) $\frac{|\alpha_k| b_{km}(\boldsymbol{\theta}'_{k-1},t)}{\sigma_k^2\sqrt{\epsilon_{km}(t)}}$ is independent of $\boldsymbol{\theta}'_{k-1}$, therefore, from (3.94) $g(\boldsymbol{d}_m(t),t)$ reduces to

$$g(\boldsymbol{d}_m(t),t)=\prod_{k=0}^{L-1} I_0\left(\frac{|\alpha_k|\left|b_{km}(\boldsymbol{\theta}'_{k-1},t)\right|}{\sigma_k^2\sqrt{\epsilon_{km}(t)}}\right)=\prod_{k=0}^{L-1} I_0(V_{km}(t))$$

where $V_{km}(t)$ is given by (3.98). Hence the function $g(\boldsymbol{d}_m(t),t)$ is independent of $\vartheta_{km}(t)$ and from (3.112), $V'_{km}(t)e^{j\vartheta'_{km}(t)}=\frac{\frac{\partial g(\boldsymbol{d}_m(t),t)}{\partial V_{km}(t)}}{g(\boldsymbol{d}_m(t),t)}$. Equivalently $V'_{km}(t)=\frac{I_1(V_{km}(t))}{I_0(V_{km}(t))}$ and $\vartheta'_{km}(t)=0$ and $\breve{v}_m(t)$ is given by (3.132) where $\widehat{a'_k(t)}$ is given by (3.146), $\widehat{e^{j\theta'_k}(t)}$ is given by

$$\widehat{e^{j\theta'_k}(t)}=\frac{I_1(V_{km}(t))}{I_0(V_{km}(t))}e^{j\vartheta_{km}(t)} \tag{3.150}$$

$V_{km}(t)$ and $\vartheta_{km}(t)$ are given by (3.98) and (3.99) and $l_{km}(s,t)$ is given by (3.147).

Hence whenever the multipath is resolved over $[0,t]$, no decorrelation is performed since the signals $\{\tilde{s}_m(s-\tau_k)\}_{k=0,\ldots,L-1}$ are already orthogonal. The estimate of a'_k employs only the information related to the k^{th} path and the effect of fading is taken into account similarly to the unresolved case (3.133) with the signal $\tilde{s}_m(s-\tau_k)/\sqrt{\epsilon_{km}(t)\tilde{E}_m}$ replacing $\phi_{km}(s,t)$.

From (3.150) only the terms $V_{km}(t)$ and $\vartheta_{km}(t)$ are involved in the estimation of the phasor. In that case $V_{km}(t)e^{j\vartheta_{km}(t)}$ can be interpreted as the correlation of the preenvelope of the whitened noiseless received signal (excluding the random phase) with the whitened received signal $\dot{z}_*(s)-v^d_{*k}(s)$ (instead of $\dot{z}_*(s)-\widehat{v^d_{*k}(s)}$) as shown in the following. From (3.139a), (3.140a) and (3.144)

$$\begin{aligned}\int_0^t\left(\int_0^t H_{*m}(s,v,t)\,|\alpha_k|\,\tilde{s}^*_m(v-\tau_k)e^{-j\omega_c v}dv\right)\left[\dot{z}_*(s)-v^d_{*k}(s)\right]ds&\\ =\int_0^t\left[\int_0^t Q_{*m}(u,v,t)\,|\alpha_k|\,\tilde{s}^*_m(v-\tau_k)e^{-j\omega_c v}dv\right]\left[dz(u)-v^d_{km}(u)du\right]&\\ =V_{km}(t)e^{j\vartheta_{km}(t)}\quad\text{from (3.143a)}&\end{aligned}$$

since the term $\left\{\int_0^t\left[\int_0^t Q_{*m}(u,v,t)\,|\alpha_k|\,\tilde{s}_m(v-\tau_k)e^{j\omega_c v}dv\right]v^d_{km}(u)du\right\}^*=0$ as shown in Appendix F.1.

The value of $V_{km}(t)$ gives an indication on the accuracy of the phase estimate $\vartheta_{km}(t)$. Assume that $V_{km}(t)e^{j\vartheta_{km}(t)} = Ke^{j\theta_k'} + \epsilon\, e^{j\phi}$ and all quantities are deterministic for these explanations, then it can be shown that if $|V_{km}(t)| \gg |\epsilon|$, $\vartheta_{km}(t) \approx \theta_k'$. Since the terms are in fact random, the larger $V_{km}(t)$ is, the more likely the phase estimate is good. In order to take into account the possible cases of very bad phase estimates, the estimate of the signal $e^{j\theta_k'}$ is obtained by scaling $e^{j\vartheta_{km}(t)}$. The scaling factor $\frac{I_1(V_{km}(t))}{I_0(V_{km}(t))}$ acts as a soft limiter whose value is always less than 1. Indeed using Taylor expansion and approximation expansion of $I_0(x)$ and $I_1(x)$, yields the following; if $x \ll 1$, $\frac{I_1(x)}{I_0(x)} \approx \frac{x}{2}$ and if $x \gg 1$, $\frac{I_1(x)}{I_0(x)} \approx 1$. This function is illustrated in Fig. 3.3. The purpose of the soft limiter is to reduce the amplitude of the phasor estimate in

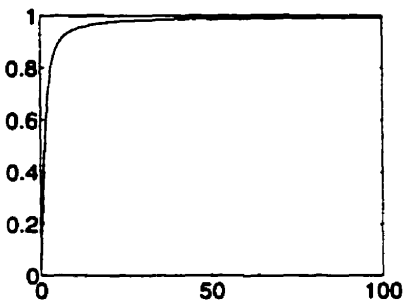

Fig. 3.3 The function $\frac{I_1(x)}{I_0(x)}$

case $V_{km}(t)$ is small and the phase estimate is likely to be far from the actual value of θ_k'. Thus as seen by Fig. 3.4, the soft limiter reduces the difference between the phasor estimate and the actual phasor when the phase estimate is poor. There are relationships between $V_{km}(t)$ and the SNR of the whitened received signal $\dot{z}_*(s) - v_{*k}^d(s)$ where $v_{*k}^d(s)$ is given by (3.140). The evaluation of $E\left[V_{km}^2(t)|H_m\right]$ is carried out in Appendix F.2 for unresolved multipath. From (3.148) when the multipath is resolved, $\forall\, k \neq n\; e_{kn}^m(t) = 0$, hence from (3.102a) $E\left[V_{km}^2(t)|H_m\right]$ given by (F.7) reduces to

$$E\left[V_{km}^2(t)|H_m\right] = \frac{2}{N_0}\int_0^t l_{km}(s,t)\,|\alpha_k|\,\tilde{s}_m^*(s-\tau_k)ds + \left|\frac{1}{N_0}\int_0^t l_{km}(s,t)\,|\alpha_k|\,\tilde{s}_m^*(s-\tau_k)ds\right|^2 \qquad (3.151)$$

where $l_{km}(s,t)$ is given by (3.147). From (3.139b) the whitened received signal $\dot{z}_*(s) -$

$v_{*k}^d(s)$ is given by

$$\dot{z}_*(s) - v_{*k}^d(s) = \int_0^t H_{*m}(s,u,t)\Re\left\{\left(|\alpha_k|\,\tilde{s}_m(u-\tau_k)e^{j\theta_k'}\right)e^{j\omega_c u}\right\}du + n_{*c}(s) \quad (3.152)$$

where $\int_0^t H_{*m}(s,u,t)\Re\left\{\left(|\alpha_k|\,\tilde{s}_m(u-\tau_k)e^{j\theta_k'}\right)e^{j\omega_c u}\right\}du$ is the signal component and $n_{*c}(s)$ is a white Gaussian noise with unit power spectral density. Therefore the SNR of $\dot{z}_*(s) - v_{*k}^d(s)$ is given by

$$\mathrm{SNR}_k \triangleq \frac{E\left[\int_0^t\left[\int_0^t H_{*m}(s,u,t)\Re\left\{\left(|\alpha_k|\,\tilde{s}_m(u-\tau_k)e^{j\theta_k'}\right)e^{j\omega_c u}\right\}du\right]^2 ds\right]}{1} \quad (3.153)$$

The evaluation of the average signal energy of $\dot{z}_*(s) - v_{*k}^d(s)$ is carried out in Appendix F.3. Substituting (F.8) into (3.153), the SNR of $\dot{z}_*(s) - v_{*k}^d(s)$ is given by

$$\mathrm{SNR}_k = \frac{\frac{1}{N_0}\int_0^t l_{km}(u,t)\,|\alpha_k|\,\tilde{s}_m^*(u-\tau_k)du}{1} = \frac{1}{N_0}\int_0^t l_{km}(u,t)\,|\alpha_k|\,\tilde{s}_m^*(u-\tau_k)du$$

Therefore from (3.151) at high SNR ($\mathrm{SNR}_k \gg 1$), $E\left[V_{km}^2(t)|H_m\right] \gg 1$. Since $V_{km}(t) \geq 0$, with a high probability $V_{km}(t) \gg 1$ and $\frac{I_1(V_{km}(t))}{I_0(V_{km}(t))} \approx 1$.

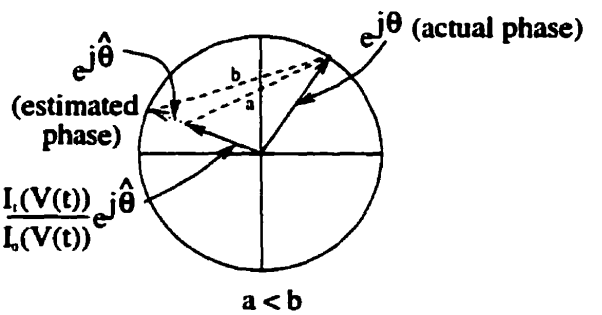

Fig. 3.4 Phasor diagram

To conclude this section on resolved multipath, substituting (3.150) into (3.132) shows that the conditional mean for a resolved multipath channel is the sum of L terms. Each term, $\Re\left\{\left(\widehat{a_k'(t)}\,\tilde{s}_m(t-\tau_k) + |\alpha_k|\,\frac{I_1(V_{km}(t))}{I_0(V_{km}(t))}e^{j\vartheta_{km}(t)}\tilde{s}_m(t-\tau_k)\right)e^{j\omega_c t}\right\}$ is the conditional mean of a one-path Ricean channel with complex path gain a_k.

Next three channels of practical interest will be considered, the mixed mode Ricean/Rayleigh channel that may represent transmission with a line-of-sight, the purely Rayleigh channel that may represent transmission without a line-of-sight and

finally the 2 Ricean/L-2 Rayleigh channel that may represent transmission with a line-of-sight and a strong reflection. Besides their practical interests, these channels will provide much insight on the operations performed by the optimum receiver for Ricean channels.

3.4 Non-coherent optimal decision rule for a mixed mode Ricean/Rayleigh channel

3.4.1 Mixed mode Ricean/Rayleigh log-likelihood

A multipath fading channel is said to be mixed mode Ricean/Rayleigh if the first path gain is Ricean distributed and the other path gains are Rayleigh distributed, i.e. $\boldsymbol{\alpha} = [\alpha_0, 0, \ldots, 0]^T$. For a mixed mode Ricean/Rayleigh channel, since $\forall\, k \neq 0, \alpha_k = 0$ (3.64) reduces to $f_m(\boldsymbol{\theta}) = \exp\left\{\frac{|\alpha_0||b_{0m}|}{\sigma_0^2\sqrt{\epsilon_{0m}}}\cos(\theta_0 - \varphi_{0m})\right\}$ where b_{0m} and φ_{0m}, given respectively by (3.65) and (3.66), are independent of $\boldsymbol{\theta}$. Since $f_m(\boldsymbol{\theta})$ is independent of $\theta_1, \ldots, \theta_{L-1}$ the log-likelihood ratio (3.67) reduces to

$$\begin{aligned}\ln\left[\Lambda_m\left(\dot{z}; T_o\right)\right] &= \ln\left(J_m\right) + \ln\left[\frac{1}{2\pi}\int_{-\pi}^{\pi}\exp\left\{\frac{|\alpha_0|\,|b_{0m}|}{\sigma_0^2\sqrt{\epsilon_{0m}}}\cos(\theta_0 - \varphi_{0m})\right\}d\theta_0\right] \\ &= \ln\left(J_m\right) + \ln\left[I_0\left(\frac{|\alpha_0|\,|b_{0m}|}{\sigma_0^2\sqrt{\epsilon_{0m}}}\right)\right] = \ln\left(J_m\right) + \ln\left[I_0(V_{0m})\right] \qquad (3.154)\end{aligned}$$

where V_{0m} is given by (3.73) and J_m is given by (3.63). Equation (3.154) is obtained by using the integral definition of the modified Bessel function and noting from (3.70) and (3.73) that $\frac{|\alpha_0||b_{0m}|}{\sigma_0^2\sqrt{\epsilon_{0m}}} = V_{0m}$. Using (3.73) with (3.68a), V_{0m} can also be written as

$$\begin{aligned}V_{0m} &= \frac{|\alpha_0|}{\sigma_0^2\sqrt{\epsilon_{0m}}}\left|\left[\boldsymbol{X}_m^T\boldsymbol{Q}_m\boldsymbol{r}_m\right]_0\right| = \left[4\left|\frac{\alpha_0}{2\sigma_0^2\sqrt{\epsilon_{0m}}}\sum_{k=0}^{L-1}\frac{\frac{\lambda_{km}}{2N_0}}{1+\frac{\lambda_{km}}{2N_0}}x_{k0}^m\left[\boldsymbol{r}_m\right]_k\right|^2\right]^{1/2} \\ &= 2\left[\left(\boldsymbol{X}_m^T\boldsymbol{Q}_m\boldsymbol{r}_m\right)^\dagger\left(\boldsymbol{\epsilon}_m^{1/2}\boldsymbol{C}\right)^{-1}\boldsymbol{\alpha}\boldsymbol{\alpha}^\dagger\left(\boldsymbol{\epsilon}_m^{1/2}\boldsymbol{C}\right)^{-1}\boldsymbol{X}_m^T\boldsymbol{Q}_m\boldsymbol{r}_m\right]^{1/2} \qquad (3.155)\end{aligned}$$

since $[\boldsymbol{C}]_{kk} = 2\sigma_k^2$ and $\boldsymbol{\alpha}$ has only one non-zero element. Similarly to results obtained in Section 3.3.2, for low γ_m regardless of $\boldsymbol{\alpha}$, $\ln(J_m) \approx \gamma_m^2\boldsymbol{u}_m^\dagger\boldsymbol{\epsilon}_m\boldsymbol{C}\boldsymbol{u}_m - \gamma_m\boldsymbol{\alpha}^\dagger\boldsymbol{\epsilon}_m\boldsymbol{\alpha}$, $\boldsymbol{X}_m^T\boldsymbol{Q}_m\boldsymbol{r}_m \approx \gamma_m\boldsymbol{\epsilon}_m\boldsymbol{C}\boldsymbol{u}_m$, hence $V_{0m} \approx 2\gamma_m\left[\boldsymbol{u}_m^\dagger\boldsymbol{\epsilon}_m^{1/2}\boldsymbol{\alpha}\boldsymbol{\alpha}^\dagger\boldsymbol{\epsilon}_m^{1/2}\boldsymbol{u}_m\right]^{1/2}$. This shows that the decorrelation operation on the input signal (present through the matrix $\boldsymbol{X}_m$) vanishes at low SNR. Note that for mixed mode Ricean/Rayleigh, the bias

term $\gamma_m \left\{ \boldsymbol{X}_m^T \boldsymbol{Q}_m \left(\boldsymbol{X}_m^T \right)^{-1} \boldsymbol{\epsilon}_m^{1/2} \right\}_l \boldsymbol{\varrho}(\boldsymbol{\theta})$ or equivalently its high SNR approximation $\gamma_m \left\{ \boldsymbol{\epsilon}_m \boldsymbol{C} \boldsymbol{\Gamma}_m^* \boldsymbol{\epsilon}_m^{1/2} \right\}_l \boldsymbol{\varrho}(\boldsymbol{\theta})$ do not appear in the likelihood ratio. This term is part of the decorrelation performed on the specular component of the received signal before the averaging over the random phases. In a mixed mode Ricean/Rayleigh channel, the specular component is composed of only one random phase signal hence no further decorrelation is needed on the specular component.

3.4.2 Limiting forms of the log-likelihood ratio

Substituting (3.68a) into (3.73) with $k = 0$ shows that V_{0m} is proportional to $|\alpha_0|$. Therefore, assume that $|\alpha_0|$ is small, then V_{0m} is small and using the first terms of the Taylor 's series expansion of the modified Bessel function of the first kind, (3.154) can be approximated by

$$\ln\left[\Lambda_m\left(\dot{z};T_o\right)\right] \approx \ln\left(J_m\right) + \ln\left[1 + \frac{V_{0m}^2}{4}\right] \approx \ln\left(J_m\right) + \frac{V_{0m}^2}{4} \approx \ln\left(J_m\right) \tag{3.156}$$

Assume now that $|\alpha_0|$ is large in (3.154), then V_{0m} is large and the asymptotic expansion of the modified Bessel function of the first kind, yields $\ln\left(I_0(V_{0m})\right) \approx V_{0m}$. If γ_m is small then $V_{0m} \gg \ln\left(J_m\right)$ and the log-likelihood ratio can be approximated by V_{0m}. An equivalent decision rule can be based on

$$\chi_m^{\mathrm{e}}\left(\dot{z};T_o\right) = V_{0m}^2 \tag{3.157}$$

If γ_m is large then $\ln(J_m) \gg V_{0m}$ and the log-likelihood ratio can be approximated by

$$\ln\left[\Lambda_m\left(\dot{z};T_o\right)\right] \approx \ln\left(J_m\right) \tag{3.158}$$

The limiting forms of the log-likelihood ratio will help to design suboptimum structures as will be seen in Section 3.7. Similarly to the non-coherent optimum receiver for general Ricean channels, the mixed mode non-coherent optimum receiver can be interpreted as an estimator-correlator which will be investigated next.

3.4.3 Non-coherent estimator-correlator for a mixed mode Ricean/Rayleigh channel

Interpretation of the MMSE estimate (mixed mode Ricean/Rayleigh channels)

For a mixed mode Ricean/Rayleigh channel, from (D.15) the likelihood ratio over $[0,t]$ is given by

$$\Lambda_m(\dot{z};t) = J_m(t) I_0\big(V_{0m}(t)\big)$$

where $J_m(t)$ is given by (3.93) and $V_{0m}(t)$ is given by (3.98). Hence $g\big(\boldsymbol{d}_m(t),t\big) \triangleq \frac{\Lambda_m(\dot{z};t)}{J_m(t)} = g\big(V_{0m}(t)\big) = I_0\big(V_{0m}(t)\big)$. From [21], the likelihood ratio $\Lambda_m(\dot{z};T_o)$ can be expressed as (3.82) where from (3.111) (direct method) or from (3.124a, 3.125b) assuming $\alpha_1 = \ldots = \alpha_{L-1} = 0$ and $g\big(V_{0m}(t)\big) = I_0\big(V_{0m}(t)\big)$ (Itô differentiation), the conditional mean for a mixed mode Ricean/Rayleigh channel is given by

$$\breve{v}_m(t) = \Re\left\{\left(2\int_0^t \mathcal{H}_m^*(s,t,t)e^{-j\omega_c s}dz(s) + \frac{I_1\big(V_{0m}(t)\big)}{I_0\big(V_{0m}(t)\big)} l_{0m}(t,t)e^{j\vartheta_{0m}(t)}\right)e^{j\omega_c t}\right\} \tag{3.159a}$$

$$= \Re\left\{\left(2\int_0^t \mathcal{H}_m^*(s,t,t)e^{-j\omega_c s}dy_m^{\mathrm{nc}}(s) + |\alpha_0|\,\frac{I_1\big(V_{0m}(t)\big)}{I_0\big(V_{0m}(t)\big)} e^{j\vartheta_{0m}(t)}\tilde{s}_m(t-\tau_0)\right)e^{j\omega_c t}\right\} \tag{3.159b}$$

where from (3.128) $y_m^{\mathrm{nc}}(s)$ is given by

$$dy_m^{\mathrm{nc}}(s) = dz(s) - \Re\left\{\frac{I_1\big(V_{0m}(t)\big)}{I_0\big(V_{0m}(t)\big)} e^{j\vartheta_{0m}(t)}\,|\alpha_0|\,\tilde{s}_m(s-\tau_0)e^{j\omega_c s}\right\} ds \tag{3.160}$$

and $\mathcal{H}_m(s,t,t)$, $V_{0m}(t)$, $l_{0m}(t,t)$ and $\vartheta_{0m}(t)$ are respectively given by (3.41), (3.98), (3.103) and (3.99).

Following the methodology used in Section 3.3.3, from (3.132) the conditional mean can be viewed as

$$\breve{v}_m(t) = \Re\left\{\left(\sum_{k=0}^{L-1} \widehat{a_k'(t)}\,\tilde{s}_m(t-\tau_k) + |\alpha_0|\,\widehat{e^{j\theta_0'(t)}}\,\tilde{s}_m(t-\tau_0)\right)e^{j\omega_c t}\right\} \tag{3.161}$$

where $\widehat{a'_k(t)}$ is given by (3.131) and from (3.127) $\widehat{e^{j\theta'_0(t)}} = \frac{I_1(V_{0m}(t))}{I_0(V_{0m}(t))} e^{j\vartheta_{0m}(t)}$ since $g(\boldsymbol{d}_m(t), t) = I_0(V_{0m}(t))$. The amplitude estimate $\widehat{a'_k(t)}$ is obtained by filtering of the unknown part of the received signal $\dot{z}(s) - \Re\left\{|\alpha_0| \widehat{e^{j\theta'_0(t)}} \tilde{s}_m(s-\tau_0) e^{j\omega_c s}\right\}$ by the filter $\frac{2\sigma_k^2}{N_0} \frac{l^*_{km}(s,t)}{|\alpha_k|} e^{-j\omega_c s}$. Note from (3.103b) that $\forall k$, $\frac{l^*_{km}(s,t)}{|\alpha_k|}$ is independent of α_k so is well defined. As shown in Section 3.3.3 this filter takes into account both the multipath unresolvability and fading. First the effect of unresolvability is removed yielding a decorrelated channel with zero mean path gains $\{a''_{lm}(t)\}_{l=0,\ldots,L-1}$, and then estimation of the zero mean path gains $\{a''_{lm}(t)\}_l$ is done as for a resolved multipath channel.

As seen in Section 3.3.3, the MMSE estimate of the specular component is obtained by estimating the specular component phasors. Each specular component phasor estimate involves a phase estimator of the k^{th} random phase that is substituted for θ'_k. But the k^{th} obtained signal estimate is then scaled by a factor $V'_{km}(t)$ that takes into account the presence of all the other randomly phase shifted specular components since the multipath is not resolved. For a mixed mode Ricean/Rayleigh channel, however, only one phasor has to be estimated ($e^{j\theta'_0}$) so no other specular components have to be taken into account. Therefore the phasor scaling factor has the same form as the one obtained when the multipath is resolved $\left(\text{i.e. } \frac{I_1(V_{0m}(t))}{I_0(V_{0m}(t))}\right)$. The scaling factor for resolved multipath does not take into account the presence of the other specular components. As seen in the study of resolved multipath in Section 3.3.3 that term acts as a soft limiter whose value is always less than 1. The purpose of the soft limiter is to reduce the amplitude of the phasor estimate whenever $V_{0m}(t)$ is small which occurs when the phase estimate is likely to be far from the actual value. Similarly to results obtained in Section 3.3.3 for L-path Ricean channels, the filter $\frac{2}{N_0} l_{0m}(s,t) e^{j\omega_c s}$ can be interpreted as the concatenation of the inverse kernel (3.144) with a filter matched to the first specular component ("0^{th}" path). Since only the first path has a specular component, from (3.140b) $v^d_{*k}(s) = 0$ and the whitened received signal $\dot{z}_*(s) - v^d_{*k}(s)$ defined in Section 3.3.3 is equal to $\dot{z}_*(s)$. Since $\forall k \neq 0, |\alpha_k| = 0$, from (F.6)

$$E\left[V^2_{0m}(t)|H_m\right] = \frac{2}{N_0}\int_0^t l_{0m}(s,t)\,|\alpha_0|\,\tilde{s}^*_m(s-\tau_0)ds + \left|\frac{1}{N_0}\int_0^t l_{0m}(s,t)\,|\alpha_0|\,\tilde{s}^*_m(s-\tau_0)ds\right|^2 \tag{3.162}$$

and from (3.139b) and (F.8) the SNR of the whitened received signal $\dot{z}_*(s)$ is given

by

$$\mathrm{SNR}_0 = \frac{E\left[\int_0^t \left[\int_0^t H_{*m}(s,u,t)\Re\left\{\left(|\alpha_0|\,\tilde{s}_m(u-\tau_0)e^{j\theta_0'}\right)e^{j\omega_c u}\right\}du\right]^2 ds\right]}{1}$$
$$= \frac{1}{N_0}\int_0^t l_{0m}(u,t)\,|\alpha_0|\,\tilde{s}_m^*(u-\tau_0)du$$

Therefore from (3.162) at high SNR ($\mathrm{SNR}_0 \gg 1$), $E\left[V_{0m}^2(t)|H_m\right] \gg 1$. Hence since $V_{0m}(t) \geq 0$, with a high probability $V_{0m}(t) \gg 1$ and $\frac{I_0(V_{0m}(t))}{I_1(V_{0m}(t))} \approx 1$.

Structure of the MMSE estimate for mixed mode Ricean/Rayleigh channels

The mixed mode Ricean/Rayleigh channel MMSE estimator $\check{v}_m(t)$, given by (3.159), can conceptually be implemented as illustrated in Fig. 3.5, where $\check{v}_{Rm}(t)$ denotes the term of the conditional mean corresponding to the Rayleigh part of the channel,

$$\check{v}_{Rm}(t) = \Re\left\{\left(2\int_0^t \mathcal{H}_m^*(s,t,t)e^{-j\omega_c s}dy_m^{\mathrm{nc}}(s)\right)e^{j\omega_c t}\right\} \tag{3.163}$$

the filter $\mathcal{H}_m(s,t,t)$ is given by (3.41) and $y_m^{\mathrm{nc}}(s)$ is given by (3.160), and $\check{v}_{Sm}(t)$ denotes the term of the conditional mean corresponding to the specular component

$$\check{v}_{Sm}(t) = \Re\left\{\left(|\alpha_0|\,\frac{I_1(V_{0m}(t))}{I_0(V_{0m}(t))}e^{j\vartheta_{0m}(t)}\tilde{s}_m(t-\tau_0)\right)e^{j\omega_c t}\right\}.$$

As seen in Fig. 3.5, implementation of $\check{v}_m(t)$ requires $\{V_{0m}(t);\vartheta_{0m}(t)\}$ and $\widehat{a_k'(t)}$ (or equivalently $\int_0^t \mathcal{H}_m^*(s,t,t)e^{-j\omega_c s}dy_m^{\mathrm{nc}}(s)$) defined respectively in (3.98-3.99) and (3.131). Therefore the system uses the linear time varying filters $\mathcal{H}_m(s,t,t)$ and $Q_{*m}(s,v,t) = \frac{2}{N_0}\left[\delta(s-v) - H_m(s,v,t)\right]$. Since $\forall\, s,v > t$, $H_m(s,v,t) = 0$ and $\mathcal{H}_m(s,t,t) = 0$, $\mathcal{H}_m(s,t,t)$ and $Q_{*m}(s,v,t)$ are causal and hence physically realizable. The structure of Fig. 3.5 works as follows. First the conditional mean corresponding to the specular component $\check{v}_{Sm}(t)$ is calculated at a certain time t_0 by passing the received signal $\dot{z}(s)$ through the causal linear time varying filter with complex impulse response $\frac{2}{N_0}l_{0m}^*(s,t)e^{-j\omega_c s}$, and extracting the magnitude and phase from its output. The phase $\vartheta_{0m}(t)$ is passed through the complex exponential device with transfer function $e^{j(\cdot)}$ to generate its associated phasor. The magnitude is passed through a nonlinear device

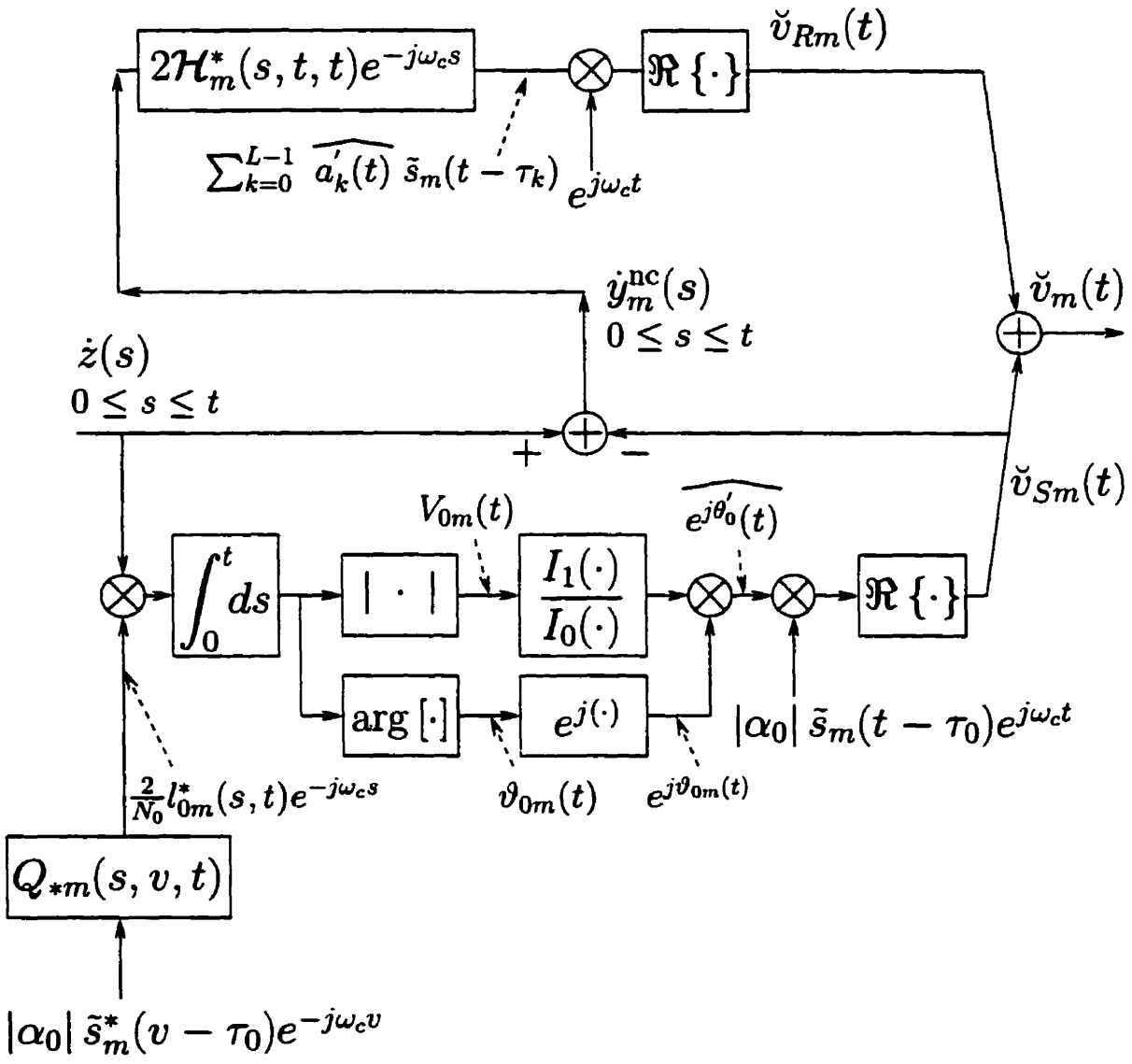

Fig. 3.5 Structure of $\breve{v}_m(t)$ for a mixed mode Ricean/Rayleigh channel, where $\mathcal{H}_m(s,t,t)$ is given by (3.41).

with transfer function $\frac{I_1(\cdot)}{I_0(\cdot)}$ and multiplied by the phasor $e^{j\vartheta_{0m}(t)}$ and the specular component $|\alpha_0|\,\tilde{s}_m(t-\tau_0)e^{j\omega_c t}$. The filter $\frac{2}{N_0}l^*_{0m}(s,t)e^{-j\omega_c s}$ is obtained by passing the conjugate of the specular component $(|\alpha_0|\,\tilde{s}^*_m(v-\tau_0)e^{-j\omega_c v})$ through the causal linear filter $Q_{*m}(s,v,t)$ (inverse kernel of $K_{cm}(v,s)$). After these operations $\{\check{v}_{Sm}(s), 0 \leq s < t\}$ is stored in memory. The second stage consists of subtracting $\check{v}_{Sm}(t)$ from the received signal, yielding $\dot{y}^{\rm nc}_m(t)$ and then $\{\dot{y}^{\rm nc}_m(s), 0 \leq s < t\}$ is stored in memory. Note the occurrence of a delay since the bottom operations and the top operations in Fig. 3.5 cannot be done in parallel. The third stage consists of passing the signal $\dot{y}^{\rm nc}_m(s) = \dot{z}(s) - \check{v}_{Sm}(s)$ through the causal linear time varying filter $2\mathcal{H}^*_m(s,t,t)e^{-j\omega_c s}$, multiplying the output by $e^{j\omega_c t}$ and then taking its real part. This real part is then added to $\check{v}_{Sm}(t)$, hence the reason for holding the value $\check{v}_{Sm}(t)$. For convenience complex filters such as $\mathcal{H}^*_m(s,t,t)e^{-j\omega_c(s-t)}$ are used in Fig. 3.5 but a completely equivalent structure can be derived using only real filters. For example for the first stage, the structure can be expressed in terms of $h_m(t,s) = 2\Re\left\{\mathcal{H}^*_m(s,t,t)e^{-j\omega_c(s-t)}\right\}$.

The conditional mean when the multipath is resolved has been derived in Section 3.3.3 for L-path Ricean channels. Mixed Ricean/Rayleigh channels are a special case of L-path Ricean channels when $\alpha_1 = \alpha_2 = \ldots = \alpha_{L-1} = 0$. Therefore results for mixed mode Ricean/Rayleigh channels can be easily deduced.

Expression of the conditional mean when $\forall k \quad \sigma_k^2 = 0$

For sake of simplicity, all σ_k^2 are assumed equal, therefore $\forall r = 1, \ldots, L-1$ $\boldsymbol{C}_r \triangleq \sigma \boldsymbol{I}_r$, where $\sigma = 2\sigma_k^2$. Defining $\forall t > T'_m + \tau_0$ $\boldsymbol{D}'_{i_t m}(t) = \frac{\boldsymbol{D}_{i_t m}(t)}{\sigma}$, (3.35b) reduces to $\boldsymbol{\epsilon}_{i_t m}(t)\boldsymbol{\Gamma}^*_{i_t m}(t)\boldsymbol{X}^T_{i_t m}(t) = \boldsymbol{X}^T_{i_t m}(t)\boldsymbol{D}'_{i_t m}(t)$. Let $\lambda'^{i_t}_{km}(t)$ be the k^{th} diagonal entry of $\boldsymbol{D}'_{i_t m}(t)$, then $\lambda'^{i_t}_{km}(t) = \frac{\lambda^{i_t}_{km}(t)}{\sigma \tilde{E}_m}$ which is independent of σ. Let us define $\lambda'_{km}(t) = \frac{\lambda_{km}(t)}{\sigma \tilde{E}_m}$ where $\lambda_{km}(t)$ is given by (3.37). Then $\lambda'_{km}(t)$ is also independent of σ as well as $x^m_{lk}(t)$. Hence $\forall t \geq 0$ (3.131a) reduces to

$$\widehat{a'_k(t)} = \frac{2}{\sqrt{\epsilon_{km}(t)\tilde{E}_m}} \sum_{l=0}^{L-1} \frac{\frac{\sigma\lambda'_{lm}(t)\tilde{E}_m}{2N_0}}{1 + \frac{\sigma\lambda'_{lm}(t)\tilde{E}_m}{2N_0}} x^m_{lk}(t) \int_0^t \phi^*_{lm}(s,t)e^{-j\omega_c s} dy^{\rm nc}_m(s)$$

Therefore

$$\lim_{\sigma \to 0} \widehat{a'_k(t)} = 0 \tag{3.164}$$

Furthermore, (3.103b) reduces to

$$l_{km}(s,t) = 2N_0 \frac{|\alpha_k|}{\sigma\sqrt{\epsilon_{km}(t)\tilde{E}_m}} \sum_{l=0}^{L-1} \frac{\sigma\lambda'_{lm}(t)\frac{\tilde{E}_m}{2N_0}}{1+\sigma\lambda'_{lm}(t)\frac{\tilde{E}_m}{2N_0}} [x_{lk}^m(t)]^* \phi_{lm}(s,t)$$

$$= 2N_0 \frac{|\alpha_k|}{\sqrt{\epsilon_{km}(t)\tilde{E}_m}} \sum_{l=0}^{L-1} \frac{\lambda'_{lm}(t)\frac{\tilde{E}_m}{2N_0}}{1+\sigma\lambda'_{lm}(t)\frac{\tilde{E}_m}{2N_0}} [x_{lk}^m(t)]^* \phi_{lm}(s,t)$$

From (C.12)

$$\mathcal{K}_m(s,r) = \sum_{j=0}^{L-1} \lambda_{jm}(t)\phi_{jm}(s,t)\phi_{jm}^*(r,t) = \sum_{j=0}^{L-1} \sigma\lambda'_{jm}(t)\tilde{E}_m\phi_{jm}(s,t)\phi_{jm}^*(r,t)$$

Therefore from (C.25)

$$l_{km}(s,t) = |\alpha_k|\tilde{s}_m(s-\tau_k) - \frac{1}{2N_0}\int_0^t \mathcal{K}_m(s,r)l_{km}(r,t)dr$$

$$= |\alpha_k|\tilde{s}_m(s-\tau_k) - \sum_{j=0}^{L-1} \sigma\lambda'_{jm}(t)\tilde{E}_m \sum_{l=0}^{L-1} \frac{|\alpha_k|}{\sqrt{\epsilon_{km}(t)\tilde{E}_m}} \frac{\lambda'_{lm}(t)\frac{\tilde{E}_m}{2N_0}}{1+\sigma\lambda'_{lm}(t)\frac{\tilde{E}_m}{2N_0}} [x_{lk}^m(t)]^*$$

$$\cdot \int_0^t \phi_{jm}(s,t)\phi_{jm}^*(r,t)\phi_{lm}(r,t)dr$$

$$= |\alpha_k|\tilde{s}_m(s-\tau_k) - \sigma \sum_{l=0}^{L-1} \frac{|\alpha_k|\tilde{E}_m}{\sqrt{\epsilon_{km}(t)\tilde{E}_m}} \frac{\left(\lambda'_{lm}(t)\right)^2\frac{\tilde{E}_m}{2N_0}}{1+\sigma\lambda'_{lm}(t)\frac{\tilde{E}_m}{2N_0}} [x_{lk}^m(t)]^* \phi_{lm}(s,t)$$

Hence

$$\lim_{\sigma\to 0} l_{km}(s,t) = |\alpha_k|\tilde{s}_m(s-\tau_k) \tag{3.165}$$

From (3.164) the conditional mean (3.161) reduces to

$$\check{v}_m(t) = \Re\left\{\frac{I_1(V_{0m}(t))}{I_0(V_{0m}(t))}|\alpha_0|\tilde{s}_m(t-\tau_0)e^{j\vartheta_{0m}(t)}e^{j\omega_c t}\right\} \tag{3.166}$$

where from (3.98-3.99) and (3.165)

$$V_{0m}(t)e^{j\vartheta_{0m}(t)} = \frac{2}{N_0}\int_0^t l_{0m}^*(s,t)e^{-j\omega_c s}dz(s) = \frac{2}{N_0}\int_0^t |\alpha_0|\tilde{s}_m^*(s-\tau_0)e^{-j\omega_c s}dz(s)$$

When $\boldsymbol{C} = \sigma\boldsymbol{I} = \boldsymbol{0}$, the path gains are not random anymore and are equal to their mean; only the first path gain has non-zero mean, hence from (3.1) the received signal is given by

$$\dot{z}(s) = \Re\left\{|\alpha_0|\tilde{s}_m(s-\tau_0)e^{j\theta_0'}e^{j\omega_c s}\right\} + \dot{w}(s) \tag{3.167}$$

This a typical received signal over a random phase channel. As expected (3.166) corresponds to the conditional mean found in [21] for a signal corrupted with a random phase and an additive Gaussian noise such as (3.167).

The limiting case when the specular components vanish resulting in Rayleigh channels will be investigated next. Section 3.2.2 showed that the matrix $\boldsymbol{X}_m$ is a decorrelating matrix in the case of specular coherent detection. From (3.67), it is seen that the matrix $\boldsymbol{X}_m$ is present in the non-coherent likelihood ratio associated with the general Ricean channel since $\boldsymbol{r}_m = \boldsymbol{X}_m^*\boldsymbol{u}_m$. Furthermore the dependence on $\boldsymbol{X}_m$ is maintained when the specular components vanish (Rayleigh channels). Therefore the study of Rayleigh channels will provide confirmation of the decorrelation purpose of the matrix $\boldsymbol{X}_m$ and generally much insight on the operations performed by the non-coherent optimum receiver for Ricean channels. Furthermore Rayleigh channels are of significant interest since they model transmission without a line-of-sight, and as such they represent a severely fading channel.

3.5 Non-coherent optimal decision rule for an L-path Rayleigh channel

3.5.1 L-path Rayleigh log-likelihood

For a Rayleigh multipath channel, $\alpha_0 = \alpha_1 = \ldots = \alpha_{L-1} = 0$. The log-likelihood ratio (3.67) reduces to

$$\ln\left[\Lambda_m\left(\dot{z};T_o\right)\right] = \ln\left(J_m\right) = \gamma_m^2\boldsymbol{u}_m^\dagger\left[\left(\boldsymbol{\epsilon}_m\boldsymbol{C}\right)^{-1} + \gamma_m\boldsymbol{\Gamma}_m^*\right]^{-1}\boldsymbol{u}_m - \ln\left[\det(\boldsymbol{I} + \gamma_m\boldsymbol{\epsilon}_m\boldsymbol{C}\boldsymbol{\Gamma}_m^*)\right] \tag{3.168a}$$

or to the equivalent form

$$\ln\left[\Lambda_m\left(\dot{z};T_o\right)\right] = \ln\left(J_m\right) = \gamma_m^2 \boldsymbol{r}_m^{\dagger}\left[\boldsymbol{D}_m^{-1} + \gamma_m \boldsymbol{I}\right]^{-1}\boldsymbol{r}_m - \ln\left[\det(\boldsymbol{I} + \gamma_m \boldsymbol{D}_m)\right] \tag{3.168b}$$

From (3.168a) and (3.168b), it is seen that the non-coherent optimum receiver for a multipath Rayleigh fading channel, denoted R OPT, is quadratic in the sampled matched filter output $\boldsymbol{u}_m$ or equivalently in the transform of these samples $\boldsymbol{r}_m$. The first form of the log-likelihood (3.168a) is essentially the receiver derived in [84], assuming a zero Doppler path shift and $\boldsymbol{\epsilon}_m = \boldsymbol{I}$. Similarly to the results of Section 3.2.2 for the SPECCOH scheme, the second form (3.168b) provides an important insight to the operations performed by the non-coherent optimal receiver as seen next.

3.5.2 R OPT over Rayleigh channels: a quadratic decorrelator

For a Rayleigh multipath channel, $\forall k = 0, \ldots, L-1\ \alpha_k = 0$. Therefore from (3.45) an equivalent model for such a channel is given by $H_m : \dot{z}(s) = \Re\left\{\sum_{k=0}^{L-1} a_k' \tilde{s}_m(s-\tau_k)e^{j\omega_c s}\right\}$ $+\dot{w}(s)$, $m = 1, 2, \ldots, M$, where a_k' are zero mean circularly complex Gaussian random variables with variance $E\left[a_k' a_k'^{*}/2\right] = \sigma_k^2$. Similar to (3.19), the m^{th} hypothesis can be equivalently expressed (since the linear transformation (3.7) is invertible) as

$$\begin{aligned}\dot{z}(s) &= \Re\left\{\sum_{k=0}^{L-1} a_k'\left[\sqrt{\tilde{E}_m}\sum_{l=0}^{L-1}\sqrt{\epsilon_{km}}\, y_{kl}^m \phi_{lm}(s)\right] e^{j\omega_c s}\right\} + \dot{w}(s) \\ &= \Re\left\{\sum_{l=0}^{L-1} a_{lm}'' \sqrt{\epsilon_{lm}\tilde{E}_m}\,\phi_{lm}(s) e^{j\omega_c s}\right\} + \dot{w}(s)\end{aligned} \tag{3.169}$$

where $y_{kl}^m = \left[\boldsymbol{X}_m^{-1}\right]_{kl}$[19] and $a_{lm}'' = \sum_{k=0}^{L-1} a_k' \frac{\sqrt{\epsilon_{km}}}{\sqrt{\epsilon_{lm}}} y_{kl}^m$. Note that $a_{lm}'' \triangleq a_{lm}''(T_o)$ where $a_{lm}''(t)$ is given by (3.52). Under each hypothesis the new random vector $\left[a_{0m}'', \ldots, a_{L-1m}''\right]^T$ is Gaussian with zero mean and covariance $\boldsymbol{\epsilon}_m^{-1}\boldsymbol{D}_m$ as shown in the following, using the proof of (3.20):

$$E\left[a_{rm}''\left(a_{lm}''\right)^{*}\right] = \sum_{k=0}^{L-1} 2\sigma_k^2 \epsilon_{km} \frac{y_{kr}^m}{\sqrt{\epsilon_{rm}}} \frac{\left(y_{kl}^m\right)^{*}}{\sqrt{\epsilon_{lm}}} = \left[\boldsymbol{\epsilon}_m^{-1}\boldsymbol{D}_m\right]_{rl} = 0 \quad \text{if } r \neq l$$

[19]The superscript m is not an exponent and refers to the hypothesis H_m.

Therefore, under each hypothesis, the received signal can be represented as a linear combination of orthogonal functions weighted by uncorrelated Gaussian random variables, similar to the resolvable multipath case. The log-likelihood ratio for a resolved multipath Rayleigh fading channel is given by

$$\gamma_m^2 \boldsymbol{u}_m^\dagger \left[(\boldsymbol{\epsilon}_m \boldsymbol{C})^{-1} + \gamma_m \boldsymbol{I} \right]^{-1} \boldsymbol{u}_m - \ln \left[\det(\boldsymbol{I} + \gamma_m \boldsymbol{\epsilon}_m \boldsymbol{C}) \right] \tag{3.170}$$

Note that (3.170) with $\boldsymbol{\epsilon}_m = \boldsymbol{I}$ is presented in [4, 88]. From (3.168b) and (3.170) it is seen that the Rayleigh channel non-coherent optimal receiver for unresolved multipath channels consists of an orthogonalization (or decorrelation) stage that transforms $\boldsymbol{u}_m$ into $\boldsymbol{r}_m = \boldsymbol{X}_m \boldsymbol{u}_m$ and then implements a resolved multipath channel non-coherent optimal decision rule for $\boldsymbol{r}_m$.

3.5.3 Non-coherent estimator-correlator for an L-path Rayleigh channel

A Rayleigh multipath channel can be viewed as a limiting form of a mixed mode Ricean/Rayleigh channel, when $\alpha_0 = 0$ in addition to $\alpha_1 = \alpha_2 = \ldots = \alpha_{L-1} = 0$. Hence results of Section 3.4.3 apply. From [21], the likelihood ratio $\Lambda_m(\dot{z}; T_o)$ can be expressed as (3.82) where the conditional mean (3.159a) reduces to

$$\check{v}_m(t) = \Re \left\{ \left(2 \int_0^t \mathcal{H}_m^*(s,t,t) e^{-j\omega_c s} dz(s) \right) e^{j\omega_c t} \right\} = \int_0^t h_m(t,s) dz(s)$$

where $\mathcal{H}_m(s,t,t)$ is given by (3.41) and $h_m(t,s) = \Re \left\{ 2\mathcal{H}_m^*(s,t,t) e^{j\omega_c(t-s)} \right\}$ is the unique square integrable solution of (3.28). Following the same method as in Section 3.3.3, from (3.161) the conditional mean is also given by

$$\check{v}_m(t) = \Re \left\{ \left(\sum_{k=0}^{L-1} \widehat{a_k'(t)}\, \tilde{s}_m(t - \tau_k) \right) e^{j\omega_c t} \right\}$$

where from (3.131) and (3.160) $\widehat{a_k'(t)}$ is given by

$$\widehat{a_k'(t)} = \frac{2}{\sqrt{\epsilon_{km}(t) \tilde{E}_m}} \sum_{l=0}^{L-1} \frac{\frac{\lambda_{lm}(t)}{2N_0}}{1 + \frac{\lambda_{lm}(t)}{2N_0}} x_{lk}^m(t) \int_0^t \phi_{lm}^*(s,t) e^{-j\omega_c s} dz(s) \tag{3.171a}$$

$$= \frac{2\sigma_k^2}{N_0} \int_0^t \frac{l_{km}^*(s,t)}{|\alpha_k|} e^{-j\omega_c s} dz(s) \quad \text{from (3.103b)} \tag{3.171b}$$

Since $\frac{l_{km}^{*}(s,t)}{|\alpha_k|}$ is independent of α_k, (3.171b) is well defined. Since the problem is Gaussian, the conditional mean is linear and the estimates of the path gains are MAP or MMSE estimators. The interpretation of the Rayleigh channel conditional mean is similar to the interpretation given in Section 3.3.3 and Section 3.4.3 for the Rayleigh part of Ricean and mixed mode Ricean/Rayleigh channel conditional means except that the remaining unknown part of the observation $y_m^{nc}(s)$ is equal to the received signal since there is no specular component.

3.6 Non-coherent optimal decision rule for a 2 Ricean/L-2 Rayleigh channel

3.6.1 2 Ricean/L-2 Rayleigh likelihood

A multipath fading channel is said to be a 2 Ricean/L-2 Rayleigh channel if the first two path gains are Ricean distributed and the other path gains are Rayleigh distributed, i.e. $\boldsymbol{\alpha} = [\alpha_0, \alpha_1, 0 \ldots, 0]^T$. For a 2 Ricean/$L$-2 Rayleigh channel, from Appendix B.3.2, the likelihood ratio is given by

$$\Lambda_m(\dot{z};T_o) = J_m\Big[I_0(V_{0m})\, I_0(V_{10}^m)\, I_0(V_{1m}) + 2\sum_{p=1}^{\infty}(-1)^p I_p(V_{0m})\, I_p(V_{10}^m)\, I_p(V_{1m})\cos\big(p(\vartheta_{0m}+\vartheta_{10}^m-\vartheta_{1m})\big)\Big] \quad (3.172)$$

where J_m is given by (3.63), V_{km} and ϑ_{km} are given by (3.73) and (3.74), V_{10}^m and ϑ_{10}^m are given by (3.75) and (3.76). It is seen that the likelihood ratio is independent of the phase of $\boldsymbol{\alpha}$.

3.6.2 Non-coherent estimator-correlator for a 2 Ricean/L-2 Rayleigh channel

From (D.21) the likelihood ratio over $[0,t]$ for a 2 Ricean/L-2 Rayleigh channel is given by

$$\Lambda_m(\dot{z};t) = J_m(t)\Big[I_0\big(V_{0m}(t)\big)I_0\big(V_{10}^m(t)\big)I_0\big(V_{1m}(t)\big) + 2\sum_{p=1}^{\infty}(-1)^p I_p\big(V_{0m}(t)\big)\, I_p\big(V_{10}^m(t)\big)\, I_p\big(V_{1m}(t)\big)\cos\big[p\big(\vartheta_{0m}(t)+\vartheta_{10}^m(t)-\vartheta_{1m}(t)\big)\big]\Big]$$

where $J_m(t)$ is given by (3.93), $V_{km}(t)$ and $\vartheta_{km}(t)$ are given by (3.98) and (3.99), $V_{10}^m(t)$ and $\vartheta_{10}^m(t)$ are given by (3.114) and (3.115). From [21], the likelihood ratio $\Lambda_m(\dot{z};T_o)$ can be expressed as (3.82) where from (3.113) (direct method) or from (3.124a, 3.125b) assuming $\alpha_2 = \ldots = \alpha_{L-1} = 0$ (Itô differentiation), the conditional mean for a 2 Ricean/L-2 Rayleigh channel is given by

$$\check{v}_m(t) = \Re\left\{\left(2\int_0^t \mathcal{H}_m^*(s,t,t)e^{-j\omega_c s}dz(s) + \sum_{k=0}^{1} V_{km}'(t)e^{j\vartheta_{km}'(t)}l_{km}(t,t)e^{j\vartheta_{km}(t)}\right)e^{j\omega_c t}\right\} \tag{3.173a}$$

$$= \Re\left\{\left(2\int_0^t \mathcal{H}_m^*(s,t,t)e^{-j\omega_c s}dy_m^{\mathrm{nc}}(s) + \sum_{k=0}^{1} |\alpha_k|\, V_{km}'(t)e^{j\vartheta_{km}'(t)}e^{j\vartheta_{km}(t)}\tilde{s}_m(t-\tau_k)\right)e^{j\omega_c t}\right\} \tag{3.173b}$$

where $dy_m^{\mathrm{nc}}(s) = dz(s) - \Re\left\{\sum_{k=0}^{1}|\alpha_k|\, V_{km}'(t)e^{j\vartheta_{km}'(t)}e^{j\vartheta_{km}(t)}\tilde{s}_m(s-\tau_k)e^{j\omega_c s}\right\}ds$, $\mathcal{H}_m(s,t,t)$ is given by (3.41), $V_{km}'(t)e^{j\vartheta_{km}'(t)}$ is given by (3.112), $l_{km}(t,t)$ is given by (3.103) and $\vartheta_{km}(t)$ is given by (3.99).

The interpretation of $\check{v}_m(t)$ for a 2 Ricean/L-2 Rayleigh channel follows the same lines of thought as in Section 3.3.3 for an L-path Ricean channel.

3.7 Non-coherent suboptimal receiver structures for a mixed mode Ricean/Rayleigh channel

3.7.1 The SPECCOH over resolved Ricean channels (SPECCOHR)

To assess the improvement due to the decorrelation stage for specular coherent detection, a receiver similar to SPECCOH except that it does not perform decorrelation is considered. This is the specular coherent optimum receiver over resolved Ricean channels (SPECCOHR) whose decision variable is given by (3.21).

3.7.2 The Quadratic Decorrelation Receiver (QDR)

The limiting forms of the log-likelihood ratio of the OPT scheme for a mixed mode Ricean/Rayleigh channel help to design suboptimum structures. Such a structure is

derived in the following. For extreme values of $|\alpha_0|$ the decision variables (3.156)-(3.158) can be viewed as linear combinations of $\ln(J_m)$ and V_{0m}^2. Therefore a suboptimal receiver based on the functional

$$\chi_m(\dot{z};T_o) = \ln(J_m) + cV_{0m}^2 \tag{3.174}$$

is proposed in this thesis where c is a constant to be determined, J_m is given by (3.63) and $V_{0m} = |\alpha_0|\,|b_{0m}|/(\sigma_0^2\sqrt{\epsilon_{0m}})$. For large values of $|\alpha_0|$, the constant c should vanish as γ_m increases since in that case the log-likelihood ratio can be approximated by $\ln(J_m)$. The simplest function achieving this goal is $c \propto \gamma_m^{-\beta}$. With this, the decision variable $\chi_m(\dot{z};T_o)$ tends to the true log-likelihood ratio as $|\alpha_0|$ assumes small or large values. Furthermore since $\boldsymbol{\alpha}$ has only one non-zero element, V_{0m} can be written as (3.155) hence V_{0m}^2 is a quadratic form. Thus a family of receivers of the form (3.174) called Quadratic Decorrelation Receivers (QDR) whose decision variables are given by

$$\chi_m(\dot{z};T_o) = \ln(J_m) + \frac{1}{\gamma_m^{\beta}}V_{0m}^2 \tag{3.175a}$$

$$= \ln(J_m) + \frac{4}{\gamma_m^{\beta}}\boldsymbol{r}_m^{\dagger}\boldsymbol{Q}_m\boldsymbol{X}_m^{*}\left(\boldsymbol{\epsilon}_m^{1/2}\boldsymbol{C}\right)^{-1}\boldsymbol{\alpha}\boldsymbol{\alpha}^{\dagger}\left(\boldsymbol{\epsilon}_m^{1/2}\boldsymbol{C}\right)^{-1}\boldsymbol{X}_m^{T}\boldsymbol{Q}_m\boldsymbol{r}_m \tag{3.175b}$$

is obtained. These receivers exploit the decorrelation performed on the input samples similar to the non-coherent optimal receiver. However, the nonlinear term due to the specular component is replaced by a quadratic form that is more suitable for implementation and analysis of performance. Furthermore the QDR requires knowledge of $|\alpha_0|$ only. It is to be noted that the QDR reduces to Aiken's receiver [84] when the path magnitudes are Rayleigh distributed and $\boldsymbol{\epsilon}_m = \boldsymbol{I}$.

When the observation interval $[0, T_o]$ is assumed to be much longer than the inter-path delays ($T_o \gg \tau_l$ for all l) and $\epsilon_{lm} = 1$ for all l, the QDR receiver is illustrated in Fig. 3.6. Calculation of the probability of error for several values of β shows that a good choice is $\beta = 1.3$ [188]. This value gives a low probability of error at high SNR as well as at low SNR.

The QDR decision variable depends only on $\ln(J_m)$ and V_{0m}. At low γ_m, $V_{0m} \approx 2\gamma_m\left[\boldsymbol{u}_m^{\dagger}\boldsymbol{\epsilon}_m^{1/2}\boldsymbol{\alpha}^{\dagger}\boldsymbol{\alpha}\boldsymbol{\epsilon}_m^{1/2}\boldsymbol{u}_m\right]^{1/2}$, thus it can be seen that the QDR, although suboptimal, has the property that the decorrelation on the input signal vanishes at low γ_m. Similarly to Proposition 3.3.1 in Section 3.3.1, it can be shown that the QDR decision

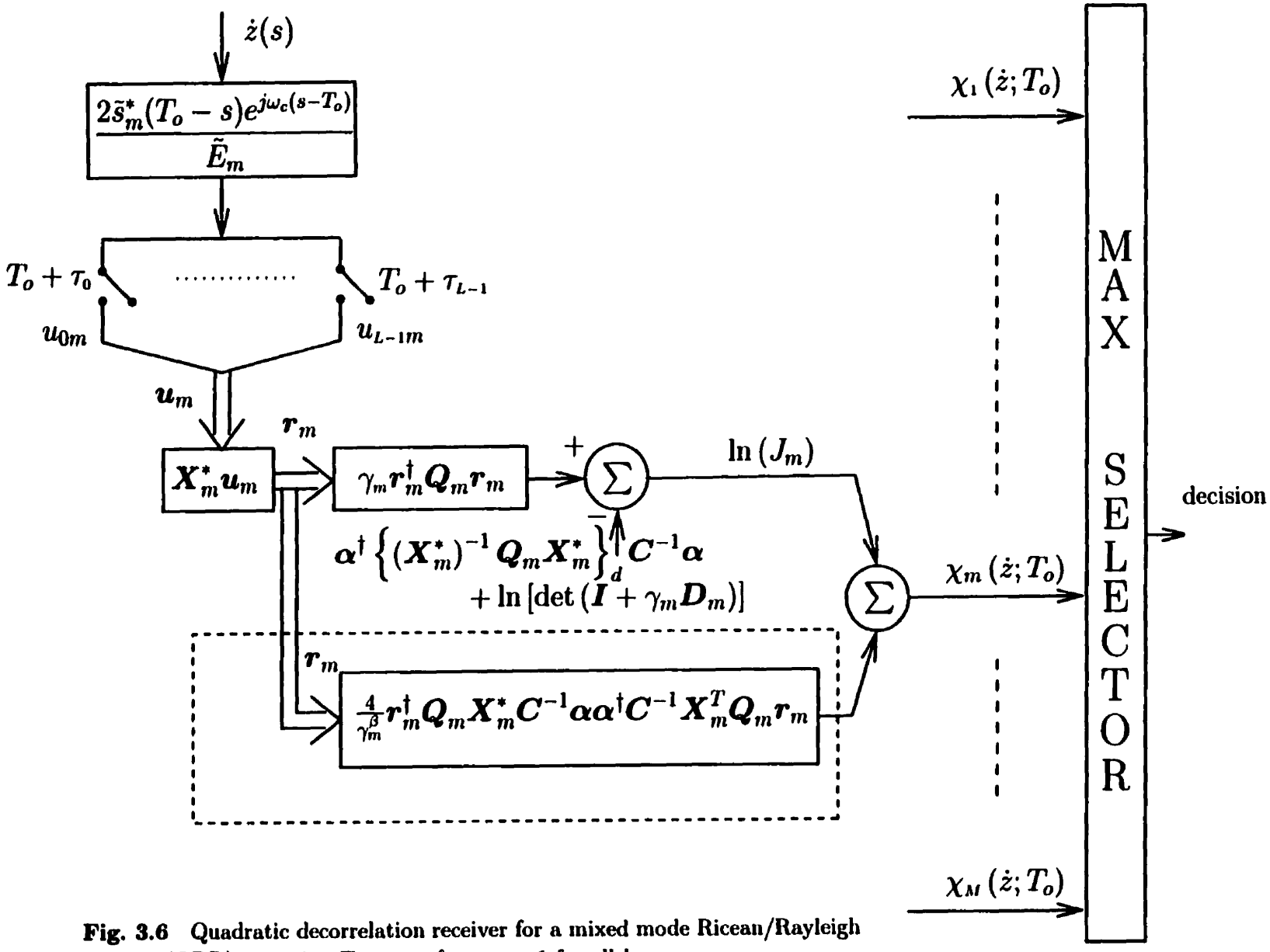

Fig. 3.6 Quadratic decorrelation receiver for a mixed mode Ricean/Rayleigh channel (QDR) assuming $T_o \gg \tau_l$ & $\epsilon_{lm} = 1$ for all l

variable and the OPT scheme log-likelihood ratio converge almost surely to the same term as γ_m goes to infinity, i.e.

$$\lim_{\gamma_m \to \infty} \text{a.s. } \frac{1}{\gamma_m} \ln\left[\Lambda_m(\dot{z}; T_o)\right] = \lim_{\gamma_m \to \infty} \text{a.s. } \frac{1}{\gamma_m} \ln\left[\chi_m(\dot{z}; T_o)\right] = \boldsymbol{r}_m^{\dagger} \boldsymbol{r}_m$$

This asymptotical property will also be confirmed analytically and numerically in terms of the receivers performance in Chapter 4.

3.7.3 The linear estimator-correlator form for the QDR

Over the observation interval $[0, T_o]$, the decision variable $\chi_m(\dot{z}; T_o)$ is given by (3.175a). Therefore considering an observation interval of $[0, t]$ instead of $[0, T_o]$, $\exp\{\chi_m(\dot{z}; t)\} = J_m(t) g\big(\boldsymbol{d}_m(t), t\big)$, where $g\big(\boldsymbol{d}_m(t), t\big) = \exp\left\{\gamma_m^{-\beta} V_{0m}^2(t)\right\}$. Therefore results from Appendix E can be applied. Let us denote $\chi_m'(\dot{z}; t) = \exp\{\chi_m(\dot{z}; t)\}$. Similarly to the optimum decision rule over mixed mode Ricean/Rayleigh channels, the function $g\big(\boldsymbol{d}_m(t), t\big)$ does not depend directly on t, and does not depend either on $V_{km}(t), k = 1, \ldots, L-1$ and $\vartheta_{km}(t), k = 0, \ldots, L-1$, thus from (3.112), $V_{km}'(t) e^{j\vartheta_{km}'(t)}$ is given by

$$V_{km}'(t) e^{j\vartheta_{km}'(t)} = 0 \quad k = 1, \ldots, L-1 \tag{3.176a}$$

$$V_{0m}'(t) e^{j\vartheta_{0m}'(t)} = \frac{\dfrac{\partial g\left(\boldsymbol{d}_m(t), t\right)}{\partial V_{0m}(t)}}{g\left(\boldsymbol{d}_m(t), t\right)} + j \frac{\dfrac{1}{V_{0m}(t)} \dfrac{\partial g\left(\boldsymbol{d}_m(t), t\right)}{\partial \vartheta_{0m}(t)}}{g\left(\boldsymbol{d}_m(t), t\right)} = \frac{2}{\gamma_m^{\beta}} V_{0m}(t) \tag{3.176b}$$

$$\text{i.e.} \quad V_{0m}'(t) = \frac{2}{\gamma_m^{\beta}} V_{0m}(t) \quad \vartheta_{0m}'(t) = 0$$

Substituting (3.176) into (E.53) yields

$$d\chi_m'(\dot{z}; t) = \frac{2}{N_0} \chi_m'(\dot{z}; t) \left[\Re\left\{ \left(2 \int_0^t \mathcal{H}_m^*(s, t, t) e^{-j\omega_c s} dz(s) + \frac{2}{\gamma_m^{\beta}} V_{0m}(t) l_{0m}(t, t) e^{j\vartheta_{0m}(t)} \right) e^{j\omega_c t} \right\} \right] dz(t) + \mathcal{R}_{2m}(t) \chi_m'(\dot{z}; t)\, dt \tag{3.177}$$

where $\mathcal{H}_m(s,t,t)$ and $l_{0m}(s,t)$ are respectively given by (3.41) and (3.103) and by substituting (C.36) and (E.3) into (E.50) $\mathcal{R}_{2m}(t)$ is given by

$$\begin{aligned}\mathcal{R}_{2m}(t) &= \frac{1}{2}\frac{N_0}{2}\left(\frac{2}{N_0}\right)^2 |l_{0m}(t,t)|^2 \cos^2\left(\omega_c t + \psi_{0m}(t,t) + \vartheta_{0m}(t)\right) \frac{\frac{\partial^2 g}{\partial V_{0m}^2}}{g\left(\boldsymbol{d}_m(t),t\right)} \\ &\quad + \frac{|l_{0m}(t,t)|^2}{2N_0}\left(\frac{\frac{1}{V_{0m}}\frac{\partial g}{\partial V_{0m}}}{g\left(\boldsymbol{d}_m(t),t\right)} - 1\right) \\ &= \frac{1}{2}\frac{N_0}{2}\left(\frac{2}{N_0}\right)^2 |l_{0m}(t,t)|^2 \cos^2(\omega_c t + \psi_{0m}(t,t) + \vartheta_{0m}(t)) \frac{2}{\gamma_m^\beta}\left(1 + \frac{2}{\gamma_m^\beta} V_{0m}^2(t)\right) \\ &\quad + \frac{|l_{0m}(t,t)|^2}{2N_0}\left(\frac{2}{\gamma_m^\beta} - 1\right) \end{aligned} \tag{3.178}$$

since $\chi_m'(\dot{z};t) = J_m(t)\exp\left\{\gamma_m^{-\beta} V_{0m}^2(t)\right\}$. Therefore from (3.177) $d\chi_m'(\dot{z};t)$ is of the form (3.118), so from Proposition 3.3.2 in Section 3.3.3 and using (3.176b), the linear estimator of the signal associated with the QDR scheme is given by

$$\widehat{v_m(t)} = \Re\left\{\left(2\int_0^t \mathcal{H}_m^*(s,t,t)e^{-j\omega_c s}dz(s) + \frac{2}{\gamma_m^\beta} V_{0m}(t) l_{0m}(t,t) e^{j\vartheta_{0m}(t)}\right) e^{j\omega_c t}\right\} \tag{3.179a}$$

$$= \Re\left\{\left(2\int_0^t \mathcal{H}_m'^*(s,t,t)e^{-j\omega_c s}dz(s)\right) e^{j\omega_c t}\right\} \quad \text{from (3.98-3.100)} \tag{3.179b}$$

where

$$\mathcal{H}_m'(\tau,s,t) = \mathcal{H}_m(\tau,s,t) + \frac{1}{\gamma_m^\beta}\frac{2}{N_0} l_{0m}(\tau,t) l_{0m}^*(s,t) \tag{3.180}$$

From (3.178), neglecting integrals containing double frequency terms yields

$$\int_0^{T_o} \mathcal{R}_{2m}(t)dt = \frac{2}{N_0}\int_0^{T_o} |l_{0m}(t,t)|^2 \left[\frac{1}{\gamma_m^\beta}\left(1 + \frac{1}{\gamma_m^\beta} V_{0m}^2(t)\right) - \frac{1}{4}\right] dt \tag{3.181}$$

Therefore from (3.119) and (3.177), the quasi estimator-correlator form of the QDR is given by

$$\chi_m'(\dot{z};T_o) = \exp\left\{\frac{2}{N_0}\left[\int_0^{T_o} \widehat{v_m(t)}\, dz(t) - \frac{1}{2}\int_0^{T_o}\left(\widehat{v_m(t)}\right)^2 dt + \frac{N_0}{2}\int_0^{T_o} \mathcal{R}_{2m}(t)dt\right]\right\}$$

or equivalently

$$\chi_m(\dot{z};T_o) = \frac{2}{N_0}\left[\int_0^{T_o} \widehat{v_m(t)}\, dz(t) - \frac{1}{2}\int_0^{T_o} \left(\widehat{v_m(t)}\right)^2 dt + \frac{N_0}{2}\int_0^{T_o} \mathcal{R}_{2m}(t)dt\right]$$

where $\widehat{v_m(t)}$ is given by (3.179) and $\mathcal{R}_{2m}(t)$ is given by (3.181). From (3.179b) it is seen that the obtained estimator is linear. Comparing (3.179a) with the MMSE estimate given by (3.159a) shows that $\widehat{v_m(t)}$ is obtained by linearizing the nonlinear scaling factor $\frac{I_1(V_{0m}(t))}{I_0(V_{0m}(t))}$ in (3.159a), yielding a linear estimator (3.179b). Specifically $\frac{I_1(x)}{I_0(x)}$ has been replaced by $\frac{2x}{\gamma_m^\beta}$, which is equivalent to the approximation

$$\ln\left[I_0(u)\right] \approx \frac{u^2}{\gamma_m^\beta} \tag{3.182}$$

since $I_1(x) = I_0'(x)$. Note that (3.182) has been used to approximate the term $\ln\left[I_0(V_{0m})\right]$ in the log-likelihood ratio of the mixed mode Ricean/Rayleigh channel to obtain the QDR decision variable $\chi_m(\dot{z};T_o)$. Therefore to each approximation of the likelihood ratio corresponds an approximation to the MMSE estimate that yields a suboptimum estimate. The decision variable obtained by approximation of the likelihood ratio can be expressed as a quasi-estimator-correlator form where the estimate is given by the corresponding approximation of the MMSE estimate. In general the new decision variable is not a likelihood ratio. Other suboptimum decision variables can be obtained by substituting the MMSE estimate in the estimator-correlator form of the likelihood ratio by an approximation. For example it is shown in Section 3.7.5 that the decision variable of R OPT is obtained when the MMSE estimate is replaced by the linear estimate $\int_0^t h_m(t,s)dz(s)$. The linear MMSE (LMMSE) estimator-correlator over Ricean channels is derived in Section 3.7.6.

To provide insight on the linear estimate used by the QDR scheme, let us consider its limiting form when the path resolvability assumption is satisfied over $[0,t]$ (i.e. (3.58) holds). In that case $\widehat{v_m(t)}$ is given by (3.179b) where substituting (3.59-3.61)

and (3.147) into (3.180) yields

$$\mathcal{H}'_m(s,t,t) = \sum_{l=1}^{L-1} \frac{2\sigma_l^2 \epsilon_{lm}(t)\gamma_m}{1+2\sigma_l^2\epsilon_{lm}(t)\gamma_m} \frac{\tilde{s}_m(s-\tau_l)}{\sqrt{\epsilon_{lm}(t)\tilde{E}_m}} \frac{\tilde{s}_m^*(t-\tau_l)}{\sqrt{\epsilon_{lm}(t)\tilde{E}_m}} + \frac{2\sigma_0^2\epsilon_{0m}(t)\gamma_m}{1+2\sigma_0^2\epsilon_{0m}(t)\gamma_m} \left(1 + \frac{4|\alpha_0|^2}{\gamma_m^\beta 2\sigma_0^2(1+2\sigma_0^2\epsilon_{0m}(t)\gamma_m)}\right) \frac{\tilde{s}_m(s-\tau_0)}{\sqrt{\epsilon_{0m}(t)\tilde{E}_m}} \frac{\tilde{s}_m^*(t-\tau_0)}{\sqrt{\epsilon_{0m}(t)\tilde{E}_m}} \tag{3.183}$$

Such a linear estimator will be compared to the linear estimator of the LMMSE scheme derived in Section 3.7.6.

3.7.4 The Quadratic Receiver (QR)

In order to assess the performance improvement due to the decorrelation operation for non-coherent detection, receivers that are very similar to QDR except that they do not employ decorrelation are considered. Therefore simple Quadratic Receivers (QR) that are a limiting form of the QDR (3.175) when the multipath is resolved (i.e. when $\boldsymbol{X}_m = \boldsymbol{\Gamma}_m = \boldsymbol{I}$) are also studied in this thesis. The decision variable for the QR is then

$$\begin{aligned}\chi''_m(\dot{z};T_o) &= \ln(J_m) + \frac{1}{\gamma_m^\beta} V_{0m}^2 \\ &= \gamma_m^2 \boldsymbol{u}_m^\dagger \left[(\boldsymbol{\epsilon}_m \boldsymbol{C})^{-1} + \gamma_m \boldsymbol{I}\right]^{-1} \\ &\quad \cdot \left[\boldsymbol{I} + \frac{4}{\gamma_m^{\beta+1}} \left(\boldsymbol{\epsilon}_m^{1/2}\boldsymbol{C}\right)^{-1} \boldsymbol{\alpha}\boldsymbol{\alpha}^\dagger \left(\boldsymbol{\epsilon}_m^{1/2}\boldsymbol{C}\right)^{-1} \gamma_m \left[(\boldsymbol{\epsilon}_m\boldsymbol{C})^{-1} + \gamma_m\boldsymbol{I}\right]^{-1}\right] \boldsymbol{u}_m \\ &\quad - \boldsymbol{\alpha}^\dagger \gamma_m \left[(\boldsymbol{\epsilon}_m\boldsymbol{C})^{-1} + \gamma_m\boldsymbol{I}\right]^{-1} \boldsymbol{C}^{-1}\boldsymbol{\alpha} - \ln\left[\det(\boldsymbol{I} + \gamma_m \boldsymbol{\epsilon}_m \boldsymbol{C})\right] \end{aligned} \tag{3.184}$$

where $V_{0m} = |\alpha_0| \left|\left[\gamma_m \left[(\boldsymbol{\epsilon}_m\boldsymbol{C})^{-1} + \gamma_m\boldsymbol{I}\right]^{-1} \boldsymbol{u}_m\right]_0\right| / \left(\sigma_0^2\sqrt{\epsilon_{0m}}\right)$. The QR's schemes can be considered as suboptimum receivers with respect to Turin's resolved multipath optimum receiver [4]. When the path magnitudes are Rayleigh distributed, they reduce to the optimum receiver for a resolved multipath Rayleigh fading channel. Calculation of the bit error probabilities shows that for QR, $\beta = 0$ is best [188].

3.7.5 The non-coherent optimal receiver over Rayleigh channels (R OPT)

The non-coherent optimal receiver over Rayleigh multipath channels can be viewed as a suboptimal receiver for mixed mode Ricean/Rayleigh channels. Its decision rule is given by (3.168). Since the Itô differentiation of any $\mathcal{F}_m(\dot{z};t)$ is independent of whether the fading is Ricean or Rayleigh, the estimator-correlator form obtained in Section 3.5.3 by Itô differentiation is also valid for Ricean channels. From Section 3.5.3, it is seen that the likelihood ratio $\Lambda_m(\dot{z};T_o)$ given by (3.168) can also be expressed as

$$\Lambda_m(\dot{z};T_o) = \exp\left\{\frac{2}{N_0}\left[\int_0^{T_o} \widehat{v_m(t)}\, dz(t) - \frac{1}{2}\int_0^{T_o}\left(\widehat{v_m(t)}\right)^2 dt\right]\right\}$$

where $\widehat{v_m(t)}$ is a linear estimator given by

$$\widehat{v_m(t)} = \int_0^t \Re\left\{\left(2\int_0^t \mathcal{H}_m^*(s,t,t)e^{-j\omega_c s}dz(s)\right)e^{j\omega_c t}\right\} = \int_0^t h_m(t,s)dz(s)$$

where $\mathcal{H}_m(s,t,t)$ is given by (3.41). Note however that for Ricean channels, $\int_0^t h_m(t,s)dz(s)$ is not the MMSE estimator.

3.7.6 The linear MMSE estimator-correlator (LMMSE)

In this section, the linear MMSE estimator-correlator over Ricean channels is investigated. This receiver has the following decision rule

$$\Lambda_m(\dot{z};T_o) = \exp\left\{\frac{2}{N_0}\left[\int_0^{T_o} \widehat{[v_m(t)|\dot{z}(s),0\le s\le t,H_m]}\, dz(t) - \frac{1}{2}\int_0^{T_o}\left(\widehat{[v_m(t)|\dot{z}(s),0\le s\le t,H_m]}\right)^2 dt\right]\right\} \tag{3.185}$$

where $\widehat{[v_m(t)|\dot{z}(s),0\le s\le t,H_m]}$ is the MMSE linear estimator of $v_m(t)$ based on the observation $\{\dot{z}(s),0\le s\le t\}$, where $\dot{z}(t) = v_m(t) + \dot{w}(t)$. Here a form similar to (3.82) employing the Itô integral is considered.

Proposition 3.7.1. *The linear MMSE estimator-correlator for Ricean channels decision variable is given by (3.185) where*

$$\widehat{[v_m(t)|\dot{z}(s), 0 \le s \le t, H_m]} = \int_0^t h_m''(t,s)dz(s) \tag{3.186a}$$

$$= \Re\left\{\left(2\int_0^t \mathcal{H}_m''^*(s,t,t)e^{-j\omega_c s}dz(s)\right)e^{j\omega_c t}\right\} \tag{3.186b}$$

$h_m''(t,s)$ is the unique square integrable solution of the Wiener Hopf equation

$$h_m''(t,s) + \frac{2}{N_0}\int_0^t h_m''(t,u)K_m''(u,s)du = \frac{2}{N_0}K_m''(t,s) \quad 0 \le s \le t \tag{3.187}$$

and $K_m''(u,v) \triangleq E[v_m(u)v_m(v)]$ is given by

$$K_m''(u,v) = \left[K_m(u,v) + K_m^s(u,v)\right] = \Re\left\{\frac{1}{2}\mathcal{K}_m''(u,v)e^{j\omega_c(u-v)}\right\} \tag{3.188}$$

where $\mathcal{K}_m''(u,v) \triangleq E[\tilde{v}_m(u)\tilde{v}_m^*(v)]$ satisfies

$$\mathcal{K}_m''(u,v) = \mathcal{K}_m(u,v) + \mathcal{K}_m^s(u,v) = \sum_{k=0}^{L-1}\left(|\alpha_k|^2 + 2\sigma_k^2\right)\tilde{s}_m(u-\tau_k)\tilde{s}_m^*(v-\tau_k) \tag{3.189}$$

since $\mathcal{K}_m(u,v)$ is given by (3.6), $\mathcal{K}_m^s(u,v) = \sum_{k=0}^{L-1}|\alpha_k|^2\tilde{s}_m(u-\tau_k)\tilde{s}_m^*(v-\tau_k)$, and

$$K_m^s(u,v) = E\Big[E\big[v_m(u)|\boldsymbol{\theta}\big]E\big[v_m(v)|\boldsymbol{\theta}\big]\Big] = \Re\left\{\frac{1}{2}\mathcal{K}_m^s(u,v)e^{j\omega_c(u-v)}\right\} \tag{3.190}$$

It can be shown that $h_m''(t,s) = \Re\left\{2\mathcal{H}_m''^*(s,t,t)e^{j\omega_c(t-s)}\right\}$ where $\mathcal{H}_m''(\tau,s,t)$ is given by

$$\mathcal{H}_m''(\tau,s,t) \triangleq \begin{cases} \displaystyle\sum_{l=0}^{L-1}\frac{\frac{\lambda_{lm}''(t)}{2N_0}}{1+\frac{\lambda_{lm}''(t)}{2N_0}}\phi_{lm}''(\tau,t)\phi_{lm}''^*(s,t) & \begin{matrix}0 \le \tau, s \le t \\ 0 \le t < \infty\end{matrix} \\ 0 & \text{else.}\end{cases} \tag{3.191}$$

with $\lambda_{lm}''(t)$ and $\phi_{lm}''(s,t)$ defined similar to $\lambda_{lm}(t)$, (3.37), and $\phi_{lm}(s,t)$, (3.39), except that they are associated with $\mathcal{K}_m''(\tau,s)$ instead of $\mathcal{K}_m(\tau,s)$.

It is seen from (3.189) that the LMMSE estimator-correlator scheme treats the randomly phase-shifted specular component as an additional Gaussian component whose power is added to the Rayleigh component.

Proof. As seen in Appendix F.2, the random process $v_m(s)$ is zero mean with covariance function $K_m''(\tau, s)$ given by

$$K_m''(\tau, s) \triangleq E[v_m(\tau)v_m(s)] = K_m(\tau, s) + K_m^s(\tau, s)$$

where $K_m(\tau, s)$ is given by (3.5) and from (F.1) $K_m^s(\tau, u)$ is given by (3.190).

Following [189, p. 67] and [187, pp. 198-202], a linear estimate of $v_m(\tau)$ at time τ based on the values of the received signal under H_m for the interval of time $[0, t]$ can be written as

$$\widehat{[v_m(\tau)|\dot{z}(s), 0 \le s \le t, H_m]} = \int_0^t H_m''(\tau, s, t)\dot{z}(s)ds = \int_0^t H_m''(\tau, s, t)dz(s) \quad (3.192)$$

where $H_m''(\tau, s, t)$ is a linear filter and the dependence on the observation interval t has been introduced as an extra parameter to the filter. The linear MMSE estimate satisfies [187, p. 201], [189, p. 67]

$$\frac{N_0}{2}H_m''(\tau, s, t) + \int_0^t H_m''(\tau, u, t)K_m''(u, s)du = K_m''(\tau, s) \qquad 0 \le \tau, s \le t$$

Setting $\tau = t$ into (3.192) yields

$$\widehat{[v_m(t)|\dot{z}(s), 0 \le s \le t, H_m]} = \int_0^t h_m''(t, s)dz(s)$$

where $h_m''(t, s) \triangleq H_m''(t, s, t)$ satisfies the Wiener Hopf equation (3.187). **Q.E.D**

To compare the linear estimators of the LMMSE and the QDR schemes, let us consider the special case of resolved mixed mode Ricean/Raleigh channels, where a simple closed-form solution of $H_m''(\tau, s, t)$ can be found. When the path resolvability assumption is satisfied on $[0, t]$ (i.e. (3.58) holds), $\widehat{v_m(t)}$ is given by (3.186b) where

$\mathcal{H}_m''(s,t,t)$ is given by

$$\mathcal{H}_m''(s,t,t) = \sum_{l=1}^{L-1} \frac{2\sigma_l^2 \epsilon_{lm}(t)\gamma_m}{1+2\sigma_l^2\epsilon_{lm}(t)\gamma_m} \frac{\tilde{s}_m(s-\tau_l)}{\sqrt{\epsilon_{lm}(t)\tilde{E}_m}} \frac{\tilde{s}_m^*(t-\tau_l)}{\sqrt{\epsilon_{lm}(t)\tilde{E}_m}} + \frac{\left(|\alpha_0|^2+2\sigma_0^2\right)\epsilon_{0m}(t)\gamma_m}{1+\left(|\alpha_0|+2\sigma_0^2\right)\epsilon_{0m}(t)\gamma_m} \frac{\tilde{s}_m(s-\tau_0)}{\sqrt{\epsilon_{0m}(t)\tilde{E}_m}} \frac{\tilde{s}_m^*(t-\tau_0)}{\sqrt{\epsilon_{0m}(t)\tilde{E}_m}} \quad (3.193)$$

Equation (3.193) is obtained by noting that since the signals $\tilde{s}_m(s-\tau_l)$ are orthogonal, from (3.189) the eigenvalues and eigenfunctions of $\mathcal{K}_m''(s,u)$ are respectively equal to $\left\{\left(|\alpha_l|^2+2\sigma_l^2\right)\epsilon_{lm}(t)\tilde{E}_m\right\}_{l=0,\ldots,L-1}$ and $\left\{\frac{\tilde{s}_m(s-\tau_l)}{\sqrt{\epsilon_{lm}(t)\tilde{E}_m}}\right\}_{l=0,\ldots,L-1}$. Comparing (3.193) with (3.183) shows how the QDR handles the specular component close to the way that the LMMSE scheme does. Basically the weighting factor in front of the eigenfunction associated with the first path is different. It is seen that at high SNR, both factors converge to one showing that the QDR and the LMMSE schemes perform the same operations on the received signal at high SNR and thus yield similar performance. At low SNR however, the factor for the QDR tends to $4\cdot\epsilon_{0m}(t)\left|\alpha_0\right|^2\gamma_m^{1-\beta}$ whereas the LMMSE factor tends to $\left(|\alpha_0|^2+2\sigma_0^2\right)\epsilon_{0m}(t)\gamma_m$.

3.8 Non-coherent suboptimal receiver structure for an L-path Rayleigh channel: the QR over resolved Rayleigh channels (R QR)

To assess the improvement due to the decorrelation stage over Rayleigh channels, a receiver similar to R OPT except that it does not perform decorrelation is considered. This is the Quadratic Receiver for Rayleigh fading channels (R QR) whose decision variable is based on (3.170). Note that (3.170) is also obtained by setting $\boldsymbol{\alpha}=\mathbf{0}$ into the QR decision variable (3.184).

Performance of the various receivers studied in this chapter will be presented next over the two channels of focus, i.e. over two-path mixed mode Ricean/Rayleigh and two and three-path Rayleigh channels assuming a long observation interval and signals time-limited to $[0,T]$.

Chapter 4

Performance analysis with binary modulation schemes (FSK, DPSK)

4.1 Performance evaluation

4.1.1 Performance evaluation of the OPT scheme over mixed mode Ricean/Rayleigh channels

The non-linearities of the non-coherent optimum receiver (OPT) for Ricean multi-path channels, (3.67), make its performance analysis very tedious, if not impossible. Therefore, upper and lower-bounds for the bit-error probability of the OPT scheme are employed. Upper-bounds are obtained by evaluating the performance of suboptimum quadratic receivers such as the QDR (for various β), R OPT or QR schemes. For each SNR, the lowest probability of error among all suboptimum receivers is retained to provide the tightest upper-bound. An example that considers FSK with frequency deviation $f_1 - f_2 = 1/2T$ is illustrated in Fig. 4.1. The bit-error probabilities of the various suboptimum receivers considered in this case are calculated as a function of the received SNR per bit E_b/N_0 over a two-path mixed mode Ricean/Rayleigh fading channel. Then, for each value of E_b/N_0, the minimum among the calculated curves is used to form the upper-bound for the bit-error probability of the OPT scheme with FSK signaling. The considered channel is characterized by three parameters, $s \triangleq \frac{\sigma_1^2}{\sigma_2^2}$, $\mathsf{K} \triangleq \frac{|a_0|^2}{2\sigma_0^2}$ and $\tau = \tau_1 - \tau_0$. For convenience K is expressed in decibels (dB) and τ is expressed as a percentage of the duration of the signaling waveform, T. More details on channel labeling are given in Section 4.2.

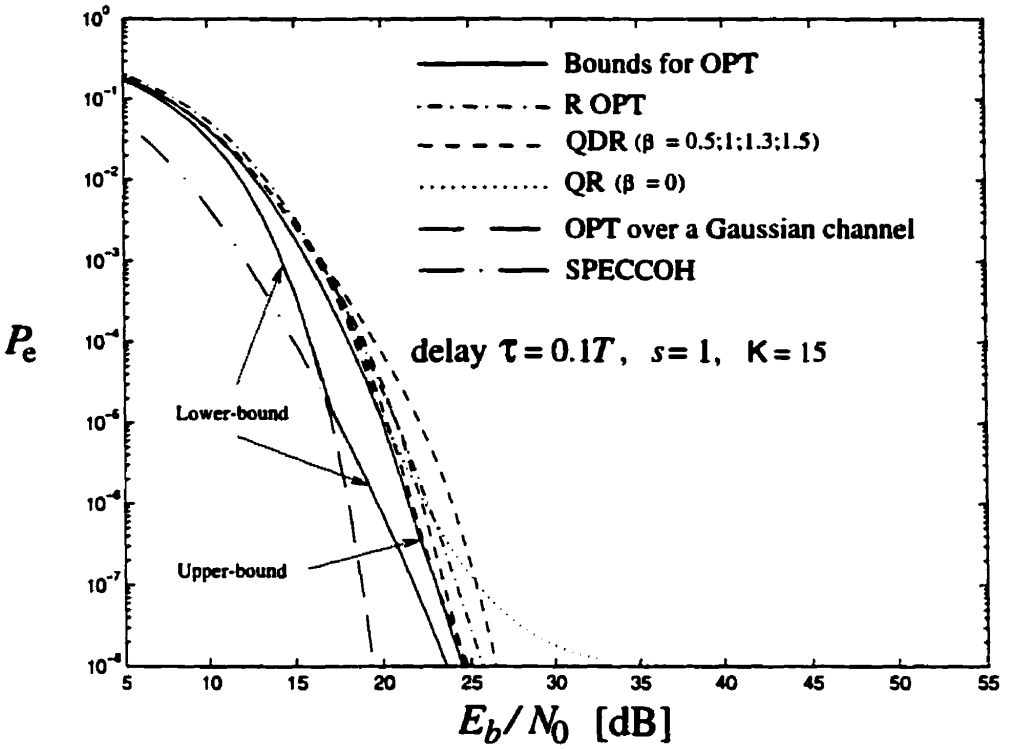

Fig. 4.1 Performance of FSK signaling with $f_1 - f_2 = 1/2T$ over a 2-path mixed mode Ricean/Rayleigh channel ($\tau = 0.1T$, $s = 1$ and K = 15dB)

Lower-bounds are obtained by evaluating the performance of the non-coherent optimum receiver over a Gaussian non-fading channel, and the performance of the optimum receiver that assumes perfect knowledge of the amplitude and phase of the specular term over the considered mixed mode Ricean/Rayleigh multipath fading channel (SPECCOH) from Section 3.2.1. For each SNR, the highest probability of error is retained to provide the tightest lower-bound as seen by the example of Fig 4.1. Fig 4.1 shows that the lower-bound is equal to the bit-error probability of the Gaussian channel non-coherent optimum receiver for low SNR, and to the SPECCOH one for high SNR. This rule is quite general for the cases of this thesis, although the SNR "threshold" varies with the channel parameters and modulation schemes. For example for low values of the Ricean parameter, since the SNR "threshold" is very low, the lower-bound is equal to the performance of the SPECCOH scheme for the entire range of SNR considered in this thesis. As seen in Section 3.2.1, the SPECCOH

scheme is also quadratic. Therefore, the technique of upper and lower bounding the performance of the OPT receiver for the various modulation schemes requires the evaluation of quadratic receivers performance.

4.1.2 Performance evaluation of quadratic receivers

This section presents the method used to compute the bit-error probability of any quadratic receivers with a Gaussian statistic. This method can be applied to the SPECCOH, SPECCOHR, QDR, R OPT and QR schemes. Let $\chi_m(\dot{z};T_o) \triangleq \chi_m$ be the decision variable under hypothesis H_m associated with the considered receiver. When the receiver is coherent as for the SPECCOH and SPECCOHR schemes, the decision variables employ $\boldsymbol{\theta}$. When the receiver is non-coherent as for the QDR, R OPT and QR schemes, the decision variables do not use $\boldsymbol{\theta}$. However, in both cases they may depend on $\boldsymbol{\theta}$ through the received signal. With equiprobable equal energy binary signals, the probability of error (bit-error probability) with $\boldsymbol{\theta}$ held fixed is

$$\begin{aligned} P_e(\boldsymbol{\theta}) &= \frac{1}{2}\left(\Pr[\chi_1 < \chi_2 | H_1, \boldsymbol{\theta}] + \Pr[\chi_2 < \chi_1 | H_2, \boldsymbol{\theta}]\right) \\ &= \frac{1}{2}\left(\Pr[\chi_1 - \chi_2 < 0 | H_1, \boldsymbol{\theta}] + \Pr[\chi_2 - \chi_1 < 0 | H_2, \boldsymbol{\theta}]\right) \\ &= \frac{1}{2}\left(\Pr[\Delta < A | H_1, \boldsymbol{\theta}] + \Pr[\Delta > A | H_2, \boldsymbol{\theta}]\right) \end{aligned} \tag{4.1}$$

where $\chi_1 - \chi_2 = \Delta - A$, $\Delta \triangleq \boldsymbol{r}^\dagger \begin{pmatrix} \boldsymbol{Q}_1' & \boldsymbol{0} \\ \boldsymbol{0} & -\boldsymbol{Q}_2' \end{pmatrix} \boldsymbol{r}$ is a Hermitian quadratic form in jointly Gaussian random variables, and A is a bias term. The probability of error, P_e is then obtained by averaging (4.1) over the phases $\boldsymbol{\theta}$. The expressions of $\boldsymbol{Q}_m'$, $m = 1, 2$ and $\boldsymbol{r}$ for the various receivers studied in this thesis assuming equal energy and a long observation interval are presented in Table 4.1. The expressions of the bias term A are presented in Table 4.2.

It is well known that (4.1) can be evaluated by inverting the characteristic function, $\varphi_{\Delta|H_k}(jt) \triangleq E\left[e^{jt\Delta} | H_k, \boldsymbol{\theta}\right]$, of Δ [88],

$$\varphi_{\Delta|H_k}(jt) = [\det(\boldsymbol{I} - jt\boldsymbol{R}_k\boldsymbol{Q})]^{-1} \exp\left\{-\overline{\boldsymbol{r}}^{k\dagger}\boldsymbol{R}_k^{-1}[\boldsymbol{I} - (\boldsymbol{I} - jt\boldsymbol{R}_k\boldsymbol{Q})^{-1}]\overline{\boldsymbol{r}}^k\right\} \tag{4.2}$$

where $\overline{\boldsymbol{r}}^k = E[\boldsymbol{r}|H_k, \boldsymbol{\theta}]$, $\boldsymbol{R}_k = E\left[(\boldsymbol{r} - \overline{\boldsymbol{r}})(\boldsymbol{r} - \overline{\boldsymbol{r}})^\dagger | H_k, \boldsymbol{\theta}\right]$ and $\boldsymbol{Q} = \begin{pmatrix} \boldsymbol{Q}_1' & \boldsymbol{0} \\ \boldsymbol{0} & -\boldsymbol{Q}_2' \end{pmatrix}$.

Table 4.1 Characterization of the quadratic form Δ associated with the probability of error of the various quadratic receivers.
$\boldsymbol{Q}_m$, $\boldsymbol{X}_m$, $\boldsymbol{\varrho}(\boldsymbol{\theta})$, $\boldsymbol{\alpha}$, $\boldsymbol{r}_m, \boldsymbol{u}_m, m = 1, 2$ are respectively given by (3.16), (3.8), (3.12), (3.13), (3.14) and (3.18a).

receivers	$\boldsymbol{Q}'_m$, $m = 1, 2$	$\boldsymbol{r}$
SPECCOH	$\boldsymbol{Q}_m$	$\begin{pmatrix} \boldsymbol{r}_1 + \frac{1}{\gamma}\boldsymbol{X}_1^* \boldsymbol{C}^{-1}\boldsymbol{\varrho}(\boldsymbol{\theta}) \\ \boldsymbol{r}_2 + \frac{1}{\gamma}\boldsymbol{X}_2^* \boldsymbol{C}^{-1}\boldsymbol{\varrho}(\boldsymbol{\theta}) \end{pmatrix}$
SPECCOHR	$\boldsymbol{C}'' = \gamma\left(\boldsymbol{C}^{-1} + \gamma \boldsymbol{I}\right)^{-1}$	$\begin{pmatrix} \boldsymbol{u}_1 + \frac{1}{\gamma}\boldsymbol{C}^{-1}\boldsymbol{\varrho}(\boldsymbol{\theta}) \\ \boldsymbol{u}_2 + \frac{1}{\gamma}\boldsymbol{C}^{-1}\boldsymbol{\varrho}(\boldsymbol{\theta}) \end{pmatrix}$
QDR	$\boldsymbol{Q}_m\left(\boldsymbol{I} + \frac{4}{\gamma^{\beta+1}}\boldsymbol{X}_m^* \boldsymbol{C}^{-1}\boldsymbol{\alpha}\boldsymbol{\alpha}^\dagger \boldsymbol{C}^{-1}\boldsymbol{X}_m^T \boldsymbol{Q}_m\right)$ where $\gamma = \gamma_1 = \gamma_2$	$\begin{pmatrix} \boldsymbol{r}_1 \\ \boldsymbol{r}_2 \end{pmatrix}$
R OPT	$\boldsymbol{Q}_m$	$\begin{pmatrix} \boldsymbol{r}_1 \\ \boldsymbol{r}_2 \end{pmatrix}$
QR	$\boldsymbol{C}''\left(\boldsymbol{I} + \frac{4}{\gamma^{\beta+1}}\boldsymbol{C}^{-1}\boldsymbol{\alpha}\boldsymbol{\alpha}^\dagger \boldsymbol{C}^{-1}\boldsymbol{C}''\right)$	$\begin{pmatrix} \boldsymbol{u}_1 \\ \boldsymbol{u}_2 \end{pmatrix}$

The pdf of Δ is given by the Fourier transform of $\varphi_{\Delta|H_k}(jt)$, and $\Pr[\Delta < A|H_1, \boldsymbol{\theta}]$, $\Pr[\Delta > A|H_2, \boldsymbol{\theta}]$ are obtained by integrating this pdf:

$$P_{e1}(\boldsymbol{\theta}) = \Pr[\Delta < A|H_1, \boldsymbol{\theta}] = \frac{1}{2\pi j}\int_{-\infty}^{A}\int_{-j\infty}^{j\infty} \varphi_{\Delta|H_1}(z)e^{-zu}dz\,du$$
$$= -\frac{1}{2\pi j}\int_{-j\infty-\epsilon}^{j\infty-\epsilon} \frac{\varphi_{\Delta|H_1}(z)}{z}e^{-zA}dz \triangleq -\frac{1}{2\pi j}\int_{C_1} \mathrm{h}_1(z)dz \tag{4.3}$$
$$P_{e2}(\boldsymbol{\theta}) = \Pr[\Delta > A|H_2, \boldsymbol{\theta}]$$
$$= \frac{1}{2\pi j}\int_{-j\infty+\epsilon}^{j\infty+\epsilon} \frac{\varphi_{\Delta|H_2}(z)}{z}e^{-zA}dz \triangleq \frac{1}{2\pi j}\int_{C_2} \mathrm{h}_2(z)dz \tag{4.4}$$

where a small positive number ϵ has been inserted in order to move the path of integration away from the singularity at $z = 0$ and allows for the interchange in the order of integration. The contours C_1 and C_2 can be closed to include the left-half plane without changing the value of the integral (see Fig. 4.2). For Rayleigh

Table 4.2 Expression of the bias A for the various quadratic receivers. $\boldsymbol{D}_m, m = 1, 2$ is given by (3.8).

receivers	A
SPECCOH	$\frac{1}{\gamma} \ln \left(\frac{\det (\boldsymbol{I} + \gamma \boldsymbol{D}_1)}{\det (\boldsymbol{I} + \gamma \boldsymbol{D}_2)} \right)$
SPECCOHR	0
QDR	$\frac{1}{\gamma} \left[\ln \left(\frac{\det (\boldsymbol{I} + \gamma \boldsymbol{D}_1)}{\det (\boldsymbol{I} + \gamma \boldsymbol{D}_2)} \right) + \boldsymbol{\alpha}^\dagger \boldsymbol{C}^{-1} \left\{ \boldsymbol{X}_1^T \boldsymbol{D}_1 \boldsymbol{Q}_1 \boldsymbol{X}_1^* - \boldsymbol{X}_2^T \boldsymbol{D}_2 \boldsymbol{Q}_2 \boldsymbol{X}_2^* \right\}_d \boldsymbol{C}^{-1} \boldsymbol{\alpha} \right]$
R OPT	$\frac{1}{\gamma} \ln \left(\frac{\det (\boldsymbol{I} + \gamma \boldsymbol{D}_1)}{\det (\boldsymbol{I} + \gamma \boldsymbol{D}_2)} \right)$
QR	0

channels (i.e. $\overline{\boldsymbol{r}}^k = \boldsymbol{0}, {}_{k=1,2}$), $\varphi_{\Delta|H_k}(jt) = [\det (\boldsymbol{I} - jt\boldsymbol{R}_k\boldsymbol{Q})]^{-1}$. Hence in this case within those positively oriented closed contours C_1 and C_2 and on those contours the functions $\{\mathsf{h}_k(z)\}_{k=1,2}$ are analytic except for a finite number of isolated singular points, namely the eigenvalues of the matrices $(\boldsymbol{R}_k\boldsymbol{Q})^{-1}, k = 1, 2$ plus the pole $z = 0$. Therefore for Rayleigh channels, the integrals (4.3) and (4.4) can be evaluated by using the residue theorem [190, p. 89]. The residue theorem states that the integral of a complex function over a contour is equal to $2\pi j$ times the sum of its residues at the singular points interior to the contour [190, p. 89]. Then from (4.3) and (4.4)

$$\Pr[\Delta < A|H_1, \boldsymbol{\theta}] = - \sum_{\substack{r \\ \eta_r^{-1} < 0}} \operatorname{res} \left(\mathsf{h}_1(z), z = \eta_r^{-1} \right)$$

$$\Pr[\Delta > A|H_2, \boldsymbol{\theta}] = \sum_{\substack{r \\ \eta_r'^{-1} \leq 0}} \operatorname{res} \left(\mathsf{h}_2(z), z = \eta_r'^{-1} \right)$$

where η_r^{-1} and $\eta_r'^{-1}$ are respectively the singular points of $\mathsf{h}_1(z)$ and $\mathsf{h}_2(z)$. Moreover, since all the singular points of $\mathsf{h}_1(z)$ and $\mathsf{h}_2(z)$ are in fact finite order poles, the residues

at those points are easy to evaluate by use of the following formula [190, p. 90].

$$\text{res } (\mathsf{h}_k(z), z = z_0) = \lim_{z \to z_0} \left\{ \frac{1}{(n-1)!} \frac{d^{n-1}}{dz^{n-1}} [(z - z_0)^n \mathsf{h}_k(z)] \right\} \quad \text{where } n \text{ is the order of the pole } z_0$$

Furthermore, since for Rayleigh channels, $\boldsymbol{\varrho}(\boldsymbol{\theta}) = [0, \ldots, 0]^T$, Δ is independent of $\boldsymbol{\theta}$ for all the receivers considered in this thesis (coherent and non-coherent) and integration over the phases $\boldsymbol{\theta}$ is not needed to evaluate the probability of error.

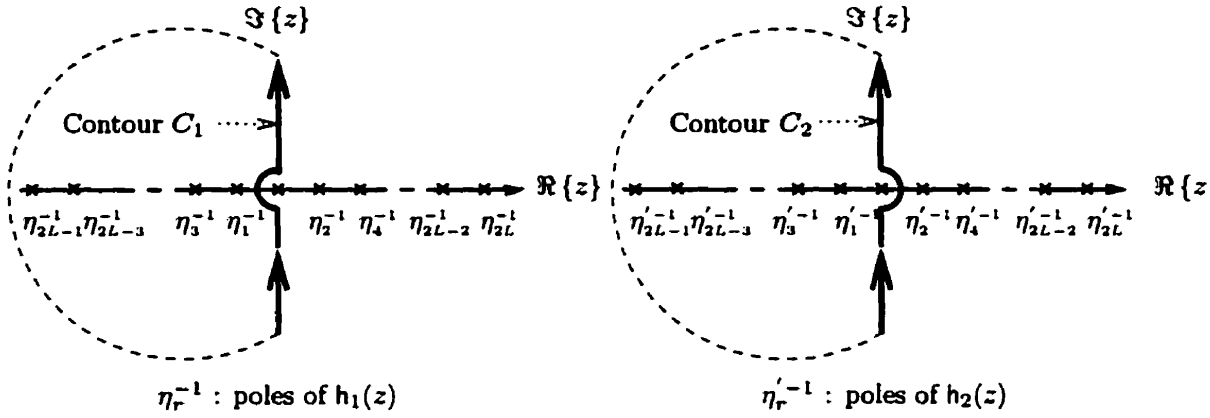

Fig. 4.2 Contours C_1 and C_2 of the residue method used in performance evaluation over Rayleigh channels

In fact in the numerical routine used in this thesis, $\Pr[\Delta < A|H_1]$ is not evaluated directly. Instead $\Pr[\Delta' > A'|H_1] = \Pr[\Delta < A|H_1]$ is evaluated where $\Delta' = -\Delta$ and $A' = -A$. The residues were found using the MATLAB routine "residue". Such routine can be applied to the ratio of two polynomials. First the poles are found then the residues are determined by evaluating the polynomial with individual roots removed.

When $\overline{\boldsymbol{r}}^k \neq \mathbf{0}, k = 1, 2$ (i.e. for Ricean channels), two difficulties arise. First the probability of error is generally difficult to obtain analytically because of the complicated nature of the exponential factor in the characteristic function, $\varphi_{\Delta|H_k}(jt)$. Secondly $\varphi_{\Delta|H_k}(jt)$ generally depends on the phases $\boldsymbol{\theta}$ through the mean $\overline{\boldsymbol{r}}^k \triangleq E[\boldsymbol{r}|H_k, \boldsymbol{\theta}]$, thus in order to evaluate the probability of error, the pdf of Δ needs to be integrated over Δ and over the phases $\boldsymbol{\theta}$.

A characteristic function $\varphi_{\Delta|H_k}(jt)$ of the form (4.2) may be diagonalized by use

of the transformation $\boldsymbol{v}^k = \boldsymbol{S}_k^{-1}\overline{\boldsymbol{r}}^k$ [89]. For sake of simplicity, the index k will be omitted in the following, but dependence of $\boldsymbol{v}^k$ on $\boldsymbol{\theta}$ is specified explicitly. The matrix $\boldsymbol{S}$ is to be chosen such that it diagonalizes the matrix $\boldsymbol{RQ}$ while satisfying $\boldsymbol{SS}^\dagger = \boldsymbol{R}$. Since $\boldsymbol{R}$ is Hermitian, there exists an unitary matrix $\boldsymbol{U}_1$ which diagonalizes $\boldsymbol{R}$ (i.e. $\boldsymbol{U}_1^\dagger \boldsymbol{R}\boldsymbol{U}_1 = \boldsymbol{R}_d$). Let $\boldsymbol{R}_{sq}$ be the square root of $\boldsymbol{R}_d$ ($\boldsymbol{R}_d = \boldsymbol{R}_{sq}\boldsymbol{R}_{sq}^\dagger$), $\boldsymbol{R}_{sq}$ exists since $\boldsymbol{R}$ is positive definite. Form the Hermitian matrix $\boldsymbol{N} = \boldsymbol{R}_{sq}^\dagger \boldsymbol{U}_1^\dagger \boldsymbol{Q}\boldsymbol{U}_1\boldsymbol{R}_{sq}$. Let $\boldsymbol{U}_2$ denote the unitary matrix which diagonalizes the matrix $\boldsymbol{N}$, $\boldsymbol{U}_2^\dagger \boldsymbol{N}\boldsymbol{U}_2 = \boldsymbol{N}_d$ and $\eta_r \triangleq [\boldsymbol{N}_d]_{rr}$. The matrix $\boldsymbol{S}$ is given by $\boldsymbol{S} = \boldsymbol{U}_1\boldsymbol{R}_{sq}\boldsymbol{U}_2$. The matrices $\boldsymbol{R}$ and $\boldsymbol{Q}$ satisfy $\boldsymbol{R} = \boldsymbol{SS}^\dagger$, $\boldsymbol{Q} = \left(\boldsymbol{S}^\dagger\right)^{-1}\boldsymbol{N}_d\boldsymbol{S}^{-1}$ and $\boldsymbol{RQ} = \boldsymbol{SN}_d\boldsymbol{S}^{-1}$. The diagonalized characteristic function is given by

$$\begin{aligned}\varphi_{\Delta|H_k}(jt) &= \left[\det(\boldsymbol{I} - jt\boldsymbol{N}_d)\right]^{-1} \exp\left\{-\boldsymbol{v}^\dagger(\boldsymbol{\theta})\left[\boldsymbol{I} - (\boldsymbol{I} - jt\boldsymbol{N}_d)^{-1}\right]\boldsymbol{v}(\boldsymbol{\theta})\right\} \\ &= \prod_{r=0}^{2L-1}(1 - jt\eta_r)^{-1} \exp\left\{jt\frac{|v_r(\boldsymbol{\theta})|^2\eta_r}{1 - jt\eta_r}\right\} \qquad (4.5)\end{aligned}$$

where $\boldsymbol{v}(\boldsymbol{\theta}) = \boldsymbol{S}^{-1}\overline{\boldsymbol{r}}$ and $v_r(\boldsymbol{\theta}) = [\boldsymbol{v}(\boldsymbol{\theta})]_r$.

In theory, (4.3-4.4) can be evaluated by using the residue method. However, as shown in Appendix G.1, such a method is not practical in that case since each residue consists of an infinite series. Therefore, when the multipath component magnitudes are Ricean distributed, the probability of error will be evaluated by performing numerical inversion of the characteristic function.

Now let's consider the dependency of $\varphi_{\Delta|H_k}(jt)$ on the phases $\boldsymbol{\theta}$. This dependency is via the mean $\overline{\boldsymbol{r}}$. Note that even for the SPECCOH and SPECCOHR schemes, $\boldsymbol{R}$ is independent of $\boldsymbol{\theta}$. For a mixed mode Ricean/Rayleigh channel when only one single multipath component is Ricean, it will be shown that $\varphi_{\Delta|H_k}(jt)$ is independent of $\boldsymbol{\theta}$. It can be shown that the mean $\overline{\boldsymbol{r}} \triangleq E[\boldsymbol{r}|H_k, \boldsymbol{\theta}]$ for the SPECCOH, SPECCOHR, QDR, R OPT and QR schemes is given by the expressions written in Table 4.3. When all α_r are null but one (for example the one corresponding to the r_0^{th} path, i.e. $\alpha_{r_0} \neq 0$), $\boldsymbol{\varrho}(\boldsymbol{\theta}) = [0, \ldots, 0, \alpha_{r_0}\exp\{j\theta_{r_0}\}, 0, \ldots, 0]^T$, and $\alpha_{r_0}\exp\{j\theta_{r_0}\}$ can be factored out in $\overline{\boldsymbol{r}}$. Then $v_r(\boldsymbol{\theta})$ satisfies $v_r(\boldsymbol{\theta}) \triangleq \left[\boldsymbol{S}^{-1}\overline{\boldsymbol{r}}\right]_r = \left[\boldsymbol{S}^{-1}\left(\alpha_{r_0}\exp\{j\theta_{r_0}\}\overline{\boldsymbol{r}}'\right)\right]_r = \alpha_{r_0}\exp\{j\theta_{r_0}\}\left[\boldsymbol{S}^{-1}\overline{\boldsymbol{r}}'\right]_r$ where $\overline{\boldsymbol{r}}'$ is independent of $\boldsymbol{\theta}$. Since $|v_r(\boldsymbol{\theta})|^2$ is independent of $\boldsymbol{\theta}$, the characteristic function is, in this special case only, independent of $\boldsymbol{\theta}$ and from

Table 4.3 Mean $\overline{r} \triangleq E[r|H_k, \theta]$ of the various quadratic receivers. Γ_{k1} and Γ_{k2} are $L \times L$ matrices defined by $[\Gamma_{kl}]_{rj} = \frac{1}{\sqrt{\tilde{E}_k \tilde{E}_l}} \int_0^{T_o} \tilde{s}_k(t-\tau_r)\tilde{s}_l^*(t-\tau_j)dt$.

SPECCOH	SPECCOHR	QDR & R OPT	QR
$\begin{pmatrix} X_1^* \left(\Gamma_{k1}^T + \frac{1}{\gamma}C^{-1}\right)\varrho(\theta) \\ X_2^* \left(\Gamma_{k2}^T + \frac{1}{\gamma}C^{-1}\right)\varrho(\theta) \end{pmatrix}$	$\begin{pmatrix} \left(\Gamma_{k1}^T + \frac{1}{\gamma}C^{-1}\right)\varrho(\theta) \\ \left(\Gamma_{k2}^T + \frac{1}{\gamma}C^{-1}\right)\varrho(\theta) \end{pmatrix}$	$\begin{pmatrix} X_1^*\Gamma_{k1}^T\varrho(\theta) \\ X_2^*\Gamma_{k2}^T\varrho(\theta) \end{pmatrix}$	$\begin{pmatrix} \Gamma_{k1}^T\varrho(\theta) \\ \Gamma_{k2}^T\varrho(\theta) \end{pmatrix}$

(4.5) it is given by

$$\varphi_{\Delta|H_k}(jt) = \prod_{r=0}^{2L-1} (1 - j\eta_r t)^{-1} \exp\left\{ j \frac{|v_r|^2 \eta_r t}{1 - j\eta_r t} \right\} \tag{4.6}$$

Therefore in order to evaluate the probability of error for the mixed mode channel it is not necessary to integrate over the phases and, the numerical inversion method proposed by Imhof in [90] can be used. Instead of the standard inversion formula $\Pr[\Delta > A|H_2] = \frac{1}{2\pi j} \int_{-j\infty+\epsilon}^{j\infty+\epsilon} \frac{\varphi_{\Delta|H_2}(z)}{z} e^{-zA} dz$, Imhof uses

$$\Pr[\Delta > A|H_2] = \frac{1}{2} + \frac{1}{\pi} \int_0^\infty \frac{\Im\left(e^{-jtA}\varphi_{\Delta|H_2}(jt)\right)}{t} dt \tag{4.7}$$

Substituting (4.6) into (4.7) and using the relations

$$\arg\left[(1-jbt)^{-1}\right] = \tan^{-1}(bt) \qquad \arg\left[\exp\left\{\frac{jat}{1-jbt}\right\}\right] = \frac{at}{1+b^2t^2}$$

$$\left|(1-jbt)^{-1}\right| = (1+b^2t^2)^{-1/2} \qquad \left|\exp\left\{\frac{jat}{1-jbt}\right\}\right| = \exp\left\{-\frac{abt^2}{1+b^2t^2}\right\}$$

the pairwise probability of error P_{e2} can be rewritten as

$$P_{e2} = \Pr[\Delta > A|H_2] = \Pr[\Delta > A|H_2, \theta] = \frac{1}{2} + \frac{1}{\pi} \int_0^\infty \frac{\sin(\Theta_1(t))}{t\Theta_2(t)} dt \tag{4.8}$$

where

$$\Theta_1(t) = \sum_{r=0}^{2L-1} \left[\tan^{-1}(\eta_r t) + \frac{|v_r|^2 \eta_r t}{1 + \eta_r^2 t^2} \right] - tA$$

$$\Theta_2(t) = \prod_{r=0}^{2L-1} (1+\eta_r^2 t^2)^{1/2} \exp\left\{\frac{|v_r|^2\eta_r^2 t^2}{1+\eta_r^2 t^2}\right\}$$

It is seen that the problem of evaluating a line integral over a contour is reduced to evaluating an improper integral of a real function (4.8). Furthermore, it appears that the function $\frac{\sin(\Theta_1(t))}{t\Theta_2(t)}$ is quite suitable for numerical integration. An example of such a function is plotted in Fig. 4.3 for the performance of QDR scheme for orthogonal FSK over a two-path mixed mode Ricean/Rayleigh channel for various received SNR per bit, E_b/N_0. Moreover the point at $t = 0$ is a removable singularity since the function $\frac{\sin(\Theta_1(t))}{t\Theta_2(t)}$ has a finite limit when $t \to 0$. Since the function $t\Theta_2(t)$ increases monotonically towards $+\infty$, the integration is carried over a finite range $0 \leq t \leq \mathcal{T}$. The error of truncation is given by

$$|e_{\mathcal{T}}| = \pi^{-1}\left|\int_{\mathcal{T}}^{\infty} [t\Theta_2(t)]^{-1}\sin(\Theta_1(t))dt\right|$$

and can be bounded above by $E_{\mathcal{T}}$, where

$$E_{\mathcal{T}}^{-1} = \pi\mathcal{T}^{2L}(2L)\prod_{r=0}^{2L-1}|\eta_r|\exp\left\{\frac{|v_r|^2\eta_r^2\mathcal{T}^2}{1+\eta_r^2\mathcal{T}^2}\right\}.$$

$\mathcal{T}$ is chosen such that the error of truncation $E_{\mathcal{T}}$ is less than the desired absolute error. In this thesis, an absolute error of 10^{-9} is considered. The probability of error obtained numerically using (4.8) differs from the true probability of error by the sum of two errors (not counting rounding-off errors):

- the error of truncation $e_{\mathcal{T}}$ due to the fact that the truncated integral $\frac{1}{\pi}\int_0^{\mathcal{T}} \frac{\sin(\Theta_1(t))}{t\Theta_2(t)}dt$ is computed instead of the integral $\frac{1}{\pi}\int_0^{\infty} \frac{\sin(\Theta_1(t))}{t\Theta_2(t)}dt$.
- the error of integration $e'_{\mathcal{T}}$ due to the fact that the truncated integral is numerically calculated.

To be more precise, the true value of the probability of error can be written as follows:

$$P_{e2} = \frac{1}{2} + \frac{1}{\pi}I_{\text{comp}} + e_{\mathcal{T}} + e'_{\mathcal{T}}$$

where $|e_{\mathcal{T}}| \leq 10^{-9}$, I_{comp} is the numerical value of the truncated integral and $e'_{\mathcal{T}}$ is the absolute error of integration. The value of this error depends on the method used to

evaluate numerically the truncated integral.

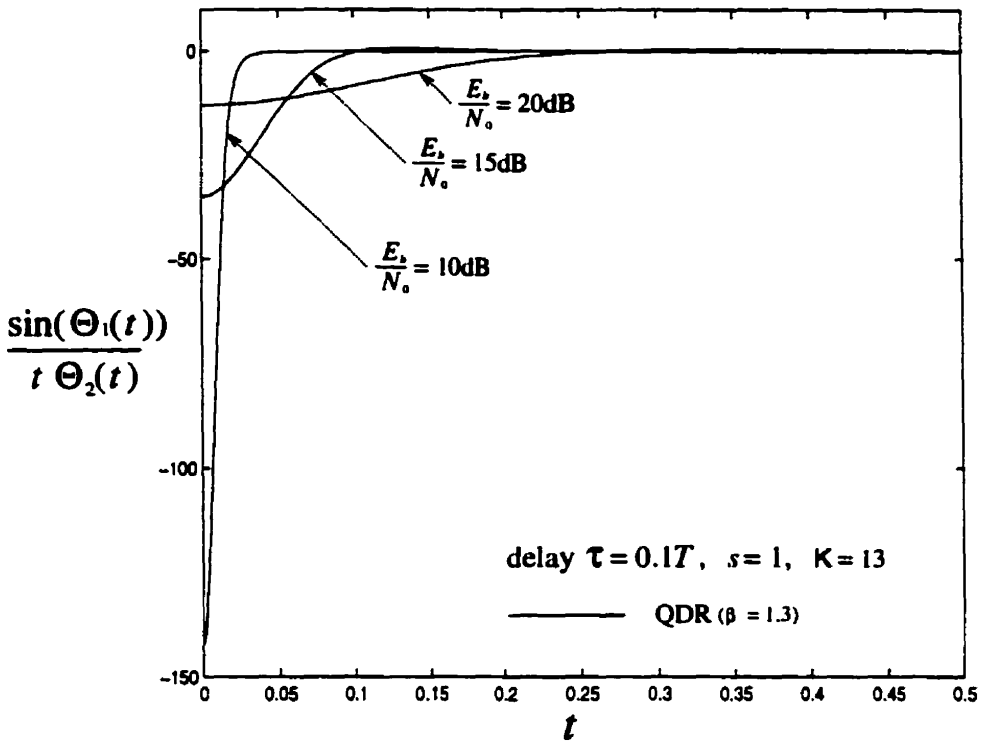

Fig. 4.3 Graph of the function $\frac{\sin(\Theta_1(t))}{t\Theta_2(t)}$ for orthogonal FSK signaling over a 2-path mixed mode Ricean/Rayleigh channel ($\tau = 0.1T$, $s = 1$ and K = 13dB)

As shown in Fig. 4.3 the function $\frac{\sin(\Theta_1(t))}{t\Theta_2(t)}$ contributes to the integral mostly around $t = 0$, thus it is appropriate to use non-uniform sub-intervals for integration. The integration interval $[0, \mathcal{T}]$ is subdivided into sub-intervals chosen by inspection such they take into consideration the shape of $\frac{\sin(\Theta_1(t))}{t\Theta_2(t)}$. These sub-intervals depend on $\mathcal{T}$. For example if $\mathcal{T} = 1$, the sub-intervals are defined as follows, $[0, 0.001], [0.001, 0.002], \ldots,$ $[0.009, 0.01], [0.01, 0.03], [0.03; 0.05], [0.05, 0.1], [0.1, 0.3], [0.3; 0.5], [0.5, 1]$. If $10 \leq \mathcal{T} <$ 100, then the first sub-intervals are identical to those with $\mathcal{T} = 1$ and the last are $[1, 2], [2, 4], [4, 10], [10, \mathcal{T}]$. The MATLAB numerical routine "quad8" is used to evaluate all the integrals over the sub-intervals. The probability of error is then the summation of all the sub-integrals. The routine "quad8" uses a adaptive recursive Newton-Cotes 8 panel rule. The sub-intervals are chosen such that the recursion level limit of ten is never reached in each of the sub-intervals. The pairwise probability of

error P_{e2} is given by

$$P_{e2} = \frac{1}{2} + \frac{1}{\pi}\sum_{n=1}^{N(\mathcal{T})} I_n + \frac{1}{\pi}\sum_{n=1}^{N(\mathcal{T})} I_n e_n' + e_{\mathcal{T}}$$

where $N(\mathcal{T})$ is the number of sub-intervals, I_n is the computed value of $\int_{\mathcal{T}_n}^{\mathcal{T}_{n+1}} \frac{\sin(\Theta_1(t))}{t\Theta_2(t)}dt$ (integral over the n^{th} sub-interval) and e_n' represents the relative error associated with calculation of $\int_{\mathcal{T}_n}^{\mathcal{T}_{n+1}} \frac{\sin(\Theta_1(t))}{t\Theta_2(t)}dt$. An estimate of P_{e2} is therefore given by

$$\frac{1}{2} + \frac{1}{\pi}\sum_{n=1}^{N(\mathcal{T})} I_n$$

The absolute error corresponding to the calculation of P_{e2} is given by

$$\left| P_{e2} - \frac{1}{2} - \frac{1}{\pi}\sum_{n=1}^{N(\mathcal{T})} I_n \right| \leq \frac{1}{\pi}\sum_{n=1}^{N(\mathcal{T})} |I_n| \left|e_n'\right| + 10^{-9}$$

since $|e_{\mathcal{T}}| < 10^{-9}$. Given the choice of sub-intervals, $\sum_{n=1}^{N(\mathcal{T})} |I_n| < 2.17$. This result was checked numerically for all the curves plotted in this thesis. The program is designed such that $\forall n, |e_n'| \leq 10^{-9}$, hence

$$\left| P_{e2} - \frac{1}{2} - \frac{1}{\pi}\sum_{n=1}^{N(\mathcal{T})} I_n \right| < \frac{2.17}{\pi} \cdot 10^{-9} + 10^{-9} < 1.7 \cdot 10^{-9}$$

Therefore the absolute error corresponding to the calculation is less than $1.7 \cdot 10^{-9}$.

Now that the method of evaluation of the probability of error of quadratic receivers has been explained, let us study (4.8). From (4.8) the probability (cumulative) distribution function (cdf) of a Hermitian quadratic form Δ in Gaussian random variables, taken at A, is expressed as the sum of a constant and an improper integral of a real function. Beside the advantage of being more suitable for numerical calculation, this form enables us to draw conclusions on the error probabilities of the various schemes at high SNR as shown next.

4.1.3 High SNR performance comparison of the SPECCOH, OPT, QDR and R OPT schemes derived from the performance evaluation analysis

Recall from (3.16) and (3.8) that $\boldsymbol{Q}_m = \gamma\left(\boldsymbol{D}_m^{-1} + \gamma\boldsymbol{I}\right)^{-1}$, and $\boldsymbol{X}_m$ and $\boldsymbol{D}_m$ are independent of γ. Therefore Table 4.1 shows that, as γ tends to infinity, the matrix $\boldsymbol{Q}_m'$, $m = 1, 2$ of the SPECCOH, QDR and R OPT schemes converges to the same matrix, namely $\boldsymbol{I}$. Similarly since the term $\frac{1}{\gamma}\boldsymbol{X}_m^*\boldsymbol{C}^{-1}\boldsymbol{\varrho}(\boldsymbol{\theta}), m = 1, 2$ is deterministic, as γ tends to infinity the vector $\boldsymbol{r}$ of the SPECCOH, QDR and R OPT schemes converges almost surely to the same vector, namely $\begin{pmatrix} \boldsymbol{r}_1 \\ \boldsymbol{r}_2 \end{pmatrix}$. Therefore as γ tends to infinity, Δ for the SPECCOH, QDR and R OPT schemes converges almost surely to the same quadratic form $\Delta_\infty = \boldsymbol{r}^\dagger\begin{pmatrix} \boldsymbol{I} & \boldsymbol{0} \\ \boldsymbol{0} & -\boldsymbol{I} \end{pmatrix}\boldsymbol{r} = \boldsymbol{r}_1^\dagger\boldsymbol{r}_1 - \boldsymbol{r}_2^\dagger\boldsymbol{r}_2$. From [182, p. 20], Δ_∞ converges also in probability. Let $F_\gamma(x)$ and $F_\infty(x)$ be respectively the probability distribution functions (cdf's) of Δ and Δ_∞. Then at every continuity point x of $F_\infty(\cdot)$ the following limit is satisfied [182, p. 23]

$$\lim_{\gamma\to\infty} F_\gamma(x) = F_\infty(x)$$

which says that Δ converges in distribution. Note that the convergence will be uniform in any closed interval of continuity of F_∞ [191, p. 9]. Considering Δ_∞, and following the same steps as in Section 4.1.2, similar to (4.8), it can be shown that

$$F_\infty(x) = 1 - \Pr[\Delta_\infty > x|H_2] = 1 - \Pr[\Delta_\infty > x|H_2, \boldsymbol{\theta}] = \frac{1}{2} - \frac{1}{\pi}\int_0^\infty \frac{\sin(\Theta_1''(t,x))}{t\Theta_2''(t)}dt \tag{4.9}$$

where $\Theta_1''(t,x)$ and $\Theta_2''(t)$ are given by

$$\Theta_1''(t,x) = \sum_{r=0}^{2L-1}\left[\tan^{-1}(\eta_r''t) + \frac{|v_r''|^2\eta_r''t}{1+\eta_r''^2t^2}\right] - tx$$

$$\Theta_2''(t) = \prod_{r=0}^{2L-1}(1+\eta_r''^2t^2)^{1/2}\exp\left\{\frac{|v_r''|^2\eta_r''^2t^2}{1+\eta_r''^2t^2}\right\}$$

$\Theta_1''(t,x)$ is continuous on $[0,\infty)\times(-\infty,\infty)$ and $\Theta_2''(t)$ is continuous on $[0,\infty)$, hence $\frac{\sin(\Theta_1''(t,x))}{t\Theta_2''(t)}$ is continuous on $(0,\infty)\times(-\infty,\infty)$. However since $\frac{\sin(\Theta_1''(t,x))}{t\Theta_2''(t)}$ has a finite

limit when t tends to zero, $\frac{\sin(\Theta_1''(t,x))}{t\Theta_2''(t)}$ is also continuous on $[0,\infty)\times(-\infty,\infty)$. Let us show now that $\int_0^\infty \frac{\sin(\Theta_1''(t,x))}{t\Theta_2''(t)}dt$ is uniformly convergent for $x\in[-A_{\text{up}},A_{\text{up}}]$, and hence the continuity of the function $F_\infty(x)$ on $[-A_{\text{up}},A_{\text{up}}]$, where from Appendix G.2

$$A_{\text{up}} = L\left|\ln\left(\frac{\lambda'_{1\,\max}}{\lambda'_{2\,\min}}\right)\right| + \frac{|\alpha_0|^2}{(2\sigma_0^2)^2}\sum_{r=0}^{L-1}\left[\left|x_{r0}^1\right|^2\lambda_{r1}'^2 + \left|x_{r0}^2\right|^2\lambda_{r2}'^2\right] \tag{4.10}$$

$\lambda'_{1\,\max} = \max_r[\boldsymbol{D}_1]_{rr}$ and $\lambda'_{2\,\min} = \min_r[\boldsymbol{D}_2]_{rr}$. Let us write the integral as

$$\int_0^\infty \frac{\sin(\Theta_1''(t,x))}{t\Theta_2''(t)}dt = \int_0^1 \frac{\sin(\Theta_1''(t,x))}{t\Theta_2''(t)}dt + \int_1^\infty \frac{\sin(\Theta_1''(t,x))}{t\Theta_2''(t)}dt$$

Since $\frac{\sin(\Theta_1''(t,x))}{t\Theta_2''(t)}$ has a limit when t tends to zero, the first integral is not an improper integral. The function $\frac{1}{t\Theta_2''(t)}$ is continuous for $1\le t<\infty$, for each $x\in(-\infty,\infty)$ $\frac{\sin(\Theta_1''(t,x))}{t\Theta_2''(t)}$ is continuous in t for $1\le t<\infty$ and satisfies

$$\left|\frac{\sin(\Theta_1''(t,x))}{t\Theta_2''(t)}\right| \le \frac{1}{t\Theta_2''(t)} \quad \text{where} \quad \int_1^\infty \frac{dt}{t\Theta_2''(t)} \quad \text{converges}$$

hence from [192, p. 454], $\int_1^\infty \frac{\sin(\Theta_1''(t,x))}{t\Theta_2''(t)}dt$ is uniformly convergent for $x\in(-\infty,\infty)$. Note that the convergence of $\int_1^\infty \frac{dt}{t\Theta_2''(t)}$ comes from the fact that, since $x>y$ implies $x^2(1+x^2)^{-1} > y^2(1+y^2)^{-1}$, $\int_1^\infty \frac{dt}{t\Theta_2''(t)}$ can be bounded above by

$$\exp\left\{-\sum_{r=0}^{2L-1}\frac{|v_r''|^2\eta_r''^2}{1+\eta_r''^2}\right\}\frac{1}{2L}\left[\prod_{r=0}^{2L-1}|\eta_r''|\right]^{-1}$$

For clarity, let us denote A from Table 4.2 as A_γ. It is shown in Appendix G.2 that for all $\gamma>1$, A_γ satisfies $|A_\gamma|\le A_{\text{up}}$ where A_{up} is given by (4.10). Let us consider the closed interval $[-A_{\text{up}},A_{\text{up}}]$. Since $\int_1^\infty \frac{\sin(\Theta_1''(t,x))}{t\Theta_2''(t)}dt$ is uniformly convergent for $x\in(-\infty,\infty)$ and $\int_0^1 \frac{\sin(\Theta_1''(t,x))}{t\Theta_2''(t)}dt$ is not an improper integral, $\int_0^\infty \frac{\sin(\Theta_1''(t,x))}{t\Theta_2''(t)}dt$ is uniformly convergent for $x\in[-A_{\text{up}},A_{\text{up}}]$. Furthermore $\frac{\sin(\Theta_1''(t,x))}{t\Theta_2''(t)}$ is continuous on $[0,\infty)\times[-A_{\text{up}},A_{\text{up}}]$, therefore from (4.9) the function $F_\infty(x)$ is continuous on $[-A_{\text{up}},A_{\text{up}}]$ [192, p. 454]. Hence the convergence of $F_\gamma(x)$ as γ tends to infinity, is

uniform [191, p. 9].

$F_\gamma(x)$ converges uniformly to $F_\infty(x)$ on $[-A_{up}, A_{up}]$, for all $\gamma > 1$, $A_\gamma \in [-A_{up}, A_{up}]$ and $F_\infty(x)$ is continuous on $[-A_{up}, A_{up}]$, hence

$$\lim_{\substack{\gamma \to \infty \\ \gamma > 1}} F_\gamma(A_\gamma) = F_\infty(0)$$

since from Table 4.2 the bias term A_γ of the SPECCOH, QDR and R OPT schemes converges to 0 as γ tends to infinity. Therefore the probabilities of error for the SPECCOH, QDR and R OPT schemes converge to the same value as γ tends to infinity. Since the bit-error probabilities of SPECCOH and R OPT are respectively lower and upper-bounds to the bit-error probabilities of OPT, the bit-error probabilities of SPECCOH and OPT also converge to the same value as γ tends to infinity. In other words performance of the SPECCOH, OPT, QDR and R OPT schemes is similar at high SNR. This behavior is observed on the curves plotted in Section 4.2 when K is not too large. The larger is K, the larger the required SNR to see this trend. Note that this asymptotical result was already illustrated in Section 3.3.1 by showing that the log-likelihood ratios of the SPECCOH and OPT schemes converge to the same decision variable as γ goes to infinity. Similar proofs can be derived for the convergence of R OPT and QDR to OPT.

4.2 Performance over mixed mode Ricean/Rayleigh channels for binary FSK and DPSK

Performance of all the receivers studied in this thesis is assessed by calculating their bit-error probabilities as functions of the received SNR per bit, E_b/N_0. This section considers mixed mode Ricean/Rayleigh channels. Let us recall from Section 3.4.1 that in such a channel the first path gain is Ricean distributed with fixed component α_0 and the second path gain is Rayleigh distributed. Hence for a two-path mixed mode Ricean/Rayleigh fading channel, the received SNR is given by $\frac{E_b}{N_0} = (2\sigma_0^2 + 2\sigma_1^2 + |\alpha_0|^2)\frac{\mathcal{E}_b}{N_0} = 2\sigma_0^2(1 + s + \mathsf{K})\frac{\mathcal{E}_b}{N_0}$ where $s = \frac{\sigma_1^2}{\sigma_0^2}$, is the relative Rayleigh component strength between the first and second path, $\mathsf{K} = \frac{|\alpha_0|^2}{2\sigma_0^2}$ is the Ricean parameter and $\mathcal{E}_b$ is the energy per bit of the real signal. All two-path mixed mode Ricean/Rayleigh channels are labeled by the values of their parameters s and K, and the relative delay between the first and the second path τ. For convenience $\tau = \tau_1 - \tau_0$ is expressed as

a percentage of T and K is expressed in dB. Several values of one parameter pointing to the same curve show that corresponding curves overlap or are very close to each other. For clarity only one of those curves is plotted.

4.2.1 Modulations format

In this thesis commonly used modulation schemes such as variations of FSK and DPSK are considered. Under $H_{m,\,m=1,2}$ the complex envelope of a FSK binary signal is

$$\tilde{s}_m(t) = \sqrt{\frac{2\mathcal{E}_b}{T}} e^{j2\pi f_m t} \qquad m = 1, 2 \qquad 0 \le t \le T$$

where $f_m \ll f_c$ (carrier frequency). FSK modulation with frequency separation $f_1 - f_2$ is denoted as FSK(v), where $v = (f_1 - f_2)T$. This thesis will focus particularly on FSK(1), which is orthogonal FSK, and FSK(1/2). For FSK the observation interval is equal to T plus the maximum of the channel inter-path delay which corresponds to a long observation interval of minimum duration. The energy per bit of FSK signals is given by $\mathcal{E}_b = \tilde{E}_m/2, m = 1, 2$, i.e. $\frac{E_b}{N_0} = 2\sigma_0^2(1 + s + \mathsf{K})\gamma$. Both DPSK and SDPSK [174] will be considered in this section. Under H_1 and H_2 the complex envelope of a DPSK binary signal over a two-symbol interval is

$$\tilde{s}_1(t) = \sqrt{\frac{2\mathcal{E}_b}{T}} \qquad 0 \le t \le 2T \qquad \tilde{s}_2(t) = \begin{cases} \sqrt{\frac{2\mathcal{E}_b}{T}} & 0 \le t \le T, \\ -\sqrt{\frac{2\mathcal{E}_b}{T}} & T < t \le 2T. \end{cases}$$

Under H_1 and H_2 the complex envelope of a SDPSK binary signal over a two-symbol interval is

$$\tilde{s}_1(t) = \begin{cases} \sqrt{\frac{2\mathcal{E}_b}{T}} & 0 \le t \le T, \\ -j\sqrt{\frac{2\mathcal{E}_b}{T}} & T < t \le 2T. \end{cases} \qquad \tilde{s}_2(t) = \begin{cases} \sqrt{\frac{2\mathcal{E}_b}{T}} & 0 \le t \le T, \\ j\sqrt{\frac{2\mathcal{E}_b}{T}} & T < t \le 2T. \end{cases}$$

Since with DPSK and SDPSK, the transition between the carrier phase of consecutive bits carries the information, the observation interval needs to be equal to twice the symbol duration. Therefore for DPSK and SDPSK, $\mathcal{E}_b = \tilde{E}_m/4, m = 1, 2$, i.e. $\frac{E_b}{N_0} =$

$2\sigma_0^2(1+s+\mathsf{K})\frac{\gamma}{2}$. Note that the present definitions of FSK and DPSK waveforms are not continuous on the observation interval since they present discontinuities at $t=0$ and $t=T$. However they can be approximated arbitrarily close in terms of Euclidean distance by continuous complex waveforms on $\mathbb{R}$ with compact support since they are square integrable functions [175, p. 71]. The support of a complex function f on a topological space X is the closure of the set $\{x : f(x) \neq 0\}$. Note finally that the performance analysis of all quadratic receivers does not use the continuity assumption.

4.2.2 Performance of the SPECCOH, SPECCOHR and OPT schemes

This section considers the performance of the specular coherent optimum receiver (SPECCOH) and the non-coherent optimum receiver (OPT) over two-path mixed mode Ricean/Rayleigh channels. Performance of the specular coherent optimum receiver when the multipath is resolved (SPECCOHR) is also presented to show the improvement due to the decorrelation stage. Numerical results are presented in Figs 4.4-4.13. Figs. 4.4-4.7 consider unresolved two-path mixed mode Ricean/Rayleigh channels with $\tau = 0.1T$ and various values of the Ricean parameter K. Recall that the bit-error probability of the OPT scheme cannot be computed exactly. Instead upper-bounds and lower-bounds are obtained (see Section 4.1.1). These bounds are represented by solid lines in Figs. 4.4-4.7, 4.9-4.13. The bit-error probabilities of the non-coherent optimum receiver over a two-path Rayleigh channel with $s = 1$ and $\tau = 0.1T$ and over a single path non-fading Gaussian channel are added as references (respectively dot-dashed and long dashed lines in Figs. 4.4-4.7, 4.10-4.11). The SPECCOH scheme bit-error probabilities over two-path mixed mode Ricean/Rayleigh channels are represented by short dashed lines in Figs. 4.4-4.7. Note that when no dashed lines appear on the curves, it means that the SPECCOH scheme bit-error probability is equal to the lower-bound to the OPT bit-error probability on the entire range of received SNR presented in this thesis.

The OPT scheme assumes knowledge of the specular term only in terms of its magnitudes, while the SPECCOH scheme assumes knowledge of the magnitudes and phases of the specular term. Therefore the importance of the knowledge of the Ricean specular term phase will be assessed by comparing performance of the SPECCOH and OPT schemes. The influence of the parameter s is considered in Section 4.3. The performance analysis of this section will be restricted to channels where the Rayleigh components of the path gains have equal strengths (i.e. $s = 1$). For most of the graphs,

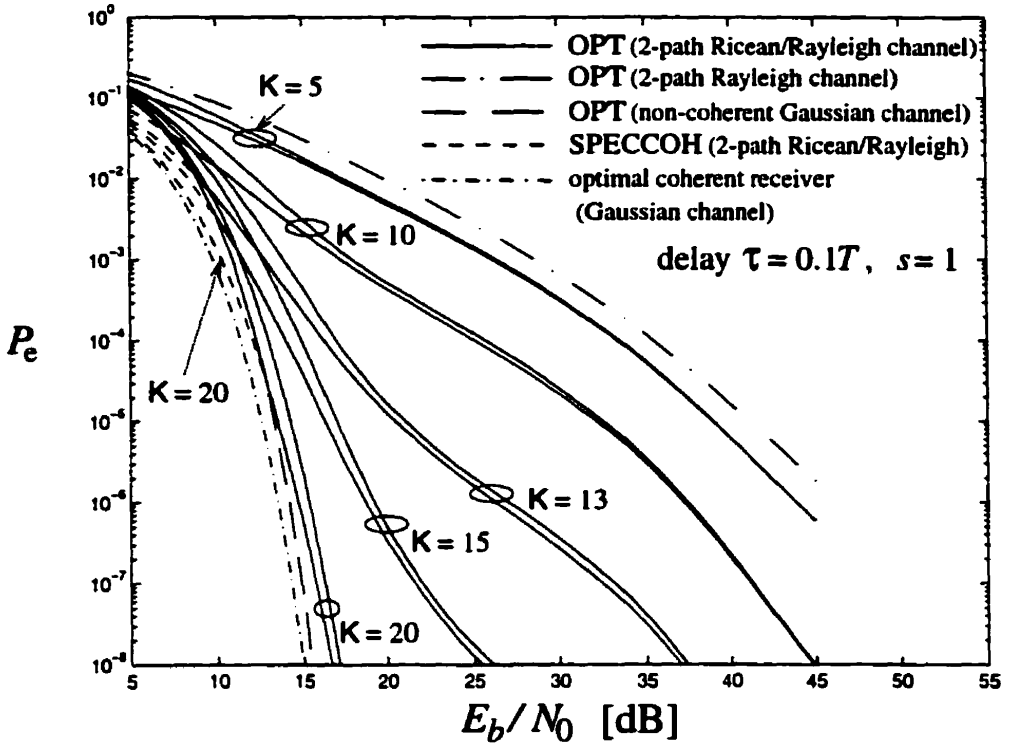

Fig. 4.4 Performance of the SPECCOH and OPT schemes with FSK(1) signaling over 2-path Ricean/Rayleigh channels ($\tau = 0.1T$, $s = 1$ and K = 5-20dB)

the inter-path delay is chosen to be $0.1T$ corresponding to a completely unresolved channel. The influence of the parameter K and the modulation scheme on the bit-error probabilities over a channel with an inter-path delay equal to $0.05T$ is quite close to the results observed with $\tau = 0.1T$, therefore only a few examples with $\tau = 0.05T$ will be provided.

Figs 4.4-4.7 show that the performance of the optimum receivers (SPECCOH and OPT) improves as the Ricean path dominates the Rayleigh path but is still worse than the performance over a Gaussian channel. Such behavior was to be expected since as K increases the channel fluctuations in amplitude are more dominated by the Ricean specular component of the first path; tending to a Gaussian channel. It is seen that when K is less than 5dB relatively small gains are obtained as compared to the performance over a two-path Rayleigh fading channel. On the other hand when K is larger than 20dB the bit-error probabilities are very close to that of the

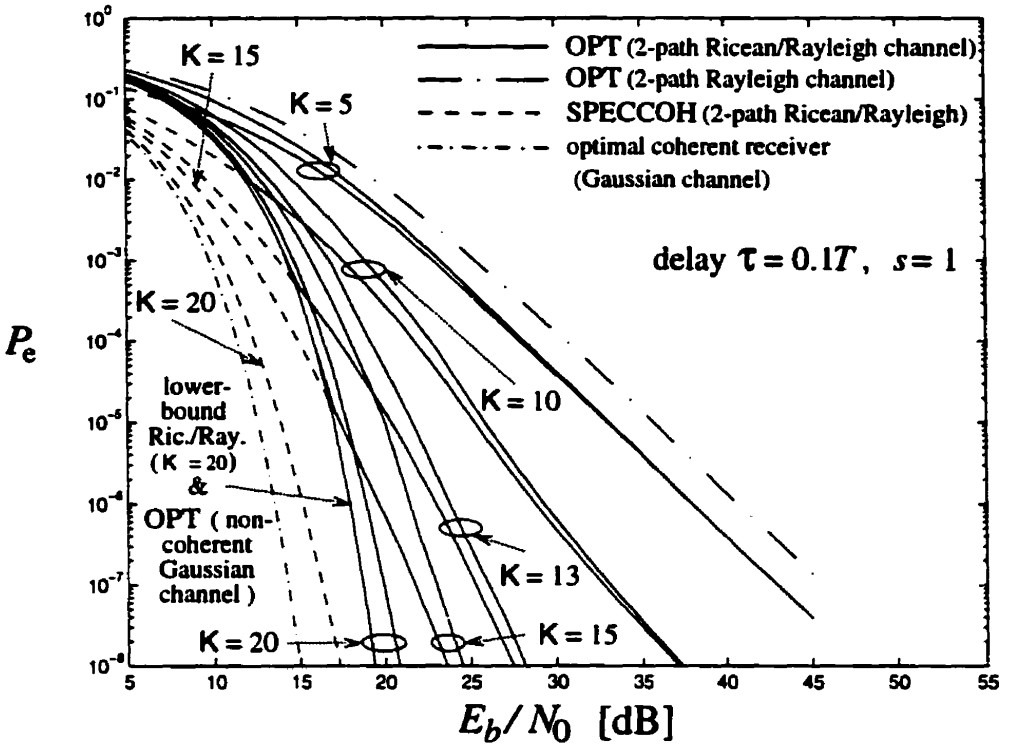

Fig. 4.5 Performance of the SPECCOH and OPT schemes with FSK(1/2) signaling over 2-path Ricean/Rayleigh channels ($\tau = 0.1T$, $s = 1$ and K = 5-20dB)

Gaussian channel. Therefore sets of curves where K is held fixed will be presented for intermediate values of K, in the range 10-15dB.

To assess the effect of the decorrelation operation on the performance of specular coherent receivers, the bit-error probabilities of the SPECCOHR scheme are presented in Fig. 4.8 for FSK(1/2) and DPSK with K = 10, 15dB with dashed lines. For purpose of comparison, corresponding bit-error probabilities of the SPECCOH scheme are plotted using solid lines in Fig. 4.8. Fig. 4.8 shows that with FSK(1/2) and DPSK the SPECCOHR scheme yields error floors which are eliminated by the SPECCOH scheme. This shows the importance of the decorrelation operation to handle path unresolvability for specular coherent detection. From Figs 4.4-4.7, the bit-error probabilities of the OPT scheme have no error floor similar to the bit-error probabilities of SPECCOH. This suggests that the decorrelation operation may also eliminate error floors for optimum non-coherent detection. As shown later in Sec-

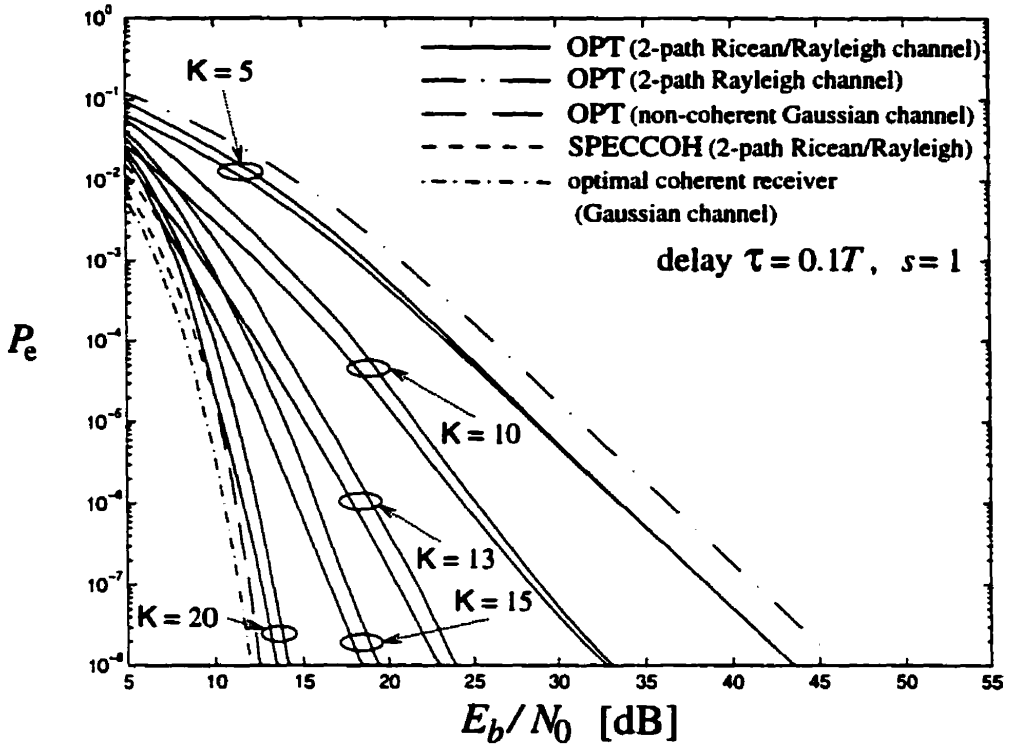

Fig. 4.6 Performance of the SPECCOH and OPT schemes with DPSK signaling over 2-path Ricean/Rayleigh channels ($\tau = 0.1T$, $s = 1$ and K = 5-20dB)

tion 4.2.3 such observation is verified for suboptimum non-coherent detection, where curves of the QDR and QR schemes, two suboptimal receivers respectively with and without decorrelation, are presented.

Next let us assess the effect of the knowledge of the Ricean specular term phase on performance by comparing the bit-error probabilities of the OPT and SPECCOH schemes. Table 4.4 provides typical examples of the SNR gains that can be obtained by using SPECCOH instead of the OPT scheme. For a given bit-error probability of the SPECCOH scheme (P_e), the numbers in Table 4.4 quantify the maximal SNR gains evaluated based on the upper-bounds to the bit-error probabilities of the OPT scheme. Using exact bit-error probabilities of OPT, these numbers would be less. SNR gains greater than 2dB are set in boldface indicating cases where specular component phase estimation may yield significant improvement. Three bit-error probabilities are considered, 10^{-3} typical of speech transmission error tolerance and $10^{-6}, 10^{-8}$ appli-

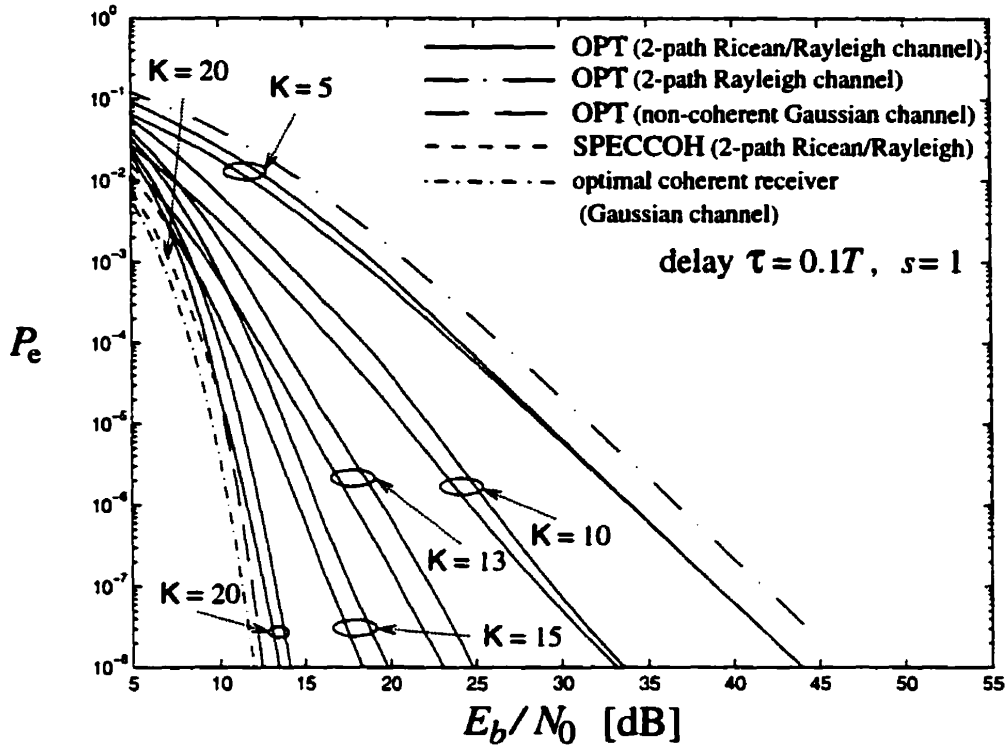

Fig. 4.7 Performance of the SPECCOH and OPT schemes with SDPSK signaling over 2-path Ricean/Rayleigh channels ($\tau = 0.1T$, $s = 1$ and K = 5-20dB)

cable for data transmission. Table 4.4 and Figs. 4.4, 4.6 show that little performance gains can be obtained for FSK(1) and to a lesser extent for DPSK by using a receiver that assumes knowledge of the magnitude and phase of the specular term instead of the knowledge of only its magnitude (for example maximal gain of $\approx$ 0.2-0.7dB for FSK(1) and 0.8-1.2dB for DPSK at $P_e = 10^{-6}$). As the probability of error decreases (or equivalently as the received SNR per bit increases) lower gains are obtained. Lower gains are also obtained for lower values of K. These observations along with the difficulties inherent to phase estimation further justify the use of non-coherent detection for FSK(1) or DPSK especially at high SNR. It may be argued here that the form of the OPT scheme is much more complex than the SPECCOH scheme. However, as shown by Table 4.4, the loss in performance obtained with the QDR scheme compared to SPECCOH is also small. And the QDR scheme is a much simpler non-coherent scheme that is quite suitable for implementation and also does not assume knowledge

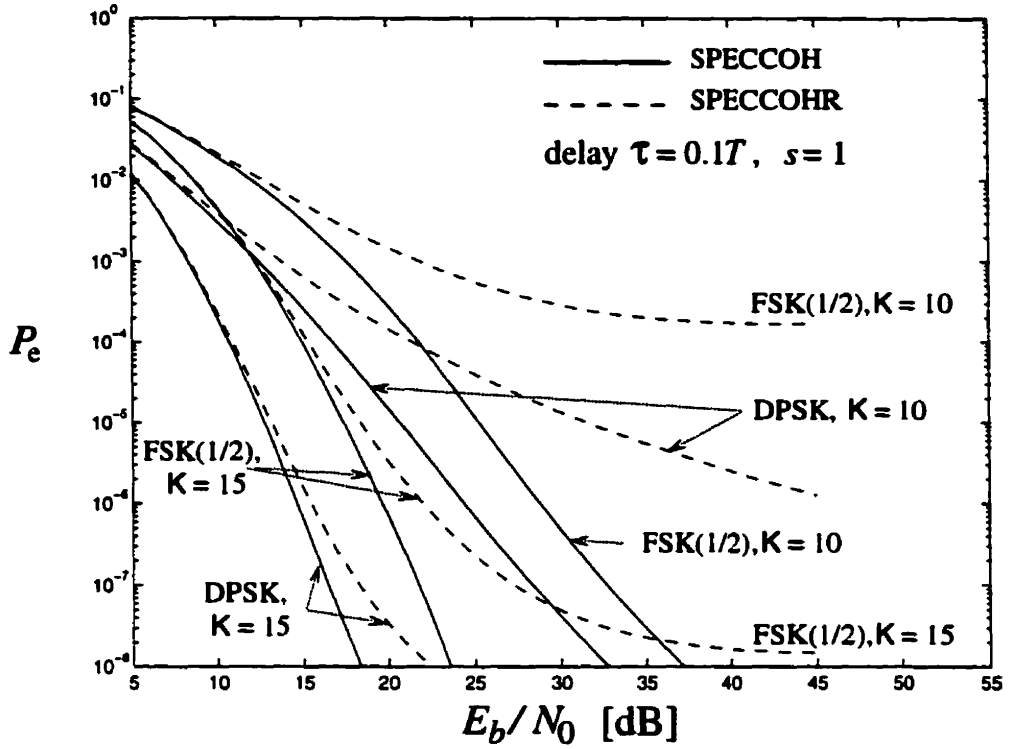

Fig. 4.8 Performance of the SPECCOH and SPECCOHR schemes with FSK(1/2) and DPSK signaling over 2-path Ricean/Rayleigh channels ($\tau = 0.1T$, $s = 1$ and K = 10, 15dB)

of the specular term phase. Table 4.4 and Figs. 4.5, 4.7 show, however, that significant gains can be obtained for FSK(1/2) and SDPSK by the knowledge of the specular component phase (for example maximal gain of 3dB at $P_e = 10^{-3}$ with K = 13dB and 1.8dB at $P_e = 10^{-6}$ with K = 15dB for FSK(1/2), 1.5dB at $P_e = 10^{-3}$ with K = 10dB and 1.8dB at $P_e = 10^{-8}$ with K = 13dB for SDPSK). Significant gains larger than 3dB are also obtained for FSK(1/2) with K = 20dB showing that the use of coherent detection may be justified for FSK(1/2).

Note that similar results (observation of little performance gains with specular term phase estimation at high SNR and lower gains with lower values of K) had been already obtained over one-path Ricean channels for binary signaling with complex cross-correlation coefficient magnitude ($|\rho_{00}^{12}|$) varying from 0 to 0.95 [193] and for binary orthogonal signaling ($\rho_{00}^{12} = 0$) [194]. The convergence of specular coherent and non-coherent performance at high SNR was explained as follows [194]. The noiseless

Table 4.4 SNR gains (in dB) obtained by SPECCOH compared to OPT and QDR. K is expressed in dB. For the comparison between the OPT and the SPECCOH schemes, these gains are "best case" gains since they are obtained using the upper-bounds to the bit-error probabilities of the OPT scheme.

SNR gains in dB		FSK(1)			FSK(1/2)				DPSK			SDPSK		
	P_e ↓, K →	10	13	15	10	13	15	20	10	13	15	10	13	15
SPECCOH /OPT	10^{-3}	0.5	1.2	1.3	1.3	**3.0**	**3.6**	**4.1**	1.4	1.4	1.3	1.5	1.4	1.3
	10^{-6}	0.2	0.7	0.5	0.5	0.8	1.8	**3.7**	0.8	1.2	1.2	1.2	1.5	1.2
	10^{-8}	≈ 0	0.4	0.6	0.2	0.7	0.9	**3.5**	0.3	0.9	1	0.4	1.8	1.4
SPECCOH /QDR(1.3)	10^{-3}	0.5	1.2	1.3	1.5	**3.2**	**4**	**4.3**	1.4	1.4	1.3	1.6	1.4	1.4
	10^{-6}	0.2	0.9	0.5	0.6	1.3	1.9	**4.3**	0.9	1.5	1.3	1.2	1.7	1.2
	10^{-8}	≈ 0	0.4	0.6	0.2	1.1	0.9	**4.3**	0.3	1.4	1	0.4	1.8	1.4

received signal over the Ricean channel is the sum of a fixed component with a fixed phase and a random component with a uniform phase. Therefore the phase of the received signal has a contribution from the random component, so knowledge of the phase of the specular term provides only partial information. The two detection techniques provide closer performance results at high SNR since in that case the fading is causing the most degradation. Note that in [193], the convergence is said to be better for large $|\rho_{00}^{12}|$. It can be shown by plotting the bit-error probabilities for FSK with several cross-correlation coefficients that the convergence for FSK(1/3) ($|\rho_{00}^{12}| \approx 0.8$) is better than the convergence for FSK(1/2) ($|\rho_{00}^{12}| \approx 0.6$) illustrating this statement. However a similar plot for FSK(1), FSK(2/3) and FSK(1/2) shows that the convergence for FSK(1) ($|\rho_{00}^{12}| = 0$) is better than the convergence for FSK(2/3) ($|\rho_{00}^{12}| \approx 0.4$) itself better than the convergence for FSK(1/2) ($|\rho_{00}^{12}| \approx 0.6$). Such observations agree with results found for mixed mode Ricean/Rayleigh channels, where the convergence for FSK(1) was shown to be much better than the convergence for FSK(1/2).

Fig. 4.9 presents the upper and lower-bounds to the bit-error probabilities of the OPT scheme with FSK(1), FSK(1/2) and DPSK over a two-path mixed mode Ricean/Rayleigh channel. For clarity, the bit-error probabilities of SDPSK which are very close to those of DPSK are not plotted in Fig. 4.9. Performance of the QDR

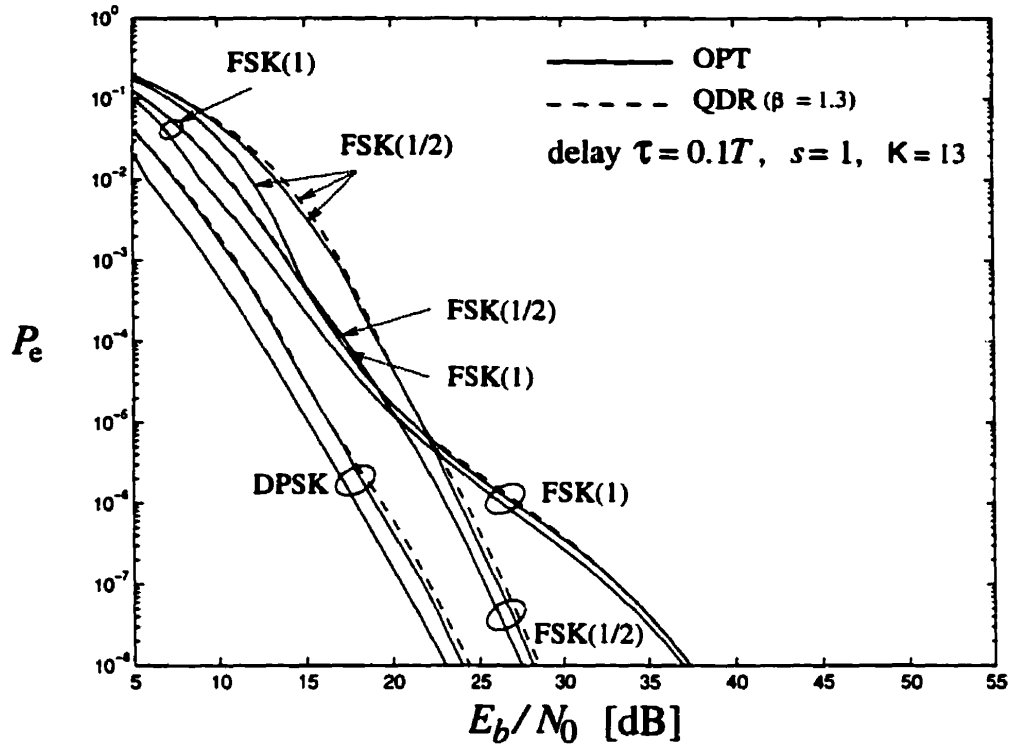

Fig. 4.9 Performance of FSK and DPSK signaling over a 2-path Ricean/Rayleigh fading channel ($\tau = 0.1T$, $s = 1$ and K = 13dB)

scheme ($\beta = 1.3$) is added as an indication to the performance of a receiver more suitable for implementation. A more thorough study of the QDR scheme will be done in Section 4.2.3. It is seen that DPSK (and SDPSK) detected with the OPT scheme give the best performance. At high SNR DPSK gives at least 3.6dB improvement compared to FSK(1/2) and at least 4.2dB compared to FSK(1) in the error probability range $10^{-5} - 10^{-8}$. However 3dB are gained because the observation interval used with DPSK is twice the one used with FSK. From Fig. 4.9, it is seen that at high SNR ($E_b/N_0 > 23$dB), performance of the OPT scheme is better with FSK(1/2) than with FSK(1). On the other hand, for lower SNR ($E_b/N_0 < 19$dB) FSK(1) performs better. For a SNR between 19dB and 23dB, the lower and upper-bounds for FSK(1) and FSK(1/2) yield ranges of possible values of the bit-error probabilities that overlap thus no conclusion can be made on which frequency deviation gives better results.

Fig. 4.9 also shows that the two bounds for the probability of error of OPT are

less tight for FSK(1/2) than for FSK(1). This can be explained intuitively as follows. When considering one-path Ricean channels, the probability of error for coherent detection depends only on the real part of the cross-correlation coefficient [193]. Hence FSK(1) and FSK(1/2) with coherent detection have the same probabilities of error. Furthermore at high SNR, the best modulus of the signal cross-correlation for non-coherent detection based on numerical performance curves is zero [193]. Therefore FSK(1/2), that has a non-zero signal cross-correlation, performs worse than FSK(1) with non-coherent detection. Consequently the gap between coherent and non-coherent detection over one-path Ricean channels is smaller for FSK(1) than for FSK(1/2). Over two-path mixed Ricean/Rayleigh channels, one can extrapolate that a similar behavior occurs with respect to the knowledge of the Ricean specular term phase. Comparing in Fig. 4.9 the lower-bounds to the OPT scheme bit-error probabilities with its upper-bounds at high SNR shows that this is the case. Note that based on Fig. 4.9 comparison can be done only at high SNR since in that case the performance curves of the SPECCOH scheme match the lower-bounds. Here high SNR means $E_b/N_0 > 8$dB for FSK(1) and $E_b/N_0 > 14$dB for FSK(1/2). Furthermore, this comparison provides only partial information since the upper-bounds are bit-error probabilities of non-coherent suboptimum receivers that yield higher bit-error probabilities than the OPT scheme. Therefore the gap between the OPT and the SPECCOH bit-error probabilities will be smaller than seen in Fig. 4.9. For all the modulation schemes considered here, although it is clearer for FSK's, there is always a region of intermediate SNRs where the bounds are less tight. This region corresponds to the range of SNRs where the suboptimum receivers derived in this thesis are the most suboptimum compared to the OPT scheme. Therefore the proposed upper-bounds are less tight in that region. Furthermore as seen in Section 3.3, the SPECCOH and the OPT schemes tend to the same receiver at high SNR, hence the lower-bounds are also more tight at high SNR.

Fig. 4.10 and Fig. 4.11 present the bounds to the OPT scheme bit-error probabilities for FSK(1) and DPSK when the inter-path delay is equal to $0.05T$. These figures should be viewed in the same context as Fig. 4.4 and Fig. 4.6. They show that the bit-error probabilities with $\tau = 0.05T$ are quite similar to those with $\tau = 0.1T$ with a similar influence of the Ricean parameter K.

Fig. 4.12 presents the bounds to the OPT scheme bit-error probability for FSK(1) over two-path mixed mode Ricean/Rayleigh fading channels with K = 13dB and

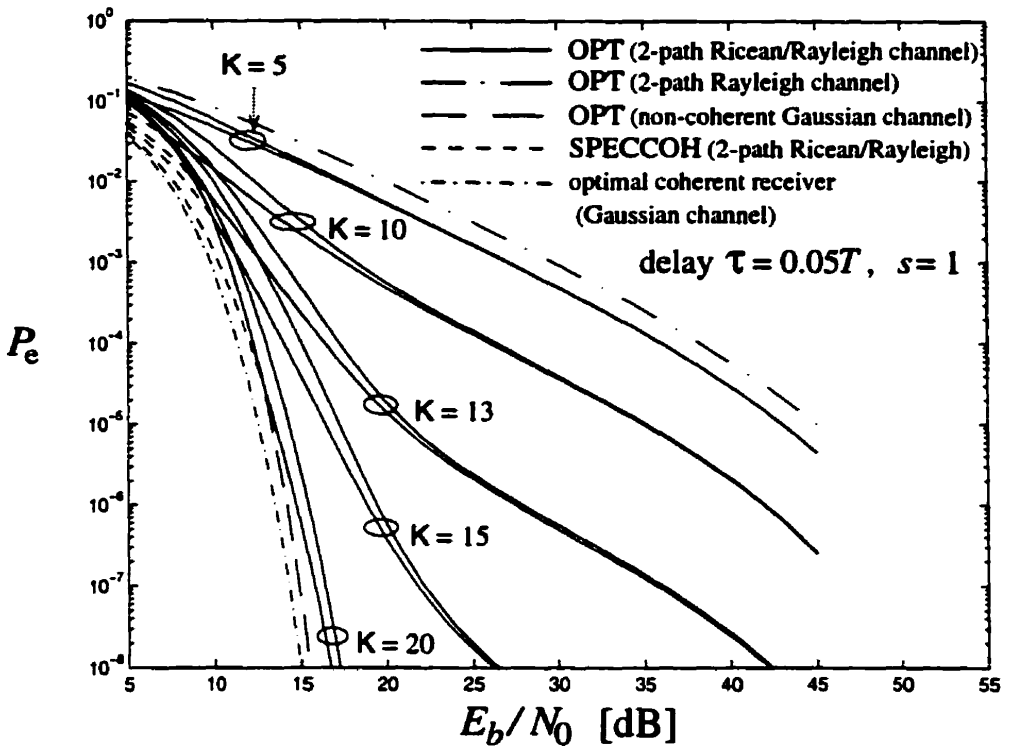

Fig. 4.10 Performance of the OPT scheme with FSK(1) signaling over 2-path Ricean/Rayleigh channels ($\tau = 0.05T$, $s = 1$ and K = 5-20dB)

various inter-path delays τ. A resolved channel corresponds to $\tau = T$. From Fig. 4.12, it is seen that for $E_b/N_0 \leq 17.3$dB, the bounds are not sufficiently tight hence no conclusion can be made on the influence of τ on the bit-error probabilities. In the following discussion, E_b $N_0 > 17.3$dB will be considered. Fig. 4.12 shows that the bounds are very tight for very small inter-path delays such as $0.1T$. When the channel inter-path delay is increased, the bounds become looser and looser until $\tau = 0.5T$ is reached. If the channel inter-path delay is further increased, the bounds become tighter; however even for resolved multipath channels they are less tight than for very small inter-path delays. From Fig. 4.12, it is seen that performance improves as the inter-path delay increases. This was to be expected since as the channel inter-path delay increases, the interference between the direct path and the first echo decreases leading to an improvement in performance. Fig. 4.12 also shows that the performance improvement is not linear. Considerable gains are obtained when the inter-path delay

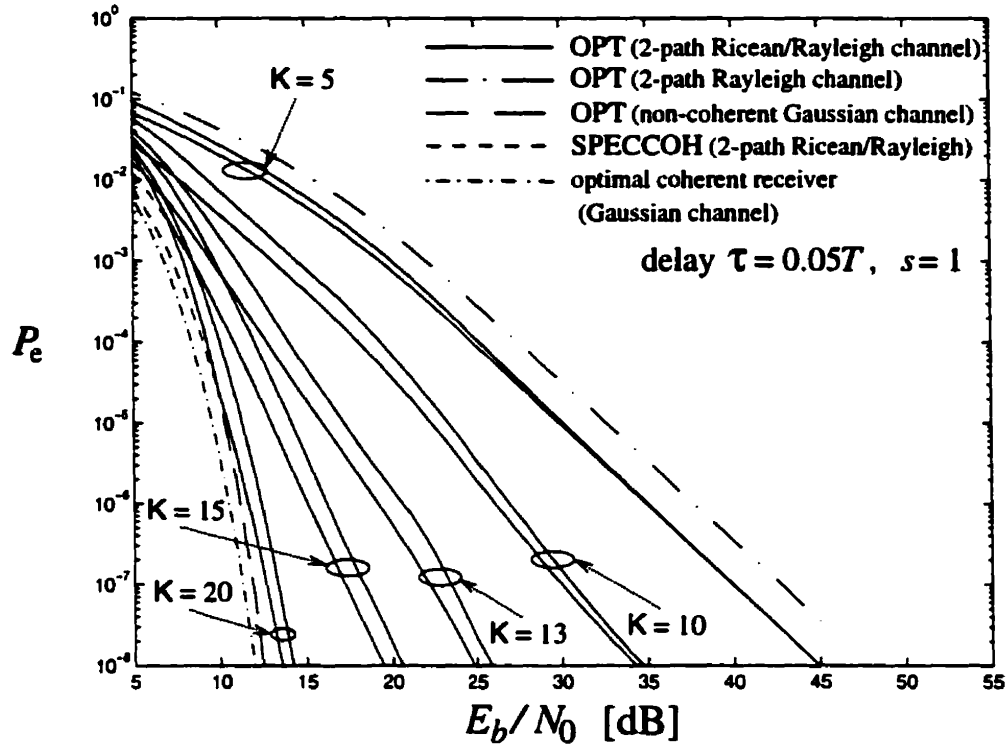

Fig. 4.11 Performance of the OPT scheme with DPSK signaling over 2-path Ricean/Rayleigh channels ($\tau = 0.05T$, $s = 1$ and K = 5-20dB)

increases from $0.1T$ to $0.3T$ (a minimum of 7dB gains at $P_e = 10^{-7}$), but less gains are obtained as the inter-path delay increases from $0.5T$ to T. For example at $P_e = 10^{-7}$ an unresolved channel with $\tau = 0.7T$ requires at most an additional 1.5dB SNR gain compared to a resolved channel ($\tau = T$). For clarity of Fig. 4.12, curves with $\tau = 0.7T$ are not plotted. Lower degradation between $0.1T$ and $0.3T$ is obtained with FSK(1/2) (less than 1.7dB). This nonlinear improvement with the channel inter-path delay is related to the expression of the cross-correlation coefficients and the way they influence the expression of the bit-error probability. The very low performance improvement as the channel inter-path delay increases from $0.5T$ to T has also been obtained in [85, 102] for two-path Rayleigh channels and various degrees of channel knowledge. It is seen from Fig. 4.12 that the bending of the curves for FSK(1) is due to unresolvability since for $\tau \geq 0.5T$, the bending disappears. Fig. 4.13 presents the bounds to the OPT scheme bit-error probability for DPSK over two-path mixed

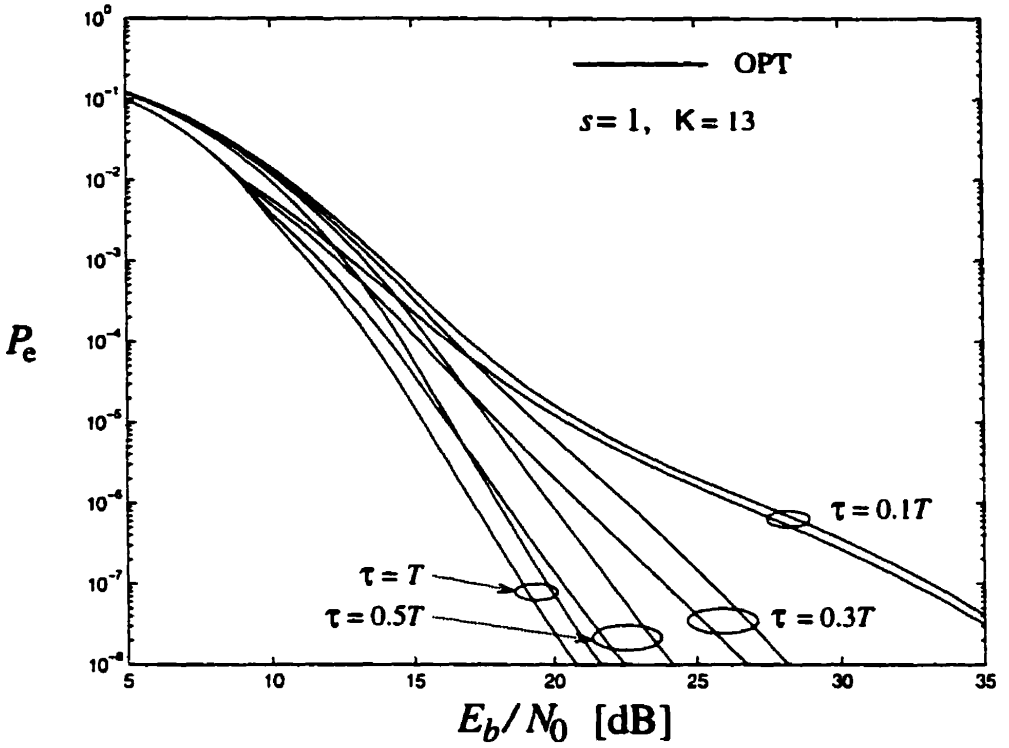

Fig. 4.12 Performance of the OPT scheme with FSK(1) signaling over 2-path Ricean/Rayleigh fading channels ($\tau = 0.1T - T$, $s = 1$ and K = 13dB)

mode Ricean/Rayleigh channels with K = 13dB and several inter-path delays. Since the observation interval for DPSK is twice that of FSK, $\tau = 2T$ corresponds to a resolved multipath channel. Similarly to FSK(1), there are some SNR ranges where no conclusion can be made. For example for $E_b/N_0 < 18.3$dB, Fig. 4.13 does not enable us to compare the performance of the OPT scheme for $\tau = 0.05T$ with its performance for $\tau = 0.1T$. Fig. 4.13 shows that the bounds are loose for very small inter-path delays such as $0.05T$ or $0.1T$. When the channel inter-path delay is increased, the bounds become tighter and tighter until $\tau \approx 1.4T$ is reached. If the channel inter-path delay is further increased, the bounds become looser. Fig. 4.13 shows that the influence of the inter-path delay on DPSK performance is quite similar to that previously observed for FSK(1) (nonlinear performance improvement as the inter-path delay increases). More important, it is seen that the degradation in performance to unresolvability is not very severe (less than 2.1dB at $P_e = 10^{-4}$ and less than 2.5dB at $P_e = 10^{-7}$) for

DPSK with $\tau \geq 0.5T$. Similar behavior was observed for SDPSK (less than 2.1dB at $P_e = 10^{-4}$ and less than 2.9dB at $P_e = 10^{-7}$).

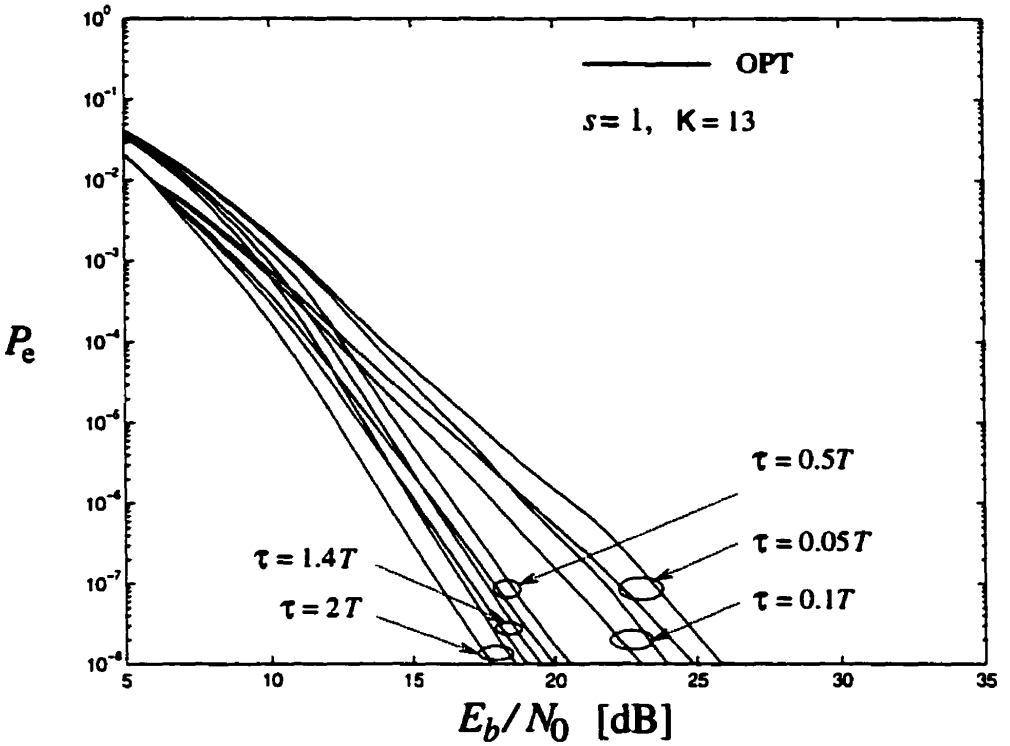

Fig. 4.13 Performance of the OPT scheme with DPSK signaling over 2-path Ricean/Rayleigh fading channels ($\tau = 0.05T - 2T$, $s = 1$ and K = 13dB)

To summarize, it is seen that similar to the SPECCOH scheme, the OPT scheme, that assumes knowledge of the specular term magnitude but not of its phase, provides good performance over unresolved multipath mixed mode Ricean/Rayleigh fading channels without any error floor. For FSK(1) and to a lesser extent for DPSK, at sufficiently high SNR, the loss in performance due to the lack of knowledge of the specular term phase is quite small (0.2-0.7dB loss with FSK(1) and 0.8-1.2 dB loss with DPSK, at $P_e = 10^{-6}$), not justifying the use of additional complex phase estimation processing. The higher the SNR, the smaller the degradation. For FSK(1/2) and SDPSK the degradation in performance is overall larger (0.5-1.8dB for FSK(1/2) and 1.2-1.5dB for SDPSK at $P_e = 10^{-6}$). Furthermore losses greater than 2dB are obtained at $P_e = 10^{-3}$ for FSK(1/2). Therefore the OPT scheme could be of interest

for modulation schemes such as FSK(1) and DPSK. If the system is operating at very high SNR it could also be of interest for FSK(1/2) and SDPSK. However the OPT receiver is difficult to implement. Performance of suboptimum receivers more suitable for implementation, such as the QDR schemes is studied next.

4.2.3 Performance of the QDR, R OPT and QR schemes

This section considers the various non-coherent suboptimum receivers derived in Chapter 3 namely the QDR, R OPT and QR schemes. Numerical results are presented in Figs. 4.14-4.23. As seen in Sections 3.7.2 and 3.7.4, the QDR and QR schemes depend on a parameter β. Figs. 4.14-4.17 present the probability of error of the various modulations schemes with QDR and QR for several values of the parameter β. To give an indication on the impact of K on the effect of β, Fig. 4.14 and Fig. 4.15 consider a channel with K = 13dB whereas Fig. 4.16 and Fig. 4.17 consider K = 15dB. The error range is chosen to be $10^{-2} - 10^{-8}$ since outside this range all QDRs perform the same. The probability of error with R OPT is included as a reference. The importance of the choice of the parameter β is shown by Figs. 4.14-4.17. From these figures it is seen that there is no single value of β that gives the best performance over the entire range of SNR. However Fig. 4.14 and Fig. 4.15 show that β should not be chosen too small (i.e. less than unity) since in that case the R OPT scheme which does not use the knowledge of the specular term outperforms the QDR scheme. Assuming a fixed value of β, the best that could be found for the QDR schemes is $\beta = 1.3$. This value gives a low probability of error at high as well as at low SNR for all the modulations schemes considered. The value $\beta = 1.3$ is chosen such that the performance degradations of the QDR scheme ($\beta = 1.3$) with respect to the best QDR scheme for each received SNR per bit are as low as possible. For example $\beta = 0.5$ is not a suitable value since for intermediate value of the received SNR, the loss with respect to QDR ($\beta = 1, 1.3, 1.5$) is not negligible as seen from Fig. 4.14. Note that the choice of β is more important for middle range of the Ricean parameter K such as K = 13dB. For example, Fig. 4.16 and Fig. 4.17 show that the probability of error is less dependent on the value of the parameter β for K = 15dB than for K = 13dB in the error range of $10^{0} - 10^{-8}$ considered in this thesis. It is to be anticipated that β has a greater influence for higher SNR. Similarly, as K decreases (i.e. the channel tending towards a Rayleigh channel), the term in the QDR schemes decision rule that depends on β decreases, hence the value of β is also less important

in that case. The dashed lines in Figs. 4.14-4.17 show that the performance of the QR scheme improves as β decreases thus the best that could be found for the QR scheme is $\beta = 0$. In the following, when the QDR and QR schemes are considered (assuming fixed β), β are respectively set to these two "best" values ($\beta = 1.3$ and $\beta = 0$).

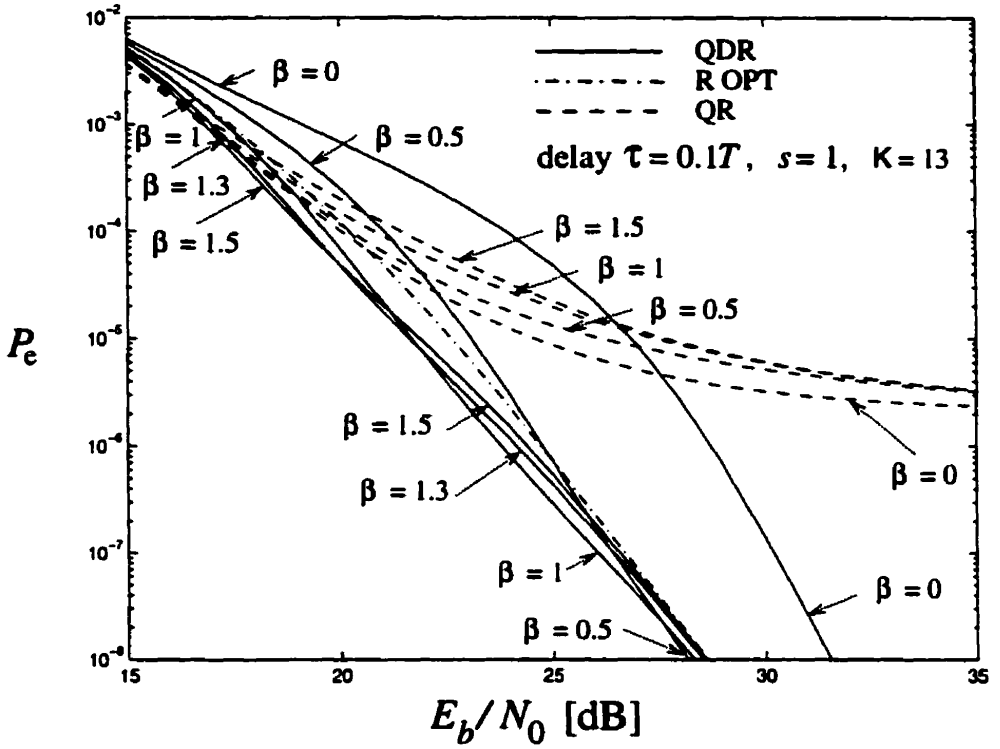

Fig. 4.14 Performance of QDR schemes ($\beta = 0 - 1.5$) with FSK(1/2) signaling over a 2-path Ricean/Rayleigh fading channel ($\tau = 0.1T$, $s = 1$ and K = 13dB)

If the parameter β is allowed, however, to assume several values, a receiver with improved performance can be designed. Specifically, let us consider the multi-receiver scheme (MQDR), composed of the QDR (with the possible values of β: 0.5, 1, 1.3, 1.5), the R OPT and the QR ($\beta = 0$) schemes, that can select a particular scheme for each received SNR per bit (E_b/N_0). Tables 4.5-4.8 give guidelines for selecting the appropriate scheme for each E_b/N_0 with the four modulations schemes considered in this thesis. These tables are closely related to the upper-bounds curves of Figs. 4.4-4.7, since the upper-bounds curves were calculated by selecting for each received SNR per bit the scheme that gave the lowest probability of error. Tables 4.5-4.8

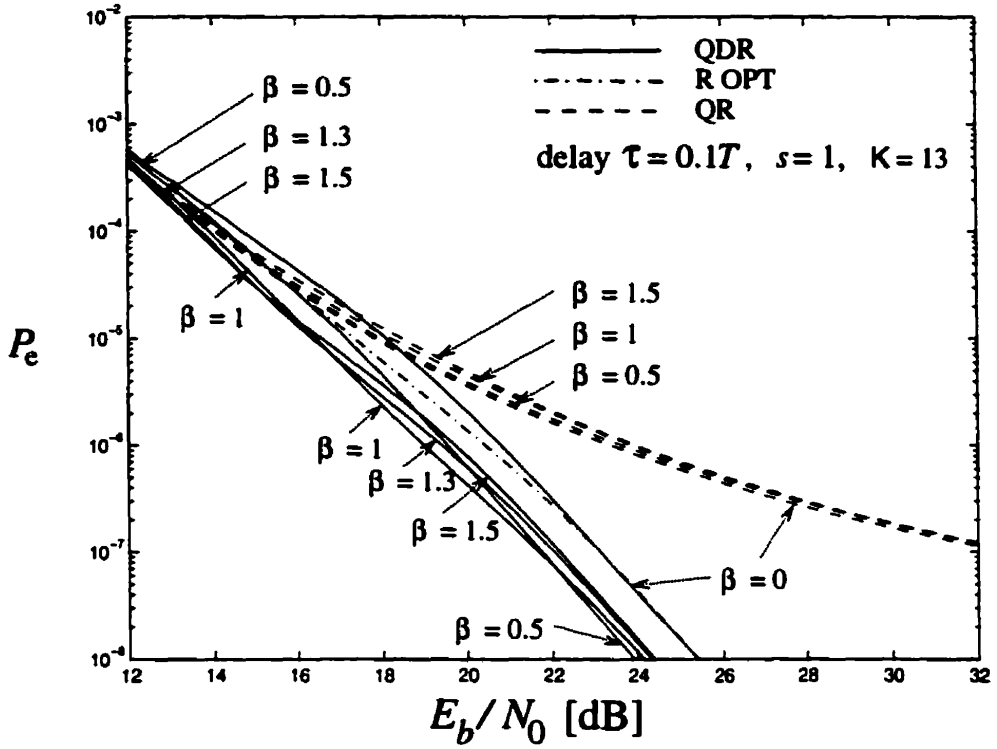

Fig. 4.15 Performance of QDR schemes ($\beta = 0 - 1.5$) with DPSK signaling over a 2-path Ricean/Rayleigh fading channel ($\tau = 0.1T$, $s = 1$ and K = 13dB)

indicate, for each value of K and for each received SNR expressed in dB, which scheme should be selected. The maximum received SNR per bit considered in these tables corresponds either to the SNR where the bit-error probability reaches $10^{-8} - 10^{-9}$ similarly to the graphs or to 45dB (whichever is lower). For some particular received SNRs per bit, several receivers are indicated in the tables. Explanations follow. Recall from Section 4.1.2 that the bit-error probabilities are numerically evaluated with an absolute error less than $1.7 \cdot 10^{-9}$. Let us consider two receivers REC1 and REC2 with respectively exact bit-error probabilities P_e' and P_e''. Let $\hat{P}_e'$ and $\hat{P}_e''$ be the computed values of P_e' and P_e''. If $\hat{P}_e' - \hat{P}_e'' > 3.4 \cdot 10^{-9}$, then $P_e' - P_e'' > 0$ and REC2 should be selected. Similarly if $\hat{P}_e' - \hat{P}_e'' < -3.4 \cdot 10^{-9}$, then $P_e' - P_e'' < 0$ and REC1 should be selected. However if $\left|\hat{P}_e' - \hat{P}_e''\right| \leq 3.4 \cdot 10^{-9}$, due to the presence of an absolute error, the numerical results do not enable us to conclude which receiver is better. In that case both receivers are indicated for that particular received SNR per bit since based

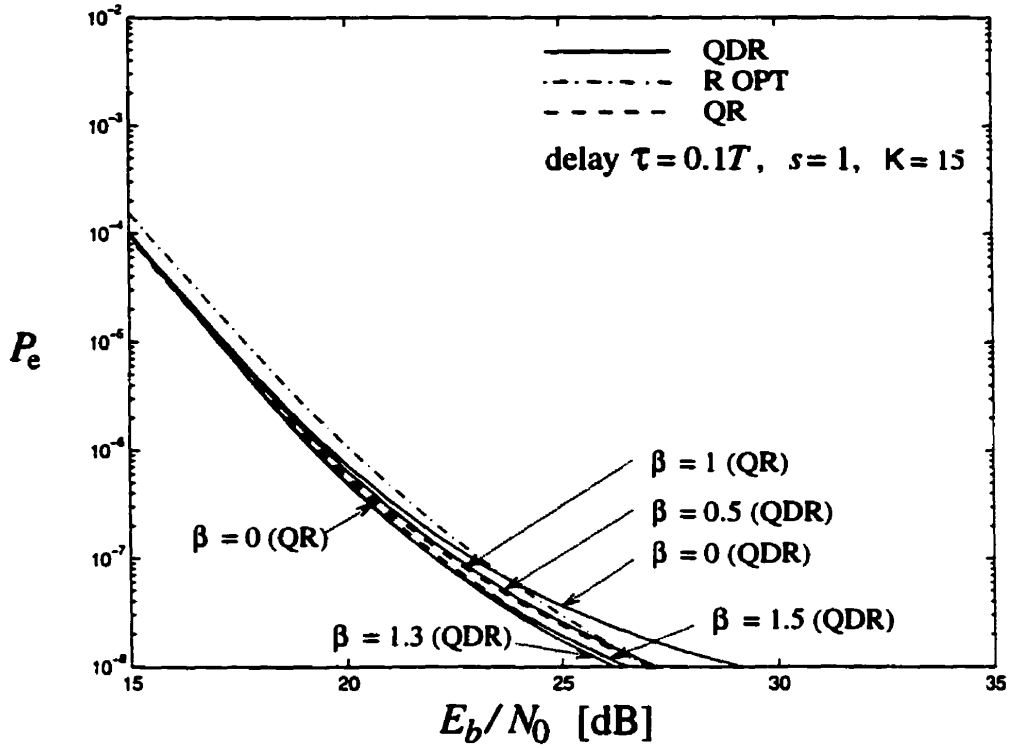

Fig. 4.16 Performance of QDR schemes ($\beta = 0 - 1.5$) with FSK(1) signaling over a 2-path Ricean/Rayleigh fading channel ($\tau = 0.1T$, $s = 1$ and K = 15dB)

on the accuracy of this thesis computation, they are equally good. The receiver name is set in boldface if the receiver to be chosen has a bit-error probability lower than the bit-error probability of the next best receiver by at least 10%. More precisely, let us assume that REC1 is the best receiver and REC2 is the next best receiver. REC1 is set in boldface if $\hat{P}_e'$ and $\hat{P}_e''$ satisfy

$$\hat{P}_e' < 0.9\hat{P}_e'' - 1.7 \cdot 10^{-9} \cdot 2.1 \qquad \text{or equivalently} \qquad \hat{P}_e'' - \hat{P}_e' > 0.1\hat{P}_e'' + 3.57 \cdot 10^{-9}$$

This ensures that the exact probabilities satisfy

$$P_e'' - P_e' > 0.1P_e''$$

In case several schemes should be selected for a particular received SNR (i.e. for $\left|\hat{P}_e' - \hat{P}_e^{(k)}\right| \leq 3.4 \cdot 10^{-9}$, $k = 1, 2, \ldots$), all these schemes are considered equivalent

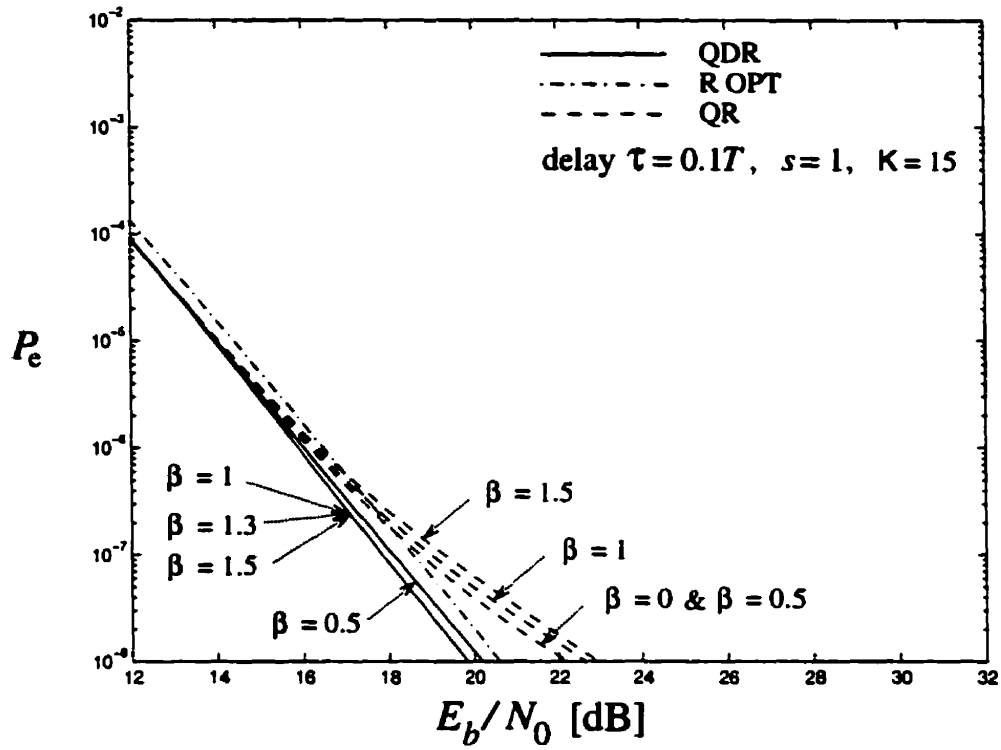

Fig. 4.17 Performance of QDR schemes ($\beta = 0 - 1.5$) with SDPSK signaling over a 2-path Ricean/Rayleigh fading channel ($\tau = 0.1T$, $s = 1$ and K = 15dB)

and comparison is with the next best receiver, excluding the equivalent ones. If these receivers perform better than the next best receiver by 10%, all of them are set in boldface. And one of the boldface receivers can be arbitrarily selected. For convenience, a QDR scheme with $\beta = 0.5$ is denoted as QDR ($\beta = 0.5$) or QDR (0.5) for short. Inside the tables, the name of the receiver is written in smaller font when it is selected by the MQDR scheme for less than two consecutive received SNR per bit values.

Tables 4.5-4.8 show that for all the modulations schemes except for DPSK and SDPSK with K = 5dB, the best receiver at low SNR (roughly for a received SNR per bit up to the value of K) is the QR scheme. However the performance of QR ($\beta = 0$) is less than 10% better than the other receivers (QR (0) is not in boldface). As shown in Section 3.4.1 at low SNR the decorrelation operation vanishes for the mixed mode Ricean/Rayleigh non-coherent optimum receiver (OPT). This may

Table 4.5 Selection of the suboptimum receiver in MQDR as a function of E_b/N_0 for FSK(1)

E_b/N_0 (dB)	5	6	7	8	9	10	11	12	13	14	15	16	17	18	19	20	21	22	23
K = 5dB	QR (0)				QDR (1.5)	QDR (1.3)	QDR (1)								QDR (0.5)				
K = 10dB	QR (0)								QDR (1.5)		QDR (1.3)		QDR (1)						
K = 13dB	QR (0)										QDR (1.5)				QDR (1.3)		QDR (1)		
K = 15dB	QR (0)														QDR (1.5)			QDR (1.3,1.5)	
K = 20dB	QR (0)												**QDR's QR (0)**	all					

E_b/N_0 (dB)	24	25	26	27	28	29	30	31	32	33	34	35	36	37	38	39	41	43	45
K = 5dB	QDR (0.5)													**QDR's & ROPT**					
K = 10dB	QDR (1)								QDR (0.5)						**QDR's & R OPT**				
K = 13dB	**QDR (1)**			QDR (1)						QDR (1,1.3,1.5) R OPT		**QDR's & R OPT**							
K = 15dB	**QDR (1,1.3,1.5) QR (0)**			QDR (1,1.3,1.5) R OPT & QR (0)															
K = 20dB																			

Table 4.6 Selection of the suboptimum receiver in MQDR as a function of E_b/N_0 for FSK(1/2)

E_b/N_0 (dB)	5	6	7	8	9	10	11	12	13	14	15	16	17	18	19	20	21	22	23	24
K = 5dB	QR (0)			QDR (1.5)			QDR (1.3)	QDR (1)				QDR (0.5)								
K = 10dB	QR (0)									QDR (1.5)		QDR (1.3)		QDR (1)		QDR (1)			QDR (0.5)	QDR (0.5)
K = 13dB	QR (0)							QR (0)					QDR (1.5)	QDR (1.5)		QDR (1.3)	QDR (1.3)	QDR (1)	QDR (1)	
K = 15dB	QR (0)								QR (0)						QDR (1.5)				QDR (1.3,1.5)	QDR (1.3)
K = 20dB	QR (0)											QR (0)								

E_b/N_0 (dB)	25	26	27	28	29	30	31	32	33	34	35	36	37	38	39	41	43	45
K = 5dB	QDR (0.5)								QDR (0.5,1)	QDR's & ROPT								
K = 10dB	QDR (0.5)				QDR (0.5)				QDR's & R OPT									
K = 13dB	QDR (1)		QDR (0.5,1)	QDR (0.5,1)	QDR's R OPT													
K = 15dB	QDR (1,1.3,1.5)																	
K = 20dB																		

Table 4.7 Selection of the suboptimum receiver in MQDR as a function of E_b/N_0 for DPSK

E_b/N_0 (dB)	5	6	7	8	9	10	11	12	13	14	15	16	17	18	19	20	21	22
K = 5dB	QDR (1.5)		QDR (1.3)		QDR (1)			QDR (0.5)										
K = 10dB	QR (0)				QDR (1.5)			QDR (1.3)	QDR (1)		QDR (1)		QDR (1)	QDR (0.5)			QDR (0.5)	
K = 13dB	QR (0)							QDR (1.5)				QDR (1.3)	QDR (1)	QDR (1)				QDR (0.5,1)
K = 15dB	QR (0)					QR (0)				QR (0)	QDR (1.5)			QDR (1.3,1.5)	QDR (1.3)	QDR (1,1.3)		
K = 20dB	QR (0)							QR (0)			QDR's ROPT, QR (0)							

E_b/N_0 (dB)	23	24	25	26	27	28	29	30	31	32	33	34	35	36	37	38	39	41	44	45
K = 5dB	QDR (0.5)							QDR's		QDR's & ROPT										
K = 10dB	QDR (0.5)			QDR (0.5)				QDR's		QDR's & R OPT										
K = 13dB	QDR (0.5)	QDR (0.5,1)																		
K = 15dB																				
K = 20dB																				

Table 4.8 Selection of the suboptimum receiver in MQDR as a function of E_b/N_0 for SDPSK

E_b/N_0 (dB)	5	6	7	8	9	10	11	12	13	14	15	16	17	18	19	20	21	22	23
K = 5dB	QDR (1.5)		QDR (1.3)	QDR (1)				QDR (0.5)											
K = 10dB	QR (0)				QDR (1.5)			QDR (1.3)	QDR (1)						QDR (0.5)				
K = 13dB	QR (0)							QDR (1.5)				QDR (1.3)	QDR (1)		**QDR (1)**		QDR (1)		
K = 15dB	QR (0)								QDR (1.5)					QDR (1.3,1.5)	QDR (1,1.3,1.5)				
K = 20dB	QR (0)								**QDR's QR (0)**		all								

E_b/N_0 (dB)	24	25	26	27	28	29	30	31	32	33	34	35	36	37	38	39	41	43	45
K = 5dB	QDR (0.5)					**QDR's & ROPT**													
K = 10dB	QDR (0.5)					**QDR's & R OPT**													
K = 13dB	QDR (0.5,1,1.3)	**QDR's R OPT**																	
K = 15dB																			
K = 20dB																			

explain why the QR outperforms the QDR schemes in some cases since the QR does not employ decorrelation. As E_b/N_0 increases, the QDR schemes outperform the QR scheme for all the modulations schemes, and the best QDR scheme becomes successively, QDR ($\beta = 1.5$), QDR ($\beta = 1.3$), QDR ($\beta = 1$) and QDR ($\beta = 0.5$). The corresponding SNR ranges of each scheme depend on both K and the modulation scheme. For larger values of K, the threshold SNR from which QDR ($\beta = 1.5$) outperforms QR ($\beta = 0$) is higher. For example for FSK(1), this threshold is equal to 9dB for K = 5dB and to 13dB for K = 10dB. At very high SNR (for example FSK(1): $E_b/N_0 \geq$ 37dB for K = 5dB and $E_b/N_0 \geq$ 38dB for K = 10dB or DPSK: $E_b/N_0 \geq$ 32dB for K = 5dB and $E_b/N_0 \geq$ 31dB for K = 10dB), all the QDR schemes and the R OPT scheme perform the same (given the tolerance error of the results) and they all outperform the QR scheme by a large value. This gives another indication of the importance of using receivers specially designed to handle multipath non-resolvability since the QDR and R OPT schemes include the decorrelation operation whereas the QR does not. These similar performances were to be expected since at high SNR, the QDR's receivers and the R OPT scheme converge to the same receiver structure. Let us consider next the case of DPSK or SDPSK with K = 5dB and low SNR. From Tables 4.7 and 4.8, it is seen that at low SNR ($E_b/N_0 \approx$ 5-6dB) the best receiver is not QR ($\beta = 0$) but QDR ($\beta = 1.5$). This is due to the fact that a low SNR for (S) DPSK with K = 5dB means a received SNR per bit lower than the value of K. But as the received SNR per bit increases, the selection of the best suboptimal receiver for (S) DPSK follows the same pattern as the other modulation schemes or as (S) DPSK with other values of K follow (i.e. as E_b/N_0 increases the best receiver is QDR ($\beta = 1.3$), QDR ($\beta = 1$) and QDR ($\beta = 0.5$)). Note that similar tables considering the QDR schemes alone show that except for K = 5dB, as E_b/N_0 increases, the best QDR scheme becomes successively QDR ($\beta = 0.5$), QDR ($\beta = 1.5$), QDR ($\beta = 1.3$), QDR ($\beta = 1$) and QDR ($\beta = 0.5$). At high SNR, all the QDR schemes perform the same, so the choice of β is not important in this case. For K = 5dB, the best receiver among the QDR schemes is QDR ($\beta = 1.5$) and as E_b/N_0 increases, the best receiver is successively QDR ($\beta = 1.3$), QDR ($\beta = 1$) and QDR ($\beta = 0.5$) similarly to the sequence for other values of K.

Fig. 4.18 presents the bounds to the bit-error probabilities of the OPT scheme and the exact bit-error probabilities of QDR ($\beta = 1.3$) with FSK(1) and DPSK signaling over two-path mixed mode Ricean/Rayleigh channels with K = 10, 15dB. Fig. 4.19

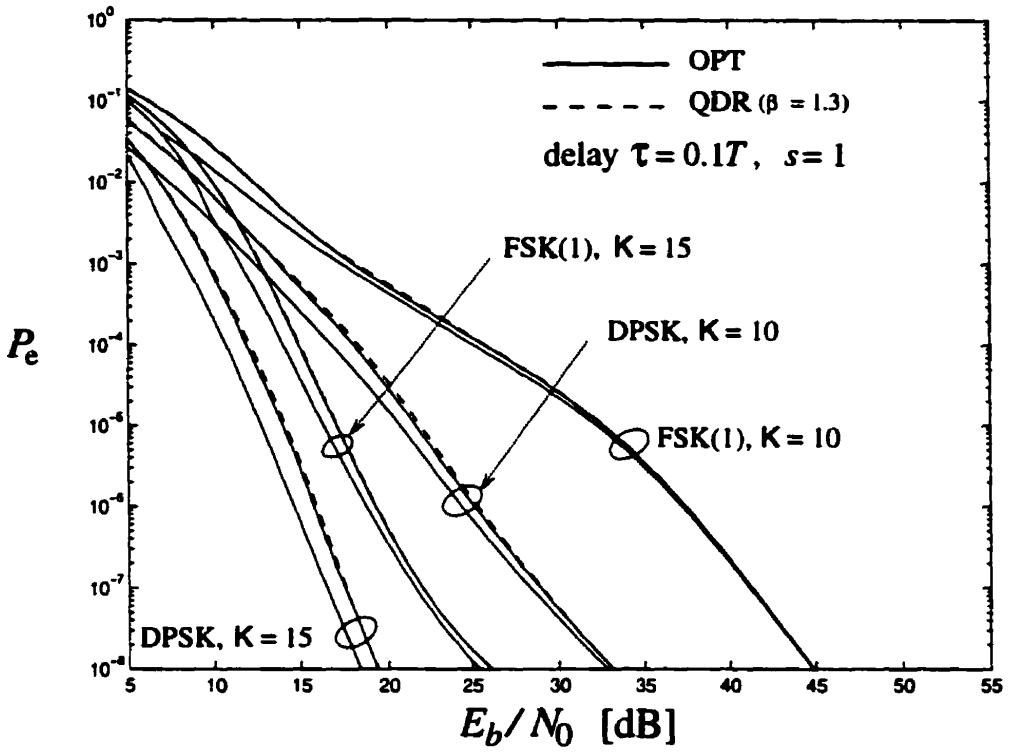

Fig. 4.18 Performance of FSK(1) and DPSK signaling over 2-path Ricean/Rayleigh fading channels ($\tau = 0.1T$, $s = 1$ and K = 10, 15dB)

presents similar curves for FSK(1/2) and SDPSK. Figs. 4.18-4.19 confirm the design specifications of the QDR scheme, particularly the fact that the QDR converges to the OPT scheme at high SNR as is explained in Section 3.7.2. However the required received SNR per bit increases with increasing K and depends on the modulation scheme. In the range of error probability of $10^0 - 10^{-8}$, the QDR is closer to OPT for smaller values of K and for FSK(1) and DPSK. Table 4.9 gives the SNR losses (in dB) yielded by the QDR ($\beta = 1.3$) compared to OPT at probabilities of error of 10^{-3}, 10^{-6} and 10^{-8}. Note that these losses are calculated with respect to the lower-bounds to the bit-error probabilities of the OPT scheme. Since the true bit-error probabilities of the OPT scheme lie between the two bounds, the actual losses are smaller. SNR losses greater than 2dB are set in boldface.

Fig. 4.18 shows that for FSK(1) and DPSK the losses yielded by QDR ($\beta = 1.3$) compared to the OPT scheme are not too severe at moderate high SNR (for example

for $E_b/N_0 \geq$ 15dB maximum losses of 1dB for FSK(1) and 1.4-1.6dB for DPSK). However as shown in Fig. 4.19 and Table 4.9, QDR ($\beta = 1.3$) exhibits larger losses compared to the OPT scheme for FSK(1/2) (2.8dB$\{P_e = 10^{-3}, \mathsf{K} = 13\text{dB}\}$ and 1.8dB$\{P_e = 10^{-6}, \mathsf{K} = 15\text{dB}\}$) and SDPSK (1.8dB$\{P_e = 10^{-6}, 10^{-8}, \mathsf{K} = 13\text{dB}\}$). But due to the looseness of the bounds for FSK(1/2), its degradation is difficult to assess (see bounds in Fig. 4.19 for $P_e \approx 10^{-5}$). Nevertheless at very high SNR (yielding probability of error of the order of 10^{-8}) the QDR relative loss compared to OPT for FSK(1/2) reaches acceptable values of the order of 1dB.

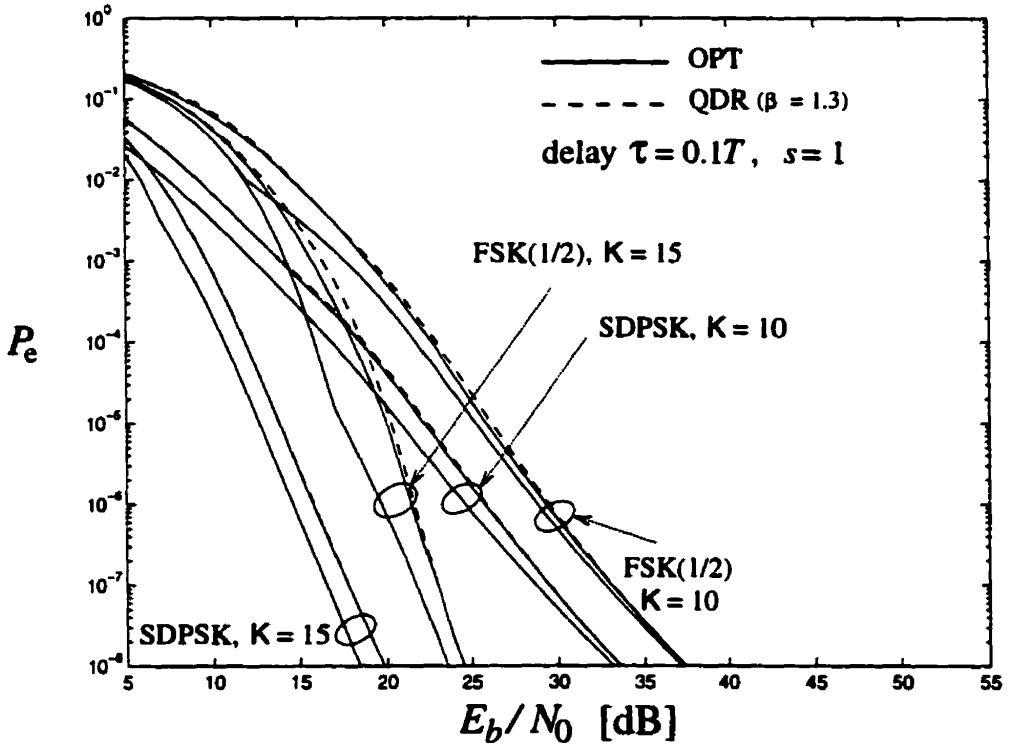

Fig. 4.19 Performance of FSK(1/2) and SDPSK signaling over 2-path Ricean/Rayleigh fading channels ($\tau = 0.1T$, $s = 1$ and K = 10, 15dB)

As seen in Section 4.2.2, the knowledge of the specular component phase shift does not provide significant gains at high SNR for FSK(1) and to a lesser extent for DPSK. However the OPT scheme, that does not use this knowledge, is not suitable for implementation. Therefore it is of interest to compare the performance of the QDR scheme with the SPECCOH scheme. Such comparison is provided by Table 4.4. From

Table 4.9 SNR losses (in dB) yielded by QDR compared to OPT. K is expressed in dB. These losses are worse cases since they are obtained using the lower-bounds to the bit-error probabilities of the OPT scheme.

SNR losses in dB		FSK(1)			FSK(1/2)				DPSK			SDPSK		
	P_e · K → ↓	10	13	15	10	13	15	20	10	13	15	10	13	15
QDR(1.3) /OPT	10^{-3}	0.5	1.1	1.3	1.4	**2.8**	**2**	0.5	1.4	1.6	1.4	1.6	1.4	1.4
	10^{-6}	0.1	1	0.5	0.6	1.2	1.8	1.4	0.9	1.5	1.4	1.3	1.8	1.2
	10^{-8}	≈ 0	0.5	0.6	0.2	0.9	0.9	**2.3**	0.4	1.4	1	0.9	1.8	1.4

Table 4.4 it is seen that similar to the OPT scheme, the losses yielded by the QDR with respect to SPECCOH are very small at high SNR for FSK(1) ($\leq$ 0.6dB at $P_e = 10^{-8}$ for K = 10-15dB). Larger losses are obtained with DPSK reaching 1.4dB values even at a very low probability of error. And losses close to 2dB are obtained for FSK(1/2) and SDPSK at high SNR. At very low SNR ($E_b/N_0 \approx$ 5-6dB) all modulation schemes yield significant losses (FSK(1):2.5dB for K = 10dB, FSK(1/2):4.6dB for K = 10dB, (S) DPSK:2.2dB for K = 10dB and 1.8dB for K = 15dB). These losses are calculated from figures similar to Figs. 4.18-4.19 but with SPECCOH bit-error probabilities instead of the lower-bounds to the bit-error probabilities of the OPT scheme. These may seem large but they represent the losses yielded by QDR ($\beta = 1.3$) with respect to SPECCOH assuming perfect estimation of the Ricean specular term phase. However it is likely that at such low SNR, the specular term phase estimate will not be perfect and this will degrade the performance of the SPECCOH scheme thus lowering the losses of QDR ($\beta = 1.3$) with respect to SPECCOH. Nevertheless, if FSK(1/2) is employed at low SNR, additional complexity required to track the Ricean specular term phase is worthwhile since significant SNR gains can be obtained.

The remainder of this section will focus on performance of implementable receivers specially designed to handle unresolvability such as the QDR ($\beta = 1.3$) scheme. Comparing the performance of the QDR scheme with the QR will show the improvement due to the decorrelation stage. Secondly, comparing the performance of the R OPT scheme with the QDR will assess the improvement yielded by the knowledge of the

Ricean specular term magnitude. Since for high SNR, the QDR performance is very close to that of OPT, the suboptimum receivers will only be compared among them. Comparison of R OPT and QR with OPT can be extrapolated from QDR curves.

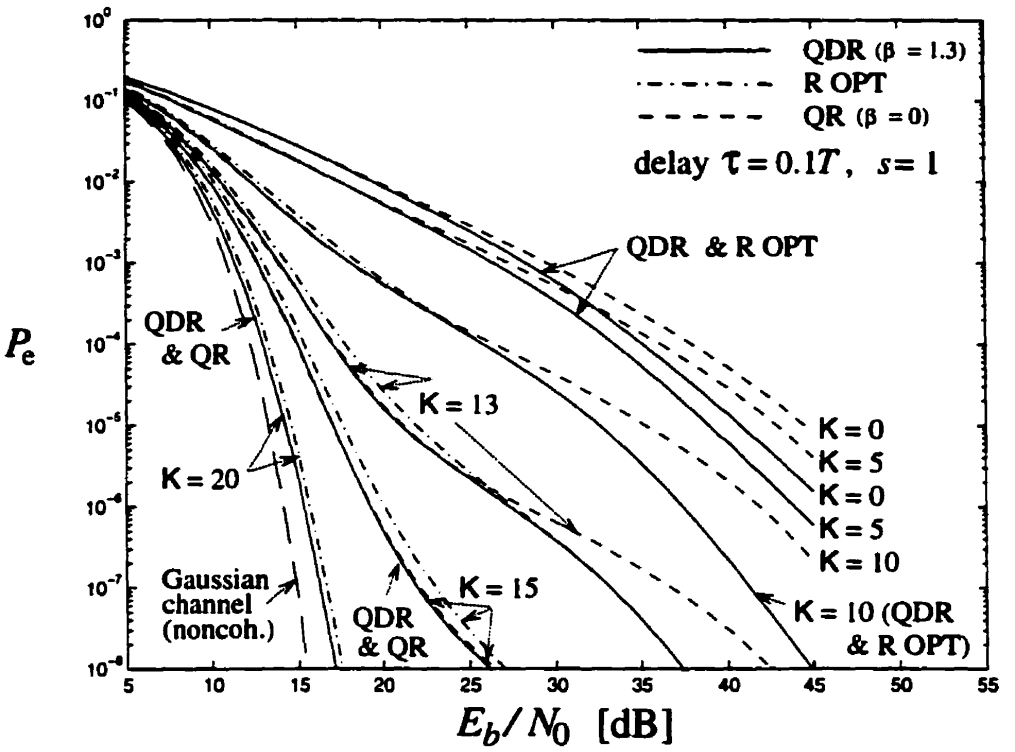

Fig. 4.20 Performance of the QDR, R OPT and QR schemes with FSK(1) signaling over 2-path Ricean/Rayleigh fading channels ($\tau = 0.1T$, $s = 1$ and K = 5-20dB)

From Figs. 4.20-4.23 it is seen that the QDR scheme performs better than the R OPT scheme over mixed mode Ricean/Rayleigh channels. Quantitatively, the QDR scheme with FSK(1) and FSK(1/2) yields up to $\approx$ 1dB gain with respect to the R OPT scheme at an error probability of $3 \cdot 10^{-5}$ for K = 13dB and at an error probability of 10^{-7} for K = 15dB. From Fig. 4.22 it is seen that the QDR scheme with DPSK yields up to 1dB gain with respect to R OPT for K = 13dB in the error probability range of $10^{-5} - 10^{-8}$ and up to 1.7dB for K = 15dB at an error probability of 10^{-8}. For SDPSK 0.8dB gain is obtained at an error probability of 10^{-8} for K = 15dB and 0.7dB is obtained at an error probability of $2 \cdot 10^{-5}$ with K = 13dB (see Fig. 4.23). This shows that SNR gains can be obtained by the use of receivers which exploit the

knowledge of the specular component magnitude.

Note that although it may appear on Figs. 4.20-4.23 that the QDR scheme yields asymptotically diversity-like gains of order higher than two, this is not actually the case. It has been verified that at sufficiently low probability of error the QDR over a two-path mixed mode Ricean/Rayleigh channel behaves asymptotically as a two-fold diversity system.

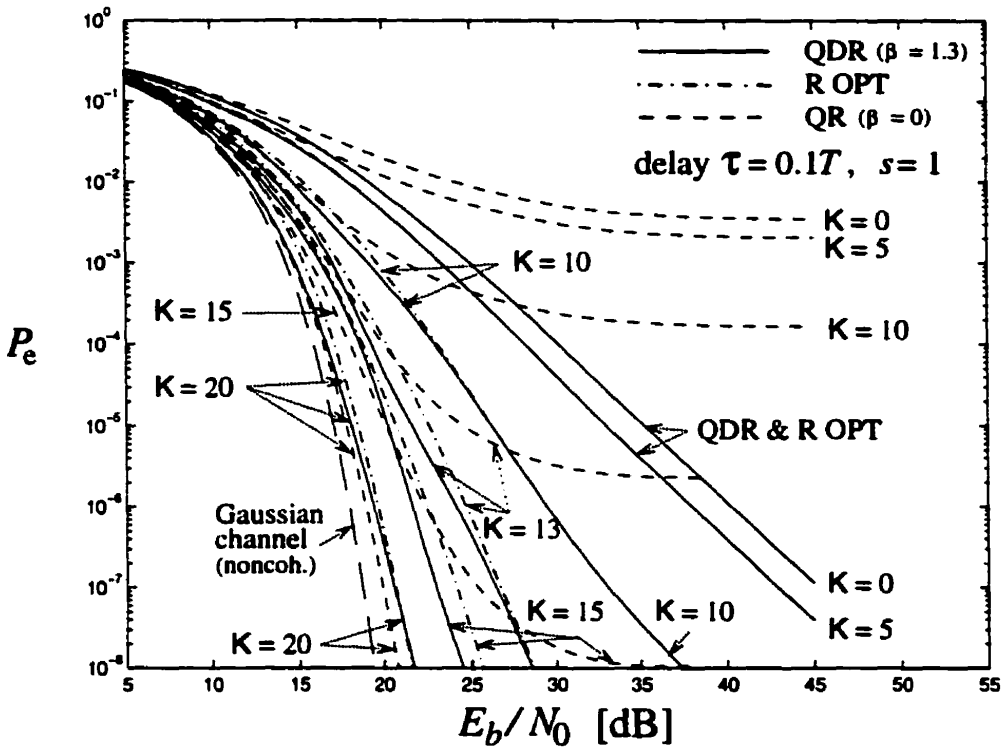

Fig. 4.21 Performance of the QDR, R OPT and QR schemes with FSK(1/2) signaling over 2-path Ricean/Rayleigh fading channels ($\tau = 0.1T$, $s = 1$ and K = 5-20dB)

Figs. 4.20-4.23 also show the superiority of the QDR scheme over the QR at high SNR, i.e. for $E_b/N_0 > 25$dB. Furthermore Fig. 4.21 and Fig. 4.22 show that with FSK(1/2) and DPSK the QR scheme yields error floors which are eliminated by the QDR. At low SNR, the QR scheme performs the same or better than the QDR. However, the performance degradation of the QDR is in general small compared with the SNR gains which can be achieved by this scheme with respect to R OPT or QR at high SNR. For example, the QDR yields 0.36dB loss for K = 13dB at an

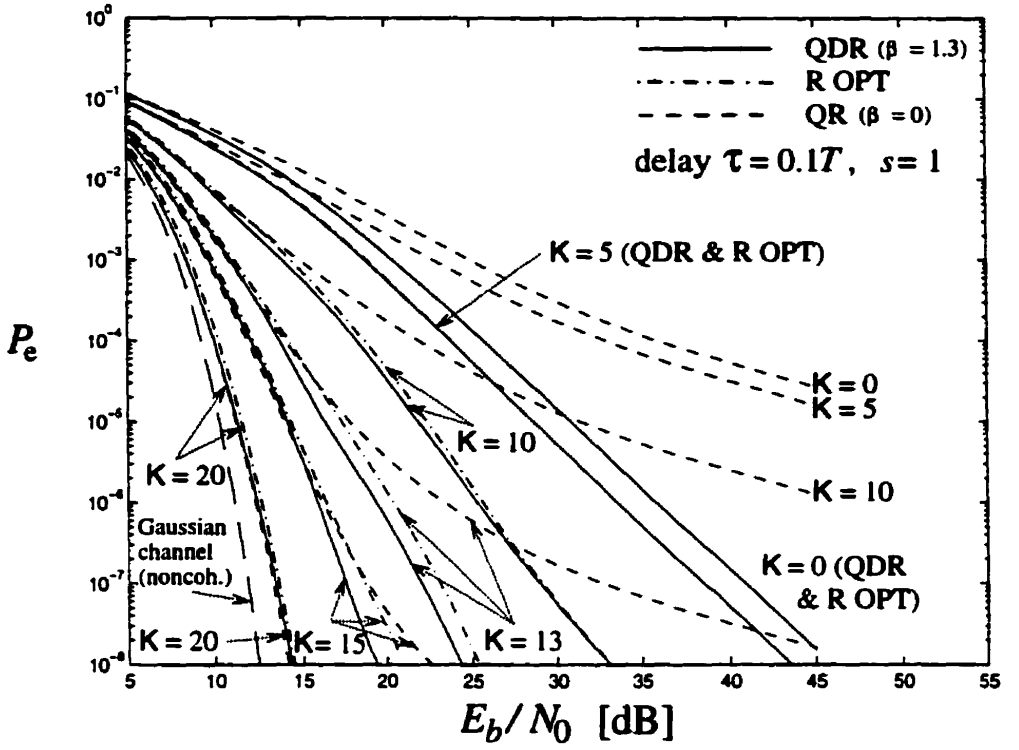

Fig. 4.22 Performance of the QDR, R OPT and QR schemes with DPSK signaling over 2-path Ricean/Rayleigh fading channels ($\tau = 0.1T$, $s = 1$ and K = 5-20dB)

error probability of $5 \cdot 10^{-3}$ for FSK(1/2) and 0.3dB loss for K = 20dB for DPSK at an error probability of 10^{-8}. Note that for K = 20dB, the QR scheme with FSK(1/2) outperforms the QDR scheme over the entire range of error probabilities considered in this thesis ($\approx$ 0dB at $P_e = 10^{-3}$, 0.5dB at $P_e = 10^{-6}$ and 0.9dB at $P_e = 10^{-8}$). As shown in Section 3.4.1, at low SNR the decorrelation vanishes for the mixed mode Ricean/Rayleigh non-coherent optimum receiver. This may explain why the QR outperforms the QDR in some cases since the QR does not employ decorrelation. Nevertheless considering the fact that the QDR eliminates the error floors, overall the superiority of the QDR over mixed mode Ricean/Rayleigh channels is clear.

To summarize, it is seen that similar to the non-coherent optimum receiver (OPT), the proposed quadratic suboptimum receiver, namely the QDR scheme, provides good performance over unresolved mixed mode Ricean/Rayleigh fading channels. At high

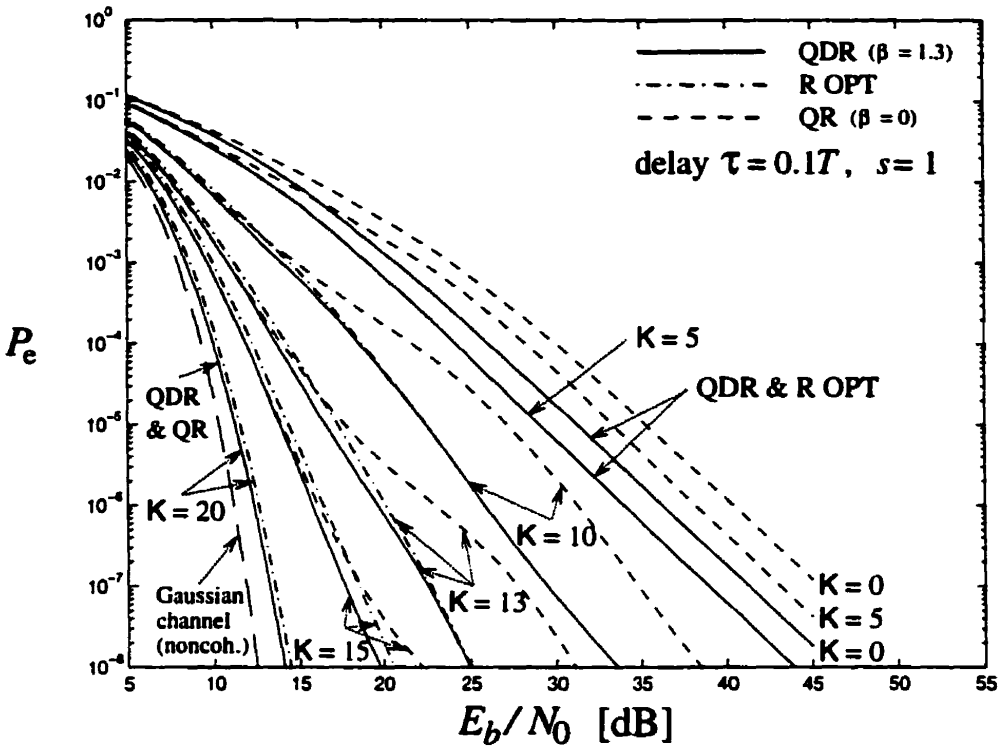

Fig. 4.23 Performance of the QDR, R OPT and QR schemes with SDPSK signaling over 2-path Ricean/Rayleigh fading channels ($\tau = 0.1T$, $s = 1$ and K = 5-20dB)

SNR ($E_b/N_0 \geq$ 15dB), QDR ($\beta = 1.3$) yields the following losses with respect to OPT: up to 0.9dB for FSK(1), 3dB for FSK(1/2), 1.5dB for DPSK, and 1.8dB for SDPSK. However for FSK(1/2) losses are difficult to assess precisely since the lower and upper-bounds of OPT are not tight. So the actual degradation may be smaller. Smaller losses are obtained for higher SNR where the bounds are tighter. Similar to the OPT scheme, the QDR scheme assumes knowledge of only the magnitude of the specular term and includes the decorrelation operation. It eliminates the error floor and provides SNR gains compared to R OPT, scheme that does not assume knowledge of the specular term (up to 1.7dB SNR gain). Since the QDR scheme is much more suitable for implementation, it represents an interesting alternative to the non-coherent optimum receiver. Furthermore it does not require the knowledge of the specular term phase. And its loss in performance compared to the optimum receiver that assumes complete knowledge of the specular term (SPECCOH) in the

range of bit-error probability $P_e = 10^0 - 10^{-8}$ was found to be small at high SNR for FSK(1) (up to 0.9dB when $E_b/N_0 \geq$ 15dB, K = 5-20dB) and to a lesser extent for DPSK (up to 1.4dB when $E_b/N_0 \geq$ 15dB, K = 5-15dB)), justifying further the use of non-coherent detection over multipath fading channels for those modulation schemes. For FSK(1/2) with large K($\geq$ 15dB) and SDPSK with K = 13dB, the degradation is significant in the order of 2dB (SDPSK) to 4dB (FSK(1/2)), making the use of Ricean specular phase estimation worthwhile in those cases. Since QDR reduces to R OPT (the unresolved Rayleigh fading channels non-coherent optimum receiver), when the fading becomes Rayleigh, the QDR will also perform well over Rayleigh fading channels as will be seen next.

4.3 Performance of the R OPT (= OPT = QDR) and R QR schemes over Rayleigh fading channels

This section considers the performance of the non-coherent optimum receiver (R OPT = OPT = QDR) and the R QR scheme over unresolved Rayleigh fading channels. Numerical results are presented in Figs. 4.24-4.27. Fig. 4.24 and Fig. 4.25 present the performance of the R OPT (= QDR) and R QR schemes over two-path Rayleigh fading channels, characterized by τ and s. These parameters are defined in Section 4.2. Comparing the solid lines with the dot-dashed lines in Figs. 4.24-4.25, it is seen that the performance degradation of the R OPT due to unresolvability is between 3 and 8.5dB in the error probability range of $10^{-5} - 10^{-8}$ without error floors for the various modulation schemes.

Fig. 4.24 and Fig. 4.25 show that the R OPT (= QDR) scheme provides two-fold diversity-like gains even when the multipath is unresolved. Moreover from Fig. 4.24 it is seen that for FSK(1/2) and DPSK the R QR scheme has a marked error floor, while the R OPT (= QDR) eliminates this effect. This shows the importance of the decorrelation operation on the input samples for Rayleigh channels. This effect was also observed over mixed mode Ricean/Rayleigh fading channels. Therefore it is seen that the decorrelation operation is very important to combat error floors over multipath fading channels when the multipath is not resolved. Specializing again to Rayleigh fading channels, Fig. 4.24 and Fig. 4.25 also show that the best performance is obtained for equal path strength channels (i.e. $s = 1$). However from Fig. 4.25 it is seen that even a low power second path (for example $s = 0.1$) should not be

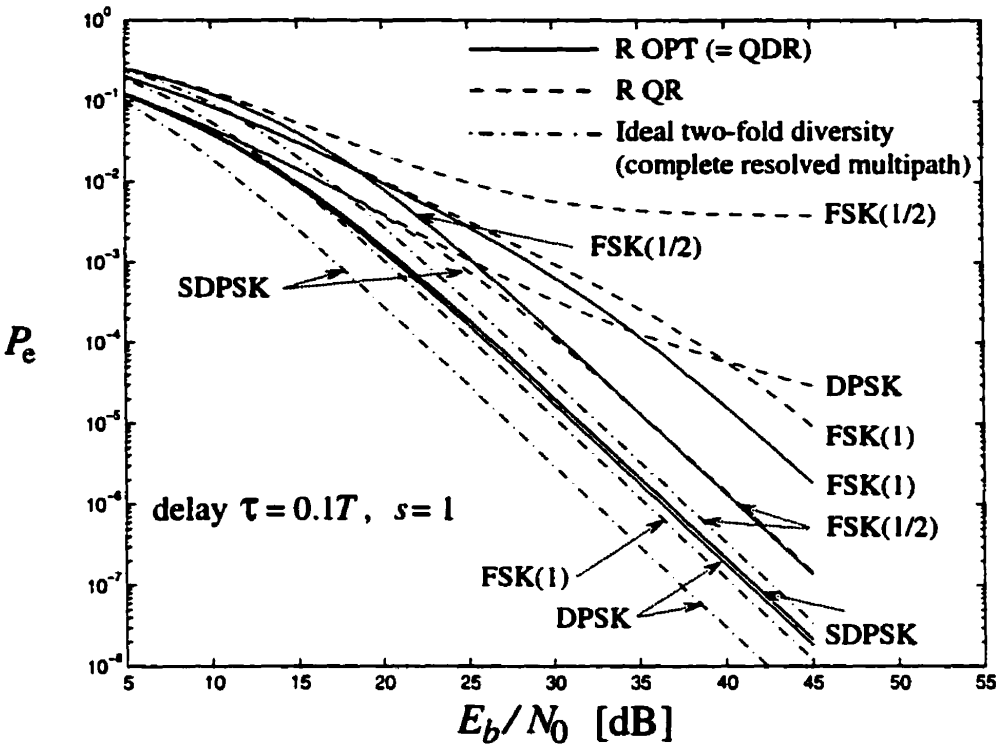

Fig. 4.24 Performance of FSK and DPSK signaling over a 2-path Rayleigh fading channel ($\tau = 0.1T$ and $s = 1$)

discarded in the detection process because the R OPT (= QDR) scheme may give some additional gain at high SNR compared to a simple non-coherent receiver, that does not exploit the second path. This is especially true for FSK(1/2), DPSK and SDPSK.

By comparing the performance of R OPT with DPSK and FSK over Rayleigh channels, remarks similar to what was noticed about the performance of OPT with DPSK and FSK over mixed mode Ricean/Rayleigh channels can be made. For example, from Fig. 4.24 it is seen that DPSK and SDPSK detected with R OPT give the best performance. At high SNR DPSK gives 4dB improvement compared to FSK(1/2) and between 10 and 13dB compared to FSK(1) in the error probability range $10^{-5} - 10^{-8}$. However as explained in Section 4.2.2, DPSK by definition gains 3dB compared to FSK because the observation interval used with DPSK is twice the one used with FSK. When the SNR is below 20dB, FSK(1) outperforms FSK(1/2)

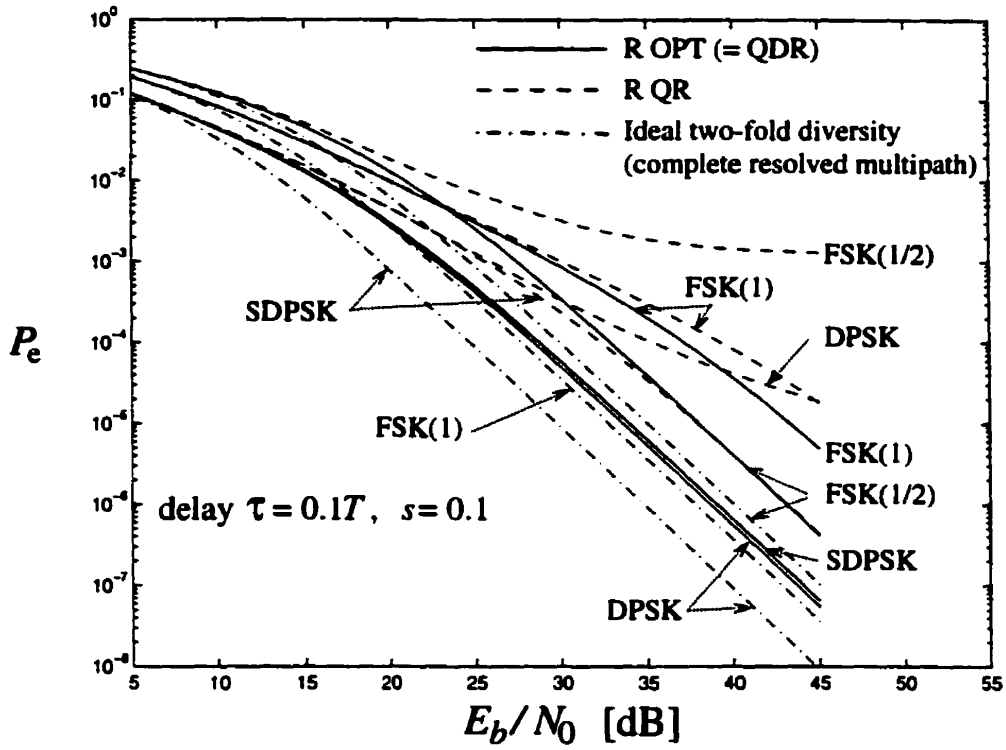

Fig. 4.25 Performance of FSK and DPSK signaling over a 2-path Rayleigh fading channel ($\tau = 0.1T$ and $s = 0.1$)

but FSK(1/2) gives better performance at higher SNR. This is similar to the behavior of FSK over mixed mode Ricean/Rayleigh channels.

Fig. 4.24 and Fig. 4.25 confirm that the performance of the R QR over two-path channels with a small inter-path delay depends heavily on the modulation schemes. For FSK(1) and SDPSK the R QR scheme performs reasonably well giving even diversity-like gains. With FSK(1/2) and DPSK, however, the R QR scheme has error floors. These error floors are eliminated by the R OPT (= QDR) scheme. The improved performance of the R OPT (= QDR) scheme can be explained as follows. Over an equal path strength channel, the performance of the R QR scheme similarly to the R OPT scheme depends on the correlation matrices $\mathbf{\Gamma}_1$ and $\mathbf{\Gamma}_2$ and the cross-correlation matrix $\mathbf{\Gamma}_{12}$. The kj^{th} entry of $\mathbf{\Gamma}_m, m = 1, 2$ is given by ρ_{kj}^{mm}, where $\rho_{kj}^{rl} = \frac{1}{\sqrt{\bar{E}_r \bar{E}_l}} \int_0^{T_o} \bar{s}_r(t - \tau_k)\bar{s}_l^*(t - \tau_j)dt$. The kj^{th} entry of $\mathbf{\Gamma}_{12}$ is ρ_{kj}^{12}. These matrices are closely related to the shape of the signals and the inter-path delay of the channel.

For SDPSK and FSK, the correlation matrices are conjugate to each other having identical eigenvalues. On the other hand, for DPSK the two correlation matrices have different eigenvalues. Let's recall that the R OPT scheme uses the eigenvalues of the matrices $\boldsymbol{C}\boldsymbol{\Gamma}_m^*, m = 1, 2$, which are equal for SDPSK and FSK and the R QR scheme uses the eigenvalues of the matrix $\boldsymbol{C}$. The relatively good performance of the R QR scheme for SDPSK can then be partly explained by the fact that although the R QR scheme does not use the appropriate eigenvalues, it uses an identical set of eigenvalues for both hypothesis similar to R OPT. The form of the cross-correlation matrix $\boldsymbol{\Gamma}_{12}$ has also an important role since although the R QR scheme uses the same set of eigenvalues for FSK(1/2) as R OPT, it yields some error floor.

The results for a two-path channel show that the performance of the R OPT (= QDR) scheme is always better than the performance of the R QR scheme. It is to be expected that the gains and the superiority of the R OPT (= QDR) scheme over R QR are even higher over a three-path channel as can be inferred from Fig. 4.26 and Fig. 4.27. With a notation similar to the two-path case, for a three-path channel, the received SNR is given by $\frac{E_b}{N_0} = (2\sigma_0^2 + 2\sigma_1^2 + 2\sigma_2^2)\frac{\mathcal{E}_b}{N_0} = 2\sigma_0^2(1 + s + s')\frac{\mathcal{E}_b}{N_0}$ where $s' = \frac{\sigma_2^2}{\sigma_0^2}$. The relative delay between the first and the third path, $\tau' = \tau_2 - \tau_0$, is expressed as a percentage of T. The three-path Rayleigh fading channel is characterized by the value of the parameters s (defined as for the two-path case) and s' which represents the Rayleigh path's strength of the third path relative to the first. Fig. 4.26 and Fig. 4.27 show that the R OPT (= QDR) scheme gives higher diversity-like gains over the three-path channel. For sufficiently high SNR, the R OPT (= QDR) bit-error probability decreases by an order of magnitude for an increase of 3.5dB in E_b/N_0, and thus yields diversity gains of order three. Furthermore from Fig. 4.26 and Fig. 4.27, it is seen that unlike over the two-path channel, the performance of R QR for FSK(1) has an error floor over the three-path channel. This shows that the error floor phenomenon in the performance of the R QR scheme is emphasized over the three-path channel. However this error floor is removed by the R OPT (= QDR). Therefore it is seen that all the effects observed over the two-path channel are enhanced over the three-path channel. It is to be expected that the same trend exists as the number of paths is increased showing that the improvement of the R OPT (= QDR) scheme might be even higher.

To summarize, it is seen that the non-coherent optimum receiver (R OPT), identical to the QDR scheme in this case performs well over unresolved Rayleigh fading

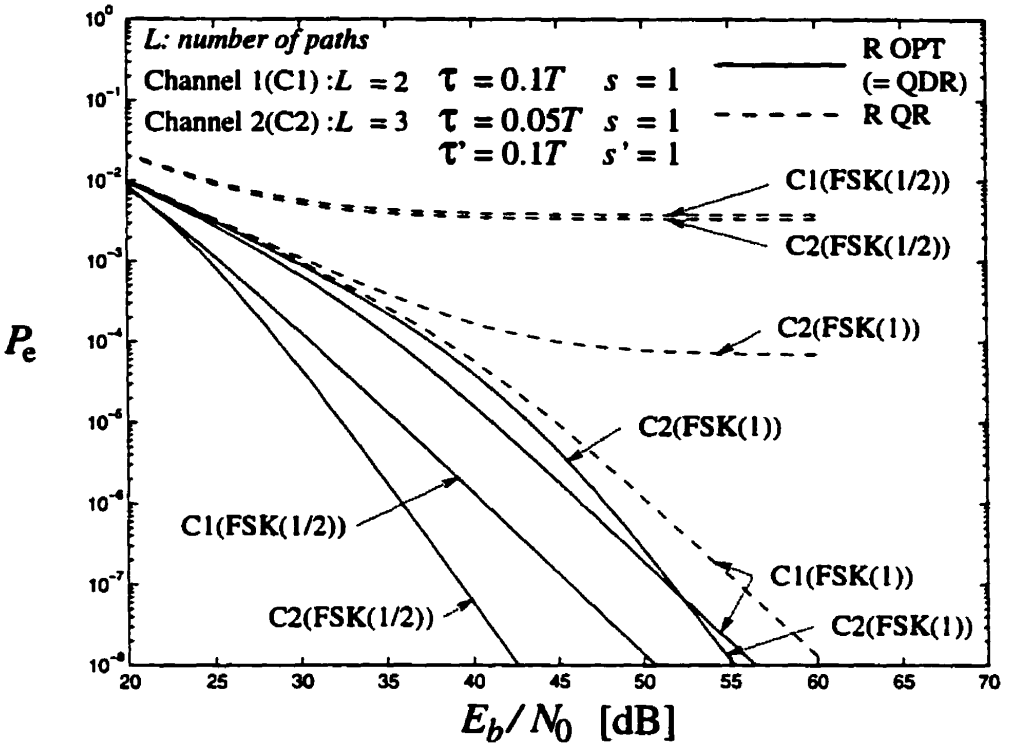

Fig. 4.26 Performance of FSK(1) and FSK(1/2) signaling over 2 and 3-path Rayleigh fading channels

channels yielding diversity gains at high SNR even if the multipath is unresolved. Due to its decorrelation operation, the R OPT (= QDR) eliminates error floors. Looking at the results on mixed mode Ricean/Rayleigh and Rayleigh fading channels as a whole, it is seen that the specular coherent and non-coherent optimum receivers yield diversity gains at high SNR and eliminate error floors over unresolved multipath fading channels. Furthermore, it was shown that the proposed non-coherent suboptimum receiver (the QDR scheme), optimum over Rayleigh channels, exhibits the same type of error floor free performance with diversity gains, while being much more suitable for implementation. Two results should be emphasized, 1) the importance of the decorrelation operation to handle unresolvability, 2) the small loss in performance due to the absence of knowledge of the specular term phase at high SNR for FSK(1) and to a lesser extent for DPSK. It can be noted however that SNR gains can be obtained by knowledge of the specular term magnitude.

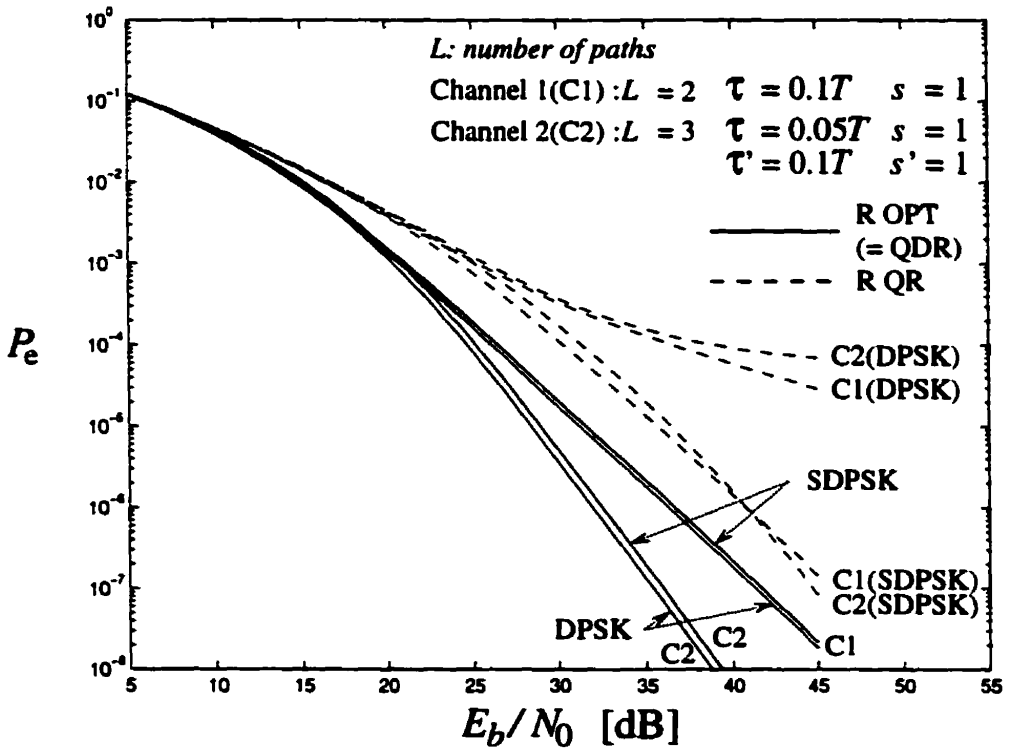

Fig. 4.27 Performance of DPSK signaling over 2 and 3-path Rayleigh fading channels

Chapter 5

A discussion on practical applications of results and extensions

The structures considered in Chapter 3 and the performance analysis of Chapter 4 show that it is possible to obtain path diversity gains without expanding bandwidth. The key to this is a decorrelation stage before Rake combining. This chapter considers key issues for practical applications of the thesis'results as well as possible extensions.

5.1 Multipath decorrelation: a "must" in detection and estimation over unresolved multipath channels

It was shown in Chapter 3 that the optimal receivers (specular coherent and non-coherent) over unresolved multipath fading channels perform an initial decorrelation (or orthogonalization) stage indicated by the presence of the decorrelating matrix $\boldsymbol{X}_m$. The effect of the decorrelation was studied in Chapter 4. It was shown that the decorrelation operation yields diversity gains over unresolved multipath channels and is essential to avoid error floors. These diversity gains can be observed, for example, in Fig. 4.18. The error floor phenomenon occurring with receivers that do not implement the decorrelation, for example the QR scheme with FSK(1/2) is shown in Fig. 4.21. Such error floor phenomenon may yield huge performance degradation, for example when K = 10dB, a received SNR per bit of 30dB yields a bit-error probability of

$\approx 7 \cdot 10^{-7}$ for the QDR scheme (with decorrelation) and a bit-error probability of $\approx 2.5 \cdot 10^{-4}$ for QR (without decorrelation).

In Chapter 2, it was shown that the path resolvability assumption is not satisfied in an indoor environment for signals based on the IS95 standard. Currently IS95 systems employ Rake receivers [162] that do assume path resolvability. However, as shown in this thesis, these receivers yield error floors in an unresolved multipath environment. Therefore receivers implementing the decorrelation operation designed in Chapter 3 could be used to replace the existing schemes in IS95 systems in an indoor environment. Furthermore even in an outdoor environment the path resolvability assumption is only approximately satisfied, so these decorrelating receivers could also be used to yield additional performance gains. In particular, the OPT or QDR schemes could be used on the reverse link (mobile-to-base or uplink) since non-coherent detection is suggested. On the forward link (base-to-mobile or downlink) a pilot signal is provided suggesting the use of coherent detection so the SPECCOH scheme could be used.

GSM was initially designed for outdoor wireless transmissions. For test purposes, the GSM standards define three channel power delay profiles, RA250, TU50 and HT100 illustrated in [34, p. 244] representing rural areas, typical urban cases and hilly terrain respectively. Furthermore, GSM includes a training sequence in the middle of each time slot suggesting the use of an equalizer. For HT100, the multipath spread is greater then 20% of the symbol duration, thus the use of the equalizer is mandatory (according to the 20% common rule of thumb [162]). For RA250 and TU50, this is not the case so an equalizer is not needed. For indoor environments, the multipath delays are even smaller than those of typical urban areas, making the use of an equalizer even less required. Because of the smaller bandwidth of GSM systems compared to IS95, the multipath channel appears flat yielding no diversity gains. One tool provided by GSM to yield diversity is the frequency hopping feature (changing frequency from time slots to time slots). If base stations use different hopping patterns, interference and fading diversity can be obtained. However, this feature may greatly complicate transmitters and receivers. An alternative solution to obtain diversity gains for narrow-band systems is provided by the multipath decorrelating schemes presented in this thesis that yield multipath diversity gains. Similarly those decorrelating receivers can also be used in IS136 systems, where an equalizer is even less required than in GSM systems due to the larger symbol duration.

DECT (Digital European Cordless Telecommunications) is a cordless standard

that is quite similar to a cellular system [162]. It has a large bandwidth of 1728kHz with a symbol duration of 868ns. Typically DECT uses antenna diversity but detection schemes presented in this thesis could also be used to yield multipath diversity gains. Since cordless services aim at low complexity handsets, non-coherent suboptimal schemes such as the QDR scheme would be suitable.

Receivers designed in Chapter 3 can also be used in third generation wireless systems proposals such as CDMA2000, Wide-CDMA (W-CDMA) and EDGE (Enhanced Data Rates for Global Evolution). CDMA2000 proposed by the North American CDMA Development Group (CDG) [167] is a third generation wireless system proposal that is backward compatible to IS95. Two proposals based on WCDMA have been made, UTRA [168] proposed by ETSI (European Telecommunications Standards Institute) and W-CDMA proposed by ARIB (Association of Radio Industries and Businesses) [169] of Japan. These third generation proposals differ from IS95, among other factors, by their (possible) higher bandwidth usage and data rates, and their demodulation methods.

CDMA2000 system can operate with two modulation techniques, single carrier with the usual spreading of the message signal (Direct Spread) and multi-carrier where the message signal is demultiplexed into N information signals which are then spread on a different carrier (Multi-Carrier). If Direct Spread is used, then the possible signal bandwidths are 1.25MHz, 3.75MHz, 7.5MHz, 11.25MHz and 15MHz corresponding to chips rate of $N \times 1.2288$Mcps, $N = 1, 3, 6, 9, 12$. If the Multi-Carrier mode is used, the demultiplexed signal bandwidth is 1.25MHz. ARIB W-CDMA systems use usual spreading techniques (equivalent to Direct Spread) with a variable spreading factor. The ARIB W-CDMA signal bandwidths are 1.25MHz, 5MHz, 10MHz or 20MHz corresponding respectively to chips rates of 1.024Mcps, 4.096Mcps, 8.192Mcps and 16.384Mcps. The UTRA bandwidth is 5MHz if the nominal chip rate of 4.096Mcps is used, but can be increased to 10MHz or 20MHz if two times or four times higher chip rates are considered.

Hence all these third generation systems may operate with larger bandwidths than the IS95 bandwidth of 1.25MHz. But as explained in Chapter 2, even these large bandwidths are not large enough to resolve the multipath in an indoor environment. Hence classical Rake receivers may yield error floors in this case. Performance can be improved by using the schemes derived in this thesis. Since pilot symbols are included on both uplinks and downlinks, coherent demodulator such as the SPECCOH scheme

could be used. Similar to the Rake receiver tested in [168], a SPECCOH scheme that uses a fixed number of fingers after the decorrelation could also be used. Such a receiver would perform the decorrelation on all the known multipath components but only the strongest paths will be used in the combining stage. Note that picking up the strongest paths from the matched filter output samples before decorrelation ($\boldsymbol{u}_m$) and then doing the decorrelation would result in performance degradation. Furthermore, when the multipath is not resolved, it is very likely that no strong peaks can be identified from the matched filter outputs samples since even without noise the peaks cannot be resolved by assumption. Methods for estimating the multipath delays without the path resolvability assumption have been discussed in Section 2.2.3 (see for example the ML approach).

EDGE [195, 196] is a TDMA data transmission standard resulting from the harmonization of technical studies on TDMA systems with higher data rates and packet data services of TIA (Telecommunications Industry Association) and ETSI. It uses a 200kHz carrier and a 8PSK modulation based radio interface. Therefore, similar to GSM and IS136 systems, multipath diversity gains can be obtained by the multipath decorrelating schemes presented in this thesis.

Multipath decorrelation can also be used as a mean to estimate the multipath component gains of an unresolved channel. As shown in Chapter 2, one of the methods for estimating the multipath gains [152] consists of passing the received signal through a matched filter matched to the sounding signal. If the inter-path delays are larger than the reciprocal of the sounding signal bandwidth (resolved multipath), the amplitudes of the peaks of the matched filter output are estimates of the multipath gains. Such method yields inaccuracy if the multipath is not resolved. However, as shown in this thesis, provided that the multipath delays are known, an equivalent resolved channel model (3.19) or (3.169) can be obtained by considering transformed transmitted signals and multipath gains (decorrelated multipath gains). Then estimates of the decorrelated multipath gains can be obtained employing the method previously mentioned using the transformed transmitted signals. Estimates of the multipath gains are then obtained from the decorrelated multipath gains estimates using the inverse linear transformation (proportional to $\boldsymbol{X}_m$).

5.2 Estimator-correlator forms

5.2.1 Optimal receiver estimator-correlator interpretation: a tool to design suboptimal receivers

It is known that the optimal receiver of any random channel corrupted by additive white Gaussian noise has an interpretation as an estimator-correlator [21], where the estimate is provided by a MMSE estimator. Suboptimal receivers can be obtained by replacing the MMSE estimate in the estimator-correlator form of the likelihood ratio by other estimates that are simpler to obtain. The R OPT scheme of Section 3.7.5 is one such example where the MMSE estimate for Ricean channels has been replaced by the MMSE estimate for Rayleigh channels. The MMSE estimate for Rayleigh channels is simpler since it is linear. Another example is the linear MMSE estimator-correlator (LMMSE) presented in Section 3.7.6 where the nonlinear MMSE estimate for Ricean channels has been replaced by the "best" (in the MMSE sense) linear estimate. These two suboptimal receivers are more suitable for implementation since they are quadratic.

5.2.2 Approximating optimal decision variables: the quasi estimator-correlator and other estimator-correlator forms

Another method to design simpler suboptimal receivers consists of directly approximating the log-likelihood ratio by simpler functionals. In that case, a quasi estimator-correlator is obtained which has a similar form as the estimator-correlator up to a correction term. The QDR scheme presented in this thesis is an example of this method for mixed/mode Ricean/Rayleigh channels. Its counterpart for 2 Ricean/L-2 Rayleigh channels could be a subject of future research although an approximation of an infinite series is needed that may present difficulties and/or may yield further performance degradations.

Let us give two examples of known suboptimal receivers for binary DPSK that are obtained by approximating the resolved multipath Rayleigh non-coherent optimal receiver. Denoted R QR in this thesis, this Rake receiver has a log-likelihood ratio given by (3.170). Let us assume a long observation interval (i.e. $\boldsymbol{\epsilon}_m = \boldsymbol{I}$). From Section 4.2.1, the two possible transmitted signals for binary DPSK can be rewritten

as $\tilde{s}_{1,2}(s) = \sqrt{\frac{2\mathcal{E}_b}{T}}\,[p(s) \pm p(s-T)]$ where $p(s) = \text{rect}\left(\frac{t}{T} - \frac{1}{2}\right)$ is a rectangular pulse[1] of duration T. From (3.170) and (3.18b) the decision rule is given by

$$\sum_{k=0}^{L-1} \frac{\gamma^2 2\sigma_k^2}{1+\gamma 2\sigma_k^2}\left[|u_{k1}|^2 - |u_{k2}|^2\right] \underset{H_2}{\overset{H_1}{\gtrless}} 0$$

or equivalently dividing by $\frac{4\gamma}{\mathcal{E}T}$ and substituting $\tilde{s}_{1,2}(s)$

$$\sum_{k=0}^{L-1} \frac{\gamma 2\sigma_k^2}{1+\gamma 2\sigma_k^2} \Re\left\{\left(2\int_0^{T_o} p(v-\tau_k)e^{j\omega_c v}dz(v)\right)\left(2\int_0^{T_o} p^*(u-T-\tau_k)e^{-j\omega_c u}dz(u)\right)\right\} \underset{H_2}{\overset{H_1}{\gtrless}} 0$$

Note that the integration limits 0 and T_o can be changed to $-\infty$ and ∞ since by definition $p(s-\tau_k) = 0$ for $s < \tau_k$ and $s > T + \tau_k$. Assuming that the carrier frequency is a multiple of $\frac{1}{T}$ the decision for the symbol transmitted between 0 and T can be rewritten then as[2]

$$\sum_{k=0}^{L-1} \frac{\gamma 2\sigma_k^2}{1+\gamma 2\sigma_k^2} J'(2T+\tau_k) = \sum_{k=0}^{L-1} \frac{\gamma 2\sigma_k^2}{1+\gamma 2\sigma_k^2} J'(t - T_m + \tau_k)\Big|_{t=2T+T_m} \underset{H_2}{\overset{H_1}{\gtrless}} 0$$

where $J'(s)$ is given by

$$J'(s) =$$
$$\Re\left\{\left(2\int_{-\infty}^{\infty} p(v-s+2T)e^{j\omega_c(v-s+2T)}dz(v)\right)\left(2\int_{-\infty}^{\infty} p^*(u-s+T)e^{-j\omega_c(u-s+T)}dz(u)\right)\right\}$$

and T_m is the multipath spread of the channel. Hence the R QR for DPSK modulation can be represented by Fig. 5.1(a), where the receiver makes the decision that $s_1(s)$ is transmitted when the output of the sampler is positive and makes the decision that $s_2(s)$ is transmitted when the output of the sampler is negative. Fig. 5.1(a) shows that $J'_F(s)$ for the R QR is obtained by multiplying $J'(s)$ with a delayed estimate of the channel impulse response featuring the known channel multipath delays with

[1] The function rect(t) is a rectangular pulse centered at the origin defined in (2.3).

[2] The term $e^{j\omega_c\tau_k}$ in $2\int_{-\infty}^{\infty} p(v-(2T+\tau_k)+2T)e^{j\omega_c(v-(2T+\tau_k)-2T)}dz(v)$ cancels with its conjugate present in $2\int_{-\infty}^{\infty} p^*(u-(2T+\tau_k)+T)e^{j\omega_c(u-(2T+\tau_k)-T)}dz(u)$ and $e^{j\omega_c T} = 1$.

estimates of the multipath gains $\left(\frac{\gamma 2\sigma_k^2}{1+\gamma 2\sigma_k^2}\right)$. This operation ensures that the decision variables take into consideration only the portions of $J'(s)$ that include signal energy. In other words, it masks the other portions of $J'(s)$ in the window corresponding to the multipath spread.

When the multipath delays are unknown but the multipath spread is known, a receiver similar to R QR can be used except that it includes all the energy corresponding to the duration of the multipath spread (the "mask" $\sum_{k=0}^{L-1}\frac{\gamma 2\sigma_k^2}{1+\gamma 2\sigma_k^2}\delta\big(s-(t-T_m+\tau_k)\big)$ has been replaced by 1. This is the Post-Detection Integrating receiver (PDI) [43, 197] illustrated in Fig. 5.1(b). However the PDI includes more noise samples than the R QR. Better suboptimal receivers can be obtained by correlating $J'(s)$ with a signal that approximates $\sum_{k=0}^{L-1}\frac{\gamma 2\sigma_k^2}{1+\gamma 2\sigma_k^2}\delta\big(s-(t-T_m+\tau_k)\big)$. Such signal could be obtained from $J'(s)$ as illustrated in Fig. 5.1(c) where $\mathbf{f}(\cdot)$ is a nonlinear function. Such receivers will be referred as Masked Post-Detection Integrating receivers (MPDI) to follow the terminology used in [198]. One such example is the Sidelobe-Masked PDI (SMPDI) that was originally designed for DPSK commutation signaling [197, 198]. In that case $\mathbf{f}\left(J'_m(s)\right) = \left|J'_m(s-NT)\right|\left|J'_m(s-N'T)\right|$, $J'_m(s)$ is given by

$$J'_m(s) =$$
$$\Re\left\{\left(2\int_{-\infty}^{\infty} p_{m-1}(v-s+2T)e^{j\omega_c(v-s+2T)}dz(v)\right)\left(2\int_{-\infty}^{\infty} p_m^*(u-s+T)e^{-j\omega_c(u-s+T)}dz(u)\right)\right\}$$

and $p_m(t)$ is the m^{th} commutation signaling codeword.

Fig. 5.1 shows that the PDI and (S)MPDI receivers can be obtained by "approximating" (not necessarily a tight approximation) the R QR receiver. Note that the same type of approximations of the QDR scheme for unresolved multipath is not feasible as will be shown in Section 5.5.2 due to the fact that the contributions of each multipath component cannot be decoupled. Similar to the PDI's schemes, the QDR scheme was designed by approximating an optimal receiver (the OPT scheme). It was shown how the QDR decision variable could be put in a quasi estimator-correlator form by Itô differentiating the corresponding decision variable expressed as a function of the observation interval. In principle, such technique could be applied to the decision variables of the PDI and (S)MPDI receivers to show that they also have a quasi estimator- correlator form. However the difficulty lies in finding the expression of the decision variable when an observation interval smaller than the symbol duration is

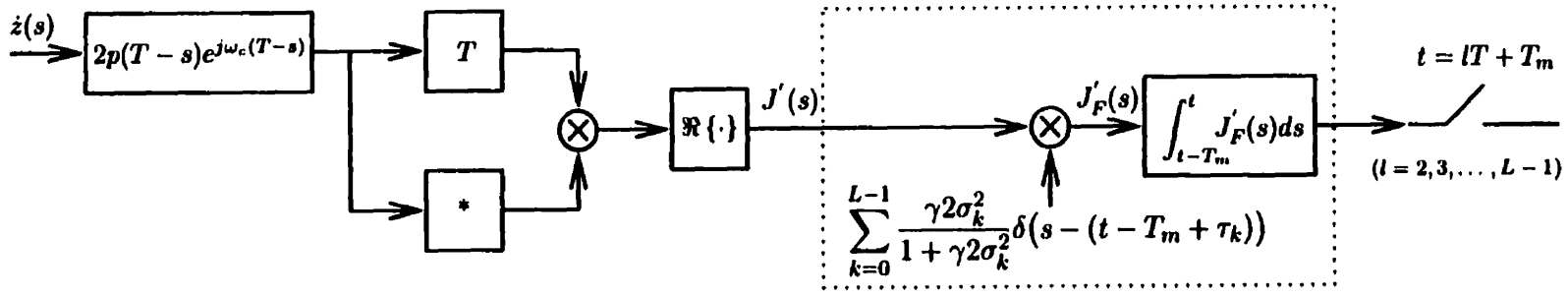

(a) Non-coherent optimum receiver for a resolved L-path Rayleigh channel (R QR) with binary DPSK signaling

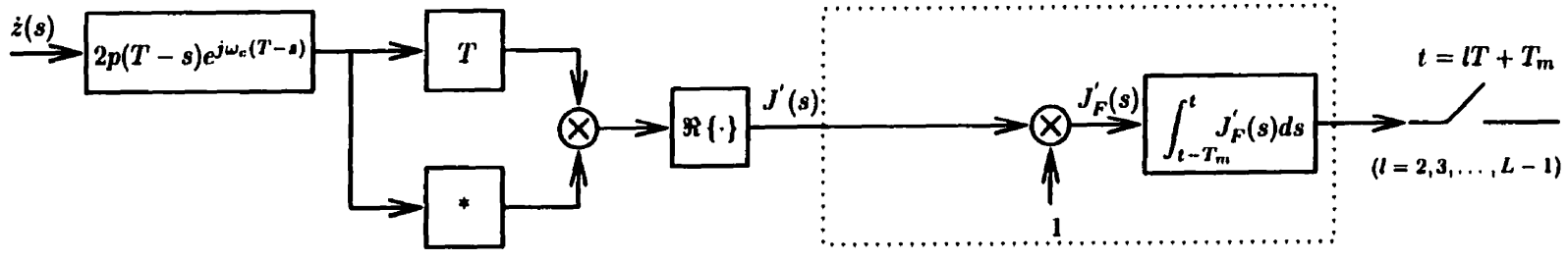

(b) Post-detection integrating receiver (PDI) with binary DPSK signaling

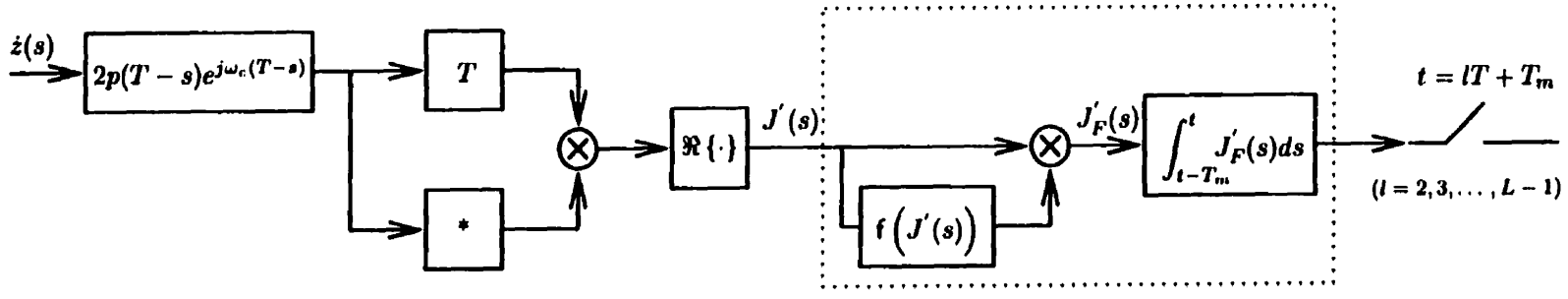

(c) Masked post-detection integrating receivers (MPDI) with binary DPSK signaling

Fig. 5.1 Non-coherent receiver structures for a resolved L-path Rayleigh channel with binary DPSK signaling

considered. For some suboptimal receivers such as the PDI or SMPDI, the dependence of the decision variable on the chosen observation interval is not straightforward. In that case, one may want to try to find simpler "estimator-correlator" interpretations of those receivers.

For example, the dotted part of the R QR scheme illustrated in Fig. 5.1(a) can be interpreted as an estimator-correlator where a channel impulse response estimate is correlated with $J'(s)$. The correlation $J'(s)$ corresponds to the part of the matched filtering outputs for DPSK that is hypothesis dependent. The correlation of $J'(s)$ with the channel estimate is equivalent to matched filtering to the estimated channel impulse response (a basic detection technique to improve performance). Similarly the PDI receiver can be interpreted as an estimator-correlator where the channel estimate is equal to a rectangular pulse of duration equal to the multipath spread. Such estimate is very simple but may not be very good. The SMPDI receiver is similar to the PDI scheme but with a better estimate. For DPSK commutation signaling the SMPDI estimate is equal to a nonlinear function $\mathrm{f}\left(J'_m(s)\right)$ such that $J'_F(s)$ has lower sidelobes. The optimal decision rule (R QR) by definition automatically discards the sidelobes. Then by lowering sidelobes, the SMPDI is closer to the optimal receiver than the PDI is, thus yields better performance.

5.3 The issue of ISI induced by multipath

Only one-shot receivers have been studied in this thesis and their single-pulse performance has been assessed. This corresponds to neglecting any ISI, a reasonable assumption for small inter-path delays. This is especially true for Spread-Spectrum systems where the multipath spread inducing ISI represents a small number of chips. ISI can also be neglected if commutation signaling is used [197], since no signal is reused until the mainlobe response of its associated matched filter corresponding to its previous use has died out. Commutation signaling can be obtained by using for each symbol a set of different frequencies or a set of various Spread-Spectrum codes. Study of ISI effects such as error floors phenomenons [199, 200] and the design of sequence detectors for unresolved multipath fading channels is beyond the scope of this thesis but may be a subject of future research. However, since the modulation schemes presented in this thesis are nonlinear, such a study may be quite involved. Practically, the bit-error probabilities curves of this thesis represent upper-bounds to

the true bit-error probabilities in the presence of ISI. How small the inter-path delays should be to yield tight upper-bounds to the bit-error probability will have to be investigated.

5.4 Implementations issues

It was mentioned in Section 5.1 that the multipath decorrelation yields diversity gains over unresolved multipath channels. However perfect multipath delays estimation has been assumed throughout this thesis. In practice such accuracy cannot be achieved, which is one of the implementation issues that remain to be considered.

5.4.1 Time delay estimation

The optimal receivers presented in this thesis have been derived assuming perfect multipath delay estimation. They yield the best performance but they do not usually provide the best robustness to delay estimation errors. Therefore performance under delay mismatch conditions should be investigated. It is to be expected that performance degradations will be small if the multipath delays errors are small since the receiver decorrelating matrix will nearly decorrelate the multipath components in that case. How small the multipath delays errors should be, or equivalently, how accurate the time delay estimation must be, remains an open issue that needs further investigation and will be the aim of future research.

In [201], an improved MMSE multi-user receiver for mismatched delay channels is presented. The conventional MMSE (CMMSE) multi-user receiver for the demodulation of DS-CDMA signals in additive white Gaussian noise is based on the decision rule

$$\hat{b}_1(0) = \text{sgn}(\boldsymbol{c}^T \boldsymbol{r}) \tag{5.1}$$

where $\hat{b}_1(0)$ is the bit estimate of the 0^{th} bit of user 1, $\boldsymbol{c}$ is an $N \times 1$ vector minimizing the MSE $E\left[\left(\boldsymbol{c}^T\boldsymbol{r} - b_1(0)\right)^2\right]$ and $\boldsymbol{r}$ is the vector composed of the N samples of the received signal at the output of the chip matched filter synchronized with the estimated delay of user 1 $\hat{\tau}_1$. Equivalently $\boldsymbol{c}$ satisfies $E_{\boldsymbol{b},\boldsymbol{n}}\left[\left(\boldsymbol{c}^T\boldsymbol{r} - b_1(0)\right)\boldsymbol{r}\right] = \boldsymbol{0}$ where $\boldsymbol{0} = [0, 0, \ldots, 0]^T$, $\boldsymbol{b} = [b_1(-1), b_1(0), b_1(1), \ldots, b_K(-1), b_K(0), b_K(1)]^T$, $\boldsymbol{n}$ is the channel noise vector (noise component of $\boldsymbol{r}$), K is the number of users and $E_{\boldsymbol{b},\boldsymbol{n}}$ represents

an average over all possible bit combinations and the noise process. The improved MMSE (IMMSE) is obtained by choosing $\boldsymbol{c}$ such that $E_{\boldsymbol{b},\boldsymbol{n},\Delta\boldsymbol{\tau}}\left[\left(\boldsymbol{c}^T\boldsymbol{r} - b_1(0)\right)\boldsymbol{r}\right] = \boldsymbol{0}$, where $\Delta\boldsymbol{\tau} = [\tau_1 - \hat{\tau}_1, \ldots, \tau_K - \hat{\tau}_K]^T$ represents the multi-user delay error and $\hat{\tau}_k$ is the estimated delay of user k. It is seen that the difference between the CMMSE and the IMMSE is the additional average over the multi-user delay error.

In this thesis, due to the fading and the possible nonlinear modulation used, the decision variables are not equal to an estimate of the transmitted bits directly, so a MMSE type of decision similar to (5.1) cannot be derived. However, from the estimator-correlator interpretation of the optimal receiver, a receiver more robust to time delay estimation errors can be obtained based on an approach similar to [201]. Assume that the multipath delays are known at the receiver with a certain uncertainty. Equivalently they are modeled as random variables with given joint probability density functions, their width with respect to the mean representing the degree of uncertainty. The larger the width, the higher is the uncertainty of the multipath delay. The optimal receiver assuming random delays has also an estimator-correlator form [21] with MMSE estimate $\check{v}_m(t) = \mathrm{f}\left(\{\dot{z}(s), 0 \leq s \leq t, H_m\}\right)$, where $\mathrm{f}(\cdot)$ is a function that minimizes $E\left[(v_m(t) - \check{v}_m(t))^2 \,|H_m\right]$, and the average is performed over all the random parameters of the channel, including the random multipath delays. Similarly to the difference between the CMMSE and the IMMSE, the difference between the optimal receiver assuming known multipath delays and the optimal receiver assuming random multipath delays resides in the additional averaging over the multipath delays. It is well known that the MMSE estimate is the conditional mean $\check{v}_m(t) = E\left[v_m(t)|\dot{z}(s), 0 \leq s \leq t, H_m\right]$ [202, p. 175]. When the multipath delays are known, all quantities calculated in this thesis such as likelihood ratios and conditional means can be interpreted as conditional over the multipath delays. Therefore the conditional mean studied in this thesis renamed here $\check{v}_m(t|\boldsymbol{\tau})$ for clarity is given by definition by $\check{v}_m(t|\boldsymbol{\tau}) = E\left[v_m(t)|\dot{z}(s), 0 \leq s \leq t, \boldsymbol{\tau}, H_m\right]$ where $\boldsymbol{\tau} = [\tau_0, \ldots, \tau_{L-1}]^T$. It is seen that in order to obtain a receiver more robust to time delay estimation errors, the conditional mean estimate $\check{v}_m(t|\boldsymbol{\tau})$ in the estimator-correlator form of the receiver likelihood ratio has to be replaced by its average over $\boldsymbol{\tau}$. The obtained estimate is also equal to the MMSE estimate assuming random delays. Therefore, such a receiver is the best receiver that can be obtained under knowledge of the multipath delays probability density function. Analysis of such a scheme, which is possibly quite involved, could be the topic of future research. Another research direction along the same lines

is to design receivers under unresolvability conditions that combine time delay estimation and detection or that adaptively update the coefficients of the decorrelating matrices.

5.4.2 Discrete time implementation

The optimal and suboptimal receivers derived in this thesis have been presented in two forms, the "likelihood ratio" form (for example (3.10) or (3.67)) and the "estimator-correlator" form (for example (3.26) or (3.119)). The "likelihood ratio" form does not present any particular implementation difficulties except for the non-coherent optimum receiver for general Ricean channels that involves infinite series not suitable for implementation. The mixed mode Ricean channels non-coherent optimum receiver involves a modified Bessel function of the first kind that also can present a difficulty, although such function is well known and tabulated. All the likelihood ratio forms depend on the variable $\boldsymbol{u}_m$ resulting from matched filtering of the received signal. If the transmitted signals contain most of their energies in a bandwidth W, from the sampling theorem they can be approximately represented by their samples. Then the matched filtering or correlation required to get $\boldsymbol{u}_m$ can be implemented in discrete-time, possibly with some modest oversampling. The vector $\boldsymbol{r}_m$ is obtained from $\boldsymbol{u}_m$ through a matrix multiplication.

The "estimator correlator" form is more involved due to the presence of the Itô integral and the linear and nonlinear time-varying functions. The Itô integral yields difficulties since it does not obey ordinary differential rules of calculus. However, such a problem can be solved as explained in the following. Itô integrals present in the estimator-correlator form of optimum receivers can be avoided by rewriting their estimator-correlator forms in terms of a Stratonovich integral (integral that does obey ordinary differential rules of calculus) and a correction term [203]. Note that transformation of [203] is possible only for a likelihood ratio function, hence does not apply to the quasi estimator-correlator form. More generally, it was shown in [204] that Itô integrals with respect to Wiener processes or with respect to Itô processes can be expressed as the limit of ordinary integrals minus a corrective integral closely related to the additional term of the Itô differential rule. Such method does not require the integrand to be a conditional mean, thus it applies to the estimator-correlator as well as the quasi estimator-correlator forms.

Once a method has been found to bypass the problem of the Itô integral, it re-

mains to evaluate the conditional mean. A conceptual implementation structure of the conditional mean $\check{v}_m(t)$ has been given in Fig. 3.5. This structure is not a real time structure due to the presence of the phase detector which hides, intrinsically, a system with a certain amount of delay such as, for example, a Phase-Lock-Loop [205, p. 336],[206]. Furthermore, as presented, the conditional mean is obtained for a specified duration of the observation interval, $[0, t]$ and the solution must be entirely re-calculated if the length of the observation interval changes (for example to $[0, t+\epsilon]$). In [207], an invariant imbedding numerical method for Fredholm integral equations of the second kind with degenerate kernels is proposed. The principle of invariant imbedding is used to derive a differential equation by regarding the solution at a fixed point as a function of the interval of integration. The knowledge of the solution for one integration interval combined with the differential equation yields solution for other integration intervals. Such a technique could be applied to yield a solution more suitable for real time implementation to compute $\mathcal{H}_m(s,t,t)$ (C.17) needed for the evaluation of $\check{v}_{Rm}(t)$ (see (3.163)). It can also be used to compute $l_{0m}(s,t)$ (C.25) present in the expression of $V_{0m}(t)$ (see (3.98)). It remains to find a real time solution for the calculation of $\vartheta_{0m}(t)$ which will be the topic of future research.

5.4.3 Receiver complexity: coherent versus non-coherent detection

Since all the receive structures presented in this thesis assume known delays and a statistical characterization of the channel impulse response, it implicitly implies the presence of a channel estimator at the receiver front end. Estimation of the multipath delays and the multipath gains statistical characteristic have been largely discussed in the literature (see Section 2.2.3). A more difficult task consists of estimating the specular component phases since phases usually do change rapidly [1, 43]. This thesis showed that for FSK(1), and to a lesser extent for DPSK, such estimation is not needed since performance degradation of non-coherent detection (using for example the QDR scheme) compared to specular coherent detection (using the SPECCOH scheme) is small at high SNR for mixed mode Ricean/Rayleigh fading channels. Quantitatively, compared to the SPECCOH scheme, the QDR scheme yields 0.2-0.7dB SNR losses for FSK(1) and 0.8-1.2dB SNR losses for DPSK, at $P_e = 10^{-6}$ with K = 10-15dB. Excluding the specular component phase estimator, these two quadratic receivers are of comparable complexity. The QDR scheme is simpler than the SPECCOH, since it does not use a phase estimator for the specular component, and thus offers an

interesting solution for FSK(1) and DPSK. For FSK(1/2) or SDPSK however this thesis showed that significant gains can be obtained by the use of specular coherent detection instead of non-coherent detection especially for large K (for example FSK(1/2):0.6-0.9dB with K = 10-15dB at $P_e = 10^{-6}$ and 4.3dB with K = 20dB, SDPSK: 1.2-1.7dB with K = 10-15dB). As seen from Section 3.3.1 and Section 4.1.3 for any modulation schemes, specular coherent and non-coherent detection yield same performance at sufficiently high SNR. However for FSK(1/2) and SDPSK, the SNR needs to be very large to see this trend. Similar high SNR convergence between specular coherent and non-coherent detection techniques has been observed for one-path Ricean channels for orthogonal binary signaling [194] and various binary signaling [193].

5.5 Extension of thesis'results to different levels of channel knowledge

Although this thesis considers only a statistical knowledge of the channel parameters with known multipath delays, results can be easily extended to the cases of

(i) known multipath gain magnitudes $|a_i|$ and delays; unknown multipath phases

(ii) unknown multipath delays

thereby generalizing results of [43][3]that were derived assuming the path resolvability assumption given by $|\tau_k - \tau_l| > \frac{1}{W}$ $k \neq l$, and

$$\left| \int_0^{T_o} \tilde{s}_m^*(\tau)\tilde{s}_m(\tau - t)d\tau \right| \ll 2E \qquad |t| > \frac{1}{W} \tag{5.2}$$

where $E = \int_0^{T_o} |s_m(\tau)|^2 d\tau$ for all m and W is the transmission bandwidth.

5.5.1 Known multipath gains magnitudes and delays; unknown multipath phases

The likelihood ratio assuming known multipath gain magnitudes and delays with uniformly distributed multipath phases (between $-\pi$ and π) can be obtained by replacing

[3]As mentioned by G.L. Turin in [43] "optimal" receivers structures derived in that paper assuming (5.2) are in fact optimal only if $|\tau_k - \tau_l| > \frac{1}{W}$ and $\left| \int_0^{T_o} \tilde{s}_m^*(\tau)\tilde{s}_m(\tau - t)d\tau \right| = 0$, $|t| > \frac{1}{W}$.

$|\alpha_k|$ by $|a_k|$, $2\sigma_k^2$ by σ (i.e. $\boldsymbol{C} = \sigma \boldsymbol{I}$) in (3.67) and taking the limit when σ goes to zero. Following the technique used in Section 3.4.3 (topic: "Expression of the conditional mean when $\forall k \quad \sigma_k^2 = 0$"), $\boldsymbol{D}_{Lm}(T_o) = \boldsymbol{D}_m$ can be expressed as $\boldsymbol{D}_m = \sigma \boldsymbol{D}_m^{'}$ where $\boldsymbol{D}_m^{'}$ and $\boldsymbol{X}_m$ satisfies the equations

$$\boldsymbol{\epsilon}_m \boldsymbol{\Gamma}_m^* \boldsymbol{X}_m^T = \boldsymbol{X}_m^T \boldsymbol{D}_m^{'} \qquad \boldsymbol{X}_m^* \boldsymbol{\Gamma}_m^* \boldsymbol{X}_m^T = \boldsymbol{I} \tag{5.3}$$

and are independent of σ. Therefore replacing $|\alpha_k|$ by $|a_k|$

$$\lim_{\sigma \to 0} J_m = \exp\left\{ -|\boldsymbol{a}|^\dagger \left\{ (\boldsymbol{X}_m^*)^{-1} \gamma_m \boldsymbol{D}_m^{'} \boldsymbol{X}_m^* \right\}_d |\boldsymbol{a}| \right\} \qquad \text{from (3.63a)}$$

$$\lim_{\sigma \to 0} l_{km}(s, T_o) = \lim_{\sigma \to 0} l_{km}(s) = |a_k| \, \tilde{s}_m(s - \tau_k) \qquad \text{from (3.165)}$$

where $|\boldsymbol{a}| \triangleq [|a_0|, \ldots, |a_{L-1}|]^T$. Thus from (3.67), the log-likelihood ratio for known multipath gain magnitudes and known multipath delays is given by

$$\ln\left[\Lambda_m(\dot{z}; T_o)\right] = -|\boldsymbol{a}|^\dagger \left\{ (\boldsymbol{X}_m^*)^{-1} \gamma_m \boldsymbol{D}_m^{'} \boldsymbol{X}_m^* \right\}_d |\boldsymbol{a}| + \ln\left[\frac{1}{(2\pi)^L} \int_{-\pi}^{\pi} \cdots \int_{-\pi}^{\pi} f_m(\boldsymbol{\theta}) \, d\boldsymbol{\theta} \right]$$

and $\frac{1}{(2\pi)^L} \int_{-\pi}^{\pi} \cdots \int_{-\pi}^{\pi} f_m(\boldsymbol{\theta}) \, d\boldsymbol{\theta}$ is the sum of multi-dimensional infinite series of products of Bessel and trigonometric functions that depends on $\left\{ V_{km} = |d_{km}|, \vartheta_{km} = \arg[d_{km}] \right\}_{k=0,\ldots,L-1}$ and $\left\{ V_{kn}^m = |e_{kn}^m|, \vartheta_{kn}^m = \arg[e_{kn}^m] \right\}_{k=0,\ldots,L-1, n<k}$, where by replacing $|\alpha_k|$ by $|a_k|$ in (3.68b-3.69b) and $l_{km}(s)$ by $|a_k| \, \tilde{s}_m(s - \tau_k)$,

$$d_{km} = \frac{2}{N_0} \int_0^{T_o} |a_k| \, \tilde{s}_m^*(s - \tau_k) e^{-j\omega_c s} dz(s)$$

$$e_{kn}^m = \frac{1}{N_0} \int_0^{T_o} |a_n| \, \tilde{s}_m(s - \tau_n) \, |a_k| \, \tilde{s}_m^*(s - \tau_k) ds$$

It is seen that the decorrelation is still performed as seen from the presence of the matrix $\boldsymbol{X}_m$ (5.3) in the log-likelihood ratio. Since $\frac{1}{(2\pi)^L} \int_{-\pi}^{\pi} \cdots \int_{-\pi}^{\pi} f_m(\boldsymbol{\theta}) \, d\boldsymbol{\theta}$ is the sum of multi-dimensional infinite series, the non-coherent optimum decision rule when the multipath is unresolved is not easily implementable even if the multipath gain magnitudes are known. For mixed mode Ricean/Rayleigh fading channels, the sum of multi-dimensional infinite series reduces to one term. Then, a similar approximation to the one that yielded the QDR scheme could be used to obtain a suboptimal receiver more suitable for implementation.

5.5.2 Unknown multipath delays

Assume that the channel model is given by (3.1) but that the L multipath delays $\tau_0, \ldots, \tau_{L-1}$ are unknown at the receiver and characterized by their joint pdf $p_{\boldsymbol{\tau}}(\boldsymbol{x})$. Then the likelihood ratio assuming unknown delays is obtained by averaging the likelihood ratio assuming known delays using the joint pdf of the multipath delays:

$$\Lambda_m''(\dot{z}; T_o) = \int \cdots \int p_{\boldsymbol{\tau}}(\boldsymbol{x}) \Lambda_m(\dot{z}; T_o)\, d\boldsymbol{x} \tag{5.4}$$

Therefore when the multipath is not resolved and an arbitrary joint pdf for the multipath delays is considered, the likelihood ratio is an L-fold integral. It was shown in [43] that when the multipath delays are independent and identically distributed $\left(\text{i.e. } p_{\boldsymbol{\tau}}(\boldsymbol{x}) = \prod_{l=0}^{L-1} p(x_l)\right)$ and the multipath is resolved in the sense that $\Pr\left(|\tau_k - \tau_l| < \frac{1}{W}\right)$ is small, the L-fold integral can be written as the product of L identical one-dimensional integrals as seen at the end of this section. Since the L integrals are positive, an equivalent decision is obtained by using only one of them yielding to a decision rule independent of the number of paths [43]. As shown in the following, such equivalent decision rule independent of the number of multipath delays cannot be found when the multipath is not resolved. This has two consequences; first, it means that the number of multipaths needs to be estimated when the multipath is not resolved. Since most estimation techniques estimate jointly the values of the inter-path delays and their number, in practice the multipath delays will be known at the receiver and results of this thesis can be used. Secondly, the presence of an L-fold integral renders approximate decision rules in the line of the PDI [43] and SMPDI [198] very difficult to find.

Let us show that the L-fold integral (5.4) cannot be simplified when the multipath is not resolved. For sake of simplicity, the case of Rayleigh fading channels will be considered but same principles apply to Ricean channels. Let us consider a long observation interval, $[0, T_o]$ (i.e. $\boldsymbol{\epsilon}_m = \boldsymbol{I}$), using (3.16a) the Rayleigh channels likelihood ratio assuming known multipath delays (3.168b) can be rewritten as

$$\Lambda_m(\dot{z}; T_o) = \prod_{l=0}^{L-1} \left[\frac{1}{1 + \gamma_m \frac{\lambda_{lm}}{E_m}} \exp\left\{ \frac{\gamma_m^2 \frac{\lambda_{lm}}{E_m} |[\boldsymbol{r}_m]_l|^2}{1 + \gamma_m \frac{\lambda_{lm}}{E_m}} \right\} \right]$$

where $[\boldsymbol{r}_m]_l$ is given by (3.14). From (3.7), $\phi_{lm}(s)$ is a function of $\tau_0, \ldots, \tau_{L-1}$ via

$\tilde{s}_m(s-\tau_k)$ and x_{lk}^m hence so is each $[\boldsymbol{r}_m]_l$. Therefore even if $p_{\boldsymbol{\tau}}(\boldsymbol{x}) = \prod_{l=0}^{L-1} p(x_l)$ (independent and identically distributed multipath delays), the L-fold integral (5.4) cannot be expressed as the product of L identical one-dimensional integrals. On the other hand, when the multipath is resolved, $\phi_{lm}(s) = \frac{\tilde{s}_m(s-\tau_l)}{\sqrt{\tilde{E}_m}}$, so from (3.14) $[\boldsymbol{r}_m]_l = \mathsf{f}(\tau_l)$ where $\mathsf{f}(x) = \frac{2}{\sqrt{\tilde{E}_m}} \int_0^{T_o} \frac{\tilde{s}_m^*(s-x)}{\sqrt{\tilde{E}_m}} e^{-j\omega_c s} dz(s)$ is independent of l and $\lambda_{lm} = 2\sigma_l^2 \tilde{E}_m \triangleq 2\sigma^2(\tau_l)\tilde{E}_m$, where $\sigma(\cdot)$ is a function independent of l defined such that $\forall l = 0, \ldots, L-1$, $\sigma(\tau_l) = \sigma_l$. Hence the L-fold integral (5.4) can be expressed as the product of L identical integrals. Since all the integrals are positive an equivalent decision rule is obtained by considering only one of them.

Chapter 6

Summary and Conclusions

This thesis has addressed the subject of detection techniques and performance analysis over multipath Ricean/Rayleigh fading channels, when the path resolvability assumption is not satisfied. Two types of path resolvability conditions have been defined in Section 2.2.1, strict and approximate path resolvability. The strict path resolvability assumption asserts that the signal autocorrelation function for a given observation interval vanishes at inter-path delays. It is equivalent to assuming that any two versions of the signal, time-shifted by different multipath delays, are orthogonal. The approximate path resolvability assumption says that the signal autocorrelation function evaluated at inter-path delays is small. For wide-band signals it is equivalent to assuming that the inter-path delays are much larger than the reciprocal of the bandwidth. As shown in Section 2.3.1, the strict path resolvability assumption is rarely satisfied and even the approximate path resolvability condition is not always satisfied in practice. For example, the later does not hold in indoor and outdoor environments for narrow-band systems such as GSM, IS136, or their third generation derivatives. Approximate path resolvability assumption is generally not satisfied in indoor environments for wide-band systems such as IS95 or the third generation systems WCDMA and CDMA2000 due to the relatively small multipath delays of these environments (order of tens to hundreds of nanoseconds [6, 7]).

As a first step in the design of receivers suitable for multipath Ricean/Rayleigh fading channels with neither the strict nor the approximate path resolvability assumptions, this thesis derived the specular coherent (SPECCOH) and non-coherent (OPT) optimal receiver structures for these unresolved channels. It was shown that they both include an orthogonalization (or decorrelation) stage that disappears when

the multipath is resolved. The decorrelation stage associated with one of the possible transmitted signals consists of a linear transformation of the samples that would be obtained at the tap outputs of the tapped-delay line used in classical Rake receivers (corresponding to the considered transmitted signal), and of an equivalent linear transformation of the channel multipath gains. Such linear transformation yields uncorrelated samples when the matched transmitted signal is sent. Applied to the multipath time-shifted versions of the transmitted signal, this linear transformation creates an orthogonal set similar to the one obtained over resolved multipath fading channels. For the SPECCOH scheme, the next and final stage following this decorrelation operation consists of a resolved multipath channel specular coherent optimal decision rule for the transformed samples and channel.

The importance of the decorrelation operation in yielding diversity gains and eliminating error floors was demonstrated for commonly used binary modulation schemes such as FSK and variants of DPSK over unresolved mixed mode Ricean/Rayleigh and Rayleigh fading channels. It was shown that classical Rake receivers such as the resolved multipath Ricean fading channels specular coherent optimum receiver (SPECCOHR) and the resolved multipath Rayleigh fading channels non-coherent optimum receiver (R QR) yield error floors over unresolved mixed mode Ricean/Rayleigh and Rayleigh fading channels. Such effects were also observed for suboptimal receivers that do not implement the decorrelation operation. This demonstrates the importance of deriving receivers especially designed to handle path unresolvability.

This thesis has proposed one such suboptimal receiver derived for unresolved mixed mode Ricean/Rayleigh fading channels, the Quadratic Decorrelation Receiver (QDR). Similar to the OPT scheme, this non-coherent suboptimal receiver implements the decorrelation operation and yields diversity gains. Unlike the OPT scheme that is nonlinear, this receiver is quadratic making it more suitable for implementation. Furthermore, the performance degradation of the QDR compared to OPT was found to be small at high SNR for binary FSK(1) (orthogonal FSK) (ex. 0.5dB with $\mathsf{K} = 15\text{dB}$ at $P_e = 10^{-6}$) and to a lesser extent for conventional DPSK. Higher degradation was observed for FSK(1/2) (frequency deviation equal to half the symbol duration) and symmetrical DPSK (SDPSK).

Furthermore, this thesis showed that the knowledge of the specular component phase shifts does not provide significant gains over two-path mixed mode Ricean/Rayleigh fading channels at high SNR for FSK(1) and, to a lesser extent,

for DPSK. However, significant diversity gains can be obtained for FSK(1/2) especially for large K. For SDPSK, the SPECCOH scheme yields larger gains than for DPSK and yields also larger gains compared to FSK(1/2) at very high SNR. Similar numbers are obtained for the SNR losses of QDR compared to SPECCOH, except for FSK(1/2) where some losses may be even larger. This justifies the use of non-coherent detection and in particular non-coherent suboptimal schemes such as QDR for FSK(1) and DPSK. It was also shown that SNR gains may be obtained by exploiting the knowledge of the specular component magnitude.

This thesis provided an interpretation as estimator-correlators for all the receivers that were derived. Generalization of the principle of optimal detection of a known signal in additive white Gaussian noise to random channels in additive white Gaussian noise asserts that a receiver first performs an estimation of the noiseless received signal and then correlates the estimate with the received signal. For optimum receivers, this estimator-correlator interpretation is well-known [21]. It was shown that the correlation involves an Itô integral and the estimate is the causal MMSE estimate of the signal from the observation. This thesis gave explicit forms of this estimate for the SPECCOH and OPT schemes. Furthermore, this thesis introduced an equivalent estimator-correlator form, denoted quasi estimator-correlator, for several suboptimal receivers as well. It was shown that suboptimal receivers do have an estimator-correlator form also involving the Itô integral but with an additional corrective term. The estimator type depends on the criteria chosen to design the suboptimal receiver. For optimal and suboptimal receivers, it was shown that the MMSE estimate of the noiseless received signal substitutes the multipath gains and the specular component phasors[1] by estimates. For specular coherent detection the specular component phasors are known, and thus they are not estimated. For non-coherent optimum detection, which corresponds to a case where the noiseless received signal is non-Gaussian, the phasor estimates are obtained by whitening the sum of the Rayleigh term and the additive white Gaussian noise term before proceeding to the estimation. The resulting causal MMSE signal estimate is non-linear in the observation. The decorrelation operation, characteristic of optimal detection over unresolved multipath fading channels appears in the multipath gains estimates, transforming the multipath channel into an equivalent decorrelated (resolved) one. Each multipath gain of the

[1]The k^{th} specular component phasor is defined in this thesis as $e^{j\theta'_k}$ where θ'_k is the k^{th} specular component phase.

equivalent channel is estimated by classical matched filtering or correlation techniques applied to the "remaining unknown" part of the observations. The "remaining unknown" part of the observations denotes the difference between the received signal and either the Ricean specular component (specular coherent detection) or the Ricean specular component estimate (non-coherent detection). The insight obtained on the operations performed by the MMSE estimate may help to the design of suboptimal receivers employing approximations to the MMSE estimate. As an example, three suboptimum receivers (LMMSE, R OPT and QDR) having a linear estimator of the noiseless received signal in their estimator-correlator forms (LMMSE and R OPT) or their quasi estimator-correlator form (QDR), have been presented.

Due to its non-linearities, the performance of the non-coherent optimum receiver (OPT) was assessed by lower and upper bounding its bit-error probabilities. Upper-bounds are obtained by evaluating the bit-error probabilities of the various suboptimum receivers considered in this thesis and retaining the lowest bit-error probability for each SNR. Lower-bounds to the bit-error probabilities of the OPT scheme are obtained by evaluating the bit-error probabilities of SPECCOH over Ricean multipath fading channels, and OPT over a non-coherent non-fading Gaussian channel, and retaining the highest bit-error probability. It was shown analytically and numerically that the lower and upper-bounds are asymptotically tight since they converge at high SNR.

Finally, practical applications of results to existing second and future third generation cellular systems have been considered. Several issues that are important for practical applications were identified as possible continuations of this work: study of receiver robustness to delay estimation errors, discrete time implementation, effects of various levels of channel knowledge, effects of ISI introduced by the channel multipath spread.

Path resolvability has been traditionally ensured by using signals of large bandwidth. This thesis, that does not assume path resolvability, has shown that diversity gains can be obtained over multipath fading channels without the need of spreading signal bandwidth to resolve the multipath. This is achieved by a decorrelation operation of the samples before Rake combining. This generalization of the Rake receiver technique is important for indoor wireless systems where the required bandwidth to ensure path resolvability is very large.

Appendix A

Stochastic integrals

This appendix presents a short overview of two types of stochastic integrals, the Wiener integral and the Itô integral (Sections A.1-A.2), as well as two non-standard properties of Wiener integrals (Sections A.1.4-A.1.5), and the proofs (Section A.3).

A.1 Wiener integrals

A.1.1 Definition of Wiener integrals

Let A be a set and let χ_A denote the characteristic function defined as

$$\chi_A(s) = \begin{cases} 1 & s \in A, \\ 0 & \text{else.} \end{cases}$$

Let $w(s)$ be a Brownian motion satisfying $E[w(s)w(u)] = \frac{N_0}{2}\min(s,u)$ and let $\mathsf{b}(s)$ be a real-valued Lebesgue measurable function square-integrable on $\mathcal{I}$, where $\mathcal{I}$ is a finite or an infinite interval of $\mathbb{R}$. The mean square stochastic integral (or second-order stochastic integral) of $\mathsf{b}(s)$ with respect to $w(s)$ on $\mathcal{I}$ is called a Wiener integral [173, 181], [208, p. 97] and was first introduced by Wiener [209]. The Wiener integral is defined as follows [182, pp. 98-99], [191, pp. 426-433]:

1. If there exist times $s_0, s_1, \ldots, s_n$, such that $-\infty < s_0 < s_1 < \ldots < s_n < \infty$ and

$$\mathsf{b}(s) = \sum_{k=0}^{n-1} \mathsf{b}(s_k)\chi_{[s_k, s_{k+1})}(s)$$

where $\chi_{[a,b)}$ is the characteristic function of $[a,b)$, then $\mathbf{b}(s)$ is called a step function on $(-\infty,\infty)$ and the Wiener integral of $\mathbf{b}(s)$ with respect to $w(s)$ is defined by

$$\int_{-\infty}^{\infty} \mathbf{b}(s)dw(s) = \sum_{k=0}^{n-1} \mathbf{b}(s_k)\left[w(s_{k+1}) - w(s_k)\right]$$

2. For a general Lebesgue measurable function $\mathbf{b}(s)$ satisfying $\int_{-\infty}^{\infty} |\mathbf{b}(s)|^2\, ds < \infty$, there exists a sequence of step functions $\{\mathbf{b}_n(s)\}$ such that $\mathbf{b}(s)$ is the limit of the sequence of step functions, that is

$$\lim_{n\to\infty} \int_{-\infty}^{\infty} |\mathbf{b}(s) - \mathbf{b}_n(s)|^2\, ds = 0 \tag{A.1}$$

It then follows that $\int_{-\infty}^{\infty} \mathbf{b}_n(s)dw(s)$ converges in mean square (or in the mean) and this mean square limit (denoted l.i.m.) is the same for any sequence of steps functions satisfying (A.1). Hence the Wiener integral of $\mathbf{b}(s)$ with respect to $w(s)$ is defined as

$$\int_{-\infty}^{\infty} \mathbf{b}(s)dw(s) \triangleq \underset{n\to\infty}{\text{l.i.m.}} \int_{-\infty}^{\infty} \mathbf{b}_n(s)dw(s)$$

where $\{\mathbf{b}_n(s)\}$ is any sequence of steps functions satisfying (A.1).

3. Let $a, b \in \mathbb{R}$ such that $a < b$

$$\int_a^b \mathbf{b}(s)dw(s) = \int_{-\infty}^{\infty} \mathbf{b}(s)\chi_{[a,b)}(s)dw(s)$$

Therefore for $\int_a^b \mathbf{b}(s)dw(s)$ to exist, $\mathbf{b}(s)$ needs to be square integrable only on $[a,b]$ (i.e. $\int_a^b |\mathbf{b}(s)|^2\, ds < \infty$).

4. If $\mathbf{b}(s)$ is continuous on $[a,b]$ then $\int_a^b \mathbf{b}(s)dw(s)$ is also defined as [191, p. 429]

$$\int_a^b \mathbf{b}(s)dw(s) = \underset{n\to\infty}{\text{l.i.m.}} \sum_{k=0}^{n-1} \mathbf{b}\left(\xi_k^{(n)}\right)\left[w\left(s_{k+1}^{(n)}\right) - w\left(s_k^{(n)}\right)\right]$$

where, for each positive integer n, $T_n = \left\{a = s_0^{(n)} < s_1^{(n)} < \ldots < s_n^{(n)} = b\right\}$ forms a partition of $[a,b]$ such that $\lim_{n\to\infty} \max_{0\le k\le n-1}\left(\left|s_{k+1}^{(n)} - s_k^{(n)}\right|\right) = 0$, and $\xi_k^{(n)} \in \left[s_k^{(n)}, s_{k+1}^{(n)}\right]$ for $k = 0, \ldots, n-1$. This latter definition will be sufficient for the scope of this thesis.

A.1.2 Definition of a Wiener integral with respect to a process $z(t)$ given by $dz(t) = \mathsf{a}(t)dt + dw(t)$ and $\mathsf{a}(t)$ is a non-anticipating real process jointly measurable in the product σ-algebra $\mathcal{L} \otimes \mathcal{F}$

Let $(\Omega, \mathcal{F}, \mathcal{P})$ be a complete probability space, consisting of a sample space, a σ-algebra of subsets of Ω, and a probability measure $\mathcal{P}$ [178, pp. 11-12]. Let $w(s)$ be a Brownian motion satisfying $E[w(s)w(u)] = \frac{N_0}{2}\min(s,u)$. Let $t \in [a,b]$. Let $\mathcal{F}_t$ be the smallest σ-algebra containing all the events $\{w(s) < x, x \in I\!R\}$ for each $s \in [0,t]$. A random function $\mathsf{b}(t)$ is said to be non-anticipating if for each t it is measurable with respect to $\mathcal{F}_t$ [178, p. 90], [180, p. 72]. In particular, a non-anticipating function $\mathsf{b}(t)$ is independent of $w(t+s) - w(t)$ for all $s > 0$ [180, p. 72]. It depends statistically at most on $w(s)$ for $s \leq t$, that is, on the "past" only but is statistically independent of future values $\{w(s), s > t\}$ [179, p. 22], [181] (if t is considered to be the present). Note that in [181], the term admissible is used instead of non-anticipating.

Let $\mathcal{L}$ be the σ-algebra of Lebesgue measurable sets in $[0,b]$. Let $\mathsf{a}(s)$ be a non-anticipating real process jointly measurable in the product σ-algebra $\mathcal{L} \otimes \mathcal{F}$ (i.e. measurable in (s,ω)). Let $t \in [a,b]$, $0 \leq a < b$ and let $\mathsf{f}(s)$ be a deterministic real-valued square integrable function on $[0,t]$ satisfying

$$\int_a^t |\mathsf{f}(s)| E\,|\mathsf{a}(s)|\,ds < \infty$$

Let $z(t)$ be a process given by

$$\begin{aligned} z(t) &= z(a) + \int_a^t \mathsf{a}(s)ds + \int_a^t dw(s) \\ dz(t) &= \mathsf{a}(t)dt + dw(t) \quad \text{(symbolic differential form)} \end{aligned} \tag{A.2}$$

The Wiener integral of $\mathsf{f}(s)$ with respect to $z(s)$ given by (A.2) is defined as

$$\int_a^t \mathsf{f}(s)dz(s) \triangleq \int_a^t \mathsf{f}(s)\mathsf{a}(s)ds + \int_a^t \mathsf{f}(s)dw(s) \tag{A.3}$$

where the first integral in the right side of (A.3) is a Lebesgue integral of the sample functions of $\mathsf{f}(s)\mathsf{a}(s)$ defined for almost all sample functions and the second integral in the right side of (A.3) is a Wiener integral defined as in Appendix A.1.1. Note that if $\mathsf{a}(s)$ is also a second order mean square continuous process and $\mathsf{f}(s)$ is continuous, then

$\int_a^t \mathsf{f}(s)\mathsf{a}(s)ds$ can also be defined as a mean square integral. Both integrals coincide [210, p. 186].

Finally let $\mathsf{f}(s)$ be a complex valued function such that the Wiener integrals $\int_a^t \Re\{\mathsf{f}(s)\}\, dz(s)$ and $\int_a^t \Im\{\mathsf{f}(s)\}\, dz(s)$ exist. Then the Wiener integral of $\mathsf{f}(s)$ with respect to $z(s)$ given by (A.2) is defined as

$$\int_a^t \mathsf{f}(s)dz(s) \triangleq \int_a^t \Re\{\mathsf{f}(s)\}\, dz(s) + j\int_a^t \Im\{\mathsf{f}(s)\}\, dz(s)$$

A.1.3 Properties of the Wiener integral related to expectation [191, pp. 427-428]

$$i) \quad E\left[\int_a^t \mathsf{b}(s)dw(s)\right] = 0$$

$$ii) \quad E\left[\int_a^t \mathsf{b}_1(s)dw(s)\int_a^t \mathsf{b}_2(r)dw(r)\right] = \frac{N_0}{2}\int_a^t \mathsf{b}_1(s)\mathsf{b}_2(s)ds$$

A.1.4 Time differentiation of a Wiener integral with respect to a Brownian motion

Assume for sake of simplicity that all functions are real. In the following, the function $\mathsf{f}(s)$ depends also on the observation interval $[0,t]$ where $t \in [a,b]$ hence is denoted as $\mathsf{f}(s,t)$.

Proposition A.1. *Let $\mathsf{f}(s,t)$ be a deterministic real-valued function defined on a closed domain $\mathcal{R}'_{ab}$ of $\mathbb{R}^2$ described by*

$$\mathcal{R}'_{ab} = \left\{(s,t) \in \mathbb{R}^2; \quad 0 \le s \le t \quad a \le t \le b\right\} \tag{A.4}$$

where $a \ge 0$. Let us assume that $\mathsf{f}(s,t)$ is continuous on $\mathcal{R}'_{ab}$ and is continuously differentiable with respect to t on $\mathcal{R}'_{ab}$ $\left(i.e.\ \dot{\mathsf{f}}(s,t) \triangleq \frac{\partial \mathsf{f}}{\partial t}(s,t)\right.$ exists and is continuous on $\left.\mathcal{R}'_{ab}\right)$. Then $\forall t \in [a,b]$, $\mathsf{c}(t) \triangleq \int_0^t \dot{\mathsf{f}}(s,t)dw(s)$ satisfies $\int_a^t E\,|\mathsf{c}(u)|\, du < \infty$ and the Wiener integral $I(t) = \int_0^t \mathsf{f}(s,t)dw(s)$ can be written as follows:

$$I(t) = I(a) + \int_a^t \left[\int_0^s \dot{\mathsf{f}}(u,s)dw(u)\right] ds + \int_a^t \mathsf{f}(s,s)dw(s) \tag{A.5}$$

which can be written in symbolic differential notation as

$$dI(t) = \left[\int_0^t \dot{\mathsf{f}}(s,t)dw(s)\right] dt + \mathsf{f}(t,t)dw(t)$$

where $dI(t)$ represents the ordinary (time) differentiation or the Itô differentiation of $I(t)$ since they both coincide due to the fact that $\mathsf{f}(s,t)$ is deterministic. The outer integral in the iterated multiple integral of (A.5) can be viewed either as a Lebesgue integral of the sample functions of $\int_0^s \dot{\mathsf{f}}(u,s)dw(u)$ defined for almost all sample functions or as a mean square integral. There is no contradiction since these two integrals coincide due to the differentiability and continuity properties of $\mathsf{f}(s,t)$. The inner integral and the second integral in (A.5) are Wiener integrals.

Proof of Proposition A.1 is given in Appendix A.3.1.

Remarks.

- $\dot{\mathsf{f}}$ is defined as the first order partial derivative of f with respect to the second variable, i.e. $\dot{\mathsf{f}}(s,u) \triangleq \frac{\partial \mathsf{f}}{\partial t}(s,t)\Big|_{t=u}$
- The continuity of $\mathsf{f}(s,t)$ ensures the existence of the Wiener integrals $\int_0^t \mathsf{f}(s,t)dw(s)$ and $\int_a^t \mathsf{f}(s,s)dw(s)$.
- The continuity of $\dot{\mathsf{f}}(s,t)$ ensures the existence of the Wiener integral $\mathsf{c}(t)$.

Since $\mathsf{f}(s,t)$ is continuous on $\mathcal{R}'_{ab}$ which is a compact set on the real surface $\mathbb{R}^2$, $\mathsf{f}(s,t)$ is bounded and hence $\forall\, t \in [a,b]$, $\int_0^t |\mathsf{f}(s,t)|^2\, ds < \infty$. This ensures the existence of the Wiener integral $\int_0^t \mathsf{f}(s,t)dw(s)$. Since $\mathsf{f}(s,t)$ is continuous on $\mathcal{R}'_{ab}$ and hence on $\mathcal{D} = \{(s,t) \in \mathcal{R}'_{ab}; s = t\}$, $\mathsf{f}(s,s)$ viewed as a function of s is continuous on $[a,b]$ which is a compact set on the real line $\mathbb{R}$, hence $\mathsf{f}(s,s)$ is bounded and thus square integrable. This ensures the existence of the Wiener integral $\int_a^t \mathsf{f}(s,s)dw(s)$. For each $t \in [a,b]$, $\dot{\mathsf{f}}(s,t)$, viewed as a function of s, is continuous on $[0,t]$ which is a compact set of $\mathbb{R}$. Therefore for each $t \in [a,b]$, $\dot{\mathsf{f}}(s,t)$ is bounded and $\int_0^t \left(\dot{\mathsf{f}}(s,t)\right)^2 ds < \infty$. Hence $\mathsf{c}(t) = \int_0^t \dot{\mathsf{f}}(s,t)dw(s)$ is well defined.

- A result along the same lines of Proposition A.1 has been obtained in [211, p. 111] for the mean square derivative of a stochastic integral $I(t) = \int_a^t \mathsf{f}'(t,s)\zeta(s)ds$ (considered as a mean square integral or equivalently as a Riemann integral

of sample functions) where $\{\zeta(s), s \in [a,b]\}$ is a zero mean stochastic process that has a covariance function continuous on $[a,b]^2$, and $\mathsf{f}'(t,s)$ is defined and continuous on $[a,b]^2$ such that $\frac{\partial \mathsf{f}'}{\partial t}$ exists and is continuous on $[a,b]^2$. The main differences between this result and Proposition A.1 are as follows:

- $\mathsf{f}'(t,s)$ is defined on $[a,b]^2$ whereas $\mathsf{f}(s,t)$ is defined only if $0 \leq s \leq t$.
- The result of [211] requires the continuity of the covariance of the stochastic process $\zeta(t)$ which is not satisfied for white noise since its covariance function is a delta function.

A.1.5 Time differentiation of a Wiener integral with respect to $z(t)$ given by $dz(t) = \mathsf{a}(t)dt + dw(t)$

Proposition A.2. *Let $z(t)$ be a process written in symbolic differential form as*

$$dz(t) = \mathsf{a}(t)dt + dw(t)$$

where $\mathsf{a}(t)$ is a real non-anticipating second order process jointly measurable in (t,ω) and mean square continuous on $[0,b]$. Let $\mathsf{f}(s,t)$ be a deterministic real-valued function defined on a closed domain $\mathcal{R}'_{ab}$ described by the inequalities

$$\mathcal{R}'_{ab} = \left\{(s,t) \in I\!R^2; \quad 0 \leq s \leq t \quad a \leq t \leq b\right\}$$

where $a \geq 0$. Let us assume that $\mathsf{f}(s,t)$ satisfies

a) $\forall t \in [a,b] \quad \int_0^t |\mathsf{f}(s,t)|\, E\,|\mathsf{a}(s)|\, ds < \infty$

b) $\mathsf{f}(s,t)$ *is continuous and continuously differentiable with respect to t on $\mathcal{R}'_{ab}$.*

Consider the Wiener integral of $\mathsf{f}(s,t)$ with respect to $z(s)$

$$I(t) = \int_0^t \mathsf{f}(s,t)dz(s) \triangleq \int_0^t \mathsf{f}(s,t)\mathsf{a}(s)ds + \int_0^t \mathsf{f}(s,t)dw(s) \tag{A.6}$$

Then $I(t)$ can be written as

$$dI(t) = \left(\int_0^t \dot{\mathsf{f}}(s,t)dz(s)\right)dt + \mathsf{f}(t,t)dz(t) \tag{A.7}$$

$$I(t) = I(a) + \int_a^t \left(\int_0^s \dot{\mathsf{f}}(u,s)dz(u) \right) ds + \int_a^t \mathsf{f}(s,s)dz(s) \qquad \text{(A.8)}$$

where $dI(t)$ represents the ordinary differentiation of $I(t)$ as well as the Itô differentiation of $I(t)$, since they both coincide due to the fact that $\mathsf{f}(s,t)$ is deterministic. The outer integral in the iterated multiple integral of (A.8) is a Lebesgue integral of sample functions, the inner integral and the second integral are Wiener integrals with respect to $z(t)$. Although $\mathsf{f}(s,s)$ is a deterministic function, by abuse of language $I(t)$ will also be referred as an Itô process with differential representation (A.7).

Proof of Proposition A.2 is given in Appendix A.3.2.

A.2 Itô stochastic integral

A.2.1 Definition of the Itô stochastic integral

Itô provided a definition for the integral of non-anticipating random processes $\{\mathsf{b}(s); a \leq s \leq t, t \in [a,b]\}$, jointly measurable in (t,ω) satisfying

$$\int_a^b E\,|\mathsf{b}(s)|^2\,ds < \infty \qquad \text{(A.9)}$$

This special integral is called Itô integral and denoted by

$$\int_a^t \mathsf{b}(s,\omega)dw(s,\omega) \qquad \text{or for short} \qquad \int_a^t \mathsf{b}(s)dw(s) \qquad a \leq t \leq b$$

where $\int$ represents Itô integration. Omitting the dependence on ω for sake of simplicity of notation, the Itô integral is defined as follows [182, pp. 141-144]:

1. If there exist times $s_0, s_1, \ldots, s_n$ independent of ω, such that $a = s_0 < s_1 < \ldots < s_n = t$ and

$$\mathsf{b}(s) = \sum_{k=0}^{n-1} \mathsf{b}(s_k)\chi_{[s_k,s_{k+1})}(s)$$

where $\chi_{[a,b)}$ is the characteristic function of $[a,b)$ then $\mathsf{b}(s)$ is called an (ω,t)-step function on $[a,t]$. For any non-anticipating (ω,t)-step function on $[a,t]$, $\mathsf{b}(s)$ satisfying

(A.9), the stochastic integral is defined by

$$\int_a^t \mathbf{b}(s)dw(s) \triangleq \sum_{k=0}^{n-1} \mathbf{b}(s_k)\left[w(s_{k+1}) - w(s_k)\right]$$

Note that the value of $\mathbf{b}(s)$ is taken at the left endpoint of the partition interval.

2. For a general non-anticipating $\mathbf{b}(s)$ satisfying (A.9), it can be shown [182, p. 142] that there exists a sequence $\{\mathbf{b}_n(s)\}$ of non-anticipating (ω, t)-step functions satisfying (A.9) such that

$$\lim_{n\to\infty} \int_a^t E\left|\mathbf{b}(s) - \mathbf{b}_n(s)\right|^2 ds = 0 \tag{A.10}$$

It then follows that $\int_a^t \mathbf{b}_n(s)dw(s)$ converges in mean square and this mean square limit is the same for any sequence of steps functions satisfying (A.10). Hence the Itô integral of $\mathbf{b}(s)$ with respect to $w(s)$ is defined as

$$\int_a^t \mathbf{b}(s)dw(s) \triangleq \underset{n\to\infty}{\text{l.i.m.}} \int_a^t \mathbf{b}_n(s)dw(s)$$

where $\{\mathbf{b}_n(s)\}$ is any sequence of steps functions satisfying (A.10).

When $\mathbf{b}(s)$ is a second order mean square continuous process, an approximating sequence of step functions $\{\mathbf{b}_n(s)\}$ can be constructed by partitioning the interval $[a, t]$ and sampling the function $\mathbf{b}(s)$. The Itô stochastic integral can be then defined as the following mean-square limit.

$$\int_a^t \mathbf{b}(s)dw(s) \triangleq \underset{n\to\infty}{\text{l.i.m.}} \sum_{k=0}^{n-1} \mathbf{b}\left(s_k^{(n)}\right)\left[w\left(s_{k+1}^{(n)}\right) - w\left(s_k^{(n)}\right)\right]$$

where, for each positive integer n, $T_n = \left\{a = s_0^{(n)} < s_1^{(n)} < \ldots < s_n^{(n)} = t\right\}$ forms a partition of $[a, t]$ such that $\lim_{n\to\infty} \max_{0\le k\le n-1}\left(\left|s_{k+1}^{(n)} - s_k^{(n)}\right|\right) = 0$.

When $\mathbf{b}(s)$ is purely deterministic, the Itô integral reduces to the Wiener integral defined in Appendix A.1.1 [181].

A.2.2 Properties of the Itô integral

Assume for sake of simplicity that all processes are real, from [181], [212, p. 149]

$$i) \quad E\left[\int_a^t \mathsf{b}(s)dw(s)\right] = 0$$

$$ii) \quad E\left[\int_a^t \mathsf{b}_1(s)dw(s)\int_a^t \mathsf{b}_2(r)dw(r)\right] = \frac{N_0}{2}\int_a^t E\left[\mathsf{b}_1(s)\mathsf{b}_2(s)\right]ds$$

A.2.3 Itô process

A process that can be written in the form

$$z(t) = z(a) + \int_a^t \mathsf{a}(s)ds + \int_a^t \mathsf{b}(s)dw(s) \quad a \le t \le b$$

$$dz(t) = \mathsf{a}(t)dt + \mathsf{b}(t)dw(t) \qquad \text{(symbolic differential form)} \tag{A.11}$$

$$\dot{z}(t) = \mathsf{a}(t) + \mathsf{b}(t)\dot{w}(t) \qquad \text{(equivalent notation when } \mathsf{b}(t) \text{ is a deterministic process)}$$

where $\mathsf{a}(t)$ and $\mathsf{b}(t)$ are non-anticipating processes jointly measurable in (t,ω) satisfying $\forall\, t \in [a,b]$, $\int_a^t E\left|\mathsf{a}(s)\right| ds < \infty$, $\int_a^t E\left|\mathsf{b}(s)\right|^2 ds < \infty$, and $\int$ is the Itô integral, is called an *Itô process* [181]. Note that in this notation $d(\cdot)$ and $\int$ are inverse operators.

Let $\{z(t), t \in [a,b]\}$ be an Itô process given by (A.11). Let $\mathsf{f}(t)$ be a non-anticipating process jointly measurable in (t,ω) such that for each $t \in [a,b]$

$$\int_a^t E\left|\mathsf{f}(s)\mathsf{a}(s)\right| ds < \infty \quad \text{and} \quad \int_a^t E\left|\mathsf{f}(s)\mathsf{b}(s)\right|^2 ds < \infty$$

The stochastic integral over the Itô process $z(t)$ (also referred as an Itô integral) is defined as [212, p. 161], [213, p. 67]

$$I(t) = \int_a^t \mathsf{f}(s)dz(s) \triangleq \int_a^t \mathsf{f}(s)\mathsf{a}(s)ds + \int_a^t \mathsf{f}(s)\mathsf{b}(s)dw(s) \quad a \le t \le b \tag{A.12}$$

Note that $I(t)$ is also an Itô process that can be written symbolically as

$$dI(t) = \mathsf{f}(t)\mathsf{a}(t)dt + \mathsf{f}(t)\mathsf{b}(t)dw(t)$$

A.2.4 The Itô differential rule

Suppose $\mathsf{f}(u,t)$ is a continuous function with continuous first order partial derivatives, $\mathsf{f}_t(u,t)$ and $\mathsf{f}_u(u,t)$, on $(-\infty,\infty)\times[a,b]$ and continuous second-order partial derivative, $\mathsf{f}_{uu}(u,t)$, on $(-\infty,\infty)\times[a,b]$. Then if $z(t)$ is an Itô process written as (A.11), Itô's differential rule states that $\mathsf{f}(z(t),t)$ is also an Itô process defined by [181]

$$\begin{aligned} d\mathsf{f}(z(t),t) &= \left(\mathsf{f}_t(z,t)+\mathsf{a}(t)\mathsf{f}_z(z,t)+\frac{1}{2}\frac{N_0}{2}\mathsf{f}_{zz}(z,t)\mathsf{b}^2(t)\right)dt+\mathsf{b}(t)\mathsf{f}_z(z,t)dw(t) \\ &= \left(\mathsf{f}_t(z,t)+\frac{1}{2}\frac{N_0}{2}\mathsf{f}_{zz}(z,t)\mathsf{b}^2(t)\right)dt+\mathsf{f}_z(z,t)dz(t) \\ \int_a^t \mathsf{f}_z(z,s)dz(s) &= \mathsf{f}(z(t),t)-\mathsf{f}(z(a),a)-\int_a^t\left(\mathsf{f}_s(z,s)+\frac{1}{2}\frac{N_0}{2}\mathsf{f}_{zz}(z,s)\mathsf{b}^2(s)\right)ds \end{aligned} \tag{A.13}$$

A.2.5 The vector Itô differential rule

A N-vector process which can be written as

$$d\boldsymbol{z}(t)=\mathbf{a}(t)dt+\mathbf{B}(t)d\boldsymbol{w}(t)$$

where $\mathbf{a}(t)$ is a column N-vector of non-anticipating processes, $\left\{\left[\mathbf{a}(t)\right]_k\right\}_{k=1,\ldots,N}$, jointly measurable in (t,ω), $\mathbf{B}(t)$ is a $N\times K$ matrix of non-anticipating processes jointly measurable in (t,ω), $\left\{\left[\mathbf{B}(t)\right]_{kj}\right\}_{k=1,\ldots,N\,j=1,\ldots,K}$, satisfying for all $t\in[a,b]$

$$\forall k=1,\ldots,N\quad\forall j=1,\ldots K\quad\int_a^t E\left|\left[\mathbf{a}(s)\right]_k\right|ds<\infty\quad\int_a^t E\left|\left[\mathbf{B}(s)\right]_{kj}\right|^2ds<\infty$$

and $\boldsymbol{w}(t)$ is a column K-vector of independent Wiener processes, $w_k(t)$, $k=1,\ldots K$ is called a vector Itô process [181]. Assume furthermore that all $w_k(t)$ have the same variance $\frac{N_0}{2}$. Let $\mathsf{f}(\boldsymbol{u},t)$ be a continuous scalar function of a column N-vector $\boldsymbol{u}$ and a scalar t. Let $\mathsf{f}_{\boldsymbol{u}}(\boldsymbol{u},t)$ (column vector) and $\mathsf{f}_t(\boldsymbol{u},t)$ (scalar) be the first order partial derivatives of $\mathsf{f}(\boldsymbol{u},t)$. Assume that the components of $\mathsf{f}_{\boldsymbol{u}}(\boldsymbol{u},t)$, $\left\{\left[\mathsf{f}_{\boldsymbol{u}}(\boldsymbol{u},t)\right]_k\right\}_{k=1,\ldots,N}$ and $\mathsf{f}_t(\boldsymbol{u},t)$ are continuous on $(-\infty,\infty)^N\times[a,b]$. Let $\mathsf{f}_{\boldsymbol{uu}}(\boldsymbol{u},t)$ (matrix) be the second order partial derivative of $\mathsf{f}(\boldsymbol{u},t)$ with respect to $\boldsymbol{u}$. Assume that the elements of $\mathsf{f}_{\boldsymbol{uu}}(\boldsymbol{u},t)$, $\left\{\left[\mathsf{f}_{\boldsymbol{uu}}(\boldsymbol{u},t)\right]_{kj}\right\}_{k,j=1,\ldots,N}$ are continuous on $(-\infty,\infty)^N\times[a,b]$. Then $\mathsf{f}(\boldsymbol{z},t)$

is also a vector Itô process and the vector Itô differential rule is [181], [208, p. 112]

$$\begin{aligned} d\mathbf{f}(\boldsymbol{z},t) &= \mathbf{f}_t(\boldsymbol{z},t)dt + \mathbf{f}_{\boldsymbol{z}}^T(\boldsymbol{z},t)\cdot\big(\mathbf{a}(t)dt + \mathbf{B}(t)d\boldsymbol{w}(t)\big) + \frac{1}{2}\frac{N_0}{2}\mathrm{tr}\big[\mathbf{B}^T(t)\mathbf{f}_{\boldsymbol{zz}}(\boldsymbol{z},t)\mathbf{B}(t)\big]dt \\ &= \left(\mathbf{f}_t(\boldsymbol{z},t) + \frac{1}{2}\frac{N_0}{2}\mathrm{tr}\big[\mathbf{B}^T(t)\mathbf{f}_{\boldsymbol{zz}}(\boldsymbol{z},t)\mathbf{B}(t)\big]\right)dt + \mathbf{f}_{\boldsymbol{z}}^T(\boldsymbol{z},t)d\boldsymbol{z}(t) \end{aligned} \tag{A.14}$$

where $\mathrm{tr}(\cdot)$ denotes the trace of a matrix.

A.3 Time differentiation of Wiener integrals: proofs

In the incoming proofs, the Lebesgue dominated convergence theorem and the Minkowski's inequality with $p = 2$ are extensively used and can be found respectively in { [214, p. 39], [182, pp. 17-18], [212, p. 22] } and [212, p. 33].

A.3.1 Proof of Proposition A.1

Let $t \in [a,b]$.

Proof that $\mathsf{c}(t) \triangleq \int_0^t \dot{\mathsf{f}}(s,t)dw(s)$ is a second order process satisfying $\int_a^t E|\mathsf{c}(u)|du < \infty$. Since $w(s)$ is a Brownian motion, $\mathsf{c}(t)$ is a Gaussian random process with zero mean and variance given by

$$E\big[\mathsf{c}^2(t)\big] = E\left[\int_0^t \dot{\mathsf{f}}(s,t)dw(s)\int_0^t \dot{\mathsf{f}}(u,t)dw(u)\right] = \frac{N_0}{2}\int_0^t \Big(\dot{\mathsf{f}}(s,t)\Big)^2 ds$$

Since $\dot{\mathsf{f}}(s,t)$ is continuous on $\mathcal{R}'_{ab}$, $\dot{\mathsf{f}}(s,t)$ is bounded on $\mathcal{R}'_{ab}$ hence $E\big[\mathsf{c}^2(t)\big] < \infty$. Furthermore, since $\mathsf{c}(t)$ is a zero mean Gaussian process, $E|\mathsf{c}(t)|$ is given by

$$E|\mathsf{c}(t)| = \sqrt{\frac{2}{\pi}E\big[\mathsf{c}^2(t)\big]} = \sqrt{\frac{2}{\pi}\frac{N_0}{2}}\left(\int_0^t \Big(\dot{\mathsf{f}}(s,t)\Big)^2 ds\right)^{1/2}$$

Hence $$\int_a^t E\,|\mathsf{c}(u)|\,du = \sqrt{\frac{2}{\pi}\frac{N_0}{2}}\int_a^t \left(\int_0^u \Big(\dot{\mathsf{f}}(s,u)\Big)^2 ds\right)^{1/2} du < \infty \qquad \textbf{Q.E.D}$$

In order to prove (A.5) the following lemmas are needed.

Lemma A.1. *Let $\{\mathbf{g}_n(t)\}$ be a sequence of deterministic square integrable functions on $[a,b]$, converging to $\mathbf{g}(t)$ for almost all $t \in [a,b]$. Assume there exists a determin-*

istic function $\phi(t)$ square integrable on $[a,b]$ for which $\forall n \quad |\mathbf{g}_n(t)|^2 \leq |\phi(t)|^2$. Then

$$\underset{n\to\infty}{\text{l.i.m.}} \int_a^b \mathbf{g}_n(s)dw(s) = \int_a^b \mathbf{g}(s)dw(s)$$

Proof of Lemma A.1.

$$E\left|\int_a^b \mathbf{g}_n(s)dw(s) - \int_a^b \mathbf{g}(s)dw(s)\right|^2$$
$$= E\left|\int_a^b [\mathbf{g}_n(s) - \mathbf{g}(s)]\,dw(s)\right|^2 = \frac{N_0}{2}\int_a^b |\mathbf{g}_n(s) - \mathbf{g}(s)|^2\,ds$$

using property *ii)* of Section A.1.3. Note that for any complex number z_1, z_2, $|\Re\{z_1 z_2^*\}| \leq |z_1|\,|z_2|$, hence

$$|\mathbf{g}_n(s) - \mathbf{g}(s)|^2 \leq |\mathbf{g}_n(s)|^2 + |\mathbf{g}(s)|^2 + 2\,|\Re\{\mathbf{g}_n(s)\mathbf{g}^*(s)\}|$$
$$\leq |\mathbf{g}_n(s)|^2 + |\mathbf{g}(s)|^2 + 2\,|\mathbf{g}_n(s)|\,|\mathbf{g}(s)| \leq 4\,|\phi(s)|^2$$

since $|\mathbf{g}_n(s)|^2 \leq |\phi(s)|^2$ and $\lim_{n\to\infty} \mathbf{g}_n(s) = \mathbf{g}(s)$ implies $|\mathbf{g}(s)|^2 \leq |\phi(s)|^2$. Furthermore $\int_a^b |\phi(s)|^2\,ds < \infty$ and $\lim_{n\to\infty} |\mathbf{g}_n(s) - \mathbf{g}(s)|^2 = 0$, thus from Lebesgue dominated convergence theorem (interchange of integration and limit) [214, p. 39]

$$\lim_{n\to\infty} \int_a^b |\mathbf{g}_n(s) - \mathbf{g}(s)|^2\,ds = 0$$

Therefore

$$\lim_{n\to\infty} E\left|\int_a^b \mathbf{g}_n(s)dw(s) - \int_a^b \mathbf{g}(s)dw(s)\right|^2 = 0 \quad \text{i.e. } \underset{n\to\infty}{\text{l.i.m.}} \int_a^b \mathbf{g}_n(s)dw(s) = \int_a^b \mathbf{g}(s)ds$$

Q.E.D

Lemma A.2. $\mathbf{c}(u) \triangleq \int_0^u \dot{\mathbf{f}}(s,u)dw(u)$, $u \in [a,b]$ *is a second order process mean square continuous hence mean square integrable.*

Proof of Lemma A.2. As proved at the beginning of this section, $\mathbf{c}(u)$ is a second order process. Since $\dot{\mathbf{f}}(s,u)$ is defined only if $0 \leq s \leq u$, right and left mean square continuity of $\mathbf{c}(u)$ have to be considered separately. Let us first consider the right mean square continuity. Let $h \geq 0$ such that $u + h \in [a,b]$. Note that if $u = b$, only

the left mean square continuity of $\mathsf{c}(u)$ has to be verified.

$$E\left|\int_0^{u+h}\dot{\mathsf{f}}\,(s,u+h)\,dw(s)-\int_0^{u}\dot{\mathsf{f}}\,(s,u)\,dw(s)\right|^2$$
$$=E\left|\int_0^{u}\left(\dot{\mathsf{f}}\,(s,u+h)-\dot{\mathsf{f}}\,(s,u)\right)dw(s)+\int_u^{u+h}\dot{\mathsf{f}}\,(s,u+h)\,dw(s)\right|^2$$
$$=\frac{N_0}{2}[I_1(h,u)+I_2(h,u)] \qquad \text{(A.15)}$$

where $I_1(h,u)$ and $I_2(h,u)$ are given by

$$I_1(h,u)=\int_0^{u}\left(\dot{\mathsf{f}}\,(s,u+h)-\dot{\mathsf{f}}\,(s,u)\right)^2 ds$$
$$I_2(h,u)=\int_u^{u+h}\left(\dot{\mathsf{f}}\,(s,u+h)\right)^2 ds$$

and (A.15) is obtained from property *ii)* of Section A.1.3 and since $[0,u]\cap[u,u+h]=u$ (set of zero measure).

Since $\dot{\mathsf{f}}\,(s,t)$ is continuous on the bounded domain $\mathcal{R}'_{ab}$, $\sup_{(s,t)\in\mathcal{R}'_{ab}}\dot{\mathsf{f}}\,(s,t)$ is finite and therefore by the Lebesgue dominated convergence theorem

$$\lim_{\substack{h\to 0\\ h\geq 0}} I_1(h,u)=\int_0^{u}\lim_{\substack{h\to 0\\ h\geq 0}}\left(\dot{\mathsf{f}}\,(s,u+h)-\dot{\mathsf{f}}\,(s,u)\right)^2 ds=0$$

From the mean value theorem for integrals, $\exists\ \zeta(h,u)\in[u,u+h]$ such that

$$I_2(h,u)=h\left(\dot{\mathsf{f}}\,(\zeta(h,u),u+h)\right)^2$$

The continuity of $\dot{\mathsf{f}}\,(s,t)$ on $\mathcal{R}'_{ab}$ and $\lim_{\substack{h\to 0\\ h\geq 0}}\zeta(h,u)=u$ yields $\lim_{\substack{h\to 0\\ h\geq 0}}\left(\dot{\mathsf{f}}\,(\zeta(h,u),u+h)\right)^2=\left(\dot{\mathsf{f}}\,(u,u)\right)^2$ and $\lim_{\substack{h\to 0\\ h\geq 0}} I_2(h,u)=0$. Therefore from (A.15)

$$\lim_{\substack{h\to 0\\ h\geq 0}} E\left|\int_0^{u+h}\dot{\mathsf{f}}\,(s,u+h)\,dw(s)-\int_0^{u}\dot{\mathsf{f}}\,(s,u)\,dw(s)\right|^2=0$$

Similarly let us check the left mean square continuity of $\mathsf{c}(u)$. Let $h\leq 0$ such that $u+h\in[a,b]$. Note that if $u=a$ only the right mean square continuity of $\mathsf{c}(u)$ has to

be checked.

$$E\left|\int_0^u \dot{\mathrm{f}}(s,u)\,dw(s) - \int_0^{u+h} \dot{\mathrm{f}}(s,u+h)\,dw(s)\right|^2$$
$$= E\left|\int_0^{u+h} \left(\dot{\mathrm{f}}(s,u) - \dot{\mathrm{f}}(s,u+h)\right) dw(s) + \int_{u+h}^u \dot{\mathrm{f}}(s,u)\,dw(s)\right|^2$$
$$= \frac{N_0}{2}\left[I_1'(h,u) + I_2'(h,u)\right] \qquad \text{(A.16)}$$

where $I_1'(h,u)$ and $I_2'(h,u)$ are given by

$$I_1'(h,u) = \int_0^{u+h} \left(\dot{\mathrm{f}}(s,u) - \dot{\mathrm{f}}(s,u+h)\right)^2 ds$$
$$I_2'(h,u) = \int_{u+h}^u \left(\dot{\mathrm{f}}(s,u)\right)^2 ds$$

and (A.16) is obtained from property *ii)* of Section A.1.3 and since $[0,u+h] \cap [u+h,u] = u+h$ (set of zero measure). Let $u \in [a,b]$ be fixed. Define the function $F(s,x)$ on the closed domain $\mathcal{R}_u'$ described by

$$\mathcal{R}_u' = \left\{(s,x) \in I\!R^2;\quad 0 \le s \le x \quad 0 \le x \le u\right\} \qquad \text{(A.17)}$$

as $F(s,x) = \left(\dot{\mathrm{f}}(s,u) - \dot{\mathrm{f}}(s,x)\right)^2$ such that $I_1'(h,u) = \int_0^{u+h} F(s,u+h)ds$. Since $\dot{\mathrm{f}}(s,t)$ is continuous on $\mathcal{R}_{ab}'$, $F(s,x)$ is continuous on $\mathcal{R}_u'$, then for $0 \le x \le u$, $\int_0^x F(s,x)ds$ is a continuous function of x [192, p. 230]. Hence

$$\lim_{\substack{h\to 0 \\ -u\le h\le 0}} I_1'(h,u) = \int_0^u F(s,u)ds = 0$$

since $F(s,u) = 0$. Since $\dot{\mathrm{f}}(s,t)$ is continuous on $\mathcal{R}_{ab}'$, from the mean value theorem for integrals, $\exists\ \zeta'(h,u) \in [u+h,u]$ such that

$$I_2'(h,u) = -h\left(\dot{\mathrm{f}}\left(\zeta'(h,u),u\right)\right)^2$$

The continuity of $\dot{\mathrm{f}}(s,t)$ on $\mathcal{R}_{ab}'$ and $\lim_{\substack{h\to 0 \\ -u\le h\le 0}} \zeta'(h,u) = u$ yields

$\lim_{\substack{h\to 0\\ -u\le h\le 0}} \left(\dot{\mathsf{f}}\left(\zeta'(h,u),u\right)\right)^2 = \left(\dot{\mathsf{f}}\left(u,u\right)\right)^2$ and $\lim_{\substack{h\to 0\\ -u\le h\le 0}} I_2'(h,u) = 0$. Therefore from (A.16)

$$\lim_{\substack{h\to 0\\ -u\le h\le 0}} E\left|\int_0^{u+h} \dot{\mathsf{f}}\left(s,u+h\right) dw(s) - \int_0^{u} \dot{\mathsf{f}}\left(s,u\right) dw(s)\right|^2 = 0$$

and $\mathsf{c}(u)$ is mean square continuous and hence mean square integrable [182, pp. 77, 80], [208, p. 67]. **Q.E.D**

Proof of (A.5). Let $T_n = \left\{a = t_0^{(n)} < t_1^{(n)} < \ldots < t_n^{(n)} = t\right\}$ be a partition of $[a,t]$ such that $\lim_{n\to\infty} \max_{0\le k\le n-1}\left(\left|t_{k+1}^{(n)} - t_k^{(n)}\right|\right) = 0$ and $t \in [a,b]$. Then

$$\begin{aligned} I(t) &= I(a) + \sum_{k=0}^{n-1}\left[I\left(t_{k+1}^{(n)}\right) - I\left(t_k^{(n)}\right)\right] \quad \text{(valid for any function } I(t)\text{)} \\ &= I(a) + \sum_{k=0}^{n-1}\left[\int_0^{t_{k+1}^{(n)}} \mathsf{f}\left(s, t_{k+1}^{(n)}\right) dw(s) - \int_0^{t_k^{(n)}} \mathsf{f}\left(s, t_k^{(n)}\right) dw(s)\right] \\ &= I(a) + S_1(n) + S_2(n) \end{aligned} \tag{A.18}$$

where

$$S_1(n) = \sum_{k=0}^{n-1} \int_{t_k^{(n)}}^{t_{k+1}^{(n)}} \mathsf{f}\left(s, t_{k+1}^{(n)}\right) dw(s) \tag{A.19}$$

$$\begin{aligned} S_2(n) &= \sum_{k=0}^{n-1} \int_0^{t_k^{(n)}} \left[\mathsf{f}\left(s, t_{k+1}^{(n)}\right) - \mathsf{f}\left(s, t_k^{(n)}\right)\right] dw(s) \\ &= \sum_{k=0}^{n-1} \int_0^{t_k^{(n)}} \left(t_{k+1}^{(n)} - t_k^{(n)}\right) \dot{\mathsf{f}}\left(s, t_k^{(n)} + \nu_k^{(n)}(s)\left[t_{k+1}^{(n)} - t_k^{(n)}\right]\right) dw(s) \end{aligned} \tag{A.20}$$

and (A.20) is obtained from the mean value theorem, since $\mathsf{f}(s,t)$ is differentiable with respect to t on $\mathcal{R}'_{ab}$, and $\nu_k^{(n)}(s) \in [0,1]$. Let $n \in N$. Recall that the interval $[a,t]$ is partitioned into n sub-intervals such that

$$[a,t] = \bigcup_{k=0}^{n-2}\left[t_k^{(n)}, t_{k+1}^{(n)}\right) \cup \left[t_{n-1}^{(n)}, t_n^{(n)}\right]$$

The last sub-interval is considered closed to include t. Let $\mathsf{g}_n(s)$ be the function

defined on $[a,t)$ as follows: $\forall\, s \in [a,t)$, s belongs to one of the sub-intervals of the partition T_n, i.e. $\exists\, k(n) \triangleq k_n \in \{0,\dots,n-1\}$ such that $s \in \left[t_{k_n}^{(n)}, t_{k_n+1}^{(n)}\right)$ and

$$\mathbf{g}_n(s) \triangleq \begin{cases} \mathrm{f}\left(s, t_{k_n+1}^{(n)}\right) & \text{for all } s \in [a,t) \ \left\{k_n \text{ is such that } s \in \left[t_{k_n}^{(n)}, t_{k_n+1}^{(n)}\right)\right\}, \\ \mathrm{f}\left(s, t_n^{(n)}\right) & \text{for } s = t, \\ 0 & \text{else.} \end{cases}$$

Let $s \in [a,t]$. Since $\mathrm{f}(s,t)$ is continuous on $\mathcal{R}'_{ab}$, $\mathrm{f}(s,t)$ is continuous on $\mathcal{D} = \{(s,t) \in \mathcal{R}'_{ab}; s = t\}$, thus

$$\forall \epsilon > 0 \quad \exists \delta > 0 \quad \text{s.t.} \quad \sqrt{|h|^2 + |h'|^2} < \delta \quad \Longrightarrow \quad \left|\mathrm{f}(s+h, s+h') - \mathrm{f}(s,s)\right| < \epsilon \tag{A.21}$$

Since $\lim_{n\to\infty} \max_{0\le k\le n-1} \left(|t_{k+1}^{(n)} - t_k^{(n)}|\right) = 0$, $\exists\, n_0$ such that

$$\forall\, n \ge n_0 \quad \forall\, k = 0,\dots,n-1 \quad \left|t_{k+1}^{(n)} - t_k^{(n)}\right| < \delta$$

If $s \in [a,t)$, then $\exists\, k(n) \triangleq k_n \in \{0,\dots,n-1\}$ such that $s \in \left[t_{k_n}^{(n)}, t_{k_n+1}^{(n)}\right)$ and

$$\forall\, n \ge n_0 \quad \left|t_{k_n+1}^{(n)} - s\right| \le \left|t_{k_n+1}^{(n)} - t_{k_n}^{(n)}\right| < \delta$$

Hence from (A.21), $(h = 0, h' = t_{k_n+1}^{(n)} - s)$, $\left|\mathrm{f}\left(s, t_{k_n+1}^{(n)}\right) - \mathrm{f}(s,s)\right| < \epsilon$. But $\mathrm{f}\left(s, t_{k_n+1}^{(n)}\right)$ $= \mathbf{g}_n(s)$, hence $\lim\limits_{n\to\infty} \mathbf{g}_n(s) = \mathrm{f}(s,s)$. If $s = t$, then the same principle applies, $s \in \left[t_{n-1}^{(n)}, t_n^{(n)}\right]$ and $\lim\limits_{n\to\infty} \mathbf{g}_n(t) = \mathrm{f}(t,t)$.

Furthermore $|\mathbf{g}_n(s)|^2 \le \sup\limits_{(s,t)\in\mathcal{R}'_{ab}} |\mathrm{f}(s,t)|^2$ and $\forall\, t \in [a,b]$, $\int_0^t \sup\limits_{(s,t)\in\mathcal{R}'_{ab}} |\mathrm{f}(s,t)|^2 ds < \infty$ since $\sup\limits_{(s,t)\in\mathcal{R}'_{ab}} |\mathrm{f}(s,t)|$ is finite by continuity of $\mathrm{f}(s,t)$ on $\mathcal{R}'_{ab}$. Therefore by Lemma A.1

$$\underset{n\to\infty}{\text{l.i.m.}} \int_a^t \mathbf{g}_n(s) dw(s) = \int_a^t \mathrm{f}(s,s) dw(s)$$

But by additivity property of Wiener integrals

$$\int_a^t \mathsf{g}_n(s)dw(s) = \sum_{k=0}^{n-1} \int_{t_k^{(n)}}^{t_{k+1}^{(n)}} \mathsf{g}_n(s)dw(s) = \sum_{k=0}^{n-1} \int_{t_k^{(n)}}^{t_{k+1}^{(n)}} \mathsf{f}\left(s, t_{k+1}^{(n)}\right) dw(s)$$

Hence from (A.19)

$$\underset{n\to\infty}{\text{l.i.m.}}\, S_1(n) = \underset{n\to\infty}{\text{l.i.m.}} \sum_{k=0}^{n-1} \int_{t_k^{(n)}}^{t_{k+1}^{(n)}} \mathsf{f}\left(s, t_{k+1}^{(n)}\right) dw(s) = \int_a^t \mathsf{f}(s,s)dw(s) \tag{A.22}$$

Note that since $\mathsf{f}(s,t)$ is continuous on $\mathcal{D}$, $\forall t \in [a,b]$, $\int_a^t |\mathsf{f}(s,s)|^2 ds < \infty$, and $\int_a^t \mathsf{f}(s,s)dw(s)$ is well defined.

Since $\dot{\mathsf{f}}(s,t)$ is continuous on $\mathcal{R}'_{ab}$

$$\lim_{n\to\infty} \sup_k \left| \dot{\mathsf{f}}\left(s, t_k^{(n)} + \nu_k^{(n)}(s)\left[t_{k+1}^{(n)} - t_k^{(n)}\right]\right) - \dot{\mathsf{f}}\left(s, t_k^{(n)}\right)\right| = 0$$

therefore from (A.20)

$$\underset{n\to\infty}{\text{l.i.m.}}\, S_2(n) = \underset{n\to\infty}{\text{l.i.m.}} \sum_{k=0}^{n-1} \left(t_{k+1}^{(n)} - t_k^{(n)}\right) \mathsf{c}\left(t_k^{(n)}\right) \tag{A.23}$$

where $\mathsf{c}(t) \triangleq \int_0^t \dot{\mathsf{f}}(s,t)dw(s)$. Note that $\forall t \in [a,b], \mathsf{c}(t)$ is well defined due to the continuity of $\dot{\mathsf{f}}(s,t)$ on $\mathcal{R}'_{ab}$. The sum $\sum_{k=0}^{n-1}\left(t_{k+1}^{(n)} - t_k^{(n)}\right)\mathsf{c}\left(t_k^{(n)}\right)$ is a regular Riemann sum of sample functions. Since $\int_a^t E\,|\mathsf{c}(u)|\,du < \infty$ (proved earlier), $\int_a^t \mathsf{c}(u)du \triangleq \int_a^t \left[\int_0^u \dot{\mathsf{f}}(s,u)dw(s)\right] du$ exists for almost all sample functions. Therefore

$$\sum_{k=0}^{n-1}\left(t_{k+1}^{(n)} - t_k^{(n)}\right)\mathsf{c}(t_k^{(n)}) \quad \begin{array}{c}\text{converges almost surely to} \\ \text{as } n \to \infty\end{array} \quad \int_a^t \left[\int_0^u \dot{\mathsf{f}}\,(s,u)\,dw(s)\right] du$$

where $\int_a^t \left[\int_0^u \dot{\mathsf{f}}\,(s,u)\,dw(s)\right] du$ is defined as an integral of the sample functions.

By Lemma A.2, $\mathsf{c}(u)$ is mean square integrable hence

$$\underset{n\to\infty}{\text{l.i.m.}} \sum_{k=0}^{n-1}\left(t_{k+1}^{(n)} - t_k^{(n)}\right)\mathsf{c}\left(t_k^{(n)}\right) = \int_a^t \left[\int_0^u \dot{\mathsf{f}}\,(s,u)\,dw(s)\right] du \tag{A.24}$$

where $\int_a^t \left[\int_0^u \dot{\mathsf{f}}(s,u)\,dw(s)\right] du$ is defined as a mean square integral. Thus from (A.23) and (A.24),

$$\underset{n\to\infty}{\text{l.i.m.}}\, S_2(n) = \int_a^t \left[\int_0^u \dot{\mathsf{f}}(s,u)\,dw(s)\right] du \tag{A.25}$$

where the integral can be defined either as a Lebesgue integral of the sample functions defined for almost all sample functions or as a mean square integral. Note there is no contradiction since the mean square continuity of $\mathsf{c}(u)$, or equivalently the continuity of its autocorrelation function $E[\mathsf{c}(u)\mathsf{c}(s)]$ [208, p. 61], [182, p. 77] implies that the mean square integral and the integral of the sample functions coincide [210, p. 186]. Grouping (A.22) and (A.25) with (A.18) yields (A.5). **Q.E.D**

A.3.2 Proof of Proposition A.2

(A.6) can be rewritten as

$$I(t) = \int_0^t \mathsf{f}(s,t)\mathsf{a}(s)ds + I_1(t) \tag{A.26}$$

where $I_1(t)$ is given by

$$I_1(t) = \int_0^t \mathsf{f}(s,t)dw(s)$$

The deterministic function $\mathsf{f}(s,t)$ satisfies all the assumptions required for Proposition A.1 to hold. Therefore from Proposition A.1, $I_1(t)$ can be written as

$$I_1(t) = \int_0^a \mathsf{f}(s,a)dw(s) + \int_a^t \left(\int_0^s \dot{\mathsf{f}}(u,s)dw(u)\right) ds + \int_a^t \mathsf{f}(s,s)dw(s) \tag{A.27}$$

It remains to find an equivalent expression for $\int_0^t \mathsf{f}(s,t)\mathsf{a}(s)ds$ which is obtained from the following lemmas.

Lemma A.3. *Let $\mathsf{f}(s,t)$ be a deterministic real-valued function continuous on $\mathcal{R}'_{ab}$ described by (A.4), where $a \geq 0$. Let $\mathsf{a}(s)$ be a real second order mean square continuous process on $[0,b]$. Then for each $t \in [a,b]$, $\mathsf{f}(s,t)\mathsf{a}(s)$ defined as a process of s is a second order mean square continuous process on $[0,t]$.*

Lemma A.4. *Let* $\mathsf{f}(s,t)$ *and* $\mathsf{a}(s)$ *be respectively a deterministic function and a random process that satisfy all the assumptions of Proposition A.2. The integral* $\int_0^t \mathsf{f}(s,t)\mathsf{a}(s)ds$ *(defined either as Lebesgue integral of the sample functions or as a mean square integral) is mean square differentiable with respect to* t *and its mean square partial derivative is given by*

$$\frac{\partial}{\partial t}\left\{\int_0^t \mathsf{f}(s,t)\mathsf{a}(s)ds\right\} = \mathsf{f}(t,t)\mathsf{a}(t) + \int_0^t \dot{\mathsf{f}}(s,t)\mathsf{a}(s)ds \tag{A.28}$$

where the integral in the right side of (A.28) is defined as a mean square integral.

Lemma A.5. $\int_0^t \dot{\mathsf{f}}(s,t)\mathsf{a}(s)ds$ *is mean square continuous. Therefore as defined in Lemma A.4,* $\frac{\partial}{\partial t}\left\{\int_0^t \mathsf{f}(s,t)\mathsf{a}(s)ds\right\}$ *is mean square continuous and hence mean square integrable.*

For convenience, proofs of Lemmas A.3-A.5 are placed after the proof of Proposition A.2. Since from Lemma A.5 $\frac{\partial}{\partial s}\left\{\int_0^s \mathsf{f}(u,s)\mathsf{a}(u)du\right\}$ is mean square integrable, the Fundamental Theorem of mean square calculus [208, p. 69], [210, p. 186] yields

$$\int_a^t \frac{\partial}{\partial s}\left\{\int_0^s \mathsf{f}(u,s)\mathsf{a}(u)du\right\} ds = \int_0^t \mathsf{f}(u,t)\mathsf{a}(u)du - \int_0^a \mathsf{f}(u,a)\mathsf{a}(u)du \tag{A.29}$$

with probability 1. Substituting (A.28) of Lemma A.4 into (A.29) and reordering terms yields

$$\begin{aligned}\int_0^t \mathsf{f}(s,t)\mathsf{a}(s)ds &= \int_0^a \mathsf{f}(s,a)\mathsf{a}(s)ds + \int_a^t \left(\mathsf{f}(s,s)\mathsf{a}(s) + \int_0^s \dot{\mathsf{f}}(u,s)\mathsf{a}(u)du\right) ds \\ &= \int_0^a \mathsf{f}(s,a)\mathsf{a}(s)ds + \int_a^t \mathsf{f}(s,s)\mathsf{a}(s)ds + \int_a^t \left[\int_0^s \dot{\mathsf{f}}(u,s)\mathsf{a}(u)du\right] ds\end{aligned} \tag{A.30}$$

where all integrals are mean square integrals. Substituting (A.27) and (A.30) into (A.26) and reordering terms yields

$$\begin{aligned}I(t) = &\int_0^a \mathsf{f}(s,a)\mathsf{a}(s)ds + \int_0^a \mathsf{f}(s,a)dw(s) + \int_a^t \left(\int_0^s \dot{\mathsf{f}}(u,s)\mathsf{a}(u)du\right) ds \\ &+ \int_a^t \left(\int_0^s \dot{\mathsf{f}}(u,s)dw(u)\right) ds + \int_a^t \mathsf{f}(s,s)\mathsf{a}(s)ds + \int_a^t \mathsf{f}(s,s)dw(s)\end{aligned}$$

$$= I(a) + \int_a^t \left(\int_0^s \dot{\mathsf{f}}(u,s)\mathsf{a}(u)du + \int_0^s \dot{\mathsf{f}}(u,s)dw(u) \right) ds$$
$$+ \int_a^t \mathsf{f}(s,s)\mathsf{a}(s)ds + \int_a^t \mathsf{f}(s,s)dw(s) \qquad \text{(A.31)}$$

Since $\dot{\mathsf{f}}(s,t)$ is continuous on $\mathcal{R}'_{ab}$ and $\mathsf{a}(s)$ is mean square continuous, by Lemma A.3 $\dot{\mathsf{f}}(s,t)\mathsf{a}(s)$ is a mean square continuous second order process. Hence $\int_0^s \dot{\mathsf{f}}(u,s)\mathsf{a}(u)du$ defined as a mean square integral coincides with $\int_0^s \dot{\mathsf{f}}(u,s)\mathsf{a}(u)du$ defined as the integral of the sample functions [210, p. 186]. Furthermore by Lemma A.5 $\int_0^s \dot{\mathsf{f}}(u,s)\mathsf{a}(u)du$ is mean square continuous and hence mean square integrable. Therefore the mean square integral $\int_a^t \left[\int_0^s \dot{\mathsf{f}}(u,s)\mathsf{a}(u)du\right] ds$ can also be defined as a Lebesgue integral of sample functions [210, p. 186]. Similarly since $\mathsf{f}(s,s)$ is continuous and $\mathsf{a}(s)$ is mean square continuous, $\mathsf{f}(s,s)\mathsf{a}(s)$ is mean square continuous and $\int_a^t \mathsf{f}(s,s)\mathsf{a}(s)ds$ exists also as an integral of the sample functions and the sample and mean square integrals coincide. By definition (see (A.12)), (A.31) can also be written as (A.8). **Q.E.D**

Proof of Lemma A.3. The function $\mathsf{f}(s,t)$ is continuous on $\mathcal{R}'_{ab}$ which is a compact set of $\mathbb{R}^2$. Therefore its range is also a compact set of $\mathbb{R}^2$. But the compact sets of $\mathbb{R}^n$ are the sets of $\mathbb{R}^n$ that are closed and bounded. Hence $\mathsf{f}(s,t)$ is bounded on $\mathcal{R}'_{ab}$. Since $\mathsf{a}(s)$ is a second order mean square continuous process, $E[\mathsf{a}(s)\mathsf{a}(u)] < \infty$. Hence for each $t \in [a,b]$, $E|\mathsf{f}(s,t)\mathsf{a}(s)|^2 < \infty$ and $\mathsf{f}(s,t)\mathsf{a}(s)$ is a second order process.

$$E\left[|\mathsf{f}(s+h,t)\mathsf{a}(s+h) - \mathsf{f}(s,t)\mathsf{a}(s)|^2\right]$$
$$= |\mathsf{f}(s+h,t)|^2 E\left[|\mathsf{a}(s+h)|^2\right] + |\mathsf{f}(s,t)|^2 E\left[|\mathsf{a}(s)|^2\right] - 2\mathsf{f}(s,t)\mathsf{f}(s+h,t)E[\mathsf{a}(s)\mathsf{a}(s+h)]$$

Since $\mathsf{a}(s)$ is mean square continuous on $[0,t]$, $E[\mathsf{a}(s)\mathsf{a}(u)]$ is continuous on $[0,t]^2$. Furthermore $\mathsf{f}(s,t)$ is also continuous on $\mathcal{R}'_{ab}$, hence

$$\lim_{h\to 0} E\left[|\mathsf{f}(s+h,t)\mathsf{a}(s+h) - \mathsf{f}(s,t)\mathsf{a}(s)|^2\right] = 0$$

Q.E.D

Proof of Lemma A.4. (A.28) is equivalent to

$$\lim_{h\to 0} E\left|\frac{1}{h}\left[\int_0^{t+h} \mathsf{f}(s,t+h)\mathsf{a}(s)ds - \int_0^t \mathsf{f}(s,t)\mathsf{a}(s)ds\right] - \left(\mathsf{f}(t,t)\mathsf{a}(t) + \int_0^t \dot{\mathsf{f}}(s,t)\mathsf{a}(s)ds\right)\right|^2 = 0$$

Since $\mathsf{a}(s)$ is mean square continuous and $\dot{\mathsf{f}}(s,t)$ is continuous on $\mathcal{R}'_{ab}$, from Lemma A.3, for each $t \in [a,b]$, $\dot{\mathsf{f}}(s,t)\mathsf{a}(s)$ viewed as a process of s is mean square continuous. Hence the mean square integral $\int_0^t \dot{\mathsf{f}}(s,t)\mathsf{a}(s)ds$ exists [208, p. 67], [210, p. 186]. Since $\mathsf{f}(s,t)$ is defined only if $0 \leq s \leq t$, right and left mean square partial differentiability of $\int_0^t \mathsf{f}(s,t)\mathsf{a}(s)ds$ have to be considered separately. Let us first consider the right mean square partial differentiability. Let $h \geq 0$ such that $t+h \in [a,b]$. If $t = b$, only the left mean square differentiability has to be considered.

$$
\begin{aligned}
&E\left|\frac{1}{h}\left[\int_0^{t+h} \mathsf{f}(s,t+h)\mathsf{a}(s)ds - \int_0^t \mathsf{f}(s,t)\mathsf{a}(s)ds\right] - \left(\mathsf{f}(t,t)\mathsf{a}(t) + \int_0^t \dot{\mathsf{f}}(s,t)\mathsf{a}(s)ds\right)\right|^2 \\
&= E\left|I_2(h,t) + I_3(h,t)\right|^2 \quad \text{(expanding integrals and reordering terms)} \\
&\leq \left(\sqrt{E\left|I_2(h,t)\right|^2} + \sqrt{E\left|I_3(h,t)\right|^2}\right)^2 \quad \text{(Minkowski's inequality, } p = 2, \text{ [212, p. 33])}
\end{aligned}
$$

where $I_2(h,t)$ and $I_3(h,t)$ are defined as

$$
\begin{aligned}
I_2(h,t) &= \frac{1}{h}\int_t^{t+h} \mathsf{f}(s,t+h)\mathsf{a}(s)ds - \mathsf{f}(t,t)\mathsf{a}(t) \\
I_3(h,t) &= \int_0^t \left[\frac{\mathsf{f}(s,t+h) - \mathsf{f}(s,t)}{h} - \dot{\mathsf{f}}(s,t)\right]\mathsf{a}(s)ds
\end{aligned}
$$

$\mathsf{a}(s)$ is mean square continuous on $[0,b]$, hence the deterministic function of two variables $E\left[\mathsf{a}(s)\mathsf{a}(u)\right]$ is continuous on $[0,b]^2$. Furthermore $\mathsf{f}(s,t)$ is continuous on $\mathcal{R}'_{ab}$ hence $E\left|I_2(h,t)\right|^2$ is given by

$$
\begin{aligned}
E\left|I_2(h,t)\right|^2 = \frac{1}{h^2}\int_t^{t+h} \mathsf{f}(s,t+h)\left[\int_t^{t+h} \mathsf{f}(u,t+h)E\left[\mathsf{a}(s)\mathsf{a}(u)\right]du\right]ds \\
+ \mathsf{f}^2(t,t)E\left[\mathsf{a}^2(t)\right] - \frac{2}{h}\int_t^{t+h} \mathsf{f}(s,t+h)\mathsf{f}(t,t)E\left[\mathsf{a}(s)\mathsf{a}(t)\right]ds
\end{aligned}
$$

Since $\mathsf{f}(u,t)E\left[\mathsf{a}(s)\mathsf{a}(u)\right]$ is continuous in u, from the mean value theorem for integrals, $\exists\, \zeta(h,t), \nu(h,t) \in [t,t+h]$ such that

$$
\begin{aligned}
E\left|I_2(h,t)\right|^2 = \frac{1}{h^2}\int_t^{t+h} \mathsf{f}(s,t+h)\Big\{h\,\mathsf{f}(\zeta(h,t),t+h)E\left[\mathsf{a}(s)\mathsf{a}(\zeta(h,t))\right]\Big\}ds \\
+ \mathsf{f}^2(t,t)E\left[\mathsf{a}^2(t)\right] - \frac{2}{h}h\,\mathsf{f}(\nu(h,t),t+h)\mathsf{f}(t,t)E\left[\mathsf{a}(\nu(h,t))\mathsf{a}(t)\right]
\end{aligned}
$$

Since $\mathsf{f}(s,t+h)E[\mathsf{a}(s)\mathsf{a}(\zeta(h,t))]$ is continuous in s, from the mean value theorem for integrals, $\exists\,\epsilon(h,t)\in[t,t+h]$ such that

$$E\left|I_2(h,t)\right|^2=\frac{1}{h}h\,\mathsf{f}(\epsilon(h,t),t+h)\mathsf{f}(\zeta(h,t),t+h)E[\mathsf{a}(\epsilon(h,t))\mathsf{a}(\zeta(h,t))]$$
$$+\mathsf{f}^2(t,t)E[\mathsf{a}^2(t)]-2\,\mathsf{f}(\nu(h,t),t+h)\mathsf{f}(t,t)E[\mathsf{a}(\nu(h,t))\mathsf{a}(t)]$$

Since $\lim_{\substack{h\to 0\\ h\geq 0}}\zeta(h,t)=\lim_{\substack{h\to 0\\ h\geq 0}}\nu(h,t)=\lim_{\substack{h\to 0\\ h\geq 0}}\epsilon(h,t)=t$ and $\mathsf{f}(u,r)$ and $E[\mathsf{a}(u)\mathsf{a}(r)]$ are respectively continuous on $\mathcal{R}'_{ab}$ and on $[0,b]^2$,

$$\forall\,t\in[a,b]\quad\lim_{\substack{h\to 0\\ h\geq 0}}E\left|I_2(h,t)\right|^2=0$$

Since $\mathsf{f}(s,t)$ and $\dot{\mathsf{f}}(s,t)$ are continuous on $\mathcal{R}'_{ab}$ and $E[\mathsf{a}(s)\mathsf{a}(u)]$ is continuous at $[0,b]^2$, $E\left|I_3(h,t)\right|^2$ is given by

$$E\left|I_3(h,t)\right|^2=\int_0^t\left(\frac{\mathsf{f}(s,t+h)-\mathsf{f}(s,t)}{h}-\dot{\mathsf{f}}(s,t)\right)$$
$$\cdot\left[\int_0^t\left(\frac{\mathsf{f}(u,t+h)-\mathsf{f}(u,t)}{h}-\dot{\mathsf{f}}(u,t)\right)E[\mathsf{a}(s)\mathsf{a}(u)]\,du\right]ds$$

From the mean value theorem, $\exists\,\eta(h,t)\in[t,t+h]$ such that

$$\frac{\mathsf{f}(s,t+h)-\mathsf{f}(s,t)}{h}-\dot{\mathsf{f}}(s,t)=\dot{\mathsf{f}}(s,\eta(h,t))-\dot{\mathsf{f}}(s,t)$$

Therefore since $\dot{\mathsf{f}}(s,t)$ is continuous on $\mathcal{R}'_{ab}$, $\dot{\mathsf{f}}(s,t)$ is bounded on $\mathcal{R}'_{ab}$ and hence so is $\frac{\mathsf{f}(s,t+h)-\mathsf{f}(s,t)}{h}-\dot{\mathsf{f}}(s,t)$. Since $\mathsf{a}(s)$ is a second order mean square continuous process, $E[\mathsf{a}(s)\mathsf{a}(u)]<\infty$. Furthermore for each $t\in[a,b]$, $\lim_{\substack{h\to 0\\ h\geq 0}}\dfrac{\mathsf{f}(s,t+h)-\mathsf{f}(s,t)}{h}-\dot{\mathsf{f}}(s,t)=0$, hence by the Lebesgue dominated convergence theorem

$$\lim_{h\to 0}E\left|I_3(h,t)\right|^2=0$$

Let us consider now the left mean square partial differentiability of $\int_0^t\mathsf{f}(s,t)\mathsf{a}(s)ds$. Let $h\leq 0$ such that $t+h\in[a,b]$. If $t=a$, only the right mean square differentiability has to be considered.

$$E\left|\frac{-1}{h}\left[\int_0^t \mathsf{f}(s,t)\mathsf{a}(s)ds - \int_0^{t+h} \mathsf{f}(s,t+h)\mathsf{a}(s)ds\right] - \left(\mathsf{f}(t,t)\mathsf{a}(t) + \int_0^t \dot{\mathsf{f}}(s,t)\mathsf{a}(s)ds\right)\right|^2$$
$$= E\left|I_2'(h,t) + I_3'(h,t)\right|^2 \quad \text{(expanding integrals and reordering terms)}$$
$$\leq \left(\sqrt{E\left|I_2'(h,t)\right|^2} + \sqrt{E\left|I_3'(h,t)\right|^2}\right)^2 \quad \text{(Minkowski's inequality, } p=2\text{)}$$

where $I_2'(h,t)$ and $I_3'(h,t)$ are defined as

$$I_2'(h,t) = \int_{t+h}^t \frac{\mathsf{f}(s,t)\mathsf{a}(s)}{-h}ds - \mathsf{f}(t,t)\mathsf{a}(t)$$
$$I_3'(h,t) = \int_0^{t+h} \frac{\mathsf{f}(s,t) - \mathsf{f}(s,t+h)}{-h}\mathsf{a}(s)ds - \int_0^t \dot{\mathsf{f}}(s,t)\mathsf{a}(s)ds \qquad \text{(A.32)}$$

Since $E\left[\mathsf{a}(s)\mathsf{a}(u)\right]$ is continuous on $[0,b]^2$ and $\mathsf{f}(s,t)$ is continuous on $\mathcal{R}_{ab}'$, $E\left|I_2'(h,t)\right|^2$ is given by

$$E\left|I_2'(h,t)\right|^2 = \frac{1}{h^2}\int_{t+h}^t \mathsf{f}(s,t)\left[\int_{t+h}^t \mathsf{f}(u,t)E\left[\mathsf{a}(s)\mathsf{a}(u)\right]du\right]ds$$
$$+ \mathsf{f}^2(t,t)E\left[\mathsf{a}^2(t)\right] + \frac{2}{h}\int_{t+h}^t \mathsf{f}(s,t)\mathsf{f}(t,t)E\left[\mathsf{a}(s)\mathsf{a}(t)\right]ds$$

Since $\mathsf{f}(u,t)E\left[\mathsf{a}(s)\mathsf{a}(u)\right]$ is continuous in u, from the mean value theorem for integrals, $\exists\zeta'(h,t), \nu'(h,t) \in [t+h,t]$ such that

$$E\left|I_2'(h,t)\right|^2 = \frac{1}{h^2}\int_{t+h}^t \mathsf{f}(s,t)\left\{-h\,\mathsf{f}(\zeta'(h,t),t)E\left[\mathsf{a}(s)\mathsf{a}(\zeta'(h,t))\right]\right\}ds$$
$$+ \mathsf{f}^2(t,t)E\left[\mathsf{a}^2(t)\right] - \frac{2}{h}h\,\mathsf{f}(\nu'(h,t),t)\mathsf{f}(t,t)E\left[\mathsf{a}(\nu'(h,t))\mathsf{a}(t)\right]$$

Since $\mathsf{f}(s,t)E\left[\mathsf{a}(s)\mathsf{a}(\zeta'(h,t))\right]$ is continuous in s, from the mean value theorem for integrals, $\exists\epsilon'(h,t) \in [t+h,t]$ such that

$$E\left|I_2'(h,t)\right|^2 = \frac{1}{h}h\,\mathsf{f}(\epsilon'(h,t),t)\mathsf{f}(\zeta'(h,t),t)E\left[\mathsf{a}(\epsilon'(h,t))\mathsf{a}(\zeta'(h,t))\right]$$
$$+ \mathsf{f}^2(t,t)E\left[\mathsf{a}^2(t)\right] - 2\,\mathsf{f}(\nu'(h,t),t)\mathsf{f}(t,t)E\left[\mathsf{a}(\nu'(h,t))\mathsf{a}(t)\right]$$

Since $\lim_{\substack{h\to 0\\ a-t\leq h\leq 0}} \zeta'(h,t) = \lim_{\substack{h\to 0\\ a-t\leq h\leq 0}} \nu'(h,t) = \lim_{\substack{h\to 0\\ a-t\leq h\leq 0}} \epsilon'(h,t) = t$ and $\mathsf{f}(u,r)$ and

$E[\mathsf{a}(u)\mathsf{a}(r)]$ are respectively continuous on $\mathcal{R}'_{ab}$ and on $[0,b]^2$,

$$\forall t \in [a,b] \quad \lim_{\substack{h\to 0 \\ a-t\le h\le 0}} E\left|I'_2(h,t)\right|^2 = 0$$

Expanding integrals and reordering terms in (A.32), $E\left|I'_3(h,t)\right|^2$ is also given by

$$\begin{aligned} E\left|I'_3(h,t)\right|^2 &= E\left|I'_4(h,t)+I'_5(h,t)\right|^2 \\ &\le \left(\sqrt{E\left|I'_4(h,t)\right|^2}+\sqrt{E\left|I'_5(h,t)\right|^2}\right)^2 \quad \text{(Minkowski's inequality, } p=2\text{)} \end{aligned}$$

where $I'_4(h,t)$ and $I'_5(h,t)$ are given by

$$\begin{aligned} I'_4(h,t) &= \int_0^{t+h}\left[\frac{\mathsf{f}(s,t)-\mathsf{f}(s,t+h)}{-h}-\dot{\mathsf{f}}(s,t)\right]\mathsf{a}(s)ds \\ I'_5(h,t) &= \int_{t+h}^{t}\dot{\mathsf{f}}(s,t)\mathsf{a}(s)ds \end{aligned} \tag{A.33}$$

Since $\mathsf{f}(s,t)$ and $\dot{\mathsf{f}}(s,t)$ are continuous on $\mathcal{R}'_{ab}$ and $E[\mathsf{a}(s)\mathsf{a}(u)]$ is continuous at $[0,b]^2$, $E\left|I'_4(h,t)\right|^2$ is given by

$$\begin{aligned} E\left|I'_4(h,t)\right|^2 = \int_0^{t+h}&\left(\frac{\mathsf{f}(s,t)-\mathsf{f}(s,t+h)}{-h}-\dot{\mathsf{f}}(s,t)\right) \\ &\cdot\left[\int_0^{t+h}\left(\frac{\mathsf{f}(u,t)-\mathsf{f}(u,t+h)}{-h}-\dot{\mathsf{f}}(u,t)\right)E[\mathsf{a}(s)\mathsf{a}(u)]\,du\right]ds \end{aligned}$$

Let $t\in[a,b]$ be fixed. Define the function $F(s,x)$ on the closed domain $\mathcal{R}'_t$ described by (A.17) as $F(s,x)=\left(\frac{\mathsf{f}(s,t)-\mathsf{f}(s,x)}{-h}-\dot{\mathsf{f}}(s,t)\right)\int_0^x G(u,s,x)du$, where $G(u,s,x)=\left(\frac{\mathsf{f}(u,t)-\mathsf{f}(u,x)}{-h}-\dot{\mathsf{f}}(u,t)\right)E[\mathsf{a}(s)\mathsf{a}(u)]$ is defined on the closed domain $\mathcal{R}''$ described by

$$\mathcal{R}'' = \left\{(u,s,x)\in\mathbb{R}^3;\quad 0\le u\le x\quad 0\le s\le x\quad 0\le x\le t\right\} \tag{A.34}$$

such that $E\left|I'_4(h,t)\right|^2=\int_0^{t+h}F(s,t+h)ds$. Since $\mathsf{f}(s,t)$ and $\dot{\mathsf{f}}(s,t)$ are continuous on $\mathcal{R}'_{ab}$ and $E[\mathsf{a}(s)\mathsf{a}(u)]$ is continuous on $[0,t]^2$, $G(u,s,x)$ is continuous on $\mathcal{R}''$, then for

$(s,x) \in \mathcal{R}'_t$ $\int_0^x G(u,s,x)du$ is a continuous function of (s,x) [192, pp. 228-234]. Hence since $\mathsf{f}(s,t)$ and $\dot{\mathsf{f}}(s,t)$ are continuous on $\mathcal{R}'_{ab}$ and $E[\mathsf{a}(s)\mathsf{a}(u)]$ is continuous on $[0,t]^2$, $F(s,x)$ is continuous on $\mathcal{R}'_t$ and $\int_0^x F(s,x)ds$ is a continuous function of x on $[0,t]$. Therefore

$$\lim_{\substack{h\to 0 \\ a-t\le h\le 0}} E\left|I'_4(h,t)\right|^2 = \int_0^t F(s,t)ds = 0$$

since $F(s,t) = 0$ as seen in the following. Since $F(s,x)$ is continuous in x

$$F(s,t) \triangleq \lim_{\substack{h\to 0 \\ a-t\le h\le 0}} \left\{\left(\frac{\mathsf{f}(s,t)-\mathsf{f}(s,t+h)}{-h} - \dot{\mathsf{f}}(s,t)\right)\right\} \lim_{\substack{h\to 0 \\ a-t\le h\le 0}} \left\{\int_0^{t+h} G(u,s,t+h)du\right\}$$

Since $\int_0^x G(u,s,x)du$ is continuous in (s,x) and $G(u,s,x)$ is continuous at (u,s,t),

$$\lim_{\substack{h\to 0 \\ a-t\le h\le 0}} \left\{\int_0^{t+h} G(u,s,t+h)du\right\} = \int_0^t G(u,s,t)du$$
$$= \int_0^t \lim_{\substack{h\to 0 \\ a-t\le h\le 0}} \left(\frac{\mathsf{f}(u,t)-\mathsf{f}(u,t+h)}{-h} - \dot{\mathsf{f}}(u,t)\right) E[\mathsf{a}(s)\mathsf{a}(u)]\,du = 0$$

From (A.33) since $E[\mathsf{a}(s)\mathsf{a}(u)]$ is continuous on $[0,b]^2$ and $\dot{\mathsf{f}}(s,t)$ is continuous on $\mathcal{R}'_{ab}$

$$E\left|I'_5(h,t)\right|^2 = \int_{t+h}^t \dot{\mathsf{f}}(s,t)\left[\int_{t+h}^t \dot{\mathsf{f}}(u,t)E[\mathsf{a}(s)\mathsf{a}(u)]\,du\right]ds$$

From the mean value theorem for integrals, $\exists\,\eta'(h,t) \in [t+h,t]$ such that

$$E\left|I'_5(h,t)\right|^2 = \int_{t+h}^t \dot{\mathsf{f}}(s,t)(-h)\dot{\mathsf{f}}\left(\eta'(h,t),t\right)E\left[\mathsf{a}(s)\mathsf{a}\left(\eta'(h,t)\right)\right]ds$$

Since $\dot{\mathsf{f}}(s,t)E\left[\mathsf{a}(s)\mathsf{a}\left(\eta'(h,t)\right)\right]$ is continuous in s, $\exists\,\gamma'(h,t) \in [t+h,t]$ such that

$$E\left|I'_5(h,t)\right|^2 = h^2\dot{\mathsf{f}}\left(\gamma'(h,t),t\right)\dot{\mathsf{f}}\left(\eta'(h,t),t\right)E\left[\mathsf{a}\left(\gamma'(h,t)\right)\mathsf{a}\left(\eta'(h,t)\right)\right]$$

Therefore since $\dot{\mathsf{f}}(s,t)$ is continuous on $\mathcal{R}'_{ab}$, $E[\mathsf{a}(s)\mathsf{a}(u)]$ is continuous on $[0,b]^2$ and

$$\lim_{\substack{h\to 0\\ a-t\le h\le 0}} \eta'(h,t) = \lim_{\substack{h\to 0\\ a-t\le h\le 0}} \gamma'(h,t) = t,$$

$$\lim_{\substack{h\to 0\\ a-t\le h\le 0}} E\left|I_5'(h,t)\right|^2 = 0 \tag{A.35}$$

Q.E.D

Proof of Lemma A.5. Similarly to the proof of Lemma A.3, it can be shown that $\mathsf{f}(t,t)\mathsf{a}(t)$ is mean square continuous on $[a,b]$ since $\mathsf{f}(s,t)$ is continuous on $\mathcal{R}'_{ab}$ and $\mathsf{a}(s)$ is mean square continuous on $[0,b]$. Let us first consider the right mean square continuity of $\int_0^t \dot{\mathsf{f}}(s,t)\mathsf{a}(s)ds$. Let $h \ge 0$ such that $t+h \in [a,b]$. If $t=b$, only the left mean square continuity has to be considered.

$$E\left|\int_0^{t+h} \dot{\mathsf{f}}(s,t+h)\mathsf{a}(s)ds - \int_0^t \dot{\mathsf{f}}(s,t)\mathsf{a}(s)ds\right|^2 = E\left|I_4(h,t)+I_5(h,t)\right|^2$$
$$\le \left(\sqrt{E\left|I_4(h,t)\right|^2} + \sqrt{E\left|I_5(h,t)\right|^2}\right)^2 \quad \text{(Minkowski's inequality, } p=2\text{)}$$

where $E\left|I_4(h,t)\right|^2$ and $E\left|I_5(h,t)\right|^2$ are given by

$$E\left|I_4(h,t)\right|^2 = E\left|\int_t^{t+h} \dot{\mathsf{f}}(s,t+h)\mathsf{a}(s)ds\right|^2$$
$$= \int_t^{t+h} \dot{\mathsf{f}}(s,t+h)\left[\int_t^{t+h} \dot{\mathsf{f}}(u,t+h)E\left[\mathsf{a}(s)\mathsf{a}(u)\right]du\right]ds$$
$$E\left|I_5(h,t)\right|^2 = E\left|\int_0^t \left(\dot{\mathsf{f}}(s,t+h)-\dot{\mathsf{f}}(s,t)\right)\mathsf{a}(s)ds\right|^2$$
$$= \int_0^t \left(\dot{\mathsf{f}}(s,t+h)-\dot{\mathsf{f}}(s,t)\right)\left[\int_0^t \left(\dot{\mathsf{f}}(u,t+h)-\dot{\mathsf{f}}(u,t)\right)E\left[\mathsf{a}(s)\mathsf{a}(u)\right]du\right]ds$$

Since $\dot{\mathsf{f}}(s,t)$ is continuous on $\mathcal{R}'_{ab}$ and $E\left[\mathsf{a}(s)\mathsf{a}(u)\right]$ is continuous on $[0,b]^2$, using the mean value theorem for integrals twice

$$\lim_{\substack{h\to 0\\ h\ge 0}} E\left|I_4(h,t)\right|^2 = 0$$

Due to its continuity, $\dot{\mathsf{f}}(s,t)$ is bounded on $\mathcal{R}'_{ab}$. $E\left[\mathsf{a}(s)\mathsf{a}(u)\right]$ is continuous on $[0,b]^2$ hence is bounded on $[0,b]^2$. Furthermore $\lim_{\substack{h\to 0\\ h\ge 0}} \dot{\mathsf{f}}(u,t+h)-\dot{\mathsf{f}}(u,t)=0$, hence

$$\lim_{\substack{h\to 0\\ h\geq 0}} E\left|I_5(h,t)\right|^2 = 0 \quad \text{(Lebesgue dominated convergence theorem)}$$

Let us consider now the left mean square continuity. Let $h \leq 0$ such that $t+h \in [a,b]$. If $t = a$, only the right mean square continuity has to be considered.

$$E\left|\int_0^t \dot{\mathsf{f}}(s,t)\mathsf{a}(s)ds - \int_0^{t+h} \dot{\mathsf{f}}(s,t+h)\mathsf{a}(s)ds\right|^2 = E\left|I_5'(h,t) + I_6'(h,t)\right|^2$$
$$\leq \left(\sqrt{E\left|I_5'(h,t)\right|^2} + \sqrt{E\left|I_6'(h,t)\right|^2}\right)^2 \quad \text{(Minkowski's inequality, } p=2\text{)}$$

where $I_5'(h,t)$ is given by (A.33) and $E\left|I_6'(h,t)\right|^2$ is given by

$$E\left|I_6'(h,t)\right|^2 = E\left|\int_0^{t+h}\left(\dot{\mathsf{f}}(s,t) - \dot{\mathsf{f}}(s,t+h)\right)\mathsf{a}(s)ds\right|^2$$
$$= \int_0^{t+h}\left(\dot{\mathsf{f}}(s,t) - \dot{\mathsf{f}}(s,t+h)\right)\left[\int_0^{t+h}\left(\dot{\mathsf{f}}(u,t) - \dot{\mathsf{f}}(u,t+h)\right)E\left[\mathsf{a}(s)\mathsf{a}(u)\right]du\right]ds$$

Define the function $F(s,x)$ on the closed domain $\mathcal{R}_t'$ described by (A.17) as $F(s,x) = \left(\dot{\mathsf{f}}(s,t) - \dot{\mathsf{f}}(s,x)\right)\int_0^x G(u,s,x)du$ such that $E\left|I_6'(h,t)\right|^2 = \int_0^{t+h} F(s,t+h)ds$, where $G(u,s,x) = \left(\dot{\mathsf{f}}(u,t) - \dot{\mathsf{f}}(u,x)\right)E\left[\mathsf{a}(s)\mathsf{a}(u)\right]$ is defined on the closed domain $\mathcal{R}''$ described by (A.34). Since $\dot{\mathsf{f}}(s,t)$ is continuous on $\mathcal{R}_{ab}'$ and $E\left[\mathsf{a}(s)\mathsf{a}(u)\right]$ is continuous on $[0,t]^2$, $G(u,s,x)$ is continuous on $\mathcal{R}''$, then for $(s,x) \in \mathcal{R}_t'$ $\int_0^x G(u,s,x)du$ is a continuous function of (s,x) [192, pp. 228-234]. Hence since $\dot{\mathsf{f}}(s,t)$ is continuous on $\mathcal{R}_{ab}'$ and $E\left[\mathsf{a}(s)\mathsf{a}(u)\right]$ is continuous on $[0,t]^2$, $F(s,x)$ is continuous on $\mathcal{R}_t'$ and $\int_0^x F(s,x)ds$ is a continuous function of x on $[0,t]$. Therefore similarly to the proof of $\lim_{\substack{h\to 0\\ a-t\leq h\leq 0}} E\left|I_4'(h,t)\right|^2$, $F(s,t) = 0$ and

$$\lim_{\substack{h\to 0\\ a-t\leq h\leq 0}} E\left|I_6'(h,t)\right|^2 = \int_0^t F(s,t)ds = 0$$

Furthermore from (A.35), $\lim_{\substack{h\to 0\\ a-t\leq h\leq 0}} E\left|I_5'(h,t)\right|^2 = 0$. Hence $\int_0^t \dot{\mathsf{f}}(s,t)\mathsf{a}(s)ds$ is mean square continuous and from (A.28), $\frac{\partial}{\partial t}\left\{\int_0^t \mathsf{f}(s,t)\mathsf{a}(s)ds\right\}$ is mean square continuous as a sum of two mean square continuous processes. **Q.E.D**

Appendix B

Receiver Structures

B.1 Linear independency of time-shifted signals

Let $n \in \mathbb{N}$ be fixed. This appendix considers the conditions under which a set of time-shifted signals $\mathsf{f}(s-\tau_0)$, $\mathsf{f}(s-\tau_1)$, $\ldots$, $\mathsf{f}(s-\tau_{n-1})$ is linearly independent over an observation interval $\mathcal{I}$. Long observation intervals of the form $[u,t]((u,t) \in \mathbb{R})$, intermediate and short observation intervals of the form $[0,t]$ $(t>0)$, as defined in Definition 3.1.1, will be considered.

B.1.1 Linear independency of n different time-shifted versions of a square integrable signal over a "long" observation interval

Theorem B.1. *Consider a square integrable complex function* $\mathsf{f}(s)$ *with* $\int_{-\infty}^{\infty}|\mathsf{f}(s)|^2 ds \neq 0$. *Let* $[u,t]$ *be a "long" observation interval as defined in Definition 3.1.1. Then the set of* n *different time-shifted versions of the signal:* $\mathsf{f}(s-\tau_0), \mathsf{f}(s-\tau_2), \ldots, \mathsf{f}(s-\tau_{n-1})$ *is linearly independent on* $[u,t]$.

Proof. The proof is by contradiction. Suppose that there exists $[\mathsf{a}_0, \ldots, \mathsf{a}_{n-1}] \neq [0, \ldots, 0]$ such that

$$\mathsf{f}_a(s) \triangleq \sum_{k=0}^{n-1} \mathsf{a}_k \mathsf{f}(s-\tau_k) = 0 \qquad \forall\, s \in [u,t] \tag{B.1}$$

Since $\mathsf{f}(s)$ is square integrable, it has a Fourier transform (denoted as $\mathsf{F}(f)$). The interval $[u,t]$ being "long" in the sense of Definition 3.1.1, it follows that $\mathsf{f}_a(\cdot)$ vanishes everywhere and its Fourier transform $\mathsf{F}_a(f)$, almost everywhere. Taking the Fourier

transform on both sides of (B.1) yields

$$\mathsf{F}_a(f) = H(j2\pi f)\mathsf{F}(f) = 0 \qquad \forall f \in \mathbb{R}$$

where

$$H(z) = \sum_{k=0}^{n-1} \mathsf{a}_k e^{-z\tau_k}$$

But $H(\cdot)$ is entire, and therefore possesses at most finitely many zeros in any bounded region of the plane [175, p.225] (Theorem 10.18). So one is forced to conclude that $\mathsf{F}(\cdot)$ itself must vanish almost everywhere, violating the requirement that f has non-zero energy [215, p.194]. **Q.E.D**

B.1.2 Linear independency of n different time-shifted versions of a continuous signal, time-limited to $[0,T]$, over an arbitrary observation interval of the form $[0,t]$, $t > 0$

Theorem B.2. *Let $\mathsf{f}(s)$ be a continuous complex function on $\mathbb{R}$, time-limited to $[0,T]$ (i.e. $\mathsf{f}(s) = 0$ for $s \notin [0,T]$) with $\tilde{E} = \int_0^T |\mathsf{f}(s)|^2\, ds \neq 0$. Let $\{\tau_k\}_{k=0,\ldots,n-1}$ be n distinct delays sorted in increasing order ($\tau_0 < \tau_1 < \ldots$), where n is an arbitrary non-zero integer. Consider the interval $[0,t]$ with $t > 0$. Let the scalar T' and the staircase t-function i_t be defined as follows:*

$$T' = \sup_v \left\{ v \in \mathbb{R},\ \int_{-\infty}^{v} |\mathsf{f}(s)|^2\, ds = 0 \right\} \tag{B.2}$$

$$i_t = \begin{cases} 0, & 0 \le t \le T' + \tau_0 \\ k, & T' + \tau_{k-1} < t \le T' + \tau_k \\ n, & t > T' + \tau_{n-1} \end{cases} \tag{B.3}$$

An example of the graph of the function i_t is illustrated in Fig. B.1 for $n = 3$.

If $0 \le t \le T' + \tau_0$, the time-shifted versions of the signal, $\left(\{\mathsf{f}(s-\tau_k)\}_{k=0,\ldots,n-1}\right)$, vanish on $[0,t]$.

If $t > T' + \tau_0$, then $i_t \ge 1$. Since $\forall k \ge i_t$, $\forall s \in [0,t]$, $\mathsf{f}(s-\tau_k) = 0$, over $[0,t]$ any functional of the signals $\mathsf{f}(s-\tau_0), \ldots, \mathsf{f}(s-\tau_{n-1})$ reduces to a functional of the signals $\mathsf{f}(s-\tau_0), \ldots, \mathsf{f}(s-\tau_{i_t-1})$ only. Furthermore the signals $\mathsf{f}(s-\tau_0)$, $\mathsf{f}(s-\tau_1), \ldots, \mathsf{f}(s-$

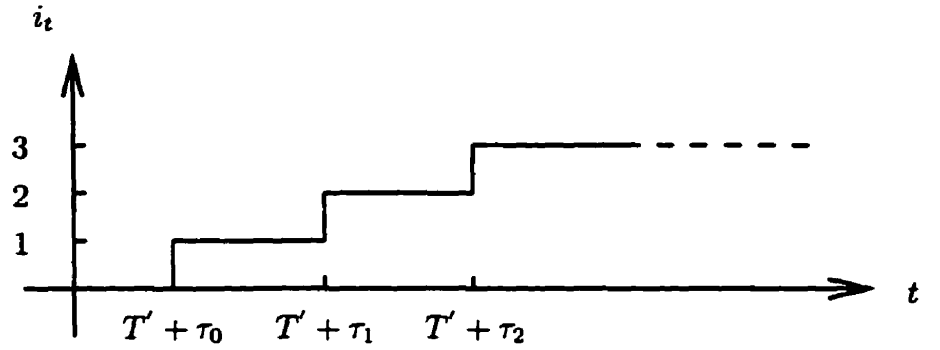

Fig. B.1 Graph of the function i_t with $n = 3$, corresponding for example to a 3-path channel

τ_{i_t-1}) *are linearly independent on* $[0,t]$. *Hence if* $t > T' + \tau_{n-1}$, *the signals* $\mathrm{f}(s-\tau_0)$, $\mathrm{f}(s-\tau_1),\ldots,\mathrm{f}(s-\tau_{n-1})$ *are linearly independent on* $[0,t]$.

Note that T' represents the "initial time" of a waveform. For example if $\mathrm{f}(s) = \sin(6\pi\frac{s-T-T_p}{T_p})\mathrm{rect}\left(\frac{s-\frac{2T-T_p}{2}}{T_p}\right)$, $T' = T - T_p$. For the continuous approximations of FSK, DPSK and SDPSK modulations defined in Section 4.2.1, $T' = 0$. To prove Theorem B.2, the following lemmas are needed.

Lemma B.1. *Let* $\mathrm{f}(s)$ *satisfy the assumptions of Theorem B.2.*

Define the set $\mathcal{A}$ *as* $\mathcal{A} = \left\{v \in [0,T],\ \int_0^v |\mathrm{f}(s)|^2\,ds = 0\right\}$ *then* $\mathcal{A} = [0,T']$

Define the set $\mathcal{B}$ *as* $\mathcal{B} = \left\{v \in [0,\infty),\ \int_0^v |\mathrm{f}(s)|^2\,ds = \tilde{E}\right\}$ *then* $\mathcal{B} = [T'',\infty)$

where T' *is defined as (B.2) and* T'' *is defined as*

$$T'' = \inf_v \left\{v \in \mathbb{R},\ \int_{-\infty}^v |\mathrm{f}(s)|^2\,ds = \tilde{E}\right\} \tag{B.4}$$

Proof of Lemma B.1. Define $\epsilon'(v) = \frac{1}{\tilde{E}}\int_{-\infty}^v |\mathrm{f}(s)|^2\,ds$. Let us first show that $\mathcal{A}$ is a connected subset of $\mathbb{R}$. $\mathcal{A}$ is non-empty since $0 \in \mathcal{A}$. Assume that $\mathcal{A}$ is not connected, then $\exists\, V_1, V_2$ open sets in $\mathbb{R}$ such that

$$\mathcal{A} \subseteq V_1 \cup V_2 \qquad \mathcal{A} \cap V_1 \cap V_2 = \emptyset \qquad \mathcal{A} \not\subseteq V_1 \ \ \& \ \ \mathcal{A} \not\subseteq V_2$$

$\mathcal{A} \not\subseteq V_1$, then $\exists v_2 \in V_2 \cap \mathcal{A}$ such that $v_2 \notin V_1$. Similarly $\exists v_1 \in V_1 \cap \mathcal{A}$ such that $v_1 \notin V_2$. For $k = 1, 2$, $v_k \in \mathcal{A}$ so $\epsilon'(v_k) = 0$. Let us assume without loss of generality that $v_1 < v_2$, then $\forall v \in [v_1, v_2]$, $0 \leq \epsilon'(v) \leq \epsilon'(v_2) = 0$, hence $\epsilon'(v) = 0$. Therefore the interval $[v_1, v_2] \subseteq \mathcal{A}$. Furthermore

$$[v_1, v_2] \subseteq V_1 \cup V_2 \quad (\text{since } [v_1, v_2] \subseteq \mathcal{A})$$
$$[v_1, v_2] \cap V_1 \cap V_2 \subseteq A \cap V_1 \cap V_2 = \emptyset \qquad \Longrightarrow [v_1, v_2] \cap V_1 \cap V_2 = \emptyset$$

Hence since the interval $[v_1, v_2]$ is connected, either $[v_1, v_2] \subseteq V_1$ or $[v_1, v_2] \subseteq V_2$, which contradicts either that $v_1 \notin V_2$ or $v_2 \notin V_1$. Therefore $\mathcal{A}$ is a connected subset of $\mathbb{R}$.

Let us show now that $\mathcal{A}$ is a closed set of $\mathbb{R}$. Let $\{v_n\}$ be a sequence of elements of $\mathcal{A}$ converging to v in $\mathbb{R}$. Since $|\mathrm{f}(s)|^2$ is continuous on $\mathbb{R}$, the function $\epsilon'(v)$ is continuous on $\mathbb{R}$. Therefore $\lim_{n\to\infty} \epsilon'(v_n) = \epsilon'(v)$, but $\forall n \in N$, $\epsilon'(v_n) = 0$ since $v_n \in \mathcal{A}$, hence $\lim_{n\to\infty} \epsilon'(v_n) = 0$. Therefore $\epsilon'(v) = 0$ and $v \in \mathcal{A}$. This is true for any sequence $\{v_n\}$ so $\mathcal{A}$ is closed.

$\mathcal{A}$ is a non-empty connected subset of $\mathbb{R}$, therefore $\mathcal{A}$ is an interval, i.e. $\mathcal{A} = [a, b]$, $a \leq b$ (it is the only closed interval type). Clearly $0 \leq a \leq b \leq T$ since $\mathcal{A} \subseteq [0, T]$, $0 \in \mathcal{A}$ so $a = 0$. Let $v \in \mathcal{A}$, then $v \leq b$, so b is an upper-bound for $\mathcal{A}$, therefore $T' \leq b$ as lowest upper-bound of $\mathcal{A}$ (see (B.2)). Since $b \in \mathcal{A}$, $b \leq T'$ hence $b = T'$.

Similarly, it can be shown that $\mathcal{B}$ is also a non-empty connected subset of $\mathbb{R}$. Hence $\mathcal{B}$ is an interval, i.e. $\mathcal{B} = (a, b), [a, b), (a, b], [a, b]$, $a \leq b$ where a or b can be ∞. Clearly $0 \leq a \leq b$ since $\mathcal{B} \subseteq [0, \infty)$. Let $v \in \mathcal{B}$, then $v \geq a$, so a is a lower-bound for $\mathcal{B}$, and $T'' \geq a$ as greatest lower-bound of $\mathcal{B}$ (see (B.4)). Since $a \in \mathcal{B}$, $a \geq T''$ hence $a = T''$. Since $\forall s \notin [0, T]\, \mathrm{f}(s) = 0$, $\forall v \geq T$, $\epsilon'(v) = 1$ so $[T, \infty) \subseteq \mathcal{B}$, hence $b = \infty$. **Q.E.D**

Lemma B.2. *Let* $\mathrm{f}(s)$ *satisfy the assumptions of Theorem B.2.*

1. *If* $0 \leq t \leq T' + \tau_r$, *then* $\forall k \geq r \quad \forall s \in [0, t] \quad \mathrm{f}(s - \tau_k) = 0$
2. *If* $t > T' + \tau_r$ *then* $\exists a_r(t), b_r(t) \in \left(T' + \tau_r, t\right], a_r(t) < b_r(t)$ *such that* $\forall s \in (a_r(t), b_r(t)) \quad \mathrm{f}(s - \tau_r) \neq 0$

Proof of Lemma B.2. Let $r \in \{0, \ldots, n-1\}$

1. Let $t \in [\tau_r, T' + \tau_r]$ then from Lemma B.1 $t - \tau_r \in \mathcal{A}$. Furthermore $\mathrm{f}(s)$ is

time-limited to $[0,T]$, therefore

$$\int_0^t |\mathsf{f}(s-\tau_r)|^2\,ds = \int_{-\tau_r}^{t-\tau_r} |\mathsf{f}(u)|^2\,du = \int_0^{t-\tau_r} |\mathsf{f}(u)|^2\,du = 0 \quad \text{(from Lemma B.1)}$$

Let $t \in [0,\tau_r)$, then $t-\tau_r < 0$ and since $\mathsf{f}(s)$ is time-limited to $[0,T]$, $\int_0^t |\mathsf{f}(s-\tau_r)|^2\,ds = 0$. Therefore if $t \in \left[0, T^{'}+\tau_r\right]$ $\mathsf{f}(s-\tau_r)$ is the "zero" function in the Hilbert space of continuous function on $[0,t]$ which is equivalent to

$$\forall r = 0,\ldots,n-1 \quad \text{if } 0 \le t \le T^{'}+\tau_r \text{ then} \qquad \forall s \in [0,t] \quad \mathsf{f}(s-\tau_r) = 0 \qquad \text{(B.5)}$$

Since $0 \le t \le T^{'}+\tau_r \implies \forall k \ge r,\ 0 \le t \le T^{'}+\tau_k$, applying result (B.5) for the index k completes the proof of '*1.*'.

2. $t > T^{'}+\tau_r \implies t-\tau_r > T^{'} \implies t-\tau_r \notin \mathcal{A} \implies t-\tau_r \notin [0,T]$ or $\{t-\tau_r \in [0,T]$ and $\epsilon^{'}(t-\tau_r) \neq 0\}$ where $\epsilon^{'}(t) = \left[\int_0^t |\mathsf{f}(s)|^2\,ds\right]/\tilde{E}$. Let us assume that $t-\tau_r \notin [0,T]$, since $t-\tau_r > T^{'} \ge 0$ it means that $t-\tau_r \in (T,\infty)$, but then $\epsilon^{'}(t-\tau_r) \ge \epsilon^{'}(T) > 0$, so in all cases $\epsilon^{'}(t-\tau_r) \neq 0$. Since $\mathsf{f}(s-\tau_r)$ is continuous on $\mathbb{R}$, from the mean value theorem for integrals $\exists\, b_r(t) \in \left(T^{'}+\tau_r, t\right)$ such that

$$\left(t-T^{'}-\tau_r\right)\left|\mathsf{f}\left(b_r(t)-\tau_r\right)\right|^2 = \int_{T^{'}+\tau_r}^{t} |\mathsf{f}(s-\tau_r)|^2\,ds = \int_{T^{'}}^{t-\tau_r} |\mathsf{f}(s)|^2\,ds = \epsilon^{'}(t-\tau_r)\tilde{E} \neq 0$$

Hence $\mathsf{f}\left(b_r(t)-\tau_r\right) \neq 0$. Furthermore continuity of $\mathsf{f}(s-\tau_r)$ also implies that $\exists\,\delta > 0$ such that $\forall\, s \in (b_r(t)-\delta, b_r(t)+\delta)$, $\mathsf{f}(s-\tau_r) \neq 0$. Define $a_r(t) = b_r(t)-\delta$. **Q.E.D**

Proof of Theorem B.2. From '*1.*' of Lemma B.2

$$0 \le t \le T^{'}+\tau_0 \implies \forall\, k = 0,\ldots,n-1 \quad \forall\, s \in [0,t] \quad \mathsf{f}(s-\tau_k) = 0$$

If $t > T^{'}+\tau_0$, $\exists\, i_t \in \{1,\ldots,n\}$ illustrated in Fig. B.1 such that $T^{'}+\tau_{i_t-1} < t \le T^{'}+\tau_{i_t}$ (with the convention that $T^{'}+\tau_n = \infty$) since the delays τ_k are all distinct and ordered. From '*1.*' of Lemma B.2

$$T^{'}+\tau_{i_t-1} < t \le T^{'}+\tau_{i_t} \implies \forall\, k \ge i_t \quad \forall\, s \in [0,t] \quad \mathsf{f}(s-\tau_k) = 0$$

hence over $[0,t]$ any functional of the signals $\mathsf{f}(s-\tau_0),\ldots,\mathsf{f}(s-\tau_{n-1})$ reduces to a functional of the signals $\mathsf{f}(s-\tau_0),\ldots,\mathsf{f}(s-\tau_{i_t-1})$ only. Let us consider $\{\mathsf{a}_k\}_{k=0,\ldots,i_t-1}$

such that

$$\forall s \in [0,t] \quad \sum_{k=0}^{i_t-1} \mathsf{a}_k \mathsf{f}(s-\tau_k) = 0 \tag{B.6}$$

Recall that $t \in \left(T' + \tau_{i_t-1}, T' + \tau_{i_t}\right]$, the observation interval $[0,t]$ can be written as

$$[0,t] = \bigcup_{k=0}^{i_t} \mathcal{I}_k \quad \text{where} \quad \begin{cases} \mathcal{I}_0 &= \left[0, T' + \tau_0\right] \\ \mathcal{I}_k &= \left(T' + \tau_{k-1}, T' + \tau_k\right] \quad k = 1, \ldots i_t - 1 \\ \mathcal{I}_{i_t} &= \left(T' + \tau_{i_t-1}, t\right] \end{cases}$$

From '*1.*' of Lemma B.2 with $t = T' + \tau_1$, $\forall s \in \mathcal{I}_1 \quad \forall k \geq 1 \ \mathsf{f}(s-\tau_k) = 0$ and on $\mathcal{I}_1$ (B.6) reduces to

$$\forall s \in \mathcal{I}_1 \quad \mathsf{a}_0 \mathsf{f}(s-\tau_0) = 0$$

From '*2.*' of Lemma B.2 with $t = T' + \tau_1$, $\exists\, a_0(t), b_0(t) \in \mathcal{I}_1$, $a_0(t) < b_0(t)$ such that

$$\forall s \in \left(a_0(t), b_0(t)\right) \subseteq \mathcal{I}_1 \quad \mathsf{f}(s-\tau_0) \neq 0$$

hence choosing $s_0 \in \left(a_0(t), b_0(t)\right)$ yields $\mathsf{a}_0 = 0$ since $\mathsf{f}(s_0 - \tau_0) \neq 0$. Substituting $\mathsf{a}_0 = 0$ into (B.6) yields the new equation

$$\forall s \in [0,t] \quad \sum_{k=1}^{i_t-1} \mathsf{a}_k \mathsf{f}(s-\tau_k) = 0 \tag{B.7}$$

Doing the same steps with $\mathcal{I}_2$ (i.e. applying Lemma B.2 with $t = T' + \tau_2$) using (B.7) yields $\mathsf{a}_1 = 0$. Such iteration can be applied successively to each interval $\mathcal{I}_k$, $k = 1, \ldots, i_t$ starting from $k = 1$, yielding $\mathsf{a}_{k-1} = 0$. Hence the signals $\mathsf{f}(s-\tau_0)$, $\mathsf{f}(s-\tau_1)$, ... $\mathsf{f}(s-\tau_{i_t-1})$ are linearly independent on $[0,t]$. If $T > T' + \tau_{n-1}$, from (B.3) $i_t = n$ hence $\mathsf{f}(s-\tau_0), \ldots, \mathsf{f}(s-\tau_{n-1})$ are linearly independent on $[0,t]$. **Q.E.D**

B.2 Eigenvalues and eigenfunctions of the signal process covariance functions $K_m(s,u)$ and $\mathcal{K}_m(s,u)$ assuming L-order linear independency

B.2.1 Expressions of $K_m(s,u)$ and $\mathcal{K}_m(s,u)$

The signal process $v_m(s)$ can be expressed in terms of its complex envelope as $v_m(s) = \frac{1}{2}\left[\tilde{v}_m(s)e^{j\omega_c s} + \tilde{v}_m^*(s)e^{-j\omega_c s}\right]$, where $\tilde{v}_m(s) = \sum_{k=0}^{L-1} a_k e^{j\theta_k}\tilde{s}_m(s-\tau_k)$. Therefore its covariance function under H_m, when $\boldsymbol{\theta}$ is held fixed, is given by

$$\begin{aligned}
K_m(s,u) &\triangleq E\Big[\big(v_m(s) - E\left[v_m(s)|\boldsymbol{\theta}\right]\big)\big(v_m(u) - E\left[v_m(u)|\boldsymbol{\theta}\right]\big)|\boldsymbol{\theta}\Big] \\
&= \frac{1}{4}\Big\{E\Big[\big(\tilde{v}_m(s) - E\left[\tilde{v}_m(s)|\boldsymbol{\theta}\right]\big)\big(\tilde{v}_m(u) - E\left[\tilde{v}_m(u)|\boldsymbol{\theta}\right]\big)|\boldsymbol{\theta}\Big]e^{j\omega_c(s+u)} \\
&\quad + E\Big[\big(\tilde{v}_m(s) - E\left[\tilde{v}_m(s)|\boldsymbol{\theta}\right]\big)\big(\tilde{v}_m(u) - E\left[\tilde{v}_m(u)|\boldsymbol{\theta}\right]\big)^*|\boldsymbol{\theta}\Big]e^{j\omega_c(s-u)} \\
&\quad + E\Big[\big(\tilde{v}_m(s) - E\left[\tilde{v}_m(s)|\boldsymbol{\theta}\right]\big)^*\big(\tilde{v}_m(u) - E\left[\tilde{v}_m(u)|\boldsymbol{\theta}\right]\big)|\boldsymbol{\theta}\Big]e^{-j\omega_c(s-u)} \\
&\quad + E\Big[\big(\tilde{v}_m(s) - E\left[\tilde{v}_m(s)|\boldsymbol{\theta}\right]\big)^*\big(\tilde{v}_m(u) - E\left[\tilde{v}_m(u)|\boldsymbol{\theta}\right]\big)^*|\boldsymbol{\theta}\Big]e^{-j\omega_c(s+u)}\Big\}
\end{aligned}$$

Since a_k are circularly complex Gaussian uncorrelated random variables, when $\boldsymbol{\theta}$ is held fixed, $\tilde{v}_m(s)$ is a circularly complex Gaussian random process. Therefore $E\left[\left(\tilde{v}_m(s) - E\left[\tilde{v}_m(s)|\boldsymbol{\theta}\right]\right)\left(\tilde{v}_m(u) - E\left[\tilde{v}_m(u)|\boldsymbol{\theta}\right]\right)|\boldsymbol{\theta}\right] = 0$ and $K_m(s,u)$ reduces to (3.5).

B.2.2 Eigenvalues and eigenfunctions of $\mathcal{K}_m(s,u)$

The eigenfunctions $\{\phi_{lm}(s)\}_{l=0,\ldots,\infty}$ of $\mathcal{K}_m(s,u)$ are solutions of the integral equation

$$\lambda_m\phi_m(s) = \int_0^{T_o}\mathcal{K}_m(s,u)\phi_m(u)du \qquad 0 \le s \le T_o \tag{B.8}$$

where from (3.6) $\mathcal{K}_m(s,u)$ is given by

$$\mathcal{K}_m(s,u) = \sum_{k=0}^{L-1} 2\sigma_k^2\tilde{s}_m(s-\tau_k)\tilde{s}_m^*(u-\tau_k) \qquad 0 \le s,u \le T_o \tag{B.9}$$

If $\lambda_m = 0$, (B.8) reduces to

$$\sum_{k=0}^{L-1} 2\sigma_k^2 \tilde{s}_m(s-\tau_k)\left[\int_0^{T_o} \tilde{s}_m^*(u-\tau_k)\phi_m(u)du\right] = 0 \qquad 0 \le s \le T_o \tag{B.10}$$

Since the signals $\tilde{s}_m(s-\tau_0), \ldots, \tilde{s}_m(s-\tau_{L-1})$ are linearly independent over $[0, T_o]$ (L-order linear independency assumption), (B.10) implies

$$\forall\, k = 0, \ldots, L-1 \qquad 2\sigma_k^2 \int_0^{T_o} \tilde{s}_m^*(u-\tau_k)\phi_m(u)du = 0$$

The eigenfunctions associated with zero eigenvalues are the functions that are orthogonal to $\{\tilde{s}_m^*(u-\tau_k)\}_{k=0,\ldots,L-1}$ over $[0, T_o]$. Hence if $\lambda_m = 0$, the projection of the signal process $v_m(s)$ on $\phi_m(s)$ is zero. Moreover, for detection in white noise, the projection of the received signal only on the signal space is used in the decision rule [216]. Therefore the eigenfunctions associated with zero eigenvalues are irrelevant. Since $\mathcal{K}_m(s,u)$ given by (B.9) is a finite dimensional kernel, the eigenfunctions associated with non-zero eigenvalues will be a linear combination of $\tilde{s}_m(s-\tau_0), \tilde{s}_m(s-\tau_1), \ldots, \tilde{s}_m(s-\tau_{L-1})$ [184, p. 56]. For convenience the eigenfunctions $\{\phi_{lm}(s)\}_{l=0,\ldots,\infty}$ are defined as

$$\phi_{lm}(s) = \frac{1}{\sqrt{\tilde{E}_m}} \sum_{r=0}^{L-1} \frac{x_{lr}^m}{\sqrt{\epsilon_{rm}}} \tilde{s}_m(s-\tau_r) \qquad 0 \le s \le T_o \tag{B.11}$$

and $\boldsymbol{x}_l^m = [x_{l0}^m, x_{l1}^m, \ldots, x_{lL-1}^m]^T$. Substituting (B.11) into (B.8) and equating the coefficients of $\tilde{s}_m(s-\tau_k)$ due to their linear independency gives (omitting the index l) $\lambda_m x_k^m = \tilde{E}_m \sum_{r=0}^{L-1} 2\sigma_k^2 \epsilon_{km} (\rho_{kr}^m)^* x_r^m$. Then the solution of (B.8) may be put into matrix form similar to Matthew [103], i.e. λ_m and $\boldsymbol{x}^m$ are solution of the algebraic system

$$\lambda_m \boldsymbol{x}^m = \tilde{E}_m \boldsymbol{\epsilon}_m \boldsymbol{C} \boldsymbol{\Gamma}_m^* \boldsymbol{x}^m \tag{B.12}$$

Moreover as shown in [184, p. 57], there is a complete equivalence between the integral equation (B.8) and the algebraic system (B.12) which is a classical eigenvalue problem. It is seen that the non-zero eigenvalues in the Karhunen-Loève expansion for $\tilde{v}_m(s)$ are the eigenvalues of the finite dimensional matrix $\tilde{E}_m \boldsymbol{\epsilon}_m \boldsymbol{C} \boldsymbol{\Gamma}_m^*$.

Although the matrices $\boldsymbol{\epsilon}_m \boldsymbol{C}$ and $\boldsymbol{\Gamma}_m$ are Hermitian, their product is not in general Hermitian. However, provided that at least one of them is positive definite, the

product has eigenvalues that have the same characteristics as eigenvalues of Hermitian matrices [217, p. 232]. The matrix $\tilde{E}_m \boldsymbol{\epsilon}_m^{1/2} \boldsymbol{\Gamma}_m \boldsymbol{\epsilon}_m^{1/2}$ is the Grammian for the L_2 inner product. Since the signals $\tilde{s}_m(s-\tau_0), \ldots, \tilde{s}_m(s-\tau_{L-1})$ are linearly independent, $\tilde{E}_m \boldsymbol{\epsilon}_m^{1/2} \boldsymbol{\Gamma}_m \boldsymbol{\epsilon}_m^{1/2}$ is positive definite Hermitian [217, p. 74]. Since $\boldsymbol{\epsilon}_m^{1/2}$ is a diagonal matrix with positive diagonal entries, it is invertible and positive definite. Furthermore $\boldsymbol{\epsilon}_m^{1/2} \boldsymbol{\Gamma}_m \boldsymbol{\epsilon}_m^{1/2}$ is positive definite. Therefore it can be easily shown that $\boldsymbol{\Gamma}_m$ is also positive definite. The covariance matrix of the channel $\boldsymbol{C}$ is diagonal with positive diagonal entries (equal to $2\sigma_k^2$), thus $\boldsymbol{C}$ is Hermitian positive definite.

Since $\boldsymbol{\epsilon}_m \boldsymbol{C}$ and $\boldsymbol{\Gamma}_m^*$ are both Hermitian positive definite, $\boldsymbol{\epsilon}_m \boldsymbol{C} \boldsymbol{\Gamma}_m^*$ has L real positive eigenvalues and L corresponding linearly independent eigenvectors [217, p. 232]. Let $\boldsymbol{D}_m$ denote the diagonal matrix with $[\boldsymbol{D}_m]_{ll} = \lambda_{lm}/\tilde{E}_m$ and let us define the matrix $\boldsymbol{X}_m$ as $[\boldsymbol{X}_m]_{lr} = x_{lr}^m$, then (B.12) is equivalent to

$$\boldsymbol{\epsilon}_m \boldsymbol{C} \boldsymbol{\Gamma}_m^* \boldsymbol{X}_m^T = \boldsymbol{X}_m^T \boldsymbol{D}_m \tag{B.13}$$

Because of the equivalence of the integral equation and the algebraic system, the eigenfunctions will be uniquely determined by the solutions $\boldsymbol{x}^m$ of (B.12) which are exactly the eigenvectors of the matrix $\tilde{E}_m \boldsymbol{\epsilon}_m \boldsymbol{C} \boldsymbol{\Gamma}_m^*$. Since $\boldsymbol{\Gamma}_m^*$ is positive definite, the eigenvalue problem (B.12) is equivalent to the generalized eigenvalue problem $\frac{\lambda_m}{\tilde{E}_m} (\boldsymbol{\Gamma}_m^*)^{-1} \boldsymbol{x}' = \boldsymbol{\epsilon}_m \boldsymbol{C} \boldsymbol{x}'$ where $\boldsymbol{x}' = \boldsymbol{\Gamma}_m^* \boldsymbol{x}^m$. From [217, p. 231], it is known that this generalized eigenvalue problem has L linearly independent eigenvectors that can be chosen to be orthogonal (or orthonormal) in the inner product defined by $(\boldsymbol{\Gamma}_m^*)^{-1}$. Therefore $\boldsymbol{x}_0', \boldsymbol{x}_1', \ldots, \boldsymbol{x}_{L-1}'$ can be chosen such that $(\boldsymbol{x}_l')^\dagger (\boldsymbol{\Gamma}_m^*)^{-1} \boldsymbol{x}_p' = \delta_{lp}$. Equivalently $\boldsymbol{x}_0^m, \boldsymbol{x}_1^m, \ldots, \boldsymbol{x}_{L-1}^m$ can be chosen such that $\boldsymbol{x}_l^{m\dagger} \boldsymbol{\Gamma}_m^* \boldsymbol{x}_p^m = \delta_{lp}$. In conclusion, the eigenvectors can be chosen to be orthonormal in the inner product defined by $\boldsymbol{\Gamma}_m^*$. It can be easily shown that this choice of eigenvectors yields orthonormal eigenfunctions. Furthermore one can show that this is equivalent to

$$\boldsymbol{X}_m^* \boldsymbol{\Gamma}_m^* \boldsymbol{X}_m^T = \boldsymbol{I} \tag{B.14}$$

B.2.3 Eigenvalues and eigenfunctions of $K_m(s,u)$

Since $K_m(s,u) = \Re\left\{\frac{1}{2} \mathcal{K}_m(s,u) e^{j\omega_c(s-u)}\right\}$, the eigenvalues and eigenfunctions of $K_m(s,u)$ can be expressed in terms of the eigenvalues and eigenfunctions of $\mathcal{K}_m(s,u)$ as shown in the following. Let us write $\Upsilon_m(s) = \Re(\phi_m(s) \exp\{j(\omega_c s + \mathsf{p})\})$ where p is an arbi-

trary number between 0 and 2π. Substituting into $\kappa_m \Upsilon_m(s) = \int_0^{T_o} K_m(s,u)\Upsilon_m(u)du$ and using $K_m(s,u) = \Re\left\{\frac{1}{2}\mathcal{K}_m(s,u)e^{j\omega_c(s-u)}\right\}$ yields

$$\begin{aligned}
&\kappa_m \Re\left\{\phi_m(s)e^{j(\omega_c s+\mathsf{p})}\right\} \\
&= \frac{1}{8}\int_0^{T_o}\left[\mathcal{K}_m(s,u)e^{j\omega_c(s-u)} + \mathcal{K}_m^*(s,u)e^{-j\omega_c(s-u)}\right]\cdot\left[\phi_m(u)e^{j(\omega_c u+\mathsf{p})} + \phi_m^*(u)e^{-j(\omega_c u+\mathsf{p})}\right]du \\
&= \frac{1}{8}\left\{e^{j(\omega_c s+\mathsf{p})}\int_0^{T_o}\mathcal{K}_m(s,u)\phi_m(u)du + e^{-j(\omega_c s+\mathsf{p})}\int_0^{T_o}\mathcal{K}_m^*(s,u)\phi_m^*(u)du\right\} \\
&\quad + \frac{1}{4}\Re\left\{e^{-j(\omega_c s-\mathsf{p})}\int_0^{T_o}\mathcal{K}_m^*(s,u)\phi_m(u)e^{2j\omega_c u}du\right\} \qquad \text{(B.15)}
\end{aligned}$$

Under each hypothesis H_m, the signal process $s_m(s)$ is narrow-band, thus its complex envelope $\tilde{s}_m(s)$ is slowly varying in s with respect to ω_c. Hence $\mathcal{K}_m^*(s,u)$ is slowly varying in s and u with respect to ω_c. This also implies that its eigenfunctions are slowly varying with respect to ω_c. Therefore the last term in (B.15) can be neglected, yielding

$$\begin{aligned}
\kappa_m \Re\left\{\phi_m(s)e^{j(\omega_c s+\mathsf{p})}\right\} &= \Re\left\{\frac{1}{4}e^{j(\omega_c s+\mathsf{p})}\int_0^{T_o}\mathcal{K}_m(s,u)\phi_m(u)du\right\} \\
\Re\left\{\kappa_m\phi_m(s)e^{j(\omega_c s+\mathsf{p})}\right\} &= \Re\left\{\frac{\lambda_m}{4}\phi_m(s)e^{j(\omega_c s+\mathsf{p})}\right\} \qquad \text{(B.16)}
\end{aligned}$$

If $\kappa_m = \frac{\lambda_m}{4}$ is required then (B.16) will be satisfied for any p. Therefore to each eigenvalue and eigenfunction of the complex process corresponds an eigenvalue and a family of eigenfunctions of the bandpass process (i.e. $\Upsilon_m(s) = \Re\left\{\phi_m(s)e^{j(\omega_c s+\mathsf{p})}\right\}_{\mathsf{p}=0,\ldots,2\pi}$). In fact only two of these can be linearly independent. By choosing $\mathsf{p} = 0$ and $\mathsf{p} = -\frac{\pi}{2}$, assuming that $\phi_{lm}(s)$ are orthonormal, the $2L$ orthonormal eigenfunctions and $2L$ eigenvalues of the bandpass signal are given by

$$\Upsilon_{lm}(s) = \Re(\sqrt{2}\phi_{lm}(s)e^{j\omega_c s}) \qquad l=0,\ldots,L-1 \qquad \text{eigenvalue: } \kappa_{lm} = \frac{\lambda_{lm}}{4} \qquad \text{(B.17a)}$$

$$\Upsilon_{lm}(s) = \Im(\sqrt{2}\phi_{l-Lm}(s)e^{j\omega_c s}) \qquad l=L,\ldots,2L-1 \qquad \text{eigenvalue: } \kappa_{lm} = \frac{\lambda_{l-Lm}}{4} \qquad \text{(B.17b)}$$

B.3 Derivation of non-coherent receiver structures assuming L-order linear independency

B.3.1 Likelihood ratio for an L-path Ricean channel

Conditional log-likelihood ratio

Recall that for detection in white noise, the projection of the received signal only on the signal space is used in the decision rule. As seen in Appendix B.2, the dimensionality of the signal space is $2L$. Let $\boldsymbol{z}_m$ be an $2L$-dimensional vector whose components are the projections of $\dot{z}(s)$ on the eigenfunctions $\{\Upsilon_{lm}(s)\}_{l=0,\ldots,2L-1}$ associated with the covariance function of the bandpass signal process $v_m(s)$, i.e.

$$[\boldsymbol{z}_m]_l = \int_0^{T_o} \Upsilon_{lm}(s)dz(s) \qquad l = 0,\ldots,2L-1 \tag{B.18}$$

where the integral in (B.18) is a Wiener integral (see Appendix A.1) and $\Upsilon_{lm}(s)$ is given by (B.17). Since $\forall\, r = 0,\ldots,L-1$, $\tilde{s}_m(s-\tau_r)$ is continuous on $[0,T_o]$, from (B.11) and (B.17), $\phi_{lm}(s)$ and $\Upsilon_{lm}(s)$ are also continuous on $[0,T_o]$. Therefore $\phi_{lm}(s)$, $\Upsilon_{lm}(s)$, $\Re\{\tilde{s}_m(s-\tau_l)e^{j\omega_c s}\}$, $\Im\{\tilde{s}_m(s-\tau_l)e^{j\omega_c s}\}$ are bounded [177, p. 72] and consequently square integrable. Furthermore from (3.2)

$$\begin{aligned}
&\int_0^{T_o} |\Upsilon_{lm}(s)|\, E\,|v_m(s)|\, ds \\
&\leq \sum_{k=0}^{L-1} E\,|a_k| \int_0^{T_o} |\Upsilon_{lm}(s)| \left[\left|\Re\left\{\tilde{s}_m(s-\tau_k)e^{j\omega_c s}\right\}\right| + \left|\Im\left\{\tilde{s}_m(s-\tau_k)e^{j\omega_c s}\right\}\right| ds\right] \\
&\leq \sum_{k=0}^{L-1} E\,|a_k| \left(\int_0^{T_o} |\Upsilon_{lm}(s)|^2\, ds\right)^{1/2} \left[\left(\int_0^{T_o} \left|\Re\left\{\tilde{s}_m(s-\tau_k)e^{j\omega_c s}\right\}\right|^2 ds\right)^{1/2}\right. \\
&\quad \left. + \left(\int_0^{T_o} \left|\Im\left\{\tilde{s}_m(s-\tau_k)e^{j\omega_c s}\right\}\right|^2 ds\right)^{1/2}\right] < \infty \quad \text{(Cauchy's Schwarz inequality)}
\end{aligned}$$

Therefore from Appendix A.1.2, the Wiener integral in (B.18) is well defined ($\Upsilon_{lm}(s)$ is square integrable and $\int_0^{T_o} |\Upsilon_{lm}(s)|\, E\,|v_m(s)|\, ds < \infty$).

Conditioned on $\boldsymbol{\theta}$, under each hypothesis, including H_0, $\dot{z}(s)$ is a Gaussian random process. Therefore $\boldsymbol{z}_m$ forms a Gaussian random vector [172, pp. 383-384]. From [187,

p. 98] and [170] the conditional likelihood ratio given $\boldsymbol{\theta}$ is found to be

$$\Lambda_m(\dot{z}; T_o|\boldsymbol{\theta}) = \Lambda_m(\boldsymbol{z}_m|\boldsymbol{\theta}) = \frac{|\boldsymbol{\Sigma}_0|^{1/2} \exp\left\{-\frac{1}{2}(\boldsymbol{z}_m - \boldsymbol{\nu}_m)^\dagger \boldsymbol{\Sigma}_m^{-1}(\boldsymbol{z}_m - \boldsymbol{\nu}_m)\right\}}{|\boldsymbol{\Sigma}_m|^{1/2} \exp\left\{-\frac{1}{2}\boldsymbol{z}_m^\dagger \boldsymbol{\Sigma}_0^{-1} \boldsymbol{z}_m\right\}} \tag{B.19}$$

The covariance matrices $\boldsymbol{\Sigma}_0$ and $\boldsymbol{\Sigma}_m$ are given by

$$\begin{aligned}
\boldsymbol{\Sigma}_0 &= E\left[\boldsymbol{z}_m \boldsymbol{z}_m^\dagger | H_0\right] = \frac{N_0}{2} \boldsymbol{I}_{2L} \\
\boldsymbol{\Sigma}_m &= E\left[(\boldsymbol{z}_m - \boldsymbol{\nu}_m)(\boldsymbol{z}_m - \boldsymbol{\nu}_m)^\dagger | \boldsymbol{\theta}, H_m\right] = \begin{pmatrix} \frac{N_0}{2}\boldsymbol{I} + \frac{\tilde{E}_m}{4}\boldsymbol{D}_m & 0 \\ 0 & \frac{N_0}{2}\boldsymbol{I} + \frac{\tilde{E}_m}{4}\boldsymbol{D}_m \end{pmatrix}
\end{aligned} \tag{B.20}$$

where $\boldsymbol{I}_{2L}$ denotes the $2L \times 2L$ identity matrix, and $\boldsymbol{\nu}_m$ is the mean of $\boldsymbol{z}_m$ when $\boldsymbol{\theta}$ is held fixed. The mean of the bandpass signal process under H_m given $\boldsymbol{\theta}$, $\nu_m(s, \boldsymbol{\theta})$, is

$$\nu_m(s, \boldsymbol{\theta}) \triangleq E[v_m(s)|\boldsymbol{\theta}] = \Re\left\{\left[\sum_{k=0}^{L-1} \alpha_k e^{j\theta_k} \tilde{s}_m(s - \tau_k)\right] e^{j\omega_c s}\right\} \triangleq \Re\left\{\mu_m(s, \boldsymbol{\theta}) e^{j\omega_c s}\right\} \tag{B.21}$$

where $\mu_m(s, \boldsymbol{\theta}) \triangleq E\left[\tilde{v}_m(s)|\boldsymbol{\theta}\right] = \sum_{k=0}^{L-1} \alpha_k e^{j\theta_k} \tilde{s}_m(s - \tau_k)$.

Expression of $\boldsymbol{\nu}_m$

From (B.18),

$$[\boldsymbol{\nu}_m]_l \triangleq E\Big[[\boldsymbol{z}_m]_l \,\Big|\boldsymbol{\theta}\Big] = \int_0^{T_o} \nu_m(s, \boldsymbol{\theta}) \Upsilon_{lm}(s) ds \qquad l = 0, \ldots, 2L-1 \tag{B.22}$$

Substituting (B.17) and (B.21) into (B.22) yields

$$[\boldsymbol{\nu}_m]_l = \int_0^{T_o} \Re\left\{\mu_m(s, \boldsymbol{\theta}) e^{j\omega_c s}\right\} \Re\left\{\sqrt{2}\phi_{lm}(s) e^{j\omega_c s}\right\} ds \qquad l = 0, \ldots, L-1 \tag{B.23a}$$

$$= \int_0^{T_o} \Re\left\{\mu_m(s, \boldsymbol{\theta}) e^{j\omega_c s}\right\} \Im\left\{\sqrt{2}\phi_{l-Lm}(s) e^{j\omega_c s}\right\} ds \quad l = L, \ldots, 2L-1 \tag{B.23b}$$

Since $\tilde{s}_m(s)$ is slowly varying with respect to ω_c, $\mu_m(s, \boldsymbol{\theta})$ is also slowly varying with respect to ω_c. As seen in Appendix B.2.3, $\phi_{lm}(s)$ is slowly varying with respect to

ω_c. Therefore from Lemma C.1, integrals containing double frequency terms can be neglected in (B.23) yielding

$$\begin{aligned}[\boldsymbol{\nu}_m]_l &= \frac{1}{\sqrt{2}}\Re\left\{\int_0^{T_o}\mu_m(s,\boldsymbol{\theta})\phi_{lm}^*(s)ds\right\} \qquad l=0,\ldots,L-1\\ &= \frac{-1}{\sqrt{2}}\Im\left\{\int_0^{T_o}\mu_m(s,\boldsymbol{\theta})\phi_{l-Lm}^*(s)ds\right\} \qquad l=L,\ldots,2L-1\end{aligned}$$

Let us define the vector $\boldsymbol{\mu}_m$ such that $[\boldsymbol{\mu}_m]_l \triangleq \int_0^{T_o}\mu_m(s,\boldsymbol{\theta})\phi_{lm}^*(s)ds$, then

$$\boldsymbol{\nu}_m = \frac{1}{\sqrt{2}}\begin{pmatrix}\Re\{\boldsymbol{\mu}_m\}\\ -\Im\{\boldsymbol{\mu}_m\}\end{pmatrix} \tag{B.24}$$

Let us simplify $\boldsymbol{\mu}_m$. From (B.11) and $\mu_m(s,\boldsymbol{\theta}) = \sum_{k=0}^{L-1}\alpha_k e^{j\theta_k}\tilde{s}_m(s-\tau_k)$

$$\begin{aligned}[\boldsymbol{\mu}_m]_l &= \int_0^{T_o}\sum_{k=0}^{L-1}\alpha_k e^{j\theta_k}\tilde{s}_m(s-\tau_k)\frac{1}{\sqrt{\tilde{E}_m}}\sum_{r=0}^{L-1}\frac{(x_{lr}^m)^*}{\sqrt{\epsilon_{rm}}}\tilde{s}_m^*(s-\tau_r)ds\\ &= \sqrt{\tilde{E}_m}\sum_{k=0}^{L-1}\left[\sum_{r=0}^{L-1}x_{lr}^m\sqrt{\epsilon_{km}}\rho_{rk}^m\right]^*\alpha_k e^{j\theta_k}\\ \boldsymbol{\mu}_m &= \sqrt{\tilde{E}_m}\boldsymbol{X}_m^*\boldsymbol{\Gamma}_m^*\boldsymbol{\epsilon}_m^{1/2}\boldsymbol{\varrho}(\boldsymbol{\theta})\end{aligned} \tag{B.25}$$

where $\boldsymbol{\varrho}(\boldsymbol{\theta}) = \left[\alpha_0 e^{j\theta_0},\ldots,\alpha_{L-1}e^{j\theta_{L-1}}\right]$ and $\boldsymbol{\epsilon}_m^{1/2}$ is a diagonal matrix with k^{th} diagonal entry equal to $\sqrt{\epsilon_{km}}$.

Conditional log-likelihood ratio

The conditional log-likelihood ratio (B.19) is given by

$$\begin{aligned}&\ln\left[\Lambda_m(\dot{z};T_o|\boldsymbol{\theta})\right]\\ &\quad= \ln\left(\frac{|\boldsymbol{\Sigma}_0|^{1/2}}{|\boldsymbol{\Sigma}_m|^{1/2}}\right)+\frac{1}{2}\left[\boldsymbol{z}_m^\dagger\left(\boldsymbol{\Sigma}_0^{-1}-\boldsymbol{\Sigma}_m^{-1}\right)\boldsymbol{z}_m+\boldsymbol{\nu}_m^\dagger\boldsymbol{\Sigma}_m^{-1}\boldsymbol{z}_m+\boldsymbol{z}_m^\dagger\boldsymbol{\Sigma}_m^{-1}\boldsymbol{\nu}_m-\boldsymbol{\nu}_m^\dagger\boldsymbol{\Sigma}_m^{-1}\boldsymbol{\nu}_m\right]\end{aligned}$$

For convenience let us define $\boldsymbol{r}_m$ as

$$[\boldsymbol{r}_m]_l \triangleq \frac{2}{\sqrt{\tilde{E}_m}}\int_0^{T_o}\phi_{lm}^*(s)e^{-j\omega_c s}dz(s) \qquad l=0,\ldots L-1 \tag{B.26}$$

where the integral is a Wiener integral of a complex function (see Appendix A.1.2). Similar to the proof for (B.18), it can be shown that $\phi_{lm}^*(s)e^{-j\omega_c s}$ is square integrable and $\int_0^t |\phi_{lm}^*(s)e^{-j\omega_c s}|\, E\, |v_m(s)|\, ds < \infty$. Therefore from Appendix A.1.2, the Wiener integral in (B.26) is well defined. Substituting (B.17) into (B.18) yields

$$\boldsymbol{z}_m = \sqrt{\frac{\tilde{E}_m}{2}} \begin{pmatrix} \Re\{\boldsymbol{r}_m\} \\ -\Im\{\boldsymbol{r}_m\} \end{pmatrix} \tag{B.27}$$

and also confirms that $\boldsymbol{r}_m$ is well defined. Let us denote

$$\boldsymbol{\Omega}_0 \triangleq N_0 \boldsymbol{I} \qquad = E\left[\frac{1}{2}\left(\sqrt{\tilde{E}_m}\boldsymbol{r}_m\right)\left(\sqrt{\tilde{E}_m}\boldsymbol{r}_m\right)^\dagger \Big| H_0\right] \tag{B.28a}$$

$$\boldsymbol{\Omega}_m \triangleq N_0 \boldsymbol{I} + \frac{\tilde{E}_m}{2}\boldsymbol{D}_m \qquad = E\left[\frac{1}{2}\left(\sqrt{\tilde{E}_m}\boldsymbol{r}_m - \boldsymbol{\mu}_m\right)\left(\sqrt{\tilde{E}_m}\boldsymbol{r}_m - \boldsymbol{\mu}_m\right)^\dagger \Big| \boldsymbol{\theta}, H_m\right] \tag{B.28b}$$

Note that $\boldsymbol{\mu}_m$ defined as $[\boldsymbol{\mu}_m]_l \triangleq \int_0^{T_o} \mu_m(s,\boldsymbol{\theta})\phi_{lm}^*(s)ds$ can be also viewed as the mean of $\sqrt{\tilde{E}_m}\boldsymbol{r}_m$ under H_m, given $\boldsymbol{\theta}$. From (B.20), (B.24) and (B.27)

$$\boldsymbol{z}_m^\dagger\left(\boldsymbol{\Sigma}_0^{-1} - \boldsymbol{\Sigma}_m^{-1}\right)\boldsymbol{z}_m = \tilde{E}_m \boldsymbol{r}_m^\dagger\left(\boldsymbol{\Omega}_0^{-1} - \boldsymbol{\Omega}_m^{-1}\right)\boldsymbol{r}_m$$

$$\boldsymbol{z}_m^\dagger \boldsymbol{\Sigma}_m^{-1}\boldsymbol{\nu}_m = \sqrt{\tilde{E}_m}\Re\left\{\boldsymbol{r}_m^\dagger \boldsymbol{\Omega}_m^{-1}\boldsymbol{\mu}_m\right\} = \frac{\sqrt{\tilde{E}_m}}{2}\left\{\boldsymbol{\mu}_m^\dagger \boldsymbol{\Omega}_m^{-1}\boldsymbol{r}_m + \boldsymbol{r}_m^\dagger \boldsymbol{\Omega}_m^{-1}\boldsymbol{\mu}_m\right\}$$

$$\boldsymbol{\nu}_m^\dagger \boldsymbol{\Sigma}_m^{-1}\boldsymbol{\nu}_m = \boldsymbol{\mu}_m^\dagger \boldsymbol{\Omega}_m^{-1}\boldsymbol{\mu}_m$$

where $\boldsymbol{\Omega}_m$ and $\boldsymbol{\Omega}_0$ are given by (B.28). Hence in terms of $\boldsymbol{r}_m$ and $\boldsymbol{\mu}_m$, the conditional log-likelihood ratio is given by

$$\ln \Lambda_m(\dot{z}; T_o|\boldsymbol{\theta}) = \ln\left(\frac{|\boldsymbol{\Omega}_0|}{|\boldsymbol{\Omega}_m|}\right) + \frac{\tilde{E}_m}{2}\boldsymbol{r}_m^\dagger\left(\boldsymbol{\Omega}_0^{-1} - \boldsymbol{\Omega}_m^{-1}\right)\boldsymbol{r}_m$$

$$+ \frac{\sqrt{\tilde{E}_m}}{2}\left\{\boldsymbol{\mu}_m^\dagger \boldsymbol{\Omega}_m^{-1}\boldsymbol{r}_m + \boldsymbol{r}_m^\dagger \boldsymbol{\Omega}_m^{-1}\boldsymbol{\mu}_m\right\} - \frac{1}{2}\boldsymbol{\mu}_m^\dagger \boldsymbol{\Omega}_m^{-1}\boldsymbol{\mu}_m \tag{B.29}$$

$$= \frac{\tilde{E}_m}{2}\left(\boldsymbol{r}_m + \left(\boldsymbol{\Omega}_0^{-1} - \boldsymbol{\Omega}_m^{-1}\right)^{-1}\boldsymbol{\Omega}_m^{-1}\frac{\boldsymbol{\mu}_m}{\sqrt{\tilde{E}_m}}\right)^{\dagger}\left(\boldsymbol{\Omega}_0^{-1} - \boldsymbol{\Omega}_m^{-1}\right)$$
$$\cdot\left(\boldsymbol{r}_m + \left(\boldsymbol{\Omega}_0^{-1} - \boldsymbol{\Omega}_m^{-1}\right)^{-1}\boldsymbol{\Omega}_m^{-1}\frac{\boldsymbol{\mu}_m}{\sqrt{\tilde{E}_m}}\right)$$
$$-\frac{1}{2}\boldsymbol{\mu}_m^{\dagger}\boldsymbol{\Omega}_m^{-1}\left(\boldsymbol{I} + \left(\boldsymbol{\Omega}_0^{-1} - \boldsymbol{\Omega}_m^{-1}\right)^{-1}\boldsymbol{\Omega}_m^{-1}\right)\boldsymbol{\mu}_m + \ln\left(\frac{|\boldsymbol{\Omega}_0|}{|\boldsymbol{\Omega}_m|}\right) \quad \text{(B.30)}$$

Substituting (B.28) into (B.30) and using (B.13-B.14) yields (3.10).

Likelihood ratio

The likelihood ratio $\Lambda_m(\dot{z};T_o)$ is obtained by integrating successively the conditional likelihood ratio $\Lambda_m(\dot{z};T_o|\boldsymbol{\theta})$ over all components of the vector $\boldsymbol{\theta}$ between $-\pi$ and π. To simplify the integration, it is convenient to isolate the terms inside the conditional likelihood ratio that are independent of $\boldsymbol{\theta}$ and write

$$\Lambda_m(\dot{z};T_o|\boldsymbol{\theta}) = J_m f_m(\boldsymbol{\theta}) \quad \text{(B.31)}$$

where $f_m(\boldsymbol{\theta})$ is the function that includes all factors involving $\boldsymbol{\theta}$ and J_m is everything left over. From (B.25), it is seen that the dependence on $\boldsymbol{\theta}$ of the conditional likelihood ratio is via the mean vector $\boldsymbol{\mu}_m$. From (B.29), it is seen that the mean is present in the terms $\boldsymbol{r}_m^{\dagger}\boldsymbol{\Omega}_m^{-1}\boldsymbol{\mu}_m$ and $\boldsymbol{\mu}_m^{\dagger}\boldsymbol{\Omega}_m^{-1}\boldsymbol{\mu}_m$. The second term is Hermitian, therefore it can be decomposed as a term dependent of $\boldsymbol{\theta}$ and a term independent of $\boldsymbol{\theta}$ as shown in the following. From (B.25)

$$\boldsymbol{\mu}_m^{\dagger}\boldsymbol{\Omega}_m^{-1}\boldsymbol{\mu}_m = \tilde{E}_m\boldsymbol{\varrho}^{\dagger}(\boldsymbol{\theta})\boldsymbol{B}\boldsymbol{\varrho}(\boldsymbol{\theta})$$

where $\boldsymbol{B} = \boldsymbol{\epsilon}_m^{1/2}\boldsymbol{\Gamma}_m^{*}\boldsymbol{X}_m^{T}\boldsymbol{\Omega}_m^{-1}\boldsymbol{X}_m^{*}\boldsymbol{\Gamma}_m^{*}\boldsymbol{\epsilon}_m^{1/2}$. Let us write $\boldsymbol{B}$ as the sum of a matrix composed of its diagonal elements $\{\boldsymbol{B}\}_d$, a matrix composed of its upper triangular elements $\{\boldsymbol{B}\}_u$ and a matrix composed of its lower triangular elements $\{\boldsymbol{B}\}_l$. Since $\boldsymbol{B}$ is Hermitian, $\{\boldsymbol{B}\}_u = \{\boldsymbol{B}\}_l^{\dagger}$. Therefore

$$\boldsymbol{\mu}_m^{\dagger}\boldsymbol{\Omega}_m^{-1}\boldsymbol{\mu}_m = \tilde{E}_m\Big[\boldsymbol{\varrho}^{\dagger}(\boldsymbol{\theta})\left\{\boldsymbol{\epsilon}_m^{1/2}\boldsymbol{\Gamma}_m^{*}\boldsymbol{X}_m^{T}\boldsymbol{\Omega}_m^{-1}\boldsymbol{X}_m^{*}\boldsymbol{\Gamma}_m^{*}\boldsymbol{\epsilon}_m^{1/2}\right\}_d\boldsymbol{\varrho}(\boldsymbol{\theta})$$
$$+2\Re\Big\{\boldsymbol{\varrho}^{\dagger}(\boldsymbol{\theta})\left\{\boldsymbol{\epsilon}_m^{1/2}\boldsymbol{\Gamma}_m^{*}\boldsymbol{X}_m^{T}\boldsymbol{\Omega}_m^{-1}\boldsymbol{X}_m^{*}\boldsymbol{\Gamma}_m^{*}\boldsymbol{\epsilon}_m^{1/2}\right\}_l\boldsymbol{\varrho}(\boldsymbol{\theta})\Big\}\Big]$$

where $\{\,\}_d$ and $\{\,\}_l$ are "matrix operators" defined in Section 3.1 and the real part, $\Re\{\cdot\}$, comes from interchanging the order of summation in $\boldsymbol{\varrho}^\dagger(\boldsymbol{\theta})\{\boldsymbol{B}\}_l^\dagger\boldsymbol{\varrho}(\boldsymbol{\theta})$ and grouping the terms $\boldsymbol{\varrho}^\dagger(\boldsymbol{\theta})\{\boldsymbol{B}\}_l\boldsymbol{\varrho}(\boldsymbol{\theta})$ and $\boldsymbol{\varrho}^\dagger(\boldsymbol{\theta})\{\boldsymbol{B}\}_l^\dagger\boldsymbol{\varrho}(\boldsymbol{\theta})$ together. Since $\{\boldsymbol{\epsilon}_m^{1/2}\boldsymbol{\Gamma}_m^*\boldsymbol{X}_m^T\boldsymbol{\Omega}_m^{-1}\boldsymbol{X}_m^*\boldsymbol{\Gamma}_m^*\boldsymbol{\epsilon}_m^{1/2}\}_d$ is diagonal, $\boldsymbol{\varrho}^\dagger(\boldsymbol{\theta})\{\boldsymbol{\epsilon}_m^{1/2}\boldsymbol{\Gamma}_m^*\boldsymbol{X}_m^T\boldsymbol{\Omega}_m^{-1}\boldsymbol{X}_m^*\boldsymbol{\Gamma}_m^*\boldsymbol{\epsilon}_m^{1/2}\}_d\boldsymbol{\varrho}(\boldsymbol{\theta})$ is independent of $\boldsymbol{\theta}$ and given by $\boldsymbol{\alpha}^\dagger\{\boldsymbol{\epsilon}_m^{1/2}\boldsymbol{\Gamma}_m^*\boldsymbol{X}_m^T\boldsymbol{\Omega}_m^{-1}\boldsymbol{X}_m^*\boldsymbol{\Gamma}_m^*\boldsymbol{\epsilon}_m^{1/2}\}_d\boldsymbol{\alpha}$, where $\boldsymbol{\alpha}$ is defined by (3.13). Hence from (B.29)

$$\ln J_m = \ln\left(\frac{|\boldsymbol{\Omega}_0|}{|\boldsymbol{\Omega}_m|}\right) - \frac{\tilde{E}_m}{2}\boldsymbol{r}_m^\dagger\left(\boldsymbol{\Omega}_m^{-1}-\boldsymbol{\Omega}_0^{-1}\right)\boldsymbol{r}_m - \frac{\tilde{E}_m}{2}\boldsymbol{\alpha}^\dagger\{\boldsymbol{\epsilon}_m^{1/2}\boldsymbol{\Gamma}_m^*\boldsymbol{X}_m^T\boldsymbol{\Omega}_m^{-1}\boldsymbol{X}_m^*\boldsymbol{\Gamma}_m^*\boldsymbol{\epsilon}_m^{1/2}\}_d\boldsymbol{\alpha} \tag{B.32}$$

$$\begin{aligned} f_m(\boldsymbol{\theta}) &= \exp\left[\frac{\sqrt{\tilde{E}_m}}{2}\{\boldsymbol{r}_m^\dagger\boldsymbol{\Omega}_m^{-1}\boldsymbol{\mu}_m + \boldsymbol{\mu}_m^\dagger\boldsymbol{\Omega}_m^{-1}\boldsymbol{r}_m\}\right. \\ &\qquad \left.-\tilde{E}_m\Re\left\{\boldsymbol{\varrho}^\dagger(\boldsymbol{\theta})\{\boldsymbol{\epsilon}_m^{1/2}\boldsymbol{\Gamma}_m^*\boldsymbol{X}_m^T\boldsymbol{\Omega}_m^{-1}\boldsymbol{X}_m^*\boldsymbol{\Gamma}_m^*\boldsymbol{\epsilon}_m^{1/2}\}_l\boldsymbol{\varrho}(\boldsymbol{\theta})\right\}\right] \qquad \text{(B.33)} \\ &= \exp\left[\tilde{E}_m\Re\left\{\boldsymbol{\varrho}^\dagger(\boldsymbol{\theta})\left[\boldsymbol{\epsilon}_m^{1/2}\boldsymbol{\Gamma}_m^*\boldsymbol{X}_m^T\boldsymbol{\Omega}_m^{-1}\boldsymbol{r}_m - \{\boldsymbol{\epsilon}_m^{1/2}\boldsymbol{\Gamma}_m^*\boldsymbol{X}_m^T\boldsymbol{\Omega}_m^{-1}\boldsymbol{X}_m^*\boldsymbol{\Gamma}_m^*\boldsymbol{\epsilon}_m^{1/2}\}_l\boldsymbol{\varrho}(\boldsymbol{\theta})\right]\right\}\right] \end{aligned}$$

Substituting (B.28) into (B.32) and using (B.13-B.14) yields (3.63a) and

$$\begin{aligned} f_m(\boldsymbol{\theta}) &= \exp\left[\Re\left\{\boldsymbol{\varrho}^\dagger(\boldsymbol{\theta})\left[2\boldsymbol{\epsilon}_m^{-1/2}\boldsymbol{C}^{-1}\left(\boldsymbol{X}_m^T\boldsymbol{Q}_m\boldsymbol{r}_m - \left\{\boldsymbol{X}_m^T\boldsymbol{Q}_m\left(\boldsymbol{X}_m^T\right)^{-1}\boldsymbol{\epsilon}_m^{1/2}\right\}_l\boldsymbol{\varrho}(\boldsymbol{\theta})\right)\right]\right\}\right] \\ &= \exp\left\{\sum_{k=0}^{L-1}\frac{|\alpha_k|}{\sigma_k^2\sqrt{\epsilon_{km}}}|b_{km}(\boldsymbol{\theta}_{k-1})|\cos\left(\theta_k - \arg\left[b_{km}(\boldsymbol{\theta}_{k-1})\right] + \arg\left[\alpha_k\right]\right)\right\} \qquad \text{(B.34)} \end{aligned}$$

where $\boldsymbol{Q}_m$ is given by (3.16a), $b_{km}(\boldsymbol{\theta}_{k-1})$ and $\varphi_{km}(\boldsymbol{\theta}_{k-1})$ are given by (3.65) and (3.66). The likelihood ratio $\Lambda_m(\dot{z};T_o)$ is obtained by integrating successively (B.31) with (B.34) over all components of the vector $\boldsymbol{\theta}$ between $-\pi$ and π.

$$\Lambda_m(\dot{z};T_o) = \frac{J_m}{(2\pi)^L}\int_{-\pi}^{\pi}\cdots\int_{-\pi}^{\pi} f_m(\boldsymbol{\theta})d\theta_0\ldots d\theta_{L-1} \tag{B.35}$$

where J_m is given by (3.63) and $f_m(\boldsymbol{\theta})$ is given by (B.34).

B.3.2 Likelihood ratio for a 2 Ricean/L-2 Rayleigh channel

Let us define

$$d_{km} = \frac{|\alpha_k|}{\sigma_k^2\sqrt{\epsilon_{km}}}\left[\boldsymbol{X}_m^T\boldsymbol{Q}_m\boldsymbol{r}_m\right]_k \qquad e_{kn}^m = \frac{|\alpha_k||\alpha_n|}{\sigma_k^2\sqrt{\epsilon_{km}}}\left[\boldsymbol{X}_m^T\boldsymbol{Q}_m\left(\boldsymbol{X}_m^T\right)^{-1}\boldsymbol{\epsilon}_m^{1/2}\right]_{kn}$$

$$V_{km} = |d_{km}| \qquad \vartheta_{km} = \arg\left[d_{km}\right] \tag{B.36}$$

$$V_{kn}^m = |e_{kn}^m| \qquad \vartheta_{kn}^m = \arg\left[e_{kn}^m\right] \tag{B.37}$$

$$\delta_n = \arg\left[\alpha_n\right]$$

such that

$$\frac{|\alpha_k|}{\sigma_k^2\sqrt{\epsilon_{km}}}b_{km}(\boldsymbol{\theta}_{k-1}) = d_{km} - \sum_{n=0}^{k-1} e_{kn}^m e^{j(\theta_n+\delta_n)} \qquad \frac{|\alpha_0|}{\sigma_0^2\sqrt{\epsilon_{0m}}}b_{0m} = d_{0m} \tag{B.38}$$

For a 2 Ricean/L-2 Rayleigh channel, (B.34) reduces to
$f_m(\boldsymbol{\theta}) = \exp\left\{V_{0m}\cos\left(\theta_0+\delta_0-\vartheta_{0m}\right)\right\}\exp\left\{\frac{|\alpha_1||b_{1m}(\theta_0)|}{\sigma_1^2\sqrt{\epsilon_{1m}}}\cos\left(\theta_1+\delta_1-\arg\left[b_{1m}(\theta_0)\right]\right)\right\}$
and (B.35) yields (after integration with respect to θ_1)

$$\Lambda_m(\dot{z};T_o) = \frac{J_m}{2\pi}\int_{-\pi}^{\pi} I_0\left(\frac{|\alpha_1|}{\sigma_1^2\sqrt{\epsilon_{1m}}}|b_{1m}(\theta_0)|\right)\exp\left\{V_{0m}\cos\left(\theta_0+\delta_0-\vartheta_{0m}\right)\right\}d\theta_0 \tag{B.39}$$

From (B.38)

$$\frac{|\alpha_1||b_{1m}(\theta_0)|}{\sigma_1^2\sqrt{\epsilon_{1m}}} = \sqrt{V_{1m}^2+\left(V_{10}^m\right)^2-2V_{1m}V_{10}^m\cos\left(\theta_0+\delta_0+\vartheta_{10}^m-\vartheta_{1m}\right)}$$

Hence applying Neumann's addition theorem (D.34b) [185, p. 358]

$$I_0\left(\frac{|\alpha_1|}{\sigma_1^2\sqrt{\epsilon_{1m}}}|b_{1m}(\theta_0)|\right)$$
$$= I_0\left(V_{1m}\right)I_0\left(V_{10}^m\right)+2\sum_{p=1}^{\infty}(-1)^p I_p\left(V_{1m}\right)I_p\left(V_{10}^m\right)\cos\left(p\left(\theta_0+\delta_0-\vartheta_{0m}+\psi_m\right)\right)$$

where V_{km} and ϑ_{km} are given by (B.36), V_{10}^m and ϑ_{10}^m are given by (B.37) and $\psi_m = \vartheta_{0m}+\vartheta_{10}^m-\vartheta_{1m}$ (independent of the phase of α_0). Then (B.39) yields (3.172) (after integration with respect to θ_0).

Appendix C

Collection of identities

This appendix presents a collection of identities and properties that will be used throughout this thesis.

C.1 Identities obtained by neglecting integrals containing double frequency terms

Lemma C.1. *Let* $\mathbf{f}(s,t)$ *and* $\mathbf{g}(s,t)$ *be complex functions slowly varying in* s *with respect to* ω_c *over the observation interval* $[0,t]$.

$$\int_0^t \Re\left\{\mathbf{f}(s,t)e^{j\omega_c s}\right\}\mathbf{g}(s,t)e^{j\omega_c s}ds \approx \frac{1}{2}\int_0^t \mathbf{f}^*(s,t)\mathbf{g}(s,t)ds \tag{C.1}$$

$$\int_0^t \Re\left\{\mathbf{f}(s,t)e^{j\omega_c s}\right\}\Re\left\{\mathbf{g}(s,t)e^{j\omega_c s}\right\}ds \approx \frac{1}{2}\int_0^t \Re\left\{\mathbf{f}^*(s,t)\mathbf{g}(s,t)\right\}ds \tag{C.2}$$

$$\int_0^t \Re\left\{\mathbf{f}(s,t)e^{j\omega_c s}\right\}\Im\left\{\mathbf{g}(s,t)e^{j\omega_c s}\right\}ds \approx \frac{1}{2}\int_0^t \Im\left\{\mathbf{f}^*(s,t)\mathbf{g}(s,t)\right\}ds \tag{C.3}$$

$$\int_0^t \Im\left\{\mathbf{f}(s,t)e^{j\omega_c s}\right\}\Im\left\{\mathbf{g}(s,t)e^{j\omega_c s}\right\}ds \approx \frac{1}{2}\int_0^t \Re\left\{\mathbf{f}^*(s,t)\mathbf{g}(s,t)\right\}ds \tag{C.4}$$

$$2\Re\left\{\left(\int_0^t \Re\left\{\mathbf{f}(s,t)e^{j\omega_c s}\right\}\mathbf{g}^*(s,t)e^{-j\omega_c s}ds\right)e^{j\omega_c t}\right\} \approx \Re\left\{\left(\int_0^t \mathbf{f}(s,t)\mathbf{g}^*(s,t)ds\right)e^{j\omega_c t}\right\} \tag{C.5}$$

Proof of Lemma C.1.

$$\int_0^t \Re\left\{\mathbf{f}(s,t)e^{j\omega_c s}\right\}\mathbf{g}(s,t)e^{j\omega_c s}ds = \frac{1}{2}\left[I_1(t)+I_2(t)\right] \tag{C.6}$$

where $I_1(t)$ and $I_2(t)$ are given by

$$I_1(t) = \int_0^t \mathbf{f}(s,t)\mathbf{g}(s,t)e^{j2\omega_c s}ds \tag{C.7}$$

$$I_2(t) = \int_0^t \mathbf{f}^*(s,t)\mathbf{g}(s,t)ds \tag{C.8}$$

Neglecting integrals containing double frequency terms in (C.6) (i.e. neglecting $I_1(t)$) yields (C.1). Taking the real part of both sides of (C.1) yields (C.2). Similarly taking the imaginary part of both sides of (C.1) yields (C.3).

$$\int_0^t \Im\left\{\mathbf{f}(s,t)e^{j\omega_c s}\right\}\Im\left\{\mathbf{g}(s,t)e^{j\omega_c s}\right\}ds = -\frac{1}{4}\left[I_1(t) - I_2(t) - I_2^*(t) + I_1^*(t)\right] \tag{C.9}$$

where $I_1(t)$ and $I_2(t)$ are given by (C.7) and (C.8). Neglecting integrals containing double frequency terms in (C.9) (i.e. neglecting $I_1(t)$) yields

$$\int_0^t \Im\left\{\mathbf{f}(s,t)e^{j\omega_c s}\right\}\Im\left\{\mathbf{g}(s,t)e^{j\omega_c s}\right\}ds \approx \frac{1}{4}\left[I_2(t) + I_2^*(t)\right] = \frac{1}{2}\int_0^t \Re\left\{\mathbf{f}^*(s,t)\mathbf{g}(s,t)\right\}ds$$

which is identical to (C.4). Taking the conjugate of (C.1), multiplying it by $e^{j\omega_c t}$ and taking its real part yields (C.5). **Q.E.D**

For the rest of this appendix, $\tilde{s}_m(s)$ is assumed continuous on $[0,t]$ and time-limited to $[0,T]$, T'_m is defined as (3.30) and the index m (indicating H_m) is omitted.

C.2 Definition of the resolvent kernels

From section 3.2.3 (topic: "Eigenvalues and eigenfunctions of $K_m(s,u)$ over an arbitrary observation interval $[0,t], t > T'_m + \tau_0$ assuming that $\tilde{s}_m(s)$ is time-limited"), the covariance function of the complex signal process $\tilde{v}(s) = \sum_{k=0}^{L-1} a_k e^{j\theta_k}\tilde{s}(s-\tau_k)$ can be written as[1]

$$\mathcal{K}(\tau,s) = \begin{cases} 0 & 0 \le \tau, s \le t \quad 0 \le t \le T' + \tau_0 \\ \mathcal{K}^{i_t}(\tau,s) & 0 \le \tau, s \le t \quad T' + \tau_0 < t < \infty \end{cases} \tag{C.10}$$

[1]The superscript i_t is not an exponent.

where $\mathcal{K}^{i_t}(\tau,s) = \sum_{k=0}^{i_t-1} 2\sigma_k^2 \tilde{s}(\tau-\tau_k)\tilde{s}^*(s-\tau_k)$ has eigenfunctions $\phi_l^{i_t}(s,t)$ given by (3.34) and eigenvalues $\lambda_l^{i_t}(t)$. From Mercer's theorem [182, p. 85]

$$\mathcal{K}^{i_t}(\tau,s) = \sum_{l=0}^{i_t-1} \lambda_l^{i_t}(t)\phi_l^{i_t}(\tau,t)\left[\phi_l^{i_t}(s,t)\right]^* \quad 0 \le \tau,s \le t \quad T' + \tau_0 < t < \infty \tag{C.11}$$

Therefore substituting (C.11) into (C.10) yields

$$\mathcal{K}(\tau,s) = \sum_{l=0}^{L-1} \lambda_l(t)\phi_l(\tau,t)\phi_l^*(s,t) \qquad 0 \le \tau,s \le t \qquad 0 \le t < \infty \tag{C.12}$$

where $\sqrt{\lambda_l(t)}\phi_l(s,t)$ is given by (3.39). Using $K(\tau,s) = \Re\left\{\frac{1}{2}\mathcal{K}(\tau,s)e^{j\omega_c(\tau-s)}\right\}$ and (3.44), $K(\tau,s)$ is similarly given by

$$K(\tau,s) = \sum_{l=0}^{2L-1} \kappa_l(t)\Upsilon_l(\tau,t)\Upsilon_l(s,t) \qquad 0 \le \tau,s \le t \qquad 0 \le t < \infty \tag{C.13}$$

where $\sqrt{\kappa_l(t)}\Upsilon_l(s,t)$ is given by (3.44). Let us define the kernels $\mathcal{H}(\tau,s,t)$ and $H(\tau,s,t)$ as

$$\mathcal{H}(\tau,s,t) \triangleq \begin{cases} \sum_{l=0}^{L-1} \frac{\frac{\lambda_l(t)}{2N_0}}{1+\frac{\lambda_l(t)}{2N_0}}\phi_l(\tau,t)\phi_l^*(s,t) & 0 \le \tau,s \le t \\ & 0 \le t < \infty \\ 0 & \text{else.} \end{cases} \tag{C.14}$$

$$H(\tau,s,t) \triangleq \begin{cases} \sum_{l=0}^{2L-1} \frac{\frac{2}{N_0}\kappa_l(t)}{1+\frac{2}{N_0}\kappa_l(t)}\Upsilon_l(\tau,t)\Upsilon_l(s,t) & 0 \le \tau,s \le t \\ & 0 \le t < \infty \\ 0 & \text{else.} \end{cases} \tag{C.15}$$

$$= 2\Re\left\{\mathcal{H}(\tau,s,t)e^{j\omega_c(\tau-s)}\right\} \tag{C.16}$$

where $\lambda_l(t)$, $\sqrt{\lambda_l(t)}\phi_l(s,t)$, $\kappa_l(t)$ and $\sqrt{\kappa_l(t)}\Upsilon_l(t)$ are respectively given by (3.37), (3.39), (3.43) and (3.44). It can be easily verified by straight forward substitutions of (C.12) and (C.14) that

$$\frac{1}{2N_0}\mathcal{K}(\tau,s) = \mathcal{H}(\tau,s,t) + \frac{1}{2N_0}\int_0^t \mathcal{K}(\tau,r)\mathcal{H}(r,s,t)dr \qquad 0 \le \tau,s \le t \tag{C.17}$$

$$\frac{2}{N_0}K(\tau,s) = H(\tau,s,t) + \frac{2}{N_0}\int_0^t H(\tau,r,t)K(r,s)dr \qquad 0 \le \tau,s \le t \qquad \text{(C.18)}$$

Similarly (C.18) can be checked using (C.13) and (C.15). Therefore $\mathcal{H}(\tau,s,u)$ and $H(\tau,s,u)$ are the resolvent kernels of $\mathcal{K}(s,u)$ and $K(s,u)$ on $[0,t]$ [218, pp. 141,162].

Proof of (C.16). Recall that since $\mathcal{K}(\tau,s)$ is Hermitian, $\forall T' + \tau_0 < t < \infty$, $\{\lambda_l^{i_t}(t)\}_{l=0,\dots,i_t-1}$ are real, hence $\{\lambda_l(t)\}_{l=0,\dots,L-1}$ are also real. For $0 \le \tau,s \le t$, from (C.14)

$$\begin{aligned}
&2\Re\left\{\mathcal{H}(\tau,s,t)e^{j\omega_c(\tau-s)}\right\} \\
&\quad= 2\sum_{l=0}^{L-1}\frac{\frac{1}{2N_0}}{1+\frac{\lambda_l(t)}{2N_0}}\Big[\Re\left\{\sqrt{\lambda_l(t)}\phi_l(\tau,t)e^{j\omega_c\tau}\right\}\Re\left\{\sqrt{\lambda_l(t)}\phi_l(s,t)e^{j\omega_c s}\right\} \\
&\qquad\qquad + \Im\left\{\sqrt{\lambda_l(t)}\phi_l(\tau,t)e^{j\omega_c\tau}\right\}\Im\left\{\sqrt{\lambda_l(t)}\phi_l(s,t)e^{j\omega_c s}\right\}\Big] \\
&\quad= \sum_{l=0}^{L-1}\frac{\frac{2}{N_0}}{1+\frac{2}{N_0}\frac{\lambda_l(t)}{4}}\Re\left\{\sqrt{\frac{\lambda_l(t)}{2}}\phi_l(\tau,t)e^{j\omega_c\tau}\right\}\Re\left\{\sqrt{\frac{\lambda_l(t)}{2}}\phi_l(s,t)e^{j\omega_c s}\right\} \\
&\quad\quad + \sum_{l=L}^{2L-1}\frac{\frac{2}{N_0}}{1+\frac{2}{N_0}\frac{\lambda_{l-L}(t)}{4}}\Im\left\{\sqrt{\frac{\lambda_{l-L}(t)}{2}}\phi_{l-L}(\tau,t)e^{j\omega_c\tau}\right\}\Im\left\{\sqrt{\frac{\lambda_{l-L}(t)}{2}}\phi_{l-L}(s,t)e^{j\omega_c s}\right\} \\
&\quad= \sum_{l=0}^{2L-1}\frac{\frac{2}{N_0}\kappa_l(t)}{1+\frac{2}{N_0}\kappa_l(t)}\Upsilon_l(\tau,t)\Upsilon_l(s,t)
\end{aligned}$$

where the last equation is obtained using (3.43-3.44). **Q.E.D**

C.3 Integral equations identities and others

C.3.1 Identities

Let $H(\tau,s,t)$ be the unique square integrable function satisfying (C.18) where $K(s,u)$ is symmetric, continuous and non-negative definite on $\mathbb{R}$ or an interval of $\mathbb{R}$. Then $H(\tau,s,t)$ satisfies the well known Siegert identity [52, p. 20], [219], [220]:

$$\frac{\partial H}{\partial t}(\tau,s,t) = -H(\tau,t,t)H(s,t,t) = -H(t,\tau,t)H(t,s,t) \qquad \text{(C.19)}$$

For $0 \leq s \leq t \;\&\; 0 \leq t < \infty$, the functions $\left\{\sqrt{\lambda_l(t)}\phi_l(s,t)\right\}_{l=0,\ldots,L-1}$ satisfy the following identities, $\forall\, l,j = 0,\ldots,L-1$

$$\sqrt{\lambda_l(t)\lambda_j(t)}\int_0^t \phi_l(s,t)\phi_j^*(s,t)ds = \sqrt{\lambda_l(t)\lambda_j(t)}\delta_{lj} \tag{C.20}$$

$$\frac{x_{lk}^*(t)}{\sqrt{\epsilon_k(t)}}\lambda_l(t)\lambda_j(t)\phi_j(\tau,t)\int_0^t \phi_l(s,t)\phi_j^*(s,t)ds = \frac{x_{lk}^*(t)}{\sqrt{\epsilon_k(t)}}\lambda_l(t)\lambda_j(t)\phi_j(\tau,t)\delta_{lj} \tag{C.21}$$

$$\frac{x_{lk}^*(t)}{\sqrt{\epsilon_k(t)}}\frac{x_{jk}(t)}{\sqrt{\epsilon_k(t)}}\lambda_l(t)\lambda_j(t)\int_0^t \phi_l(s,t)\phi_j^*(s,t)ds = \frac{x_{lk}^*(t)}{\sqrt{\epsilon_k(t)}}\frac{x_{jk}(t)}{\sqrt{\epsilon_k(t)}}\lambda_l(t)\lambda_j(t)\delta_{lj} \tag{C.22}$$

$\tilde{s}(s-\tau_l)$ can be expressed in terms of $\phi_j(s,t)$ as[2]

$$\tilde{s}(s-\tau_l) = \frac{1}{2\sigma_l^2\sqrt{\epsilon_l(t)\tilde{E}}}\sum_{j=0}^{L-1}\lambda_j(t)x_{jl}^*(t)\phi_j(s,t) \quad \begin{matrix} 0 \leq s \leq t \\ 0 \leq t < \infty \end{matrix} \tag{C.23}$$

The functions $\{\lambda_l(t)\}_{l=0,\ldots,L-1}$ satisfy

$$\sum_{k=0}^{L-1}\frac{\lambda_l^2(t)\,|x_{lk}(t)|^2}{2\sigma_k^2\epsilon_k(t)\tilde{E}} = \lambda_l(t) \tag{C.24}$$

The complex functions $l_k(\tau,t)$ and $\mathfrak{l}(t)$ satisfy the following identities, $\forall\, 0 \leq \tau \leq t$

$$l_k(\tau,t) = |\alpha_k|\tilde{s}(\tau-\tau_k) - \frac{1}{2N_0}\int_0^t \mathcal{K}(\tau,s)l_k(s,t)ds \tag{C.25}$$

$$= |\alpha_k|\tilde{s}(\tau-\tau_k) - |\alpha_k|\int_0^t \tilde{s}(u-\tau_k)\mathcal{H}(\tau,u,t)du \tag{C.26}$$

$$l_k(\tau,t)e^{j\omega_c\tau} = |\alpha_k|\tilde{s}(\tau-\tau_k)e^{j\omega_c\tau} - |\alpha_k|\int_0^t \tilde{s}(u-\tau_k)e^{j\omega_c u}H(\tau,u,t)du \tag{C.27}$$

$$\mathfrak{l}(t) = \sum_{k=0}^{L-1}\frac{|\alpha_k|}{2N_0}\int_0^t l_k(\tau,t)\tilde{s}^*(\tau-\tau_k)d\tau \tag{C.28}$$

Similar to (3.69), $\forall\, T' + \tau_0 < t < \infty$,

$$e_{kn}^{i_t}(t) \triangleq \frac{|\alpha_k||\alpha_n|}{\sigma_k^2\sqrt{\epsilon_k(t)}}\left[\boldsymbol{X}_{i_t}^T(t)\gamma\left[\boldsymbol{D}_{i_t}^{-1}(t)+\gamma\boldsymbol{I}_{i_t}\right]^{-1}\left(\boldsymbol{X}_{i_t}^T(t)\right)^{-1}\boldsymbol{\epsilon}_{i_t}^{1/2}(t)\right]_{kn}$$

[2]Note that (C.23) is identical to (3.40b) and reprinted in this appendix for convenience.

$$= \frac{1}{N_0} \int_0^t l_n^{i_t}(s,t) \, |\alpha_k| \, \tilde{s}^*(s-\tau_k) ds \tag{C.29a}$$

$$= \frac{1}{N_0} \int_0^t \left[l_k^{i_t}(s,t) \right]^* |\alpha_n| \, \tilde{s}(s-\tau_n) ds \tag{C.29b}$$

where $l_k^{i_t}(s,t)$ is given by (3.88).

C.3.2 Proofs

Proof of (C.20)

- Assume $0 \leq t \leq T' + \tau_0$:

  From (3.37) $\forall\, l, j = 0, \ldots, L-1$, $\lambda_l(t) = \lambda_j(t) = 0$ and from (3.39a) $\forall\, 0 \leq s \leq t$, $\sqrt{\lambda_l(t)}\phi_l(s,t) = \sqrt{\lambda_j(t)}\phi_j(s,t) = 0$, hence

$$\sqrt{\lambda_l(t)\lambda_j(t)} \int_0^t \phi_l(s,t)\phi_j^*(s,t) ds = \int_0^t 0 \, ds = 0 = 0 \cdot \delta_{lj} = \sqrt{\lambda_l(t)\lambda_j(t)}\delta_{lj}$$

- Assume $t > T' + \tau_0$ and $l \in \{0, \ldots, L-1\}$, $j \in \{i_t, \ldots, L-1\}$:

  From (3.37) $\lambda_j(t) = 0$, and from (3.39a) $\forall\, 0 \leq s \leq t$, $\sqrt{\lambda_j(t)}\phi_j(s,t) = 0$, hence

$$\begin{aligned}\sqrt{\lambda_l(t)\lambda_j(t)} \int_0^t \phi_l(s,t)\phi_j^*(s,t) ds &= \int_0^t 0 \cdot \sqrt{\lambda_l(t)}\phi_l(s,t) ds \\ &= 0 = 0 \cdot \sqrt{\lambda_l(t)}\delta_{lj} = \sqrt{\lambda_l(t)\lambda_j(t)}\delta_{lj}\end{aligned}$$

- Assume $t > T' + \tau_0$ and $l \in \{i_t, \ldots, L-1\}$, $j \in \{0, \ldots, L-1\}$:

  From (3.37) $\lambda_l(t) = 0$, and from (3.39a) $\forall\, 0 \leq s \leq t$, $\sqrt{\lambda_l(t)}\phi_l(s,t) = 0$, hence

$$\sqrt{\lambda_l(t)\lambda_j(t)} \int_0^t \phi_l(s,t)\phi_j^*(s,t) ds = 0 = \sqrt{\lambda_l(t)\lambda_j(t)}\delta_{lj}$$

- Assume $t > T' + \tau_0$ and $l, j \in \{0, \ldots, i_t - 1\}$, from (3.39a)

$$\begin{aligned}\sqrt{\lambda_l(t)\lambda_j(t)} \int_0^t \phi_l(s,t)\phi_j^*(s,t) ds &= \sqrt{\lambda_l^{i_t}(t)\lambda_j^{i_t}(t)} \int_0^t \phi_l^{i_t}(s,t) \left[\phi_j^{i_t}(s,t)\right]^* ds \\ &= \sqrt{\lambda_l^{i_t}(t)\lambda_j^{i_t}(t)}\delta_{lj} = \sqrt{\lambda_l(t)\lambda_j(t)}\delta_{lj}\end{aligned}$$

since the eigenfunctions $\phi_l^{i_t}(s,t)$ are orthonormal on $[0,t]$. **Q.E.D**

Equations (C.21) and (C.22) can be proved similarly using (3.39a) and (3.37- 3.38).

Proof of (C.24)

- Assume "$0 \le t \le T' + \tau_0$" or "$t > T' + \tau_0$ and $l \in \{i_t, \dots, L-1\}$":

  From (3.38) $\forall k$, $\sqrt{\frac{\lambda_l(t)}{\epsilon_k(t)}} x_{lk}(t) = 0$, and from (3.37) $\lambda_l(t) = 0$ hence

$$\sum_{k=0}^{L-1} \frac{\lambda_l^2(t)\,|x_{lk}(t)|^2}{2\sigma_k^2 \epsilon_k(t) \tilde{E}} = 0 = \lambda_l(t)$$

- Assume $t > T' + \tau_0$ and $l \in \{0, \dots, i_t - 1\}$:

  From (3.38) and (3.37)

$$\sum_{k=0}^{L-1} \frac{\lambda_l^2(t)\,|x_{lk}(t)|^2}{2\sigma_k^2 \epsilon_k(t) \tilde{E}} = \sum_{k=0}^{i_t-1} \frac{\left[\lambda_l^{i_t}(t)\right]^2 \left|x_{lk}^{i_t}(t)\right|^2}{2\sigma_k^2 \epsilon_k(t) \tilde{E}} = \lambda_l^{i_t}(t) = \lambda_l(t)$$

  where the step $\sum_{k=0}^{i_t-1} \frac{\left[\lambda_l^{i_t}(t)\right]^2 \left|x_{lk}^{i_t}(t)\right|^2}{2\sigma_k^2 \epsilon_k(t) \tilde{E}} = \lambda_l^{i_t}(t)$ is obtained using $\boldsymbol{X}_{i_t}(t)\left(\boldsymbol{\epsilon}_{i_t}(t)\boldsymbol{C}_{i_t}\right)^{-1} \boldsymbol{X}_{i_t}^{\dagger}(t)\boldsymbol{D}_{i_t}(t) = \boldsymbol{I}_{i_t}$ derived from (3.35). **Q.E.D**

Proof of (C.25)

From (3.103b) and (C.12)

$$\begin{aligned}
&\frac{1}{2N_0} \int_0^t \mathcal{K}(\tau, s) l_k(s,t) ds \\
&\quad = \frac{|\alpha_k|}{2\sigma_k^2} \sum_{l=0}^{L-1} \sum_{j=0}^{L-1} \frac{\frac{\lambda_l(t)}{2N_0}}{1 + \frac{\lambda_l(t)}{2N_0}} \frac{x_{lk}^*(t)}{\sqrt{\epsilon_k(t)\tilde{E}}} \lambda_j(t) \phi_j(\tau, t) \int_0^t \phi_l(s,t) \phi_j^*(s,t) ds \\
&\quad = \frac{|\alpha_k|}{2\sigma_k^2} \sum_{l=0}^{L-1} \frac{\frac{\lambda_l^2(t)}{2N_0}}{1 + \frac{\lambda_l(t)}{2N_0}} \frac{x_{lk}^*(t)}{\sqrt{\epsilon_k(t)\tilde{E}}} \phi_l(\tau, t) \quad \text{from (C.21)} \\
&\quad = \frac{|\alpha_k|}{2\sigma_k^2} \sum_{l=0}^{L-1} \frac{\lambda_l(t)\left(1 + \frac{\lambda_l(t)}{2N_0} - 1\right)}{1 + \frac{\lambda_l(t)}{2N_0}} \frac{x_{lk}^*(t)}{\sqrt{\epsilon_k(t)\tilde{E}}} \phi_l(\tau, t)
\end{aligned}$$

$$= \sum_{l=0}^{L-1} \frac{|\alpha_k|\lambda_l(t)x_{lk}^*(t)}{2\sigma_k^2\sqrt{\epsilon_k(t)\tilde{E}}}\phi_l(\tau,t) - \sum_{l=0}^{L-1} \frac{|\alpha_k|\lambda_l(t)x_{lk}^*(t)}{\sqrt{\epsilon_k(t)\tilde{E}}\,2\sigma_k^2\left(1+\frac{\lambda_l(t)}{2N_0}\right)}\phi_l(\tau,t)$$

Then substituting (3.103b) and (C.23) yields (C.25). **Q.E.D**

Proof of (C.26)

From (C.25)

$$\begin{aligned}
&|\alpha_k| \int_0^t \tilde{s}(u-\tau_k)\mathcal{H}(\tau,u,t)du \\
&\quad = \int_0^t \mathcal{H}(\tau,u,t)\left[l_k(u,t) + \frac{1}{2N_0}\int_0^t \mathcal{K}(u,s)l_k(s,t)ds\right]du \\
&\quad = \int_0^t \mathcal{H}^*(u,\tau,t)l_k(u,t)du + \int_0^t l_k(s,t)\left[\frac{1}{2N_0}\int_0^t \mathcal{K}^*(s,u)\mathcal{H}^*(u,\tau,t)du\right]ds \\
&\quad = \int_0^t \mathcal{H}^*(u,\tau,t)l_k(u,t)du + \int_0^t l_k(s,t)\left[\frac{1}{2N_0}\mathcal{K}(s,\tau) - \mathcal{H}(s,\tau,t)\right]^* ds \quad \text{from (C.17)} \\
&\quad = \frac{1}{2N_0}\int_0^t \mathcal{K}(\tau,s)l_k(s,t)ds
\end{aligned}$$

Then (C.25) yields (C.26). **Q.E.D**

Proof of (C.27)

Taking the real part of (C.26) yields

$$\begin{aligned}
&\Re\left\{l_k(\tau,t)e^{j\omega_c\tau}\right\} \\
&\quad = \Re\left\{|\alpha_k|\tilde{s}(\tau-\tau_k)e^{j\omega_c\tau}\right\} - |\alpha_k|\int_0^t \Re\left\{\tilde{s}(u-\tau_k)\left[\mathcal{H}(\tau,u,t)e^{j\omega_c\tau}\right]\right\}du \\
&\quad \approx \Re\left\{|\alpha_k|\tilde{s}(\tau-\tau_k)e^{j\omega_c\tau}\right\} - |\alpha_k|\int_0^t \Re\left\{\tilde{s}(u-\tau_k)e^{j\omega_c u}\right\}\Re\left\{2\left[\mathcal{H}(\tau,u,t)e^{j\omega_c\tau}\right]e^{-j\omega_c u}\right\}du
\end{aligned}$$

where the second equation is obtained by neglecting integrals containing double frequency terms (see (C.2)). Using (C.16) yields

$$\Re\left\{l_k(\tau,t)e^{j\omega_c\tau}\right\} = \Re\left\{|\alpha_k|\tilde{s}(\tau-\tau_k)e^{j\omega_c\tau}\right\} - |\alpha_k|\int_0^t \Re\left\{\tilde{s}(u-\tau_k)e^{j\omega_c u}\right\}H(\tau,u,t)du \tag{C.30}$$

Similarly, taking the imaginary part of (C.26) and neglecting integrals containing double frequency terms (see (C.3)) yield

$$\begin{aligned}
&\Im\left\{l_k(\tau,t)e^{j\omega_c\tau}\right\} \\
&= \Im\left\{|\alpha_k|\tilde{s}(\tau-\tau_k)e^{j\omega_c\tau}\right\} - |\alpha_k|\int_0^t \Im\left\{\tilde{s}(u-\tau_k)\left[\mathcal{H}(\tau,u,t)e^{j\omega_c\tau}\right]\right\}du \\
&\approx \Im\left\{|\alpha_k|\tilde{s}(\tau-\tau_k)e^{j\omega_c\tau}\right\} - |\alpha_k|\int_0^t \Im\left\{\tilde{s}(u-\tau_k)e^{j\omega_c u}\right\}\Re\left\{2\left[\mathcal{H}(\tau,u,t)e^{j\omega_c\tau}\right]e^{-j\omega_c u}\right\}du \\
&= \Im\left\{|\alpha_k|\tilde{s}(\tau-\tau_k)\right\} - |\alpha_k|\int_0^t \Im\left\{\tilde{s}(u-\tau_k)e^{j\omega_c u}\right\}H(\tau,u,t)du \qquad \text{(C.31)}
\end{aligned}$$

Adding (C.30) and (C.31) multiplied by j yields (C.27) since $H(\tau,u,t)$ is real. **Q.E.D**

Proof of (C.28)

From (3.105) and (C.22)

$$\begin{aligned}
\mathfrak{l}(t) &= \sum_{k=0}^{L-1}\frac{|\alpha_k|}{2N_0}\frac{N_0|\alpha_k|}{\sigma_k^2\sqrt{\epsilon_k(t)\tilde{E}}}\sum_{l=0}^{L-1}\frac{\frac{\lambda_l(t)}{2N_0}}{1+\frac{\lambda_l(t)}{2N_0}}x_{lk}^*(t)\cdot\frac{\lambda_l(t)x_{lk}(t)}{2\sigma_k^2\sqrt{\epsilon_k(t)\tilde{E}}} \\
&= \sum_{k=0}^{L-1}\frac{|\alpha_k|}{2N_0}\frac{N_0|\alpha_k|}{\sigma_k^2\sqrt{\epsilon_k(t)\tilde{E}}}\sum_{l=0}^{L-1}\sum_{j=0}^{L-1}\frac{\frac{\lambda_l(t)}{2N_0}}{1+\frac{\lambda_l(t)}{2N_0}}x_{lk}^*(t)\cdot\frac{\lambda_j(t)x_{jk}(t)}{2\sigma_k^2\sqrt{\epsilon_k(t)\tilde{E}}}\int_0^t\phi_l(\tau,t)\phi_j^*(\tau,t)d\tau \\
&= \sum_{k=0}^{L-1}\frac{|\alpha_k|}{2N_0}\int_0^t\left[\frac{N_0|\alpha_k|}{\sigma_k^2\sqrt{\epsilon_k(t)\tilde{E}}}\sum_{l=0}^{L-1}\frac{\frac{\lambda_l(t)}{2N_0}}{1+\frac{\lambda_l(t)}{2N_0}}x_{lk}^*(t)\phi_l(\tau,t)\right]\left[\sum_{j=0}^{L-1}\frac{\lambda_j(t)x_{jk}^*(t)}{2\sigma_k^2\sqrt{\epsilon_k(t)\tilde{E}}}\phi_j(\tau,t)\right]^* d\tau
\end{aligned}$$

hence (C.28) is obtained using (3.103b) and (C.23). **Q.E.D**

Proof of (C.29)

$$\begin{aligned}
e_{kn}^{i_t}(t) &\triangleq \frac{|\alpha_k||\alpha_n|}{\sigma_k^2\sqrt{\epsilon_k(t)}}\left[\boldsymbol{X}_{i_t}^T(t)\gamma\left[\boldsymbol{D}_{i_t}^{-1}(t)+\gamma\boldsymbol{I}_{i_t}\right]^{-1}\left(\boldsymbol{X}_{i_t}^T(t)\right)^{-1}\boldsymbol{\epsilon}_{i_t}^{1/2}(t)\right]_{kn} \\
&= \frac{|\alpha_k||\alpha_n|}{\sigma_k^2\sqrt{\epsilon_k(t)}}\left[\boldsymbol{X}_{i_t}^T(t)\gamma\left[\boldsymbol{D}_{i_t}^{-1}(t)+\gamma\boldsymbol{I}_{i_t}\right]^{-1}\boldsymbol{D}_{i_t}(t)\boldsymbol{X}_{i_t}^*(t)\boldsymbol{C}_{i_t}^{-1}\boldsymbol{\epsilon}_{i_t}^{-1/2}(t)\right]_{kn} \quad \text{from (3.35)} \\
&= \frac{|\alpha_k||\alpha_n|}{\sigma_k^2\sqrt{\epsilon_k(t)}}\sum_{l=0}^{i_t-1}\frac{\frac{\left(\lambda_l^{i_t}(t)\right)^2}{2N_0}}{1+\frac{\lambda_l^{i_t}(t)}{2N_0}}\frac{1}{2\sigma_n^2\sqrt{\epsilon_n(t)\tilde{E}}}x_{lk}^{i_t}(t)\left[x_{ln}^{i_t}(t)\right]^* \qquad \text{(C.32)}
\end{aligned}$$

Since $\left\{\phi_l^{i_t}(s,t)\right\}_{l=0,\dots,i_t-1}$ are orthonormal, (C.32) is also given by

$$e_{kn}^{i_t}(t) = \frac{|\alpha_k||\alpha_n|}{\sigma_k^2\sqrt{\epsilon_k(t)}} \sum_{l=0}^{i_t-1}\sum_{j=0}^{i_t-1} \frac{\frac{\lambda_j^{i_t}(t)}{2N_0}x_{lk}^{i_t}(t)}{1+\frac{\lambda_j^{i_t}(t)}{2N_0}} \frac{\left[x_{jn}^{i_t}(t)\right]^*\lambda_l^{i_t}(t)}{2\sigma_n^2\sqrt{\epsilon_n(t)\tilde{E}}} \int_0^t \left[\phi_l^{i_t}(s,t)\right]^*\phi_j^{i_t}(s,t)ds$$

$$= \frac{1}{N_0}\int_0^t \left(\frac{N_0|\alpha_n|}{\sigma_n^2\sqrt{\epsilon_n(t)\tilde{E}}} \sum_{j=0}^{i_t-1} \frac{\frac{\lambda_j^{i_t}(t)}{2N_0}}{1+\frac{\lambda_j^{i_t}(t)}{2N_0}} \left[x_{jn}^{i_t}(t)\right]^*\phi_j^{i_t}(s,t) \right)$$

$$\cdot \left(|\alpha_k| \sum_{l=0}^{i_t-1} \frac{\lambda_l^{i_t}(t)x_{lk}^{i_t}(t)}{2\sigma_k^2\sqrt{\epsilon_k(t)\tilde{E}}} \left[\phi_l^{i_t}(s,t)\right]^* \right) ds$$

Hence (C.29a) is obtained using (3.40a) and (3.88). Similarly, (C.32) is also given by

$$e_{kn}^{i_t}(t) = \frac{|\alpha_k||\alpha_n|}{\sigma_k^2\sqrt{\epsilon_k(t)}} \sum_{l=0}^{i_t-1}\sum_{j=0}^{i_t-1} \frac{\frac{\lambda_j^{i_t}(t)}{2N_0}x_{lk}^{i_t}(t)}{1+\frac{\lambda_j^{i_t}(t)}{2N_0}} \frac{\left[x_{jn}^{i_t}(t)\right]^*\lambda_l^{i_t}(t)}{2\sigma_n^2\sqrt{\epsilon_n(t)\tilde{E}}} \int_0^t \left[\phi_l^{i_t}(s,t)\right]^*\phi_j^{i_t}(s,t)ds$$

$$= \frac{1}{N_0}\int_0^t \left(\frac{N_0|\alpha_k|}{\sigma_k^2\sqrt{\epsilon_k(t)\tilde{E}}} \sum_{l=0}^{i_t-1} \frac{\frac{\lambda_l^{i_t}(t)}{2N_0}}{1+\frac{\lambda_l^{i_t}(t)}{2N_0}} x_{lk}^{i_t}(t)\left[\phi_l^{i_t}(s,t)\right]^* \right)$$

$$\cdot \left(|\alpha_n| \sum_{j=0}^{i_t-1} \frac{\lambda_j^{i_t}(t)\left[x_{jn}^*(t)\right]^*}{2\sigma_n^2\sqrt{\epsilon_n(t)\tilde{E}}} \phi_j^{i_t}(s,t) \right) ds$$

Hence (C.29b) is obtained using (3.40a) and (3.88). **Q.E.D**

C.4 Continuity and differentiability of the functions $\lambda_{lm}(t)$ and $\kappa_{lm}(t)$

Assume that $\tau_0 < \tau_1 < \dots < \tau_{L-1}$, then $\forall r = 1,\dots,L \quad \forall l = 0,\dots,r-1$ if $t \in \left(T' + \tau_{r-1}, T' + \tau_r\right]$, then $t > T' + \tau_l$ and from '2.' of Lemma B.2 applied to $\tilde{s}(s)$, there exists $a_l(t), b_l(t)$ such that $\forall s \in \left(a_l(t), b_l(t)\right)$, $\tilde{s}(s-\tau_l) \neq 0$. Therefore $\epsilon_l(t) \geq \frac{1}{\tilde{E}}\int_{a_l(t)}^{b_l(t)} |\tilde{s}(s-\tau_l)|^2 ds > 0$. Since $\tilde{s}(s-\tau_l)$ is continuous on $[0,t]$, $\epsilon_l(t) = \frac{1}{\tilde{E}}\int_0^t |\tilde{s}(s-\tau_l)|^2 ds$ and $\rho_{lj}(t) = \frac{1}{\tilde{E}\sqrt{\epsilon_l(t)\epsilon_j(t)}}\int_0^t \tilde{s}(s-\tau_l)\tilde{s}^*(s-\tau_j)ds$ are differentiable (with respect to t). Therefore $\forall r = 1,\dots,L$ the matrix $\boldsymbol{\epsilon}_r(t)\tilde{E}\boldsymbol{C}_r\boldsymbol{\Gamma}_r^*(t)$ is differentiable on $\left(T' + \tau_{r-1}, T' + \tau_r\right]$. $\forall r = 1,\dots,L \quad \forall t \in \left(T' + \tau_{r-1}, T' + \tau_r\right]$, the matrix $\boldsymbol{\epsilon}_r(t)\tilde{E}\boldsymbol{C}_r\boldsymbol{\Gamma}_r^*(t)$ is diagonalizable as product of two Hermitian positive matrices and

is an $r \times r$ matrix. Therefore similarly to results found in Appendix B.2.2, it has r real positive eigenvalues. Let $\left[\lambda_0^r(t), \lambda_1^r(t), \ldots, \lambda_{r-1}^r(t)\right]^T$ represent a r-tuple of the repeated eigenvalues of $\boldsymbol{\epsilon}_r(t)\tilde{\boldsymbol{E}}\boldsymbol{C}_r\boldsymbol{\Gamma}_r^*(t)$, then there exists r functions $\{\lambda_l^r(t)\}_{l=0,\ldots,r-1}$ representing the repeated eigenvalues of $\boldsymbol{\epsilon}_r(t)\tilde{\boldsymbol{E}}\boldsymbol{C}_r\boldsymbol{\Gamma}_r^*(t)$, which are single-valued and differentiable on $\left(T' + \tau_{r-1}, T' + \tau_r\right]$ [221, pp. 110-115]. From (3.37) $\forall r = 1, \ldots, L$ $\forall t \in \left(T' + \tau_{r-1}, T' + \tau_r\right]$, $i_t = r$, hence $\forall r = 1, \ldots, L \quad \forall t \in \left(T' + \tau_{r-1}, T' + \tau_r\right]$ $\forall l = r, \ldots, L-1 \quad \lambda_l(t) = 0$ (differentiable) and $\forall l = 0, \ldots, r-1$, $\lambda_l(t) = \lambda_l^r(t)$ (differentiable [221, pp. 110-115]). Therefore $\forall l = 0, \ldots, L-1 \quad \forall r = 1, \ldots, L$ the functions $\lambda_l(t)$ is differentiable on $\left(T' + \tau_{r-1}, T' + \tau_r\right]$. From (3.43), $\forall l = 0, \ldots, L-1$ $\forall r = 1, \ldots, L$ the function $\kappa_l(t)$ is also differentiable on $\left(T' + \tau_{r-1}, T' + \tau_r\right]$.

C.5 Identities assuming continuously differentiable $\{x_{lk}^{rm}(t)\}_{l,k=0,\ldots,r-1}$ and distinct $\{\lambda_l^r(t)\}_{l=0,\ldots,r-1}$ $\forall r = 1, \ldots, L$

The identities presented in Appendix C.2 and Appendix C.3 are valid for any continuous signal $\tilde{s}_m(s)$ time-limited to $[0, T]$. This section presents identities that are proved only under the assumptions

1. $\forall r = 1, \ldots, L$, there exists functions $\left\{x_{lk}^r(t)\right\}_{l,k=0,\ldots,r-1}$ continuously differentiable on $\left(T' + \tau_{r-1}, T' + \tau_r\right]$ such that the $r \times r$ matrix $\boldsymbol{X}_r(t)$, defined as $[\boldsymbol{X}_r(t)]_{lk} = x_{lk}^r(t)$, satisfies the equations $\boldsymbol{X}_r^*(t)\boldsymbol{\Gamma}_r^*(t)\boldsymbol{X}_r^T(t) = \boldsymbol{I}_r$ and $\boldsymbol{\epsilon}_r(t)\boldsymbol{C}_r\boldsymbol{\Gamma}_r^*(t)\boldsymbol{X}_r^T(t) = \boldsymbol{X}_r^T(t)\boldsymbol{D}_r(t)$.

2. $\forall r = 1, \ldots, L$, the eigenvalues of $\boldsymbol{\epsilon}_r(t)\tilde{\boldsymbol{E}}\boldsymbol{C}_r\boldsymbol{\Gamma}_r^*(t)$, $\left\{\lambda_l^r(t)\right\}_{l=0,\ldots,r-1}$ are distinct.

These assumptions ensure the continuity and differentiability properties of some of the kernels and functions previously defined. Furthermore they are not too restrictive. As shown in Appendix E.3.2, they are satisfied in the case of non-degenerate two-path channels (i.e. $2\sigma_0^2 \neq 0, 2\sigma_1^2 \neq 0$) such that $\forall t > T' + \tau_1$, $\rho_{01}(t) \neq 0$.

C.5.1 Differentiability of the functions $\sqrt{\lambda_{lm}(t)}\phi_{lm}(s,t)$ and $\sqrt{\kappa_{lm}(t)}\Upsilon_{lm}(s,t)$

Let us assume that Assumptions 1-2 are satisfied. Let $\{x_{lk}^r(t)\}_{l,k=0,\ldots,r-1}$ be the corresponding functions continuously differentiable on $\left(T' + \tau_{r-1}, T' + \tau_r\right]$. Recalling that i_t is an integer staircase function of t, from (3.34) and (3.35), the eigenfunctions $\left\{\phi_l^r(s,t)\right\}_{r=1,\ldots,L}$ can be expressed in terms of those continuously differentiable

functions $x_{lk}^r(t)$ as

$$\phi_l^r(s,t) = \frac{1}{\sqrt{\bar{E}}} \sum_{k=0}^{r-1} \frac{x_{lk}^r(t)}{\sqrt{\epsilon_k(t)}} \bar{s}(s-\tau_k) \quad 0 \le s \le t \quad \begin{matrix} r = 1, \dots, L \\ l = 0, \dots, r-1 \end{matrix} \tag{C.33}$$

Let $\mathcal{R}_r$ be the domain of $\mathbb{R}^2$ described by

$$\mathcal{R}_r = \left\{ (s,t) \in \mathbb{R}^2; \quad 0 \le s \le t \qquad T' + \tau_{r-1} < t \le T' + \tau_r \right\}$$

Since $\bar{s}(s-\tau_k)$ is continuous on $[0,t]$, from (C.33) $\forall r = 1, \dots, L$ the functions $\left\{ \sqrt{\lambda_l^r(t)} \phi_l^r(s,t) \right\}_{l=0,\dots,r-1}$ are continuous on $\mathcal{R}_r$ and differentiable with respect to t on $\mathcal{R}_r$. From (B.3), $\forall r = 1, \dots, L \quad \forall (s,t) \in \mathcal{R}_r \quad i_t = r$. Thus from (3.39a) $\forall r = 1, \dots, L \quad \forall l = 0, \dots, r-1 \quad \sqrt{\lambda_l(t)} \phi_l(s,t) = \sqrt{\lambda_l^r(t)} \phi_l^r(s,t)$ and $\forall l = r, \dots, L-1$ $\sqrt{\lambda_l(t)} \phi_l(s,t) = 0$. Therefore $\forall r = 1, \dots, L$ the functions $\left\{ \sqrt{\lambda_l(t)} \phi_l(s,t) \right\}_{l=0,\dots,L-1}$ are continuous on $\mathcal{R}_r$ and differentiable with respect to t on $\mathcal{R}_r$. From (3.44), $\forall r = 1, \dots, L$ the functions $\left\{ \sqrt{\kappa_l(t)} \Upsilon_l(s,t) \right\}_{l=0,\dots,2L-1}$ are also continuous on $\mathcal{R}_r$ and differentiable with respect to t on $\mathcal{R}_r$.

If the functions $\left\{ x_{lk}^r(t) \right\}_{l,k=0,\dots,r-1}$ are assumed to be continuously differentiable on $\left(T' + \tau_{r-1}, T' + \tau_r \right]$, the functions $\left\{ \sqrt{\lambda_l(t)} \phi_l(s,t) \right\}_{l=0,\dots,r-1}$ are continuously differentiable with respect to t on $\mathcal{R}_r$ as shown in the following. Let $r \in \{1, \dots, L\}$, (B.3) and (3.39a) yield

If $l \in \{r, \dots, L-1\}$, $\forall (s,t) \in \mathcal{R}_r \quad \sqrt{\lambda_l(t)} \phi_l(s,t) = 0$ so $\frac{\partial}{\partial t}\left(\sqrt{\lambda_l(t)} \phi_l(s,t) \right) = 0$ and $\frac{\partial}{\partial t}\left(\sqrt{\lambda_l(t)} \phi_l(s,t) \right)$ is continuous on $\mathcal{R}_r$.

If $l \in \{0, \dots, r-1\}$, $\forall (s,t) \in \mathcal{R}_r$

$$\begin{aligned}
&\frac{\partial}{\partial t}\left(\sqrt{\lambda_l(t)} \phi_l(s,t) \right) = \frac{\partial}{\partial t}\left(\sqrt{\lambda_l^r(t)} \phi_l^r(s,t) \right) \\
&= \frac{1}{\sqrt{\bar{E}}} \sum_{k=0}^{r-1} \frac{\partial}{\partial t} \left[\frac{\sqrt{\lambda_l^r(t)}}{\sqrt{\epsilon_k(t)}} x_{lk}^r(t) \right] \bar{s}(s-\tau_k) \quad \begin{matrix} 0 \le s \le t \\ \tau_{r-1} < t - T' \le \tau_r \end{matrix} \quad \text{from (3.34)} \\
&= \sum_{k=0}^{r-1} \left\{ \left[\frac{\dot{\lambda}_{lk}^r(t)}{2\sqrt{\lambda_l^r(t)}} x_{lk}^r(t) + \sqrt{\lambda_l^r(t)} \dot{x}_{lk}^r(t) \right] \frac{1}{\sqrt{\epsilon_k(t)}} - \sqrt{\lambda_l^r(t)} x_{lk}^r(t) \frac{\dot{\epsilon}_k(t)}{2\epsilon_k^{3/2}(t)} \right\} \frac{\bar{s}(s-\tau_k)}{\sqrt{\bar{E}}}
\end{aligned} \tag{C.34}$$

$\forall k = 0, \dots, L-1 \quad \epsilon_k(t)$ is differentiable with derivative given by $\dot{\epsilon}_k(t) = |\bar{s}(t-\tau_k)|^2$, $\bar{s}(t-\tau_k)$ are continuous on $[0,t]$, by assumption $\dot{x}_{lk}^r(t)$ are continuous on

$\left(T' + \tau_{r-1}, T' + \tau_{r-1}\right]$ hence from (C.34), $\frac{\partial}{\partial t}\left(\sqrt{\lambda_l(t)}\phi_l(s,t)\right)$ is continuous on $\mathcal{R}_\tau$.

From (3.44), $\forall r = 1, \ldots, L$ the functions $\left\{\sqrt{\kappa_l(t)}\Upsilon_l(s,t)\right\}_{l=0,\ldots,L-1}$ are also continuously differentiable with respect to t on $\mathcal{R}_\tau$.

C.5.2 Differentiability of $l_{km}(\tau,t)e^{j\omega_c\tau}$

Proposition C.1. *Let $\epsilon > 0$ and let $\mathcal{R}_\tau(\epsilon)$ be the domain of $\mathbb{R}^2$ described by*

$$\mathcal{R}_\tau(\epsilon) = \left\{(\tau,t) \in \mathbb{R}^2; \quad 0 \leq \tau \leq t \qquad T' + \tau_{r-1} + \epsilon \leq t \leq T' + \tau_r\right\}$$

For any $\epsilon > 0$, $\forall r = 1, \ldots, L$, $\forall k = 0, \ldots, L-1$ $l_k(\tau,t)e^{j\omega_c\tau}$ is continuous on $\mathcal{R}_\tau(\epsilon)$ and differentiable with respect to t on $\mathcal{R}_\tau(\epsilon)$ with partial derivative given by

$$\frac{\partial}{\partial t}\left(l_k(\tau,t)e^{j\omega_c\tau}\right) = \frac{\partial l_k(\tau,t)}{\partial t}e^{j\omega_c\tau} = -H(\tau,t,t)l_k(t,t)e^{j\omega_c t} \tag{C.35}$$

Proof of Proposition C.1. Let $\epsilon > 0$. As seen in Appendix C.4, $\forall r = 1, \ldots L$ the functions $\{\kappa_l(t)\}_{l=0,\ldots,L-1}$ are continuous on $\left[T' + \tau_{r-1} + \epsilon, T' + \tau_r\right]$ since $\left[T' + \tau_{r-1} + \epsilon, T' + \tau_r\right] \subset \left(T' + \tau_{r-1}, T' + \tau_r\right]$, and the functions $\left\{\sqrt{\kappa_l(t)}\Upsilon_l(s,t)\right\}_{l=0,\ldots,2L-1}$ are continuous and differentiable with respect to t on $\mathcal{R}_\tau(\epsilon)$ since $\mathcal{R}_\tau(\epsilon) \subset \mathcal{R}_\tau$. Therefore from (C.15), $\forall r = 1, \ldots, L$ the kernel $H(\tau,s,t)$ is continuous on $\mathcal{R}''_\tau(\epsilon)$, where $\mathcal{R}''_\tau(\epsilon)$ is the domain of $\mathbb{R}^3$ described by

$$\mathcal{R}''_\tau(\epsilon) = \left\{(\tau,s,t) \in \mathbb{R}^3; \quad 0 \leq \tau \leq t \qquad 0 \leq s \leq t \qquad T' + \tau_{r-1} + \epsilon \leq t \leq T' + \tau_r\right\}$$

Therefore from [192, p. 230], $\forall r = 1, \ldots L$ the right side of (C.27) is continuous on $\mathcal{R}_\tau(\epsilon)$ hence $\forall k = 0, \ldots, L-1$ the function $l_k(\tau,t)e^{j\omega_c\tau}$ is continuous on $\mathcal{R}_\tau(\epsilon)$. Furthermore from [220] $H(\tau,s,t)$ is differentiable with respect to t with partial derivative given by (C.19). Hence $\forall r = 1, \ldots L$ the kernel $\frac{\partial H(\tau,s,t)}{\partial t}$ is continuous on $\mathcal{R}''_\tau(\epsilon)$. Therefore from Leibnitz's Rule [192, p. 258] $\forall r = 1, \ldots L$ the right side of (C.27) is differentiable with respect to t on $\mathcal{R}_\tau(\epsilon)$ hence $\forall k = 0, \ldots, L-1$ the function $l_k(\tau,t)e^{j\omega_c\tau}$ is differentiable with respect to t on $\mathcal{R}_\tau(\epsilon)$ with first order partial derivative given by

$$\frac{\partial}{\partial t}\left(l_k(\tau,t)e^{j\omega_c\tau}\right) = -|\alpha_k|\int_0^t \tilde{s}(u-\tau_k)e^{j\omega_c u}\frac{\partial H(\tau,u,t)}{\partial t}du - |\alpha_k|\tilde{s}(t-\tau_k)e^{j\omega_c t}H(\tau,t,t)$$

Using (C.19) yields

$$\frac{\partial}{\partial t}\left(l_k(\tau,t)e^{j\omega_c\tau}\right) = -H(\tau,t,t)|\alpha_k|\left[\tilde{s}(t-\tau_k)e^{j\omega_c t} - \int_0^t \tilde{s}(u-\tau_k)e^{j\omega_c u}H(t,u,t)du\right]$$
$$= -H(\tau,t,t)l_k(t,t)e^{j\omega_c t} \qquad \text{from (C.27)}$$

Note that $l_k(\tau,t) = l_k(\tau,t)e^{j\omega_c\tau}\cdot e^{-j\omega_c\tau}$, hence $\forall r = 1,\dots,L \quad \forall k = 0,\dots,L-1$ the function $l_k(\tau,t)$ is also differentiable with respect to t on $\mathcal{R}_r''(\epsilon)$ with partial derivative given by $\frac{\partial l_k(\tau,t)}{\partial t} = -H(\tau,t,t)l_k(t,t)e^{j\omega_c(t-\tau)}$ **Q.E.D**

C.5.3 Differentiability of $\mathfrak{l}_m(t)$

Proposition C.2. *For any $\epsilon > 0$, $\forall r = 1,\dots,L$, $\mathfrak{l}(t)$ is differentiable on $\left[T' + \tau_{r-1} + \epsilon, T' + \tau_r\right]$ with derivative given by*

$$\dot{\mathfrak{l}}(t) = \sum_{k=0}^{L-1} \frac{|l_k(t,t)|^2}{2N_0} \tag{C.36}$$

Proof of Proposition C.2. Let $\epsilon > 0$. $\forall k = 0,\dots,L-1$, $\tilde{s}(s-\tau_k)$ is continuous on $[0,t]$. From Proposition C.1 $\forall r = 1,\dots L \quad \forall k = 0,\dots,L-1$ the function $l_k(s,t)$ is continuous on $\mathcal{R}_r(\epsilon)$ and differentiable with respect to t on $\mathcal{R}_r(\epsilon)$. Furthermore $\forall r = 1,\dots,L$ the kernel $H(s,t,t)$ is continuous on $\mathcal{R}_r(\epsilon)$. Hence $\forall r = 1,\dots L$ $\forall k = 0,\dots,L-1$ the partial derivative $\frac{\partial l_k(s,t)}{\partial t}$ is continuous on $\mathcal{R}_r(\epsilon)$. Therefore from Leibnitz's Rule $\forall r = 1,\dots L$ the right side of (C.28) is differentiable on $\left[T' + \tau_{r-1} + \epsilon, T' + \tau_r\right]$, so $\mathfrak{l}(t)$ is differentiable on $\left[T' + \tau_{r-1} + \epsilon, T' + \tau_r\right]$ with derivative given by

$$\dot{\mathfrak{l}}(t) = \sum_{k=0}^{L-1} \frac{|\alpha_k|}{2N_0}\left[\int_0^t \frac{\partial l_k(s,t)}{\partial t}\tilde{s}^*(s-\tau_k)ds + l_k(t,t)\tilde{s}^*(t-\tau_k)\right]$$

Using (C.35) yields

$$\dot{\mathfrak{l}}(t) = \sum_{k=0}^{L-1} \frac{|\alpha_k|}{2N_0} l_k(t,t)\left[\tilde{s}^*(t-\tau_k) - \int_0^t H(s,t,t)e^{j\omega_c(t-s)}\tilde{s}^*(s-\tau_k)ds\right]$$

Using (C.26) yields (C.36). **Q.E.D**

Appendix D

Direct derivation of the specular coherent and non-coherent MMSE estimates

D.1 Specular coherent MMSE estimate for an L-path Ricean channel

The specular coherent MMSE estimate, or equivalently, the conditional mean assuming that the specular component phases are known, is derived for an L-path Ricean channel based on the definition and properties of the conditional mean. For specular coherent detection, the conditional mean is defined as

$$\check{v}_m(t|\boldsymbol{\theta}) \triangleq E\left[v_m(t)|\dot{z}(s), 0 \leq s \leq t, H_m, \boldsymbol{\theta}\right] \tag{D.1}$$

where the expectation is with respect to $\boldsymbol{a} = [a_0, \ldots, a_{L-1}]^T$. Over the observation interval $[0, t]$, under H_m the received signal is given by

$$H_m : \dot{z}(s) = \Re\left\{\sum_{k=0}^{L-1} a_k e^{j\theta_k} \tilde{s}_m(s-\tau_k) e^{j\omega_c s}\right\} + \dot{w}(s) = v_m(s) + \dot{w}(s) \tag{D.2}$$

When $\boldsymbol{\theta}$ is held fixed, the noiseless received signal $v_m(s) = \Re\left\{\sum_{k=0}^{L-1} a_k e^{j\theta_k} \tilde{s}_m(s-\tau_k) e^{j\omega_c s}\right\}$ is Gaussian with mean $\nu_m(s,\boldsymbol{\theta}) \triangleq E\left[v_m(s)|\boldsymbol{\theta}\right] = \Re\left\{\sum_{k=0}^{L-1} |\alpha_k| e^{j\theta_k'} \tilde{s}_m(s-\tau_k) e^{j\omega_c s}\right\}$ and covariance function $K_m(s,u)$, where $\theta_k' = \theta_k +$

$\arg(\alpha_k)$. From (D.1) the specular coherent conditional mean $\check{v}_m(t|\boldsymbol{\theta})$ is given by

$$\begin{aligned}\check{v}_m(t|\boldsymbol{\theta}) &= E\left[(v_m(t) - \nu_m(t,\boldsymbol{\theta})) + \nu_m(t,\boldsymbol{\theta})|\boldsymbol{\theta}, \dot{z}(s), 0 \le s \le t, H_m\right] \\ &= E\left[v_m(t) - \nu_m(t,\boldsymbol{\theta})|\boldsymbol{\theta}, \dot{z}(s), 0 \le s \le t, H_m\right] + \nu_m(t,\boldsymbol{\theta}) \end{aligned} \tag{D.3}$$

But from (D.2)

$$\begin{aligned}&E\left[v_m(t) - \nu_m(t,\boldsymbol{\theta})|\boldsymbol{\theta}, \dot{z}(s), 0 \le s \le t, H_m\right] \\ &\quad = E\left[v_m(t) - \nu_m(t,\boldsymbol{\theta})|\boldsymbol{\theta}, \dot{z}(s) - \nu_m(s,\boldsymbol{\theta}) = v_m(s) - \nu_m(s,\boldsymbol{\theta}) + \dot{w}(s), 0 \le s \le t\right] \\ &\quad = E\left[v_m(t) - \nu_m(t,\boldsymbol{\theta})|\boldsymbol{\theta}, \dot{y}_m^c(s), 0 \le s \le t, H_m'\right] \end{aligned} \tag{D.4}$$

where $dy_m^c(s) = dz(s) - \nu_m(s,\boldsymbol{\theta})ds$ and the hypothesis H_m' is defined as $H_m' : \dot{y}_m^c(s) = v_m(s) - \nu_m(s,\boldsymbol{\theta}) + \dot{w}(s)$ For sake of simplicity let us introduce a new hypothesis H_{0m}' defined as $H_{0m}' : \dot{y}_m^c(s) = \dot{w}(s)$. When $\boldsymbol{\theta}$ is held fixed, $v_m(s) - \nu_m(s,\boldsymbol{\theta})$ is a Gaussian process with zero mean and covariance function $K_m(s,u)$. Therefore, considering the hypotheses H_{0m}' and H_m' from [173]

$$E\left[v_m(t) - \nu_m(t,\boldsymbol{\theta})|\boldsymbol{\theta}, \dot{y}_m^c(s), 0 \le s \le t, H_m'\right] = \int_0^t h_m(t,s)dy_m^c(s) \tag{D.5}$$

where $h_m(t,s)$ is the unique square integrable solution of the Wiener Hopf equation given by

$$h_m(t,s) + \frac{2}{N_0}\int_0^t h_m(t,\tau)K_m(\tau,s)d\tau = \frac{2}{N_0}K_m(t,s) \qquad 0 \le s \le t < \infty \tag{D.6}$$

Substituting (D.4) into (D.3) with (D.5) yields

$$\begin{aligned}\check{v}_m(t|\boldsymbol{\theta}) = &\int_0^t h_m(t,s)\left[dz(s) - \Re\left\{\sum_{k=0}^{L-1}|\alpha_k|e^{j\theta_k'}\tilde{s}_m(s-\tau_k)e^{j\omega_c s}\right\}ds\right] \\ &+ \Re\left\{\sum_{k=0}^{L-1}|\alpha_k|e^{j\theta_k'}\tilde{s}_m(t-\tau_k)e^{j\omega_c t}\right\}\end{aligned} \tag{D.7}$$

Using that $h_m(t,s)$ is real and that $h_m(t,s) = H_m(t,s,t)$ (see (C.18) and (D.6))

$$\begin{aligned}\breve{v}_m(t|\boldsymbol{\theta}) &= \int_0^t h_m(t,s)dz(s) \\ &\quad + \Re\left\{\sum_{k=0}^{L-1}|\alpha_k|e^{j\theta_k'}\left[\tilde{s}_m(t-\tau_k)e^{j\omega_c t} - \int_0^t H_m(t,s,t)\tilde{s}_m(s-\tau_k)e^{j\omega_c s}ds\right]\right\} \\ &= \Re\left\{\left(2\int_0^t \mathcal{H}_m^*(s,t,t)e^{-j\omega_c s}dz(s) + \sum_{k=0}^{L-1} l_{km}(t,t)e^{j\theta_k'}\right)e^{j\omega_c t}\right\} \qquad \text{(D.8)}\end{aligned}$$

where $\mathcal{H}_m(s,t,t)$ is given by (3.41), $l_{km}(t,t)$ is given by (3.49) and the last equality comes from (C.27) and $h_m(t,s) = H_m(t,s,t) = \Re\left\{2\mathcal{H}_m^*(s,t,t)e^{j\omega_c(t-s)}\right\}$.

D.2 Non-coherent MMSE estimate for an L-path Ricean channel

Section 3.3.3 (topic: "Computation of the conditional mean using its definition") presented the principles of an iterative method to derive the non-coherent conditional mean corresponding to L-path Ricean channels based on (3.110). This method involves the successive computation of conditional means. Details on how to compute these conditional means are given in this section.

Let $\Lambda_m\left(\dot{z};t|\boldsymbol{\theta}_l'\right)$ be the conditional likelihood ratio when $\boldsymbol{\theta}_l'$ is held fixed and the observation interval is $[0,t]$. By modifying results from Appendix B.3.1 to take into account the observation interval, $[0,t]$, and using Section 3.3.3 (topic: "Likelihood ratio over an arbitrary observation interval $[0,t]$ assuming that $\bar{s}_m(s)$ is time-limited") the conditional likelihood ratios are given by

$$\Lambda_m\left(\dot{z};t|\boldsymbol{\theta}_{L-1}'\right) = J_m(t)\exp\left\{\sum_{k=0}^{L-1}\frac{|\alpha_k||b_{km}(\boldsymbol{\theta}_{k-1}',t)|}{\sigma_k^2\sqrt{\epsilon_{km}(t)}}\cos\left(\theta_k - \varphi_{km}(\boldsymbol{\theta}_{k-1}',t)\right)\right\} \qquad \text{(D.9)}$$

$$\Lambda_m\left(\dot{z};t|\boldsymbol{\theta}_{l-1}'\right) = \frac{1}{2\pi}\int_{-\pi}^{\pi}\Lambda_m\left(\dot{z};t|\boldsymbol{\theta}_l'\right)d\theta_l' \quad l = 1,\ldots,L-1 \quad L \geq 2 \qquad \text{(D.10)}$$

where (D.9) is obtained from (3.92) and

$$\frac{|\alpha_k|b_{km}(\boldsymbol{\theta}_{k-1}',t)}{\sigma_k^2\sqrt{\epsilon_{km}(t)}} = d_{km}(t) - \sum_{n=0}^{k-1}e_{kn}^m(t)e^{j\theta_n'} \qquad \frac{|\alpha_0|b_{0m}(t)}{\sigma_0^2\sqrt{\epsilon_{0m}(t)}} = d_{0m}(t) \qquad \text{(D.11)}$$

$$e_{kn}^{m}(t) = \frac{1}{N_0}\int_0^t l_{nm}(s,t)\,|\alpha_k|\,\tilde{s}_m^*(s-\tau_k)ds \tag{D.12}$$

$$\varphi_{km}(\boldsymbol{\theta}_{k-1}^{'},t) = \arg\left[b_{km}(\boldsymbol{\theta}_{k-1}^{'},t)\right] - \arg\left[\alpha_k\right] \quad \varphi_{0m}(t) = \arg\left[b_{0m}(t)\right] - \arg\left[\alpha_0\right] \tag{D.13}$$

$d_{km}(t)$ is given by (3.100) and $\boldsymbol{\theta}_k^{'}$ is given by (3.90). Obviously, the likelihood ratio $\Lambda_m(\dot{z};t)$ is given by

$$\Lambda_m(\dot{z};t) = \frac{1}{2\pi}\int_{-\pi}^{\pi}\Lambda_m\left(\dot{z};t|\theta_0^{'}\right)d\theta_0^{'} = \frac{1}{2\pi}\int_{-\pi}^{\pi}\Lambda_m\left(\dot{z};t|\boldsymbol{\theta}_0^{'}\right)d\boldsymbol{\theta}_0^{'}$$

Then, from (3.110), Bayes' rule and the statistical independence of the $\theta_k^{'}$'s, the conditional mean given $\boldsymbol{\theta}_l^{'}$ $\check{v}_{lm}(t,\boldsymbol{\theta}_l^{'}) \triangleq E\left[\check{v}_{L-1m}(t,\boldsymbol{\theta}^{'})|\boldsymbol{\theta}_l^{'},\dot{z}(s),0\le s\le t,H_m\right]$ is given iteratively by

$$\begin{aligned}
\check{v}_{l-1m}(t,\boldsymbol{\theta}_{l-1}^{'}) &= \int_{-\infty}^{\infty}\check{v}_{lm}(t,\boldsymbol{\theta}_l^{'})p\left(\theta_l^{'}|\dot{z}(s),0\le s\le t,\boldsymbol{\theta}_{l-1}^{'},H_m\right)d\theta_l^{'} \\
&= \int_{-\infty}^{\infty}\check{v}_{lm}(t,\boldsymbol{\theta}_l^{'})\frac{p\left(\dot{z}(s),0\le s\le t|\theta_l^{'},\boldsymbol{\theta}_{l-1}^{'},H_m\right)p\left(\theta_l^{'}\right)}{p\left(\dot{z}(s),0\le s\le t|\boldsymbol{\theta}_{l-1}^{'},H_m\right)}d\theta_l^{'} \\
&= \frac{1}{2\pi}\int_{-\pi}^{\pi}\check{v}_{lm}(t,\boldsymbol{\theta}_l^{'})\frac{\frac{p\left(\dot{z}(s),0\le s\le t|\boldsymbol{\theta}_l^{'},H_m\right)}{p(\dot{z}(s),0\le s\le t|H_0)}}{\frac{p\left(\dot{z}(s),0\le s\le t|\boldsymbol{\theta}_{l-1}^{'},H_m\right)}{p(\dot{z}(s),0\le s\le t|H_0)}}d\theta_l^{'} \\
&= \frac{1}{2\pi}\int_{-\pi}^{\pi}\check{v}_{lm}(t,\boldsymbol{\theta}_l^{'})\frac{\Lambda_m\left(\dot{z};t|\boldsymbol{\theta}_l^{'}\right)}{\Lambda_m\left(\dot{z};t|\boldsymbol{\theta}_{l-1}^{'}\right)}d\theta_l^{'} \quad l=0,\ldots,L-1
\end{aligned} \tag{D.14}$$

with the convention that $\check{v}_{-1m} = \check{v}_m(t)$ (see (3.108)), $\boldsymbol{\theta}_{-1}^{'} = [\cdot]$ (*null set*) and $\Lambda_m\left(\dot{z};t|\boldsymbol{\theta}_{-1}^{'}\right) = \Lambda_m(\dot{z};t)$. The first conditional mean $\check{v}_{L-1m}\left(t,\boldsymbol{\theta}_{L-1}^{'}\right)$, (3.109) is by definition the specular coherent conditional mean $\check{v}_m(t|\boldsymbol{\theta})$, (D.1), and is computed in Appendix D.1. Use of (D.14) is illustrated in Appendix D.3 and Appendix D.4, where the conditional mean $\check{v}_m(t)$ is calculated for the special cases of mixed mode Ricean/Rayleigh and 2 Ricean/L-2 Rayleigh channels.

Remark. If $\check{v}_{lm}\left(t,\boldsymbol{\theta}_l^{'}\right)$ is independent of $\theta_l^{'}$, substituting (D.10) into (D.14) yields $\check{v}_{l-1m}\left(t,\boldsymbol{\theta}_{l-1}^{'}\right) = \check{v}_{lm}\left(t,\boldsymbol{\theta}_l^{'}\right)$.

D.3 Non-coherent MMSE estimate for a mixed mode Ricean/Rayleigh channel

Similar to (3.154), since $\forall k = 1, \ldots, L \quad \alpha_k = 0$, the likelihood ratio over $[0, t]$ (3.92) reduces to

$$\Lambda_m(\dot{z}; t) = J_m(t) I_0\big(V_{0m}(t)\big) \tag{D.15}$$

where $J_m(t)$ is given by (3.93) and $V_{0m}(t)$ is given by (3.98). For a mixed mode Ricean/Rayleigh channel, $\forall k \neq 0 \quad \alpha_k = 0$, hence from (3.103b) $\forall k \neq 0 \quad l_{km}(s,t) = 0$. Therefore in that case (D.8) reduces to

$$\begin{aligned}\check{v}_m(t|\boldsymbol{\theta}) &\triangleq \check{v}_{L-1m}(t, \boldsymbol{\theta}'_{L-1}) \\ &= \Re\left\{\left(2\int_0^t \mathcal{H}_m^*(s,t,t)e^{-j\omega_c s}\dot{\alpha}^*(s) + l_{0m}(t,t)e^{j\theta'_0}\right)e^{j\omega_c t}\right\}\end{aligned} \tag{D.16}$$

As seen from (D.16), $\check{v}_{L-1m}(t, \boldsymbol{\theta}'_{L-1})$ is independent of $\theta'_1, \ldots, \theta'_{L-1}$, hence from (D.16) and the remark at the end of Appendix D.2

$$\begin{aligned}\check{v}_{0m}(t,\theta'_0) &= \check{v}_{1m}(t,\boldsymbol{\theta}'_1) = \ldots = \check{v}_{L-1m}(t,\boldsymbol{\theta}'_{L-1}) \\ &= \Re\left\{\left(2\int_0^t \mathcal{H}_m^*(s,t,t)e^{-j\omega_c s}dz(s)\right)e^{j\omega_c t}\right\} + \Re\left\{l_{0m}(t,t)e^{j\theta'_0}e^{j\omega_c t}\right\}\end{aligned} \tag{D.17}$$

Substituting (D.17) into (D.14) yields

$$\begin{aligned}\check{v}_m(t) = \check{v}_{-1m}(t) &= \frac{1}{2\pi}\int_{-\pi}^{\pi}\Re\left\{\left(2\int_0^t \mathcal{H}_m^*(s,t,t)e^{-j\omega_c s}dz(s)\right)e^{j\omega_c t}\right\}\frac{\Lambda_m\left(\dot{z}; t|\theta'_0\right)}{\Lambda_m(\dot{z};t)}d\theta'_0 \\ &\quad + \frac{1}{2\pi}\int_{-\pi}^{\pi}\Re\left\{l_{0m}(t,t)e^{j\theta'_0}e^{j\omega_c t}\right\}\frac{\Lambda_m\left(\dot{z}; t|\theta'_0\right)}{\Lambda_m(\dot{z};t)}d\theta'_0 \\ &= \Re\left\{\left(2\int_0^t \mathcal{H}_m^*(s,t,t)e^{-j\omega_c s}dz(s)\right)e^{j\omega_c t}\right\} \\ &\quad + \frac{1}{2\pi}\int_{-\pi}^{\pi}\Re\left\{l_{0m}(t,t)e^{j\theta'_0}e^{j\omega_c t}\right\}\frac{\Lambda_m\left(\dot{z}; t|\theta'_0\right)}{\Lambda_m(\dot{z};t)}d\theta'_0\end{aligned} \tag{D.18}$$

For a mixed mode Ricean/Rayleigh channel, $\forall k \neq 0 \quad \alpha_k = 0$, hence (D.9) reduces to

$$\begin{aligned}\Lambda_m\left(\dot{z};t|\boldsymbol{\theta}'_{L-1}\right) &= J_m(t)\exp\left\{\frac{|\alpha_0|\,|b_{0m}(t)|}{\sigma_0^2\sqrt{\epsilon_{0m}(t)}}\cos\left(\theta_0-\varphi_{0m}(t)\right)\right\}\\ &= J_m(t)\exp\left\{V_{0m}(t)\cos\left(\theta'_0-\vartheta_{0m}(t)\right)\right\}\end{aligned}$$

since from (D.11) $\frac{|\alpha_0|b_{0m}(t)}{\sigma_0^2\sqrt{\epsilon_{0m}(t)}} = d_{0m}(t) = V_{0m}(t)e^{j\vartheta_{0m}(t)}$. Since $\Lambda_m\left(\dot{z};t|\boldsymbol{\theta}'_{L-1}\right)$ is independent of $\theta'_1,\ldots,\theta'_{L-1}$, $\Lambda_m\left(\dot{z};t|\boldsymbol{\theta}'_{L-1}\right) = \Lambda_m\left(\dot{z};t|\theta'_0\right)$. Using (D.15) yields[1]

$$\begin{aligned}&\frac{1}{2\pi}\int_{-\pi}^{\pi}\Re\left\{l_{0m}(t,t)e^{j\theta'_0}e^{j\omega_c t}\right\}\frac{\Lambda_m\left(\dot{z};t|\theta'_0\right)}{\Lambda_m\left(\dot{z};t\right)}d\theta'_0\\ &\quad=\frac{1}{2\pi}\int_{-\pi}^{\pi}\Re\left\{l_{0m}(t,t)e^{j\theta'_0}e^{j\omega_c t}\right\}\frac{e^{jV_{0m}(t)\cos\left(\theta'_0-\vartheta_{0m}(t)\right)}}{I_0\left(V_{0m}(t)\right)}d\theta'_0\\ &\quad=\frac{\Re\left\{l_{0m}(t,t)e^{j\vartheta_{0m}(t)}e^{j\omega_c t}\right\}}{2\pi I_0\left(V_{0m}(t)\right)}\int_{-\pi}^{\pi}\cos\left(\theta'_0-\vartheta_{0m}(t)\right)e^{jV_{0m}(t)\cos\left(\theta'_0-\vartheta_{0m}(t)\right)}d\theta'_0\\ &\quad=\Re\left\{\frac{I_1\left(V_{0m}(t)\right)}{I_0\left(V_{0m}(t)\right)}l_{0m}(t,t)e^{j\vartheta_{0m}(t)}e^{j\omega_c t}\right\}\end{aligned}\tag{D.19}$$

Substituting (D.19) into (D.18) yields

$$\begin{aligned}\breve{v}_m(t) &= \Re\left\{\left(2\int_0^t\mathcal{H}_m^*(s,t,t)e^{-j\omega_c s}dz(s)+\frac{I_1\left(V_{0m}(t)\right)}{I_0\left(V_{0m}(t)\right)}l_{0m}(t,t)e^{j\vartheta_{0m}(t)}\right)e^{j\omega_c t}\right\}\\ &= \Re\left\{\left(2\int_0^t\mathcal{H}_m^*(s,t,t)e^{-j\omega_c s}dz(s)+V'_{0m}(t)e^{j\vartheta'_{0m}(t)}l_{0m}(t,t)e^{j\vartheta_{0m}(t)}\right)e^{j\omega_c t}\right\}\end{aligned}\tag{D.20}$$

where $\mathcal{H}_m(s,t,t)$ is given by (3.41) and $l_{km}(t,t)$ is given by (3.103),

$$V'_{0m}(t)e^{j\vartheta'_{0m}(t)} = \frac{I_1\left(V_{0m}(t)\right)}{I_0\left(V_{0m}(t)\right)}+j\cdot 0 = \frac{\frac{\partial g\left(\boldsymbol{d}_m(t),t\right)}{\partial V_{0m}(t)}}{g\left(\boldsymbol{d}_m(t),t\right)}+j\frac{\frac{1}{V_{0m}(t)}\frac{\partial g\left(\boldsymbol{d}_m(t),t\right)}{\partial\vartheta_{0m}(t)}}{g\left(\boldsymbol{d}_m(t),t\right)}$$

[1]The second equality is obtained by expanding the real part of a product. Two integrals are then obtained, one with a cosine and another with a sine, however the integral with the sine is equal to zero since the integrand is odd.

and $g(\boldsymbol{d}_m(t),t)=\frac{\Lambda_m(\dot{z};t)}{J_m(t)} = I_0(V_{0m}(t))$. It is seen that (D.20) is identical to the conditional mean expression found by Itô differentiation (see (3.124a) assuming $l_{1m}(s,t) = \ldots = l_{L-1m}(s,t) = 0$, a property of mixed mode Ricean/Rayleigh channels).

D.4 Non-coherent MMSE estimate for a 2 Ricean/L-2 Rayleigh channel

Modifying results of Section 3.6.1 to take into account the new observation interval $[0,t]$ and using techniques of Section 3.3.3, from (3.172) the likelihood ratio over $[0,t]$ for a 2 Ricean/L-2 Rayleigh channel is given by

$$\Lambda_m(\dot{z};t) = J_m(t)g(\boldsymbol{d}_m(t),t) = J_m(t)\Big\{I_0(V_{0m}(t))I_0(V_{10}^m(t))I_0(V_{1m}(t)) + 2\sum_{p=1}^{\infty}(-1)^p I_p(V_{0m}(t))I_p(V_{10}^m(t))I_p(V_{1m}(t))\cos\left[p(\vartheta_{0m}(t)+\vartheta_{10}^m(t)-\vartheta_{1m}(t))\right]\Big\} \tag{D.21}$$

where $J_m(t)$ is given by (3.93), $V_{km}(t)$ is given by (3.98), $\vartheta_{km}(t)$ is given by (3.99), $V_{kn}^m(t) = |e_{kn}^m(t)|$, $\vartheta_{kn}^m(t) = \arg[e_{kn}^m(t)]$ and $e_{kn}^m(t)$ is given by (D.12).

D.4.1 2 Ricean/L-2 Rayleigh conditional mean when θ_0' is held fixed $(\breve{v}_{0m}(t,\theta_0'))$

For a 2 Ricean/L-2 Rayleigh channel, $\forall\, k = 2,\ldots,L-1 \;\; \alpha_k = 0$, hence from (3.103b), $\forall k \neq 0,1 \; l_{km}(s,t) = 0$. Therefore in that case (D.8) reduces to

$$\begin{aligned}\breve{v}_m(t|\boldsymbol{\theta}) &\triangleq \breve{v}_{L-1m}(t,\boldsymbol{\theta}_{L-1}')\\ &= \Re\left\{\left(2\int_0^t \mathcal{H}_m^*(s,t,t)e^{-j\omega_c s}dz(s) + \sum_{k=0}^{1} l_{km}(t,t)e^{j\theta_k'}\right)e^{j\omega_c t}\right\}\end{aligned} \tag{D.22}$$

As seen from (D.22), $\breve{v}_{L-1m}(t,\boldsymbol{\theta}_{L-1}')$ is independent of $\theta_2',\ldots,\theta_{L-1}'$, hence from (D.22) and the remark at the end of Appendix D.2

$$\breve{v}_{1m}(t,\boldsymbol{\theta}_1') = \breve{v}_{2m}(t,\boldsymbol{\theta}_2') = \ldots = \breve{v}_{L-1m}(t,\boldsymbol{\theta}_{L-1}')$$

$$\breve{v}_{1m}(t,\boldsymbol{\theta}_1') = \Re\left\{\left(2\int_0^t \mathcal{H}_m^*(s,t,t)e^{-j\omega_c s}dz(s) + l_{0m}(t,t)e^{j\theta_0'}\right)e^{j\omega_c t}\right\} + \Re\left\{l_{1m}(t,t)e^{j\theta_1'}e^{j\omega_c t}\right\} \tag{D.23}$$

Substituting (D.23) into (D.14) and simplifying yield

$$\breve{v}_{0m}(t,\boldsymbol{\theta}_0') = \Re\left\{\left(2\int_0^t \mathcal{H}_m^*(s,t,t)e^{-j\omega_c s}dz(s) + l_{0m}(t,t)e^{j\theta_0'}\right)e^{j\omega_c t}\right\} + \frac{1}{2\pi}\int_{-\pi}^{\pi}\Re\left\{l_{1m}(t,t)e^{j\theta_1'}e^{j\omega_c t}\right\}\frac{\Lambda_m(\dot{z};t|\boldsymbol{\theta}_1')}{\Lambda_m(\dot{z};t|\boldsymbol{\theta}_0')}d\theta_1' \tag{D.24}$$

For a 2 Ricean/L-2 Rayleigh channel, $\forall\, k \neq 0,1 \quad \alpha_k = 0$, therefore (D.9) reduces to

$$\Lambda_m(\dot{z};t|\boldsymbol{\theta}_{L-1}') = J_m(t)e^{\left[\frac{|\alpha_1||b_{1m}(\theta_0',t)|}{\sigma_1^2\sqrt{\epsilon_{1m}(t)}}\cos\left(\theta_1-\varphi_{1m}(\theta_0',t)\right)\right]}e^{V_{0m}(t)\cos\left(\theta_0'-\vartheta_{0m}(t)\right)} \tag{D.25}$$

since from (D.11) $\frac{|\alpha_0|b_{0m}(t)}{\sigma_0^2\sqrt{\epsilon_{0m}(t)}} = d_{0m}(t) = V_{0m}(t)e^{j\vartheta_{0m}(t)}$. Since $\Lambda_m(\dot{z};t|\boldsymbol{\theta}_{L-1}')$ is independent of $\theta_2', \ldots, \theta_{L-1}'$, $\Lambda_m(\dot{z};t|\boldsymbol{\theta}_{L-1}') = \Lambda_m(\dot{z};t|\boldsymbol{\theta}_1')$ and from (D.10)

$$\begin{aligned}\Lambda_m(\dot{z};t|\theta_0') &= \frac{1}{2\pi}\int_{-\pi}^{\pi}\Lambda_m\left(\dot{z};t|\boldsymbol{\theta}_1'\right)d\theta_1' \\ &= J_m(t)I_0\left(\frac{|\alpha_1|\,|b_{1m}(\theta_0',t)|}{\sigma_1^2\sqrt{\epsilon_{1m}(t)}}\right)\exp\left\{V_{0m}(t)\cos\left(\theta_0'-\vartheta_{0m}(t)\right)\right\}\end{aligned} \tag{D.26}$$

Using (D.26), and $\Lambda_m(\dot{z};t|\boldsymbol{\theta}_1') = \Lambda_m(\dot{z};t|\boldsymbol{\theta}_{L-1}')$ with (D.25), yield

$$\frac{1}{2\pi}\int_{-\pi}^{\pi}\Re\left\{l_{1m}(t,t)e^{j\theta_1'}e^{j\omega_c t}\right\}\frac{\Lambda_m\left(\dot{z};t|\boldsymbol{\theta}_1'\right)}{\Lambda_m(\dot{z};t|\theta_0')}d\theta_1'$$

$$= \frac{1}{2\pi}\int_{-\pi}^{\pi}\Re\left\{l_{1m}(t,t)e^{j\theta_1'}e^{j\omega_c t}\right\}\frac{e^{\left[\frac{|\alpha_1||b_{1m}(\theta_0',t)|}{\sigma_1^2\sqrt{\epsilon_{1m}(t)}}\cos\left(\theta_1-\varphi_{1m}(\theta_0',t)\right)\right]}}{I_0\left(\frac{|\alpha_1||b_{1m}(\theta_0',t)|}{\sigma_1^2\sqrt{\epsilon_{1m}(t)}}\right)}d\theta_1'$$

$$= \frac{\Re\left\{l_{1m}(t,t)e^{j\varphi_{1m}(\theta_0',t)}e^{j\delta_1}e^{j\omega_c t}\right\}}{2\pi I_0\left(\frac{|\alpha_1||b_{1m}(\theta_0',t)|}{\sigma_1^2\sqrt{\epsilon_{1m}(t)}}\right)}$$

$$\cdot \int_{-\pi}^{\pi} \cos\left(\theta_1' - \delta_1 - \varphi_{1m}(\theta_0',t)\right) e^{\left[\frac{|\alpha_1||b_{1m}(\theta_0',t)|}{\sigma_1^2\sqrt{\epsilon_{1m}(t)}}\cos\left(\theta_1'-\delta_1-\varphi_{1m}(\theta_0',t)\right)\right]} d\theta_1' \tag{D.27}$$

$$= \Re\left\{\frac{I_1\left(\frac{|\alpha_1||b_{1m}(\theta_0',t)|}{\sigma_1^2\sqrt{\epsilon_{1m}(t)}}\right)}{I_0\left(\frac{|\alpha_1||b_{1m}(\theta_0',t)|}{\sigma_1^2\sqrt{\epsilon_{1m}(t)}}\right)} l_{1m}(t,t)e^{j\varphi_{1m}(\theta_0',t)}e^{j\delta_1}e^{j\omega_c t}\right\} \tag{D.28}$$

where $\delta_1 = \arg[\alpha_1]$ and (D.27) is obtained by expanding the real part of a product. Two integrals are then obtained, one with a cosine and another with a sine, however the integral with the sine is equal to zero since the integrand is odd. Substituting (D.28) into (D.24) yields

$$\breve{v}_{0m}(t,\theta_0') = \breve{v}_{0m}(t,\boldsymbol{\theta}_0') = \Re\left\{\left(2\int_0^t \mathcal{H}_m^*(s,t,t)e^{-j\omega_c s}dz(s)\right)e^{j\omega_c t}\right\}$$

$$+ \Re\left\{l_{0m}(t,t)e^{j\theta_0'}e^{j\omega_c t}\right\} + \Re\left\{\frac{I_1\left(\frac{|\alpha_1||b_{1m}(\theta_0',t)|}{\sigma_1^2\sqrt{\epsilon_{1m}(t)}}\right)}{I_0\left(\frac{|\alpha_1||b_{1m}(\theta_0',t)|}{\sigma_1^2\sqrt{\epsilon_{1m}(t)}}\right)} l_{1m}(t,t)e^{j\varphi_{1m}(\theta_0',t)}e^{j\delta_1}e^{j\omega_c t}\right\} \tag{D.29}$$

where $b_{1m}(\theta_0',t)$ and $\varphi_{1m}(\theta_0',t)$ are given by (D.11) and (D.13) and $\delta_1 = \arg[\alpha_1]$.

D.4.2 2 Ricean/L-2 Rayleigh MMSE estimate $(\breve{v}_m(t))$: averaging of $\breve{v}_{0m}(t,\theta_0')$ over θ_0'

Substituting (D.29) into (D.14) and simplifying yield

$$\breve{v}_m(t) = \breve{v}_{-1m}(t) = \Re\left\{\left(2\int_0^t \mathcal{H}_m^*(s,t,t)e^{-j\omega_c s}dz(s)\right)e^{j\omega_c t}\right\} + l_{0m}'(t) + l_{1m}'(t) \tag{D.30}$$

where $l_{0m}'(t)$ and $l_{1m}'(t)$ are given by

$$l_{0m}'(t) = \frac{1}{2\pi}\int_{-\pi}^{\pi} \Re\left\{l_{0m}(t,t)e^{j\theta_0'}e^{j\omega_c t}\right\}\frac{\Lambda_m\left(\dot{z};t|\theta_0'\right)}{\Lambda_m\left(\dot{z};t\right)}d\theta_0' \tag{D.31}$$

$$l'_{1m}(t) = \frac{1}{2\pi}\int_{-\pi}^{\pi} \Re\left\{ \frac{I_1\left(\frac{|\alpha_1||b_{1m}(\theta'_0,t)|}{\sigma_1^2\sqrt{\epsilon_{1m}(t)}}\right)}{I_0\left(\frac{|\alpha_1||b_{1m}(\theta'_0,t)|}{\sigma_1^2\sqrt{\epsilon_{1m}(t)}}\right)} l_{1m}(t,t)e^{j\varphi_{1m}(\theta'_0,t)}e^{j\delta_1}e^{j\omega_c t}\right\} \frac{\Lambda_m\left(\dot{z};t|\theta'_0\right)}{\Lambda_m\left(\dot{z};t\right)} d\theta'_0 \tag{D.32}$$

Omitting t wherever there is no ambiguity, substituting (D.21) and (D.26) into (D.31) yield

$$l'_{0m}(t) = \frac{1}{2\pi}\int_{-\pi}^{\pi} \Re\left\{ l_{0m}(t,t)e^{j\theta'_0}e^{j\omega_c t}\right\} \exp\left\{V_{0m}\cos\left(\theta'_0 - \vartheta_{0m}\right)\right\} \frac{I_0\left(\frac{|\alpha_1||b_{1m}(\theta'_0)|}{\sigma_1^2\sqrt{\epsilon_{1m}}}\right)}{g\left(\boldsymbol{d}_m,t\right)} d\theta'_0 \tag{D.33}$$

where $g\left(\boldsymbol{d}_m,t\right) = \frac{\Lambda_m(\dot{z};t)}{J_m(t)}$ can be obtained from (D.21). From [185, pp. 358,361]

$$I_0(\omega) = I_0(Z)I_0(z) + 2\sum_{p=1}^{\infty}(-1)^p I_p(Z)I_p(z)\cos p\phi \tag{D.34a}$$

$$I_n(\omega)\cos n\psi = \sum_{p=-\infty}^{\infty}(-1)^p I_{n+p}(Z)I_p(z)\cos p\phi \tag{D.34b}$$

$$I_n(\omega)\sin n\psi = \sum_{p=-\infty}^{\infty}(-1)^p I_{n+p}(Z)I_p(z)\sin p\phi \tag{D.34c}$$

where n is an integer and Z, z, ϕ, ω and ψ are complex numbers satisfying

$$\omega = \sqrt{Z^2 + z^2 - 2Zz\cos\phi} \qquad \omega\cos\psi = Z - z\cos\phi \qquad \omega\sin\psi = z\sin\phi$$

Recall from (D.11) $\frac{|\alpha_1|b_{1m}(\theta'_0)}{\sigma_1^2\sqrt{\epsilon_{1m}}} = d_{1m} - e_{10}^m e^{j\theta'_0}$, then substituting (D.34a) with $\omega = \frac{|\alpha_1||b_{1m}(\theta'_0)|}{\sigma_1^2\sqrt{\epsilon_{1m}}}$, $Z = V_{1m}$, $z = V_{10}^m$ and $\phi = \theta'_0 + \vartheta_{10}^m - \vartheta_{1m}$ into (D.33) yields

$$l'_{0m}(t) = \frac{I_0\left(V_{1m}\right)I_0\left(V_{10}^m\right)}{g\left(\boldsymbol{d}_m,t\right)}\mathcal{A}_0 + 2\sum_{p=1}^{\infty}(-1)^p\frac{I_p\left(V_{1m}\right)I_p\left(V_{10}^m\right)}{g\left(\boldsymbol{d}_m,t\right)}\mathcal{A}_p \tag{D.35}$$

where $\mathcal{A}_0$ is given by

$$\mathcal{A}_0 = \frac{1}{2\pi}\int_{-\pi}^{\pi}\Re\left\{l_{0m}(t,t)e^{j\theta'_0}e^{j\omega_c t}\right\}e^{V_{0m}\cos\left(\theta'_0-\vartheta_{0m}\right)}d\theta'_0$$

$$= \Re\left\{ l_{0m}(t,t) e^{j\theta_0'} e^{j\omega_c t} \right\} I_0\left(V_{0m}\right) \tag{D.36}$$

and $\mathcal{A}_p$ $(p \geq 1)$ is given by[2]

$$\begin{aligned}
\mathcal{A}_p &= \frac{1}{2\pi} \int_{-\pi}^{\pi} \Re\left\{ l_{0m}(t,t) e^{j\theta_0'} e^{j\omega_c t} \right\} \cos\Big(p\big(\theta_0' + \vartheta_{10}^m - \vartheta_{1m}\big) \Big) e^{V_{0m}\cos\left(\theta_0' - \vartheta_{0m}\right)} d\theta_0' \\
&= \frac{1}{2}\frac{1}{2\pi} \int_{-\pi}^{\pi} \Re\left\{ l_{0m}(t,t) e^{j\omega_c t} e^{jp\left(\vartheta_{10}^m - \vartheta_{1m}\right)} e^{j(p+1)\theta_0'} \right\} e^{V_{0m}\cos\left(\theta_0' - \vartheta_{0m}\right)} d\theta_0' \\
&\quad + \frac{1}{2}\frac{1}{2\pi} \int_{-\pi}^{\pi} \Re\left\{ l_{0m}(t,t) e^{j\omega_c t} e^{-jp\left(\vartheta_{10}^m - \vartheta_{1m}\right)} e^{-j(p-1)\theta_0'} \right\} e^{V_{0m}\cos\left(\theta_0' - \vartheta_{0m}\right)} d\theta_0' \\
&= \frac{1}{2} \Re\left\{ l_{0m}(t,t) e^{j\omega_c t} e^{j\vartheta_{0m}} e^{jp\left(\vartheta_{10}^m - \vartheta_{1m} + \vartheta_{0m}\right)} \right\} I_{p+1}\left(V_{0m}\right) \\
&\quad + \frac{1}{2} \Re\left\{ l_{0m}(t,t) e^{j\omega_c t} e^{j\vartheta_{0m}} e^{-jp\left(\vartheta_{10}^m - \vartheta_{1m} + \vartheta_{0m}\right)} \right\} I_{p-1}\left(V_{0m}\right) \\
&= \Re\left\{ l_{0m}(t,t) e^{j\omega_c t} e^{j\vartheta_{0m}} \right\} \cos\Big(p\big(\vartheta_{10}^m - \vartheta_{1m} + \vartheta_{0m}\big) \Big) \frac{\partial I_p\left(V_{0m}\right)}{\partial V_{0m}} \\
&\quad - \Im\left\{ l_{0m}(t,t) e^{j\omega_c t} e^{j\vartheta_{0m}} \right\} (-p) \sin\Big(p\big(\vartheta_{10}^m - \vartheta_{1m} + \vartheta_{0m}\big) \Big) \frac{I_p\left(V_{0m}\right)}{V_{0m}}
\end{aligned} \tag{D.37}$$

since [185, p. 79]

$$I_{p+1}(x) + I_{p-1}(x) = 2\frac{\partial I_p(x)}{\partial x} \qquad I_{p+1}(x) - I_{p-1}(x) = -2p\frac{I_p(x)}{x}$$

Substituting (D.36) and (D.37) into (D.35) and simplifying yield

$$l_{0m}'(t) = \Re\left\{ l_{0m}(t,t) e^{j\vartheta_{0m}} e^{j\omega_c t} \right\} \frac{\dfrac{\partial g\left(\boldsymbol{d}_m, t\right)}{\partial V_{0m}}}{g\left(\boldsymbol{d}_m, t\right)} - \Im\left\{ l_{0m}(t,t) e^{j\vartheta_{0m}} e^{j\omega_c t} \right\} \frac{\dfrac{1}{V_{0m}} \dfrac{\partial g\left(\boldsymbol{d}_m, t\right)}{\partial \vartheta_{0m}}}{g\left(\boldsymbol{d}_m, t\right)} \tag{D.38}$$

where $g(\boldsymbol{d}_m, t)$ is obtained from (D.21). Substituting (D.21) and (D.26) into (D.32) yields

$$l_{1m}'(t) = \frac{1}{2\pi} \int_{-\pi}^{\pi} \Re\left\{ l_{1m}(t,t) e^{j\varphi_{1m}(\theta_0')} e^{j\delta_1} e^{j\omega_c t} \right\} \frac{I_1\left(\frac{|\alpha_1||b_{1m}(\theta_0')|}{\sigma_1^2 \sqrt{\epsilon_{1m}}} \right)}{g\left(\boldsymbol{d}_m, t\right)} e^{V_{0m}\cos\left(\theta_0' - \vartheta_{0m}\right)} d\theta_0'$$

[2]The third equality is obtained by noting that the real part of a complex number can be expressed in terms of a cosine and by using the trigonometric expansion of a product of cosine.

$$= \frac{\Re\left\{l_{1m}(t,t)e^{j\vartheta_{1m}}e^{j\omega_c t}\right\}}{g\left(\boldsymbol{d}_m,t\right)}\frac{1}{2\pi}\int_{-\pi}^{\pi} I_1\left(\frac{|\alpha_1||b_{1m}(\theta_0')|}{\sigma_1^2\sqrt{\epsilon_{1m}}}\right)\cos\left(\vartheta_{1m}-\delta_1-\varphi_{1m}(\theta_0')\right)$$
$$\cdot\exp\left\{V_{0m}\cos\left(\theta_0'-\vartheta_{0m}\right)\right\}d\theta_0'$$
$$+\frac{\Im\left\{l_{1m}(t,t)e^{j\vartheta_{1m}}e^{j\omega_c t}\right\}}{g\left(\boldsymbol{d}_m,t\right)}\frac{1}{2\pi}\int_{-\pi}^{\pi} I_1\left(\frac{|\alpha_1||b_{1m}(\theta_0')|}{\sigma_1^2\sqrt{\epsilon_{1m}}}\right)\sin\left(\vartheta_{1m}-\delta_1-\varphi_{1m}(\theta_0')\right)$$
$$\cdot\exp\left\{V_{0m}\cos\left(\theta_0'-\vartheta_{0m}\right)\right\}d\theta_0' \qquad \text{(D.39)}$$

Substituting (D.34b) and (D.34c) with $p=1$, $\omega=\frac{|\alpha_1||b_{1m}(\theta_0')|}{\sigma_1^2\sqrt{\epsilon_{1m}}}$, $Z=V_{1m}$, $z=V_{10}^m$, $\psi=\vartheta_{1m}-\delta_1-\varphi_{1m}(\theta_0')$ and $\phi=\theta_0'+\vartheta_{10}^m-\vartheta_{1m}$ into (D.39) yields

$$l_{1m}'(t)=\frac{\Re\left\{l_{1m}(t,t)e^{j\vartheta_{1m}}e^{j\omega_c t}\right\}}{g\left(\boldsymbol{d}_m,t\right)}\mathcal{A}'+\frac{\Im\left\{l_{1m}(t,t)e^{j\vartheta_{1m}}e^{j\omega_c t}\right\}}{g\left(\boldsymbol{d}_m,t\right)}\mathcal{A}'' \qquad \text{(D.40)}$$

where $\mathcal{A}'$ is given by

$$\mathcal{A}'=\sum_{p=-\infty}^{\infty}(-1)^p I_{p+1}\left(V_{1m}\right)I_p\left(V_{10}^m\right)\int_{-\pi}^{\pi}\cos\left(p\left(\theta_0'+\vartheta_{10}^m-\vartheta_{1m}\right)\right)\frac{e^{V_{0m}\cos\left(\theta_0'-\vartheta_{0m}\right)}}{2\pi}d\theta_0'$$
$$=I_1\left(V_{1m}\right)I_0\left(V_{10}^m\right)I_0\left(V_{0m}\right)$$
$$+\sum_{p=1}^{\infty}(-1)^p I_p\left(V_{10}^m\right)I_p\left(V_{0m}\right)\cos\left(p(\vartheta_{10}^m-\vartheta_{1m}+\vartheta_{0m})\right)\left[I_{p+1}\left(V_{1m}\right)+I_{p-1}\left(V_{1m}\right)\right]$$
$$=I_1\left(V_{1m}\right)I_0\left(V_{10}^m\right)I_0\left(V_{0m}\right)$$
$$+2\sum_{p=1}^{\infty}(-1)^p I_p\left(V_{10}^m\right)I_p\left(V_{0m}\right)\frac{\partial I_p\left(V_{1m}\right)}{\partial V_{1m}}\cos\left(p(\vartheta_{10}^m-\vartheta_{1m}+\vartheta_{0m})\right) \qquad \text{(D.41)}$$

and $\mathcal{A}''$ is given by

$$\mathcal{A}''=\sum_{p=-\infty}^{\infty}(-1)^p I_{p+1}\left(V_{1m}\right)I_p\left(V_{10}^m\right)\int_{-\pi}^{\pi}\sin\left(p\left(\theta_0'+\vartheta_{10}^m-\vartheta_{1m}\right)\right)\frac{e^{V_{0m}\cos\left(\theta_0'-\vartheta_{0m}\right)}}{2\pi}d\theta_0'$$
$$=\sum_{p=1}^{\infty}(-1)^p I_p\left(V_{10}^m\right)I_p\left(V_{0m}\right)\sin\left(p(\vartheta_{10}^m-\vartheta_{1m}+\vartheta_{0m})\right)\left[I_{p+1}\left(V_{1m}\right)-I_{p-1}\left(V_{1m}\right)\right]$$
$$=2\sum_{p=1}^{\infty}(-1)^p I_p\left(V_{10}^m\right)I_p\left(V_{0m}\right)\frac{I_p\left(V_{1m}\right)}{V_{1m}}(-p)(-1)\sin\left(p(\vartheta_{10}^m-\vartheta_{1m}+\vartheta_{0m})\right) \qquad \text{(D.42)}$$

Substituting (D.41) and (D.42) into (D.40) yields

$$l'_{1m}(t) = \Re\left\{l_{1m}(t,t)e^{j\vartheta_{1m}}e^{j\omega_c t}\right\}\frac{\dfrac{\partial g(\boldsymbol{d}_m,t)}{\partial V_{1m}}}{g(\boldsymbol{d}_m,t)} - \Im\left\{l_{1m}(t,t)e^{j\vartheta_{1m}}e^{j\omega_c t}\right\}\frac{\dfrac{1}{V_{1m}}\dfrac{\partial g(\boldsymbol{d}_m,t)}{\partial \vartheta_{1m}}}{g(\boldsymbol{d}_m,t)} \tag{D.43}$$

where $g(\boldsymbol{d}_m,t)$ is obtained from (D.21). Substituting (D.38) and (D.43) into (D.30) and simplifying yield

$$\check{v}_m(t) = \Re\left\{\left(2\int_0^t \mathcal{H}_m^*(s,t,t)e^{-j\omega_c s}dz(s) + \sum_{k=0}^{1} V'_{km}(t)e^{j\vartheta'_{km}(t)}l_{km}(t,t)e^{j\vartheta_{km}(t)}\right)e^{j\omega_c t}\right\} \tag{D.44}$$

where $V'_{km}(t)e^{j\vartheta'_{km}(t)}$ is given by (3.112). It is seen that (D.44) is identical to the conditional mean expression found by Itô differentiation (see (3.124a) assuming $l_{2m}(s,t) = \ldots = l_{L-1m}(s,t) = 0$, a property of 2 Ricean/L-2 Rayleigh channels).

Note that the iterative method presented in Section D.2 can be used for any number of paths using similar derivation as in this section. An increasing number of infinite series of product of Bessel and trigonometric functions is obtained as the number of Ricean paths increases.

Appendix E

Derivation of the non-coherent MMSE and other estimates by Itô differentiation of an m^{th} decision variable of the form

$$\mathcal{F}_m\left(\dot{z};t\right) = J_m(t)g\left(\boldsymbol{d}_m(t),t\right)$$

In this appendix, following Section 3.3.3 (topic: "Computation of the conditional mean by using Itô differentiation of the likelihood ratio"), Assumption 1 and Assumption 2 are made, i.e.

1. $\forall r = 1,\ldots,L$, there exists functions $\{x_{lk}^{rm}(t)\}_{l,k=0,\ldots,r-1}$ continuously differentiable on $\left(T_m' + \tau_{r-1}, T_m' + \tau_r\right]$ such that the $r \times r$ matrix $\boldsymbol{X}_{rm}(t)$ defined as $[\boldsymbol{X}_{rm}(t)]_{lk} = x_{lk}^{rm}(t)$ satisfies the equations $\boldsymbol{X}_{rm}^*(t)\boldsymbol{\Gamma}_{rm}^*(t)\boldsymbol{X}_{rm}^T(t) = \boldsymbol{I}_r$ and $\boldsymbol{\epsilon}_{rm}(t)\tilde{\boldsymbol{E}}_m\boldsymbol{C}_r\boldsymbol{\Gamma}_{rm}^*(t)\boldsymbol{X}_{rm}^T(t) = \boldsymbol{X}_{rm}^T(t)\boldsymbol{D}_{rm}(t)$.

2. $\forall r = 1,\ldots,L$, the eigenvalues of $\boldsymbol{\epsilon}_{rm}(t)\tilde{\boldsymbol{E}}_m\boldsymbol{C}_r\boldsymbol{\Gamma}_{rm}^*(t)$, $\{\lambda_{lm}^r(t)\}_{l=0,\ldots,r-1}$ are distinct.

Therefore all identities derived in Appendix C are valid. For sake of simplicity the index m indicating the hypothesis will be omitted in this appendix.

E.1 Preliminaries

E.1.1 Dependence of $\mathcal{F}_m(\dot{z};t)$ on a vector Itô process $\boldsymbol{\varpi}$: Proposition E.1

Let $\mathcal{F}(\dot{z};t)$ be defined as

$$\mathcal{F}(\dot{z};t) = J(t)g\big(\boldsymbol{d}(t),t\big) \tag{E.1}$$

where $J(t)$ is given by (3.93), g is an arbitrary function of $\boldsymbol{d}(t)$ and t that possesses continuous first and second order partial derivatives with respect to any components of $\boldsymbol{d}(t)$ and a continuous first order partial derivative with respect to t, and the vector $\boldsymbol{d}(t)$ is given by (3.95). The general expression of the Itô derivative of $\mathcal{F}(\dot{z};t)$ is linked to the following proposition.

Proposition E.1. *Let $\epsilon > 0$. Let $\boldsymbol{\varpi} = [\boldsymbol{d}(t) \quad Z(t)]^T$ where $\boldsymbol{d}(t)$ and $Z(t)$ are given by (3.95) and (3.106), then $\forall r = 1,\ldots,L \quad \forall t \in \big[T' + \tau_{r-1} + \epsilon, T' + \tau_r\big]$, $\boldsymbol{\varpi}$ is a vector Itô process that can be written as*

$$d\boldsymbol{\varpi} = \begin{pmatrix} \boldsymbol{q}'(t) \\ \boldsymbol{q}''(t) \\ q(t) \end{pmatrix} dt + \begin{pmatrix} \boldsymbol{\ell}'(t) \\ \boldsymbol{\ell}''(t) \\ \ell(t) \end{pmatrix} dw(t)$$

where

$$\boldsymbol{\ell}'(t) = \Big[\ell'_0(t),\ldots,\ell'_{L-1}(t)\Big]^T \tag{E.2}$$

$$\ell'_k(t) = \frac{2}{N_0}|l_k(t,t)|\cos\big(\omega_c t + \psi_k(t,t) + \vartheta_k(t)\big) \qquad k = 0,\ldots,L-1 \tag{E.3}$$

$$= \frac{2}{N_0}\Re\left\{l_k(t,t)e^{j\omega_c t}e^{j\vartheta_k(t)}\right\} \tag{E.4}$$

$$\boldsymbol{\ell}''(t) = \Big[\ell''_0(t),\ldots,\ell''_{L-1}(t)\Big]^T \tag{E.5}$$

$$\ell''_k(t) = -\frac{2}{N_0}\frac{|l_k(t,t)|}{V_k(t)}\sin\big(\omega_c t + \psi_k(t,t) + \vartheta_k(t)\big) \quad k = 0,\ldots,L-1 \tag{E.6}$$

$$= \frac{2}{N_0}\Im\left\{l_k(t,t)e^{j\omega_c t}e^{j\vartheta_k(t)}\right\} \tag{E.7}$$

$$\ell(t) = 2\int_0^t h(t,s)dz(s) \tag{E.8}$$

$$h(t,s) = H(s,t,t) = \begin{cases} \sum_{l=0}^{2L-1} \frac{\frac{2}{N_0}\kappa_l(t)}{1+\frac{2}{N_0}\kappa_l(t)} \Upsilon_l(t,t)\Upsilon_l(s,t) & 0 \le \tau, s \le t \\ & 0 \le t < \infty \\ 0 & else. \end{cases} \tag{E.9}$$

$l_k(s,t)$ is given by (3.103), $\psi_k(s,t) = \arg[l_k(s,t)]$, $V_k(t)$ and $\vartheta_k(t)$ are given by (3.98) and (3.99), and

$$\boldsymbol{q}'(t) = \left[q_0'(t), \ldots, q_{L-1}'(t)\right]^T \tag{E.10}$$

$$q_k'(t) = \ell_k'(t)\, v(t) + p_k'(t) + \frac{1}{2N_0}\frac{|l_k(t,t)|^2}{V_k(t)} \qquad k = 0, \ldots, L-1 \tag{E.11}$$

$$p_k'(t) = -\ell_k'(t)\left(\int_0^t h(t,s)dz(s)\right) \qquad k = 0, \ldots, L-1 \tag{E.12}$$

$$\boldsymbol{q}''(t) = \left[q_0''(t), \ldots, q_{L-1}''(t)\right]^T \tag{E.13}$$

$$q_k''(t) = \ell_k''(t)\, v(t) + p_k''(t) \qquad k = 0, \ldots, L-1 \tag{E.14}$$

$$p_k''(t) = -\ell_k''(t)\left(\int_0^t h(t,s)dz(s)\right) \qquad k = 0, \ldots, L-1 \tag{E.15}$$

$$q(t) = \ell(t)v(t) - 2\frac{N_0}{2}\frac{\dot{\Pi}(t)}{\Pi(t)} - \int_0^t\int_0^t h(t,\tau)h(t,s)dz(s)dz(\tau) \tag{E.16}$$

and $\Pi(t)$ is given by (3.104).

Since $\mathcal{F}(\dot{z};t)$ can be viewed as a scalar function of $\boldsymbol{\varpi}$ and t, from Proposition E.1 $\mathcal{F}(\dot{z};t)$ can be Itô differentiated by using the vector Itô differential rule (A.14).

E.1.2 Proof of Proposition E.1: Lemmas E.1-E.4

To prove Proposition E.1, the following lemmas are needed.

Lemma E.1. *Let $\epsilon > 0$ and*

$$V_k^c(t) = \Re\{d_k^*(t)\} = \frac{2}{N_0}\int_0^t |l_k(s,t)|\cos\big(\omega_c s + \psi_k(s,t)\big)dz(s) \quad {\scriptstyle k=0,\ldots,L-1} \tag{E.17}$$

$$V_k^s(t) = \Im\{d_k^*(t)\} = \frac{2}{N_0}\int_0^t |l_k(s,t)|\sin\big(\omega_c s + \psi_k(s,t)\big)dz(s) \quad {\scriptstyle k=0,\ldots,L-1} \tag{E.18}$$

then $\forall r = 1, \ldots, L$, $\forall t \in \left[T' + \tau_{r-1} + \epsilon, T' + \tau_r\right]$, $\boldsymbol{v}_k = \left[V_k^c(t)\ V_k^s(t)\right]^T$ is a vector

Itô process that can be written as

$$d\boldsymbol{v}_k = \begin{pmatrix} dV_k^c \\ dV_k^s \end{pmatrix} = \begin{pmatrix} \frac{2}{N_0}|l_k(t,t)|\cos\big(\omega_c t + \psi_k(t,t)\big)v(t) + p_k^c(t) \\ \frac{2}{N_0}|l_k(t,t)|\sin\big(\omega_c t + \psi_k(t,t)\big)v(t) + p_k^s(t) \end{pmatrix} dt + \boldsymbol{v}_{kw}(t)\,dw(t)$$

where

$$p_k^c(t) = -\frac{2}{N_0}|l_k(t,t)|\cos\big(\omega_c t + \psi_k(t,t)\big)\int_0^t H(s,t,t)dz(s) \tag{E.19}$$

$$p_k^s(t) = -\frac{2}{N_0}|l_k(t,t)|\sin\big(\omega_c t + \psi_k(t,t)\big)\int_0^t H(s,t,t)dz(s) \tag{E.20}$$

$$\boldsymbol{v}_{kw}(t) = \left[\frac{2}{N_0}|l_k(t,t)|\cos\big(\omega_c t + \psi_k(t,t)\big)\ \ \frac{2}{N_0}|l_k(t,t)|\sin\big(\omega_c t + \psi_k(t,t)\big)\right]^T \tag{E.21}$$

Lemma E.2. *$\forall r = 1,\ldots,L$, $\forall t \in \left[T' + \tau_{r-1} + \epsilon, T' + \tau_r\right]$, $V_k(t)$ is an Itô process that can be written as*

$$dV_k(t) = q_k'(t)dt + \ell_k'(t)dw(t) \tag{E.22}$$

where $q_k'(t)$ and $\ell_k'(t)$ are given by (E.11) and (E.3).

Lemma E.3. *$\forall r = 1,\ldots,L$, $\forall t \in \left[T' + \tau_{r-1} + \epsilon, T' + \tau_r\right]$, $\vartheta_k(t)$ is an Itô process that can be written as*

$$d\vartheta_k(t) = q_k''(t)dt + \ell_k''(t)dw(t) \tag{E.23}$$

where $q_k''(t)$ and $\ell_k''(t)$ are given by (E.14) and (E.6).

Lemma E.4. *$\forall r = 1,\ldots,L$, $\forall t \in \left[T' + \tau_{r-1} + \epsilon, T' + \tau_r\right]$, $Z(t)$ is an Itô process that can be written as*

$$dZ(t) = q(t)dt + \ell(t)dw(t) \tag{E.24}$$

where $q(t)$ and $\ell(t)$ are given by (E.16) and (E.8).

Proof of Proposition E.1. By lemmas E.2- E.4,
$\forall r = 1,\ldots,L$, $\forall t \in \left[T' + \tau_{r-1} + \epsilon, T' + \tau_r\right]$, $\boldsymbol{\varpi}$ is a vector Itô process (see Ap-

pendix A.2.5) since

$$d\boldsymbol{\varpi} = [dV_0(t) \quad dV_1(t) \quad \dots \quad dV_{L-1}(t) \quad d\vartheta_0(t) \quad d\vartheta_1(t) \quad \dots \quad d\vartheta_{L-1}(t) \quad dZ(t)]^T \tag{E.25}$$

where $\forall\, k = 0, \dots, L-1$, $V_k(t)$, $\vartheta_k(t)$ and $Z(t)$ are Itô processes. Substituting (E.22-E.24) into (E.25) yields the result of Proposition E.1. **Q.E.D**

For the rest of this appendix, k denotes an arbitrary integer number between 0 and $L-1$.

E.1.3 Proof of Lemma E.1

To prove that $\boldsymbol{v}_k$ is a vector Itô process, it is sufficient to prove that $V_k^c(t)$ and $V_k^s(t)$ are Itô processes, since $\boldsymbol{v}_k$ is given by

$$\boldsymbol{v}_k = [V_k^c(t) \;\; V_k^s(t)]^T \tag{E.26}$$

From Section 3.3.3 under each hypothesis (including H_0) the received signal is an Itô process [181] and can be written as

$$dz(t) = v_m(t)dt + dw(t) \qquad m = 0, \dots, M \tag{E.27}$$

where by convention $v_0(t) = 0$. Let us consider first $V_k^c(t)$. By assumptions (see Section 3.1), under each hypothesis, $v(t)$ is a real non-anticipating second order jointly measurable in (t,ω) and mean square continuous process on $[0, T_o]$. Let $\epsilon > 0$, $\forall\, r = 1, \dots, L$ from (3.103b), $|l_k(s,t)|\cos\big(\omega_c s + \psi_k(s,t)\big)$ is a deterministic real-valued function defined on the closed domain $\mathcal{R}_r(\epsilon)$ described by

$$\mathcal{R}_r(\epsilon) = \Big\{(s,t) \in I\!R^2; \quad 0 \le s \le t \qquad T' + \tau_{r-1} + \epsilon \le t \le T' + \tau_r\Big\}$$

Let us show that $\forall\, r = 1, \dots, L$

a) $\forall\, t \in \Big[T' + \tau_{r-1} + \epsilon, T' + \tau_r\Big] \quad \displaystyle\int_0^t \big|l_k(s,t)\cos\big(\omega_c s + \psi_k(s,t)\big)\big|\, E\,|v(s)|\, ds < \infty$

b) $|l_k(s,t)|\cos\big(\omega_c t + \psi_k(t,t)\big)$ is continuous and continuously differentiable with respect to t on $\mathcal{R}_r(\epsilon)$.

Proof of a). Let us show a slightly more general result:

Lemma E.5.

For any function $\mathrm{f}(s,t)$ *satisfying* $\int_0^t |\mathrm{f}(s,t)|^2\,ds < \infty$ *then* $\int_0^t |\mathrm{f}(s,t)|\,E\,|v(s)|\,ds < \infty$.

From (3.2)

$$\begin{aligned}
&\int_0^t |\mathrm{f}(s,t)|\,E\,|v(s)|\,ds \\
&\le \sum_{l=0}^{L-1} E\,|a_l| \left[\int_0^t |\mathrm{f}(s,t)|\,\left|\Re\left\{\tilde{s}(s-\tau_l)e^{j\omega_c s}\right\}\right| ds + \int_0^t |\mathrm{f}(s,t)|\,\left|\Im\left\{\tilde{s}(s-\tau_l)e^{j\omega_c s}\right\}\right| ds\right] \\
&\le \sum_{l=0}^{L-1} E\,|a_l| \left(\int_0^t |\mathrm{f}(s,t)|^2\,ds\right)^{1/2} \left[\left(\int_0^t \left|\Re\left\{\tilde{s}(s-\tau_l)e^{j\omega_c s}\right\}\right|^2 ds\right)^{1/2}\right. \\
&\qquad \left. + \left(\int_0^t \left|\Im\left\{\tilde{s}(s-\tau_l)e^{j\omega_c s}\right\}\right|^2 ds\right)^{1/2}\right] < \infty \quad \text{(Cauchy's Schwarz inequality)}
\end{aligned}$$

since $\tilde{s}(s-\tau_l)$ is continuous on $[0,t]$ and hence bounded and by assumption $\mathrm{f}(s,t)$ satisfies $\int_0^t |\mathrm{f}(s,t)|^2\,ds < \infty$. In particular from Proposition C.1 (Appendix C.5.2) $l_k(s,t)e^{j\omega_c s}$ is continuous on $\mathcal{R}_\tau(\epsilon)$ and hence is bounded on $\mathcal{R}_\tau(\epsilon)$. Therefore $l_k(s,t)$ satisfies $\int_0^t \left|l_k(s,t)\cos\big(\omega_c s + \psi_k(s,t)\big)\right|^2 ds < \infty$. **Q.E.D**

Proof of b). From Proposition C.1, $l_k(s,t)e^{j\omega_c s}$ is continuous and differentiable with respect to t on $\mathcal{R}_\tau(\epsilon)$, hence $|l_k(s,t)|\cos\big(\omega_c s + \psi_k(s,t)\big) \triangleq \Re\left\{l_k(s,t)e^{j\omega_c s}\right\}$ is also continuous and differentiable with respect to t on $\mathcal{R}_\tau(\epsilon)$. Using (C.35), $\frac{\partial}{\partial t}\Big(|l_k(s,t)|\cos\big(\omega_c s + \psi_k(s,t)\big)\Big)$ is given by

$$\begin{aligned}
\frac{\partial}{\partial t}\Big(|l_k(s,t)|\cos\big(\omega_c s + \psi_k(s,t)\big)\Big) &= \frac{\partial}{\partial t}\left(\Re\left\{l_k(s,t)e^{j\omega_c s}\right\}\right) = \Re\left\{\frac{\partial}{\partial t}\left(l_k(s,t)e^{j\omega_c s}\right)\right\} \\
&= -\Re\left\{H(s,t,t)l_k(t,t)e^{j\omega_c t}\right\} \\
&= -H(s,t,t)|l_k(t,t)|\cos\big(\omega_c t + \psi_k(t,t)\big) \qquad \text{(E.28)}
\end{aligned}$$

since $H(s,t,t)$ is real. As seen in the proof of Proposition C.1, $H(s,t,t)$ is continuous on $\mathcal{R}_\tau(\epsilon)$, hence from (E.28) $\frac{\partial}{\partial t}\Big(|l_k(s,t)|\cos\big(\omega_c s + \psi_k(s,t)\big)\Big)$ is continuous on $\mathcal{R}_\tau(\epsilon)$. **Q.E.D**

Proof of Lemma E.1 (cont.)

$|l_k(s,t)|\cos\big(\omega_c s + \psi_k(s,t)\big)$ in (E.17), satisfies the assumptions required for Proposition A.2 to hold. Hence from Proposition A.2, $V_k^c(t)$ is an Itô process that can be written as

$$dV_k^c(t) = p_k^c(t)dt + \frac{2}{N_0}|l_k(t,t)|\cos\big(\omega_c t + \psi_k(t,t)\big)dz(t) \tag{E.29}$$

where

$$p_k^c(t) = \frac{2}{N_0}\int_0^t \Big(-H(s,t,t)|l_k(t,t)|\cos\big(\omega_c t + \psi_k(t,t)\big)\Big)dz(s)$$

Noting that $|l_k(s,t)|\sin\big(\omega_c s + \psi_k(s,t)\big) = \Im\{l_k(s,t)e^{j\omega_c s}\}$, by using similar arguments as for $|l_k(s,t)|\sin\big(\omega_c s + \psi_k(s,t)\big)$, Proposition A.2 also holds for $|l_k(s,t)|\sin\big(\omega_c s + \psi_k(s,t)\big)$. Therefore Proposition A.2 applied to (E.18) yields

$$dV_k^s(t) = p_k^s(t)dt + \frac{2}{N_0}|l_k(t,t)|\sin\big(\omega_c t + \psi_k(t,t)\big)dz(t) \tag{E.30}$$

where

$$p_k^s(t) = \frac{2}{N_0}\int_0^t \Big(-H(s,t,t)|l_k(t,t)|\sin\big(\omega_c t + \psi_k(t,t)\big)\Big)dz(s)$$

Noting from (E.26) that $d\boldsymbol{v}_k = [dV_k^c(t)\ \ dV_k^s(t)]^T$ and substituting (E.27) into (E.29) and (E.30) complete the proof of Lemma E.1. **Q.E.D**

E.1.4 Proof of Lemma E.2

From (3.98)

$$V_k(t) = \sqrt{\big[V_k^c(t)\big]^2 + \big[V_k^s(t)\big]^2}$$

where $V_k^c(t)$ and $V_k^s(t)$ are given by (E.17) and (E.18). Thus $V_k(t)$ can be viewed as a scalar function of the vector Itô process $\boldsymbol{v}_k = [V_k^c(t)\ \ V_k^s(t)]^T$ with partial derivatives

given by

$$V_v(t) = \begin{pmatrix} \frac{V_k^c(t)}{V_k(t)} \\ \frac{V_k^s(t)}{V_k(t)} \end{pmatrix} \qquad V_{vv}(t) = \begin{pmatrix} \frac{(V_k^s(t))^2}{V_k^3(t)} & \frac{-V_k^c(t)V_k^s(t)}{V_k^3(t)} \\ \frac{-V_k^c(t)V_k^s(t)}{V_k^3(t)} & \frac{(V_k^c(t))^2}{V_k^3(t)} \end{pmatrix} \qquad V_t(t) = 0$$

The function $\mathrm{f}([x_1,x_2]^T,t) = \sqrt{x_1^2+x_2^2}$ is continuous and has continuous first order partial derivatives and continuous second order partial derivatives with respect to $\boldsymbol{x} = [x_1,x_2]^T$ on $I\!R$. Using Lemma E.1, the vector Itô differential rule (A.14) can be applied to $V_k(t) = \mathrm{f}(\boldsymbol{v}_k,t)$ yielding

$$dV_k(t) = \frac{1}{2}\frac{N_0}{2}\mathrm{tr}\left[\boldsymbol{v}_{kw}{}^T(t)\, V_{vv}(t)\, \boldsymbol{v}_{kw}(t)\right] dt + \frac{V_k^c(t)}{V_k(t)}dV_k^c(t) + \frac{V_k^s(t)}{V_k(t)}dV_k^s(t) \qquad \text{(E.31)}$$

Let us simplify $\mathrm{tr}\left[\boldsymbol{v}_{kw}{}^T(t)\, V_{vv}(t)\, \boldsymbol{v}_{kw}(t)\right]$. From (E.21)

$$\begin{aligned}
&\mathrm{tr}\left[\boldsymbol{v}_{kw}{}^T(t)\, V_{vv}(t)\, \boldsymbol{v}_{kw}(t)\right] \\
&= \left(\frac{2}{N_0}\right)^2 \frac{|l_k(t,t)|^2}{V_k(t)}\left[\left(\frac{V_k^s(t)}{V_k(t)}\right)^2 \cos^2\left(\omega_c t + \psi_k(t,t)\right) + \left(\frac{V_k^c(t)}{V_k(t)}\right)^2 \sin^2\left(\omega_c t + \psi_k(t,t)\right)\right. \\
&\qquad\qquad \left. - 2\frac{V_k^c(t)}{V_k(t)}\frac{V_k^s(t)}{V_k(t)}\cos\left(\omega_c t + \psi_k(t,t)\right)\sin\left(\omega_c t + \psi_k(t,t)\right)\right] \\
&= \left(\frac{2}{N_0}\right)^2 \frac{|l_k(t,t)|^2}{2V_k(t)}\left[1 - \cos\left[2\left(\omega_c t + \psi_k(t,t) + \vartheta_k(t)\right)\right]\right] \qquad \text{(E.32)}
\end{aligned}$$

where $\vartheta_k(t) = \arg\left[d_k(t)\right] = -\tan^{-1}\left[V_k^s(t)/V_k^c(t)\right]$, $V_k^c(t) = V_k(t)\cos\vartheta_k(t)$. Substituting (E.29-E.30) and (E.32) into (E.31) yields

$$\begin{aligned}
dV_k(t) = &\left\{p_k'(t) + \frac{1}{2N_0}\frac{|l_k(t,t)|^2}{V_k(t)}\left[1 - \cos\left[2\left(\omega_c t + \psi_k(t,t) + \vartheta_k(t)\right)\right]\right]\right\} dt \\
&+ \frac{2}{N_0}|l_k(t,t)|\cos\left(\omega_c t + \psi_k(t,t) + \vartheta_k(t)\right)dz(t) \qquad \text{(E.33)}
\end{aligned}$$

where from (E.19-E.20)

$$\begin{aligned}
p_k'(t) &\triangleq p_k^c(t)\frac{V_k^c(t)}{V_k(t)} + p_k^s(t)\frac{V_k^s(t)}{V_k(t)} \\
&= -\frac{2}{N_0}\left(\int_0^t H(s,t,t)dz(s)\right)\left[\Re\left\{l_k(t,t)e^{j\omega_c t}\right\}\cos\vartheta_k(t) - \Im\left\{l_k(t,t)e^{j\omega_c t}\right\}\sin\vartheta_k(t)\right]
\end{aligned}$$

$$= -\frac{2}{N_0}\left(\int_0^t H(s,t,t)dz(s)\right)|l_k(t,t)|\cos\left(\omega_c t + \psi_k(t,t) + \vartheta_k(t)\right)$$

After substitution of (E.3) and (E.9), $p_k'(t)$ is given by (E.12) . Substituting (E.27) into (E.33) shows that $V_k(t)$ is an Itô process which can be written as (E.22) where $q_k'(t) = \ell_k'(t)\,v(t) + p_k'(t) + \frac{1}{2N_0}|l_k(t,t)|^2/V_k(t)\left[1-\cos\left(2\left[\omega_c t + \psi_k(t,t) + \vartheta_k(t)\right]\right)\right]$ and $\ell_k'(t)$ is given by (E.3). Recall from Appendix A.2.3 that (E.22) is a symbolic notation for

$$V_k(t) = \int_0^t q_k'(s)\,ds + \int_0^t \ell_k'(s)\,dw(s) \tag{E.34}$$

Hence assuming that ω_c is very large, integrals containing double frequency terms can be neglected in (E.34) which completes the proof of Lemma E.2. **Q.E.D**

E.1.5 Proof of Lemma E.3

From (3.99)

$$\vartheta_k(t) = -\tan^{-1}\left[\frac{V_k^s(t)}{V_k^c(t)}\right] \tag{E.35}$$

where $V_k^c(t)$ and $V_k^s(t)$ are given by (E.17) and (E.18). Thus $\vartheta_k(t)$ can be viewed as a scalar function of $\boldsymbol{v}_k = [V_k^c(t)\ \ V_k^s(t)]^T$ with partial derivatives given by

$$\vartheta_v(t) = \begin{pmatrix} \frac{V_k^s(t)}{V_k^2(t)} \\ \frac{-V_k^c(t)}{V_k^2(t)} \end{pmatrix} \qquad \vartheta_{vv}(t) = \begin{pmatrix} \frac{-2V_k^c(t)V_k^s(t)}{V_k^4(t)} & \frac{\left(V_k^c(t)\right)^2-\left(V_k^s(t)\right)^2}{V_k^4(t)} \\ \frac{\left(V_k^c(t)\right)^2-\left(V_k^s(t)\right)^2}{V_k^4(t)} & \frac{2V_k^c(t)V_k^s(t)}{V_k^4(t)} \end{pmatrix} \qquad \vartheta_t(t) = 0$$

The function $\mathrm{f}([x_1,x_2]^T,t) = -\tan^{-1}\left[\frac{x_1}{x_2}\right]$ is continuous and has continuous first order partial derivatives and continuous second order partial derivatives with respect to $\boldsymbol{x} = [x_1,x_2]^T$ on $I\!R$. Using Lemma E.1, the vector Itô differential rule (A.14) can be applied to $\vartheta_k(t) = \mathrm{f}(\boldsymbol{v}_k,t)$ yielding

$$d\vartheta_k(t) = \frac{1}{2}\frac{N_0}{2}\mathrm{tr}\left[\boldsymbol{v}_{kw}{}^T(t)\,\vartheta_{vv}(t)\,\boldsymbol{v}_{kw}(t)\right]dt + \frac{V_k^s(t)}{V_k^2(t)}dV_k^c(t) - \frac{V_k^c(t)}{V_k^2(t)}dV_k^s(t) \tag{E.36}$$

Let us simplify $\mathrm{tr}\left[\boldsymbol{v}_{kw}{}^T(t)\,\vartheta_{vv}(t)\,\boldsymbol{v}_{kw}(t)\right]$. From (E.21)

$$\begin{aligned}
&\mathrm{tr}\left[\boldsymbol{v}_{kw}{}^T(t)\,\vartheta_{vv}(t)\,\boldsymbol{v}_{kw}(t)\right] \\
&= \left(\frac{2}{N_0}\right)^2 \frac{|l_k(t,t)|^2}{V_k^2(t)}\left[-2\frac{V_k^c(t)}{V_k(t)}\frac{V_k^s(t)}{V_k(t)}\Big(\cos^2\big(\omega_c t+\psi_k(t,t)\big)-\sin^2\big(\omega_c t+\psi_k(t,t)\big)\Big)\right. \\
&\qquad\qquad \left. +\left(\left(\frac{V_k^c(t)}{V_k(t)}\right)^2-\left(\frac{V_k^s(t)}{V_k(t)}\right)^2\right)\sin\Big(2\big[\omega_c t+\psi_k(t,t)\big]\Big)\right] \\
&= \left(\frac{2}{N_0}\right)^2 \frac{|l_k(t,t)|^2}{V_k^2(t)}\sin\Big(2\big[\omega_c t+\psi_k(t,t)+\vartheta_k(t)\big]\Big) \qquad \text{(E.37)}
\end{aligned}$$

where $\vartheta_k(t)$ is given by (E.35). Substituting (E.29-E.30) and (E.37) into (E.36) yields

$$\begin{aligned}
d\vartheta_k(t) = &\left[p_k''(t)+\frac{1}{N_0}\frac{|l_k(t,t)|^2}{V_k^2(t)}\sin\Big(2\big[\omega_c t+\psi_k(t,t)+\vartheta_k(t)\big]\Big)\right]dt \\
&-\frac{2}{N_0}\frac{|l_k(t,t)|}{V_k(t)}\sin\big(\omega_c t+\psi_k(t,t)+\vartheta_k(t)\big)dz(t) \qquad \text{(E.38)}
\end{aligned}$$

where from (E.19-E.20)

$$\begin{aligned}
p_k''(t) &\triangleq p_k^c(t)\frac{V_k^s(t)}{V_k^2(t)}-p_k^s(t)\frac{V_k^c(t)}{V_k^2(t)} \\
&= -\frac{2}{N_0}\left(\int_0^t H(s,t,t)dz(s)\right) \\
&\qquad\cdot\left[\Re\left\{l_k(t,t)e^{j\omega_c t}\right\}\frac{-\sin\vartheta_k(t)}{V_k(t)}-\Im\left\{l_k(t,t)e^{j\omega_c t}\right\}\frac{\cos\vartheta_k(t)}{V_k(t)}\right] \\
&= \frac{2}{N_0}\left(\int_0^t H(s,t,t)dz(s)\right)\frac{|l_k(t,t)|}{V_k(t)}\sin\big(\omega_c t+\psi_k(t,t)+\vartheta_k(t)\big)
\end{aligned}$$

After substitution of (E.6) and (E.9), $p_k''(t)$ is given by (E.15). Substituting (E.27) into (E.38) shows that $\vartheta_k(t)$ is an Itô process which can be written as (E.23) where $q_k''(t) = \ell_k''(t)\,v(t)+p_k''(t)+\frac{1}{N_0}|l_k(t,t)|^2/V_k^2(t)\sin\left(2\big[\omega_c t+\psi_k(t,t)+\vartheta_k(t)\big]\right)$ and $\ell_k''(t)$ is given by (E.6). Recall from Appendix A.2.3 that (E.23) is a symbolic notation for

$$\vartheta_k(t) = \int_0^t q_k''(s)\,ds + \int_0^t \ell_k''(s)\,dw(s) \qquad \text{(E.39)}$$

Hence assuming that ω_c is very large, integrals containing double frequency terms can be neglected in (E.39) which completes the proof of Lemma E.3. **Q.E.D**

E.1.6 Proof of Lemma E.4

From (3.106), $Z(t)$ is a scalar function of $\boldsymbol{z}'(t)$, where

$$\boldsymbol{z}'(t) = \left[\sqrt{\kappa_0(t)}z_1(t), \ldots, \sqrt{\kappa_{2L-1}(t)}z_{2L-1}(t)\right]^T$$

Hence in order to prove Lemma E.4 using the vector Itô differential rule, the first step consists to prove that $z'_k(t) = \sqrt{\kappa_k(t)}z_k(t)$ are Itô processes. Recall from (3.107)

$$z'_k(t) \triangleq \sqrt{\kappa_k(t)}z_k(t) = \int_0^t \sqrt{\kappa_k(t)}\Upsilon_k(s,t)dz(s) \tag{E.40}$$

From Section 3.3.3 that under each hypothesis(including H_0) the received signal is an Itô process [181] and can be written as (E.27). By assumptions (see Section 3.1), under each hypothesis, $v(t)$ is a real non-anticipating second order jointly measurable in (t,ω) and mean square continuous process on $[0,T_o]$. Let $\epsilon > 0$, $\forall r = 1,\ldots,L$ from (3.44), $\forall k = 0,\ldots,2L-1$ $\sqrt{\kappa_k(t)}\Upsilon_k(s,t)$ is a deterministic real-valued function defined on the closed domain $\mathcal{R}_r(\epsilon)$. Let us show that $\forall r = 1,\ldots,L$ $\forall k = 0,\ldots,2L-1$

a) $\forall t \in \left[T' + \tau_{r-1} + \epsilon, T' + \tau_r\right]$ $\int_0^t \left|\sqrt{\kappa_k(t)}\Upsilon_k(s,t)\right| E\left|v(s)\right| ds < \infty$

b) $\sqrt{\kappa_k(t)}\Upsilon_k(s,t)$ is continuous and continuously differentiable with respect to t on $\mathcal{R}_r(\epsilon)$.

Proof. From Appendix C.5.1, $\forall k = 0,\ldots,2L-1$ $\sqrt{\kappa_k(t)}\Upsilon_k(s,t)$ is continuous on $\mathcal{R}_r(\epsilon)$ since $\mathcal{R}_r(\epsilon) \subset \mathcal{R}_r$ and hence bounded. Therefore $\sqrt{\kappa_k(t)}\Upsilon_k(s,t)$ satisfies $\int_0^t \left|\sqrt{\kappa_k(t)}\Upsilon_k(s,t)\right|^2 ds < \infty$. Hence using Lemma E.5, proof of a) is completed. From Appendix C.5.1, $\forall k = 0,\ldots,2L-1$ $\sqrt{\kappa_k(t)}\Upsilon_k(s,t)$ is continuous and continuously differentiable with respect to t on $\mathcal{R}_r(\epsilon)$. **Q.E.D**

Proof of Lemma E.4 (cont.)

$\forall k = 0,\ldots,2L-1$ $\sqrt{\kappa_k(t)}\Upsilon_k(s,t)$ in (E.40) satisfies the assumptions required for Proposition A.2 to hold. Hence from Proposition A.2, $\forall k = 0,\ldots,2L-1$ $z'_k(t)$ is

an Itô process that can be written as

$$dz_k'(t) = \left(\int_0^t \frac{\partial}{\partial t}\left(\sqrt{\kappa_k(t)}\Upsilon_k(s,t)\right)dz(s)\right)dt + \sqrt{\kappa_k(t)}\Upsilon_k(t,t)dz(t)$$

Therefore using (E.27), $\boldsymbol{z}'(t)$ is a vector Itô process that can be written as

$$d\boldsymbol{z}'(t) = \begin{pmatrix} \sqrt{\kappa_0(t)}\Upsilon_0(t,t)v(t) + \int_0^t \frac{\partial}{\partial t}\left(\sqrt{\kappa_0(t)}\Upsilon_0(s,t)\right)dz(s) \\ \vdots \\ \sqrt{\kappa_{2L-1}(t)}\Upsilon_{2L-1}(t,t)v(t) + \int_0^t \frac{\partial}{\partial t}\left(\sqrt{\kappa_{2L-1}(t)}\Upsilon_{2L-1}(s,t)\right)dz(s) \end{pmatrix} dt + \boldsymbol{z}_w'(t)dw(t) \tag{E.41}$$

where $\boldsymbol{z}_w'(t) = \left[\sqrt{\kappa_0(t)}\Upsilon_0(t,t),\ldots,\sqrt{\kappa_{2L-1}(t)}\Upsilon_{2L-1}(t,t)\right]^T$. From (3.106), $Z(t)$ is a scalar function of $\boldsymbol{z}'$ and t with partial derivatives given by

$$Z_{z'}(t) = \left(\frac{\frac{2}{N_0}2z_0'(t)}{1+\frac{2}{N_0}\kappa_0(t)},\ldots,\frac{\frac{2}{N_0}2z_{2L-1}'(t)}{1+\frac{2}{N_0}\kappa_{2L-1}(t)}\right)^T$$

$$Z_{z'z'}(t) = \begin{pmatrix} \frac{2\frac{2}{N_0}}{1+\frac{2}{N_0}\kappa_0(t)} & 0 & \cdots & 0 \\ 0 & \frac{2\frac{2}{N_0}}{1+\frac{2}{N_0}\kappa_1(t)} & \cdots & 0 \\ \vdots & \vdots & \ddots & \vdots \\ 0 & 0 & \cdots & \frac{2\frac{2}{N_0}}{1+\frac{2}{N_0}\kappa_{2L-1}(t)} \end{pmatrix}$$

$$Z_t(t) = -\sum_{k=0}^{2L-1}\frac{\left(\frac{2}{N_0}\right)^2\dot{\kappa}_k(t)\left[z_k'(t)\right]^2}{\left(1+\frac{2}{N_0}\kappa_k(t)\right)^2}$$

and

$$\mathrm{tr}\left[\left(\boldsymbol{z}_w'(t)\right)^T Z_{z'z'}(t)\boldsymbol{z}_w'(t)\right] = \sum_{k=0}^{2L-1}\frac{2\frac{2}{N_0}\left[\sqrt{\kappa_k(t)}\Upsilon_k(t,t)\right]^2}{1+\frac{2}{N_0}\kappa_k(t)} = \sum_{k=0}^{2L-1}\frac{2\frac{2}{N_0}\kappa_k(t)\Upsilon_k^2(t,t)}{1+\frac{2}{N_0}\kappa_k(t)}$$

where $\dot{\kappa}_k(t)$ denotes the derivative of $\kappa_k(t)$ with respect to t. By applying the vector Itô differential rule (A.14) to $Z(t)$ and using (E.41), $Z(t)$ is an Itô process that can

be written as (E.24) where $q(t)$ and $\ell(t)$ are given by

$$q(t) - \ell(t)v(t) = -\sum_{k=0}^{2L-1} \frac{\left(\frac{2}{N_0}\right)^2 \dot{\kappa}_k(t)}{\left(1+\frac{2}{N_0}\kappa_k(t)\right)^2}\left[z_k'(t)\right]^2 + \frac{1}{2}\frac{N_0}{2}\sum_{k=0}^{2L-1}\frac{2\frac{2}{N_0}\kappa_k(t)}{1+\frac{2}{N_0}\kappa_k(t)}\Upsilon_k^2(t,t)$$
$$+\sum_{k=0}^{2L-1}\frac{\frac{2}{N_0}}{1+\frac{2}{N_0}\kappa_k(t)}2z_k'(t)\int_0^t\frac{\partial}{\partial t}\left(\sqrt{\kappa_k(t)}\Upsilon_k(s,t)\right)dz(s) \qquad \text{(E.42)}$$

$$\ell(t) = \sum_{k=0}^{2L-1} 2\sqrt{\kappa_k(t)}\Upsilon_k(t,t)z_k'(t)\frac{\frac{2}{N_0}}{1+\frac{2}{N_0}\kappa_k(t)} \qquad \text{(E.43)}$$

Substituting (E.40) into (E.42) and using $\dot{\kappa}_k(t) = \kappa_k(t)\Upsilon_k^2(t,t)$ [187, pp. 204-205] yield

$$\begin{aligned}
&q(t) - \ell(t)v(t)\\
&= \sum_{k=0}^{2L-1}\left\{\frac{-\left(\frac{2}{N_0}\right)^2\dot{\kappa}_k(t)}{\left(1+\frac{2}{N_0}\kappa_k(t)\right)^2}\left[\int_0^t\sqrt{\kappa_k(t)}\Upsilon_k(\tau,t)dz(\tau)\right]\left[\int_0^t\sqrt{\kappa_k(t)}\Upsilon_k(s,t)dz(s)\right]\right.\\
&\left.+\frac{\dot{\kappa}_k(t)}{1+\frac{2}{N_0}\kappa_k(t)}+\frac{2\frac{2}{N_0}}{1+\frac{2}{N_0}\kappa_k(t)}\left[\int_0^t\sqrt{\kappa_k(t)}\Upsilon_k(\tau,t)dz(\tau)\right]\left[\int_0^t\frac{\partial}{\partial t}\left(\sqrt{\kappa_k(t)}\Upsilon_k(s,t)\right)dz(s)\right]\right\}\\
&= \sum_{k=0}^{2L-1}\frac{\dot{\kappa}_k(t)}{1+\frac{2}{N_0}\kappa_k(t)}+\int_0^t\int_0^t\left\{\sum_{k=0}^{2L-1}\left[\frac{-\left(\frac{2}{N_0}\right)^2\dot{\kappa}_k(t)}{\left(1+\frac{2}{N_0}\kappa_k(t)\right)^2}\sqrt{\kappa_k(t)}\Upsilon_k(\tau,t)\sqrt{\kappa_k(t)}\Upsilon_k(s,t)\right.\right.\\
&\quad+\frac{\frac{2}{N_0}}{1+\frac{2}{N_0}\kappa_k(t)}\left(\sqrt{\kappa_k(t)}\Upsilon_k(\tau,t)\frac{\partial}{\partial t}\left(\sqrt{\kappa_k(t)}\Upsilon_k(s,t)\right)\right.\\
&\left.\left.\left.\quad+\sqrt{\kappa_k(t)}\Upsilon_k(s,t)\frac{\partial}{\partial t}\left(\sqrt{\kappa_k(t)}\Upsilon_k(\tau,t)\right)\right)\right]\right\}dz(s)dz(\tau)\\
&= \sum_{k=0}^{2L-1}\frac{\dot{\kappa}_k(t)}{1+\frac{2}{N_0}\kappa_k(t)}\\
&\quad+\int_0^t\int_0^t\frac{\partial}{\partial t}\left(\sum_{k=0}^{2L-1}\frac{\frac{2}{N_0}}{1+\frac{2}{N_0}\kappa_k(t)}\sqrt{\kappa_k(t)}\Upsilon_k(\tau,t)\sqrt{\kappa_k(t)}\Upsilon_k(s,t)\right)dz(s)dz(\tau)
\end{aligned}$$

Using (3.104) and (3.42)

$$q(t) - \ell(t)v(t) = -2\frac{N_0}{2}\frac{\dot{\Pi}(t)}{\Pi(t)} + \int_0^t \int_0^t \frac{\partial H(\tau,s,t)}{\partial t} dz(s)dz(\tau) \qquad \text{(E.44)}$$

By using the Siegert identity (C.19) in (E.44) with (E.9), $q(t)$ is also given by (E.16). Substituting (E.40) into (E.43) with (E.9) yields (E.8). **Q.E.D**

E.2 Itô derivative of $\mathcal{F}_m(\dot{z};t)$

$\mathcal{F}(\dot{z};t)$ given by (E.1) is a scalar function of $\boldsymbol{\varpi} = [\boldsymbol{d}(t)\ Z(t)]^T = [\boldsymbol{V}(t)\ \boldsymbol{\vartheta}(t)\ Z(t)]$ and t with partial derivatives given by

$$\mathcal{F}_{\boldsymbol{\varpi}}(\dot{z};t) = \left[\left(\frac{\partial \mathcal{F}}{\partial \boldsymbol{V}}\right)^T \left(\frac{\partial \mathcal{F}}{\partial \boldsymbol{\vartheta}}\right)^T \frac{\partial \mathcal{F}}{\partial Z}\right]^T = \mathcal{F}(\dot{z};t)\left[\frac{\left(\frac{\partial q}{\partial \boldsymbol{V}}\right)^T}{g(\boldsymbol{d},t)} \frac{\left(\frac{\partial q}{\partial \boldsymbol{\vartheta}}\right)^T}{g(\boldsymbol{d},t)} \frac{\frac{\partial J}{\partial Z}}{J(t)}\right]^T$$

$$\mathcal{F}_{\boldsymbol{\varpi}\boldsymbol{\varpi}}(\dot{z};t) = \begin{pmatrix} \frac{\partial^2 \mathcal{F}}{\partial \boldsymbol{V}^2} & \frac{\partial^2 \mathcal{F}}{\partial \boldsymbol{V}\partial \boldsymbol{\vartheta}} & \frac{\partial^2 \mathcal{F}}{\partial \boldsymbol{V}\partial Z} \\ \frac{\partial^2 \mathcal{F}}{\partial \boldsymbol{\vartheta}\partial \boldsymbol{V}} & \frac{\partial^2 \mathcal{F}}{\partial \boldsymbol{\vartheta}^2} & \frac{\partial^2 \mathcal{F}}{\partial \boldsymbol{\vartheta}\partial Z} \\ \frac{\partial^2 \mathcal{F}}{\partial Z\partial \boldsymbol{V}} & \frac{\partial^2 \mathcal{F}}{\partial Z\partial \boldsymbol{\vartheta}} & \frac{\partial^2 \mathcal{F}}{\partial Z^2} \end{pmatrix} = \mathcal{F}(\dot{z};t)\begin{pmatrix} \frac{\frac{\partial^2 q}{\partial \boldsymbol{V}^2}}{g(\boldsymbol{d},t)} & \frac{\frac{\partial^2 q}{\partial \boldsymbol{V}\partial \boldsymbol{\vartheta}}}{g(\boldsymbol{d},t)} & \frac{\frac{\partial q}{\partial \boldsymbol{V}}\frac{\partial J}{\partial Z}}{g(\boldsymbol{d},t)J(t)} \\ \frac{\frac{\partial^2 q}{\partial \boldsymbol{\vartheta}\partial \boldsymbol{V}}}{g(\boldsymbol{d},t)} & \frac{\frac{\partial^2 q}{\partial \boldsymbol{\vartheta}^2}}{g(\boldsymbol{d},t)} & \frac{\frac{\partial q}{\partial \boldsymbol{\vartheta}}\frac{\partial J}{\partial Z}}{g(\boldsymbol{d},t)J(t)} \\ \frac{\frac{\partial q}{\partial \boldsymbol{V}}\frac{\partial J}{\partial Z}}{g(\boldsymbol{d},t)J(t)} & \frac{\frac{\partial q}{\partial \boldsymbol{\vartheta}}\frac{\partial J}{\partial Z}}{g(\boldsymbol{d},t)J(t)} & \frac{\frac{\partial^2 J}{\partial Z^2}}{J(t)} \end{pmatrix}$$

$$\mathcal{F}_t(\dot{z};t) = \frac{\partial \mathcal{F}}{\partial t} = \mathcal{F}(\dot{z};t)\left[\frac{\dot{\Pi}(t)}{\Pi(t)} - \dot{\mathrm{i}}(t) + \frac{\dot{g}(\boldsymbol{d},t)}{g(\boldsymbol{d},t)}\right]$$

where $g\big(\boldsymbol{d}(t),t\big)$ (or for short $g(\boldsymbol{d},t)$) is an arbitrary function of $\boldsymbol{d}(t)$ and t that possesses continuous first and second order partial derivatives with respect to any components of $\boldsymbol{d}(t)$ and a continuous first order partial derivative with respect to t. The vector $\boldsymbol{d}(t)$ is defined as $\boldsymbol{d}(t) = [\boldsymbol{V}(t)\ \boldsymbol{\vartheta}(t)]^T$ (see 3.95-3.100), $J(t)$, $\Pi(t)$ and $Z(t)$ are respectively given by (3.93), (3.104) and (3.106). From Proposition E.1 and using the vector Itô differential rule (A.14) $\mathcal{F}(\dot{z};t) = \mathcal{F}(\boldsymbol{\varpi},t)$ is an Itô process which can be written as

$$d\mathcal{F}(\dot{z};t) = \mathcal{F}(\dot{z};t)\left\{\left[\frac{\dot{\Pi}(t)}{\Pi(t)} - \dot{\mathrm{i}}(t) + \frac{\dot{g}(\boldsymbol{d},t)}{g(\boldsymbol{d},t)} + \frac{1}{2}\frac{N_0}{2}\frac{\mathrm{tr}\left(\boldsymbol{\ell}_{\mathcal{F}}^T(t)\mathcal{F}_{\boldsymbol{\varpi}\boldsymbol{\varpi}}\boldsymbol{\ell}_{\mathcal{F}}(t)\right)}{\mathcal{F}(\dot{z};t)} + \frac{\left(\frac{\partial q}{\partial \boldsymbol{V}}\right)^T}{g(\boldsymbol{d},t)}\boldsymbol{q}'(t)\right.\right.$$
$$\left.\left. + \frac{\left(\frac{\partial q}{\partial \boldsymbol{\vartheta}}\right)^T}{g(\boldsymbol{d},t)}\boldsymbol{q}''(t) + \frac{\frac{\partial J}{\partial Z}}{J(t)}q(t)\right]dt + \left(\frac{\left(\frac{\partial q}{\partial \boldsymbol{V}}\right)^T}{g(\boldsymbol{d},t)}\boldsymbol{\ell}'(t) + \frac{\left(\frac{\partial q}{\partial \boldsymbol{\vartheta}}\right)^T}{g(\boldsymbol{d},t)}\boldsymbol{\ell}''(t) + \frac{\frac{\partial J}{\partial Z}}{J(t)}\ell(t)\right)dw(t)\right\}$$

where $\boldsymbol{\ell}_{\mathcal{F}}(t) = \left[\left[\boldsymbol{\ell}'(t)\right]^T \left[\boldsymbol{\ell}''(t)\right]^T \ell(t)\right]^T$. Substituting $\boldsymbol{\ell}_{\mathcal{F}}(t)$ and using (E.27) yields

$$\frac{d\mathcal{F}(\dot{z};t)}{\mathcal{F}(\dot{z};t)} = \left(\frac{\left(\frac{\partial g}{\partial \boldsymbol{V}}\right)^T}{g(\boldsymbol{d},t)}\boldsymbol{\ell}'(t) + \frac{\left(\frac{\partial g}{\partial \boldsymbol{\vartheta}}\right)^T}{g(\boldsymbol{d},t)}\boldsymbol{\ell}''(t) + \frac{\frac{\partial J}{\partial Z}}{J(t)}\ell(t)\right)dz(t) + \mathcal{R}(t)dt \tag{E.45}$$

where $\mathcal{R}(t)$ is given by

$$\begin{aligned}\mathcal{R}(t) = {} & \frac{\dot{\Pi}(t)}{\Pi(t)} - \dot{\mathrm{i}}(t) + \frac{\dot{g}(\boldsymbol{d},t)}{g(\boldsymbol{d},t)} + \frac{\frac{\partial J}{\partial Z}}{J(t)}\left(q(t) - \ell(t)v(t)\right) + \frac{\left(\frac{\partial g}{\partial \boldsymbol{V}}\right)^T}{g(\boldsymbol{d},t)}\left(\boldsymbol{q}'(t) - \boldsymbol{\ell}'(t)v(t)\right) \\ & + \frac{\left(\frac{\partial g}{\partial \boldsymbol{\vartheta}}\right)^T}{g(\boldsymbol{d},t)}\left(\boldsymbol{q}''(t) - \boldsymbol{\ell}''(t)v(t)\right) + \frac{1}{2}\frac{N_0}{2}\left[\left(\boldsymbol{\ell}'(t)\right)^T \frac{\frac{\partial^2 g}{\partial \boldsymbol{V}^2}}{g(\boldsymbol{d},t)}\boldsymbol{\ell}'(t)\right. \\ & + 2\left(\boldsymbol{\ell}'(t)\right)^T \frac{\frac{\partial^2 g}{\partial \boldsymbol{V}\partial \boldsymbol{\vartheta}}}{g(\boldsymbol{d},t)}\boldsymbol{\ell}''(t) + 2\left(\boldsymbol{\ell}'(t)\right)^T \frac{\frac{\partial g}{\partial \boldsymbol{V}}\frac{\partial J}{\partial Z}}{g(\boldsymbol{d},t)\,J(t)}\ell(t) + \left(\boldsymbol{\ell}''(t)\right)^T \frac{\frac{\partial^2 g}{\partial \boldsymbol{\vartheta}^2}}{g(\boldsymbol{d},t)}\boldsymbol{\ell}''(t) \\ & \left. +2\left(\boldsymbol{\ell}''(t)\right)^T \frac{\frac{\partial g}{\partial \boldsymbol{\vartheta}}\frac{\partial J}{\partial Z}}{g(\boldsymbol{d},t)\,J(t)}\ell(t) + \frac{\frac{\partial^2 J}{\partial Z^2}}{J(t)}\ell^2(t)\right]\end{aligned} \tag{E.46}$$

and $q(t)$, $\ell(t)$, $\boldsymbol{q}'(t)$, $\boldsymbol{\ell}'(t)$, $\boldsymbol{q}''(t)$, $\boldsymbol{\ell}''(t)$ are respectively given by (E.16), (E.8), (E.10), (E.2), (E.13) and (E.5).

Simplification of $\mathcal{R}(t)$

Recall that (E.45) is a symbolic differential notation for

$$\int_a^b \frac{d\mathcal{F}(\dot{z};s)}{\mathcal{F}(\dot{z};s)} = \int_a^b \left(\frac{\left(\frac{\partial g}{\partial \boldsymbol{V}}\right)^T}{g(\boldsymbol{d},s)}\boldsymbol{\ell}'(s) + \frac{\left(\frac{\partial g}{\partial \boldsymbol{\vartheta}}\right)^T}{g(\boldsymbol{d},s)}\boldsymbol{\ell}''(s) + \frac{\frac{\partial J}{\partial Z}}{J(s)}\ell(s)\right)dz(s) + \int_a^b \mathcal{R}(s)ds$$

thus double frequency terms can be neglected in $\mathcal{R}(s)$ since when integrated they are vanishing if the carrier frequency is large. Note from (3.93) that $\frac{\partial J}{\partial Z} = \frac{1}{2}\frac{2}{N_0}J$ and $\frac{\partial^2 J}{\partial Z^2} = \left(\frac{1}{2}\frac{2}{N_0}\right)^2 J$. Substituting (E.10), (E.13), (E.2) and (E.5) into (E.46) yields

$$\mathcal{R}(t) = \mathcal{R}_1(t) + \sum_{k=0}^{L-1}\frac{\frac{\partial g}{\partial V_k}}{g(\boldsymbol{d},t)}\mathcal{R}_k'(t) + \sum_{k=0}^{L-1}\frac{\frac{\partial g}{\partial \vartheta_k}}{g(\boldsymbol{d},t)}\mathcal{R}_k''(t) + \mathcal{R}_2(t)$$

where $\mathcal{R}_1(t)$, $\mathcal{R}_k'(t)$, $\mathcal{R}_k''(t)$ and $\mathcal{R}_2(t)$ are given by

$$\mathcal{R}_1(t) = \frac{1}{2}\frac{2}{N_0}\left(q(t) - \ell(t)v(t) + \frac{1}{4}\ell^2(t)\right) + \frac{\dot{\Pi}(t)}{\Pi(t)} \tag{E.47}$$

$$\mathcal{R}_k'(t) = q_k'(t) - \ell_k'(t)v(t) - \frac{1}{2N_0}\frac{|l_k(t,t)|^2}{V_k(t)} + \frac{1}{2}\ell_k'(t)\ell(t) \tag{E.48}$$

$$\mathcal{R}_k''(t) = q_k''(t) - \ell_k''(t)v(t) + \frac{1}{2}\ell_k''(t)\ell(t) \tag{E.49}$$

$$\mathcal{R}_2(t) = \frac{1}{2}\frac{N_0}{2}\left\{\sum_{j=0}^{L-1}\sum_{k=0}^{L-1}\left[\ell_k'(t)\ell_j'(t)\frac{\frac{\partial^2 g}{\partial V_k \partial V_j}}{g(\boldsymbol{d},t)} + \ell_k''(t)\ell_j''(t)\frac{\frac{\partial^2 g}{\partial \vartheta_k \partial \vartheta_j}}{g(\boldsymbol{d},t)} + 2\ell_k'(t)\ell_j''(t)\frac{\frac{\partial^2 g}{\partial V_k \partial \vartheta_j}}{g(\boldsymbol{d},t)}\right]\right\}$$
$$+ \sum_{k=0}^{L-1}\frac{\frac{\partial g}{\partial V_k}}{g(\boldsymbol{d},t)}\frac{|l_k(t,t)|^2}{2N_0V_k(t)} + \frac{\dot{g}(\boldsymbol{d},t)}{g(\boldsymbol{d},t)} - \dot{\mathrm{i}}(t) \tag{E.50}$$

where the term $-\frac{1}{2N_0}\frac{|l_k(t,t)|^2}{V_k(t)}$ has been artificially introduced in $\mathcal{R}_k'(t)$ for convenience, and its equivalent positive term has been included in $\mathcal{R}_2(t)$. Then as shown in the following, $\mathcal{R}_1(t)$, $\mathcal{R}_k'(t)$ and $\mathcal{R}_k''(t)$ are equal to zero.

Proof that $\mathcal{R}_1(t) = 0$. Substituting (E.16) and (E.8) into (E.47) yields

$$\mathcal{R}_1(t) = \frac{1}{2}\frac{2}{N_0}\left\{-2\frac{N_0}{2}\frac{\dot{\Pi}(t)}{\Pi(t)} - \int_0^t\int_0^t h(t,\tau)h(t,s)dz(s)dz(\tau) + \frac{1}{4}4\left(\int_0^t h(t,s)dz(s)\right)^2\right\}$$
$$+ \frac{\dot{\Pi}(t)}{\Pi(t)} = 0$$

Q.E.D

Proof that $\mathcal{R}_k'(t) = 0$. Substituting (E.11) and (E.8) into (E.48) yields

$$\mathcal{R}_k'(t) = p_k'(t) + \ell_k'(t)\left(\int_0^t h(t,s)dz(s)\right) = 0 \qquad \text{using (E.12)}$$

Q.E.D

Proof that $\mathcal{R}_k''(t) = 0$. Substituting (E.14) and (E.8) into (E.49) yields

$$\mathcal{R}_k''(t) = p_k''(t) + \ell_k''(t)\left(\int_0^t h(t,s)dz(s)\right) = 0 \qquad \text{using (E.15)}$$

Q.E.D

Itô derivative of $\mathcal{F}(\dot{z};t)$ with simplified $\mathcal{R}(t)$

Substituting (E.2), (E.5) and (E.8) into (E.45) and using $\mathcal{R}(t) = \mathcal{R}_2(t)$ yield

$$\frac{d\mathcal{F}(\dot{z};t)}{\mathcal{F}(\dot{z};t)} = \mathcal{R}_2(t)\,dt + \left[\sum_{k=0}^{L-1}\left(\frac{\frac{\partial g}{\partial V_k}}{g(\boldsymbol{d},t)}\ell_k'(t) + \frac{\frac{\partial g}{\partial \vartheta_k}}{g(\boldsymbol{d},t)}\ell_k''(t)\right) + \frac{1}{2}\frac{2}{N_0}\ell(t)\right]dz(t) \quad \text{(E.51)}$$

where $\mathcal{R}_2(t)$ is given by (E.50). Define $V_k'(t)e^{j\vartheta_k'(t)}$ as[1]

$$V_k'(t)e^{j\vartheta_k'(t)} = \frac{\dfrac{\partial g(\boldsymbol{d},t)}{\partial V_k(t)}}{g(\boldsymbol{d},t)} + j\frac{\dfrac{1}{V_k(t)}\dfrac{\partial g(\boldsymbol{d},t)}{\partial \vartheta_k(t)}}{g(\boldsymbol{d},t)} \quad V_k'(t)\text{: real, positive.} \quad \text{(E.52)}$$

Substituting (E.4), (E.7) and (E.8) into (E.51) yields

$$\frac{d\mathcal{F}(\dot{z};t)}{\mathcal{F}(\dot{z};t)} = \mathcal{R}_2(t)\,dt + \frac{2}{N_0}\left[\int_0^t h(t,s)dz(s) + \Re\left\{\left(\sum_{k=0}^{L-1}V_k'(t)e^{j\vartheta_k'(t)}l_k(t,t)e^{j\vartheta_k(t)}\right)e^{j\omega_c t}\right\}\right]dz(t)$$

Using (E.9) and $h(t,s) = \Re\left\{2\mathcal{H}^*(s,t,t)e^{j\omega_c(t-s)}\right\}$

$$\frac{d\mathcal{F}(\dot{z};t)}{\mathcal{F}(\dot{z};t)} = \mathcal{R}_2(t)dt + \frac{2}{N_0}\Re\left\{\left(2\int_0^t \mathcal{H}^*(s,t,t)e^{-j\omega_c s}dz(s) + \sum_{k=0}^{L-1}V_k'(t)e^{j\vartheta_k'(t)}l_k(t,t)e^{j\vartheta_k(t)}\right)e^{j\omega_c t}\right\}dz(t) \quad \text{(E.53)}$$

Note that (E.53) is valid $\forall\,\epsilon > 0, \forall\, r = 1,\ldots,L \;\; \forall\, t \in \left[T' + \tau_{r-1} + \epsilon, T' + \tau_r\right]$. Since ϵ can be arbitrarily small, (E.53) is also valid $\forall\, r = 1,\ldots,L$ and $\forall\, t \in \left(T' + \tau_{r-1}, T' + \tau_r\right]$. From (3.117) in Section 3.3.3, it is seen that whenever $\mathcal{F}(\dot{z};t)$ is a likelihood ratio, $\mathcal{R}_2(t) = 0$ and $\frac{N_0}{2}\frac{d\mathcal{F}(\dot{z};t)}{\mathcal{F}(\dot{z};t)dz(t)}$ is equal to the conditional mean or MMSE estimate. As an example, verification that $\mathcal{R}_2(t)$ for mixed mode Ricean/Rayleigh channels is presented next.

[1] (E.52) is identical to (3.112) and reprinted here for convenience.

E.3 Consistency of results

E.3.1 Verification that $\forall \epsilon > 0$, $\forall r = 1, \ldots, L-1 \quad \int_{T'+\tau_{r-1}+\epsilon}^{T'+\tau_r} \mathcal{R}_2(t)dt = 0$ for the likelihood ratio of a mixed mode Ricean/Rayleigh channel

From (D.15) the likelihood ratio over $[0,t]$ for a mixed mode Ricean/Rayleigh channel is given by

$$\Lambda(\dot{z};t) = J(t)I_0(V_0(t))$$

Hence $g(\boldsymbol{d},t) \triangleq \frac{\Lambda(\dot{z};t)}{J(t)} = g(V_0) = I_0(V_0)$. For a mixed mode Ricean/Rayleigh channel, $\forall k = 1, \ldots, L-1 \quad \alpha_k = 0$, hence from (3.103b), (3.98- 3.100) and (3.102b) $\forall k \neq 0$ $l_k(s,t) = 0$, $V_k(t) = 0$, $\vartheta_k(t) = 0$ and $e_{kn}(t) = 0$. Therefore using Proposition C.2 (E.50) reduces to

$$\mathcal{R}_2(t) = \frac{1}{2}\frac{N_0}{2}\left\{\left(\ell_0'(t)\right)^2 \frac{\frac{\partial^2 g}{\partial V_0^2}}{g(\boldsymbol{d},t)} + \left(\ell_0''(t)\right)^2 \frac{\frac{\partial^2 g}{\partial \vartheta_0^2}}{g(\boldsymbol{d},t)} + 2\ell_0'(t)\ell_0''(t)\frac{\frac{\partial^2 g}{\partial V_0 \partial \vartheta_0}}{g(\boldsymbol{d},t)}\right\}$$
$$+ \frac{|l_0(t,t)|^2}{2N_0}\frac{\frac{\partial g}{\partial V_0}}{g(\boldsymbol{d},t)V_0(t)} - \frac{|l_0(t,t)|^2}{2N_0} + \frac{\dot{g}(\boldsymbol{d},t)}{g(\boldsymbol{d},t)} \tag{E.54}$$

where $\ell_0'(t)$ and $\ell_0''(t)$ are given by (E.3) and (E.6). Since for mixed mode Ricean/Rayleigh channels $g(\boldsymbol{d},t)$ is independent of t besides the dependence through $V_0(t)$, $\dot{g}(\boldsymbol{d},t) = 0$. Similarly $g(\boldsymbol{d},t)$ is independent of ϑ_0, thus $\frac{\partial^2 g}{\partial \vartheta_0^2} = \frac{\partial^2 g}{\partial V_0 \partial \vartheta_0} = 0$. Therefore substituting (E.3) and (E.6) and omitting the index t for clarity, (E.54) reduces to

$$\mathcal{R}_2(t) = \frac{1}{2}\frac{N_0}{2}\left(\frac{2}{N_0}\right)^2 |l_0(t,t)|^2 \cos^2\left(\omega_c t + \psi_0(t,t) + \vartheta_0(t)\right)\frac{\frac{\partial^2 I_0(V_0)}{\partial V_0^2}}{I_0(V_0)}$$
$$+ \frac{I_1(V_0)}{I_0(V_0)}\frac{|l_0(t,t)|^2}{2N_0V_0} - \frac{1}{2N_0}|l_0(t,t)|^2$$
$$\int_{T'+\tau_{r-1}+\epsilon}^{T'+\tau_r} \mathcal{R}_2(t)dt = \frac{1}{2N_0}\int_{T'+\tau_{r-1}+\epsilon}^{T'+\tau_r} |l_0(t,t)|^2 \frac{I_0(V_0) - \frac{I_1(V_0)}{V_0}}{I_0(V_0)}dt$$
$$+ \frac{1}{2N_0}\frac{I_1(V_0)}{I_0(V_0)}\frac{|l_0(t,t)|^2}{V_0} - \frac{1}{2N_0}|l_0(t,t)|^2 = 0 \tag{E.55}$$

where (E.55) is obtained by neglecting integrals containing double frequency terms and using $\frac{\partial^2 I_0(x)}{\partial x^2} = I_0(x) - \frac{I_1(x)}{x}$ [185, p. 79].

The validity of the assumptions of continuously differentiable $x_{kl}^r(t)$ and distinct $\lambda_k^r(t)$ is studied next for the special case of two-path Ricean channels.

E.3.2 Continuous differentiability of the functions $\{x_{lk}^{rm}(t)\}_{l,k=0,\ldots,r-1}$ $(r=1,2)$ for a two-path Ricean channel

In this appendix, a two-path Ricean channel is considered with ordered multipath delays $\tau_0 < \tau_1$. The signals are assumed to be time-limited to $[0,T]$ and continuous over any finite observation $[0,t]$ $(0 \le t < \infty)$.

Existence of functions $x_{00}^1(t)$ continuously differentiable on $(T'+\tau_0, T'+\tau_1]$

Assume that $T'+\tau_0 < t \le T'+\tau_1$. From (B.3), $i_t = 1$ and from (3.32) the covariance function $\mathcal{K}^{i_t}(s,u) \triangleq \mathcal{K}^1(s,u)$ is given by[2]

$$\mathcal{K}^1(s,u) = 2\sigma_0^2 \tilde{s}(s-\tau_0)\tilde{s}^*(u-\tau_0) \quad 0 \le s,u \le t \quad T'+\tau_0 < t \le T'+\tau_1$$

Using Mercer's theorem [182, p. 85] ($\mathcal{K}^1(s,u) = \lambda_0^1(t)\phi_0^1(s,t)\,[\phi_0^1(u,t)]^*$), the only non-zero eigenvalue $\lambda_0^1(t)$ and its corresponding eigenfunction $\phi_0^1(s,t)$, found by inspection, are given by

$$\lambda_0^1(t) = 2\sigma_0^2\epsilon_0(t)\tilde{E} \qquad T'+\tau_0 < t \le T'+\tau_1$$

$$\phi_0^1(s,t) = \frac{\tilde{s}(s-\tau_0)}{\sqrt{\tilde{E}\epsilon_0(t)}} \quad 0 \le s \le t \qquad T'+\tau_0 < t \le T'+\tau_1$$

Comparing with (3.34) yields $x_{00}^1(t) = 1$.

Existence of functions $\{x_{lk}^2(t)\}_{l,k=0,1}$ continuously differentiable on $(T'+\tau_1, \infty)$

Assume that $T'+\tau_1 < t \le \infty$. From (B.3), $i_t = 2$ and the 2-dimensional matrices $\boldsymbol{\Gamma}_{i_t}(t) \triangleq \boldsymbol{\Gamma}_2(t)$ and $\boldsymbol{\epsilon}_{i_t}(t)\tilde{E}\boldsymbol{C}_{i_t}\boldsymbol{\Gamma}_{i_t}^*(t) \triangleq \boldsymbol{\epsilon}_2(t)\tilde{E}\boldsymbol{C}_2\boldsymbol{\Gamma}_2^*(t)$ are given by

$$\boldsymbol{\Gamma}_2(t) = \begin{pmatrix} 1 & \rho_{01}(t) \\ \rho_{01}^*(t) & 1 \end{pmatrix} \quad \boldsymbol{\epsilon}_2(t)\tilde{E}\boldsymbol{C}_2\boldsymbol{\Gamma}_2^*(t) = \tilde{E}\begin{pmatrix} 2\sigma_0^2\epsilon_0(t) & 2\sigma_0^2\epsilon_0(t)\rho_{01}^*(t) \\ 2\sigma_1^2\epsilon_1(t)\rho_{01}(t) & 2\sigma_1^2\epsilon_1(t) \end{pmatrix}$$

[2]The superscript 1 is not an exponent.

where $\rho_{01}(t) = \frac{1}{\tilde{E}\sqrt{\epsilon_0(t)\epsilon_1(t)}} \int_0^t \tilde{s}(s-\tau_0)\tilde{s}^*(s-\tau_1)ds$. Hence the eigenvalues of $\boldsymbol{\epsilon}_2(t)\tilde{E}\boldsymbol{C}_2\boldsymbol{\Gamma}_2^*(t)$, $\left\{\lambda_l^{i_t}(t) \triangleq \lambda_l^2(t)\right\}_{l=1,2}$, satisfy the equation[3]

$$\left(2\sigma_0^2\epsilon_0(t)\tilde{E} - \lambda\right)\left(2\sigma_1^2\epsilon_1(t)\tilde{E} - \lambda\right) - 2\sigma_0^2\epsilon_0(t)\tilde{E}\,2\sigma_1^2\epsilon_1(t)\tilde{E}\,|\rho_{01}(t)|^2 = 0$$

$$\lambda^2 - \tilde{E}\left(2\sigma_0^2\epsilon_0(t) + 2\sigma_1^2\epsilon_1(t)\right)\lambda + 2\sigma_0^2\epsilon_0(t)\tilde{E}\,2\sigma_1^2\epsilon_1(t)\tilde{E}\left(1 - |\rho_{01}(t)|^2\right) = 0$$

and can be expressed as

$$\lambda_0^2(t) = \frac{\tilde{E}}{2}\left[2\sigma_0^2\epsilon_0(t) + 2\sigma_1^2\epsilon_1(t) + \sqrt{\Delta_2(t)}\right] \tag{E.56a}$$

$$\lambda_1^2(t) = \frac{\tilde{E}}{2}\left[2\sigma_0^2\epsilon_0(t) + 2\sigma_1^2\epsilon_1(t) - \sqrt{\Delta_2(t)}\right] \tag{E.56b}$$

where $\Delta_2(t)$ is defined as

$$\Delta_2(t) \triangleq \left(2\sigma_0^2\epsilon_0(t) - 2\sigma_1^2\epsilon_1(t)\right)^2 + 4\cdot 2\sigma_0^2\epsilon_0(t)2\sigma_1^2\epsilon_1(t)\,|\rho_{01}(t)|^2 \tag{E.57}$$

If $\forall\, t \in \left(T' + \tau_1, \infty\right)$, $|\rho_{01}(t)| \neq 0$, then $\forall\, t \in \left(T' + \tau_1, \infty\right)$, from (E.57) $\Delta_2(t) \neq 0$ and the eigenvalues $\lambda_0^2(t)$ and $\lambda_1^2(t)$ are distinct. Furthermore $|\rho_{01}|^2$ is differentiable on $\left(T' + \tau_1, \infty\right)$. From (E.57) and (E.56), $\lambda_0^2(t)$ and $\lambda_1^2(t)$ are continuously differentiable on $\left(T' + \tau_1, \infty\right)$.

If $\forall\, t \in \left(T' + \tau_1, \infty\right), |\rho_{01}(t)| \neq 0$, then it can be shown that the functions $\left\{x_{lk}^{i_t}(t) \triangleq x_{lk}^2(t)\right\}_{l,k=0,1}$ such that the matrix $\boldsymbol{X}_2(t) = \begin{pmatrix} x_{00}^2(t) & x_{01}^2(t) \\ x_{10}^2(t) & x_{11}^2(t) \end{pmatrix}$ satisfies (3.35), are given up to phase rotation by

$$x_{00}^2(t) = \frac{2\sigma_0^2\epsilon_0(t)\,|\rho_{01}(t)|}{\sqrt{\Delta_{00}^2(t)}} = \frac{\left(\lambda_0'^2(t) - 2\sigma_1^2\epsilon_1(t)\right)}{\sqrt{\Delta_{01}^2(t)}} \tag{E.58a}$$

$$x_{01}^2(t) = \frac{\frac{\rho_{01}(t)}{|\rho_{01}(t)|}\left(\lambda_0'^2(t) - 2\sigma_0^2\epsilon_0(t)\right)}{\sqrt{\Delta_{00}^2(t)}} = \frac{2\sigma_1^2\epsilon_1(t)\rho_{01}(t)}{\sqrt{\Delta_{01}^2(t)}} \tag{E.58b}$$

$$x_{10}^2(t) = \frac{-2\sigma_0^2\epsilon_0(t)\,|\rho_{01}(t)|}{\sqrt{\Delta_{10}^2(t)}} = \frac{-\left(2\sigma_1^2\epsilon_1(t) - \lambda_1'^2(t)\right)}{\sqrt{\Delta_{11}^2(t)}} \tag{E.58c}$$

$$x_{11}^2(t) = \frac{\frac{\rho_{01}(t)}{|\rho_{01}(t)|}\left(2\sigma_0^2\epsilon_0(t) - \lambda_1'^2(t)\right)}{\sqrt{\Delta_{10}^2(t)}} = \frac{2\sigma_0^2\epsilon_0(t)\rho_{01}(t)}{\sqrt{\Delta_{11}^2(t)}} \tag{E.58d}$$

[3]The superscript 2 of $\{\lambda_l^2(t)\}_{l=0,1}$ is not an exponent.

where $\forall l = 0,1, \lambda_l'^2(t) = \dfrac{\lambda_l^2(t)}{\tilde{E}}$ and $\{\Delta_{lk}^2(t)\}_{l,k=0,1}$ are given by[4]

$$\Delta_{00}^2(t) = \left(2\sigma_0^2\epsilon_0(t) - \lambda_0'^2(t) - 2\sigma_0^2\epsilon_0(t)\left|\rho_{01}(t)\right|^2\right)^2 + \left(2\sigma_0^2\epsilon_0(t)\right)^2\left|\rho_{01}(t)\right|^2\left(1-\left|\rho_{01}(t)\right|^2\right)$$

$$\Delta_{01}^2(t) = \left(2\sigma_1^2\epsilon_1(t) - \lambda_0'^2(t) - 2\sigma_1^2\epsilon_1(t)\left|\rho_{01}(t)\right|^2\right)^2 + \left(2\sigma_1^2\epsilon_1(t)\right)^2\left|\rho_{01}(t)\right|^2\left(1-\left|\rho_{01}(t)\right|^2\right)$$

$$\Delta_{10}^2(t) = \left(2\sigma_0^2\epsilon_0(t) - \lambda_1'^2(t) - 2\sigma_0^2\epsilon_0(t)\left|\rho_{01}(t)\right|^2\right)^2 + \left(2\sigma_0^2\epsilon_0(t)\right)^2\left|\rho_{01}(t)\right|^2\left(1-\left|\rho_{01}(t)\right|^2\right)$$

$$\Delta_{11}^2(t) = \left(2\sigma_1^2\epsilon_1(t) - \lambda_1'^2(t) - 2\sigma_1^2\epsilon_1(t)\left|\rho_{01}(t)\right|^2\right)^2 + \left(2\sigma_1^2\epsilon_1(t)\right)^2\left|\rho_{01}(t)\right|^2\left(1-\left|\rho_{01}(t)\right|^2\right)$$

Since $\tau_0 \neq \tau_1$ and $\tilde{s}(s)$ are time-limited, $|\rho_{01}(t)|^2 \neq 1$, therefore since $|\rho_{01}(t)| \neq 0$ all denominators are strictly positive. Note that without the continuous differentiability condition, valid functions $\{x_{lk}^2(t)\}_{l,k=0,1}$ satisfying (3.35) can be obtained by phase rotation of (E.58) according to the following rule. If $x_{00}^2(t)$ is phase rotated, $x_{01}^2(t)$ should be rotated by the same phase and the opposite also holds. Similarly, if $x_{10}^2(t)$ is phase rotated, $x_{11}^2(t)$ should be rotated by the same phase and vice versa. And $x_{00}^2(t)$ and $x_{10}^2(t)$ can be rotated by two different phases.

Recall that since $\forall, t \in \left(T' + \tau_1, \infty\right), |\rho_{01}(t)| \neq 0$, the arguments of the square root present in the denominators of $x_{lk}^2(t)$ are strictly positive. Furthermore $\rho_{01}(t)$, $\epsilon_l(t)$ and $\lambda_l'^2(t)$ are continuously differentiable on $\left(T' + \tau_0, \infty\right)$ therefore $\{x_{lk}^2(t)\}_{l,k=0,1}$ given by (E.58) are continuously differentiable on $\left(T' + \tau_0, \infty\right)$.

[4]The superscript 2 of $\{\Delta_{lk}^2(t)\}_{l,k=0,1}$ is not an exponent.

Appendix F

Interpretation of the MMSE estimate (mathematical details)

In this appendix, only the first section assumes path resolvability.

F.1 Proof of $\int_0^t \left[\int_0^t Q_{*m}(u,v,t)\,|\alpha_k|\,\tilde{s}_m(v-\tau_k)e^{j\omega_c v}dv\right] v_{km}^d(u)du = 0$ when the multipath is resolved

This section shows that when the multipath is resolved the term $\int_0^t \left[\int_0^t Q_{*m}(u,v,t)\,|\alpha_k|\,\tilde{s}_m(v-\tau_k)e^{j\omega_c v}dv\right] v_{km}^d(u)du$ vanishes regardless of the nature of $\{\theta_r'\}_{r\neq k}$ (known or random). From (3.137)

$$\int_0^t \left[\int_0^t Q_{*m}(u,v,t)\,|\alpha_k|\,\tilde{s}_m(v-\tau_k)e^{j\omega_c v}dv\right] v_{km}^d(u)du$$

$$= \int_0^t \left[\int_0^t Q_{*m}(u,v,t)\,|\alpha_k|\,\tilde{s}_m(v-\tau_k)e^{j\omega_c v}dv\right] \Re\left\{\left(\sum_{\substack{r=0\\r\neq k}}^{L-1} |\alpha_r|\,\tilde{s}_m(u-\tau_r)e^{j\theta_r'}\right) e^{j\omega_c u}\right\} du$$

$$= \frac{2}{N_0}\int_0^t l_{km}(u,t)e^{j\omega_c u}\Re\left\{\left(\sum_{\substack{r=0\\r\neq k}}^{L-1} |\alpha_r|\,\tilde{s}_m(u-\tau_r)e^{j\theta_r'}\right) e^{j\omega_c u}\right\} du \quad \text{from (3.141)}$$

$$\approx \frac{1}{N_0}\int_0^t \sum_{\substack{r=0\\r\neq k}}^{L-1} |\alpha_r|\,\tilde{s}_m^*(u-\tau_r)e^{-j\theta_r'} l_{km}(u,t)du \qquad \text{from}^1\text{(C.1)}$$

[1]This approximation corresponds to neglecting integrals containing double frequency terms.

$$= \frac{1}{N_0}\int_0^t \sum_{\substack{r=0\\ r\neq k}}^{L-1} |\alpha_r|\,\tilde{s}_m^*(u-\tau_r)e^{-j\theta_r'}\frac{|\alpha_k|}{1+2\sigma_k^2\epsilon_{km}(t)\gamma_m}\tilde{s}_m(u-\tau_k)du \qquad \text{from (3.147)}$$

$$= \frac{1}{N_0}\frac{|\alpha_k|}{1+2\sigma_k^2\epsilon_{km}(t)\gamma_m}\sum_{\substack{r=0\\ r\neq k}}^{L-1} |\alpha_r|\,e^{-j\theta_r'}\int_0^t \tilde{s}_m(u-\tau_k)\tilde{s}_m^*(u-\tau_r)du = 0 \qquad \text{from (3.58a)}$$

F.2 Close form expression of $E\left[V_{km}^2(t)|H_m\right]$

From Section 3.2.1 when $\boldsymbol{\theta}$ is held fixed, $v_m(s) = \Re\left\{\sum_{k=0}^{L-1} a_k e^{j\theta_k}\tilde{s}_m(s-\tau_k)e^{j\omega_c s}\right\}$ has a covariance function $K_m(s,u)$ given by (3.5) and a mean given by $E\left[v_m(s)|\boldsymbol{\theta}\right] = \Re\left\{\left(\sum_{k=0}^{L-1}\alpha_k e^{j\theta_k}\tilde{s}_m(s-\tau_k)\right)e^{j\omega_c s}\right\}$. Hence $v_m(s)$ has zero mean since $\{\theta_k\}_k$ are uniformly distributed between $-\pi$ and π. Therefore the covariance function of $v_m(s)$ is given by[2]

$$\begin{aligned}
K_m''(s,u) &\triangleq E\left[\left(v_m(s)-\overline{v_m(s)}\right)\left(v_m(u)-\overline{v_m(u)}\right)\right] = E\left[v_m(s)v_m(u)\right]\\
&= E\Big[E\left[v_m(s)v_m(u)|\boldsymbol{\theta}\right]\Big]\\
&= E\Big[E\left[\left(v_m(s)-\nu_m(s,\boldsymbol{\theta})\right)\left(v_m(u)-\nu_m(u,\boldsymbol{\theta})\right)|\boldsymbol{\theta}\right]\Big] + E\Big[\nu_m(s,\boldsymbol{\theta})\nu_m(u,\boldsymbol{\theta})\Big]\\
&= E\Big[K_m(s,u)\Big] + E\left[\Re\left\{\sum_{k=0}^{L-1}\alpha_k e^{j\theta_k}\tilde{s}_m(s-\tau_k)e^{j\omega_c s}\right\}\Re\left\{\sum_{r=0}^{L-1}\alpha_r e^{j\theta_r}\tilde{s}_m(u-\tau_r)e^{j\omega_c u}\right\}\right]\\
&= K_m(s,u) + \Re\left\{\frac{1}{2}\mathcal{K}_m^s(s,u)e^{j\omega_c(s-u)}\right\} \qquad \text{(F.1)}
\end{aligned}$$

$$\text{where}^3 \quad \mathcal{K}_m^s(s,u) = \sum_{k=0}^{L-1}|\alpha_k|^2\,\tilde{s}_m(s-\tau_k)\tilde{s}_m^*(u-\tau_k) \qquad \text{(F.2)}$$

and (F.1) is obtained since $K_m(s,u)$ given by (3.5) is independent of $\boldsymbol{\theta}$ and $\{\theta_k\}_k$ are independent uniformly distributed between $-\pi$ and π. Under hypothesis H_m, since

[2] $\nu_m(s,\boldsymbol{\theta}) \triangleq E\left[v_m(s)|\boldsymbol{\theta}\right]$ (see Appendix B).

[3] The superscript s in (F.2) is not an exponent and indicates that $\Re\left\{\frac{1}{2}\mathcal{K}_m^s(s,u)e^{j\omega_c(s-u)}\right\}$ is the specular component part of $K_m''(s,u)$.

$E[v_m(u)] = 0$ from (3.98-3.100)

$$E\left[V_{km}^2(t)|H_m\right] = \left(\frac{2}{N_0}\right)^2 \int_0^t \int_0^t l_{km}(s,t)e^{j\omega_c s} l_{km}^*(u,t)e^{-j\omega_c u} E\left[dz(s)dz(u)\right]$$
$$= \left(\frac{2}{N_0}\right)^2 \int_0^t \int_0^t l_{km}(s,t)e^{j\omega_c s} l_{km}^*(u,t)e^{-j\omega_c u} \left\{K_m''(s,u) + \frac{N_0}{2}\delta(s-u)\right\} ds\, du$$
$$= \left(\frac{2}{N_0}\right)^2 \left[\int_0^t \int_0^t l_{km}(s,t)e^{j\omega_c s} l_{km}^*(u,t)e^{-j\omega_c u} K_m''(s,u) ds\, du + \frac{N_0}{2}\int_0^t |l_{km}(s,t)|^2 ds\right] \tag{F.3}$$

$$\int_0^t \int_0^t l_{km}(s,t)e^{j\omega_c s} l_{km}^*(u,t)e^{-j\omega_c u} K_m''(s,u) ds\, du$$
$$= \int_0^t l_{km}(s,t)e^{j\omega_c s} \left[\int_0^t \Re\left\{\left[\frac{1}{2}\mathcal{K}_m^*(s,u)e^{-j\omega_c s}\right] e^{j\omega_c u}\right\} l_{km}^*(u,t)e^{-j\omega_c u} du\right] ds$$
$$+ \int_0^t l_{km}(s,t)e^{j\omega_c s} \left[\int_0^t \Re\left\{\left[\frac{1}{2}\left[\mathcal{K}_m^s(s,u)\right]^* e^{-j\omega_c s}\right] e^{j\omega_c u}\right\} l_{km}^*(u,t)e^{-j\omega_c u} du\right] ds \tag{F.4}$$

where (F.4) is obtained from (F.1) and (3.5). Applying conjugate of (C.1) to the inner integrals of (F.4) and substituting (F.4) into (F.3) yields

$$E\left[V_{km}^2(t)|H_m\right] \approx \frac{2}{N_0}\int_0^t |l_{km}(s,t)|^2 ds \quad \text{(i.e. neglecting double frequency integrals)}$$
$$+ \left(\frac{2}{N_0}\right)^2 \int_0^t l_{km}(s,t)e^{j\omega_c s} \left\{\frac{1}{2}\int_0^t \left[\frac{1}{2}\mathcal{K}_m^*(s,u)e^{-j\omega_c s}\right] l_{km}^*(u,t) du\right\} ds$$
$$+ \left(\frac{2}{N_0}\right)^2 \int_0^t l_{km}(s,t)e^{j\omega_c s} \left\{\frac{1}{2}\int_0^t \left[\frac{1}{2}\left[\mathcal{K}_m^s(s,u)\right]^* e^{-j\omega_c s}\right] l_{km}^*(u,t) du\right\} ds$$
$$= \frac{2}{N_0}\int_0^t |l_{km}(s,t)|^2 ds + \frac{1}{4}\left(\frac{2}{N_0}\right)^2 \int_0^t l_{km}(s,t)\left[\int_0^t l_{km}^*(u,t)\mathcal{K}_m^*(s,u) du\right] ds$$
$$+ \frac{1}{4}\left(\frac{2}{N_0}\right)^2 \int_0^t l_{km}(s,t)\left[\int_0^t l_{km}^*(u,t)\left[\mathcal{K}_m^s(s,u)\right]^* du\right] ds$$
$$= \frac{2}{N_0}\int_0^t |l_{km}(s,t)|^2 ds + \frac{1}{4}\left(\frac{2}{N_0}\right)^2 \int_0^t l_{km}(s,t) 2N_0 \left[|\alpha_k|\,\tilde{s}_m^*(s-\tau_k) - l_{km}^*(s,t)\right] ds$$
$$+ \frac{1}{4}\left(\frac{2}{N_0}\right)^2 \sum_{r=0}^{L-1} |\alpha_r|^2 \left[\int_0^t l_{km}(s,t)\tilde{s}_m^*(s-\tau_r) ds\right]\left[\int_0^t l_{km}^*(u,t)\tilde{s}_m(u-\tau_r) du\right] \tag{F.5}$$

$$= \frac{2}{N_0}\int_0^t l_{km}(s,t)\,|\alpha_k|\,\tilde{s}_m^*(s-\tau_k)ds + \sum_{r=0}^{L-1}\left|\frac{1}{N_0}\int_0^t l_{km}(s,t)\,|\alpha_r|\,\tilde{s}_m^*(s-\tau_r)ds\right|^2 \tag{F.6}$$

$$= 2e_{kk}^m(t) + \sum_{r=0}^{L-1}\left|\left[e_{kr}^m(t)\right]^*\right|^2 = 2e_{kk}^m(t) + \sum_{r=0}^{L-1}|e_{kr}^m(t)|^2 \tag{F.7}$$

where (F.5) is obtained from (C.25) and (F.2) and $e_{kr}^m(t)$ is given by (3.102).

F.3 Average signal energy of the whitened received signal $\dot{z}_*(s) - v_{*k}^d(s)$

Since $\{\theta_k'\}_k$ are uniformly distributed between $-\pi$ and π, from (3.152) the expected value of the energy of $\dot{z}_*(s) - v_{*k}^d(s)$ is given by

$$\begin{aligned}
&E\left[\int_0^t\left[\int_0^t H_{*m}(s,u,t)\Re\left\{\left(|\alpha_k|\,\tilde{s}_m(u-\tau_k)e^{j\theta_k'}\right)e^{j\omega_c u}\right\}du\right]^2 ds\right] \\
&= \int_0^t\int_0^t\int_0^t H_{*m}(s,u,t)H_{*m}(s,v,t)E\left[\Re\left\{|\alpha_k|\,\tilde{s}_m(u-\tau_k)e^{j\theta_k'}e^{j\omega_c u}\right\}\right. \\
&\qquad\left.\cdot\,\Re\left\{|\alpha_k|\,\tilde{s}_m(v-\tau_k)e^{j\theta_k'}e^{j\omega_c v}\right\}\right]du\,dv\,ds \\
&= \int_0^t\int_0^t\int_0^t H_{*m}(s,u,t)H_{*m}(s,v,t)\frac{1}{2}\Re\left\{|\alpha_k|^2\,\tilde{s}_m(u-\tau_k)\tilde{s}_m^*(v-\tau_k)e^{j\omega_c(u-v)}\right\}du\,dv\,ds \\
&= \frac{1}{2}\int_0^t\int_0^t Q_{*m}(u,v,t)\Re\left\{|\alpha_k|^2\,\tilde{s}_m(u-\tau_k)\tilde{s}_m^*(v-\tau_k)e^{j\omega_c(u-v)}\right\}du\,dv \quad \text{from (3.144)} \\
&= \frac{1}{2}\int_0^t\int_0^t Q_{*m}(u,v,t)\left[\Re\left\{|\alpha_k|\,\tilde{s}_m(v-\tau_k)e^{j\omega_c v}\right\}\Re\left\{|\alpha_k|\,\tilde{s}_m(u-\tau_k)e^{j\omega_c u}\right\}\right. \\
&\qquad\left.+\,\Im\left\{|\alpha_k|\,\tilde{s}_m(v-\tau_k)e^{j\omega_c v}\right\}\Im\left\{|\alpha_k|\,\tilde{s}_m(u-\tau_k)e^{j\omega_c u}\right\}\right]du\,dv \\
&= \int_0^t\frac{1}{N_0}\Re\left\{l_{km}(u,t)e^{j\omega_c u}\right\}\Re\left\{|\alpha_k|\,\tilde{s}_m(u-\tau_k)e^{j\omega_c u}\right\}du \\
&\qquad+\int_0^t\frac{1}{N_0}\Im\left\{l_{km}(u,t)e^{j\omega_c u}\right\}\Im\left\{|\alpha_k|\,\tilde{s}_m(u-\tau_k)e^{j\omega_c u}\right\}du \qquad \text{from (3.141)} \\
&= \frac{1}{N_0}\int_0^t\Re\left\{l_{km}(u,t)\,|\alpha_k|\,\tilde{s}_m^*(u-\tau_k)\right\}du = \frac{1}{N_0}\int_0^t l_{km}(u,t)\,|\alpha_k|\,\tilde{s}_m^*(u-\tau_k)du
\end{aligned} \tag{F.8}$$

since from (3.102), $\int_0^t l_{km}(u,t)\,|\alpha_k|\,\tilde{s}_m^*(u-\tau_k)du$ is real.

Appendix G

Performance analysis

G.1 Proof that the residues of $h_k(z)$ consist of infinite series for an L-path Ricean channel

As seen in Section 4.1.2, the probability of error of the SPECCOH, SPECCOHR, QDR, R OPT and QR schemes involves the evaluation of integrals (4.3-4.4) over a contour. In theory these integrals can be evaluated by using the residue method. However as shown in this appendix, such a method is not practical in the case of Ricean channels since each residue consists of an infinite series.

Proof. Omitting for sake of simplicity the dependence on $\boldsymbol{\theta}$ and the index k representing the hypothesis considered, from (4.3-4.5) , the function to integrate is given by

$$\mathsf{h}(z) \triangleq \frac{\varphi_{\Delta}(z)}{z} e^{-zA} = \mathsf{f}_l(z)\mathsf{g}_l(z) \tag{G.1}$$

where all terms not defined at $z = \eta_l^{-1}$ have been included in one function $\mathsf{f}_l(z)$,

$$\mathsf{f}_l(z) = (1 - z\eta_l)^{-1} \exp\left\{\frac{z\eta_l|v_l|^2}{1 - z\eta_l}\right\} = (1 - z\eta_l)^{-1} \exp\left\{-|v_l|^2\right\} \exp\left\{\frac{|v_l|^2}{1 - z\eta_l}\right\}$$

and $\mathsf{g}_l(z)$ is everything left over

$$\mathsf{g}_l(z) = \frac{e^{-zA}}{z} \prod_{\substack{j=0 \\ j \neq l}}^{2L-1} \mathsf{f}_j(z)$$

Note that the function $\mathbf{g}_l(z)$ is analytic at the point $z = \eta_l^{-1}$. For sake of simplicity, all η_l will be assumed distinct, however, similar reasoning may be followed with eigenvalues of multiplicity greater than one, provided that the part of $\mathsf{h}(z)$ with singularities is isolated from the analytical part as done in (G.1). From (G.1), it is seen that $\mathsf{h}(z)$ is the product of two analytic functions on the entire complex plane with the exception of a finite number of isolated points, corresponding, similar to the zero mean case, to the eigenvalues of the matrix $(\boldsymbol{RQ})^{-1}$, $\{\eta_l^{-1}\}_{l=0,\ldots,2L-1}$. For Ricean channels, the Laurent series of $\mathsf{f}_l(z)$ in the neighborhood of η_l^{-1} is given by

$$\mathsf{f}_l(z) = \exp\left\{-|v_l|^2\right\} \sum_{s=0}^{\infty} \frac{(|v_l|^2)^s}{(1 - z\eta_l)^{s+1} s!} \tag{G.2}$$

which reduces to $\mathsf{f}_l(z) = \frac{1}{1-z\eta_l}$ for Rayleigh channels. From (G.2) it is seen that the principal part of the Laurent series of $\mathsf{f}_l(z)$ at $z = \eta_l^{-1}$ has an infinite number of non-zero terms, hence the points $z = \eta_l^{-1}$ are not poles but essential singular points [190, pp. 83-93]. By expanding the function $\mathbf{g}_l(z)$ in a Mac Laurin series in the neighborhood of $z = \eta_l^{-1}$ and using (G.2), the Laurent series of $\mathsf{h}(z)$ is given by

$$\begin{aligned}
\mathsf{h}(z) &= \exp\left\{-|v_l|^2\right\} \sum_{s=0}^{\infty} \frac{(|v_l|^2)^s}{(-\eta_l)^{s+1}(z - \eta_l^{-1})^{s+1} s!} \cdot \sum_{n=0}^{\infty} \frac{\mathbf{g}_l^{(n)}(\eta_l^{-1})(z - \eta_l^{-1})^n}{n!} \\
&= \exp\left\{-|v_l|^2\right\} \sum_{n=0}^{\infty} \sum_{s=0}^{\infty} \frac{\mathbf{g}_l^{(n)}(\eta_l^{-1})\,(|v_l|^2)^s}{(-1)^{s+1}\eta_l^{s+1} n! s! (z - \eta_l^{-1})^{s-n+1}}
\end{aligned}$$

where $\mathbf{g}_l^{(n)}(z)$ denotes the n^{th} derivative of $\mathbf{g}_l(z)$. The residue of $\mathsf{h}(z)$ at the essential singular point $z = \eta_l^{-1}$ is the coefficient of the term $(z - \eta_l^{-1})^{-1}$ of the Laurent series of $\mathsf{h}(z)$ in a neighborhood of that point [190, p. 92] and is given by

$$\text{res}\ \left(\mathsf{h}(z), z = \eta_l^{-1}\right) = \exp\left\{-|v_l|^2\right\} \sum_{n=0}^{\infty} \frac{\mathbf{g}_l^{(n)}(\eta_l^{-1})\,(|v_l|^2)^n}{(-1)^{n+1}(n!)^2 \eta_l^{n+1}}$$

which is an infinite series. **Q.E.D**

G.2 Bounding the bias term A for the SPECCOH, QDR and R OPT schemes

To emphasize the dependence of the bias term A on γ, let us denote A as A_γ. From Table 4.2, the bias term $A \triangleq A_\gamma$ of the SPECCOH, QDR and R OPT schemes satisfies

$$|A_\gamma| \leq \frac{1}{\gamma}\left|\ln\left(\frac{\det(\boldsymbol{I}+\gamma\boldsymbol{D}_1)}{\det(\boldsymbol{I}+\gamma\boldsymbol{D}_2)}\right)\right| + \frac{1}{\gamma}\left|\boldsymbol{\alpha}^\dagger\boldsymbol{C}^{-1}\left\{\boldsymbol{X}_1^T\boldsymbol{D}_1\boldsymbol{Q}_1\boldsymbol{X}_1^* - \boldsymbol{X}_2^T\boldsymbol{D}_2\boldsymbol{Q}_2\boldsymbol{X}_2^*\right\}_d\boldsymbol{C}^{-1}\boldsymbol{\alpha}\right|$$

Substituting the values of $\boldsymbol{C}$, $[\boldsymbol{C}]_{rj} = 2\sigma_r^2\delta_{rj}$, $\boldsymbol{D}_m$, $[\boldsymbol{D}_m]_{rj} = \frac{\lambda_{rm}}{E}\delta_{rj} \triangleq \lambda'_{rm}\delta_{rj}$ (where δ_{rj} is the Kronecker operator) and $\boldsymbol{\alpha} = [\alpha_0\, 0 \ldots 0]^T$ yields

$$|A_\gamma| \leq \frac{1}{\gamma}\left|\ln\left(\frac{\prod_{r=0}^{L-1}(1+\gamma\lambda'_{r1})}{\prod_{r=0}^{L-1}(1+\gamma\lambda'_{r2})}\right)\right| + \frac{1}{\gamma}\left|\frac{\alpha_0^*}{2\sigma_0^2}\left[\boldsymbol{X}_1^T\boldsymbol{D}_1\boldsymbol{Q}_1\boldsymbol{X}_1^* - \boldsymbol{X}_2^T\boldsymbol{D}_2\boldsymbol{Q}_2\boldsymbol{X}_2^*\right]_{00}\frac{\alpha_0}{2\sigma_0^2}\right|$$

Substituting $\boldsymbol{Q}_m$ and $\boldsymbol{X}_m$ yields

$$\begin{aligned}|A_\gamma| &\leq \frac{1}{\gamma}\left|\sum_{r=0}^{L-1}\ln\left(\frac{1+\gamma\lambda'_{r1}}{1+\gamma\lambda'_{r2}}\right)\right| + \frac{1}{\gamma}\frac{|\alpha_0|^2}{(2\sigma_0^2)^2}\sum_{r=0}^{L-1}\left|\left|x_{r0}^1\right|^2\lambda'_{r1}\frac{\lambda'_{r1}\gamma}{1+\lambda'_{r1}\gamma} - \left|x_{r0}^2\right|^2\lambda'_{r2}\frac{\lambda'_{r2}\gamma}{1+\lambda'_{r2}\gamma}\right| \\ &\leq \frac{L}{\gamma}\left|\ln\left(\frac{1+\gamma\lambda'_{1\max}}{1+\gamma\lambda'_{2\min}}\right)\right| + \frac{|\alpha_0|^2}{(2\sigma_0^2)^2}\sum_{r=0}^{L-1}\left[\left|x_{r0}^1\right|^2\lambda'^2_{r1}\frac{1}{1+\lambda'_{r1}\gamma} + \left|x_{r0}^2\right|^2\lambda'^2_{r2}\frac{1}{1+\lambda'_{r2}\gamma}\right]\end{aligned}$$

where $\lambda'_{1\max} = \max_r\lambda'_{r1}$ and $\lambda'_{2\min} = \min_r\lambda'_{r2}$. Since $\left|\ln\left(\frac{1+xa}{1+xb}\right)\right| \leq \left|\ln\left(\frac{a}{b}\right)\right|$, for all $x \geq 0$, $|A_\gamma| \leq \frac{A_{\text{up}}}{\gamma}$, where A_{up} is given by

$$A_{\text{up}} = L\left|\ln\left(\frac{\lambda'_{1\max}}{\lambda'_{1\min}}\right)\right| + \frac{|\alpha_0|^2}{(2\sigma_0^2)^2}\sum_{r=0}^{L-1}\left[\left|x_{r0}^1\right|^2\lambda'^2_{r1} + \left|x_{r0}^2\right|^2\lambda'^2_{r2}\right]$$

Therefore

$$\forall\gamma > 1 \quad |A_\gamma| \leq A_{\text{up}}$$

References

[1] H. Hashemi, "The indoor radio propagation channel," *Proceedings of the IEEE*, vol. 81, pp. 943–968, July 1993.

[2] J. Proakis, *Digital communications*. New York: McGraw-Hill, 1989.

[3] R. Price, "Optimum detection of random signals in noise, with application to scatter-multipath communication, I," *IRE Trans. Inform. Theory*, vol. 2, pp. 125–135, Dec. 1956.

[4] G. Turin, "Communication through noisy, random-multipath channels," *1956 I.R.E. National Convention record*, vol. pt. 4, pp. 154–166, Mar. 1956.

[5] R. Price and P. Green Jr., "A communication technique for multipath channels," *Proceedings of the IRE*, vol. 46, pp. 555–570, Mar. 1958.

[6] W. Lee, *Mobile communications engineering, 2nd edition*. New York: McGraw-Hill, 1998.

[7] D. Devasirvatham, M. Krain, and D. Rappaport, "Radio propagation measurements at 850 MHz, 1.7 GHz and 4 GHz inside two dissimilar office buildings," *Electronics Letters*, vol. 26, pp. 445–447, Mar. 1990.

[8] J. Shapira, "Channel characteristics for land cellular radio, and their systems implications," *IEEE Antennas and Propagation Magazine*, vol. 34, pp. 7–16, Aug. 1992.

[9] A. Levy, J.-P. Rossi, J.-P. Barbot, and J. Martin, "An improved channel sounding technique applied to wideband mobile 900 MHz propagation measurements," in 40^{th} *IEEE Vehicular Technology Conference (VTC90')*, (Orlando FL USA), pp. 513–519, 1990.

[10] T. Manabe and H. Takai, "Superresolution of multipath delay profiles measured by PN correlation method," *IEEE Trans. Antennas and Propagation*, vol. 40, pp. 500–509, May 1992.

[11] Z. Kostić, M. Sezan, and E. Titlebaum, "Estimation of the parameters of a multipath channel using set-theoretic deconvolution," *IEEE Trans. Communications*, vol. 40, pp. 1006–1011, June 1992.

[12] L. Dumont, M. Fattouche, and G. Morrison, "Super-resolution of multipath channels in a spread spectrum location system," *Electronics Letters*, vol. 30, pp. 1583–1584, Sept. 1994.

[13] T. Manickam, R. Vaccaro, and D. Tufts, "A least-squares algorithm for multipath time-delay estimation," *IEEE Trans. Signal Processing*, vol. 42, pp. 3229–3233, Nov. 1994.

[14] T. Korhonen, M. Hall, and S.-G. Häggman, "Superresolution multipath channel parameter estimation by matched filter deconvolution and sequential bin tuning," in *2nd International Workshop on Multi-Dimensional Mobile Communications*, (Seoul, Korea), July 1996.

[15] T. Korhonen and S.-G. Häggman, "Location of subchip radio channel multipath components from direct sequence sounding data," in *IEEE International Conference on Personal Wireless communications*, (Bombay, India), pp. 43–47, 1997.

[16] G. Morrison and M. Fattouche, "Super-resolution modeling of the indoor radio propagation channel," *IEEE Trans. Vehicular Technology*, vol. 47, pp. 649–657, May 1998.

[17] J. Kivinen and al., "Wideband radio channel measurement system at 2 GHz," *IEEE Trans. Instrumentation and Measurement*, vol. 48, pp. 39–44, Feb. 1999.

[18] R. Vaughan and N. Scott, "Super-resolution of pulsed multipath channels for delay spread characterization," *IEEE Trans. Communications*, vol. 47, pp. 343–347, Mar. 1999. see also same title, PIRMC'96, pp. 781-785, 1996.

[19] Z. Kostić and G. Pavlović, "Resolving subchip-spaced multipath components in CDMA communication systems," *IEEE Trans. Vehicular Technology*, vol. 48, pp. 1803–1808, Nov. 1999.

[20] F. Danilo and H. Leib, "Detection techniques for fading multipath channels with unresolved components," *IEEE Trans. Inform. Theory*, vol. 44, pp. 2848–2863, Nov. 1998.

[21] T. Kailath, "A general likelihood-ratio formula for random signals in Gaussian noise," *IEEE Trans. Inform. Theory*, vol. 15, pp. 350–361, May 1969.

[22] S. Gupta, R. Viswanathan, and R. Muammar, "Land mobile radio systems-a tutorial exposition," *IEEE Communications Magazine*, vol. 23, pp. 34–45, June 1985.

[23] L. Pickering and J. De Rosa, "Refractive multipath model for line-of-sight microwave relay links," *IEEE Trans. Communications*, vol. 27, pp. 1174–1182, Aug. 1979.

[24] C. Bianchi and K. Sivaprasad, "A channel model for multipath interference on terrestrial line-of-sight digital radio," *IEEE Trans. Antennas and Propagation*, vol. 46, pp. 891–901, June 1998.

[25] C. Loo, "A statistical model for a land mobile satellite link," *IEEE Trans. Vehicular Technology*, vol. 34, pp. 122–127, Aug. 1985.

[26] G. Corazza and F. Vatalaro, "A statistical model for land mobile satellite channels and its application to nongeostationary orbit systems," *IEEE Trans. Vehicular Technology*, vol. 43, pp. 738–742, Aug. 1994.

[27] J. Lodge, M. Moher, and S. Crozier, "A comparison of data modulation techniques for land mobile satellite channels," *IEEE Trans. Vehicular Technology*, vol. 36, pp. 28–35, Feb. 1987.

[28] I. Korn, "Error probability of digital modulation in satellite mobile, land mobile, and Gaussian channels with narrow-band receiver filter," *IEEE Trans. Communications*, vol. 40, pp. 697–707, Apr. 1992.

[29] M. Schwartz, W. Bennett, and S. Stein, *Communication systems and techniques.* New York: McGraw-Hill, 1966.

[30] R. Kennedy, *Fading dispersive communication channels.* New York: Wiley-Interscience, 1969.

[31] P. Bello, "Characterization of randomly time-variant linear channels," *IEEE Trans. Communications Systems*, vol. 11, pp. 360–393, Dec. 1963.

[32] J. Parsons and A. Bajwa, "Wideband characterisation of fading mobile radio channels," *IEE Proceedings*, vol. 129, Pt. F, pp. 95–101, Apr. 1982.

[33] E. Biglieri, J. Proakis, and S. Shamai, "Fading channels: information-theoretic and communications aspects," *IEEE Trans. Inform. Theory*, vol. 44, pp. 2619–2692, Oct. 1998.

[34] S. Saunders, *Antennas and propagation for wireless communication systems.* New York: John Wiley, 1999.

[35] S. Stein and J. Jones, *Modern communication principles, with application to digital signaling.* New York: McGraw-Hill, 1967.

[36] W. Gardner, "A sampling theorem for nonstationary random processes," *IEEE Trans. Inform. Theory*, vol. 18, pp. 808–809, Nov. 1972.

[37] S. Stein, "Fading channel issues in system engineering," *IEEE Journal on Selected Areas in Communications*, vol. 5, pp. 68–89, Feb. 1987.

[38] G. Turin and al., "A statistical model of urban multipath propagation," *IEEE Trans. Vehicular Technology*, vol. 21, pp. 1–9, Feb. 1972.

[39] H. Suzuki, "A statistical model for urban radio propagation," *IEEE Trans. Communications*, vol. 25, pp. 673–680, July 1977.

[40] H. Hashemi, "Impulse response modeling of indoor radio propagation channels," *IEEE Journal on Selected Areas in Communications*, vol. 11, pp. 967–978, Sept. 1993.

[41] A. Hewitt and E. Vilar, "Selective fading on LOS microwave links: classical and spread-spectrum measurement techniques," *IEEE Trans. Communications*, vol. 36, pp. 789–796, July 1988.

[42] J. Parsons, D. Demery, and A. Turkmani, "Sounding techniques for wideband mobile radio channels: a review," *IEE Proceedings-I*, vol. 138, pp. 437–446, Oct. 1991.

[43] G. Turin, "Introduction to spread-spectrum antimultipath techniques and their application to urban digital radio," *Proceedings of the IEEE*, vol. 68, pp. 328–353, Mar. 1980.

[44] A. Saleh and R. Valenzuela, "A statistical model for indoor multipath propagation," *IEEE Journal on Selected Areas in Communications*, vol. 5, pp. 128–137, Feb. 1987.

[45] S.-C. Kim, H. Bertoni, and M. Stern, "Pulse propagation characteristics at 2.4 GHz inside buildings," *IEEE Trans. Vehicular Technology*, vol. 45, pp. 579–592, Aug. 1996.

[46] N. Papadakis, A. Kanatas, and P. Constantinou, "Microcellular propagation measurements and simulation at 1.8 GHz in urban radio environment," *IEEE Trans. Vehicular Technology*, vol. 47, pp. 1012–1026, Aug. 1998.

[47] Y. Zhang and Y. Hwang, "Characterization of UHF radio propagation channels in tunnel environments for microcellular and personal communications," *IEEE Trans. Vehicular Technology*, vol. 47, pp. 283–296, Feb. 1998.

[48] U. Charash, "Reception through Nakagami fading multipath channels with random delays," *IEEE Trans. Communications*, vol. 27, pp. 657–670, Apr. 1979.

[49] M. Pätzold, U. Killat, and F. Laue, "An extended Suzuki model for land mobile satellite channels and its statistical properties," *IEEE Trans. Vehicular Technology*, vol. 47, pp. 617–630, May 1998.

[50] D. Polydorou and C. Capsalis, "A new theoretical model for the prediction of rapid fading variations in an indoor environment," *IEEE Trans. Vehicular Technology*, vol. 46, pp. 748–754, Aug. 1997.

[51] J. Hancock and P. Wintz, *Signal detection theory.* New York: McGraw-Hill, 1966.

[52] H. Van Trees, *Detection, estimation, and modulation theory, part III.* New York: John Wiley & Sons, 1968.

[53] A. Mämmela, *Diversity receivers in a fast fading multipath channel.* Ph.D. thesis, University of Oulu, Technical Research Centre of Finland (VTT), Espoo, Dec. 1995.

[54] T. Kailath, "Adaptive matched filters," in *Mathematical optimization techniques* (R. Bellman, ed.), pp. 109–140, Berkeley: University of California Press, 1963.

[55] G. Turin, "On optimal diversity reception," *IRE Trans. Inform. Theory*, vol. 7, pp. 154–166, July 1961.

[56] G. Turin, "On optimal diversity reception II," *IRE Trans. Communications Systems*, vol. 10, pp. 22–31, Mar. 1962.

[57] W. Lindsey, "Error probabilities for Ricean fading multichannel reception of binary and N-ary signals," *IEEE Trans. Inform. Theory*, vol. 10, pp. 339–350, Oct. 1964.

[58] D. Brennan, "Linear diversity combining techniques," *Proceedings of the IRE*, vol. 47, pp. 1075–1102, June 1959.

[59] J. Pierce, "Theoretical diversity improvement in frequency-shift keying," *Proceedings of the IRE*, vol. 46, pp. 903–910, May 1958.

[60] T. Kailath, "On multilink and multidimensional channels," *IRE Trans. Inform. Theory*, vol. 8, pp. 260–262, Apr. 1962.

[61] J. Pierce, "Theoretical limitations on frequency and time diversity for fading binary transmissions," *IRE Trans. Communications Systems*, vol. 9, pp. 186–187, June 1961.

[62] J. Pierce and S. Stein, "Multiple diversity with nonindependent fading," *Proceedings of the IRE*, vol. 48, pp. 89–104, Jan. 1960.

[63] B. Barrow, "Diversity combination of fading signals with unequal mean strengths," *IEEE Trans. Communications Systems*, vol. 11, pp. 73–78, Mar. 1963.

[64] P. Bello and B. Nelin, "The effect of frequency selective fading on the binary error probabilities of incoherent and differentially coherent matched filter receivers," *IEEE Trans. Communications Systems*, vol. 11, pp. 170–186, June 1963. see also corrections, *IEEE Trans. Communications Technology*, vol. 12, pp. 230-231, Dec. 1964.

[65] P. Bello, "Binary error probabilities over selectively fading channels containing specular components," *IEEE Trans. Communication Technology*, vol. 14, pp. 400–406, Aug. 1966.

[66] W. Lindsey, "Error probability for incoherent diversity reception," *IEEE Trans. Inform. Theory*, vol. 11, pp. 491–499, Oct. 1965.

[67] J. Jones, "Multichannel FSK and DPSK reception with three-component multipath," *IEEE Trans. Communication Technology*, vol. 16, pp. 808–821, Dec. 1968.

[68] J. Proakis, "Probabilities of error for adaptive reception of m-phase signals," *IEEE Trans. Communication Technology*, vol. 16, pp. 71–81, Feb. 1968.

[69] N. Beaulieu and A. Abu-Dayya, "Analysis of equal gain diversity on Nakagami fading channels," *IEEE Trans. Communications*, vol. 39, pp. 225–234, Feb. 1991.

[70] N. Beaulieu, "An infinite series for the computation of the complementary probability distribution function of a sum of independent random variables and its application to the sum of Rayleigh random variables," *IEEE Trans. Communications*, vol. 38, pp. 1463–1474, Sept. 1990.

[71] Q. Zhang, "A simple approach to probability of error for equal gain combiners over Rayleigh channels," *IEEE Trans. Vehicular Technology*, vol. 48, pp. 1151–1154, July 1999.

[72] Q. Zhang, "Maximal-ratio combining over Nakagami fading channels with an arbitrary branch covariance matrix," *IEEE Trans. Vehicular Technology*, vol. 48, pp. 1141–1150, July 1999.

[73] Q. Zhang, "Exact analysis of postdetection combining for DPSK and NFSK systems over arbitrarily correlated Nakagami channels," *IEEE Trans. Communications*, vol. 46, pp. 1459–1467, Nov. 1998.

[74] M. Simon and M.-S. Alouini, "A unified approach to the performance analysis of digital communication over generalized fading channels," *Proceedings of the IEEE*, vol. 86, pp. 1860–1877, Sept. 1998.

[75] M. Simon and M.-S. Alouini, "A unified approach to the probability of error for noncoherent and differentially coherent modulations over generalized fading channels," *IEEE Trans. Communications*, vol. 46, pp. 1625–1638, Dec. 1998.

[76] G. Vitetta, U. Mengali, and D. Taylor, "Error probability with incoherent diversity reception of FSK signals transmitted over fast Ricean fading channels," *IEEE Trans. Communications*, vol. 46, pp. 1443–1447, Nov. 1998.

[77] X. Dong, N. Beaulieu, and P. Wittke, "Signaling constellations for fading channels," *IEEE Trans. Communications*, vol. 47, pp. 703–714, May 1999.

[78] S. Sussman, "A matched filter communication system for multipath channels," *IRE Trans. Inform. Theory*, vol. 6, pp. 367–373, June 1960.

[79] H. Ochsner, "Direct-sequence spread-spectrum receiver for communication on frequency-selective fading channels," *IEEE Journal on Selected Areas in Communications*, vol. 5, pp. 188–193, Feb. 1987.

[80] F. Hagmanns and V. Hespelt, "On the detection of bandlimited direct-sequence spread-spectrum signals transmitted via fading multipath channels," *IEEE Journal on Selected Areas in Communications*, vol. 12, pp. 891–899, June 1994.

[81] U. Fawer, "A coherent spread-spectrum diversity-receiver with AFC for multipath fading channels," *IEEE Trans. Communications*, vol. 42, pp. 1300–1311, Feb.-Apr. 1994.

[82] T. Eng and L. Milstein, "Partially coherent DS-SS performance in frequency selective multipath fading," *IEEE Trans. Communications*, vol. 45, pp. 110–118, Jan. 1997.

[83] H. Abdel-Ghaffar and S. Pasupathy, "Partially coherent, suboptimal detectors over Rayleigh fading diversity channels," in *Proc. of the GLOBECOM94, 3rd Comm. Theory Mini-Conf (CTMC)*, (San Francisco, CA), pp. 76–80, Nov.-Dec. 1994.

[84] R. Aiken, "Communication over the discrete-path fading channel," *IEEE Trans. Inform. Theory*, vol. 13, pp. 346–347, Apr. 1967.

[85] M. Alles and S. Pasupathy, "Channel knowledge and optimal performance for two-wave Rayleigh fading channels," *IEEE Trans. Vehicular Technology*, vol. 43, pp. 8–20, Feb. 1994. see also correction, vol. 44, p. 202, Feb. 1995.

[86] M. Alles and S. Pasupathy, "Suboptimum detection for the two-wave Rayleigh-fading channel," *IEEE Trans. Communications*, vol. 42, pp. 2947–2958, Nov. 1994.

[87] H. Abdel-Ghaffar and S. Pasupathy, "Performance of the noncoherent bi-quadratic and GLRT receivers over two-path channels with known amplitudes and Rayleigh fading," *IEEE Trans. Vehicular Technology*, vol. 44, pp. 715–728, Nov. 1995.

[88] G. Turin, "Some computations of error rates for selectively fading multipath channels," in *Proc. of the National Electronics Conference*, vol. 15, pp. 431–440, Mar. 1959.

[89] G. Turin, "The characteristic function of Hermitian quadratic forms in complex normal variables," *Biometrika*, vol. 47, pp. 199–201, June 1960.

[90] J. Imhof, "Computing the distribution of quadratic forms in normal variables," *Biometrika*, vol. 48, no. 3-4, pp. 419–426, 1961.

[91] J. Proakis, "On the probability of error for multichannel reception of binary signals," *IEEE Trans. Communication Technology*, vol. 16, pp. 68–71, Feb. 1968.

[92] K. Biyari and W. Lindsey, "Statistical distributions of Hermitian quadratic forms in complex Gaussian variables," *IEEE Trans. Inform. Theory*, vol. 39, pp. 1076–1082, May 1993.

[93] E. Biglieri, G. Caire, G. Taricco, and J. Ventura-Traveset, "Simple method for evaluating error probabilities," *Electronics Letters*, vol. 32, pp. 191–192, Feb. 1996.

[94] E. Biglieri, G. Caire, G. Taricco, and J. Ventura-Traveset, "Computing error probabilities over fading channels: a unified approach," *European Trans. Telecommunications and related Technologies*, vol. 9, pp. 15–25, Jan.-Feb. 1998.

[95] J. Lehnert and M. Pursley, "Multipath diversity reception of spread-spectrum multiple-access communications," *IEEE Trans. Communications*, vol. 35, pp. 1189–1198, Nov. 1987.

[96] K. Cheun, "Performance of direct-sequence spread-spectrum rake receivers with random spreading sequences," *IEEE Trans. Communications*, vol. 45, pp. 1130–1143, Sept. 1997.

[97] M. Win and Z. Kostić, "Impact of spreading bandwidth on rake reception in dense multipath channels," *IEEE Journal on Selected Areas in Communications*, vol. 17, pp. 1794–1806, Oct. 1999.

[98] R. Aiken, "Error probability for binary signaling through a multipath channel," *Bell System Technical Journal*, vol. 46, pp. 1601–1631, Sept. 1967.

[99] H. Abdel-Ghaffar and S. Pasupathy, "Asymptotical performance of m-ary and binary signals over multipath/multichannel Rayleigh and Ricean fading," *IEEE Trans. Communications*, vol. 43, pp. 2721–2731, Nov. 1995.

[100] S. Fechtel and H. Meyr, "Matched filter bound for trellis-coded transmission over frequency-selective fading channels with diversity," *European Trans. Telecommunications and related Technologies*, vol. 4, pp. 343–354, May-June 1993.

[101] F. Ling, "Matched filter-bound for time-discrete multipath Rayleigh fading channels," *IEEE Trans. Communications*, vol. 43, pp. 710–713, Feb.-Apr. 1995.

[102] J. Mazo, "Exact matched filter bound for two-beam Rayleigh fading," *IEEE Trans. Communications*, vol. 39, pp. 1027–1030, July 1991.

[103] J. Matthews, "Eigenvalues and troposcatter multipath analysis," *IEEE Journal on Selected Areas in Communications*, vol. 10, pp. 497–505, Apr. 1992.

[104] M. Clark, L. Greenstein, W. Kennedy, and M. Shafi, "Matched filter performance bounds for diversity combining receivers in digital mobile radio," *IEEE Trans. Vehicular Technology*, vol. 41, pp. 356–362, Nov. 1992.

[105] V.-P. Kaasila and A. Mämmelä, "Bit error probability of a matched filter in a Rayleigh fading multipath channel," *IEEE Trans. Communications*, vol. 42, pp. 826–828, Feb.-Apr. 1994.

[106] C. Schlegel, "Error probability calculation for multibeam Rayleigh channels," *IEEE Trans. Communications*, vol. 44, pp. 290–293, Mar. 1996.

[107] K.-W. Yip and T.-S. Ng, "Matched filter bound for multipath Ricean-fading channels," *IEEE Trans. Communications*, vol. 46, pp. 441–445, Apr. 1998.

[108] K. Pahlavan and J. Matthews, "Performance of adaptive matched filter receivers over fading multipath channels," *IEEE Trans. Communications*, vol. 38, pp. 2106–2113, Dec. 1990.

[109] V.-P. Kaasila and A. Mämmelä, "Bit error probability of a matched filter in a Rayleigh fading multipath channel in the presence of interpath and intersymbol interference," *IEEE Trans. Communications*, vol. 47, pp. 809–812, June 1999.

[110] A. Kansal, S. Batalama, and D. Pados, "Adaptive maximum SINR rake filtering for DS-CDMA multipath fading channels," *IEEE Journal on Selected Areas in Communications*, vol. 16, pp. 1765–1773, Dec. 1998.

[111] J. Wozencraft, "Sequential reception of time-variant dispersive transmissions," in *Lectures on communication system theory* (E. Baghdady, ed.), pp. 279–320, New York: McGraw-Hill, 1961.

[112] R. Chang and J. Hancock, "On receiver structures for channels having memory," *IEEE Trans. Inform. Theory*, vol. 12, pp. 463–468, Oct. 1966.

[113] K. Abend and B. Fritchman, "Statistical detection for communication channels with intersymbol interference," *Proceedings of the IEEE*, vol. 58, pp. 779–785, May 1970.

[114] L. Bahl, J. Cocke, F. Jelinek, and J. Raviv, "Optimal decoding of linear codes for minimizing symbol error rate," *IEEE Trans. Inform. Theory*, vol. 20, pp. 284–287, Mar. 1974.

[115] Y. Li, B. Vucetic, and Y. Sato, "Optimum soft-output detection for channels with intersymbol interference," *IEEE Trans. Inform. Theory*, vol. 41, pp. 704–713, May 1995.

[116] D. Williamson, R. Kennedy, and G. Pulford, "Block decision feedback equalization," *IEEE Trans. Communications*, vol. 40, pp. 255–264, Feb. 1992.

[117] J. Omura, "Optimal receiver design for convolutional codes and channels with memory via control theoretical concepts," *Inform. Sci.*, vol. 3, pp. 243–266, 1971.

[118] G. Forney Jr., "Maximum-likelihood sequence estimation of digital sequences in the presence of intersymbol interference," *IEEE Trans. Inform. Theory*, vol. 18, pp. 363–378, May 1972.

[119] G. Ungerboeck, "Adaptive maximum-likelihood receiver for carrier-modulated data-transmission systems," *IEEE Trans. Communications*, vol. 22, pp. 624–636, May 1974.

[120] A. Viterbi, "Error bounds for convolutional codes and an asymptotically optimum decoding algorithm," *IEEE Trans. Inform. Theory*, vol. 13, pp. 260–269, Apr. 1967.

[121] G. Bottomley and S. Chennakeshu, "Unification of MLSE receivers and extension to time-varying channels," *IEEE Trans. Communications*, vol. 46, pp. 464–472, Apr. 1998.

[122] B. Hart and D. Taylor, "Extended MLSE diversity receiver for the time- and frequency-selective channel," *IEEE Trans. Communications*, vol. 45, pp. 322–333, Mar. 1997.

[123] K. Chugg and A. Polydoros, "MLSE for an unknown channel-part I: optimality considerations," *IEEE Trans. Communications*, vol. 44, pp. 836–846, July 1996.

[124] Q. Dai and E. Shwedyk, "Detection of bandlimited signals over frequency selective Rayleigh fading channels," *IEEE Trans. Communications*, vol. 42, pp. 941–950, Feb.-Apr. 1994.

[125] W.-H. Sheen and G. Stüber, "MLSE equalization and decoding for multipath-fading channels," *IEEE Trans. Communications*, vol. 39, pp. 1455–1464, Oct. 1991.

[126] D. Dzung and W. Braun, "Performance of coherent data transmission in frequency-selective Rayleigh fading channels," *IEEE Trans. Communications*, vol. 41, pp. 1335–1341, Sept. 1993.

[127] P. Monsen, "Feedback equalization for fading dispersive channels," *IEEE Trans. Inform. Theory*, vol. 17, pp. 56–64, Jan. 1971.

[128] R. Iltis, "A Bayesian maximum-likelihood sequence estimation algorithm for a priori unknown channels and symbol timing," *IEEE Journal on Selected Areas in Communications*, vol. 10, pp. 579–588, Apr. 1992.

[129] W. Leon and D. Taylor, "An adaptive receiver for the time- and frequency-selective fading channel," *IEEE Trans. Communications*, vol. 45, pp. 1548–1555, Dec. 1997.

[130] S. Chen, B. Mulgrew, and S. McLaughlin, "Adaptive Bayesian equalizer with decision feedback," *IEEE Trans. Signal Processing*, vol. 41, pp. 2918–2927, Sept. 1993.

[131] S. Chen, S. McLaughlin, B. Mulgrew, and P. Grant, "Adaptive Bayesian decision feedback equalizer for dispersive mobile radio channels," *IEEE Trans. Communications*, vol. 43, pp. 1937–1946, May 1995.

[132] K. Giridhar, J. Shynk, R. Iltis, and A. Mathur, "Adaptive MAPSD algorithms for symbol and timing recovery of mobile radio TDMA signals," *IEEE Trans. Communications*, vol. 44, pp. 976–987, Aug. 1996.

[133] J. Proakis, "Adaptive equalization for TDMA digital mobile radio," *IEEE Trans. Vehicular Technology*, vol. 40, pp. 333–341, May 1991.

[134] S. Qureshi, "Adaptive equalization," *Proceedings of the IEEE*, vol. 73, pp. 1349–1387, Sept. 1985.

[135] P. Monsen, "Fading channel communications," *IEEE Communications Magazine*, vol. 18, pp. 16–25, Jan. 1980.

[136] M. Stojanovic, J. Proakis, and J. Catipovic, "Analysis of the impact of channel estimation errors on the performance of a decision-feedback equalizer in fading multipath channels," *IEEE Trans. Communications*, vol. 43, pp. 877–886, Feb.-Apr. 1995.

[137] N. Lo, D. Falconer, and A. Sheikh, "Adaptive equalization and diversity combining for mobile radio using interpolated channel estimates," *IEEE Trans. Vehicular Technology*, vol. 40, pp. 636–645, Aug. 1991.

[138] P. Balaban and J. Salz, "Optimum diversity combining and equalization in digital data transmission with applications to cellular mobile radio, part I & II," *IEEE Trans. Communications*, vol. 40, pp. 885–907, May 1992.

[139] E. Baccarelli and R. Cusani, "Combined channel estimation and data detection using soft statistics for frequency-selective fast-fading digital links," *IEEE Trans. Communications*, vol. 46, pp. 424–427, Apr. 1998.

[140] W. Zhuang and W. Huang, "Phase precoding for frequency-selective Rayleigh and Ricean slowly fading channels," *IEEE Trans. Vehicular Technology*, vol. 46, pp. 129–142, Feb. 1997.

[141] B. Hart and D. Taylor, "Maximum-likelihood synchronization, equalization, and sequence estimation for unknown time-varying frequency-selective Ricean channels," *IEEE Trans. Communications*, vol. 46, pp. 211–221, Feb. 1998.

[142] R. Lupas and S. Verdú, "Linear multiuser dectectors for synchronous code-division multiple-access channels," *IEEE Trans. Inform. Theory*, vol. 35, pp. 123–136, Jan. 1989.

[143] R. Lupas and S. Verdú, "Near-far resistance of multiuser detectors in asynchronous channels," *IEEE Trans. Communications*, vol. 38, pp. 496–508, Apr. 1990.

[144] Z. Zvonar and D. Brady, "Coherent and differentially coherent multiuser detectors for asynchronous CDMA frequency-selective channels," in *Proc. IEEE Milcom Conf.*, (San Diego, CA USA), pp. 442–446, Oct. 1992.

[145] Z. Zvonar and D. Brady, "Linear multipath-decorrelating receivers for CDMA frequency-selective fading channels," *IEEE Trans. Communications*, vol. 44, pp. 650–653, June 1996.

[146] T. Kailath, "Correlation detection of signals perturbed by a random channel," *IRE Trans. Inform. Theory*, vol. 6, pp. 361–366, June 1960. see also correction, vol. 7, p. 50, Jan. 1961.

[147] T. Kailath and H. Poor, "Detection of stochastic processes," *IEEE Trans. Inform. Theory*, vol. 44, pp. 2230–2259, Oct. 1998.

[148] R. Morley Jr. and D. Snyder, "Maximum likelihood sequence estimation for randomly dispersive channels," *IEEE Trans. Communications*, vol. 27, pp. 833–839, June 1979.

[149] R. Haeb and H. Meyr, "A systematic approach to carrier recovery detection of digitally phase modulated signals on fading channels," *IEEE Trans. Communications*, vol. 37, pp. 748–754, July 1989.

[150] R. De Gaudenzi, "Direct-sequence spread-spectrum chip tracking in the presence of unresolvable multipath components," *IEEE Trans. Vehicular Technology*, vol. 48, pp. 1573–1583, Sept. 1999.

[151] D. Cox, "Delay Doppler characteristics of multipath propagation at 910 MHz in a suburban mobile radio environment," *IEEE Trans. Antennas and Propagation*, vol. 20, pp. 625–635, Sept. 1972.

[152] J. Ehrenberg, T. Ewart, and R. Morris, "Signal-processing techniques for resolving individual pulses in a multipath signal," *Journal Acoustical Society of America*, vol. 63, pp. 1861–1865, June 1978.

[153] B. Hunt, "Deconvolution of linear systems by constrained regression and its relationship to the Wiener theory," *IEEE Trans. Automatic Control*, vol. 17, pp. 703–705, Oct. 1972.

[154] G. Turin, "On the estimation in the presence of noise of the impulse response of a random, linear filter," *IRE Trans. Inform. Theory*, vol. 3, pp. 5–10, Mar. 1957.

[155] R. De Figueiredo and C.-L. Hu, "Waveform feature extraction based on Tauberian approximation," *IEEE Trans. Pattern Analysis and Machine Intelligence*, vol. 4, pp. 105–116, Mar. 1982.

[156] S. Kay, *Modern spectral estimation: theory and application.* Englewood Cliffs, New Jersey: Prentice Hall, 1988.

[157] J. Burg, "Maximum entropy spectral analysis," *Proc. 37th Meet. Soc. Exploration Geophysicists*, 1967.

[158] R. Schmidt, "Multiple emitter location and signal parameter estimation," *IEEE Trans. Antennas and Propagation*, vol. 34, pp. 276–280, Mar. 1986.

[159] E. Robinson, "A historical perspective of spectrum estimation," *Proceedings of the IEEE*, vol. 70, pp. 885–906, Sept. 1982.

[160] "Special issue on Spectral Estimation," *Proceedings of the IEEE*, vol. 70, Sept. 1982.

[161] T. Korhonen and S.-G. Häggman, "Novel recursive deconvolution noise compensation method for direct sequence radio channel sounding," in 48^{th} *IEEE Vehicular Technology Conference (VTC98')*, (Ottawa, Canada), pp. 688–692, 1998.

[162] J. Padgett, C. Günther, and T. Hattori, "Overview of wireless personal communications," *IEEE Communications Magazine*, vol. 33, pp. 28–41, Jan. 1995.

[163] B. Sklar, "Rayleigh fading channels in mobile digital communication systems part I: characterization," *IEEE Communications Magazine*, vol. 35, pp. 136–146, Sept. 1997.

[164] B. Sklar, "Rayleigh fading channels in mobile digital communication systems part II: mitigation," *IEEE Communications Magazine*, vol. 35, pp. 148–155, Sept. 1997.

[165] M. Fitz and al., "The 220 MHz ITS spectral allocation: potential, pitfalls, and applications," *IEEE Communications Magazine*, vol. 34, pp. 42–54, Oct. 1996.

[166] A. Fukasawa and al., "Wideband CDMA system for personal radio communications," *IEEE Communications Magazine*, vol. 34, pp. 116–123, Oct. 1996.

[167] "The CDMA2000 (ITU-R) RTT candidate submission," tech. rep., CDG, June 1998. available at http://www.cdg.org/3GPavilion/Detailed_Info/IMT_2000/TR455_RTT_V17.pdf.

[168] "The ETSI UMTS Terrestrial Radio Access (UTRA) ITU-R RTT candidate submission," tech. rep., ETSI, Jan. 1998. available at http://www.etsi.org/smg/utra/utra.pdf.

[169] "Japan's proposal for candidate radio transmission technology on IMT-2000:W-CDMA," tech. rep., ARIB, June 1998. available at http://www.itu.int/imt/2-radio-dev/proposals/j/j.pdf.

[170] W. McGee, "Complex Gaussian noise moments," *IEEE Trans. Inform. Theory*, vol. 17, pp. 149–157, Mar. 1971.

[171] R. Steele, *Mobile radio communications*. New York: IEEE Press, 1992.

[172] H. Poor, *An introduction to signal detection and estimation*. New York: Springer-Verlag, 1988.

[173] T. Kailath, "Likelihood ratios for Gaussian processes," *IEEE Trans. Inform. Theory*, vol. 16, pp. 276–288, May 1970.

[174] J. Winters, "Differential detection with intersymbol interference and frequency uncertainty," *IEEE Trans. Communications*, vol. 32, pp. 25–33, Jan. 1984.

[175] W. Rudin, *Real and complex analysis, 2nd edition.* New York: Tata McGraw-Hill, 1974.

[176] L. Brandenburg, "Approximation of finite-energy random processes by continuous processes," *IEEE Trans. Inform. Theory*, vol. 20, pp. 653–654, Sept. 1974.

[177] J. Magnus and H. Neudecker, *Matrix differential calculus with applications in statistics and econometrics.* New York: John Wiley & Sons, 1988.

[178] R. Liptser and A. Shiryayev, *Statistics of random processes I, General Theory.* New York: Springer-Verlag, 1977.

[179] B. Øksendal, *Stochastic differential equations, 4th edition.* New York: Springer, 1995.

[180] Z. Schuss, *Theory and applications of stochastic differential equations.* New York: John Wiley & Sons, 1980.

[181] T. Kailath and P. Frost, "Mathematical modeling of stochastic processes," in *Stochastic Problems in Control (A symposium of the American Automatic Control Council)*, (Ann Arbor, MI USA), pp. 1–38, June 1968.

[182] E. Wong and B. Hajek, *Stochastic processes in engineering systems.* New York: Springer-Verlag, 1985.

[183] J. Thomas, *An introduction to applied probability and random processes.* New York: John Wiley & Sons, 1971.

[184] F. Tricomi, *Integral equations.* New York: Interscience Publishers, 1957.

[185] G. Watson, *A Treatise on the Theory of Bessel Functions, second edition.* Cambridge University Press, 1966.

[186] T. Kailath, "A note on least-squares estimates from likelihood ratios," *Information and Control*, vol. 13, pp. 534–540, 1968.

[187] H. Van Trees, *Detection, estimation, and modulation theory, part I.* New York: John Wiley & Sons, 1968.

[188] F. Danilo and H. Leib, "Receivers structures and performance for unresolved Ricean/Rayleigh multipath fading channels," in 48^{th} *IEEE Vehicular Technology Conference*, vol. 3, (Ottawa, Canada), pp. 1979–1983, May 1998.

[189] T. Kailath, *Lectures on Wiener and Kalman filtering.* New York: Springer-Verlag, 1981.

[190] M. Evgrafov, *Analytic functions.* Philadelphia: Saunders Mathematics books, 1966.

[191] J. Doob, *Stochastic processes.* New York: John Wiley & Sons, 1953.

[192] W. Kaplan, *Advanced calculus.* Reading, Massachusetts: Addison-Wesley Publishing Company, 1984.

[193] G. Turin, "Error probabilities for binary symmetric ideal reception through nonselective slow fading and noise," *Proceedings of the IRE*, vol. 46, pp. 1603–1619, Sept. 1958. see also correction, same volume, p. 1913, 1958.

[194] P. Kam, "On orthogonal signaling over the slow nonselective Ricean fading channel with unknown specular component," *IEEE Trans. Communications*, vol. 41, pp. 817–819, June 1993.

[195] A. Furuskär, S. Mazur, F. Müller, and H. Olofsson, "EDGE: Enhanced Data Rates for GSM and TDMA/IS136 Evolution," *IEEE Personal Communications*, vol. 6, pp. 56–66, June 1999.

[196] R. Pirhonen, T. Rautava, and J. Penttinen, "TDMA convergence for packet data services," *IEEE Personal Communications*, vol. 6, pp. 68–73, June 1999.

[197] G. Turin, "Commutation signaling-an antimultipath technique," *IEEE Journal on Selected Areas in Communications*, vol. 2, pp. 548–562, July 1984.

[198] Y. Qian and H. Leib, "An enhanced anti-multipath modulation approach (SDPSK/SMPDI)," in *Proc. IEEE Int. Conf. Communications (ICC)*, vol. 1, (Dallas, TX USA), pp. 369–373, June 1996.

[199] I. Crohn, G. Schultes, R. Gahleitner, and E. Bonek, "Irreducible error performance of a digital portable communication system in a controlled time-dispersion indoor channel," *IEEE Journal on Selected Areas in Communications*, vol. 11, pp. 1024–1033, Sept. 1993.

[200] A. Molisch, L. Lopes, M. Paier, J. Fulh, and E. Bonek, "Error floor of unequalized wireless personal communications systems with MSK modulation and training-sequence-based adaptive sampling," *IEEE Trans. Communications*, vol. 45, pp. 554–562, May 1997.

[201] L.-C. Chu and U. Mitra, "Performance analysis of an improved MMSE multiuser receiver for mismatched delay channels," *IEEE Trans. Communications*, vol. 46, pp. 1369–1380, Oct. 1998.

[202] A. Papoulis, *Probability, random variables, and stochastic processes, 3rd edition.* New York: McGraw-Hill, 1991.

[203] R. Mazumdar and A. Bagchi, "On the relation between filter maps and correction factors in likelihood ratios," *IEEE Trans. Inform. Theory*, vol. 41, pp. 833–836, May 1995.

[204] E. Wong and M. Zakai, "On the convergence of ordinary integrals to stochastic integrals," *The Annals of Mathematical Statistics*, vol. 36, pp. 1560–1564, 1965.

[205] A. Whalen, *Detection of signals in noise.* New York: Academic Press, 1971.

[206] A. Viterbi, *Principles of coherent communication.* New York: McGraw-Hill, 1966.

[207] H. Kagiwada, R. Kalaba, and B. Vereeke, "The invariant imbedding numerical method for Fredholm integral equations with degenerate kernels," *Journal Approximation Theory*, vol. 1, pp. 355–364, 1968.

[208] A. Jazwinski, *Stochastic processes and filtering theory.* New York: Academic Press, 1970.

[209] N. Wiener, "Generalized harmonic analysis," *Acta Math.*, vol. 55, pp. 117–258, 1930.

[210] M. Loève, *Probability Theory II, 4nd edition.* New York: Springer-Verlag, 1978.

[211] K. Miller, *Complex Stochastic Processes an introduction to theory and application.* Reading, Massachusetts: Addison-Wesley Publishing Company, 1974.

[212] V. Krishnan, *Nonlinear filtering and smoothing: An introduction to martingales, stochastic integrals and estimation.* New York: John Wiley & Sons, 1984.

[213] I. Gihman and A. Skorohod, *The theory of stochastic processes III.* New York: Springer-Verlag, 1979.

[214] F. Riesz and B. SZ.-Nagy, *Functional Analysis, translated from the 2nd French edition by L.F. Boron.* New York: Frederick Ungar Publishing, 1955.

[215] O. Nielsen, *An Introduction to Integration and Measure Theory.* New York: John Wiley & Sons, 1997.

[216] C. Helstrom, *Elements of signal detection, and estimation.* Englewood Cliffs, New Jersey: Prentice Hall, 1995.

[217] J. Ortega, *Matrix theory: a second course.* New York: Plenum Press, 1987.

[218] R. Courant and D. Hilbert, *Methods of mathematical physics, Vol. I.* New York: Interscience Publishers, 1953.

[219] R. Bellman, "Functional equations in the theory of dynamic programming-VII. A partial differential equation for the Fredholm resolvent," *Proc. of the American Mathematical Society*, vol. 8, pp. 435–440, June 1957.

[220] A. Siegert, "A systematic approach to a class of problems in the theory of noise and other random phenomena, part II, examples," *IRE Trans. Inform. Theory*, vol. 3, pp. 38–43, Mar. 1957.

[221] T. Kato, *Pertubation theory for linear operators.* New York: Springer, 1980.